THE APOLLO 15 LUNAR SAMPLES

EDITED BY

J. W. CHAMBERLAIN

AND

C. WATKINS

THE LUNAR SCIENCE INSTITUTE

HOUSTON, TEXAS

THE APOLLO 15 LUNAR SAMPLES

EDITED BY

J. W. CHAMBERLAIN
AND
C. WATKINS

Reproduced and Distributed by
The Lunar Science Institute
3303 NASA Rd. 1
Houston, Texas 77058

Library of Congress Card No. 72-93377

PREFACE

Apollo 15 was launched on 26 July 1971, and it was an outstanding scientific success. However, the lunar rocks and soil returned by that mission were, with few exceptions, not analyzed to the point where useful results could be reported at the Third Lunar Science Conference held at Houston, 10-13 January 1972. On the other hand, Apollo 16, also highly productive, will likely dominate the Fourth Lunar Science Conference in March 1973, and Apollo 15, in some respects, could become the forgotten mission.

Consequently, the Lunar Science Institute, at the suggestion of NASA's Lunar Sample Analysis Planning Team, undertook to produce this volume of short papers, similar in scope to the expanded abstracts of the Conference papers that we published immediately after the Third Conference. These short papers are in no way intended to substitute for more detailed discussions published in the Proceedings of the Lunar Science Conferences and in the standard journals. This volume is, however, intended to focus attention on the variety of research being conducted on Apollo 15 samples.

These manuscripts were received by the editors in the four-week period before mid-September 1972.

J. W. C.

C. W.

Houston
6 October 1972

TABLE OF CONTENTS

V. CARBON CHEMISTRY

VI. ISOTOPES, AGING, AND TRACKS

XI. INDEXES

PETROLOGY OF THE 2-4 mm SIZED SOIL FRAGMENTS FROM APOLLO 15; K. L. Cameron, J. W. Delano, A. E. Bence, and J. J. Papike, State Univ. of New York, Stony Brook, N. Y. 11790

A petrologic examination has been made of the 2-4 mm sized soil fragments from Apollo 15 sample stations 2 (St. George Crater) and 6 (east of Spur Crater) on the Apennine Front, and stations 4 (Dune Crater) and 9A (edge of Hadley Rill) on the Mare plains. Polished thin sections, suitable for electron microprobe analysis, were made of each fragment; furthermore, a number of the fragments were also dated by the ^{40}Ar-^{39}Ar incremental heating method.(1)

The Apennine Front samples are composed largely of brown glass microbreccias (Table 1), whereas those from the plains are dominated by fragments of mare basalts. In addition, individual 2-4 mm fragments of a gabbroic anorthosite, a KREEP basalt, and a recrystallized polymict breccia have also been found.

The brown glass microbreccias typically contain monomineralic grains of plagioclase, pyroxene and olivine, green glass spheres and sphere fragments, angular fragments of other glasses, and clasts of mare and non-mare crystalline rocks set in a matrix of fine particles of brown glass. The microbreccias from the Apennine Front are believed to be post-Imbrium regolith breccias because of their high content of matrix glass. However, their abundant trapped argon content(1) precludes $^{40}Ar/^{39}Ar$ age measurements.

Two major textural-compositional types of mare basalts observed in the larger rocks(2) can also be distinguished in the 2-4 mm soil fragments. These are the (1) pyroxene-porphyritic (e.g., rocks 15499, 15058) and (2) poikilitic plagioclase types (e.g., rock 15555). The pyroxene porphyritic basalts are characterized by composite, zoned clinopyroxene phenocrysts (pigeonite cores and augite rims) with variable degrees of form development set in a groundmass that ranges from glassy to aphanitic/variolitic to subophitic. One variant of this basalt type (similar to rock 15016) contains abundant vesicles lined with ilmenite plates. The poikilitic plagioclase basalts contain phenocrysts of olivine and clinopyroxene (pigeonite zoned to augite) in a groundmass of smaller euhedral augite and olivine crystals enclosed by large poikilitic plagioclase (An_{85-92}). The pyroxene porphyritic basalts are the most common type and are found in the soil at all four stations; the poikilitic plagioclase type dominates in the 2-4 mm soil fragments at station 9A, but is also present in lesser amounts at the other stations. No "new" textural-compositional types of mare basalts, that is, types not found in the large basalt samples, have been recognized. Thirteen of the 2-4 mm fragments of mare basalts have been dated.(1) Most cluster near 3.3 G.y., and there is no obvious correlation of age with textural type. Basalt fragments, texturally identical to those from the mare, are present in the front samples (Table 1), and these undoubtedly were thrown up on the Apennine Front by meteoritic impacts on the Mare plains.

Only three 2-4 mm fragments of non-mare crystalline rocks have been found (Table 1). Crystalline rock fragments are also uncommon in the brown glass

Apollo 15 Coarse Fines

K. L. Cameron

microbreccias. Nevertheless, the non-mare crystalline rocks can be divided into four general categories; (1) anorthositic rocks, (2) KREEP basalts, (3) recrystallized noritic fragments, and (4) recrystallized polymict microbreccias.

The anorthositic rock fragments (∿ 5 fragments > 0.25 mm) are composed primarily of calcic plagioclase (> An_{90} with most near An_{95}), and most contain a Ca-rich pyroxene ($En_{48}Wo_{42}Fs_{10}$ to $En_{35}Wo_{42}Fs_{23}$) plus olivine (Fa_{30-35}) and/or orthopyroxene (∿ $En_{50}Wo_5Fs_{45}$).

About eight fragments (> 0.25 mm) of KREEP basalt[3] have been found. These have subophitic to intersertal texture (average grain size < ½ mm) and are composed primarily of Ca-poor pyroxene ($En_{85}Wo_2Fs_{12}$ to $En_{50}Wo_{15}Fs_{35}$) and plagioclase (An_{80} to An_{90}), and commonly contain interstitial glass of "granitic" composition (e.g., 77% SiO_2, 6% K_2O).

The recrystallized noritic fragments (∿ 10 fragments > 0.25 mm) appear to have been both brecciated and thermally annealed. They have an average grain size of 20-50μ and contain olivine (Fo_{65} to Fo_{75}), Ca-poor pyroxene ($En_{80}Wo_3Fs_{17}$ to $En_{60}Wo_{20}Fs_{20}$), plagioclase (An_{85} to An_{95}) and scattered grains of ilmenite. These fragments are more aluminous (∿ 19 to 26 wt.% Al_2O_3) and less potassic (K_2O < 0.15 wt.%) than the KREEP basalts (Al_2O_3 = 16-19 wt.%, K_2O = 0.5 to 1.0 wt.%). All recrystallized noritic fragments have similar mineralogy, but rocks of several different bulk compositions (e.g., Highlands basalts and Low-K Fra Mauro basalts[4]) may be included in this category.

The recrystallized polymict breccias (∿ 5 fragments > 0.25 mm) contain little or no glass, have a fine-grained granoblastic texture which suggests thermal metamorphism and usually contain recognizable rock fragments. One such breccia, which encloses an anorthositic rock fragment, was dated at 3.99 G.y.[1]

Spheres and sphere fragments of green glass are abundant in the brown-glass microbreccias. The spheres and fragments which are entirely glass are transparent and emerald green when viewed megascopically. Others, which are identical in bulk composition, contain feathery quench olivine crystals and appear a more translucent milky green. The emerald green glass is extremely uniform in composition (avg. of 13 analyses-SiO_2 = 45.4 wt.%, Al_2O_3 = 7.48 wt.%, TiO_2 = 0.43 wt.%, Cr_2O_3 = 0.55 wt.%, FeO = 19.9 wt.%, MnO = 0.26 wt.%, MgO = 17.5 wt.%, CaO = 8.22 wt.%, Na_2O = 0.12 wt.%, K_2O = 0.01 wt.%) and has the normative composition of a feldspathic peridotite (plagioclase = 21.1%, olivine 30.2%, orthopyroxene = 29.3%, calcic pyroxene = 17.7, ilmenite = 0.7). There are at least two possible origins for the green glass spheres: magmatic and impact melting. The extreme uniformity in composition, the absence of enclosed relict shock crystals, and the absence of rock fragments of composition similar to the green glass argue against an impact melt origin. Similar green glass spheres and sphere fragments from 15426 have been dated at 3.79 G.y.[1] and the green glass thus may be related to extrusive igneous activity caused by the Imbrium impact event.

Figure 1 shows the composition of pyroxenes that occur as single crystals in the size range 5-200μ, in four brown-glass microbreccias from the Apennine Front (two from Station 6 and two from Station 2). Ca-rich pyroxenes which plot near the diopside-hedenbergite join are very rare. About half of the pyroxenes are Ca-poor, have Fe-Mg ratios less than 1/3, and thus are similar in

composition to the pyroxenes from the KREEP basalts and recrystallized noritic fragments. Pyroxenes more Fe-rich than Fe:Mg = 1/3 are dominantly subcalcic augites; many of these are probably contaminants derived from the mare basalts. No differences were found between the pyroxenes from Stations 2 and 6.

At present only about 20 analyses of single crystals of plagioclase from the brown-glass microbreccias have been made. These, however, are dominantly more calcic than An_{93} and suggest a significant contribution of anorthositic material.

In summary:

(1) The 2-4 mm soil fragments from the Mare plains (Stations 4 and 9A) are composed dominantly of Mare basalts. These fragments are texturally and mineralogically similar to the large Mare basalt samples. The ^{40}Ar-^{39}Ar ages of the 2-4 mm fragments cluster at about 3.3 G.y. with no apparent correlation of textural-mineralogical type with age.

(2) About 90% of the 2-4 mm fragments from the Apennine Front (Stations 2 and 6) are brown-glass microbreccias. These are probably post-Imbrian regolith breccias developed on Imbrium ejecta.

(3) Non-Mare crystalline rock fragments are rare in the samples examined, but the compositions of pyroxene and plagioclase crystals in the brown-glass (regolith) microbreccias from the Apennine Front suggest that the Imbrium ejecta below the regolith is composed of an intimate mixture of comminuted noritic material (KREEP basalt and/or recrystallized norites) probably of volcanic and/or hypabysal origin and anorthositic (Highlands) material. With the exception of the high calcium plagioclase single crystals and rare clinopyroxenes with optically visible exsolution lamellae, no recognizable derivatives of plutonic rocks were found.

(4) The emerald green spheres and sphere fragments are extremely uniform in composition and may be of extrusive magmatic origin. This activity occurred at 3.79 G.y.[(1)]

References

(1) Husain, L., 1972, The ^{40}Ar-^{39}Ar and cosmic ray exposure ages of Apollo 15 crystalline rocks, breccias and glasses. "The Apollo 15 Lunar Samples" ed. J. W. Chamberlain and C. Watkins (Houston: Lunar Science Institute).

(2) Bence, A. E. and J. J. Papike, 1972, Pyroxenes as recorders of lunar basalt petrogenesis: Chemical trends due to crystal-liquid interaction. Proc. Third Lunar Sci. Conf., Geochim. Cosmochim. Acta, in press.

(3) Meyer, Charles, Jr., 1972, Mineral assemblages and the origin of non-mare lunar rock types. Lunar Science-III, pp. 542-544. Lunar Sci. Inst. Contr. No. 88.

(4) Reid, A. M., J. Warner, W. I. Ridley, R. W. Brown, 1972, Major element composition of glasses in three Apollo 15 soils. Preprint of paper submitted to Geochim. Cosmochim. Acta.

Apollo 15 Coarse Fines
K. L. Cameron

Table 1. 2-4 mm sized soil fragments from Apollo 15.

Station	Location	Sample number	Glassy fragments*	Mare basalts	Others	Total
2	Apennine Front	15103	24 (89%)	2 (7%)	1[a] (4%)	27
6	Apennine Front	15263	29 (88%)	3 (9%)	1[b] (3%)	33
4	Mare Surface	15473	14 (32%)	26 (63%)	2[c] (5%)	42
9A	Mare Surface	15603	10 (27%)	27 (73%)	0	37

Total number of fragments = 139

*Mostly brown-glass microbreccias.
a = one KREEP basalt.
b = one recrystallized polymict breccia.
c = one gabbroic anorthosite, one single pyroxene crystal.

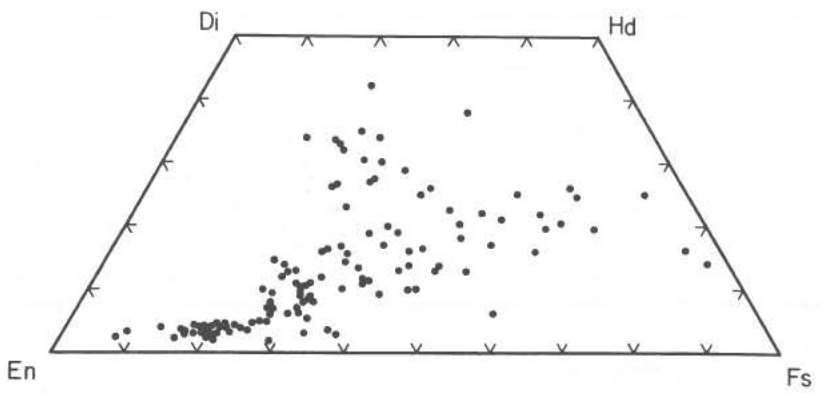

Figure 1

THE SOURCE AREA OF APOLLO 15 "GREEN GLASSES".

Carusi A.,Ist.Geol.Univ.Roma, Cavarretta G.,Ist.Geol.Univ.Roma, Cinotti F.,Ist.Geol.Univ.Roma,Civitelli G.,Ist.Geol.Univ.Roma, Coradini A.,Ist.Geol.Univ.Roma, Fulchignoni M.,Lab.Astrofis.,CNR, Frascati, Funiciello R.,Ist.Geol.Univ.Roma, Taddeucci A.,Ist.Geochim.Univ.Roma,Trigila R.,Ist.Min.Petr.Univ.Roma.

The Q-mode analysis was performed on chemical data of 1249 glassy particles contained in the samples returned from Apollo 11, 12,14 and Luna 16 missions.

Three end-members has been derived from multifactorial analysis,viz. (a) mare basalt, (b) anorthosite, (c) KREEP component.

Assuming for the chemical composition of the end-members the data from LINDSAY (1971) (basalt),LSPET (1972) Apollo 15 rock 15415 (anorthosite), and LSPET (1970) Apollo 12 rock 12013 (KREEP) a mixing model has been used in order to determine the concentration of each end-member in a single particle.

In a triangular diagram with the vertices representing 100% of each end-member the composition has been plotted of the glasses taken into account. Within each triangle (figs.1,2,3,4) the samples are clustered in different areas, corresponding to a particular chemistry. The most populated group reflects the mean chemical composition of the main geological unit of the sampled areas, whereas the less populated ones have to be related to farther material as well as to less abundant local material.

The evidence arises that the glassy particles may also reflect the lithology of the impacted area lying far away from the landing site.

On the ground of these considerations, a dynamical model can be sketched out accounting for the displacement of the glassy particles during an impact event. By applying the model to a homogeneous family of glassy particles their source areas can be detected.

We had the opportunity to test this method in the area of the Apennines front. In fact the Apollo 15 "pyroxenitic green glasses",as they will be described, can be really considered a very peculiar and homogeneous group.

Six samples of fines from Apollo 15 mission, with diameter

THE SOURCE AREA OF APOLLO 15 "GREEN GLASSES"

Carusi A.

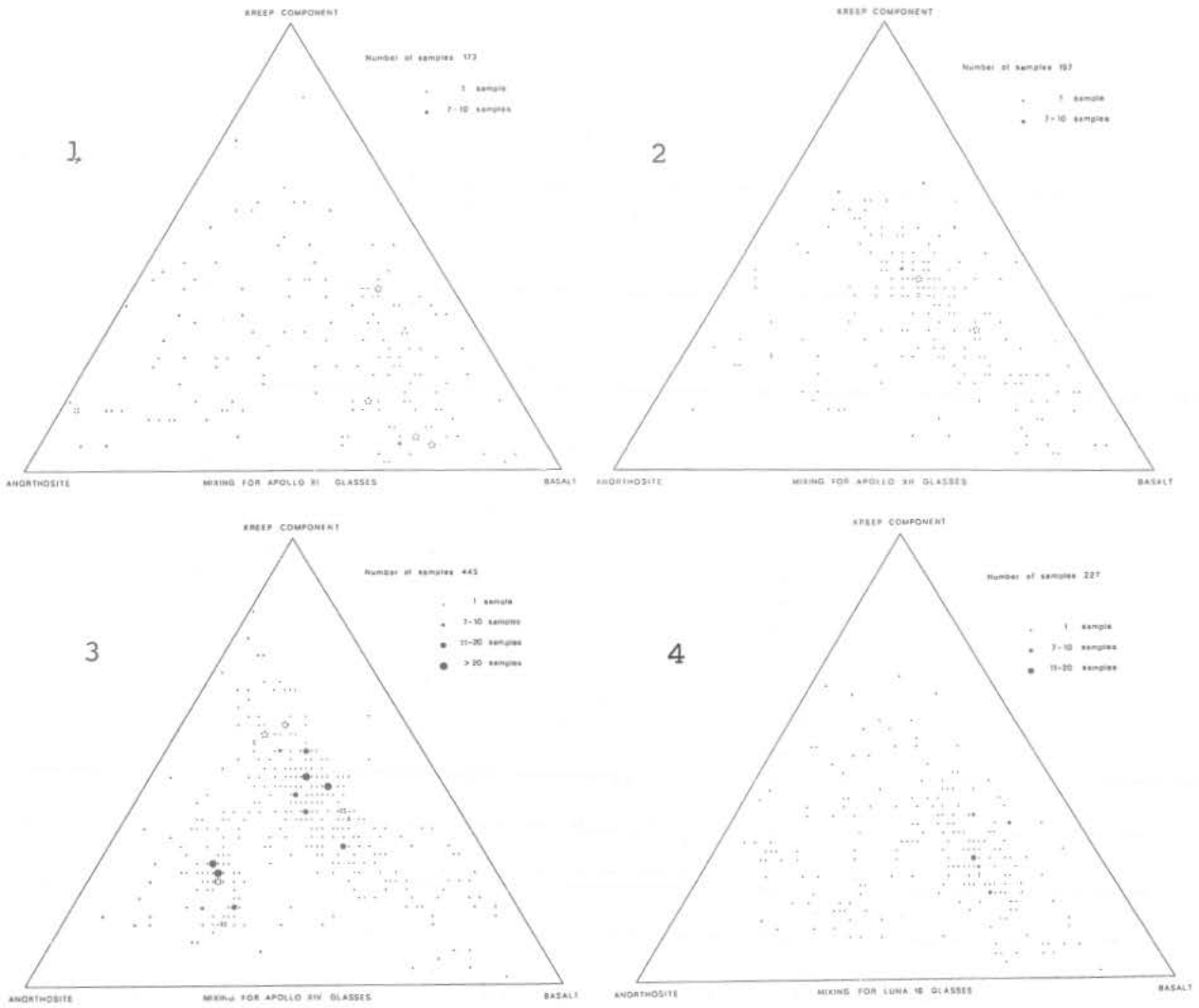

Figs. 1,2,3,4 - Composition of the glassy particles with respect to the end-members. About 46% of glasses from Mare Tranquillitatis (Apollo 11) are grouped in the area with more than 50% of basaltic component. The remaining samples are quite spread on the triangle. The glasses from Apollo 12 mission are substantially grouped in a cluster shifted toward the KREEP component corner. The KREEP group appears as a well defined one in the Apollo 14 triangle, together with a cluster of glasses that contains more than 50% of anorthositic component (26% of the particles). In the samples from Luna 16 probe, 42% of glasses contains more than 50% of basaltic component and results very well defined.

Courtesy of Geologica Romana.

THE SOURCE AREA OF APOLLO 15 "GREEN GLASSES"

Carusi A.

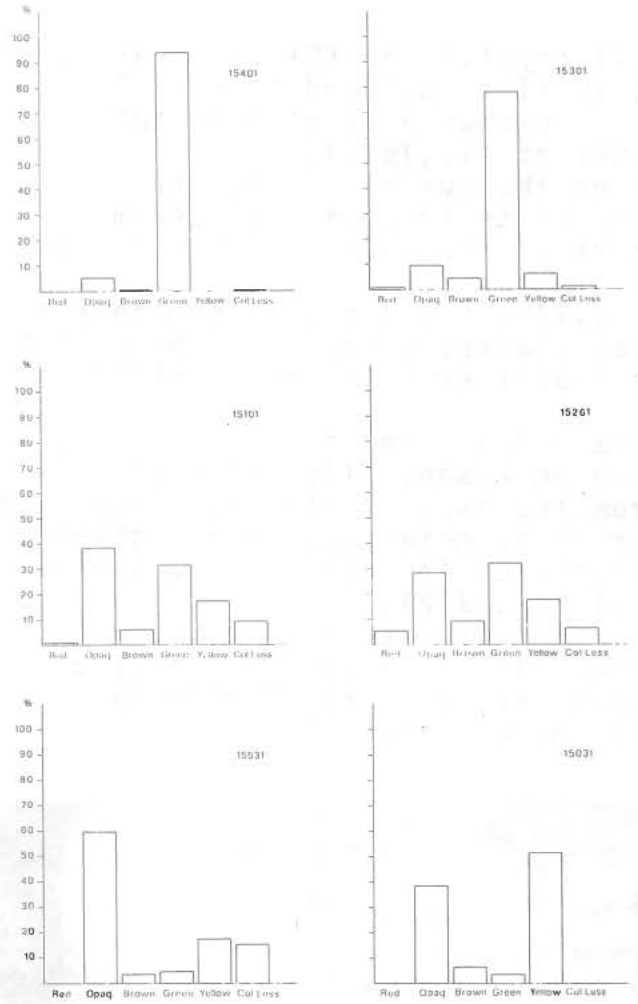

Fig.5 - Distribution of the glassy rotational particles in samples 15031,74, 15101,129, 15261,86, 15301,115, 15401,59, 15531,61 with respect to their colour.

less than 1 mm were examined: sample 15031,74, 15531,61, 15101,29, 15301,115, 15261,86 15401,59.

Regarding the grain size distribution, no significant differences were revealed. The abundance of glassy rotational forms in the soils shows a wide range of variations. The range is essentially due to the contribution of the green spheroids distinctive of several soils of Apollo 15 mission. The distribution follows a trend decreasing from sample 15401 (from a fillet on a boulder crater by green material near the front of Apennines, station 6A) (fig.5).

Major element chemistry of green spheroids was obtained by means of ARL microprobe at NASA MSC by A. Reid. Some green particles of our samples 15401, 15101, 15531 and more than one hundred green particles of other Apollo 15 samples show an absolute homogeneity. Particles are supposed to derive from pyroxenitic material in the Apennine front (REID et Al.,1972). By means of SEM non-dispersive detector the occurrence has been observed as well as the chemical composition of the surface coating, the occurrence of fractures, low velocity and high velocity impacts on samples 15101, 15401, 15301, 15261, where the abundance of green forms is significant.

The coating has been roughly analyzed by means of SEM non-dispersive system, and has generally shown the same composition of the green glasses. However in few cases and particularly in samples 15101 and 15261, KREEP or anorthositic coating has been detected.

Figure 5 - Courtesy of Geologica Romana.

THE SOURCE AREA OF APOLLO 15 "GREEN GLASSES"

Carusi A.

On 10% of the surfaces small crystals of KCl are present (fig.6) and some blebs enriched in Ti or KCl and S (Fig.7). The presence of these particles is probably related to the vapour phase crystalization (McKAY et Al.,1971).

Low velocity impacts occur on the surface of 20% of rotational forms, whereas high velocity impacts are random events, observable on the 1% to 2% of the cases. Other fractures are present on 20% of the cases.

According to RIDLEY et Al. (1972) the chemical homogeneity and the distribution of the green glasses allow to suppose that they derive from a single large impact event on pyroxenitic material.

The displacement of these materials from the source areas toward the front of Apennines can be essentially produced by impact of small meteoroids. From the experimental relationships related to the ejection of material by meteoroid impact given by GAULT et Al. (1963) and SHOEMAKER et Al. (1970), the source area can be determined (CARUSI et Al.,1972).

The source areas of such glasses can be located in two different sites of Hadley δ . However it is possible that a complete analysis of all the soils returned from Apollo 15 mission could cover the complete source area.

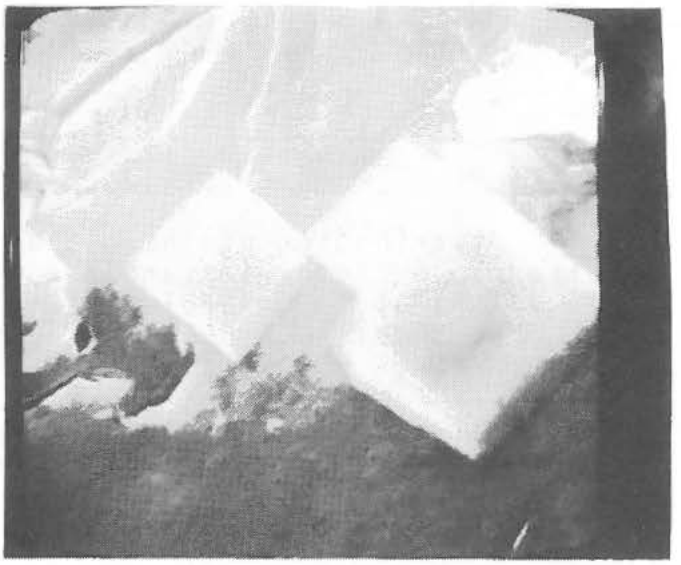

Fig. 6 - Probable sylvite crystals on the surface of a green glass sphere from the sample 15301, x8000.

THE SOURCE AREA OF APOLLO 15 "GREEN GLASSES"

Carusi A.

Fig.7 - Blebs of KCL and Ti on and around the fracture surface of a green sphere (sample 15101) probably related to the vapour phase crystalization, x1000.

R e f e r e n c e s

A.CARUSI,G.CAVARRETTA,F.CINOTTI,G.CIVITELLI,A.CORADINI,M. FULCHIGNONI,R.FUNICIELLO,A.TADDEUCCI; Geol.Rom.,Vol 11,137(1972).
D.E.GAULT,E.M.SHOEMAKER,H.J.MOORE; NASA-TN D 1767 (1963).
J.F.LINDSAY; Earth Planetary Sci. Letters. Vol 12, 67 (1971).
LSPET; NASA-SP, 235 (1970).
LSPET; NASA-SP, 289 (1972).
A.M.REID,W.I.RIDLEY,R.W.BROWN; LSI contr. (1972).
W.I.RIDLEY,A.M.REID,J.L.WARNER,R.W.BROWN; submitted to Science (1972).
E.M. SHOEMAKER, M.H.HAIT,G.A.SWANN,D.L.SCHLEIKER,G.G.SCHABER, R.L.SUTTON,D.H.DAHLEM,E.N.GODDARD,A.C.WATERS; Geochim.Cosmochim. Acta, Proc.Apollo 11 Lunar Sci. Conf.,Vol 3, 2399 (1970).
D.S.McKAY,D.A.MORRISON,U.S.CLANTON,H.G.LADLE,J.F.LINDSAY;Geochim. Cosmochim.Acta,Proc Second Lunar Sci. Conf.,Vol 1,755 (1971)

OPTICAL EVIDENCE FOR AVERAGE PYROXENE COMPOSITION OF APOLLO 15 SAMPLES: John B. Adams, West Indies Laboratory, Fairleigh Dickinson University, St. Croix, U.S.V.I. 00820; and Thomas B. McCord, Department of Earth and Planetary Sciences, M.I.T., Cambridge, Mass. 02139.

The diffuse reflection spectra (0.35-2.5 μm) of four rocks, four breccias and 19 soil samples from the Apollo 15 site were measured to determine the wavelength positions of the two crystal-field absorption bands that are contributed by the pyroxenes. The bands occur near 1 μm and 2 μm and arise from Fe^{2+} on a highly distorted octahedral site in pyroxene (1). Band positions vary in wavelength as a regular function of pyroxene composition (2), and previous work (3) has shown that the bands in lunar samples are related to the average pyroxene composition of the soils and rocks.

Apollo 15 samples show well-defined pyroxene band structure in their spectra in diffuse reflected light. The only exception is anorthosite 15415 which contains less than 2% pyroxene (4), and yields only the plagioclase Fe^{2+} band at 1.3 μm. Most Apollo 15 samples plot along the pyroxene compositional trend (2,3) as shown in Figure 1. The trend is defined by plotting the wavelengths of the two pyroxene bands, the band near 1 μm on the vertical axis, and the band near 2 μm on the horizontal axis. Orthopyroxenes fall at the short-wavelength end of the curve, and the bands generally shift to longer wavelengths with increasing calcium in the pyroxene structure.

We interpret the position of a given Apollo 15 sample on the trend to be a function of the average pyroxene composition. It is recognized that individual pyroxene grains are inhomogeneous on submicroscopic and microscopic scales, and that several varieties of pyroxenes may occur in a sample, especially the soils. The bulk optical properties nonetheless are some average of the many contributing pyroxene crystals.

For Apollo 15 materials there is a clear distinction between the bands for samples from the mare area and those from the Apennine front (Figure 2). Mare samples typically plot at longer wavelengths, in keeping with the calcic pyroxenes of mare rocks and soils. The most calcium-rich (augitic) average composition occurs in samples 15499 (basalt from Dune Crater) and 15601 (an unusually crystalline, pyroxene-rich soil from the rim of Hadley Rille). The least calcic (pigeonitic) pyroxenes predominate in samples 15205 and 15459 (breccias from "front" stations 2 and 7 respectively). These breccias are similar optically to some of the Apollo 14 breccias (3). Apollo 15 soil samples fall between the mare basalt and "front" breccia end-members, which implies that none of the soils correspond in pyroxene composition to the end member rocks, but rather that the soils are contaminated by one another. Further evidence for mixing of the mare and "front"

OPTICAL EVIDENCE FOR PYROXENE COMPOSITION
Adams

soils is seen in the clustering of band plots for samples from sites 1 (Elbow Crater) and 2 ("front" near St. George Crater).

Two samples have anomalous positions on the pyroxene trend. Rock 15065 (Station 1) was tentatively identified as a mare-type basalt (5) but its bands indicate a preponderance of pigeonite, similar to the front breccias. Breccia 15255 is from Station 6 but it is rich in mare-basalt fragments (5) and has bands indicative of calcic pyroxene. Both samples occur near the "front"–mare boundary and are likely to have been transported.

Four samples fall above the pyroxene trend. Two of these, 15401 and 15301, contain abundant green glass. A separate of green glass from 15401 shows Fe^{2+} absorption bands at 1.02 μm and 1.94 μm. These band positions are typical for iron-bearing silicate glasses (6), however, the bands in the green glass are strong compared to those in glass from other lunar samples. The effect of the green glass is to move the bands in the soil mixture up and to the left on the diagram. (Figure 2). Soil 15401 with the green glass removed has bands at .955 μm and 2.09 μm, which places it with the typical mare soils. If soil 15401 was in fact partly derived from the adjacent rock (5) found at station 6a it seems likely from our evidence that the rock and perhaps the green glass were derived from a mare area.

Rock 15555 contains approximately 15% olivine in addition to pyroxene, and the band positions fall above the pure pyroxene trend. These band locations are expectable in view of the single strong Fe^{2+} band in olivine near 1.03 μm. Extrapolation back to the pyroxene trend however places 15555 among "front" like materials rather than among the points for typical mare basalt. Breccia 15086 also falls above the trend, however petrographic data are not available at this writing to explain this departure.

We showed previously (3) that there is an excellent correspondence between the telescopic curve of the landing site (8 km) and the curve for soil 15021 from the LM site.

REFERENCES

1. G.M. Bancroft and R.G. Burns, Amer. Mineral. 52, 1278-1287 (1967)
2. J.B. Adams, in preparation
3. J.B. Adams and T.B. McCord, Proceedings of Third Lunar Science Conference, M.I.T. Press. (1972)
4. R.B. Hargraves and L.S. Hollister, Science 175 430-432 (1972)
5. Apollo 15 Preliminary Science Report, NASA SP-289 (1972)
6. D.B. Nash and J.E. Conel, Lunar Science-III, C. Watkins, ed., Lunar Science Institute (1972)
7. We are grateful to M. Charette of M.I.T. for his assistance with the data reduction. Research supported by NASA.

OPTICAL EVIDENCE FOR PYROXENE COMPOSITION

Adams

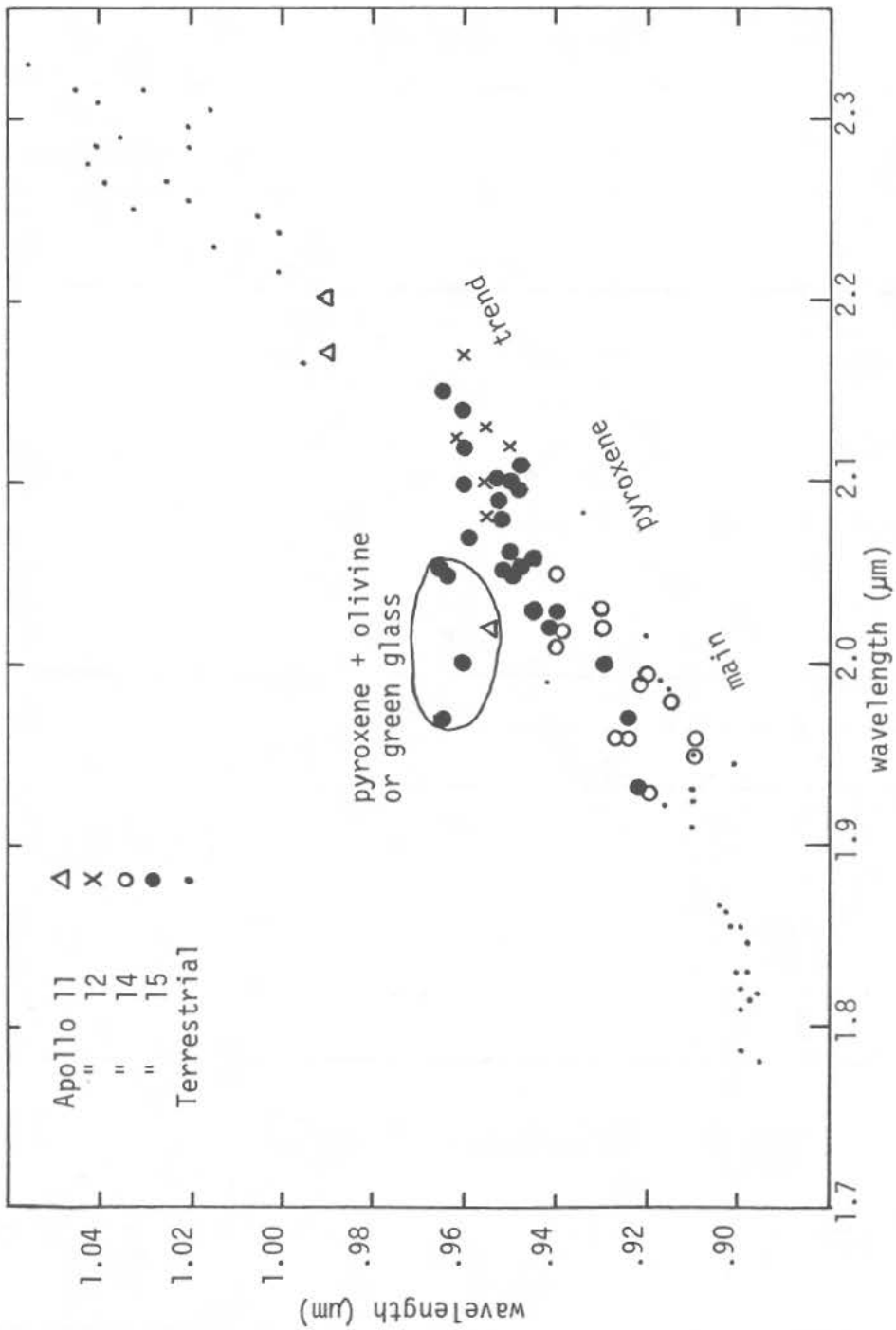

Fig 1: Pyroxenes have two absorption bands in their diffuse reflection spectra. The wavelength position of the band near 1 μm is plotted against that of the band near 2 μm for Apollo samples and for several terrestrial pyroxenes. The points define a trend along which the composition changes, calcium increasing toward the longer wavelengths. Apollo 15 samples fall on the trend except for samples containing pyroxene plus olivine or green glass.

OPTICAL EVIDENCE FOR PYROXENE COMPOSITION

Adams

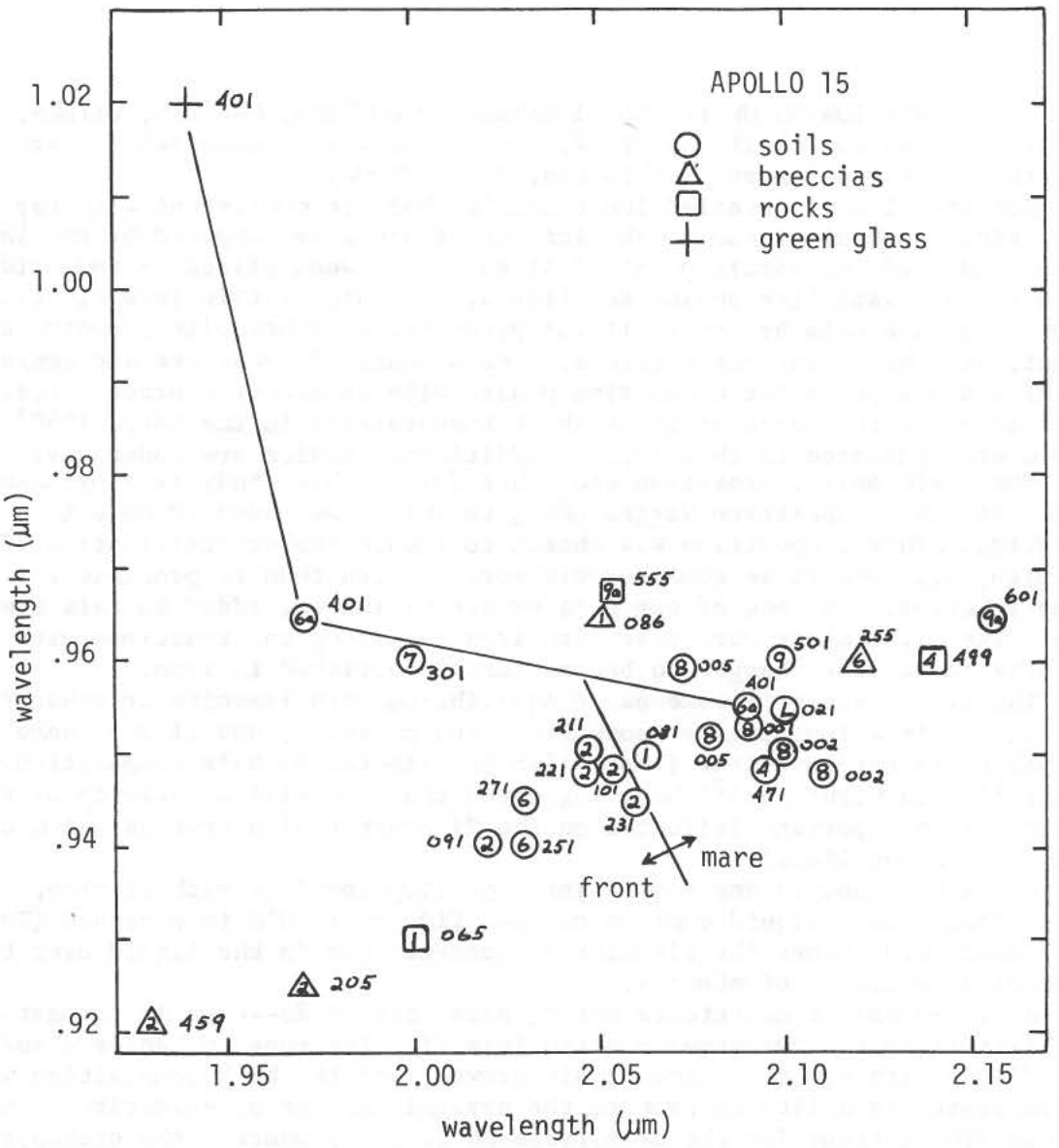

Fig 2: Similar to figure 1 but with only Apollo 15 samples shown on an expanded scale. The numbers contained within the symbols are the sample locations, and the numbers on the outsides of the symbols are the sample identification-numbers with "15" omitted (e.g. 15401 = 401).

PARTITIONING OF Ti AND Al BETWEEN PYROXENES, GARNETS, OXIDES, AND LIQUID, Jagannadham Akella and F. R. Boyd, Geophysical Laboratory, Carnegie Institution of Washington, Washington, D. C. 20008.

Construction of detailed lunar models that are consistent with rapidly increasing geochemical and geophysical constraints is hampered by the lack of knowledge of the partitioning of Al and Ti between silicates and oxides and between crystalline phases and liquid. The aim of this investigation is to provide such data by crystallizing pyroxenes together with ilmenite and garnet, or other aluminous minerals, over a range of pressures and temperatures and analyzing the coexisting phases with an electron probe. Preliminary data for the range up to 40 kb at temperatures in the range 1050°-1350°C are presented in this report; additional studies are under way.

The basic bulk composition used thus far in this study is a pyroxene glass with the composition $Wo_{25}Fs_{30}En_{45}$ to which was added 10 mole % $CaAl_2TiO_6$. This composition was chosen to insure the crystallization of ilmenite, although it is considerably more Fe-rich than is probable for the lunar interior. In some of our runs excess silica was added to this composition. The experiments were made with iron capsules, and reactions with the capsules caused the charges to become further enriched in iron.

The Ti content of pyroxenes in equilibrium with ilmenite or other Ti-rich phases is a function of temperature and pressure, and if the phase assemblage is not invariant it may also be affected by bulk composition. Kushiro[1] and Verhoogen[2] have suggested that the silica activity of the liquid has an important influence on the Ti content of pyroxenes which crystallize from the liquid.

Ca-rich clinopyroxene containing 2.5% TiO_2 coexists with olivine, plagioclase, and a liquid containing 9.4% TiO_2 at 1110°C in a vacuum (Table 1). Under these conditions the titanium is concentrated in the liquid over the pyroxene by a factor of about 4.

At comparable temperatures but at pressures of 25-40 kb in the garnet stability field the pyroxenes contain less Ti. The runs in Tables 2 and 3 were fluxed with H_2O to enhance grain growth, and the bulk composition was oversaturated in silica to promote the crystallization of enstatite. The maximum TiO_2 content for the clinopyroxene is 1.5%, whereas the orthopyroxene contains 0.4-0.6% TiO_2. In both of the runs in Tables 2 and 3 the garnet contains only about 1.5% TiO_2. Rutile replaces ilmenite as the Ti-rich phase in runs made at and above 30 kb with the oversaturated composition in the presence of H_2O. This reaction is not a subsolidus phase transformation; it apparently involves the liquid phase and the iron capsule. We have not thus far been successful in analyzing the small amounts of liquid present in the high-pressure runs.

Table 4 shows a dry run with the undersaturated composition at 1350°C and 30 kb. Under these conditions the TiO_2 contents of the garnet and clinopyroxene coexisting with ilmenite are increased to the range 2-3 wt %.

Partitioning of Ti and Al

Jagannadham Akella

The TiO_2 contents of the pyroxenes in these and other runs we have made increase with decreasing pressure, increasing temperature, and decreasing silica activity in the melt. Our data are not yet sufficiently complete to evaluate the relative importance of these variables. Atomic proportions for Al in pyroxenes synthesized at high pressure are more than twice the proportions for Ti; thus there is a small Tschermak component in all these pyroxenes. In the pyroxene synthesized at 1 atm the Al:Ti ratio is slightly less than 2. There is a deficiency in the sum of Al + Ti in the synthetic garnets that is approximately balanced by a surplus in the sum of divalent ions. Evidently Ti is present in these garnets in a substitution of the type $Ti^{4+} + R^{2+}$ for $2Al^{3+}$.

The ilmenites we have synthesized in the pressure range 15-30 kb contain 7-19 mole % geikilite ($MgTiO_3$), an amount that is greater than that found in ilmenites from rocks of the terrestrial crust[3] but less than is commonly found in ilmenites from kimberlites.

The results outlined show concentrations of TiO_2 and Al_2O_3 in pyroxenes at high pressures that are comparable to the values reported by Ringwood,[4] on which he based his model lunar pyroxenite. Our data show that synthetic garnets coexisting with ilmenite or rutile have TiO_2 contents similar to those of the Ca-rich pyroxenes. Data must be obtained for the partition of Ti between crystalline phases and liquid at high pressures, comparable to those we have obtained in runs in a vacuum (e.g. Table 1), before we can quantitatively assess the possibilities of deriving mare basalts from pyroxenites by partial fusion.

(1) Kushiro, I., Si-Al relation in clinopyroxenes from igneous rocks, Amer. J. Sci., 258, 548-554, 1960.
(2) Verhoogen, J., Distribution of titanium between silicates and oxides in igneous rocks, Amer. J. Sci., 260, 211-220, 1962.
(3) Howie, R. A., The geochemistry of the charnockite series of Madras, India, Trans. Roy. Soc. Edinburgh, 62, 725-768, 1955.
(4) Ringwood, A. E., Petrogenesis of Apollo 11 basalts and implications for lunar origin, J. Geophys. Res., 75, 6453-6479, 1970.

Partitioning of Ti and Al

Jagannadham Akella

TABLE 1. Coexisting phases in a run made at 1110°C in an iron capsule in an evacuated silica glass tube

Phase	Clinopyroxene		Plagioclase		Olivine		Glass	
SiO_2	50.4	(1.1)*	44.69	(0.7)	36.54	(0.2)	39.41	(0.4)
TiO_2	2.5	(0.4)	0.06	(0.03)	0.14	(0.02)	9.40	(0.3)
Al_2O_3	3.0	(0.6)	35.21	(0.6)	0.04	(0.01)	9.76	(0.3)
Fe_2O_3	...		...		...		...	
FeO	9.1	(0.4)†	0.64	(0.1)†	29.84	(0.3)†	24.07	(1.3)†
MgO	14.9	(0.8)	0.34	(0.01)	32.24	(0.3)	4.25	(0.4)
CaO	20.1	(0.2)	19.65	(0.4)	0.62	(0.04)	12.37	(0.6)
Totals	100.00		100.58		99.41		99.27	
	0 = 6		0 = 32		0 = 4			
Si	1.876	2.000	8.227		0.995	0.995		
Al	0.124		7.640		...			
Al	0.008	1.989				2.011		
Ti	0.070		0.009		0.006			
Fe	0.283		0.099		0.679			
Mg	0.826		0.093		1.308			
Ca	0.802		3.876		0.018			
Ca	42.0				Fo 65.8			
Mg	43.2				Fa 34.2			
Fe	14.8							
$\frac{Mg}{(Mg+Fe)}$	0.755				0.658		0.239	

*Numbers in parentheses are standard deviations for analyses of a number of grains.

†Total Fe as FeO or Fe^{2+}.

Partitioning of Ti and Al

Jagannadham Akella

TABLE 2. Analyses of coexisting crystalline phases in a run at 1050°C and 25 kb; metallic iron and minor glass oversaturated in SiO_2 are also present

Phase	Clinopyroxene		Orthopyroxene		Garnet		Ilmenite	
SiO_2	50.5	(0.6)*	51.2	(0.4)	39.4	(0.4)	0.5	(0.2)
TiO_2	1.5	(0.3)	0.2	(0.2)	1.4	(0.4)	50.8	(0.8)
Al_2O_3	2.7	(0.7)	1.5	(0.2)	20.6	(0.6)	0.4	(0.05)
Fe_2O_3	...		...		...		2.7†	
FeO	14.9‡	(0.7)	25.1‡	(1.1)	22.0‡	(1.0)	42.0	(0.2)
MgO	13.6	(0.5)	19.5	(0.5)	9.2	(0.7)	2.1	(0.1)
CaO	15.8	(0.7)	1.8	(0.6)	7.3	(0.6)	0.5	(0.1)
Totals	99.0		99.3		99.9		99.0	
	O = 6		O = 6		O = 12		O = 3	
Si	1.923	2.000	1.954	2.000	3.005	3.005	0.014	2.000§
Al	0.077		0.046		...		0.012	
Al	0.045	1.974	0.018	2.004	1.854	1.934	...	
Ti	0.042		0.006		0.080		0.955	
Fe	0.473		0.800		1.405		0.879(2+) 0.050(3+)	
Mg	0.771		1.109		1.050	3.051	0.077	
Ca	0.643		0.071		0.596		0.013	
Ca	34.1	32.5‖	3.6		19.5		Ilm = 89.6	
Mg	40.8	41.8	56.0		34.4		Geik = 7.8	
Fe	25.1	25.6	40.4		46.1		Hem = 2.6	
$\frac{Mg}{(Mg+Fe)}$	0.62		0.58		0.43		0.08	

*Numbers in parentheses are standard deviations for analyses of a number of grains.

†Calculated from total Fe and from structural formula.

‡Total Fe as FeO or Fe^{2+}.

§Cation total normalized in the course of Fe^{3+} calculation.

‖Values underlined were obtained after correcting for $CaTiAl_2O_6$ and $CaAl_2SiO_6$.

TABLE 3. Analyses of coexisting phases in a run at 1100°C and 40 kb; metallic iron and minor glass oversaturated in SiO_2 are also present

Phase	Clinopyroxene		Orthopyroxene		Garnet		Rutile
SiO_2	51.7 (0.4)*		52.8 (0.6)		39.4 (0.8)		0.7 (0.07)
TiO_2	0.5 (0.3)		0.4 (0.2)		1.5 (0.2)		94.0 (2.1)
Al_2O_3	1.5 (0.5)		1.3 (0.4)		19.7 (0.5)		0.9 (0.06)
FeO	12.6 (0.5)†		21.2 (0.6)†		21.6 (0.7)†		2.7 (1.4)†
MgO	14.7 (0.5)		21.6 (0.9)		9.3 (0.5)		0.2 (0.05)
CaO	17.6 (0.5)		1.7 (0.4)		7.4 (0.7)		0.6 (0.02)
Totals	98.6		99.0		98.9		99.1
	O = 6		O = 6		O = 12		
Si	1.960	2.000	1.975	2.000	3.036	3.036	
Al	0.040		0.025		...		
Al	0.028	1.992	0.032	1.985	1.793	1.878	
Ti	0.015		0.012		0.085		
Fe	0.401		0.665		1.390	3.068	
Mg	0.834		1.206		1.067		
Ca	0.714		0.070		0.611		
Ca	36.7		3.6		19.9		
Mg	42.8		62.2		34.8		
Fe	20.6		34.3		45.3		
$\frac{Mg}{(Mg+Fe)}$	0.68		0.65		0.43		

*Numbers in parentheses are standard deviations for analyses of a number of grains.

†Total Fe as FeO or Fe^{2+}.

Partitioning of Ti and Al

Jagannadham Akella

TABLE 4. Coexisting phases in a run made at 1350°C and 30 kb; metallic iron and a minute amount of glass are also present

Phase	Clinopyroxene		Olivine		Garnet		Ilmenite	
SiO_2	48.2	(0.3)*	36.6	(0.8)	39.4	(0.4)	0.92	(0.3)
TiO_2	2.32	(0.1)	0.32	(0.06)	2.9	(0.2)	53.4	(0.4)
Al_2O_3	6.05	(0.3)	0.43	(0.1)	20.8	(0.04)	1.6	(0.1)
Fe_2O_3	...		...		...		...	
FeO	11.6	(0.6)†	35.9	(0.7)†	16.0	(0.3)†	38.2	(0.2)†
MgO	13.0	(0.6)	25.1	(0.6)	12.2	(0.3)	5.1	(0.1)
CaO	19.0	(0.4)	1.04	(0.3)	9.3	(0.1)	0.84	(0.1)
Totals	100.17		99.39		100.60		100.06	
	0 = 6		0 = 4		0 = 12		0 = 3	
Si	1.808	2.000	1.024	1.024	2.931	2.931	0.022	
Al	0.192		0.014		...			
Al	0.076				1.824	1.987	0.045	1.994
Ti	0.065		0.007		0.163		0.961	
Fe	0.364	1.993	0.839	1.939	0.991	3.076	0.764	
Mg	0.725		1.048		1.347		0.180	
Ca	0.762		0.031		0.738		0.022	
Ca	41.2		Fo 55.5		Ca 24.0		Ilm 80.9	
Mg	39.2		Fa 44.5		Mg 43.8		Geik 19.1	
Fe	19.7				Fe 32.2		Hem 0.0	
$\frac{Mg}{(Mg+Fe)}$	0.666		0.555		0.576		0.191	

*Numbers in parentheses are standard deviations for analyses of a number of grains.

†Total Fe as FeO or Fe^{2+}.

PETROLOGY OF APOLLO 15 SAMPLE 15486. A. L. Albee, A. A. Chodos and A. J. Gancarz, California Institute of Technology, Pasadena, Calif. 91109.*

Sample 15486 is one of three samples—15485, 15486 and 15499—collected from a large (>1m) vesicular block at station 4 on the south rim of Dune Crater. $^{40}Ar/^{39}Ar$ studies by Huneke et al. [1] show that 15499 has an age of 3.40 AE and a Rb-Sr model age has been reported [2]. Silver and Jakes [3] describe 15486 as a blocky, angular porphyritic basalt fragment (47 gm), 5.6 x 3 x 2.5 cm, with a grey coating on fracture surfaces and some zap pits on the exterior surfaces. They describe pyroxene prisms up to 10mm in length and about 5% vugs.

The sample was studied in polished thin section 15486,20(area $\approx 75mm^2$). It is a porphyritic, clinopyroxene vitrophyre composed of elongate pyroxene prisms (53%) in a matrix of opaque devitrified glass (44%) with 3% globulose vugs and about 0.1% each of spinel and Fe-metal. Olivine phenocrysts are reported in other samples from this block [4-5], but are not present in this sample.

The matrix appears to be a devitrified glass composed of extremely fine-grained segregations of crystallites. It is predominantly opaque, but a "fingerprint-like" pattern is visible under reflected light at high magnification. The striations in the "fingerprint" pattern are made up of alternating subparallel segregations about 1μm wide, consisting of crystallites of either pyroxene or plagioclase and opaque minerals. At their edges light is partially transmitted and the opacity appears to be due to a myriad of wormlike rods, about 0.2μm in diameter, of opaque minerals, predominantly troilite.

Despite the devitrification-segregation the matrix is quite homogeneous at the 20μm level. Five analyses of 20μm diameter spots are nearly identical (analysis 9). The matrix contains about 53% normative feldspar, 35% pyroxene, 7% SiO_2, and 4% opaque minerals. This may be compared to the norm for a chemical analysis of 15499 [4] which contains about 28% feldspar, 68% pyroxene and 0.4% SiO_2. A devitrified glass inclusion within a pyroxene prism (analysis 10) has an intermediate composition.

Pyroxene occurs as elongate skeletal prisms, which commonly enclose matrix (see photomicrographs of 15485 [4] and 15499[5]). Many of the larger grains contain low-Ca clinopyroxene cores enclosed by high-Ca clinopyroxene (figs. 2 and 3). As illustrated, $CaAlAlSiO_6$, $NaAlSi_2O_6$, and $CaTiAl_2O_6$ increase outward and $CaCrAlSiO_6$ decreases outward. This minor element variation is similar to that described for 15499 by Bence and Papike [5], who note that Al/Si increases in lunar pyroxene continuously until the onset of plagioclase crystallization, which never began in this rock. Some areas of the slide contain many small pyroxene grains with rather uniform augitic composition similar to that of the rims of larger pyroxene phenocrysts.

Spinels and Fe-metal are present in minor amounts (<0.5%), but ilmenite and troilite are absent as phenocrysts and are present only in the devitrified matrix. Cr-spinel occurs in euhedral grains, 20-100μm, both in pyroxene and in the matrix. These grains become more Al-rich and more Fe-rich from the core outward and many of them are rimmed by Fe-rich ulvöspinel (fig. 1). These rims

Table 1: Selected electron microprobe analyses from sample 15486,20

	Pyroxene				Spinel				"Glass"			
wt.%	1	2	3	4	5	6	7	8		9		10
SiO_2	52.08	50.45	48.14	44.61	0.26	0.72	1.12	0.35	SiO_2	48.84	±0.62	43.98
Al_2O_3	2.32	4.09	6.33	9.23	11.25	7.93	12.42	11.27	Al_2O_3	16.83	±0.95	14.99
Cr_2O_3	1.14	1.20	0.76	0.06	53.40	9.44	30.82	51.15	Cr_2O_3	0.01	±0.01	0.04
TiO_2	0.50	1.22	1.67	2.23	2.35	24.72	11.11	5.93	TiO_2	2.30	±0.23	3.05
MgO	23.12	13.96	11.89	7.41	7.76	0.61	1.32	7.19	MgO	0.77	±0.10	2.83
FeO	17.14	14.10	16.01	26.53	24.32	54.16	42.47	26.07	FeO	20.34	±1.80	22.98
MnO	0.28	0.30	0.27	0.35	0.72	0.35	0.49	0.72	MnO	0.21	±0.02	0.30
CaO	3.43	15.39	16.45	10.89	n.a.	n.a.	n.a.	n.a.	CaO	9.98	±0.43	10.99
Na_2O	0.02	0.05	0.07	0.08	n.a.	n.a.	n.a.	n.a.	BaO	0.02	±0.03	0.02
									Na_2O	0.88	±0.09	0.44
Total	100.03	100.76	101.59	101.39	100.06	97.93	99.75	102.63	K_2O	0.15	±0.01	0.09
									P_2O_5	0.18	±0.03	0.14
									SO_3	0.15	±0.11	0.05
									NiO	<0.01		<0.01
									ZrO_2	<0.01		<0.01
Formula proportions									Total	100.66	±0.85	99.90
Si	1.91	1.89	1.81	1.74	0.01	0.03	0.04	0.01				
Al	0.10	0.18	0.28	0.42	0.44	0.34	0.51	0.43		"Glass Norms"		
Cr	0.03	0.04	0.02	<0.01	1.41	0.27	0.85	1.32	an	44.11		41.49
Ti	0.01	0.03	0.05	0.07	0.06	0.68	0.29	0.15	ab	8.40		4.24
Mg	1.27	0.78	0.67	0.43	0.39	0.03	0.07	0.35	or	0.94		0.57
Fe	0.53	0.44	0.50	0.87	0.68	1.64	1.23	0.71	cel	0.04		0.04
Mn	0.01	0.01	0.01	0.01	0.02	0.01	0.01	0.02	en	2.26		8.22
Ca	0.14	0.62	0.66	0.46	n.a.	n.a.	n.a.	n.a.	fs	30.20		33.37
Na	0.01	<0.01	0.01	0.01	n.a.	n.a.	n.a.	n.a.	wo	2.90		6.43
									fo	0.0		0.13
Total	4.01	3.99	4.01	4.01	3.01	3.00	3.00	2.99	fa	0.0		0.53
									Q	7.12		0.0
									C	0.0		0.0
									il	3.41		4.54
									cm	0.01		0.05
									FeS	0.22		0.08
									ap	0.40		0.31
									Z	0.0		0.0
									NiO	0.0		0.0

n.a. ≡ not analyzed for

Petrology of Apollo 15 Sample 15486

A. L. Albee

tend to be broader on grains in the matrix than on grains enclosed in pyroxene. Fe-metal occurs as equidimensional spherical blebs or aggregates of equidimensional blebs. It is both associated with spinel and independent of spinel in the matrix. An average of 8 analyses gives the following composition: $Fe_{92.16}$ wt%, $Ni_{6.28}$, and $Co_{1.42}$. A computer printout of all electron microprobe analyses from sample 15486,20 is available upon request.

REFERENCES

[1] J.C. Huneke, F.A. Podosek, and G.J. Wasserburg, personal communication.
[2] D.A. Papanastassiou and G.J. Wasserburg, Rb-Sr ages and initial strontium in basalts from Apollo 15 (in press).
[3] Lunar Sample Information Catalog: Apollo 15, NASA pub. MSC 03209 (1971).
[4] Lunar Sample Preliminary Examination Team, Preliminary examination of lunar samples in: Apollo 15: Preliminary Science Report NASA SP-289 (1972).
[5] A.E. Bence and J.J. Papike, Pyroxenes as recorders of lunar basalt petrogenesis: I. Chemical data for liquidus trends (in press).

*Contribution number 2211

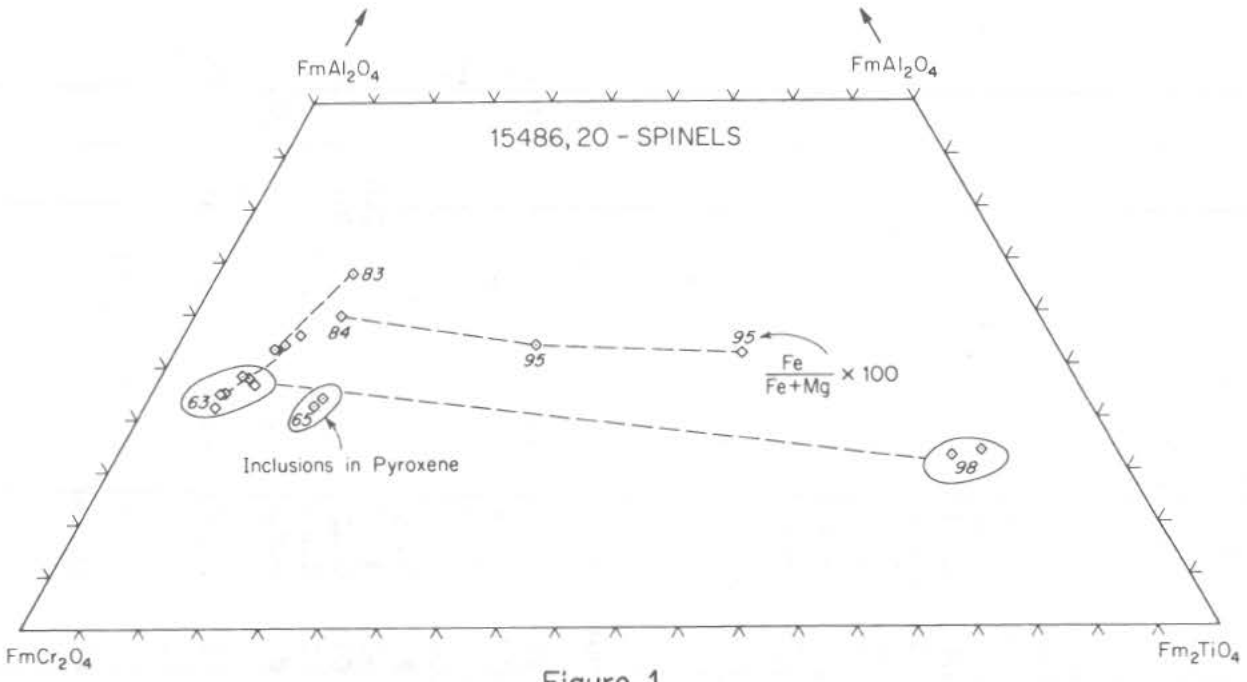

Figure 1

Petrology of Apollo 15 Sample 15486

A. L. Albee

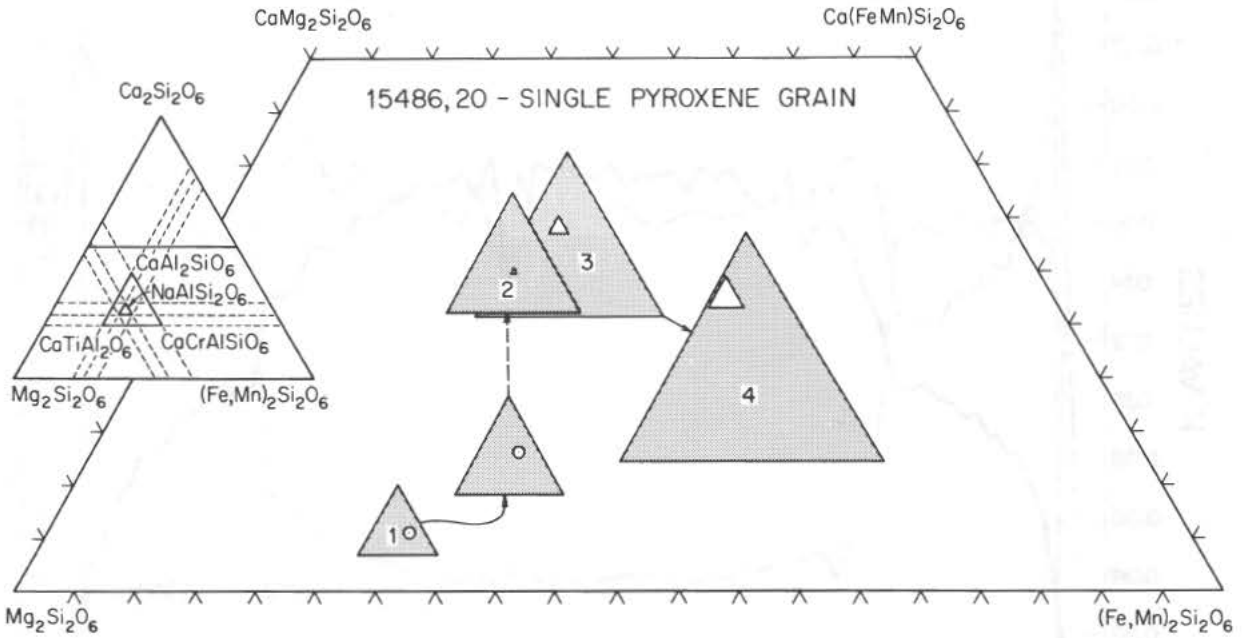

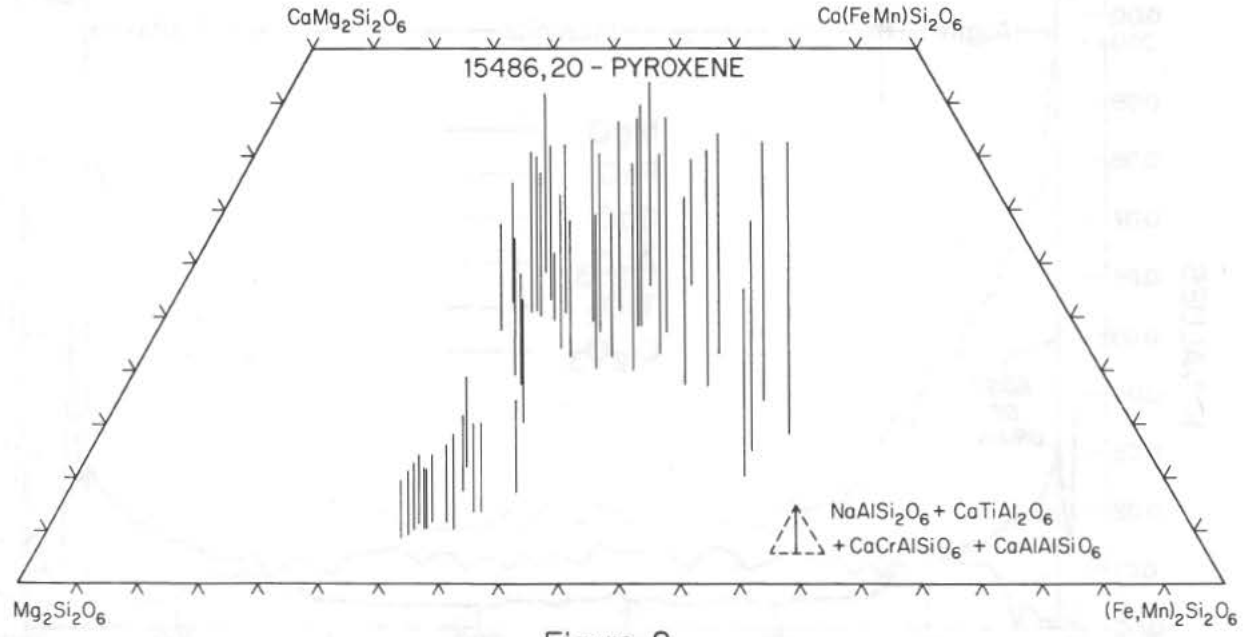

Figure 2

Petrology of Apollo 15 Sample 15486

A. L. Albee

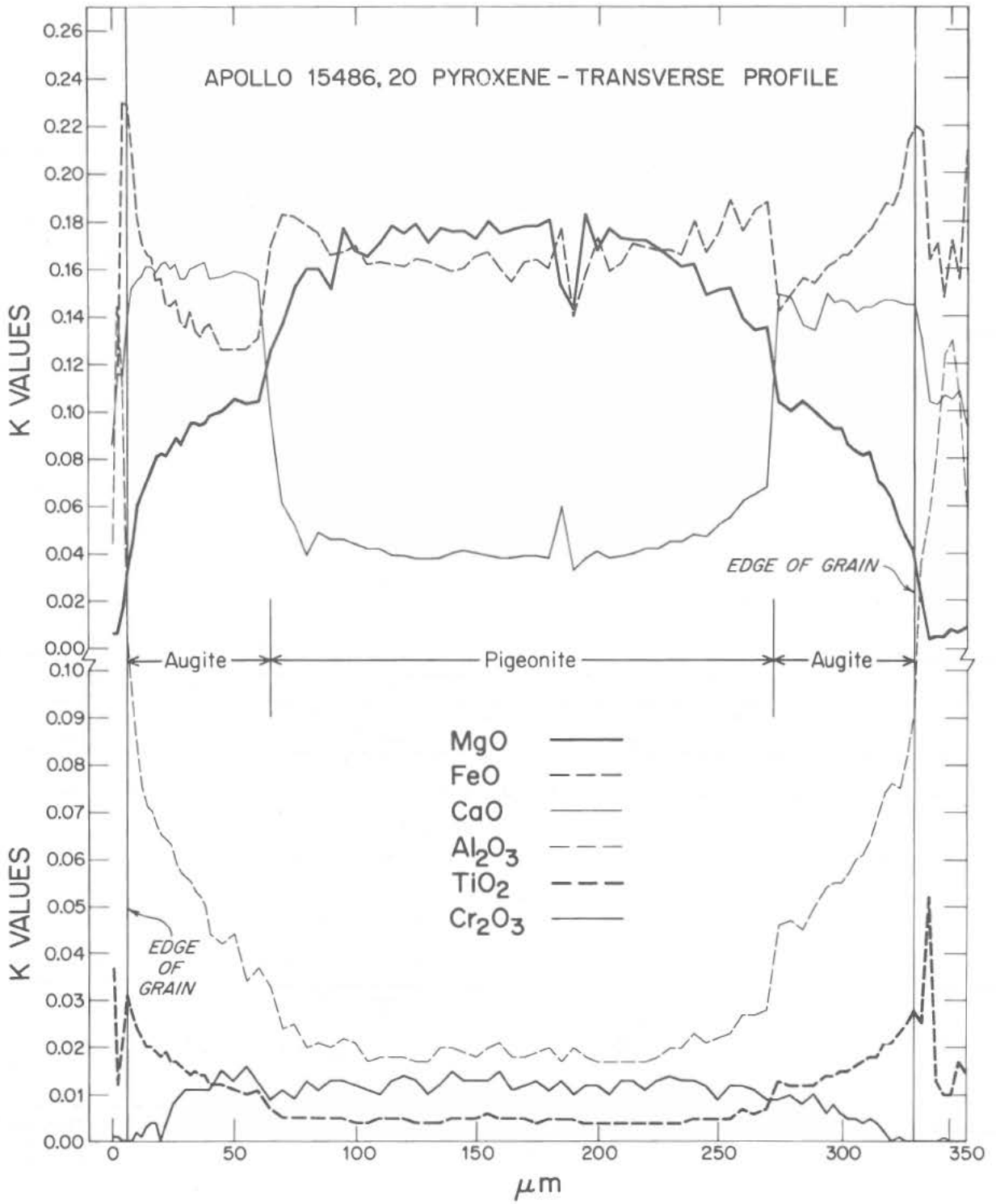

Figure 3

Petrology of Apollo 15 Sample 15486

A. L. Albee

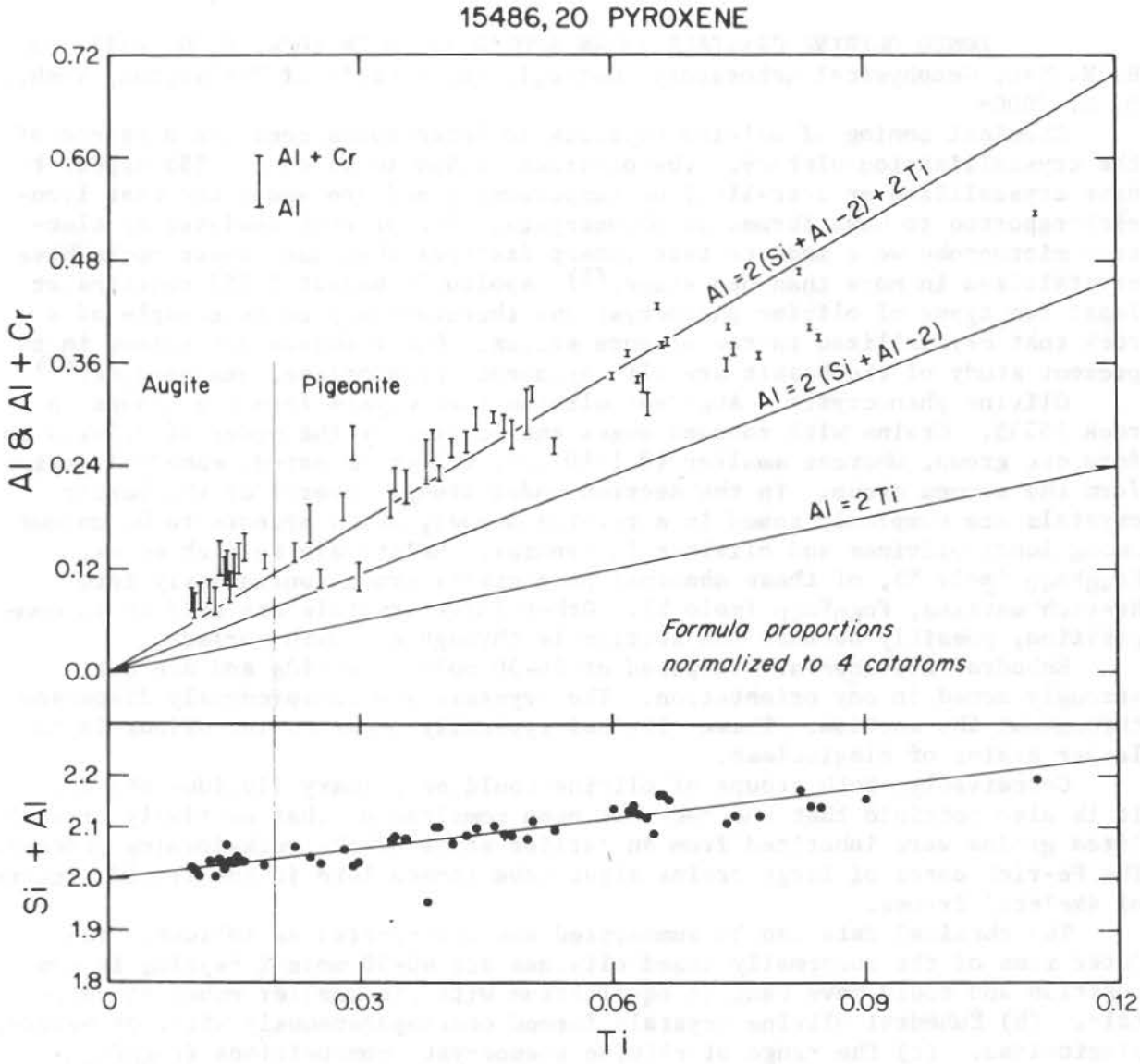

Figure 4

ZONED OLIVINE CRYSTALS IN AN APOLLO 15 LUNAR ROCK, P. M. Bell and H. K. Mao, Geophysical Laboratory, Carnegie Institution of Washington, Wash., D. C. 20008.

Chemical zoning of olivine crystals in lunar rocks contains a record of the crystallization history. The olivines in Apollo 15 rock 15555 appear to have crystallized at near-liquidus temperatures and are among the most iron-rich reported to have formed as phenocrysts. The present analyses by electron microprobe were made to test interpretations that many lunar rocks have crystallized in more than one stage.(1) Apollo 15 basalt 15555 contains at least two types of olivine phenocryst and therefore may be an example of a rock that crystallized in two or more stages. Other phases determined in the present study of the basalt are clinopyroxene, plagioclase, and opaques.(2)

Olivine phenocrysts: Abundant olivine phenocrysts form two groups in rock 15555. Grains with rounded edges and lengths of the order of 0.5-1.5 mm form one group, whereas smaller (0.1-10 μm), well-terminated, euhedral grains form the second group. In the section under study, several of the larger crystals are complexly zoned in a reverse manner, which appears to be unique among lunar olivines and olivines in general. Relatively Fe-rich cores, $Fo_{40}Fa_{60}$ (mole %), of these abnormal phenocrysts grade continuously into Mg-rich margins, $Fo_{60}Fa_{40}$ (mole %). Other large crystals are uniform in composition, possibly because the section is through a growth surface.

Euhedral olivines are composed of 40-50 mole % Fe_2SiO_4 and are not strongly zoned in any orientation. The crystals are conspicuously dispersed throughout the section. These olivines typically occur as inclusions in much larger grains of plagioclase.

Conceivably, both groups of olivine could be primary liquidus phases. It is also possible that the rock has been remelted or that partially crystallized grains were inherited from an earlier stage of the rock-forming process. The Fe-rich cores of large grains might have formed late in the liquid centers of skeletal frames.

The chemical data can be summarized and interpreted as follows: (a) Outer rims of the abnormally zoned olivines are 40-50 mole % Fe_2SiO_4 in composition and could have been in equilibrium with the smaller euhedral crystals. (b) Euhedral olivine crystals formed contemporaneously with, or before, plagioclase. (c) The range of olivine phenocryst compositions ($Fo_{60}Fa_{40}$-$Fo_{40}Fa_{60}$) is among the most Fe-rich ever reported for a basalt, reflecting a remarkably high Fe/Mg for the rock as a whole.

Reverse zoning: The fact that chemically reversed zoning occurs in several of the larger grains seems to preclude, although not eliminate, explanations based on fortuitous growth and sectioning of these aberrant crystals. One of the larger (1 mm length × 0.4 mm maximum width) reversely zoned crystals was analyzed in detail by electron microprobe. Data averages are given in Table 1. Fifty points on this crystal were analyzed for the eight elements Fe, Mg, Si, Ca, Cr, Mn, Al, and Ti, and contours of Fe/Mg were

ZONED OLIVINE CRYSTALS

P. M. Bell

constructed.

A central core (Fig. 1), dimensionally 0.15 × 0.15 mm in section, averages $Fo_{40}Fa_{60}$ in composition, with deviations of less than 1 mole % Fe_2SiO_4. Toward the margins of this elongate grain, steep compositional gradients of approximately 15 mole % Fe_2SiO_4 occur in less than 0.1 mm. Lengthwise, the gradients are smaller, averaging 2-4 mole % Fe_2SiO_4 in 0.1 mm, and appear to be continuous. The crystal-field spectra of iron-rich cores of similar olivines from 15555 are compared with the spectra of olivine and plagioclase from rock 15601 in a study to be published elsewhere.(3)

The olivine binary system is like the plagioclase feldspar melting loop, and the zoning could have resulted from a process of fast quench and readjustment in composition along the solidus after a rise in temperature from release of the enthalpy (heat) of crystallization. Bowen,(4) who considered this a possible mechanism to explain reverse zoning in plagioclase, also considered the effects of changing liquid compositions.

However, many other conceivable paths in the crystallization history could have caused the zoning to be reversed. For example, if adiabatic decompression occurred during passage of the lava to the surface, it would not be possible to determine the magnitude of the pressure release unless the combined enthalpy and entropy changes during the process were known. Whatever the cause of their reverse zoning, these crystals attest to a compositional trend dominated by high values of Fe/Mg.

Euhedral olivines: Outlines of these crystals in section show prism and domal traces, exhibiting well developed terminations. Mean compositions determined by electron microprobe are listed in Table 1. Zoning is usually very slight or not detectable by electron microprobe. In most of the crystals the composition changes by no more than 1 mole % Fe_2SiO_4 from margin to interior. A number of crystals fall in narrow ranges close to the mean compositions $Fo_{51}Fa_{49}$, $Fo_{54}Fa_{46}$, and $Fo_{60}Fa_{40}$, and in crystals in which slight zoning was observed, the margins were more Fe-rich than the interiors.

Because of the distinct crystal form and chemical composition, the euhedral olivines appear to have crystallized apart from the larger, irregular olivines, probably on or near the liquidus. All the evidence implies at least two stages of crystallization for this rock--one for the large reversely zoned olivines and the other for the smaller euhedral olivines.

(1) Bell, P. M., and H. K. Mao, Initial findings of a study of chemical composition and crystal-field spectra of selected grains from Apollo 14 and 15 rocks, glasses and fine fractions (less than 1 mm) (abstract), in "Lunar Science--III," C. Watkins, ed., Lunar Sci. Inst. Contrib., 88, 55-57, 1972.

(2) Boyd, F. R., Zoned pyroxenes in lunar rock 15555, Carnegie Inst. Wash. Year Book 71, in press, 1972; Haggerty, S. E., Solid solution characteristics of lunar spinels, ibid.

(3) Bell, P. M., and H. K. Mao, Crystal-field studies of lunar samples, Carnegie Inst. Wash. Year Book 71, in press, 1972.

(4) Bowen, N. L., The melting phenomena of the plagioclase feldspars, Amer. J. Sci., 34, 577-599, 1913.

ZONED OLIVINE CRYSTALS

P. M. Bell

TABLE 1. Electron Microprobe Analyses of Typical Olivines* from Apollo Rock 15555, average wt %

	FeO	MgO	SiO_2	CaO	Cr_2O_3	MnO	Al_2O_3	TiO_2
a	strongly zoned		33.32	0.40	0.16	0.44	0.05	0.09
b	32.79	30.70	35.38	0.32	0.23	0.37	0.05	0.05
c	40.84	23.46	35.23	0.96	0.20	0.52	0.12	0.08
d	38.97	25.27	34.79	0.44	0.22	0.50	0.09	0.03
e	34.43	28.26	34.57	0.35	0.25	0.41	0.02	0.05

*(a) Reversely zoned crystal shown in Fig. 1. The zoning of FeO and MgO are too great for averaging. (b) Another reversely zoned olivine. The zoning was not so great as in (a). (c-e) Three typical euhedral olivines.

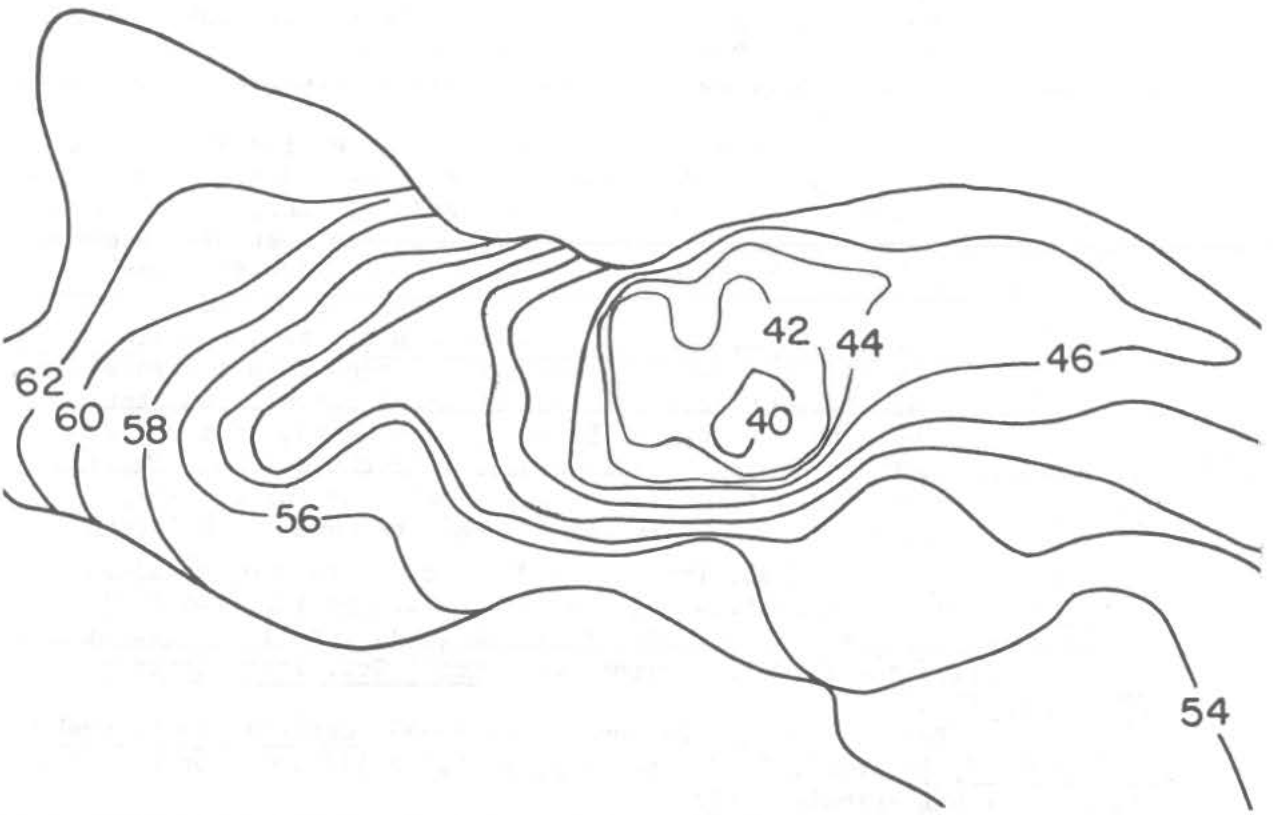

FIG. 1. Compositional contours of forsterite on reversely zoned olivine in section of Apollo 15 rock 15555. Chemical analysis was by electron microprobe; contour interval, 2 mole % forsterite. Length ~2 mm.

Crystallography of Lunar Feldspars and Pyroxenes from 15076,55

B.Berking and H.Jagodzinski; Institut für Kristallographie und Mineralogie, Universität München, 8 München 2, Theresienstr. 41, BRD
M.Korekawa; Institut für Kristallographie, Universität Frankfurt, 6 Frankfurt, Senckenberg Anlage 30, BRD
R. Schmid; Institut für Kristallographie u. Petrographie der ETH, 8006 Zürich, Sonneggstr. 5, Switzerland.

1. Feldspars

1.1. Optical and chemical investigations

Two plagioclase crystals from Apollo 15 sample (15076,55) show peculiar features which can barely be observed by means of optical microscopy. The pecularity of crystal No. 1 is shown in Fig. 1. On the (010) surface of this plagioclase crystal, we observed a segment of a spherical surface and a circular area of opaque material on its top. There is no observable difference in color between the host crystal and the area of the spherical surface except the opaque part itself. A similar feature was also observed on the opposite surface $(0\bar{1}0)$. The connecting line between the centres of the two opaque spots (I) is slightly tilted both from the b-axis and the b^*-axis.

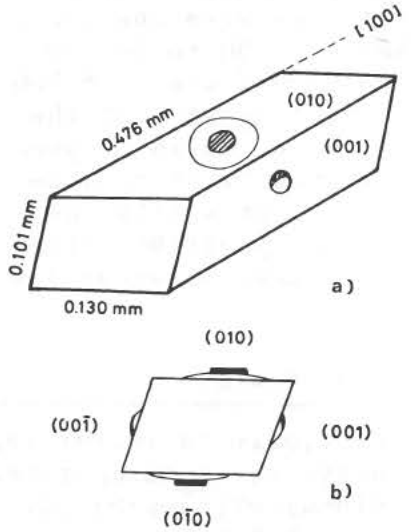

Fig. 1. Schematic representation of crystal 15076,55 No.1 (plagioclase An 85 ± 3).
a) Peculiar features on (010) and (001). Corresponding features exist on $(0\bar{1}0)$ and $(00\bar{1})$. The hatched circle and arch on the planes (010) and (001), respectively, are areas of opaque material.

b) Schematic view parallel to [100]. The thick lines and arches (overemphasized) correspond to the four areas of the opaque material. The heights of all sphere segments are about 1μ measured by optical microscopy.

On the surface (001) another segment of a spherical surface with a curvature larger than that on (010) and $(0\bar{1}0)$ was observed. The segment is also covered by opaque material like that on (010) and $(0\bar{1}0)$, but in arched form. The same feature is found on the opposite surface $(00\bar{1})$; the connecting line between these two opaque spots (II) is slightly tilted from the c^*-axis of the host crystal. The two connecting lines (I and II) cross approximately. The anorthite contents of the host crys-

tal was optically determined using the tables of BURRI et al.(1) and is found to be An 85±3 Mol %.

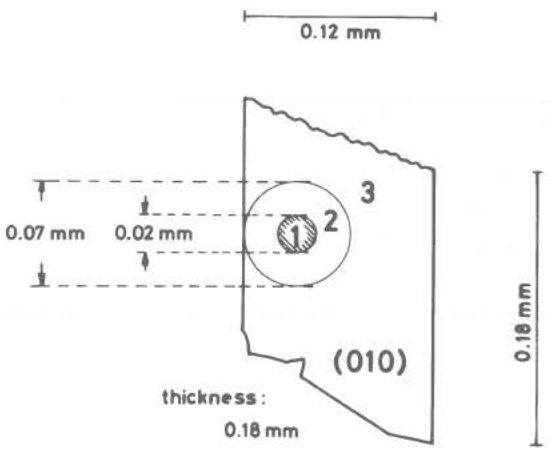

Fig. 2. Schematic view on (010) of crystal 15076,55 No.2 of An-rich low-temperature plagioclase.
1: Circular area of opaque material on top of the sphere segment.
2: Area of the sphere segment, colourless and transparent.
3: (010) surface of host crystal.

The crystal No.2 shows a similar segment of a spherical surface and an opaque circle on its top (Fig.2), but only on (010).The specimen was studied by means of scanning electron microscopy (SEM) and energy dispersion X-ray analysis (EDAX). SEM photos show many coneshaped pillars of very different lengths in area 1 (Fig.2). The biggest one is ca. 20 000 Å in height and ca. 5000 Å in diameter at its base. On the top of these big pillars, needles (three, four or more) pointing upwards are observed. They are 3000 to 5000 Å long and ab. 500 Å in diameter. The nature of this material could not be identified. Similar pillars on ilmenite surface from Apollo 12 sample 12036,2 were reported by Jedwab (2) and described as silicate. At the border of area 1, long parallel orientated cristallites were observed. They are about 20 000 to 30 000 Å long, 4000 to 5000 Å wide and 2000 to 3000 Å thick. There are three orientations of the long axis of the crystallites forming angles of 120° approximately; one of these is parallel to [100] of the host crystal, some are morphologically interpenetrated. These crystallites could not yet be identified crystallographically. The details of these SEM photographs will be published elsewhere (KOREKAWA, in preparation). The results of the EDAX of areas 1,2 and 3 (Fig. 2) are given in Fig. 3 and in Table 1.

areas	Al	Si	P,Zr	K	Ca	Ti	Fe	minerals
1		++	++		+++	+	+	ilmenite, perovskite, rutile, baddeleyite, zircon, apatite, whitelockite? (compare (2))
2	+	+++		+				glass with K-feldspar composition?
3	++	+++			++			An-rich plagioclase

Table 1. Distribution of elements in three areas (see Fig. 2) of sample 15076,55 No. 2 from energy dispersion X-ray analysis (EDAX). + small, ++ medium, +++ predominant contents.

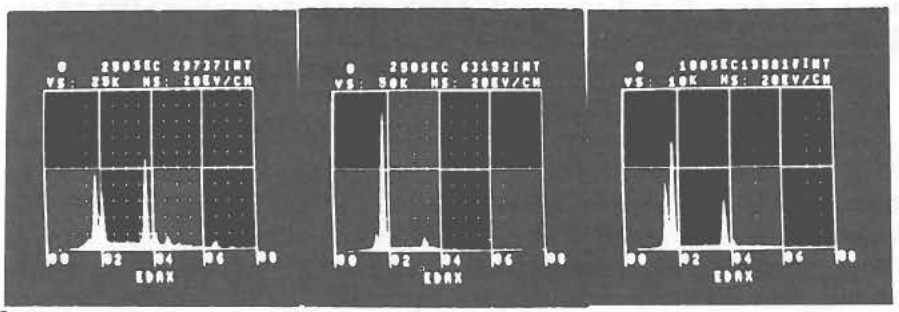

Fig.3.Energy dispersion X-ray analysis (EDAX) of areas 1,2 and 3 (see Fig.2) of crystal No.2. Units in KeV. left=area 1: 1.739 Si(Kα), 2.013 P (Kα1) or 2.042 Zr (Lα1) or both of them, 3.690 Ca(Kα), 4.012 Ca(Kß), 4.508 Ti(Kα), 4.931 (Kß1), 6.398 Fe(Kα), 7.057 Fe(Kß1). middle = area 2: 1.486 Al(Kα), 1.739 Si(Kα), 3.312 K(Kα), right = area 3: 1.486 Al(Kα), 1.739 Si(Kα), 3.690 Ca(Kα), 4.012 Ca(Kß).

1.2 X-ray investigations

Three feldspar crystals from lunar sample Nr. 15076,55 have been investigated by X-rays using Weissenberg-techniques with filtered CuKα- and strictly monochromatic CuKα1-radiation. Crystals Nos.1 and 2 were untwinned while crystal No.3 showed twinning according to the albite- and Karlsbad-laws as previously described (4) for other lunar and terrestrial feldspars.

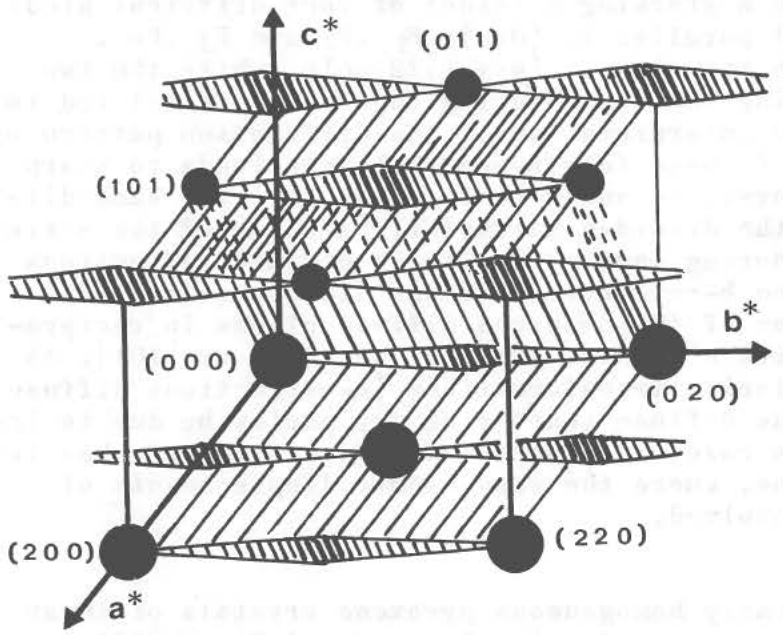

Fig.4: Schematic picture of diffuse scattering of lunar feldspars. Type of reflections: a: b: c: d:

a-reflections (h+k=2n, l=2n) and b-reflections (h+k=2n+1,l=2n+1) are sharp,while c-reflections (h+k=2n,l=2n+1) and d-reflections (h+k=2n+1, l=2n) are very diffuse. The integrated intensities of c- and d- reflections do not vanish as is described by various authors (5).Instead, the integrated intensities remain roughly constant. Thus we can conclude that the bytownite structure(ab.An 80) previonsly described (6) is an averaged structure only. The diffuse c- and d- reflections were studied with the aid of strictly monochromatic Laue-photographs (standing crystal in a cylindrical camera). The results are given in Fig.4. The c- and d-reflections are dominantly diffuse in the b*-direction, but streaks extend also in the remaining two

dimensions of reciprocal space. The latter diffuseness is approximately one order of magnitude smaller than the b^*-diffuseness. Planes of weak diffuse intensity in reciprocal space are found for (hko,hk1) etc.and (h+0,k,h), (h+1,k,h) etc. (Fig.4). They can clearly be observed as "ribbons" connecting c-reflections or a- and b-reflections. In addition, these diffuse streaks are anisotropic extending into the ($\underline{a}^*$- $\underline{c}^*$) direction, thus generating the diffuse planes (h,k,h). It could also be shown, that sharp a-reflections "sit" on weak peaks elongated in b^*.
A terrestrial specimen with the same anorthite contents within the limits of experimental error has kindly been provided by Dr. H.U.Nissen, Zürich. This crystal showed a very similar behavior of c- and d-reflections. The diffuseness into b^* was equal, but there was a distinctly smaller diffuseness into the other two dimensions of reciprocal space. Extrapolating the results of Laves et al. (7), who measured the diffuseness of c-reflections as a function of temperature down to 90 mole% anorthite contents, to our averaged composition of 85 mole%, we may conclude that this diffuseness may be due to a higher temperature of formation of feldspars or to their different thermal history. However,it can not be excluded that the difference in diffuseness is a secondary effect of radiation damage.
A qualitative interpretation of these effects shall be given here. In a first approximation we have a stacking disorder of four different kinds of layers (F_1 ,F_2 ,F_3 ,F_4) parallel to (010); F_1 ,F_2 and F_3 ,F_4 , respectively, differ by the translation $(\underline{a} + \underline{c})/2$ only, while the two pairs are different. Assuming that neighboring layers are translated to each other by $(\underline{a} + \underline{c})/2$,the interpretation of the diffraction pattern by a statistical arrangement of these four types of layers leads to sharp a- and b-reflections; moreover, c- and d-reflections have the same diffuseness as determined by the disorder parameter. Omission of the strict displacement rule of neighboring layers results in diffuse reflections superimposed on sharp a- and b-reflections. These diffuse reflections could be observed. Inclusion of the observed diffuse planes in reciprocal space involves statistics of chains parallel to [001] or [101]. As we are concerned with displacive transformations (c-reflections diffuse at higher temperatures), the diffuse scattering may partly be due to inelastic scattering. In this case the static model discussed here has to be replaced by a dynamic one, where the same atomic displacements of the layers (F_1 ,F_4) are involved.

2. Pyroxenes

Five yellow and microscopically homogeneous pyroxene crystals of lunar sample 15076,55 Nos.11-15 were investigated by means of X-ray diffraction methods. Four of these crystals were found to be pigeonites ($P2_1/c$). The lattice parameters a = 9.60-9.68,b = 8.86-8.96,c = 5.20-5.22 Å ß = 71.3-71.7° are in the usual range and indicate rather high Mg- and Fe- and low Ca- contents (8). The crystal No.15 shows remarkably different parameters: a = 9.38(3), b = 8.91(3), c = 5.33 (2) Å; its chemical composition has not yet been identified. In contrast to Apollo 12

and 14 samples (4), our X-ray photos show no splitting of reflections and no additional distinct reflections of augite. Beginning augite exsolution, however, is indicated by diffuse streaks originating from the pigeonite reflections and pointing towards the expected positions of the augite reflections. Reflections with h+k=2n+1 which are absent in the augite and diopside structures (C2/c) are generally less intense, but show the same streaks. Inhomogeneties within the crystal No.13 are apparent on Weissenberg photographs taken with monochromatic radiation focussed on different parts of the crystal. The photographs yielded different shapes of the diffuse streaks.

The diffuseness of the reflections is highly anisotropic. While the reflections are nearly sharp in the b^*-direction leaving the Cu Kα1 - α2 separation visible, they are rather diffuse in the a^*- and most diffuse in the c^*-direction where the Kα1 - α2 splitting is totally smeared out. This is due to well known lamellar (100)- and (001)- augite exsolutions (9), i.e. (100) and (001) are planes of intergrowth between the lamellae of pigeonite and augite. The curvatures of the streaks indicate incongruent planes of intergrowth with partly coherent scattering (4).

Quite often straight streaks are observed. In these areas of the reciprocal lattice the theory may be reduced to the simpler equations for lamellae with a congruent plane of intergrowth which is described by equation (4) in the paper cited. The characteristic values $\lambda_i = |\lambda_i| e^{i\varphi_i}$ of this equation describe the behavior of reflections. Here $e^{i\varphi}$ represents the displacement of reflections in reciprocal space, while $|\lambda_i|$ stands for their diffuseness (continous streaks for $|\lambda| = 0$, sharp reflections for $|\lambda| = 1$). As the reflections of the new phase are not visible, the constant ß describing the probability that exsolution layers are continued in the stacking order of layers should lie in the range $0 < ß < 0{,}5$. On the other hand, the main reflections of the host structure are partly diffuse, therefore the corresponding probability α for the host structure must differ from unity. In this case $|\lambda|$ is a function of all variables α, ß and $\exp\left[2\pi i (h\Delta_1 + k\Delta_2 + l\Delta_3)\right]$; $\Delta_1, \Delta_2, \Delta_3$ are the deviations of the lattice constants of the host and exolution lamellae from their average values. In this way, the anisotropic behavior of diffuse reflections can easily be understood. A quantitative treatment of this problem will be given in a later paper.

References

(1) C.Burri, R.L.Rarker and E.Wenk; Die optische Orientierung der Plagioklase. Birkhäuser, Basel and Stuttgart, p.334 (1967).
(2) J.Jedwab; Proceedings of the Second Lunar Science Conference, Geochim. Cosmochim. Acta, Suppl.2, Vol.1, 923 (1971).
(3) B.Mason and W.G.Nelson; The Lunar Rocks. Wiley-Interscience, 33 (1970).
(4) H.Jagodzinski, M.Korekawa; Proc.of the Third Lunar Science Conf., Geochim.Cosmochim.Acta, Suppl.3, Vol.1, in press (1972).
(5) F.Laves, M.Czank, H.Schulz; Schweizer.Min.Petrogr.Mitt. 50, 519 (1970).
(6) S.G.Fleet, S.Chandrasekhar, H.D.Megaw; Acta Cryst., 21, 782 (1966).
(7) F.Laves and J.R. Goldschmith; Acta Cryst., 7, 465 (1954).
(8) LSPET; Science 173, 681 (1971).
(9) P.Robinson, H.W.Jaffee, M.Ross, C.Klein; Amer.Mineral., 56, 909 (1971).

APOLLO 15 GLASSES OF IMPACT ORIGIN by Judith B. Best and Jean A. Minkin, U. S. Geological Survey, Washington, D. C. 20242

The Apollo 15 fines and breccias contain a strikingly large and varied assemblage of impact-produced glass particles. We have determined chemical compositions by electron microprobe analysis for more than 130 glass particles from fines (15101,94, 15251,47, 15261,65, 15271,107, 15301,82, and 15501,26--all <1 mm) and polished thin sections of breccias (15025,6, 15286,35, 15298,22, 15306,5, and 15466,14). Refractive indices were measured for all non-opaque particles selected from the fines. In order to ascertain whether the glass compositions cluster into distinctive groups and to determine possible parent rock types, we have compiled frequency distribution curves of refractive indices, and we have calculated CIPW norms and plotted major and minor element variation diagrams using our chemical data. Chemical analyses from the literature have also been included for comparison[1,2,3].

Color and Refractive Index

We selected over 100 glass particles at random from Apollo 15 fines for detailed study. Their range in color is given in Table 1. Refractive indices (R.I.) of these particles were measured using an interference microscope. Precision of measurement by this technique is $\pm$0.0002 in the range below 1.700 and $\pm$0.0005 for R.I.'s greater than 1.700. The particles were later embedded in epoxy, polished and analyzed.

R.I.'s of Apollo 15 glasses that we measured range from 1.5717 to 1.733. As was previously observed in our studies of Apollo 11, 12, and 14 glasses[4,5] the variation of R.I. is discontinuous. A frequency distribution of R.I.'s for Apollo 15 glasses shows a very prominent peak at 1.649, corresponding to a group of homogeneous emerald-green glasses. Green glasses with an R.I. peak at 1.649 also occur among Apollo 14 glasses[5], but in less abundance. Another important peak occurs at 1.671, representing a group of orange to reddish-brown glasses also found in Apollo 11 samples[4]. A peak at 1.597 is associated with a group of pale green glasses. This is slightly shifted from the peak at 1.595 previously observed as common to Apollo 11, 12 and 14 glasses[5]. A minor peak occurs at 1.572 and is associated with a group of colorless fragments.

Brown glasses, varying in R.I. from 1.631 to 1.655, are fairly abundant among Apollo 15 glasses. Brown glasses with a similar range in R.I. were also found for Apollo 12[4]. In addition, among the Apollo 15 fines, as well as in Apollo 11 and 12, there is a distinct lack of glasses with R.I.'s in the range 1.604 to 1.630, the range that contains a broad major group of gold glasses in Apollo 14 fines[6].

Chemical Groups

The CIPW norms of all of our Apollo 15 glass analyses, plus norms computed from published chemical analyses of Apollo 15 basalts, fines and glasses, were plotted on three types of ternary diagrams that use common lunar minerals as apices. Feldspar and pyroxene are two of the components in all three plots; the third apex is (respectively) olivine, quartz, or ilmenite (plus chromite). To

APOLLO 15 GLASSES

J. B. Best

complement the norm plots and check the consistency of grouping, oxide variation diagrams were also prepared.

From the plots and R.I. data we distinguish 12 apparent chemical groups. Their physical and compositional characteristics are summarized in Table 1 and discussed in some detail below. Group numbers have been assigned in approximate order of increasing average R.I.

Group 1. Anorthite. The colorless angular fragments of this group are approximately An_{96} in composition and are the only Apollo 15 mineral glasses we have found. Their R.I.'s range from 1.5717 to 1.5724. Since the R.I. associated with normal plagioclase glass of the same composition is 1.5710[7] these are probably dense thetomorphic glasses identical to those found in Apollo 11 fines (see [4]: Apollo 11 group 1).

Group 2. Anorthosite. This group of colorless and pale green glasses contains the most abundant normative feldspar and lowest normative ilmenite and pyroxene of all the Apollo 15 rock glasses we have analyzed. They have low alkali contents and vary from low normative olivine to very low normative quartz. Compared to other Apollo 15 glass groups, the normative pyroxenes of this group are high in magnesium, low in iron and lowest of all in calcium, and their olivines are highly magnesian. The average composition of these glasses is similar to that of Chao et al.'s Apollo 14 "anorthositic" group ([5]: group 2). Reid et al.'s average "highland basalt" analysis[3] falls just outside the boundaries of this group on our normative diagrams.

Group 3. Anorthositic gabbro. In general, the normative mineral assemblage of this pale green glass group shows feldspar dominant over pyroxene, low olivine, and very low ilmenite. The average FeO/MgO ratio is nearly identical to that of group 2, although their normative pyroxenes are slightly richer in calcium and their alkali contents are higher. Glasses with similar R.I. and composition have been reported for all Apollo sites[3,5,8].

Group 4. Feldspathic basalt. Most heterogeneous glasses fall within the boundaries of this large and varied group. Some particles in this group are quartz normative but most contain low to moderate amounts of normative olivine. Group 4 glasses contain about equal amounts of normative feldspar and pyroxene and have minor ilmenite. Their average normative pyroxene has about the same calcium level as that of group 3, but it is more iron-rich; their normative olivines are also richer in iron. In addition, the alkali and P_2O_5 contents of glasses within this group are slightly higher than those of group 3. Glasses with similar compositions have been reported at the Apollo 14 site (see [5]: group 4, [10], and [11]). Reid et al.'s average analysis of Apollo 15 "moderate K Fra Mauro basalt" glass[3] corresponds to this group as do the analyses of fines samples 15101,87 and 15291,32[1].

Subgroup 4A. These highly homogeneous pale green glasses, all from Station 6, have a normative mineral assemblage similar to that of group 4 except that ilmenite is slightly lower and all are olivine normative. In addition, P_2O_5 is slightly lower. FeO/MgO ratios are very low (.59-.74) and this group is characterized by having the most highly magnesian normative pyroxenes (En_{67-73}) and olivines (Fo_{72-76}) of all the groups. Reid et al.'s Apollo 15 "low K Fra Mauro basalt" glass[3] has many of the same characteristics as our subgroup 4A glasses.

Group 5. KREEP. The glasses of this group, four from near the LM and one from

APOLLO 15 GLASSES

J. B. Best

Hadley Rille (Sta. 9), are characterized by the highest silica (52.8-57.7 wt. %), potash (0.8-1.7%) and soda (0.8-1.4%) contents of any group, and they contain extremely variable P_2O_5 (0.1-1.3%). Their normative mineral assemblages show feldspar dominant over pyroxene; ilmenite is minor but distinctly higher than in groups 2,3,4 and 4A. The very high FeO/MgO ratio (average value 2.8) is reflected in the normative pyroxenes which are richest in iron of all Apollo 15 groups. The normative plagioclase is the least calcic of all the groups, with an average composition of An_{66}. Several glasses in this group are comparable to Apollo 12 KREEP glass fragments[9] and to some "basaltic" glasses from the Apollo 14 fines analyzed by Chao et al. (see [5]: group 4). They are also similar in composition to the Apollo 15 "high K Fra Mauro basalt" glasses of Reid et al.[3].

Group 6. Olivine-bearing feldspathic basalt. Compared to the preceding groups, the average normative ilmenite content for these two greenish-gold spheres is high relative to their high normative feldspar. They contain moderate amounts of normative olivine and very low alkalies and P_2O_5. Their normative pyroxenes have calcium contents a bit higher than those of groups 3 and 4.

Group 7. Troctolite. The three gold spheres of this group show an even higher normative ilmenite content relative to feldspar than does group 6. In addition, they have low pyroxene and the highest normative olivine of all the Apollo 15 glass groups. Normative pyroxenes for group 7 glasses are the most calcic of all the groups (average Wo_{29}). They have very low alkali and P_2O_5 contents, and, except for slightly lower TiO_2 levels, these glasses are identical to Chao et al.'s Apollo 14 "troctolitic" glasses (see [5]: group 6).

Group 8. Ilmenite-bearing basalt. This rather homogeneous group of golden-brown particles is the first Apollo 15 group for which normative pyroxene is more abundant than feldspar. The range of the latter constituent is very narrow (36-42%). These glasses vary from moderately high normative olivine to minor normative quartz and have ilmenite levels slightly higher than the glasses in group 4. Alkali and P_2O_5 contents are variable, but are generally low. The normative pyroxenes of this group are richer in calcium, and their olivines are richer in iron, than those of group 4. The average composition of group 8 is almost identical to Reid et al.'s Apollo 15 "mare 1 basalt" glass[3] and it is similar to Chao et al.'s Apollo 12 group 5 glasses[4].

Group 9. Peridotite. Our largest group of Apollo 15 glasses is very homogeneous, and except for breccias 15025,6 and 15286,35, glasses from this group are found in all the Apollo 15 fines and breccia samples we studied. They are especially abundant in fines sample 15301,82 which was collected on the rim of Spur Crater (Sta. 7). These glasses have the highest MgO and lowest Al_2O_3 contents of any Apollo 15 glasses analyzed; FeO is very high, Cr_2O_3 is high, and titania is very low. Alkalies and P_2O_5 are also low. Normative olivine for this group is very abundant, second only to group 7, and normative pyroxene is greatly dominant over feldspar. (Feldspar levels are constant at about 20% and are the lowest of all Apollo 15 groups.) The normative pyroxene of group 9 contains moderately high calcium and more magnesium than iron. Only two glasses with similar composition were analyzed in the Apollo 11 and 12 fines by Chao et al. (see [4]: Apollo 11 group 8). However, the Apollo 14 fines produced many glass particles with peridotite compositions[5,12]; in fact Chao et al.'s Apollo 14 group 7a[5] is identical in composition and R.I. to these group 9

APOLLO 15 GLASSES

J. B. Best

glasses. Several other investigators have reported "green glass" in Apollo 15 fines with compositions corresponding to group 9[3,13,14].

Group 10. Ilmenite-bearing olivine basalt (Apollo 12-or 15-type mare basalt). These reddish-brown glasses contain very low Al_2O_3, moderate MgO, very high FeO (about 21%), and a nearly constant TiO_2 level of almost 4%. Alkalies and P_2O_5 are highly variable, and Cr_2O_3 is the highest of all the groups. The normative mineral assemblage for this group is dominated by pyroxene with slightly more feldspar than group 9, about 7% ilmenite, and minor to abundant olivine. Normative pyroxene shows magnesium slightly greater than iron and a calcium content similar to that of group 9. Normative olivine is the most iron-rich of any group (Fo_{47-57}). Except for slightly higher TiO_2 levels, group 10 glasses correspond in composition to Apollo 15 basalts 15557,27 and 15659,4[2] and to the "mare 3 basalt" glass of Reid et al.[3]. Futhermore, by adding about 0.5 to 1.0% TiO_2, the average composition of group 10 approximates that of Apollo 12 mare basalts[15].

Group 11. Ilmenite basalt (Apollo 11-type mare basalt). The reddish-brown glasses of this group are characterized by moderate to high TiO_2, moderately high FeO, low Al_2O_3, and moderate amounts of P_2O_5 and alkalies. Normative mineral assemblages show pyroxene dominant over feldspar and abundant ilmenite. Only one particle is olivine normative; the rest contain minor normative quartz. The normative pyroxenes of this group are variable in composition, but they generally contain high calcium and more magnesium than iron. Table 1 includes two analyses for this group since it is so heterogeneous. Several glasses in this group closely approximate the average composition of Apollo 11 ilmenite basalts[15] and have analogues in both the Apollo 11 and 14 fines (see [4]: Apollo 11 group 5, and [5]: group 8).

Group 12. Olivine-bearing ilmenite basalt. This group of nine dark reddish-brown to black spheres have the lowest silica (36.7-38.9 wt. %) and highest TiO_2 (10.6-14.3%) and FeO (19.8-22.2%) contents of any Apollo 15 group, and they contain very low Al_2O_3. In addition, they have abundant Cr_2O_3 and alkalies; P_2O_5 is variable. Their normative chemical composition is distinct, with pyroxene greatly dominating feldspar and ilmenite the highest of all Apollo 15 groups. They vary from low to moderate normative olivine. The normative pyroxenes of group 12 glasses have high calcium, second only to those of group 7, and much more magnesium than iron. Normative olivines are Mg-rich. Glasses with similar characteristics have been reported for the Apollo 14 fines (see [5]: group 8) as well as in other Apollo 15 investigations[3].

Discussion

The trends exhibited by the Apollo 15 chemical groups on the normative and variation diagrams are similar to those of the Apollo 11 and 12 glasses[4] and identical to those of Apollo 14[5]. This implies that similar petrogenetic processes are involved at different localities on the moon.

Thirty-five percent of the Apollo 15 glasses we have analyzed are mare-type basalt glasses (groups 8, 10, 11 and 12); another 25% are "green glass" (group 9), probably of highland origin. The rest of the glasses, apart from group 1, are probably also of highland affinity. Thus it is apparent that the Apollo 15 regolith is an intimate mixture of both mare and highland materials.

APOLLO 15 GLASSES

J. B. Best

Acknowledgments. This study has been carried out as part of an investigation of the impact metamorphism of lunar materials for which E. C. T. Chao, U. S. Geological Survey, Washington, D. C., is principal investigator. We are grateful to Dr. Chao for providing the samples for analysis. The work was done under NASA Contracts T-2357A and W-13130.

References

[1] Carron, M. K., Annell, C. S., Christian, R. P., Cuttitta, F., Dwornik, E. J., Ligon, D. T. Jr., and Rose, H. J. Jr. (1972) Elemental analyses of lunar soil samples from Apollo 15 mission. In The Apollo 15 Lunar Samples (ed. J. W. Chamberlain and C. Watkins), Lunar Sci. Inst., Houston.

[2] Christian, R. P., Annell, C. S., Carron, M. K., Cuttitta, F., Dwornik, E. J., Ligon, D. T. Jr., and Rose, H. J. Jr. (1972) Chemical composition of some Apollo 15 igneous rocks. In The Apollo 15 Lunar Samples (ed. J. W. Chamberlain and C. Watkins), Lunar Sci. Inst., Houston.

[3] Reid, A. M., Warner, J., Ridley, W. I., and Brown, R. W. (1972) Major element composition of glasses in three Apollo 15 soils. Meteoritics, in press.

[4] Chao, E. C. T., Boreman, J. A., Minkin, J. A., James, O. B., and Desborough, G. A. (1970) Lunar glasses of impact origin: Physical and chemical characteristics and geologic implications. J. Geophys. Res. 75, No. 35, pp. 7445-7479.

[5] Chao, E. C. T., Best, J. B., and Minkin, J. A. (1972) Apollo 14 glasses of impact origin and their parent rock types. Proc. Third Lunar Sci. Conf., Geochim. Cosmochim. Acta, Suppl. 3, in press.

[6] Cavarretta, G., Coradini, A., Fulchignoni, M., Funiciello, R. Taddeucci, A., and Trigila, R. (1972) Glassy particles in Apollo 14 soil 14163,88: peculiarities and genetic considerations (Abstr.). In Lunar Science-III (ed. C. Watkins), pp. 128-130, Lunar Science Contr. No. 88.

[7] Shairer, J. F., Smith, J. R., and Chayes, F. Refractive indices of plagioclase glasses. Carnegie Inst. Wash. Yr. Book 55-56, pp. 195-197.

[8] Glass, B. P. (1972) Apollo 14 glasses (Abstr.). In Lunar Science-III (ed. C. Watkins), pp. 312-314, Lunar Science Contr. No. 88.

[9] Meyer, C., Jr., Brett, R., Hubbard, N. J., Morrison, D. A., McKay, D. S., Aitken, F. K., Takeda, H., and Schonfeld, E. (1971) Mineralogy, chemistry, and origin of the KREEP component in soil samples from the Ocean of Storms. Proc. Apollo 11 Lunar Sci. Conf., Geochim. Cosmochim. Acta, Suppl. 1, Vol. 1, pp. 393-411. Pergamon.

[10] Reid, A. M., Ridley, W. I., Warner, J., Russell, S. H., Brett, R., Jakes, P., and Brown, R. (1972) Chemistry of highland and mare basalts as inferred from glasses in the lunar soils (Abstr.). In Lunar Science-III (ed. C. Watkins), pp. 640-642, Lunar Science Contr. No. 88.

[11] Quaide, W. (1972) Mineralogy and origin of Fra Mauro fines and breccias (Abstr.). In Lunar Science-III (ed. C. Watkins), pp. 627-629, Lunar Science Contr. No. 88.

[12] Marvin, U. B., Reid, J. B. Jr., Taylor, G. J., and Wood, J. A. (1972) Lunar mafic green glasses, howardites, and the composition of undifferentiated lunar material (Abstr.) In Lunar Science-III (ed. C. Watkins), pp. 507-509, Lunar Science Contr. No. 88.

[13] Carusi, A., Cavarretta, G., Cinotti, F., Civitelli, G., Coradini, A., Funiciello, R., Fulchignoni, M., and Taddeucci, A. (1972) Lunar glasses as an index of the impacted sites lithology: The source area of Apollo 15 "green glasses." Geol. Rom. 11, pp. 137-151.

[14] Bence, A. E., Delano, J. W., and Papike, J. J. (1972) Apollo 15 (2-4 mm) coarse fines: A mineralogical and petrogeologic study (Abstr.). EOS Transactions, Am. Geophys. U., Vol. 53, No. 4, p. 551.

[15] Hubbard, N. J., and Gast, P. W. (1971) Chemical composition and origin of nonmare lunar basalts. Proc. Second Lunar Sci. Conf., Geochim. Cosmochim. Acta, Suppl. 2, Vol. 2, pp. 999-1020. MIT Press.

Table 1. The Chemical Groups of Apollo 15 Glasses

Group	1	2	3	4	4A	5	6	7	8	9	10	11	12
Color	Color-less	Color-less, Pale green	Pale green	Pale green, Yellowish-green, Yellow, Gold, Brown, Opaque	Pale green	Pale brown, Gold	Greenish-gold	Gold	Gold, Greenish-gold, Brown, Gray, Opaque	Yellowish-green, Green, Greenish-gold	Dark red, Reddish-brown, Orange	Dark red, Reddish-brown	Dark Reddish-brown, Black
Range of Refractive Index	1.5717-1.5724	1.5783-1.5940	1.5879-1.5976	1.5953-1.6240	1.6012-1.6037	1.582	1.6208-1.6309	1.6242-1.6350	1.6305-1.6543	1.6473-1.6532	1.6690-1.6719	1.6728-1.6966	1.733
Number Analyzed	3	6	5	21	7	5	2	3	15	32	16	6	9
Chemical Composition (in weight percent)													
Representative Sample	15-3	15-27	15-56	15-60 15-93A	15-76	15025, 6-2	15-16	15-55	15-50	15-51	15306, 5-7	15-44 15025, 6-7	15298, 22-16
SiO_2	45.2	46.2	46.6	49.9 45.9	48.4	57.4	43.6	40.6	44.8	45.7	44.3	45.4 42.5	37.4
TiO_2	0.03	0.23	0.46	1.28 1.29	0.68	2.28	1.15	1.65	2.01	0.41	3.57	5.9 9.6	13.6
Al_2O_3	36.3	30.0	23.9	16.4 16.6	16.5	12.9	20.3	19.4	14.6	7.2	7.5	9.7 9.2	8.0
FeO	0.15	3.6	6.5	9.9 12.5	8.8	11.8	10.4	10.9	15.0	19.3	21.1	20.2 18.2	21.2
MgO	0.10	4.4	8.1	9.2 12.6	14.9	3.5	11.0	11.6	11.4	16.9	12.6	6.4 7.0	9.2
CaO	19.1	16.7	14.2	10.1 10.4	9.5	9.0	12.9	13.1	11.6	8.3	8.5	10.7 11.6	9.0
Na_2O	0.42	0.06	0.17	0.62 0.42	0.46	0.86	0.05	0.03	0.05	0.15	0.40	0.41 0.43	0.65
K_2O	--	0.04	0.21	0.63 0.37	0.20	1.04	--	0.13	0.19	0.18	0.16	0.17 0.20	0.27
P_2O_5	0.07	0.05	0.06	0.29 0.19	0.08	0.08	0.05	0.05	0.05	0.07	0.15	0.09 0.14	0.14
MnO	--	0.05	0.08	0.13 0.16	0.11	0.13	0.15	0.10	0.17	0.17	0.30	0.19 0.26	0.28
Cr_2O_3	--	0.09	0.15	0.27 0.27	0.09	0.07	0.21	0.24	0.31	0.52	0.55	0.26 0.46	0.50
NiO	--	--	--	-- --	--	--	--	0.04	0.03	0.07	0.05	0.06 --	0.04
Total	101	101	100	99 101	100	99	100	98	100	99	99	100 100	100
CIPW Norms													
Q	1.75	0.83	0	3.82 0	0	19.51	0	0	0	0	0	3.74 3.67	0
C	1.04	0	0	0 0	0	0	0	0	0	0	0	0 0	0
Or	0	0.23	1.24	3.78 2.17	1.18	6.20	0	0.78	1.12	1.08	0.95	1.01 1.19	1.59
Ab	3.51	0.50	1.43	5.31 3.53	3.90	7.35	0.42	0.26	0.42	1.28	3.41	3.49 3.65	5.48
An	93.02	80.30	63.56	40.62 42.02	42.48	28.54	55.27	53.57	38.97	18.63	18.35	24.25 22.68	18.06
Wo	0	0.43	2.59	3.43 3.33	1.78	6.68	3.56	5.23	7.57	9.40	9.68	11.91 14.28	10.67
En	0.25	10.80	17.10	23.21 17.36	28.60	8.80	12.46	4.80	18.08	22.51	21.76	16.02 17.50	18.43
Fs	0.22	6.23	9.49	16.28 11.56	11.68	18.26	7.86	2.88	15.49	18.58	22.89	27.73 17.73	13.38
Fo	0	0	2.10	0 9.67	6.04	0	10.50	17.32	7.19	14.03	6.93	0 0	3.10
Fa	0	0	1.28	0 7.10	2.72	0	7.31	11.46	6.79	12.77	8.03	0 0	2.48
Cm	0	0.13	0.22	0.40 0.40	0.13	0.10	0.31	0.36	0.46	0.77	0.82	0.39 0.68	0.73
Il	0.06	0.43	0.87	2.46 2.43	1.30	4.37	2.19	3.20	3.81	0.79	6.84	11.26 18.31	25.76
Ap	0.16	0.11	0.14	0.70 0.45	0.19	0.19	0.12	0.12	0.12	0.17	0.36	0.21 0.33	0.33
Feldspar													
Or	0	0.3	1.9	7.5 4.5	2.5	14.6	0	1.4	2.8	5.1	4.2	3.5 4.3	6.2
Ab	3.8	0.6	2.3	11.3 7.8	8.7	18.3	0.8	0.5	1.1	6.5	15.8	12.8 14.0	22.8
An	96.2	99.1	95.8	81.2 87.7	88.8	67.1	99.2	98.1	96.1	88.4	80.0	83.7 81.7	71.0
Pyroxene													
Ca	0	2.4	8.4	7.7 9.9	3.9	20.3	14.3	39.2	18.0	18.1	17.6	21.7 28.5	24.4
Mg	59.2	67.8	64.4	60.2 59.8	73.3	30.9	57.9	41.7	49.6	50.3	45.8	33.8 40.4	48.7
Fe	40.8	29.8	27.2	32.1 30.3	22.8	48.8	27.8	19.1	32.4	31.6	36.6	44.5 31.1	26.9
Olivine													
Mg	0	0	70.3	0 66.4	76.3	0	67.6	68.6	60.5	61.4	55.5	0 0	64.4
Fe	0	0	29.7	0 33.6	23.7	0	32.4	31.4	39.5	38.6	44.5	0 0	35.6

-- Below limit of detection

PETROLOGY, MINERALOGY AND CLASSIFICATION OF APOLLO 15 MARE BASALTS. G.M. Brown, C.H. Emeleus, J.G. Holland, A. Peckett and R. Phillips. Geology Dept., Durham Univ., England.

Preliminary data on three basalts, a new zirkelite-type mineral and a strontian whitlockite have been published (1,2). This account is concerned chiefly with 11 mare basalts that can be grouped into 3 contrasted types. The Apollo 15 PET description (1971) gave a possible grouping into 4 types of mare basalt. This is valid and we extend it to other samples, except that their Type 4 is probably a textural variant of Type 3.

Mare basalt I (15058, 15065, 15076, 15085, 15475). Stations 8 (LM), 1 (Elbow, traverse of 3 samples) and 4 (Dune), respectively. Pyroxene-rich, tridymite gabbro. Most notably this suite contains no early-phase olivine (except 2% of Fo60 in 15065 which may be transitional to Type III), is low in opaque phases (2-4%) and all rocks contain prismatic tridymite (2-6%). Clinopyroxene is abundant (64-68%) and plagioclase (24-32%) more abundant than in most Apollo 12 mare basalts. An exceptional member (15076) must be heterogeneous because our sample contains only 53% Cpx with 36% Pl, whereas the PET analysis gives normative values as for the rest of Type I modes. Similar evidence for crystal sorting at the source of the suite is shown by 15085 where pigeonite is much more abundant than in the others (1). The pyroxenes are all zoned discontinuously from fairly large, zoned pigeonite cores (up to 60% in 15085) to zoned augite mantles and (?) pyroxferroite rims. The calcic trends for 15085 (1) and 15065 are closer to the subcalcic augite field. Al:Ti ratios are moderately high (4-6) in the pigeonites and decrease to about 3 (augites) and to 1 or less in the mesostasis phases (i.e. Ti^{3+} common). Large fayalites occur in sieve-texture with K-rhyolite glass, and rare phases are common in the mesostasis (see mineralogy). Chrome-alumina spinels (to 53% Cr_2O_3) have only moderate Mg:Fe ratios and zone, sometimes continuously, to ulvospinel. Plagioclases range An92-72, the commonest zoning being normal continuous (92 → 80) or normal oscillatory in 15076 (89 → 82 → 89 → 72). They often contain small Cpx inclusions (subcalcic augite) with low Al:Ti (2:1).

Mare basalt II (15485, 15596). Stations 4 (Dune) and 9A (Rille) respectively. They are strikingly similar in containing long (1-6mm) clinopyroxene prisms, with originally hollow cores, as phenocrysts. However, 15485 has a glass, whereas 15596 has a plumose intergrowth of Cpx and Pl, as groundmass. The distance between their localities suggested a widespread flow from which chilled edge and more central parts had been sampled. This is difficult to reconcile with the modes, where the glass contains more phenocryst volume (53%) than the rock in which

slower crystallization should have added to the phenocrysts (41%). Crystal sorting at depth is more likely, as shown by the mineralogy. The plumose groundmass of 15596 adds 32% Cpx, 20% Pl (An83-87) and 6% opaques, giving a very high total Cpx content of 73%. Rare zoned olivine (Fo66→37) and chrome-spinel microphenocrysts occur in 15596 and Fe-Ni spheres in the glass of 15485. The major phenocryst assemblage in both rocks is the most "primitive" of the three basalt groups. The pyroxene phenocrysts consist of zoned magnesian pigeonite cores (as in Type I) but with very sharp discontinuities against the narrow augite mantles. Small Opx (?) kernels need confirmation. Al:Ti ratios are very high (7-10) in the cores, and quite high (5-7) in the mantles, although metastable subcalcic augite in vesicles of the glass are much lower(2). The pyroxene trends are quite different in each rock. Narrow phenocryst mantles in the glassy rock trend towards hedenbergite (Ca44 Mg14 Fe42) compared with augite mantles in the coarser rock. The hedenbergitic mantle-rim is remarkably rich in Al_2O_3 (11.7%) and TiO_2 (4.3%). The plumose groundmass pyroxenes in the coarser rock (15596) are chemically discontinuous with the phenocryst mantles and approach pyroxferroite compositions. Presumably the glassy rock would have produced this additional trend with slower cooling because the glass normative pyroxene is Ca11 Mg5 Fe84. The glass is rich in occult plagioclase (adding 24% Pl, 21% Px, 2% Qz, 2% Ilm, normatively), but gives a total phenocryst + "groundmass" pyroxene content of about 74% (cf. 73% in the coarser rock). The spinel grains show a sharp discontinuity between chrome-spinel core (within Cpx) and ulvospinel mantle (outside Cpx), the chemical break being extreme. Cr_2O_3 (54%), Al_2O_3 (11%) and MgO (7.5%), with Mg/Mg + Fe = 0.36, indicate a more primitive spinel-core assemblage than in both the other mare basalt types and in Apollo 12 samples. The glass of 15485 shows normative plagioclase of An78 (1% Na_2O, 0.2% K_2O), suggesting a more sodic nature for basalt liquids prior to eruptive crystallization.

Mare basalt III (15016, 15536, 15555, 15598). Stations 3 (Seatbelt) and 9A (Rille, 3 specimens), respectively. Although PET viewed 15016 as a Type IV (scoriaceous) it is mineralogically a vesicular, quickly cooled equivalent of Type III. Also it is isochemical with 15555 (PET Report). These rocks are olivine basalts, with a granular texture and finer grainsize than Type I. Cristobalite rather than tridymite, and fairly abundant opaques, also distinguish them. Modally they show olivine (6-10%), clinopyroxene (59-63%), plagioclase (21-27%), opaques (4-7%) and cristobalite(1-2%). 15016 contains 45% vesicles. Although olivine phenocrysts could signify a primitive lava, this is not the case here. Not only are the olivine cores (Fo66) more iron-rich than those in Apollo 12 (Fo78), but the pyroxene and spinel assemblage is more advanced, in terms of crystal-liquid fractionation, than in the pigeonite-phyric basalts of Types I and II. The pyroxenes show non-extreme pigeonite cores at Ca12 Mg58 Fe30, while 15016 contains no detectable pigeonite. The trends show only a slight break between pigeonite cores and augite mantles, and the "shallow" augite trends are

PETROLOGY OF MARE BASALTS

G.M. BROWN

towards hedenbergite or subcalcic ferroaugite. Residual phases rich in $FeSiO_3$ were not found, and the published trend for 15555 (1) is typical of Type III. The pigeonite cores show very low Al:Ti (2-3), and the low values throughout the augite-ferroaugite trend (1-4) is in contrast to Types II (especially) and I. This suggests proximity in temperatures to plagioclase coprecipitation with pyroxene. Plagioclase shows both normal and irregular reversed zoning (range An93-83), but 15016 is markedly reversed (An83→92), probably due to the strong vesiculation and alkali loss. The olivines show continuous zoning but with a break between phenocrysts (Fo66 → 30) and mesostasis (Fo18 → 1). The spinels are less primitive than in Types I and II, the cores showing maxima of 48% Cr_2O_3, Mg/Mg+Fe = 0.21. Ulvospinel is more abundant in this type, showing zoning from Cr-rich to Cr-poor variants.

Other mineralogical features. The patterns for major and minor elements (all by electron probe) in the pyroxenes, plagioclases, olivines, spinels, ilmenites, silica-phases, irons and troilites are generally similar to other Apollo mare basalt suites. There is an overall trend from "primitive" pigeonites and chrome spinels; to early-intermediate augites and olivines; to late-intermediate ilmenite, ulvospinel and plagioclase; to late-stage ferropyroxenes, ferro-olivines, phosphates, Zr-rich minerals (high in REE) and rhyolitic glass. K-Ba feldspar was not detected. The crystallization stage of the irons (varying in Ni from 0.2 to 25%, and Co from 0.8 to 6%), tridymite and cristobalite is not clear, but the Type I basalts show some evidence for early tridymite, and the Type III basalts for late cristobalite. Mesostasis apatite, tranquillityite and strontian whitlockite (1) were analysed from Type I rocks, and tranquillityite, whitlockite and a new zirkelite-type mineral (2) with 10% Y_2O_3, 12% RE_2O_3 from Type III rocks. In spinels, V_2O_3 decreases from chrome-spinel (1%) to ulvospinel (0.15%). In plagioclases, FeO increases regularly with decreasing An content (e.g. 0.4% in An90 to 1.1% in An80).

Residual glasses. Interstitial patches of glass differ between Types III and I basalts. The Type III (olivine basalt) glasses are mostly pale-brown, K-rhyolite (75% SiO_2, 8% K_2O) with one barian example (1), similar to those in other Apollo suites. The vesicular basalt member (15016) is exceptional in containing a heterogeneous assemblage of K-poor (0.3% K_2O, 79% SiO_2, 6% CaO) and K-rich (as above) glasses. This is further evidence for local alkali loss during vesiculation. The Type I (pigeonite-phyric basalt), K-rhyolite glasses are intergrown with large fayalites in a "swiss-cheese" texture. However, the more usual, interstitial brown glass in this basalt-type is a more calcic rhyolite than in Type III (e.g. 4% CaO, 4% K_2O). Cloudy vermicular areas associated with the latter are normatively pyroxferroite (Ca8 Mg2 Fe90) but modally a breakdown intergrowth of Fe-Ca Px, fayalite and silica.

Microbreccia and Green Glasses (15086, Station 1, Elbow Crater). A soil breccia because of several mare basalt fragments, preserved glass spheres, and friable nature. A Cpx fragment identical in high Al and Ti to Type II basalt pyroxene (see above) is proof of local regolith

PETROLOGY OF MARE BASALTS

G. M. Brown

derivation. The glasses are chiefly the "green glass" common in the Front soils. We cannot accept the uncritical use of "pyroxenite" for these compositions (3) which show only 50% Px (28% olivine, 22% plagioclase). They are normatively neither monomineralic nor of the (magnesian) peridotite clan. Normative olivine (Fo50) and pyroxene (Ca20 Mg45 Fe35) are gabbroic rather than ultrabasic, and the source is probably a mafic cumulate of troctolitic nature. Other glasses include yellow KREEP-basalt glass and a highly titaniferous (10.4% TiO_2) type that is too low in MgO for the Mare Basalt Glass 4 group (3). Crystal fragments are much more abundant than lithic and include "primitive" highland assemblages of plagioclase (An97), orthopyroxene (Ca2 Mg83 Fe15, Al_2O_3 3.5%), chromian pleonaste (63% Al_2O_3, 22% MgO, 8% Cr_2O_3) and extreme chrome-spinel (54% Cr_2O_3). An unusual olivine (0.5mm) is Fo93, the most magnesian recorded from the Moon. It differs from breccia/soil magnesian olivines previously recorded (Fo88-90) in its low Cr_2O_3 (0.03%) and CaO ($< 0.01\%$). This characterises meteoritic olivine whereas the Fo88-90 range (0.25% Cr_2O_3) is probably of lunar-mantle origin.

Coarse Fines. A suite (ca. 2mm) from 7 stations can be divided into groups according to relative amounts of mare basalt and highlands debris. A method of semi-quantitative, X-ray fluorescence analysis was devised to categorize the samples in an uncrushed state prior to population survey. All the data (Table 1) were obtained using untreated samples (0.25g each) on a Mylar-sheet container in an air path. Although the poor cross-section of the particles gives results inferior to those on finely crushed powders (see correction, Table 1), the method is so rapid that it can be recommended for studies on extensive suites of coarse-fragment samples. The results show grouping according to relative enrichment in KREEP-basalt elements (Ba, Nb, Zr, Y, Rb) relative to mare basalt, plagioclase-rich (Sr control) and green-glass (mare basalt-type diluent) fragments. Samples from LM-Station 8 (15022,32,42) are KREEP-enriched probably due to the ray of highlands debris from the Aristillus area. Front material (Station 2, St. George) gives high values also in Sr, from plagioclase-enriched KREEP material (102). Sample 502 (Rille Scarp, Stn.9) is a regolith mean. Fairly low values in 302 (Spur, Stn.7) are due to "dilution" of ray and Front material by abundant green-glass (troctolitic) spheres. The lowest values occur in samples at Elbow crater (072,082), Dune (472) and Hadley Rille rim (602). In these, either mare basalt or green glasses are abundant. Further petrographic correlation is in progress. No KREEP-basalts have yet been detected, the high KREEP-element contents being associated chiefly with brown glass and microbreccia concentrations.

Basalt relationships

No evidence permits grouping of any samples as definable parts of a particular lava flow. Primitive pigeonite-basalts (Type II) vary according to deep-level crystal sorting, and pigeonite-rich gabbros (Type I) are influenced by higher-level crystal sorting. Olivine

PETROLOGY OF MARE BASALTS

G. M. Brown

basalts (Type III) are the least primitive and may be associated at source with more mafic, troctolitic cumulates fused by impact to green glasses. Alkali losses during basalt vesiculation (Type III) and high retention during chilling to basalt glass (Type II), indicate differences in initial magma volatile contents.

TABLE I

Semi-quantitative XRF analyses of Apollo 15 coarse fines (ca. 2mm) generally in decreasing order of KREEP components

	22	32	42	102	502	302	82	472	602	72
Ba	147	169	179	139	119	75	88	85	65	54
Nb	18	17	20	16	13	14	10	10	8	6
Zr	328	350	383	327	260	215	209	199	152	135
Y	74	77	81	70	56	47	49	43	34	32
Sr	103	114	107	129	90	101	108	110	81	109
Rb	5	6	5	6	3	3	2	3	1	2

Note: Amounts (ppm) probably about 30% under-value (except Rb) due to method (see text) and comparison with a few similar-locality soils analysed by PET. Table to be used for inter-site variations, where inter-element consistency is valid.

References:

(1) Brown, G.M., Emeleus, C.H., Holland, J.G., Peckett, A., and Phillips, R. (1972). Mineral-chemical variations in Apollo 14 and Apollo 15 basalts and granitic fractions. Proc. Third Lunar Sci. Conf. (in press).

(2) Peckett, A., Phillips, R., and Brown, G.M. (1972). New zirconium-rich minerals from Apollo 14 and 15 lunar rocks. Nature, 236, 215-217.

(3) Reid, A.M., Warner, J., Ridley, W.I., and Brown, R.W. (1972). Major element composition of glasses in three Apollo 15 soils. Science (in press).

SIZE FREQUENCY DISTRIBUTIONS AND PETROGRAPHIC OBSERVATIONS OF APOLLO 15 SAMPLES, J. C. Butler, E. A. King and M. F. Carman, Department of Geology, University of Houston, Houston, Texas, 77004

The size frequency distributions of nine Apollo 15 samples have been determined by dry sieving. The size frequency distributions of these samples have the same general characteristics that have been reported previously from samples collected at other lunar sites(1). The samples are slightly bimodal and mostly have low values of negative skewness (Table 1., Figs. 1 & 2). The average median grain size of the nine samples is 4.15ϕ and the average graphic mean size is 4.17ϕ.

Table 1. Quantitative Statistical Parameters of Apollo 15 Size Frequency Distributions.*

Sample Number	Weight gm	Graphic Mean	Graphic Std. Deviation	Graphic Skewness	ϕ_{50}
15101,103	0.4467	4.30ϕ	2.10ϕ	0.000	4.30ϕ
15231,67	0.4559	4.45ϕ	1.98ϕ	-0.012	4.45ϕ
15201,17	0.4479	4.13ϕ	2.00ϕ	-0.100	4.32ϕ
15221,57	0.4806	4.43ϕ	2.10ϕ	-0.047	4.50ϕ
15221,24	0.9532	4.53ϕ	2.07ϕ	-0.036	4.25ϕ
15071,47	0.4592	3.33ϕ	1.75ϕ	+0.143	3.20ϕ
15601,81	0.9711	3.68ϕ	1.80ϕ	-0.050	3.65ϕ
15091,41	0.9363	4.30ϕ	1.88ϕ	-0.040	4.35ϕ
15021,117	1.0520	4.37ϕ	2.02ϕ	-0.012	4.35ϕ

* For the less than 1 mm size fraction only; determined by dry sieving with controlled relative humidity and precision sieves.

Samples from the Apennine Front mostly are finer than plains samples at the Apollo 15 site. Apennine Front samples have similar mean sizes and other size frequency distribution characteristics to undisturbed plains samples from Fra Mauro, indicating that the Fra Mauro Formation and the Apennine Front have been exposed to meteoroid bombardment for similar lengths of time(2). Fines samples from on, under and around the boulder near St. George Crater have virtually identical size frequency distributions (Fig. 2), indicating that the boulder has been in its present location for a relatively short time. If the boulder had been at its present site for more than approximately 1×10^5 years, we should observe a fraction of coarser detritus, eroded from the boulder onto the nearby surface by meteoroid impacts. Furthermore, it appears that the boulder picked up the fines on its surface during rolling to rest on the Apennine Front regolith.

The plains fines samples at the Apollo 15 site are complicated by ray material(3), Apennine Front regolith that has been ejected onto the plains and by crater rim material. However, if obviously disturbed samples are eliminated from consideration, the samples tend to be coarser than the samples

from the Apennine Front. The coarsest of these samples are comparable to the fines samples from the Apollo 12 site in their size parameters, but more samples from the plains must be analyzed before this suggestion can be confirmed or rejected.

Chondrules have been reported in the Apollo 14 lunar samples by a number of investigators(e.g.,2,4,5,6,7). Similar chondrules have been found in the Apollo 15 samples 15426 and 15425. Specifically, chondrules are abundant to common in sections 15426,18; 15436,19; 15426,20; 15426,23; 15426,72 and 15425,16. In contrast to the Apollo 14 chondrules, the Apollo 15 chondrules are dominated strongly by the crystallized glass spherule chondrule type (See Figs. 3 & 4). However, this observation is based on a relatively small total area of thin sections examined and should be reconsidered after more sections have been described. A few chondrules that are composed of rounded mineral grains and lithic fragments do occur in the Apollo 15 samples (Fig. 5). The apparent lesser abundance of this chondrule type in the Apollo 15 samples may reflect the shorter distance of travel with base surge from the Imbrium Basin, hence less opportunity for abrasion, than the travel distance required for the material deposited at Fra Mauro.

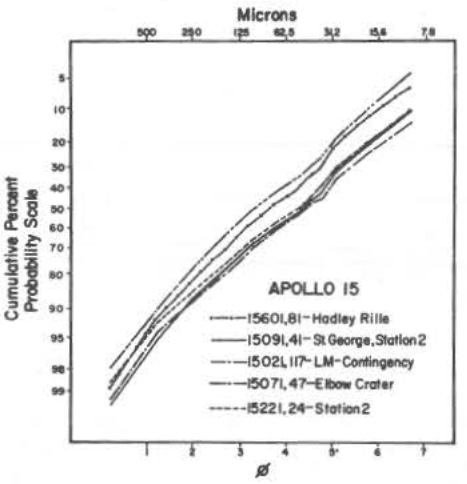

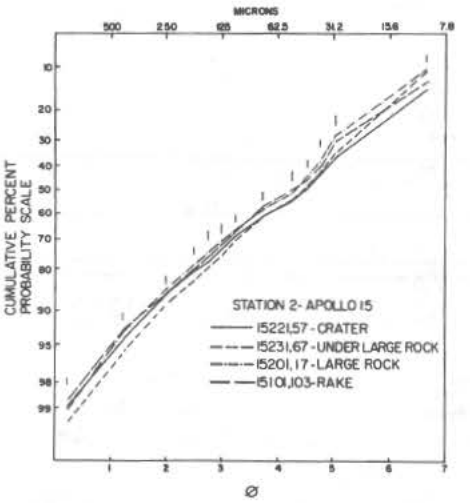

Figure 1, left; Size frequency distributions of five Apollo 15 samples from both the Apennine Front and plains localities.

Figure 2, right; Size frequency distributions of four Apollo 15 samples from on, under and around the boulder sampled Station 2, near St. George Crater. The size frequency distributions are virtually identical. Vertical hashes indicate the sieve sizes actually used.
Courtesy of MIT Press.

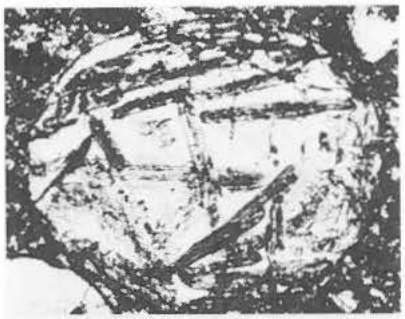

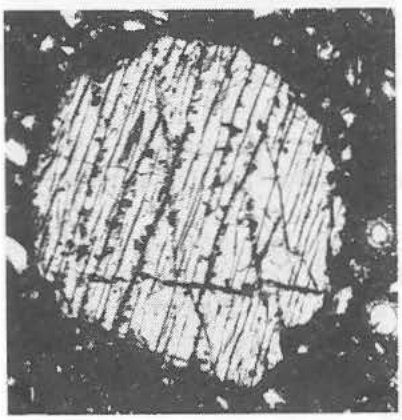

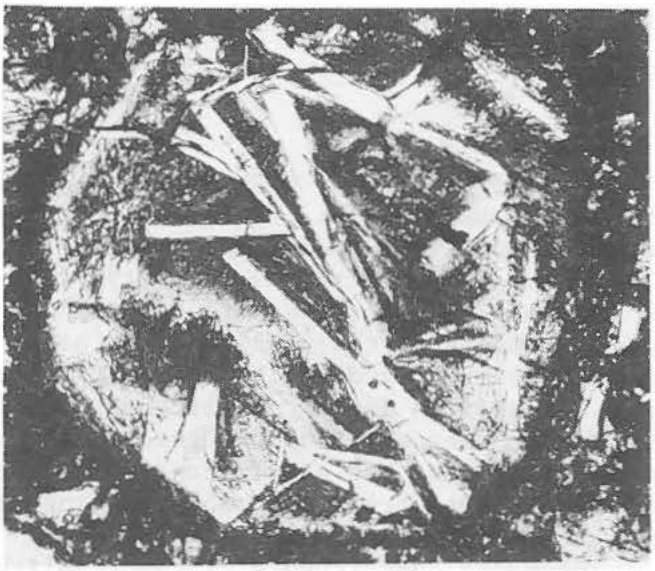

Fig. 3. Plagioclase-pyroxene-glass chondrule in 15426,20, max. diam.=0.35 mm (upper left). Fig. 4. Same in 15425,16, max. diam.=0.45 mm (above). Fig. 5. Single crystal pyroxene chondrule, 15426,18, 0.30 mm diameter, (lower left).

References

(1) King, E. A., Jr., J. C. Butler and M. F. Carman, Jr. (1971) The lunar regolith as sampled by Apollo 11 and Apollo 12: Grain size analyses, modal analyses and origins of particles: Proc. Second Lunar Sci. Conf., Geochim. Cosmochim. Acta, Suppl. 2, Vol. 1, p. 737-746.

(2) King, E. A., Jr., J. C. Butler and M. F. Carman (1972) Chondrules in Apollo 14 samples and size analyses of Apollo 14 and 15 fines: Proc. Third Lunar Sci. Conf., Geochim. Cosmochim. Acta, Suppl. 3, Vol. 1, p. 673-686.

(3) Howard, K. A. (1971) Geologic map of part of the Apennine-Hadley region of the Moon: U.S.G.S., Map I-723, Sheet 2.

(4) King, E. A., Jr., M. F. Carman and J. C. Butler (1972) Chondrules in Apollo 14 samples: Implications for the origin of chondritic meteorites: Science, Vol. 175, p. 59-60.

(5) Kurat, G., K. Keil, M. Prinz and C. E. Nehru (1972) Chondrules of lunar origin: Proc. Third Lunar Sci. Conf., Geochim. Cosmochim. Acta, Suppl. 3, Vol. 1, p. 707-721.

(6) Fredriksson, K., J. Nelen, A. Noonan and F. Kraut (1972) Apollo 14: Glasses, breccias, chondrules: in Lunar Science-III (editor C. Watkins), p. 280-282, Lunar Sci. Inst. Contr. No. 88, abstract.

(7) Juan, V. C., J. C. Chen, C. K. Huang, P. Y. Chen and C. M. Wang Lee (1972) Petrology and chemistry of some Apollo 14 samples: Proc. Third Lunar Sci. Conf., Geochim. Cosmochim. Acta, Suppl. 3, Vol. 1, p. 687-705.

CHEMICAL AND PETROGRAPHIC CHARACTERISTICS OF THE REGOLITH AT THE APOLLO 15 LANDING SITE. Michael H. Carr and Charles E. Meyer, U.S. Geological Survey, Menlo Park, California 94025.

Fines (< 1 mm) from the LM site, Dune and Elbow craters and Stations 9 and 9a close to the rille were examined to determine how the various particulate components of the regolith vary according to sample location. The samples can be conveniently described in terms of two major components, one locally derived, consisting largely of lithic and mineral debris, and a much smaller exotic component of clear homogeneous glass. The local component shows only minor variations, but significant variations are apparent in the exotic component and these are ascribed to varying amounts of Aristillus or Autolycus ray material.

The major constituents of the regolith are what one would anticipate from gardened basalt, i.e., basaltic fragments, basaltic mineral fragments and dark glass laden with lithic and mineral debris. The LM, Elbow and Station 9 samplea are very similar to each other with respect to the relative proportions and composition of the major components (fig. 1). Dark glassy agglutinates constitute 53-57% of the sample, mineral debris 25-30%, homogeneous glass 8-10%. In the Dune crater sample, the mineral debris is enhanced at the expense of the glassy agglutinates. At Station 9a at the rille edge, basalt and mineral fragments are more than twice as abundant as at the other sites, making up 65-70% of the sample. The mineral debris in all the samples is mostly subcalcic augite, pigeonite, and feldspar (An_{86-97}) with minor amounts of orthopyroxene (Fs_{70}), olivine (Fo_{60}) and opaque minerals. The lithic fragments are 50-80% basalt and the rest metabreccias except at Station 9a, where they are nearly all basalts. For all samples except 15531, the bulk analyses[1] and the compositions reconstructed from relative proportions and compositions of the mineral debris give elemental values intermediate between those for the local mare basalts and those for the Apollo 14 metabreccias. The values suggest a mixing ratio approximately of 3:1 in favor of the mare basalts. The bulk composition of sample 15531 corresponds very closely to the local basalts.

Homogeneous glasses range from colorless, through light yellow and green to a deep red and may occur as angular fragments or spheres. They show a significant variation from location to location. Two types of glasses are found. First, a dark green glass and its devitrified counterpart with a very restricted compositional range; second, an array of glasses similar to those at the Apollo 14 site[2], consisting mostly of the Fra Mauro Basalt Glass[3]. The green glass is compositionally equivalent to a mafic olivine basalt with 43% sub-calcic augite, 35% olivine, 21% plagioclase and 1% ilmenite. It has not been recognized as a local igneous rock. Figure 2 shows CaO-Al_2O_3 plots for homogeneous glasses at each location and shows the clustering of green glass analyses at 7.5% Al_2O_3, 8.0% CaO. The clusters at 17% Al_2O_3 and 10.3% CaO are glasses of the Fra Mauro basalt type. The diagrams indicate that the green glass is abundant at the two locations close to the rille (15531, 15501) and at

CHEMICAL AND PETROGRAPHIC CHARACTERISTICS OF THE REGOLITH AT THE APOLLO 15---

Michael H. Carr

Dune Crater (15471) but is poorly represented at Elbow crater (15081) and the LM site (15021, 15031). One striking characteristic of the homogeneous glasses is the lack of compositions corresponding to the local basalts.

The green glasses are interpreted as originating from either Autolycus or Aristillus, prefereably Aristillus. Ridley[4] and Reid[5] have suggested that the green glass originates from mafic-rich layer brought close to the surface by the formation of the Apennine front. We are skeptical of a local origin because of the absence locally of rocks with green glass composition (other than green glass clods) and because of the absence of this material in the non-homogeneous glass components which constitute the bulk of the regolith. The whole Hadley region is crossed by rays from both Aristillus and Autolycus and the cluster of craters around Dune crater have been interpreted as secondaries from one of these craters [6]. The green glass at Stations 6 and 7 [4] occurs where "plumes" characteristically occur down range from secondary crater clusters, in this case the cluster around Dune crater. The area sampled near the rille is also heavily cratered suggesting possible secondaries. The main problem with interpreting the green glass as Aristillus/Autolycus secondaries is the absence of green glass at the LM where a bright streak on the photographs suggests a ray. The LM landed, however, on a narrow ridge about 10 meters high and the high albedo may result from the ridge rather than the presence of ray material. Numerous small positive relief features occur within the mare throughout the Hadley region and these have been interpreted as areas where the mare is either thin or absent and the topography of the pre-mare surface is showing through [6]. This interpretation is consistent with the bulk composition of the regolith being intermediate between the local mare basalts and the Apollo 14 metabreccias since it implies that the pre-mare rocks are at a shallow depth and readily incorporated into the regolith. The high albedo at the LM site is thus interpreted as due not to ray material but partly to topography and partly to incorporation of the pre-mare materials into the regolith. With an Aristillus or Autolycus origin for the green glass, two possibilities are immediately suggested. Either the green glass is what remains of the projectile that formed the primary crater or the green glass represents the composition of a deep layer excavated by the formation of the primary crater.

References

1. Preliminary Examination Team, Apollo 15, 1972, Preliminary examination of lunar samples, in NASA SP-289, p. 6-1, 6-17.
2. Carr, M. H. and Meyer, C. E., 1972, Chemical and petrographic characterization of soils from the Apollo 14 landing site: Abstracts Third Lunar Sci. Conf., Lunar Science Institute, Contrib. No. 88, p. 116.
3. Apollo Soil Survey, 1971, Apollo 14: Nature and origin of rock types in soil from the Fra Mauro Formation: Earth and Planetary Sci. Letters, v. 12, p. 49-54.
4. Ridley, W. I., Reid, A. M., Warner, J. L., and Brown, R. W., 1972, Apollo 15 green glass: submitted to Science.
5. Reid, A. M., Warner, J., Ridley, W . I., and B rown, R. W., 1972, Major element composition of glasses in three Apollo 15 soils: (in press).
6. Carr, M. H., Howard, K. A., and El-Baz, F., 1971, Geologic maps of the Apennine Hadley Region of the Moon: U.S. Geol. Survey Misc. Geol. Inv. Map I-723.

REGOLITH CHARACTERISTICS

Michael H. Carr

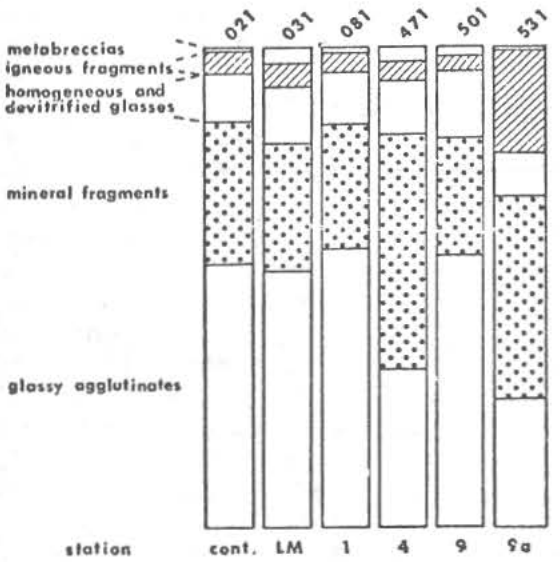

Figure 1. (above) Relative proportions of various regolith components in the six samples examined.

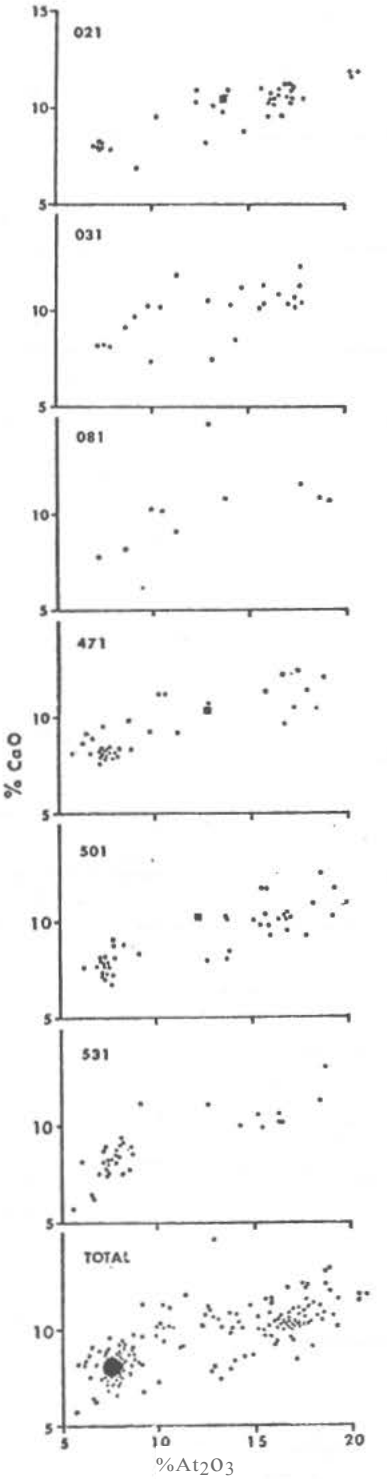

Figure 2. (right) CaO - Al_2O_3 plot for the six samples examined. Solid circles are homogeneous and devitrified glasses, solid squares are bulk soil compositions (Preliminary Examination Team, Apollo 15, 1972).

MORPHOLOGY AND CHEMISTRY OF GLASS SURFACE OF BRECCIA 15015,36. James L. Carter, University of Texas at Dallas, Geosciences Division, Dallas, Texas 75230. Contribution no. 220.

Two types of glassy materials occur in the lunar samples: glass spheres found in the soil and glassy coatings found on rocks. It has been proposed that the craters on the glass spheres occurred mainly in an impact-generated debris cloud (1). The craters on the glassy coating on rocks have been interpreted as arising from micrometeroid bombardment of the glassy surface while in place on the lunar surface (2). The various types of mounds found on the surface of the glass spheres are considered as resulting from both vapor condensation and reduction processes (1,3). The mounds and other similar features on the spheres and the glassy coatings have been compared in an attempt to determine whether the glassy surface coatings were in place on the lunar surface when impacted or if they were produced in an impact-generated debris cloud.

A 62 mm^2 glass surface was coated with gold and examined with a JSM-1 scanning electron microscope and an ARL scanning electron microprobe with an energy dispersive X-ray analyzer. A mosaic of the entire surface was made at 60X (Fig. 1). The glass surface is very frothy or hummocky consisting of a series of depressions and blisters connected by valleys. Many of the blisters are ruptured. Two major areas occur in which large depressions are absent. An enlarged mosaic view of one of the areas (Fig. 2) reveals a wrinkled surface that probably represents a collapse structure. The diameter of the depressions in the wrinkled areas are less than for the overall surface (Fig. 3). This is consistent with a collapse of blisters and continued out-gassing of the host silicate material during cooling.

The glass surface has an assortment of mound types. The larger mounds are primairly concentrated in the valleys with mound size decreasing towards a depression. This suggests that iron migrated from the sides of a depression towards the valleys and due to surface tension mound growth took place there. The larger mounds consist of a central area of metallic iron surrounded by a waist of iron sulfide (Fig. 4). The iron sulfide incompletely wets the mound.

A mosaic of one cluster of mounds is shown by Fig. 4 which is an enlarged view of the central bottom portion of Fig. 1. The surface of the glass area scanned (0.47 mm^2) is covered with mounds over approximately 25 to 30% of its surface with a distribution as shown in Fig. 4. A histogram of the percentage of surface area covered by the various sizes of mounds is shown in Fig. 5. A histogram of the number of mounds versus mound diameter, Fig. 6, reveals that the number of mounds rapidly decreases with an increase in mound diameter. A measurement at 11,500X of 45 square microns (Fig. 7, lower right, Fig. 4) gave approximately 2×10^7 mounds greater than 0.04 microns in diameter and less than 0.5 microns in diameter per square millimeter of the glass surface. A plot of the volume of material in a mound assuming a sphere for the shape of a mound reveals that there are three grouping (Fig. 8).

The less than 4 microns-in-diameter spheres are predominately metallic iron, whereas those larger than 12 microns in diameter are entirely a mixture

of iron sulfide and metallic iron. In the case of dimples for which the mounds are absent the adherance of fragments of iron sulfide to the surface of the dimples (Fig. 4; see also 1,3,5) shows that they were originally mixtures of iron sulfide and metallic iron as suggested by Fig. 8. With the exception of the larger dimples and those near the left margin of the sample, which probably resulted due to the stress of breaking the sample, the dimples are concentrated around a low velocity impact crater.

The mounds do not represent splashes but were grown on the silicate surface. The larger mounds grew at the expense of the smaller mounds. The area immediately surrounding the larger mounds is devoid of smaller mounds. The area of paucity of smaller mounds is elliptical not circular suggesting longitudional migration of molten material on a liquid silicate surface.

The distribution of mounds (Fig. 4) and the mound volume (Fig. 8) suggests that there are different sources for the iron and sulfur. A nucleation site was initiated and the degree of mound growth was a function of the available iron and sulfur at the growth site. A large portion of the metallic iron probably resulted from in situ reduction of the silicate surface (Fig. 7; see also 3), whereas the sulfur was supplied mainly from an external source such as an impact-generated cloud. Additional iron probably was also supplied by this source.

Another interesting feature of this glass surface is the concentration of irregular or amoeboid-shaped mounds around hills of silicate minerals. An example is seen in the central right portion of Fig. 4. The reason for this type of mound is not known but it may be speculated that in this case there was not sufficient heat to allow the material to coalesce into a sphere by surface tension. It may be that the silicate hill effectively quenched the growth process. This may explain also the paucity of small mounds near the silicate hills.

Possibly the most striking feature of the glass surface is a series of patches ranging from 0.4 to 400 microns in longest dimension that distort the electron beam as it passes over a patch suggesting that they are magnetic. Fig. 7 shows the relationship of this type of structure to other mounds. This is an enlargment of an area just to the right bottom of Fig. 4. The structures appear to be composed of a series of approximately 0.1 to 0.2 micron in diameter spherules and rods. It is thought that this material is metallic iron.

A detailed examination of the mosaic at 60X revealed no hypervelocity craters. 1.07 mm^2 was scanned at 1,150X and again no hypervelocity craters were observed. However, two low velocity craters were noted; one 25 microns in diameter and the other 35 microns in diameter. These data suggest that this glass surface was never exposed to either bombardment by micrometeroids or high velocity projectiles in an impact-generated debris cloud.

References:

1. Carter J. L. and MacGregor I. D., Ap. 11 Lun. Sci. Conf., 247-275, 1970.
2. Hartung J. B. et al., 3 Lun. Sci. Conf., 363-365, 1972.
3. Carter J. L. and McKay D. S., In Press, 1972.
4. Carter J. L. and McKay D. S., 2 Lun. Sci. Conf., 2653-2670, 1971.
5. Carter J. L., 2 Lun. Sci. Conf., 873-892, 1971.

Morphology of Glass Surface

James L. Carter

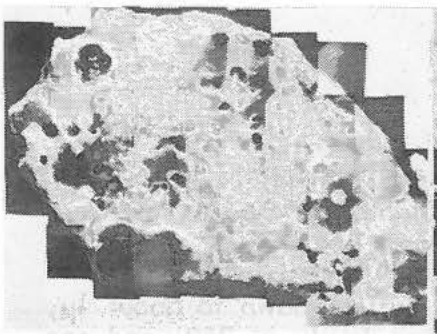

Fig. 1. SEM image, 40X.

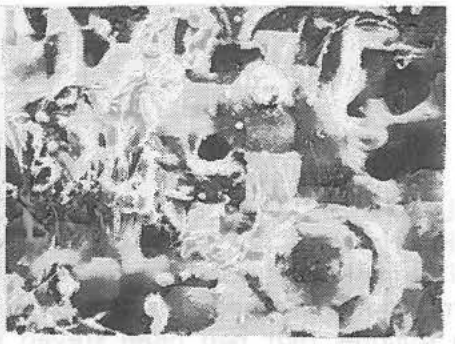

Fig. 2. SEM image, central left, Fig. 1, 1,150X.

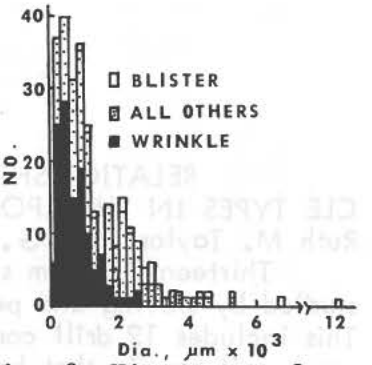

Fig. 3. Histogram of dia. of depressions.

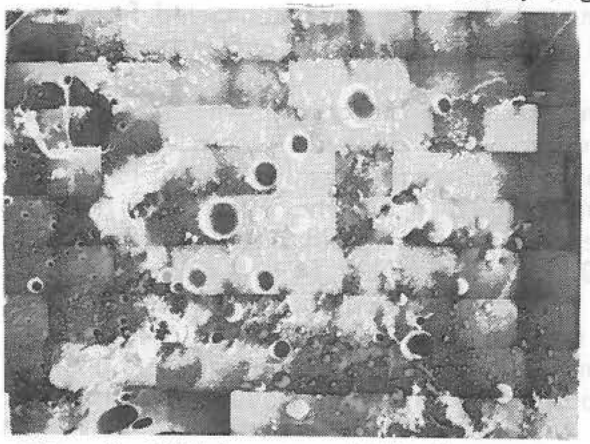

Fig. 4. SEM image, middle bottom of Fig. 1, 1,150X.

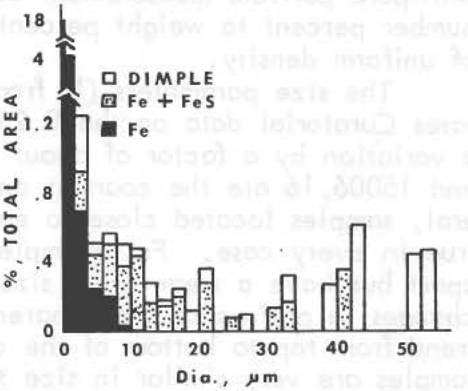

Fig. 5. Histogram of mound dia. versus % of total area.

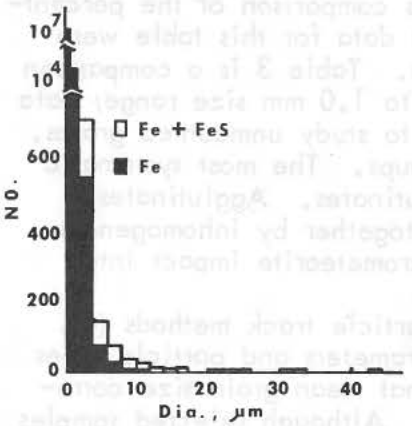

Fig. 6. Histogram of mounds versus dia.

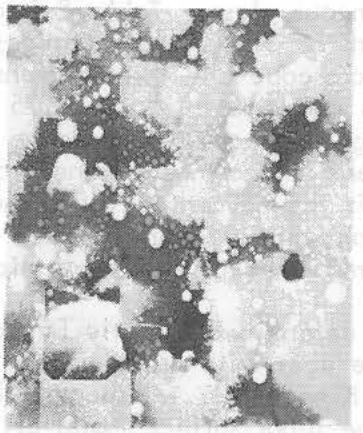

Fig. 7. Enlarged view, lower right of Fig. 4, 11,500X.

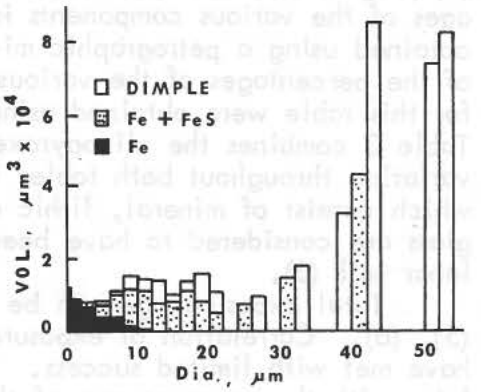

Fig. 8. Histogram of Vol. of mounds versus dia.

RELATIONSHIP OF EXPOSURE AGE TO SIZE DISTRIBUTION AND PARTICLE TYPES IN THE APOLLO 15 DRILL CORE. Uel S. Clanton, David S. McKay, Ruth M. Taylor, and G. H. Heiken, NASA-MSC, Houston, Texas 77058

Thirteen 0.25 gm soil samples returned by the Apollo 15 mission have been studied by sieving and petrographic methods for size distributions down to about 1μ. This includes 12 drill core samples that had been sieved previously at 250μ and one green soil sample that had been sieved at 1 mm. Size distribution was determined by sieving down to 20μ. Particles less than 20μ in diameter were analyzed using a Millipore particle measurement computer system and the data were converted from number percent to weight percent by graphical integration assuming spherical particles of uniform density.

The size parameters (1) from this data are presented in Table 1 which incorporates Curatorial data on the 0.25 to 1 mm fraction of the deep-drill core. There is a variation by a factor of about 2 in the graphic mean grain size. Sample 15006,24 and 15006,16 are the coarsest and 15003,26 and 15003,19 are the finest. In general, samples located close to each other have similar mean grain size but this is not true in every case. For example, samples 15006,17 and 15006,24 are only 2 cm apart but have a mean grain size differing by a factor of about 1.5. Rather abrupt changes in grain size are apparent throughout the length of the core (2). No overall trend from top to bottom of the core is apparent in any of the size parameters. The samples are very similar in size to previous Apollo soils. Sample 15003,26 is the finest lunar soil that we have ever measured.

The particles were divided into eight general groups: (1) agglutinates, (2) vitric breccias, (3) recrystallized breccias, (4) basalt, (5) orthopyroxene, (6) clinopyroxene, (7) plagioclase, and (8) miscellaneous glass. Table 2 is a comparison of the percentages of the various components in the 90-150μ size range; data for this table were obtained using a petrographic microscope and thin sections. Table 3 is a comparison of the percentages of the various components in the 0.25 to 1.0 mm size range; data for this table were obtained using a binocular microscope to study unmounted grains. Table 3 combines the clinopyroxene and orthopyroxene groups. The most systematic variation throughout both tables is the percentage of agglutinates. Agglutinates, which consist of mineral, lithic and glassy debris bonded together by inhomogeneous glass are considered to have been formed primarily by micrometeorite impact into lunar soil (3).

Total exposure age can be determined directly by particle track methods (4), (5), (6). Correlation of exposure ages with grain size parameters and particle types have met with limited success. King et al. (7) suggest that mean grain size correlates with the exposure age of the lunar surface material. Although selected samples from Apollo 14 can be forced to establish such a trend, data from the drill core show no such correlation. The agglutinate content as suggested by McKay et al. (8) continues to correlate closely with particle track methods for indicating relative age relationships.

Figure 1 is a plot of the depth of the sample versus percentage of agglutinates, particle track density (9) and ^4He (10) and Hg (11) concentrations. Except for the

Relationship of Exposure Age

Uel S. Clanton

40 cm points for ^4He and Hg, the plots are remarkably similar. Both ^4He and Hg are subject to volatilization and the analytical techniques are sensitive to variations in grain size. The lack of correlation for these two points may reflect a real difference; it may, however, be due to a difference in grain size of the sample analyzed or some difference in sample handling.

There is some indication that we may not yet fully understand agglutinate production, micrometeoroid flux and their relationship to particle track density. Crozaz et al. (6) present track density data for Apollo 14 and 15 samples. The highest track densities in the Apollo 14 samples are in the high 10^8 t/cm^2 and low 10^9 t/cm^2 range. These values were obtained from samples that contained on the average of about 50% agglutinates in the 90 to 150 μ fraction (3). All six Apollo 15 core samples show track density values in excess of 10^8 t/cm^2 with maximum values approaching 10^{10} t/cm^2 (6). If the micrometeoroid mass and flux rate were constant through time then agglutinate production would be proportional to exposure age based on track density measurements and one would expect to find a higher percentage of agglutinates in the Apollo 15 core sample than seen in the Apollo 14 samples. The percentage of agglutinates, however, is less than predicted based on the higher track densities of the core, indeed the percentage of agglutinates is lower than observed for the Apollo 14 samples. The correlation between agglutinate content and exposure age is clearly demonstrated (Figure 1). The data suggest a variation in agglutinate production or micrometeoroid flux during the history of the Moon. This concept has been suggested previously by Gault et al. (12) based on studies of microcraters on rock surfaces.

Based on these observations, agglutinate content and exposure age are related but the relationship has been modified by changes in the mass and flux of the micrometeoroids impacting the lunar surface. However, once a correlation between track density and agglutinate content has been established in an area, agglutinate content can be used to extend the relative age relationships to other samples. It is not yet clear to what distance either horizontally or vertically that the agglutinate content-exposure age relationship can be extrapolated.

Conclusions: a. Based on twelve samples from six textural units of the 42 known major textural units in the 2.4 meter long core, there are wide variations in the percentage of the various components.

b. Agglutinate content and exposure age are related but the relationship has not remained constant through the history of the regolith at this site.

c. Variations in agglutinate content and exposure ages supports the theory that the mass and flux of meteoroids impacting the Moon has changed with time.

d. The regolith is formed by a series of random erosional and depositional events of various magnitudes and is composed of a series of fossil surfaces which have been covered by younger layers, but only after each surface has been exposed for some appreciable time.

References

1. Folk, R. L. and Ward, W. C. (1957) J. Sediment. Petrol. 27, 3-26.
2. Heiken, G. H., et al. (1972) NASA Tech Memo (in prep.).
3. McKay, D. S., et al. (1972) Proc. Third Lunar Sci. Conf., 3, (in press).
4. Arrhenius, G., et al. (1971) Proc. Second Lunar Sci. Conf., 3, 2583-2598.
5. Crozaz, G., et al. (1971) Proc. Second Lunar Sci. Conf., 3, 2543-2558.
6. Crozaz, G., et al. (1972) Lunar Science III, 167-169.
7. King, E. A., et al. (1972) Lunar Science III, 449-451.
8. McKay, D. S., et al. (1971) Proc. Second Lunar Sci. Conf., 1, 755-774.
9. Phakey, P. P., et al. (1972) Lunar Science III, 608-610.
10. Bogard, D. D. and Nyquist, L. E. (1972) The Apollo 15 Lunar Samples, LSI.
11. Jovanovic, S. and Reed, G. W. (1972) Earth and Planetary Science Letters (in press).
12. Gault, D. E., et al. (1972) Proc. Third Lunar Sci. Conf., 3, (in press).

Table 1. Graphical size parameters (Folk and Ward, 1957) for the <1 mm fraction of the Apollo 15 deep-drill core.

Sample No.	Approximate Depth cm	Median Grain Size Md		Graphic Mean Mz		Inclusive Graphic Standard Deviation σ_I	Inclusive Graphic Skewness SK_I	Graphic Kurtosis KG
Core		ϕ	μ	ϕ	μ	ϕ		
15001,21	240	4.17	55.9	3.94	65.1	1.63	-.23	.98
15001,28	240	4.11	58.1	3.88	68.0	1.62	-.10	..86
15002,17	200	3.82	72.0	3.71	76.8	1.59	-.10	1.09
15002,24	200	4.10	58.8	3.90	67.1	1.83	-.14	1.08
15003,19	160	4.30	51.0	4.18	55.0	1.84	-.11	1.04
15003,26	160	4.48	45.0	4.52	43.8	1.82	-.01	.96
15004,17	120	4.17	55.8	4.05	60.8	1.77	-.09	1.04
15004,24	120	3.80	72.0	3.77	73.2	1.78	-.05	1.03
15005,16	80	3.63	81.0	3.50	88.9	1.85	-.00	.97
15005,23	80	4.12	58.0	3.91	67.0	1.63	-.14	1.02
15006,17	40	4.10	58.8	4.06	60.2	1.62	-.02	1.02
15006,24	40	3.50	88.9	3.25	105.0	1.78	-.19	.93
Green Sphere Split 15401,61	Surface	3.72	76.1	3.93	65.8	1.80	+.14	.94

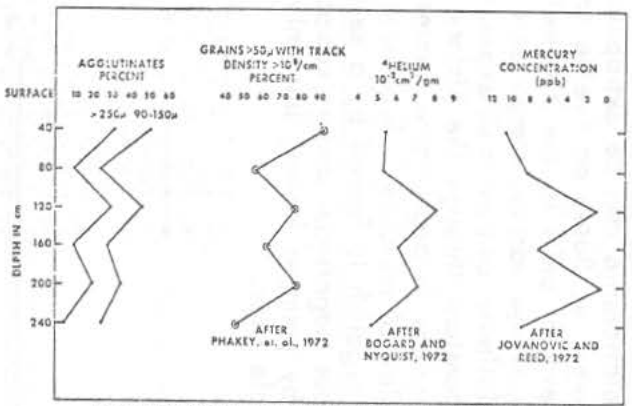

FIGURE 1 COMPARISON OF AGGLUTINATE CONTENT, PARTICLE TRACK DENSITY, ⁴HELIUM CONCENTRATION AND MERCURY CONCENTRATION IN THE APOLLO 15 CORE.

Table 2. Comparison of the 90-150μ fractions of the Apollo 15 deep drill samples.

Sample No.	15001,21	15001,28	15002,17	15002,24	15003,19	15003,26	15004,17	15004,24	15005,16	15005,23	15006,17	15006,24
Approximate Depth (cm)	240	240	200	200	160	160	120	120	80	80	40	40
Component	Values in percent.											
Agglutinates	25.1	19.9	35.0	40.5	27.2	25.0	46.5	33.6	23.6	33.1	51.0	41.0
Vitric breccia	4.2	8.6	3.1	7.5	5.6	9.0	0.5	3.6	7.9	8.9	4.5	5.2
Recrystallized breccia	7.8	5.2	4.1	3.5	4.2	3.5	3.0	2.9	2.6	4.8	6.3	2.3
Basalt	10.1	5.7	14.4	6.0	2.8	5.5	6.0	3.6	7.9	4.8	2.5	6.4
Orthopyroxene	17.4	12.6	10.3	8.5	10.3	15.0	11.0	14.3	9.9	6.5	11.5	12.9
Clinopyroxene	16.8	21.8	11.3	13.0	17.8	20.0	19.5	24.3	27.7	20.2	12.7	11.0
Plagioclase	6.6	12.7	8.2	11.5	5.6	9.0	5.5	7.1	9.9	8.1	5.7	4.0
Glass	11.4	17.0	13.4	9.0	26.3	13.5	8.0	8.6	10.5	11.3	3.8	16.0
Total grains counted	167	174	97	200	213	200	200	140	191	124	157	173

Table 3. Comparison of >250μ fractions of the Apollo 15 deep drill samples.

Sample No.	15001,34	15001,38	15002,32	15002,37	15003,34	15003,37	15004,32	15004,36	15005,123	15005,127	15005,30	15006,33
Approximate Depth (cm)	240	240	200	200	160	160	120	120	80	80	40	40
Component	Values in percent											
Agglutinates	5.2	4.2	19.9	19.8	10.0	16.8	29.4	30.8	10.2	6.7	32.7	35.0
Vitric breccia	5.5	1.7	17.4	11.0	9.4	4.1	5.7	5.7	6.0	6.7	9.2	5.4
Recrystallized breccia	20.0	24.6	14.2	15.1	19.0	14.9	14.2	13.7	24.8	20.0	19.6	17.0
Basalt	34.0	35.5	15.1	30.8	31.5	25.8	30.8	20.8	25.0	23.1	12.6	16.7
Pyroxene	11.8	7.9	12.6	10.0	11.3	18.7	9.9	12.8	16.4	18.0	12.6	9.7
Plagioclase	8.7	6.3	5.3	2.7	3.0	7.8	3.9	4.2	4.9	5.6	3.0	4.0
Glass	13.8	19.4	15.4	10.3	15.8	12.0	9.9	10.3	13.1	20.0	10.4	10.2
Total grains counted	253	239	436	338	439	268	282	357	433	195	500	423

VISCOUS FLOW OF LUNAR COMPOSITIONS, M. Cukierman and D. R. Uhlmann, Dept. of Metallurgy and Materials Science, Massachusetts Institute of Technology, Cambridge, Massachusetts 02139

The flow behavior of lunar composition 15418 has been determined over a wide range of viscosity. This material, a gabbroic anorthosite rich in anorthite, was selected because of the interesting crystallization morphologies noted in the lunar sample and because of its compositional similarity to the Apollo 14 liquids (14259 and 14310) investigated previously.[1] Relative to those compositions, the 15418 material is richer in Al_2O_3 and somewhat poorer in SiO_2 and FeO. The present report will be concerned only with its flow characteristics and with a comparison of its flow behavior with that of other lunar compositions. In a subsequent paper[2], the viscosity data will be used to interpret the crystallization behavior.

Specimens of the 15418 composition (SiO_2, 45 wt %; Al_2O_3, 26.7; MgO, 5.4; FeO, 5.4; CaO, 16.1; TiO_2, 0.3; Na_2O, 0.3) were prepared from reagent grade raw material powders. The initial melting as well as the viscosity measurements were carried out under conditions of low oxygen activity to simulate the ferrous/ferric iron conditions of the lunar material. These conditions have been described previously[1], as have the details of the specimen preparation procedure and the viscosimeters employed. For viscosities in the molten range, a rotating-cylinder instrument was used; for viscosities greater than about 10^9 poise, the bending-beam viscosimeter was preferred. In both cases, the viscosimeters were calibrated against reference materials.

The viscosity vs. temperature relation for the 15418 composition is shown in the figure on the following page. As shown there, reliable data could be obtained only at temperatures above 1275°C and below 835°C. Determinations at intermediate temperatures were prevented by the occurrence of crystallization during the time required for the viscosity measurements. In the low temperature range below 835°C, the measurements could be completed in times which were short relative to those required for significant crystallization. In the portion of the high temperature range below the liquidus, data could be obtained after superheating the specimen well above the liquidus temperature prior to cooling.

The apparent activation energy for viscous flow in the high temperature region is about 60 kcal $(gm\ at)^{-1}$. This is similar to those derived from the corresponding high-temperature data on the 14259 and 14310 compositions. The glass transition temperature (viscosity=10^{13} poise) for the 15418 composition is about 730°C. The flow behavior appears to be non-Arrhenian as the glass transition is approached. At the lowest measurement temperatures in this

range, the apparent activation energy for flow is about 210 kcal $(gm\ at)^{-1}$. This value is somewhat higher than those observed for the previous lunar compositions, 160-170 kcal $(gm\ at)^{-1}$, where Arrhenian flow behavior was found in the vicinity of the glass transition.

Considering the full range of viscosity shown in the figure, it is apparent that appreciable curvature exists in the log (viscosity) vs. 1/T relation for the 15418 composition; and similar curvature was noted for the 14259 and 14310 liquids. This curvature, together with the magnitudes of the derived apparent activation energies, indicate that viscous flow in the lunar compositions should not be regarded as a simply-activated process.

It has been suggested[3] that free volume models can provide a useful representation of liquid flow in the high temperature region (viscosities less than 10^4-10^5 poise), and that such models are best applied in this region rather than in the vicinity of the glass transition. The data on the lunar compositions investigated to date are in accord with this suggestion, although the occurrence of crystallization in the intermediate temperature range limits the details of the comparison which can be effected.

The high temperature data on the 15418 composition can also be well described by the semi-empirical model of Bottinga and Weill[4]. The agreement in this case is within ± 0.10 in log (viscosity). This agreement, together with that found previously for the 14259 and 14310 compositions in the same range of viscosity, lend support to the model for describing the high temperature flow behavior of other similar compositions, and increase the impetus for extending the model over a wider range of temperature and viscosity.

The variability in form of the viscosity vs. temperature relations for the lunar compositions in the high viscosity region is in accord with recent results on other liquids (Ref. 5, e.g.). The flow behavior in this region cannot be well represented by any of the available theoretical models, although an extensive degree of cooperative motion seems indicated.

REFERENCES

1. M. Cukierman, P.M. Tutts & D.R. Uhlmann, Viscous flow behavior of lunar compositions 14259 and 14310, to appear in Proceedings of Third Lunar Science Conference Vol. III.

2. G. Scherer, L. Klein & D.R. Uhlmann, Crystallization morphologies and crystallization kinetics of lunar composition 15418, to be published.

3. D.R. Uhlmann, Viscous flow in glass-forming liquids, in Amorphous Materials (ed. R.W. Douglas & B. Ellis), Wiley, 1972, pp. 205-214.

4. Y. Bottinga & D.F. Weill, The viscosity of magmatic silicate liquids: A model for calculation, Amer. J. Sci. 272 (1972) 438-475.

5. W.T. Laughlin & D.R. Uhlmann, Viscous flow in liquids, J.Phys.Chem. 76 (1972)2317-2325.

Viscous Flow in Lunar Compositions

Cukierman

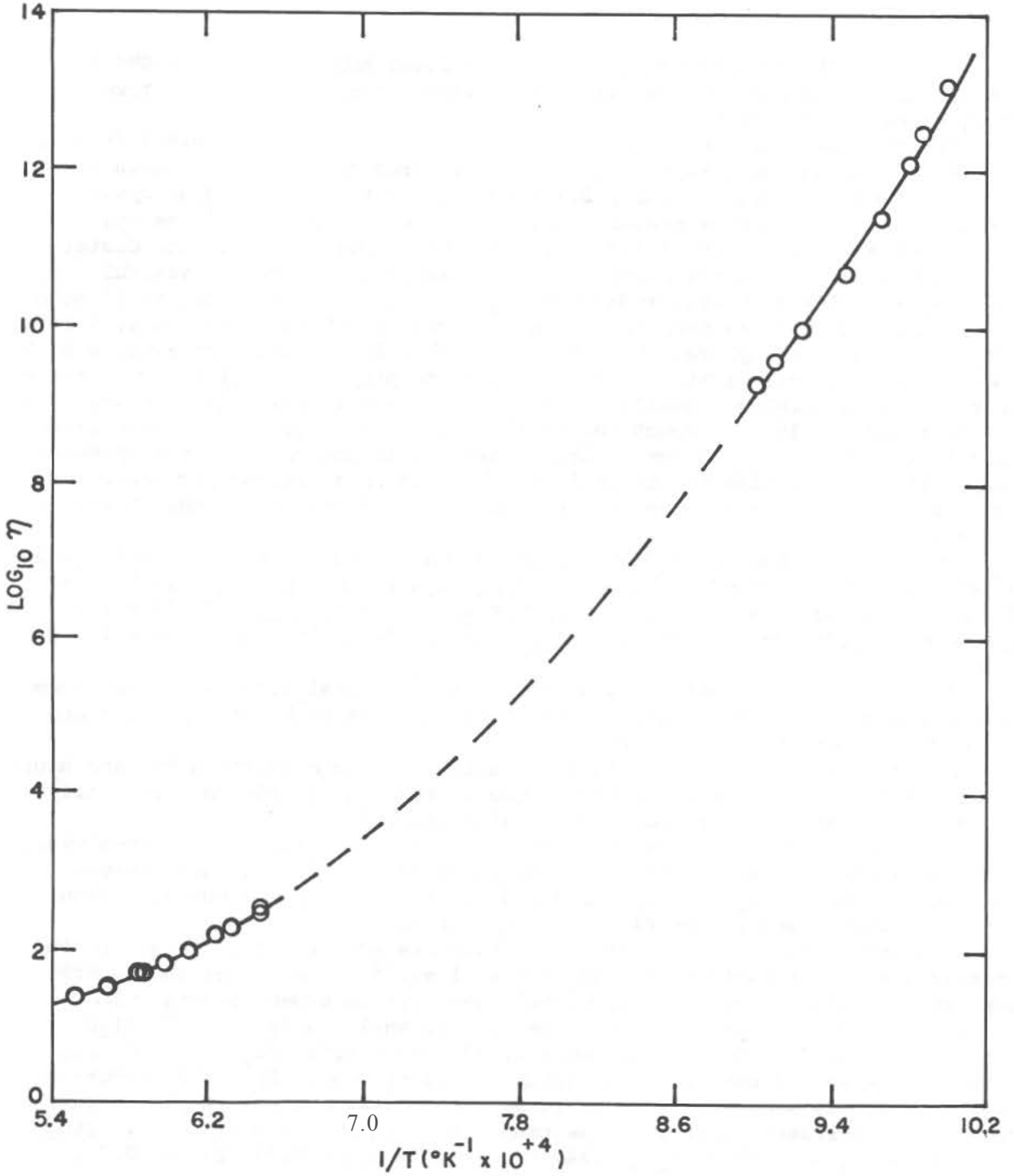

PETROLOGIC EXAMINATION OF BRECCIA 15465 AND ITS IMPLICATIONS AS TO THE NATURE OF THE APENNINE FRONT; J. W. Delano, State Univ. of New York, Stony Brook, N. Y. 11790

Twenty-three polished thin sections of the consortium breccia 15465, 7, 1 have been studied petrographically and by electron microprobe techniques. The sample allocation weighed nearly 2.7 grams of the total 374.8 gram specimen and the individual pieces measured $\leq$ 1 centimeter in maximum dimension.

Breccia 15465 was collected on the north-northwest rim of Spur Crater.(1) It is a brown-glass matrix breccia with a variety of clasts and vesicular dark green splash glass. Visual modal percent estimations of the various lithologies within the breccia samples studied indicate 5-10% rock fragments, 5-10% glass fragments and spheres, 60-70% plagioclase, 10-20% orthopyroxene, and 5% clinopyroxene single crystals. The approximate proportions of the rock fragments including highland basalts, mare basalts, and recrystallized clasts are 7:5:1, respectively. Although the modal percent of plagioclase single crystals in the breccia indicates a large anorthositic component in the Apennine Front, its contribution is difficult to estimate in a microscopic search of small fragments ($\geq$ ¼ mm) due to its coarse-grained and nearly monomineralic character.

The highland basalt fragments have subophitic to ophitic textures and approximate modes of 50-60% plagioclase ($An_{80}Ab_{19}Or_1$ to $An_{85}Ab_{14}Or_1$), 20-30% Ca-poor pyroxene ($En_{79}Wo_3Fs_{18}$ to $En_{69}Wo_6Fs_{25}$ to $En_{58}Wo_9Fs_{33}$), 5-15% clinopyroxene ($En_{49}Wo_{21}Fs_{30}$ to $En_{37}Wo_{34}Fs_{29}$), and $\leq$ 10% tan to dark interstitial glass.

The mare basalt clasts consist of the two textural types which are common to the 2-4 mm coarse-fine samples.(2) These are the poikilitic plagioclase and pyroxene porphyritic basalts.

Recrystallized clasts of highland basalt, gabbroic anorthosite, and anorthosite are observed. Some of the fragments texturally and mineralogically resemble samples from the Apollo 16 landing site.(3)

Although most of the basaltic rock fragments are extrusive or hypabysal, occasional clinopyroxene single crystals that may be plutonic are present. One such crystal ($En_{52}Wo_{38}Fs_{10}$) measured about 0.5 mm in maximum dimension with exsolution lamellae nearly 10 microns in width.

Two compositional groups of glass fragments are present. These are the emerald green ultramafic glass and high-K glass.(2) The former ranges texturally from glass spheres to completely devitrified brown spheres. The chemical composition is as follows (weight percent): SiO_2 = 45.17, Al_2O_3 = 7.11, TiO_2 = 0.35, FeO = 21.55, MgO = 17.37, CaO = 8.53, Na_2O = 0.00, K_2O = 0.01. The second compositional group is high-K, possibly KREEP, occurring as irregular, flow-banded greenish glass with occasional relict plagioclase and/or orthopyroxene crystals. The composition in weight percent is: SiO_2 = 48.91, Al_2O_3 = 17.87, TiO_2 = 1.14, FeO = 9.27, MgO = 9.42, CaO = 10.77, Na_2O = 0.35, K_2O = 1.20, Cr_2O_3 = 0.23.

Breccia 15465

J. W. Delano

The bulk of the material comprising this breccia is similar to that observed in the Hadley Delta 2-4 mm coarse-fines.[2] From these observations, it appears that the Apennine Front consists dominantly of granulated anorthosite, gabbroic anorthosite, highland basalt, and recrystallized equivalents. Most of the vesicular splash glass and the mare basalt clasts may have been added by the Spur Crater event during the Copernican Period to give the breccia its presently observed character. The K-Ar minimum age of about 1.0 G.y.[4] for the splash glass on 15465 is consistent with this interpretation.

The large abundance of glass fragments in the breccia, particularly the nearly 3.79 G.y.[4] green ultramafic glass spheres which seem to be thoroughly mixed into the Apennine Front and thereby pre-date or date the Imbrium event, strongly indicate that metamorphism in a hot ejecta blanket did not occur in the sampled levels of the Apennine Mountains. The recrystallized clasts observed in 15465 were probably produced in a mature, pre-Imbrian regolith and were mixed to a minor extent with more deeply-derived ejecta during the Imbrium event. Deeper levels of the 20-25 kilometer thick brecciated outer zone of the moon[5] yielded the granulated anorthosites, gabbroic anorthosites, and highland basalts comprising most of the Apennine Front at the Apollo 15 landing site.

References

(1) G. A. Swann, M. H. Hait, G. G. Schaber, V. L. Freeman, G. E. Ulrich, E. W. Wolfe, V. S. Reed, and R. L. Sutton (1971), Preliminary description of Apollo 15 sample environments: NASA-CR-124730; 255 p.

(2) K. L. Cameron, J. W. Delano, A. E. Bence, and J. J. Papike, Petrology of the 2-4 mm sized soil fragments from Apollo 15. "The Apollo 15 Lunar Samples," ed. J. W. Chamberlain and C. Watkins (Houston: Lunar Science Institute), 1972.

(3) J. W. Delano, A. E. Bence, and J. J. Papike (1972), Apollo 16 coarse fines (2-4 mm): Interstation variations in lithologies (abstract): 1972 Annual Meeting of The Geological Society of America.

(4) Liaquat Husain, The ^{40}Ar-^{39}Ar and cosmic-ray exposure ages of Apollo 15 crystalline rocks, breccias, and glasses. "The Apollo 15 Lunar Samples," ed. J. W. Chamberlain and C. Watkins (Houston: Lunar Science Institute), 1972

(5) M. N. Toksoz, F. Press, K. Anderson, A. Dainty, G. Latham, M. Ewing, et al. (1972), Lunar crust: Structure and composition: Science, 176, 1012-1016.

ANORTHOSITE IN THE APOLLO 15 RAKE SAMPLE FROM SPUR CRATER

Eric Dowty, Klaus Keil and Martin Prinz, Dept. of Geology and Inst. of Meteoritics, Univ. of New Mexico, Albuquerque, N. M. 87106, U.S.A.

Introduction Anorthosite 15362,1 is one of the Apollo 15 rake sample specimens collected on the inner side of the rim of Spur Crater, on the lowermost slope of Hadley Delta, part of the Apennine Front. Material from this locality is rich in members of the ANT (anorthositic-noritic-troctolitic) group of rocks, as they have been termed [1]. Some of the Apollo 15 ANT hand specimens are anorthosite (rock 15415, the "genesis rock") and anorthositic norite (e.g. rocks 15418 and 15455). Smaller ANT lithic fragments are also found in the microbreccias [2]; we are presently studying some of them and results will be published elsewhere.

Texture Rock 15362 consists mostly of plagioclase, so that we are primarily concerned with its intergranular relationships. The texture is variable, and at least four different types of local texture may be distinguished: (1) Coarse, irregularly shaped plagioclase grains; (2) smaller polygonal plagioclase grains; (3) small to very small angular fragments of plagioclase; and (4) opaque veins or blotches. The first three types of texture have been previously described for anorthosite 15415 [3,4], and we shall not go into these in detail here. However, anorthosite 15362 appears to differ from 15415 in that types (1) and (2) are distinctly subordinate to types (3) and (4), suggesting a greater degree of cataclasis.

The opaque veins, not previously described for lunar anorthosite, are similar to features sometimes found in meteorites, and are probably caused by shock [5]. In meteorites, such opaque veins often contain minute, finely dispersed troilite and nickel-iron grains. We have noted the same effect in another rake sample specimen from Spur Crater, 15308, and in this rock, troilite can be seen on grain boundaries in the opaque regions. We were unable to detect troilite optically or by microprobe in the opaque regions of rock 15362. Analyses of portions of the opaque areas which present a smooth surface in reflected light show that they are pure plagioclase, identical to the large clear grains (Table 1). The opaque areas seem to be made up of very finely granulated material. Evidently the loss of transparency must be attributed to the presence of many small voids caused by the fine granulation.

No areas or grains of clear glass were definitely identified.

Bulk composition and mineralogy The bulk composition, determined by broad-beam electron microprobe methods, is given in Table 1. Oxide concentrations appear to be essentially identical to those of hand specimen anorthosite 15415 [2], except for magnesium, which is higher in 15362.

Compositions and modal abundances of the principal minerals, namely plagioclase and accessory pyroxene and ilmenite, are very similar to those of 15415 [6-8]. We have, in addition, found chromite (two grains) and troilite (one grain), which have not been reported from 15415, and a few tiny grains of a silica mineral, as reported for 15415 [3]. Olivine and apatite were

Anorthosite in the Apollo 15 rake sample

Eric Dowty

tentatively reported from 15415 [4] but were not found in our sample of 15362.

Modal plagioclase content is 97 to 98% (by volume). The average of nine complete plagioclase analyses is given in Table 1, and in terms of end members, this agrees well with the average of 92 partial analyses (Ca,Na,K) of plagioclase ($An_{96.7\pm0.6}Ab_{3.1\pm0.6}Or_{0.2\pm0.1}$).

Heavily exposed X-ray precession photographs of a crystal of plagioclase showed a, b, c and weak d reflections, none of which appeared to be diffuse; this finding indicates that the structure is ordered. Universal stage studies show that the twin law of plagioclase is predominantly pericline, with subsidiary albite, similar to 15415 [3].

Pyroxene constitutes about 2% by volume of the rock. Two types of pyroxene have been found, augite and hypersthene. Smaller grains of pyroxene (<0.05 mm) included in single grains of plagioclase appear to be exclusively augite, but larger grains (up to 0.5 mm) are present between large plagioclase grains and are commonly complex intergrowths, either lamellar or patchy, of augite and hypersthene. Augite and hypersthene analyses are projected onto the pyroxene quadrilateral in Fig. 1, and average compositions are given in Table 1. The pyroxene compositions are very similar to the augite and hypersthene from anorthosite 15415 [3,6-8]. No homogeneous (single-phase) grains intermediate in composition between augite and hypersthene were found. Augite dominates over hypersthene by a ratio of at least 3 to 1.

Minor elements appear to be strongly partitioned between the two pyroxenes in anorthosite 15362. Manganese prefers hypersthene, and chromium, titanium and aluminum prefer augite. The combination of chromium and manganese partitioning is especially noteworthy (Fig. 2). Also noteworthy is the fact that the Cr/(Al+Ti) ratio falls in the same range for the two pyroxenes (Fig. 3), although the absolute amounts of chromium and titanium are distinctly different. However, each type of pyroxene has a range of aluminum content, and the two overlap to some extent (Fig. 4). Minor element patterns in the pyroxenes of anorthosite 15415 appear from the published analyses [6-8] to be much the same.

X-ray precession photographs of two augite grains gave average cell dimensions (the two were identical within experimental error) a = 9.722, b = 8.884, c = 5.259 Å, β = 106° 11'. These cell dimensions are different from those reported by Stewart et al. [8], and furthermore the photos showed no evidence for exsolved, epitaxial low-calcium pyroxene.

Ilmenite is found both interstitially and as inclusions in plagioclase. Its modal abundance is 0.3% or less. Our ilmenite analyses (Table 1) differ somewhat from Hargraves and Hollister's [7] from rock 15415 in almost all elements determined. However, their analyses are considerably below 100% (97.5 and 96.8%).

Two grains of aluminous chromite, about 15 x 35 μm, were found adjacent to large pyroxene grains (Table 1). It is basically similar to many Cr-rich spinels previously reported from lunar mare-type rocks [9,10], but its combination of low TiO_2 (3.23%) and low MgO (1.27%) make it unique for lunar spinels. The chromite grains are homogeneous and show no signs of exsolution.

A small troilite grain, too small to analyze quantitatively, was found adjacent to a small pyroxene grain, both being entirely included within a large clear plagioclase.

Discussion The high plagioclase content of the anorthosites 15362 and

Anorthosite in the Apollo 15 rake sample

Eric Dowty

15415 is most readily explained as a result of the original formation of these rocks as cumulates. However, in both rocks there appear to be no definite remnants of the textures normally associated with cumulates. In fact, the textural relations indicate only a history of cataclasis and metamorphism. The superposition of various stages of fracture, granulation, and recrystallization in 15415 have been described by James [3] and Wilshire et al. [4]. The same features are present in 15362, and we concur that the texture indicates more than one episode of cataclasis and annealing, although we hesitate to deduce a strict chronological series of events.

The mineralogical data also indicate that the rock was held for some time at sub-igneous temperatures. The predominance in the plagioclase of pericline twinning, which appears to be more characteristic of metamorphic than igneous rocks [11], suggests that even the large crystals may have formed under metamorphic conditions, as pointed out by James [3] for 15415. The low content of calcium in hypersthene, the high content of calcium in augite, and the fact that the Mg/(Fe+Mg) ratio is higher in augite than in hypersthene, are all features which are usually associated in terrestrial rocks with metamorphic conditions, and form a marked contrast to the type of pyroxenes found in lunar mare-type rocks. The strong partitioning of minor elements in the pyroxenes is also suggestive of low-temperature equilibration.

Acknowledgements We are indebted to G. Moreland for preparation of polished thin sections, J. Green and G. Conrad for assistance in electron microprobe analyses, and J. Hultzen for data reduction. Work supported in part by NASA Grant NGL 32-004-063.

References [1] Keil, K., Kurat, G., Prinz, M., and Green, J. A. (1972) Earth Planet. Sci. Lett. 13, 243; Kurat, G., Keil, K., Prinz, M., and Nehru, C. E., Proc. Third Lunar Science Conf. (in press); [2] PET (Apollo 15 Preliminary Examination Team) (1972) Science 175, 363; ALGIT (Apollo Lunar Geology Investigation Team) (1972) Science 175, 307; [3] James, O. B. (1972) Science 175, 432; [4] Wilshire, H. B., Schaber, G. G., Silver, L. T., Phinney, W. C., and Jackson, E. D. (1972) Bull. Geol. Soc. Amer. 83, 1083 [5] Fredriksson, K., De Carli, P., and Aaramae, A. (1963) Space Research, Proc. Intern. Space Sci. Symp., 3rd, North Holland, Amsterdam; [6] Steele, I. M., and Smith, J. V. (1971) Nature 234, 138; [7] Hargraves, R. B., and Hollister, L. S. (1972) Science 175, 430; [8] Stewart, D. B., Ross, M., Morgan, B. A., Appleman, D. E. Huebner, J. S., and Commeau, R. F. (1972) Lunar Science III, Ed. C. Watkins, Lunar Science Institute Cont. No. 88, pp. 726-728; [9] Haggerty, S. E. (1972) Lunar Science III, Ed. C. Watkins, Lunar Science Institute, Cont. No. 88, pp. 348-349; [10] Busche, F. D., Prinz, Martin, Keil, Klaus, and Bunch, T. E., Amer. Mineral. (in press); [11] Gorai, M. (1950) J. Geol. Soc. Japan 56, 149.

Anorthosite in the Apollo 15 rake sample

Eric Dowty

Table 1: Electron microprobe analyses of minerals and bulk rock from rake sample anorthosite 15362,1 (in weight percent)

	Mineral Analyses					Bulk Analyses	
	Plagio-clase	Augite	Hypers-thene	Ilmenite	Spinel	Opaque areas	bulk rock
SiO_2	43.8	52.4	52.5	0.27	0.37	44.0	44.0
TiO_2	0.02	0.51	0.30	51.6	3.23	n.d.	0.03
Al_2O_3	35.8	1.34	0.93	1.61	9.14	36.6	35.1
Cr_2O_3	n.d.	0.25	0.14	0.07	48.8	n.d.	0.01
V_2O_3	n.d.	n.d.	n.d.	n.d.	0.86	n.d.	n.d.
FeO	0.09	11.4	26.0	42.9	35.1	0.04	0.29
MnO	n.d.	0.24	0.48	0.72	0.41	n.d.	0.01
MgO	0.03	13.8	20.2	1.86	1.27	n.d.	0.31
CaO	19.6	20.9	1.45	0.77	n.d.	19.7	19.8
Na_2O	0.37	n.d.	n.d.	n.d.	n.d.	0.27	0.35
K_2O	0.04	n.d.	n.d.	n.d.	n.d.	0.03	0.04
Total	99.71	100.8	102.0	99.8	99.2	100.6	100.0*
No. of analyses	9	14	12	4	2		
	Structural formulae on the basis of					CIPW Norm for bulk rock	
	32(0)	6(0)	6(0)	6(0)	32(0)		
Si	8.128	1.934	1.956	0.013	0.106	ap	0.14
Al	7.832	0.059	0.040	0.094	3.072	il	0.05
Ti	-	0.014	0.008	1.922	0.692	or	0.26
Cr	-	0.007	0.004	0.003	10.997	ab	2.51
V	-	-	-	-	0.197	an	94.0
Fe	0.016	0.356	0.810	1.777	8.368	ne	0.38
Mn	-	0.008	0.015	0.030	0.099	wo	0.13
Mg	0.008	0.767	1.122	0.137	0.540	di-wo	1.24
Ca	3.900	0.835	0.058	0.041	0.0	di-en	0.85
Na	0.132	-	-	-	0.0	di-fs	0.40
K	0.08	-	-	-	0.0		
Z	15.960	1.993	1.996	2.032	-		
X	4.064	1.987	2.017	1.985	-		
Σ	20.024	3.980	4.013	4.017	24.071		
An	3.3	En 39.2	En 56.4		Cm 71.5		
Ab	96.5	Fs 18.2	Fs 40.7		Pc 0.0		
Or	0.2	Wo 42.6	Wo 2.9		Sp 0.6		
					Hc 19.0		
					Uv 8.8		

n.d. = not determined

*Includes 0.06 P_2O_5. Normalized to 100%. Al_2O_3 adjusted to account for contamination from polishing.

Anorthosite in the Apollo 15 Rake Sample

Eric Dowty

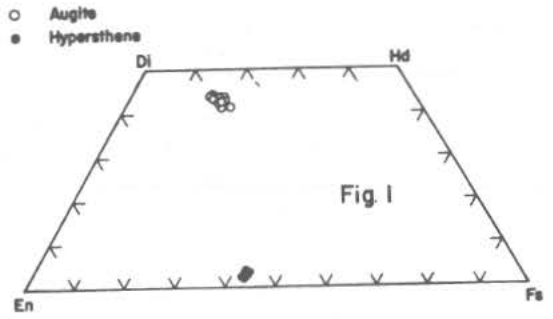

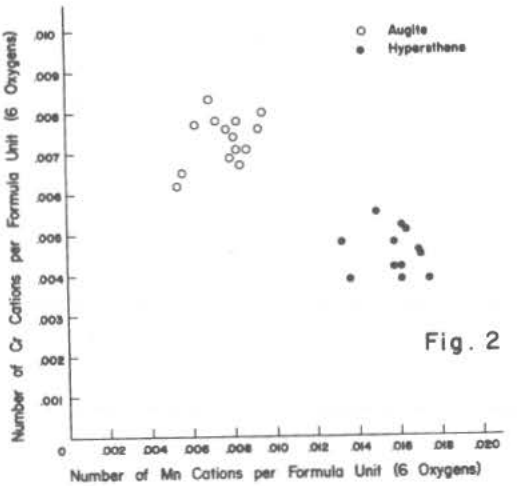

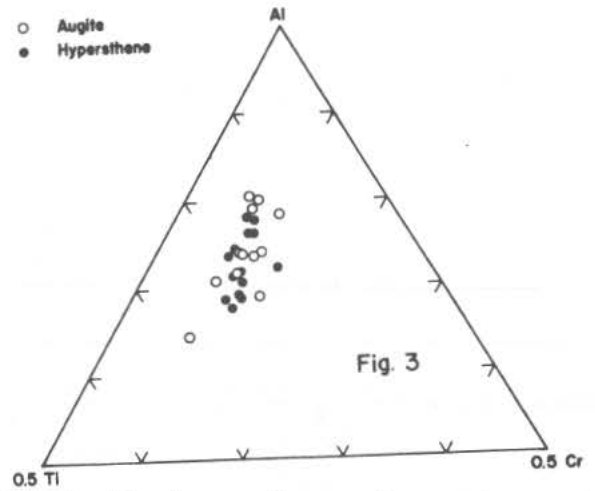

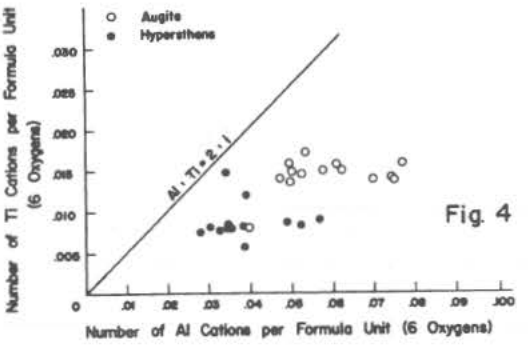

Fig. 1: Electron microprobe analyses of augite and hypersthene from rake sample anorthosite 15362,1, expressed as mole percent end members enstatite (En;$Mg_2Si_2O_6$); ferrosilite (Fs;$Fe_2Si_2O_6$); and wollastonite ($Ca_2Si_2O_6$). Di=diopside($MgCaSi_2O_6$):Hd=hedenbergite($FeCaSi_2O_6$).

Fig. 2: Electron microprobe analyses of Cr plotted against Mn, for augite and hypersthene from rake sample anorthosite 15362,1. Chromium and manganese are strongly partitioned between the two pyroxenes.

Fig. 3: Electron microprobe analyses of Al, Ti, and Cr for augite and hypersthene from rake sample anorthosite 15362,1, expressed as the number of cations per formula unit. Cr/(Al+Ti) ratios are about the same in augite and hypersthene.

Fig. 4: Electron microprobe analyses of Ti and Al for augite and hypersthene from rake sample anorthosite 15362,1. In general, augite has more Ti and Al than hypersthene. In both augite and hypersthene, the variation in Al is, in general, higher than in Ti.

MINERALOGICAL AND CHEMICAL STUDIES OF BRECCIA 15086. J. C. Drake* and C. Klein, Jr.**, Dept. Geological Sciences, Harvard Univ., Cambridge, Mass. 02138 (present addresses:*Univ. of Vermont, Burlington, Vt. 05401, **Indiana Univ., Bloomington, Ind. 47401)

Breccia section 15086,39 which displays an unusually diverse range of lithic fragments, glass types, and textures has been studied in detail by optical and electron microprobe techniques. A bulk chemical analysis has been made on the < 74 microns fraction of material broken off rock fragment 15086, 21 (Table 1, #1). The detrital texture, the abundance of unrecrystallized glass fragments, and the presence of matrix glass indicate that this breccia has undergone little to no metamorphism (similar to group I, Warner, 1972, for Apollo 14). Analyses of 291 glasses (173 rounded, 118 angular and irregular), 58 pyroxenes, 27 feldspars, 4 olivines and 12 lithic fragments (by broad beam technique) have been made. The clasts consist of lithic fragments, monomineralic crystal fragments and various types of glass set in a fine-grained, granular, glassy matrix. Lithic clasts include intersertal basalts, subophitic and recrystallized breccias. Only traces of anorthosite were noted and no noritic fragments were observed. Representative chemical analyses for several of these rock types are given in Table 1 (analyses 2-6). Pyroxenes from lithic clasts and individual crystal fragments show gross compositional charactertistics similar to those reported for lunar pyroxenes. Pigeonites, subcalcic augites, augites, ferroaugites and pyroxferroite were observed. Pronounced chemical zonation of single crystals was not detected, and compositions trend towards pyroxferroite rather than hedenbergite (see fig. 1E). The highest analyzed TiO_2 content in pyroxene was 2.13 wt. %, and in the majority of pyroxenes TiO_2 was less than 1 wt. %. No pronounced chemical dissimilarity was observed between pyroxenes from lithic clasts and pyroxene crystal fragments.

Glass, the most abundant constituent of 15086,39 occurs in rounded shapes, as angular fragments, as large patches occasionally showing flow features, and as angular glass associated with pyroxene fragments. Compositional relationships for the various types are shown in figures 1 and 2 which reveal several distinct compositional groupings. Most obvious is the highly restricted compositional range of most rounded glass particles (figs. 1B, 1D, 2A). A representative analysis of this composition is given in table 1, #8. Angular glasses with compositions similar to that of the most common rounded type undoubtably represent fragments of spherules. Another chemically distinct glass type, associated with pyroxene fragments, is shown in figure 1A at approximate coordinates CaO = 40, MgO = 5, FeO = 55. A representative analysis of this glass type is #7, table 1. Coexisting pyroxenes are indicated in figure 1E by ■ . A third glass type is apparent in fig. 2B by the clustering of compositions near TiO_2 = 2%, Al_2O_3 = 18%.

BRECCIA 15086: MINERALOGY AND CHEMISTRY.

J. C. Drake

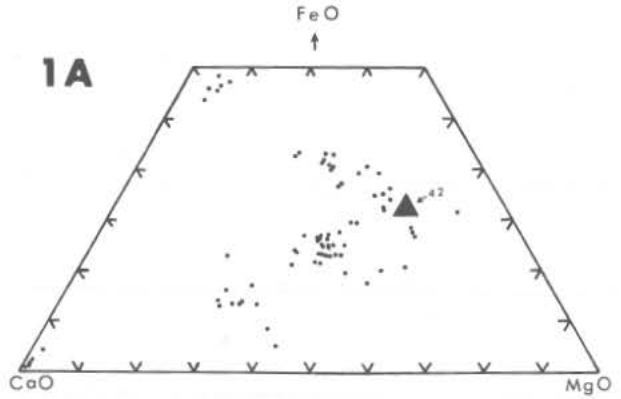

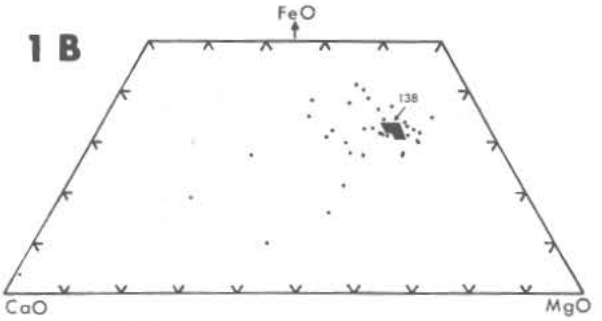

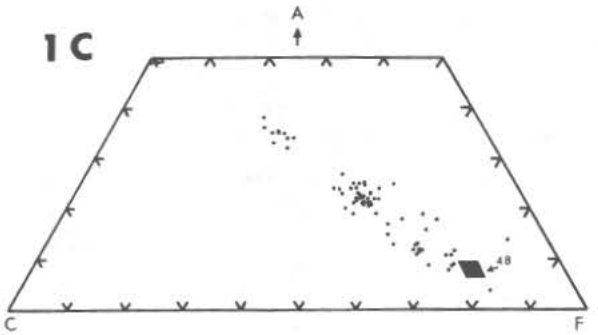

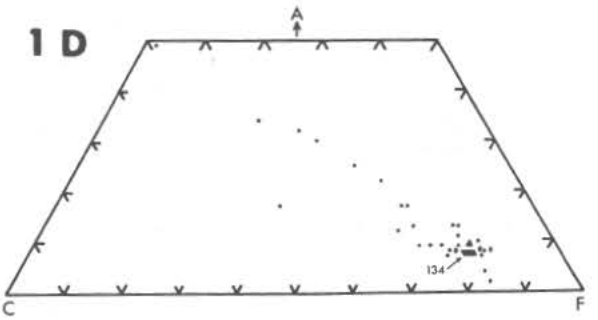

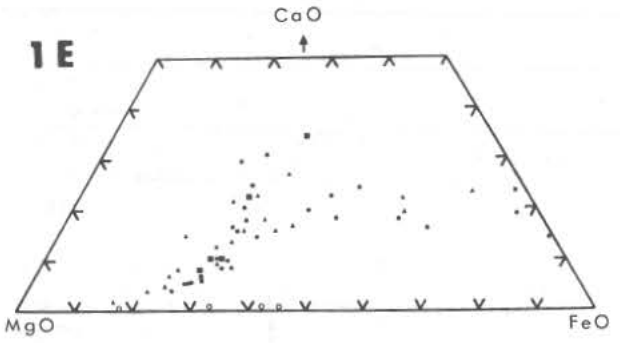

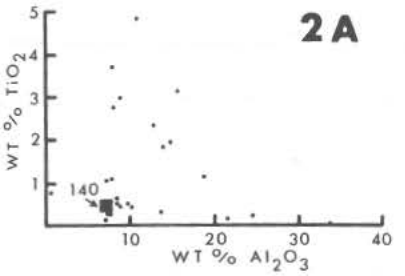

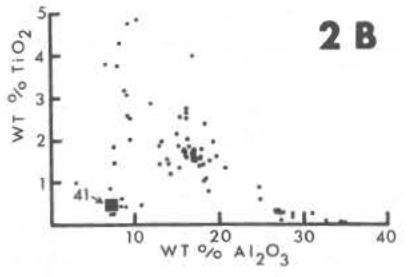

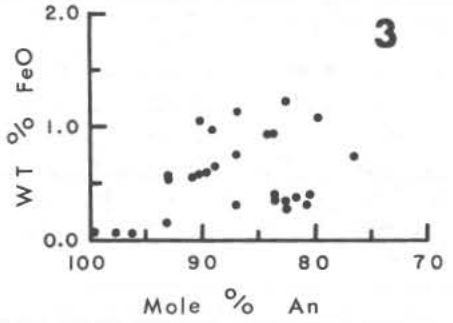

BRECCIA 15086: MINERALOGY AND CHEMISTRY.

J. C. Drake

Figure 1A: Relative molecular proportions of CaO, MgO, and FeO in 118 angular glass particles; 42 analyses plot within shaded triangle. Figure 1B: Relative molecular proportions of CaO, MgO and FeO in 173 rounded glass particles; 138 analyses plot within the shaded area. Figure 1C: ACF diagram of 118 angular glass particles; 48 analyses plot within the shaded area. Figure 1D: ACF diagram for 173 rounded glass particles; 134 analyses plot within the shaded area. Figure 1E: Relative molecular proportions of CaO, MgO, and FeO in pyroxenes and olivines, o = olivine, ▲ = pyroxene in lithic fragments, ● = pyroxene crystal fragments, ■ = pyroxene coexisting with angular glass plotting near CaO = 40, MgO = 5, FeO = 55 in figure 1A. Figure 2A: Weight percent TiO_2 vs. weight percent Al_2O_3 in rounded glass particles; 140 analyses plot in shaded area. Figure 2B: Weight percent TiO_2 vs. weight percent Al_2O_3 in angular glass; 41 analyses plot in shaded area. Figure 3: Weight percent FeO vs. anorthite content of 27 plagioclase grains.

Table 1

	1	2	3	4	5	6	7	8
SiO_2	46.7	49.25	53.35	50.01	51.36	51.25	48.90	45.19
TiO_2	1.6	2.26	2.36	1.22	0.82	1.47	2.64	0.50
Al_2O_3	15.2	13.68	21.15	10.20	25.32	18.00	16.23	7.10
Cr_2O_3	0.47	0.18	0.26	0.51	0.21	0.27	0.01	0.59
FeO	14.8	19.68	4.44	17.52	2.62	9.80	20.66	20.85
MgO	10.2	3.18	3.31	7.87	1.75	8.04	1.05	17.17
CaO	10.4	9.97	11.97	10.74	14.30	9.80	9.97	7.95
K_2O	0.17	0.14	1.08	0.10	0.37	0.91	0.02	0.09
Na_2O	0.38	0.66	1.13	0.42	1.51	1.00	0.78	0.08
Total	100.37*	99.00	99.05	98.59	98.26	100.54	100.26	99.52

1)15086,21 (<74 μ) includes 0.20% MnO, 0.02% NiO, 0.22% P_2O_5 and 0.01% CoO - Jun Ito, analyst; 2) intersertal basalt fragment; 3) subophitic basalt fragment; 4) pyroxenite fragment; 5) subophitic basalt fragment; 6) recrystallized breccia; 7) glass coexisting with pyroxene; 8) composition typical of dominant rounded glass type.

MINERALOGY AND PETROLOGY OF TWO APOLLO 15 MARE BASALTS

P. Gay, I.D. Muir and G.G. Price, Department of Mineralogy and Petrology, University of Cambridge, England.

Two specimens of Apollo 15 mare basalts (15058 and 15065) have been examined; in each case a polished thin section and rock chip were available. Both specimens belong to the porphyritic clinopyroxene basalts of the textural type 1 (1) though 15065 has a more gabbroic aspect than 15058. Although most of our detailed work so far has been carried out on the latter specimen it seems unlikely that the results for 15065 will differ significantly.

Petrographically 15058 can be described as a porphyritic dolerite or very coarse grained basalt in which large phenocrysts of a complexly zoned pyroxene, some of which may reach 2cm in length, are set in a finer-grained groundmass composed of a yellow lime-poor ferroaugite, calcic plagioclase of bytownite-anorthite compositions, Fe-Ti oxide minerals, minor sulphides and a few specks of iron. Apatite is a prominent accessory and in the residuum there are pools of cristobalites and tridymites. 15065 is generally similar differing only in the coarser grain size and in the presence of olivine.

As in the Apollo 12 basalts, the pyroxenes have cores of magnesia-rich pigeonite, $Ca_5Mg_{68}Fe_{27}$ (anal. 1 Table I) with the characteristic curved fractures. This pyroxene is strongly zoned to compositions around $Ca_{17}Mg_{43}Fe_{40}$ (anal. 2 Table I) but we have found no evidence of sector zoning. The pigeonite cores are sharply mantled by subcalcic augite $Ca_{33}Mg_{43}Fe_{24}$ (anal. 3 Table I) which is also strongly zoned to margins that are subcalcic ferroaugites, ($Ca_{26}Mg_{34}Fe_{40}$, anal. 4 Table I). In the groundmass still more iron rich compositions are found and the pyroxenes here become distinctly yellow in colour (anal. 5 Table I). There appears to be a small amount of scatter in the range of compositions encountered in this groundmass pyroxene but most lie close to the compositions quoted; pyroxferroite has not been detected. The pyroxenes found as cores to the plagioclase crystals seem to form a separate group. These are iron-rich pigeonites and the composition of anal. 6 Table 1, $Ca_{14}Mg_{38}Fe_{48}$ seems to be representative of this group. Exsolution lamellae $\parallel$ {001} can sometimes be detected optically, though these are less distinct in 15065. Single-crystal diffraction patterns of both augite and pigeonite crystals removed from the surfaces of the rock chips show {001} exsolution of the minor component, though in a few cases incipient exsolution only can be inferred from the streaks running from the host maxima towards the expected positions of the exsolved maxima. Individual patterns are often complex with features that are characteristic of most lunar clinopyroxenes with strong zoning and involved crystallisation histories. The pyroxenes are crowded with inclusions which occur as rounded (50μ

diameter) grains of coffee brown spinel and specks of Ni-iron ($Fe_{96}Ni_4$). Optically they also seem to contain some brown translucent lamellae apparently exsolved || {100} and elongated || to [001]; such plates are about 250μ in length and about 10μ wide and look as if they are barely 5μ in thickness. In terrestrial pyroxenes such lamellae would be regarded as ilmenite but in these rocks their nature and significance is at present uncertain. Diffraction patterns often show the presence of disoriented inclusions (presumably of spinel and iron) but so far no unusual oriented product has been detected (though this may not be unexpected given the nature of such lamellae). Orthopyroxene has not been found in either of these two samples, though we have found crystals in a fine (15292) where it often shows exsolution of twinned augite on {100}.

Plagioclase is of composition around An_{90} (anal. 7 Table I) and relatively unzoned, though with variable twinning. As expected diffraction patterns of feldspar crystals from the rock chips show transitional anorthite structures with little or no variation in the intensity and diffuseness of type (c) reflections. A curious feature of some of the small plagioclase crystals is the presence of rectangular cores of iron-rich pigeonite; similar minute pyroxene grains within plagioclase have been reported in rock 15415(2). We have been unable to find any oriented crystallographic relationships between felspar and pyroxene and must conclude that, as for 15415, the pyroxenes must have been trapped within the growing feldspar crystals.

Texturally these rocks seem to be derived from the lower parts of thick flows or from shallowly emplaced minor intrusions. There appears to be some evidence for cumulate pyroxene. As mare basalts they have strong chemical and mineralogical affinities with the Apollo 12 suite although the types so far analysed seem to be distinctly poorer in TiO_2. The normative pyroxene of 15058 is slightly more iron rich than the Apollo 12 average but has the same lime content. In harmony with this the pyroxenes generally are slightly more iron-rich.

A superficial glance at the thin sections of these rocks reveals an abundance of translucent and opaque inclusions in the pyroxenes and olivines. These might suggest the existence of post crystallization oxidation or reduction reactions similar to those reported in some Apollo 14 breccias (3) The irregular distribution of the inclusions, their lack of orientation (with the possible exception of the brown lamellae described above), and their Mg and Cr-rich compositions indicate that they are early crystallizing phases trapped within the rapidly growing ferromagnesian silicate phases.

REFERENCES

(1) LSPET, 1972. Science, 175, 363.

(2) R.B. Hargraves and L.S. Hollister, 1972. Science, 175, 430.

(3) P. Gay, M.G. Bown and I.D. Muir, 1972. Proc. Third Lunar Science Conf., Suppl. 3, Geochim. Cosmochim. Acta, vol.1 (in the press).

Table 1
Selected mineral analyses (wt%) from 15058.18

	1	2	3	4	5	6	7
SiO_2	53.30	49.70	49.75	49.53	47.06	48.95	48.81
TiO_2	0.27	0.27	0.70	0.69	1.34	0.72	-
Al_2O_3	1.13	1.11	2.84	2.89	1.32	1.14	32.70
Cr_2O_3	0.90	0.88	1.03	0.99	0.24	0.34	-
FeO	16.96	23.87	14.28	23.34	27.68	29.26	-
MnO	0.31	0.30	0.17	0.17	0.43	0.43	-
MgO	24.17	14.17	13.94	11.30	8.60	13.40	-
CaO	2.47	7.58	15.17	11.77	13.57	6.79	17.65
Na_2O	-	-	-	-	-	-	1.18
Total	99.51	97.88	97.88	100.68	100.24	101.03	100.24
Composition							
Ca	5.1	16.5	32.9	25.6	28.8	14.0	An_{90}
Mol.%Mg	67.8	42.9	42.6	34.4	25.5	38.6	
Fe	27.1	40.6	24.5	40.0	45.7	47.4	

1. Low Ca pigeonite core of pyroxene phenocryst.
2. Outer part of pigeonite core of same crystal.
3. Inner part of augite jacket of same crystal.
4. Subcalcic ferroaugite, outer margin to jacket of same crystal.
5. Groundmass pyroxene.
6. Iron-rich pigeonite, core to feldspar crystal.
7. Plagioclase.

MAJOR ELEMENT COMPOSITION OF APOLLO 15 GLASSES, Billy P. Glass, Geology Dept., Univ. of De., Newark, Delaware 19711

Previous studies have shown that glass compositions provide a useful guide for determining the major rock types (and abundances) contributing to the lunar soil (1,2,3). Because some of the glass particles may have been derived from as far away as several hundred kilometers, the investigation of glass particles recovered from a single sample of <1mm fines can yield a great deal of information about the composition and variability of the lunar surface within a radius of several hundred kilometers of the collection site. This paper reports on the investigation of glass particles from three Apollo 15 soil samples: 15041,85; 15101,128 and 15301,117. Sample 15041 is the <1mm fines taken on the mare surface between the LM and the ALSEP site. Sample 15101 is the <1mm fines from station 2 located near the base of the Apennine Front near St. George Crater. Sample 15301 is the <1mm fines from station 7 from the rim of Spur Crater on the lower slope of Hadley Delta. Thus the three samples investigated are from widely separated sampling points at the Apollo 15 site.

Each sample was sieved into five size fractions (<74μm, 74-149μm, 149-295μm, 295-505μm, 505 to 1000μm). The percent abundance of each major component was determined using a binocular microscope, for each size fraction >149μm. The three Apollo 15 samples are somewhat finer grained than most of the Apollo 12, 14 and 16 soil samples that I have investigated (Table 1). They also contain a large percentage of glass, particularly regular forms (Table 1). This is especially true of Sample 15301 which contains ~40% glass fragments and spherules. This sample contains 10 times as many spherules as soils from the Apollo 12, 14 and 16 sites (Table 1). This unusually high concentration of glass spherules is due mostly to the presence of the transparent green glass as first reported by LSPET (4). The glass contents of the three Apollo 15 samples have been characterized according to size, color, transparency, shape and surface texture.

Approximately 150 glass particles from 15101, 15301 and 15041 were then described and individually mounted in epoxy in 1/4" metal cylinders ground down to expose a flat surface and polished for electron microprobe analysis. Each particle was examined with a petrographic microscope in reflected and transmitted light and then analyzed for Si,Ti,Al,Fe,Mn,Mg,Ca,Na and K using an ARL microprobe analyzer (see (2) for method of analysis). Although the glasses exhibit a wide range in composition, histograms of oxide abundance and various oxide plots for ~130 homo-

APOLLO 15 GLASSES

Billy P. Glass

geneous glasses show that the analyses tend to cluster into groups. Based on the histograms and oxide plots, the glasses were divided into five main groups (Table 2). These groups are similar to those proposed by Reid et al. (5) for Apollo 15 glasses.

Green(Pyroxenitic) Glasses - The glasses in this group can be distinguished by their high FeO (~20%) and MgO (~18%) and low Al_2O_3 (~7.5%) and TiO_2 (~0.5%) contents. These glasses are remarkably homogeneous not only within a single grain, but from grain to grain and from sample to sample. The green glasses all seem to be nonvesicular spherules or fragments of spherules. Some of the green glasses have partly devitrified to crystallites of olivine (Fo_{76}) (6). Some translucent yellow to orange spherules, with the same compositions as the green glasses, appear to be devitrified green glass spherules. X-ray diffraction analysis indicates that the crystalline material in the translucent spherules is olivine (~Fo_{85}). One spherule contains a rather large (~50μm dia.) Ni-Fe spherule. Other than the olivine crystallites and Ni-Fe spherule the green glasses appear to be free of crystalline inclusions.

The green glasses are most abundant in the soils from the Apennine Front, especially in soil from Spur Crater (4,6). The >149um size fractions of samples 15301,117, 15101,128 and 15041, 85, contain approximately 18%, 2% and 0.3% green glasses respectively. Glasses with similar compositions have been reported from the Apollo 11 site (6). Glasses with this composition have not been reported from the Apollo 12 site, but transparent green glasses with similar compositions have been recovered from Apollo 14 soils (7) (Table 2). The Apollo 14 green glasses have somewhat higher Al_2O_3 and CaO and lower FeO and MgO contents than the Apollo 15 green glasses; however, they are more similar to the Apollo 15 green glasses than to any other known major lunar glass types. The Apollo 14 green glasses are not only similar in composition, but like the Apollo 15 green glasses, are remarkably homogeneous and free of relict crystalline inclusions and vesicles (7). It has been suggested that the Apollo 15 green glasses were derived from material of pyroxenitic composition (6). It is possible that the source of the green glasses may be some deep seated material excavated by the Imbrian event. Likewise, the Apollo 14 site is located on the Fra Mauro Formation which is believed to be material ejected by the Imbrian event.

Feldspathic Glasses - These glasses are characterized by high Al_2O_3 (>22%) and CaO (>13%) and low FeO (<9%) and MgO (<11%) contents. Most of the glasses in this group are yellowish-green spherules or fragments without vesicles or crystalline inclusions. Glasses with similar compositions have been found in all lunar soils investigated to date (8). Reid et al. (8) refer to them as highland basalt glasses. They have compositions similar to anorthositic gabbros (Table 2) and are probably derived from the lunar highlands. This suggestion is supported by preliminary data on Apollo 16 samples that indicate that glasses with this compo-

APOLLO 15 GLASSES

Billy P. Glass

sition make up the bulk of the glasses at this highland site. It is also supported by X-ray fluorescence data from lunar orbit(9).

High Fe Basaltic (Mare-Derived) Glasses - The glasses in this group are distinguished from the green glasses by their lower MgO (<15%) and higher TiO_2 (>1%) and Al_2O_3 (>8%) contents and from the feldspathic glasses by their lower Al_2O_3 (<16%) contents. Glasses in this group all have FeO contents greater than 14% and thus are similar to the glasses that the Apollo Soil Survey (10) refer to as mare-derived glasses. The glasses in this group can be subdivided based on their Fe and Ti contents, into three subgroups: Subgroup I - The glasses in this subgroup are characterized by high FeO (>20%). These glasses also have rather high TiO_2 contents (generally >3%). They are generally transparent dark brown to deep red spherules without vesicles or crystalline inclusions. Subgroup II - This subgroup has glasses with FeO contents >14% but <18%. Five are opaque grey or brown vesicular fragments with crystalline inclusions and the rest are generally transparent brown spherules without vesicles or crystalline inclusions. The glasses in this subgroup are quite similar to the soils and breccias from the Apollo 15 site (Table 2). Subgroup III-This subgroup is characterized by very high TiO_2 content (~13%) and low SiO_2 (~37%). Only one glass spherule has been assigned to this subgroup. However, this spherule is similar in composition to glasses that Reid et al. (5) refer to as MARE 4 glasses which according to them, make up about 1% of the glasses in the Apollo 15 soils.

Low Fe, High K (KREEP) Glasses - The glasses in this group have low FeO (<13%) and high K_2O (>0.2%) and Na_2O (>0.5%) and generally high SiO_2 (46-51%) contents. These glasses have been divided into three subgroups based on their K_2O and FeO contents. Subgroup I - The glasses in this subgroup are distinguished by having high K_2O contents (>0.4%). These glasses are all light colored (yellow to grey) transparent to opaque fragments with or without vesicles and/or mineral inclusions. Subgroups II and III-These two subgroups both have lower K_2O contents (between 0.2 and 0.4%). One of these subgroups (II), has FeO > 10% and the other (III), has FeO < 10%; otherwise they are quite similar. The glasses in both subgroups are mostly fragments, but some are spherules. They are generally opaque to translucent and various shades of grey, brown or yellow. Many of them have vesicles and/or crystalline inclusions. The glasses in these three subgroups are similar to the most abundant group of glasses at the Apollo 14 site and to the high K_2O basaltic glasses at the Apollo 12 site. Material with this composition has been variously called KREEP, norite, grey mottled fragments, non-mare basalts and Fra Mauro basalts.

Low Alkali, Low Fe Basaltic Glasses - The glasses in this group are distinguished from the green glasses and the high iron (mare-derived) basaltic glasses by their lower FeO content (<14%), and from the feldspathic glasses by their lower Al_2O_3 con-

APOLLO 15 GLASSES

Billy P. Glass

tent (<22%) and from the high K_2O (KREEP) glasses by their lower K_2O content (<0.2%). These glasses are all fairly small (<300μm dia.) transparent spherules without vesicles or crystalline inclusions. These glasses could possibly have been produced from the low FeO, high K_2O (KREEP) glasses by selective volatization. Similar small transparent nonvesicular glass spherules with low alkali content have been found in the Apollo 12 and 14 soils (2, 7).

REFERENCES

1) E.C.T. Chao, et al. J. Geophys. Res., 75, 7445 (1970).
2) B.P. Glass. NASA Goddard Space Flight Center Doc. X-644-71-414 (1971).
3) A.M. Reid, et al. Proc. Third Lunar Sci. Conf. Geochim. Cosmochim. Acta. (in press).
4) Lunar Sample Preliminary Examination Team. Science, 175, 363 (1972).
5) A.M. Reid, et al. Major element composition of glasses in three Apollo 15 soils (preprint - 1972).
6) W.I. Ridley, et al. Apollo 15 green glass (preprint - 1972).
7) B.P. Glass. Proc. Third Lunar Sci. Conf., Geochim. Cosmochim. Acta. (in press).
8) A.M. Reid, et al. Geochim. Cosmochim. Acta. (in press).
9) I. Adler, et al. Goddard Space Flight Center Preprint X-641-72-57 (1972).I. Adler, et al, Goddard Space Flight Center Preprint X-641-72-198 (1972).
10) Apollo Soil Survey. Earth Planet Sci. Lett., 12, 49 (1971).

TABLE I

Percent >149μm and Glass Content of Various Apollo Soil Samples.

Sample	%>149μm	% Glass (74-295μm)	% Spherules >149μm	No. Spherules/gm 74-149μm
12001,59	20	22	0.8	1705
12057,54	21	28	0.6	2151
12070,129	26	23	0.4	2633
14148,44	18	27	1.2	4544
14149,55	25	20	0.8	3272
14156,41	21	21	1.2	4507
14163,49	19	30	0.9	4296
14230,75	19	25	1.9	-
14230,82	17	19	0.5	-
15041,85	16	24	1.4	3631
15101,128	16	21	2.5	3762
15301,117	18	41	14.0	58485
63501,23	29	12	0.2	2356
68501,29	29	7	0.7	2779

APOLLO 15 GLASSES

Billy P. Glass

TABLE II - Range and average compositions of glass types in Apollo 15 soils with other lunar rocks, soils and glasses for comparison.

	SiO_2	TiO_2	Al_2O_3	FeO	MnO	MgO	CaO	Na_2O	K_2O
				Green (Pyroxenitic) Glasses (35)					
low	43.0	0.49	6.63	19.0	0.19	16.9	7.14	0.09	0.17
high	47.1	0.62	8.22	22.0	0.24	20.5	8.46	0.29	0.25
ave.	45.2	0.54	7.45	20.3	0.22	18.1	8.19	0.20	0.21
				Feldspathic Glasses (6)					
low	37.6	0.20	22.7	4.52	0.03	2.49	13.5	0.05	0.12
high	48.4	1.00	26.4	8.47	0.11	10.6	15.5	0.70	0.35
ave.	45.3	0.51	24.9	6.64	0.07	8.00	14.1	0.39	0.20
				High Fe Basaltic (Mare-Derived) Glasses					
				Subgroup I (19)					
low	41.6	2.27	8.08	19.8	0.20	8.78	8.04	0.21	0.26
high	45.5	4.81	10.6	23.6	0.25	14.4	9.71	0.84	0.49
ave.	43.1	3.63	8.98	21.9	0.23	12.3	8.73	0.54	0.32
				Subgroup II (13)					
low	41.4	1.58	11.5	14.5	0.15	9.26	9.80	0.04	0.17
high	47.7	3.24	15.6	18.0	0.20	14.1	11.8	0.70	0.46
ave.	45.0	1.90	13.9	16.0	0.17	11.4	10.8	0.26	0.29
				Subgroup III (1)					
	36.7	13.1	8.97	20.4	0.21	10.3	8.40	0.78	0.38
				Low Fe, High K Basaltic (KREEP) Glasses					
				Subgroup I (22)					
low	48.0	0.98	13.6	7.94	0.10	7.87	10.2	0.54	0.45
high	51.2	2.07	20.7	12.1	0.17	11.4	12.0	1.32	0.85
ave.	49.7	1.39	17.3	9.97	0.12	9.47	10.8	0.84	0.62
				Subgroup II (8)					
low	42.9	0.98	14.9	10.6	0.10	10.3	10.8	0.48	0.20
high	47.2	1.85	19.1	13.0	0.17	14.6	11.6	0.96	0.36
ave.	46.1	1.35	17.0	12.0	0.13	11.7	11.1	0.64	0.30
				Subgroup III (6)					
low	46.3	0.80	17.3	8.05	0.09	10.7	10.6	0.52	0.23
high	47.3	1.29	18.9	8.60	0.12	13.4	11.9	1.03	0.43
ave.	47.1	0.99	18.0	8.32	0.10	12.4	11.2	0.69	0.36
				Low Alkali Basaltic Glasses (6)					
low	40.4	0.34	16.1	6.71	0.08	10.9	11.4	0.03	0.12
high	44.2	1.59	21.7	13.6	0.15	14.2	13.9	0.30	0.20
ave.	42.5	1.27	19.8	10.8	0.12	12.0	12.4	0.12	0.16
				Apollo 15 Basalts (7)*					
	46.07	2.13	8.95	21.19	0.29	9.51	10.21	0.26	0.03
				Apollo 15 Gabbroic Anorthosite *					
	44.97	0.27	26.73	5.37	0.08	5.38	16.10	0.31	0.03
				Apollo 15 Soils and Breccias (10)*					
	46.09	1.55	14.16	15.76	0.20	10.88	10.71	0.38	0.17
				Apollo 14 Green Glasses (17)					
	46.1	0.70	9.89	17.8	0.20	14.6	9.38	0.37	0.25

*LSPET (4)

METALLIC PARTICLES FROM 3 APOLLO 15 SOILS, J. I. Goldstein and H. J. Axon, Metallurgy and Materials Science Dept., Lehigh University, Bethlehem, Pa. 18015.

We have made a metallographic and electron probe study of the metal in 584 of the most magnetic particles in 18g of the <1mm Apollo 15 soil. Pairs of samples from three sites were analyzed: (1) 15031,40 and 15041,44 from a trench at the LM/ALSEP site, (2) 15071,23 and 15081,18 from 25m and 60m East of the Elbow crater rim, respectively, and (3) 15261,50-51 from a trench dug into S. rim of a 12m crater, and 15271,52 from about 10-15m SE of this trench, station 6, at the Apennine Front.

Each soil sample was separated into 4 sieve fractions, >74μm, >125μm, >354μm, >707μm and then separated magnetically to obtain the most magnetic particles. Almost all the metal in the magnetic fraction was 50 to 250μm in the largest dimension and only about 10 metal particles were larger than 300μm in size. The proportion of clean magnetic particles was 0.02 ± 0.005 wt% at the LM/ALSEP site, 60m from Elbow crater and 10-15m from the 12m crater at the Front. Larger amounts of metal 0.045 ± 0.005 wt% were found in soils closer to crater rims; that is at 25m from Elbow crater rim and at the rim of the 12m crater at the Front. These weight fractions greatly underestimate the total metallic content of the soil since the metal in the <74μm sieve fraction was not measured and also some metal is present as small inclusions in the less magnetic soil particles.

The metal particles were mounted in epoxy and electron microprobe analyses for Fe, Ni, Co, P and S were obtained. Significant differences were not observed in the Co-Ni distributions from the pairs of samples at the LM/ALSEP site nor at Elbow crater. The Co and Ni point analyses of the metallic portion of the one phase particles and also of those two phase particles with minor amounts of second phase are plotted as circles, and the bulk compositions of the remelted globules are plotted as crosses in Fig. 1a for the LM/ALSEP site, Fig. 1b for the Elbow crater site, and Fig. 1c and d for the two Apennine Front sites 15261, 15271 respectively. The distribution of metal particles is summarized in Table I. Most are either one phase or contain minor amounts of second phase. A few of these particles have high Ni and/or high Co contents and these, as well as the 2 phase particles and the special cases (Table I) are <u>not</u> plotted in Fig. 1.

About 5% of our metal particles are two phase $\alpha + \gamma$ or α + phosphide. A few of the two phase $\alpha + \gamma$ particles have a recognizable chondritic-metal microstructure but most have Co and S contents greater than the meteoritic range. It is noteworthy that most of the two phase $\alpha + \gamma$ particles were collected at the Apennine Front. The distribution of Ni and P between the 2 phases of the α + phosphide particles can provide a measure of the last temperature of heat treatment or equilibration for the metal. Using the α/Ph interface compositions in the appropriate Fe-Ni-P phase diagrams as discussed

METALLIC PARTICLES FROM 3 APOLLO 15 SOILS

J. I. Goldstein and H. J. Axon

by Axon and Goldstein (1) temperatures for the analyzed particles were estimated at 550°C or below.

TABLE I - Distribution of Metal Particles

Soil Location	Essentially Single Phase		Two Phase Particles			Special Cases	Total
	Ni<25 wt%/ Co<3.2 wt%	Ni>25 wt%/ Co>3.2 wt%	α+γ	α+Phosphide	Globules		
15031-041	96	2	4	1	7	5	115
15071-081	133	4	5	1	8	3	154
15261	140	4	4	5	12	2	167
15271	112	6	12	3	14	1	148

A few special particles were also analyzed including 2 Cr rich fragments, 2 melted phosphide particles and 2 particles with Ni contents exceeding 90 wt% attached to an almost pure Fe phase.

The Ni-Co range for meteoritic metal as given by Goldstein and Yakowitz (2) is plotted on Fig. 1. A second range called the high Fe group with low Ni (≤1%) and low Co (≤0.5 wt%) and appropriate to metal in Apollo 11 lunar basalts is also plotted. A third range which is defined on Fig. 1 includes the high Co particles and encompasses the Ni-Co contents of metal from Apollo 12 lunar basalts. Four metallic particles that we have analyzed within the crystalline-breccia portions of thin section 15205,61 also lie within this composition range. Using these 3 Ni-Co ranges and the data of Fig. 1, it is possible to chemically group the Apollo 15 metal particles. Table II summarizes the distribution of metal in the 3 composition ranges both for Apollo 15 and also for previous missions. Elbow crater soils contain a large amount of the high Co particles with only a small amount of the meteoritic group. Apennine Front soils contain a large amount of the meteoritic group and a small but significant amount of the high Co and high Fe groups. The metal content of the LM/ALSEP site is intermediate to the other two sites and is very similar in character to that encountered at the Apollo 12 site. As previously suggested it is probably a mixture of ray materials thrown from distant locations.

TABLE II - Composition Ranges of Metal Particles in Lunar Soils

Location	Number of Particles	Chemical Group		
		% Meteoritic	% High Fe	% High Co
15031-041 LM/ALSEP	103	43	6	35
15071-081 Elbow Crater	141	28	5	63
15261 Apennine Front	152	46	15	26
15271 Apennine Front	126	55	12	22
15601 Hadley Rille (Wlotzka et al)[3]	66	11	11	64
14003-14163(Goldstein et al)[4]	190	78	8.5	2.5
14163 (Wlotzka et al)[3]	98	78	12	0
12001 (Wlotzka et al)[3]	87	40	9	42
10084 (Wlotzka et al)[3]	99	60	8.5	2.5

After the Imbrium impact the Imbrium basin appears to have been flooded by lava and there is no reason to expect metal of meteoritic composition in

METALLIC PARTICLES FROM 3 APOLLO 15 SOILS

J. I. Goldstein and H. J. Axon

such lava flows. This is in agreement with results on soil (15601), Table II (3) from the Hadley Rille, which cuts into these lava flows. Elbow crater also appears to have been excavated from these lava flows and this is in keeping with the large proportion of high Co metal encountered at this site as well as at the Hadley Rille. The higher content of meteoritic metal at Elbow crater compared to Hadley Rille arises because Elbow crater is the target area for recent meteoritic infall. The Apennine Front provides a location from which metallic particles that originally formed deep inside the lunar crust may now be eroded. In this context the large number of 2 phase $\alpha + \gamma$ particles of non-meteoritic, high Co contents at the (uncratered) location 12571 is noteworthy. At location 15261 the situation is complicated by recent cratering activity.

The majority (65-75%) of metal particles in the Apollo 15 soils have sulfur contents $\geq$0.02 wt%. This is to be contrasted with the Apollo 14 metal in which S contents were almost always less than 0.02 wt%. In addition, a direct relationship was observed between measured Co and S contents.

Metallic spheroids, globules, were identified at all the sites forming ~7% of our sample (Fig. 1, Table I) with a larger fraction at the Apennine Front. The composition of the Apollo 15 globules vary more widely (0.2-22.5 wt% Ni, 0.1-2.35 wt% Co, 0.02-13.2 wt% P, and 0.02-25.5 wt% S) than for the other Apollo sites. For the first time metallic globules of non-meteoritic composition (0.2-3.3 Ni, 0.2-2.35 Co) were observed, collected at the Apennine Front.

The silicate associated with the high Fe group of metal particles is mainly idiomorphic-well crystallized while the silicate associated with the high Co group of metal particles is of various types (idiomorphic, breccia and glass) in about equal proportions. The metal of meteoritic composition is mostly associated with glass and somewhat less with breccia. The surrounding glass is of two types: vesicular or with small metal droplets embedded within it. When in association with glass much of the metal of meteoritic composition also shows, metallographically, signs of reheating such as the development of blocky martensite, polycrystalline kamacite and α_2, and shows, chemically, enrichment of P (>0.05 wt%) over that of meteoritic metal. More extensive reheating of the metal is usually encountered when the glass contains metal droplets.

References

(1) H. J. Axon and J. I. Goldstein, Earth and Planetary Science Letters, to be published (1972).
(2) J. I. Goldstein and H. Yakowitz, Proc. Second Lunar Sci. Conf., Geochim. Cosmochim. Acta Suppl. 2, 1, pp. 177-191, MIT Press (1971).
(3) F. Wlotzka, E. Jagoutz, B. Spettel, H. Baddenhausen, A. Balacescu, and H. Wanke, Lunar Science-III (editor C. Watkins), pp. 806-808 (1972).
(4) J. I. Goldstein, H. J. Axon and F. Yen, Proc. Third Lunar Sci. Conf., Geochim. Cosmochim Acta Suppl. 3, 1, MIT Press, to be published (1972).

Fig. 1a - Co-Ni analyses for the LM/ALSEP site, soil 15031, 15041.

Fig. 1b - Co-Ni analyses for the Elbow crater site, soil 15071, 15081.

Fig. 1c - Co-Ni analyses for the S rim of 12m crater, Apennine Front, soil 15261

Fig. 1d - Co-Ni analyses for soil 15271, 10-15m from the 12m crater, Apennine Front.

SIGNIFICANCE OF APOLLO 15 MARE BASALTS AND 'PRIMITIVE' GREEN GLASSES IN LUNAR PETROGENESIS

D.H. Green and A.E. Ringwood
Dept. of Geophysics and Geochemistry
Australian National University.

The Apollo 15 mare basalts fall petrographically and chemically into two distinct groups (1,2). The olivine basalts are characterized by high normative and modal olivine contents whereas the pyroxene or quartz basalts are characterized by normative quartz and either the absence or rarity of magnesian olivine. Within analyzed samples of the olivine basalt group, normative olivine contents vary from 4 to 20 percent (approx.) whilst TiO_2 contents vary sympathetically from 2.8% to 2.2%. These variations are believed to be caused by local olivine crystallization, accumulation and fractionation in several distinct but closely related lava flows or small intrusions (2). We do not yet have sufficient information to deduce the olivine content and Mg-value (100Mg/Mg+Fe) of the probable parent magma. However, the latter differs from the parent magma for the Apollo 12 olivine basalts (3,4,5) in having higher normative olivine and lower TiO_2 content for a given Mg-value (e.g. at Mg-value = 50, Apollo 12 magma contains 11% normative olivine and TiO_2 $\sim$2.9%, whereas Apollo 15 basalt contains 22% normative olivine and 2.2% TiO_2).

The Apollo 15 quartz basalts (or pyroxene basalts) form a coherent group and clear evidence for crystal fractionation within the group is lacking. The group is distinctive in low TiO_2 content (1.8%) and in the combination of relatively high Mg-value (43-45) coupled with quartz normative character. Olivine basalts of Apollo 12 type with Mg-value of 43-45 contain 2-5% normative olivine and Apollo 15 olivine basalts with Mg-value of 43-45 contain 11-15% normative olivine. It has been shown (2) that Apollo 15 quartz basalts cannot be derived by low pressure crystal fractionation from a parent basalt of either Apollo 15 olivine basalt or Apollo 12 olivine basalt type. It can equally be shown that these basalts are not genetically related to Apollo 11 basalts or 'Highland basalts' (6).

From experimental studies of the natures and compositions of the near-liquidus phases of lunar basalts under high pressures it is possible to draw conclusions regarding the nature and degrees of partial melting of their source regions and of their

APOLLO 15 MARE BASALTS & GREEN GLASSES

D.H. GREEN

depths (pressures) of origin within the moon(7).We have applied these methods and conclude that the parental magmas of Apollo 12 olivine basalts, Apollo 15 olivine basalts and Apollo 15 quartz basalts may all be derived from a source rock with solidus mineralogy dominated by sub-calcic clinopyroxene, orthopyroxene and olivine and further that the Mg-value of the source rock is ∿75. Variations in the chemical compositions of these three magma series which prohibit their genetic relationship by processes of low pressure crystal fractionation, can be used to infer specific melting conditions. Thus we infer that the parental basalt for Apollo 12 olivine basalts (∿12009) was derived by 5-10% melting, with magma segregation at 10-12kb, leaving residual olivine, orthopyroxene and sub-calcic clinopyroxene. Likewise, we infer that the parental basalt for Apollo 15 olivine basalts was derived by 10-15% melting with magma segregation at 15-17kb, leaving residual olivine, orthopyroxene and less sub-calcic clinopyroxene, whilst the parental basalt for Apollo 15 quartz basalts was derived by ∿20% melting with magma segregation at 7-9kb leaving residual olivine, orthopyroxene and little or no clinopyroxene. The extrusion temperatures of parental olivine basalt were probably around 1250°C (Apollo 12), and 1300°C (Apollo 15). Because of adiabatic cooling and the possibility of limited crystal fractionation en route to the surface, these represent minimum temperatures for the source regions deep in the lunar interior. Consideration of relevant factors suggests that appreciably higher temperatures (1300-1400°C) could have been reached during magma genesis.

These high temperatures in conjunction with the variability in degrees of melting inferred above lead us to suggest that at the time of flooding of the mare-basins extensive regions of the lunar interior at depths ≥300km were at temperatures in excess of 1350°C and that there were at this time massive diapiric (convective) movements within the lunar mantle leading to high degrees of melting and varying depths of magma segregation, much as in terrestrial basaltic volcanism (8).

Significance of 'Green Glass' compositions:

The presence of widespread spherules and fragments of green glass of distinctive, olivine-rich (30%), magnesian (100Mg/Mg+Fe = 61) picritic compositions, and relatively depleted in rare earths and Ti, has been reported (9,10). The character, uniformity and distribution of this material argues that it is representative of a significant lunar formation, possibly pre-mare filling or an early mare-filling rock type, at the lunar surface. We have shown (11) that this rock type cannot be genetically related to any of the Apollo 11, 12 or 15 mare

APOLLO 15 MARE BASALTS & GREEN GLASSES

D.H. GREEN

basalts by processes of low pressure crystal fractionation. The nature of the liquidus phases at high pressure and their composition relative to Apollo 12-15 olivine basalts however suggest that this composition is a product of a very high degree of partial melting (30-50%)of a similar source rock to that yielding the other mare basalts (11). The partial melting process followed by magma segregation to form the antecedent of green glass probably occurred at a pressure >15kb, and a temperature of about 1450°C, with olivine and orthopyroxene only remaining as residual phases. (The nature of melting of the postulated pyroxenite source (sub-calcic clinopyroxene, orthopyroxene, minor olivine) is such that the subcalcic clinopyroxene provides the major contribution to the melt by an incongruent melting equilibrium leaving residual orthopyroxene and olivine). The high degree of melting produces very low REE abundances, very small europium anomaly and leaves highly magnesian residual minerals (Mg value 82; initially 75).

While this discussion accounts for the chemical variation among lunar mare compositions within a framework of constant source mineralogy and chemical composition, the latter constraint may be relaxed to allow variation of factors of 2-3 on concentration of incompatible elements. This would allow reduction in the range of degrees of partial melting required (to account for Ti and REE abundances in parental magmas) and some decrease in the maximum temperatures required for magma production (from ∿1450 to ∿1350 or 1300°C). However the main conclusions on mare basalt genesis would not materially change.

References

1. Lunar Sample Preliminary Examination Team (1972) Apollo 15 Preliminary Science Report 6.1
2. B.W. Chappell and D.H. Green (1972) In preparation.
3. W. Compston, H. Berry, M.Vernon, B.Chappell and M. Kay (1971) Proc.2nd.Lunar Science Conference 2, 1471-1485.
4. D.H.Green, A.E.Ringwood, N.Ware, W.Hibberson, A.Major & E.Kiss (1971) Proc.2nd. Lunar Science Conference 1,601-615.
5. D.H.Green, N.Ware, W.Hibberson and A.Major (1971) Earth Planet. Sci. Letters 13, 85-96.
6. D.H.Green, A.E.Ringwood, N.Ware and W.Hibberson (1972) Proc. 3rd.Lunar Science Conference. In Press.
7. A.E.Ringwood and E. Essene (1970) Proc. Apollo 11 Lunar Science Conference 1, 769-799.
8. D.H. Green and A.E. Ringwood (1967) Contrib. Min. and Petrol. 15 15, 103-190.
9. I. Ridley (1972) Preprint
10. J.A.Wood (1972) Preprint
11. D.H.Green and A.E. Ringwood (1972) In preparation.

AN ENSTATITE CHONDRITE FROM HADLEY RILLE. S. E. Haggerty, Geology Department, University of Massachusetts, Amherst, Mass. 01002

An enstatite chondrite, free of chondrules, and with the following mineral assemblage: enstatite (≈75%), kamacite (≈20%), a SiO_2 polymorph (≈2%), troilite (≈1%), schreibesite (≈1%), and niningerite (≈1%) was found in the 1-2 mm. size fraction of soil sample 15602,29. The sample was collected at station 9 in close proximity to Hadley Rille. This is the first reported occurrence of an enstatite chondrite in the lunar samples and only 16 are known in the world's meteorite collections (1). The meteoritic fragment is a Type 1 enstatite chondrite according to the Keil (1) classification; this is based on the presence and composition of niningerite (MgS), and the high Si content of the kamacite (>3 wt % Si). Of the 15 enstatite chondrites studied in detail by Keil (1), six are characterized by the assemblage niningerite (MgS) + oldhamite (CaS) and the remainder by alabandite (MnS) + CaS. The calcium monosulfide was not identified in the lunar fragment and although there is the possibility that the mineral was lost during polished section preparation, because of its high solubility in water, no obvious solution or plucking voids are present. In all other respects, however, the unusual mineral chemistry appears to compare favorably with other enstatite chondrites studied (1,2,3).

Enstatite: Enstatite is present in euhedral-subhedral crystals that range in length from 25-250 μm. Crystals are compositionally homogeneous although a range of 0.4-2.3% FeO was determined for the 5 grains analyzed. Ca, Al, Ni, P, Mn and Ti were detected but the total concentration of these elements amounts to <1%.

Kamacite: Kamacite is present in 3 modes: (1) as large (400 μm) discrete rectangular grains; (2) as interlacing stringers along silicate grain boundaries; and (3) as spherules (<1-20 μm) in eutectic intergrowth with troilite. Only the first of these types were satisfactorily analyzed; the large grains contain between 6.4 and 6.9% Ni. Phosphorous varies between .05 and 0.1%; Mn, Ti, Cr, Al, and Ca are present in concentrations of <.1%. Silicon is relatively constant and values between 2.9 and 3.2% were determined. Fe-Ni-Si solid solution is unique to the highly reduced enstatite chondrites (1,2) and the 3% Si content is characteristic of the Type 1 and intermediate types as defined by Keil (1).

SiO_2 polymorph: The SiO_2 polymorph is present in discrete grains (20-50 μm) and as inclusions in troilite and enstatite. Minute high reflectivity particles are observed in most SiO_2 grains. As much as 0.6% TiO_2 and 0.4% FeO were determined in "inclusion-free" areas and although it is unlikely that these oxides are in solid solution it is noteworthy that the phase emits a blue luminescence under the electron beam, reaffirming Keil's (1) observation for the unusual nature of SiO_2 in enstatite chondrites.

Schreibesite: $(Fe\ Ni)_3P$ is sparsely distributed; it is included in kamacite

An Enstatite Chondrite from Hadley Rille

S. E. Haggerty

and is present along kamacite grain boundaries. Fe varies between 64 and 65.9%; Ni between 19.3 and 19.5% and P between 14.3 and 14.7%. Ca, Ti, Mg and Mn were detected in concentrations of <0.1% and Si is present in concentrations of 0.3%.

Troilite: FeS is present in irregularly shaped grains (intensely shocked), and in eutectic intergrowth with kamacite. Minor elements in concentrations of >0.1% are Cr (1.1-1.3%), Ti (0.4-0.6%) and Si (0.2-0.3%).

Niningerite: Niningerite (Nss) occurs in discrete subrectangular or angular fragments with maximum dimensions of 250 x 100 μm. Two of 15 grains identified contain troilite lamellae (5 μm width) in a widmanstatten-like pattern. Bordering these lamellae is an unidentified light-gray transitional phase rich in Mg, Mn, Ca and S but depleted in Fe, relative to the Nss host. Niningerite is not stoichiometric MgS but contains MnS (9.9%), FeS (33.3%), and CaS (1.5%) in solid solution; CrS (1.1%), TiS (0.12%) and NiS (0.29%) are also present. Of the six niningerite-bearing enstatite chondrites studied by Keil (1) the Nss in the Hadley Rille fragment is closest in composition to the Type 1 Indach meteorite (Fig. 1). Application of the geothermometric data of Skinner and Luce (4) for solid solutions in the MgS-CaS-MnS-FeS systems provides an estimate of minimum temperatures of formation for Nss. Determinations are illustrated graphically, firstly in Fig. 1 where T is between 500 and 600°C, and secondly in Fig. 2 where T is between 590 and 625°C. Exsolved FeS and FeS in Nss suggest cooling rates of <0.01°C/sec.

References

(1) Keil, K., (1968) Mineralogical and chemical relationships among enstatite chondrites. Jour. Geophys. Res. 73, 6945-6976.

(2) Ringwood, A.E., (1961) Silicon in the metal phase of enstatite chondrites and some geochemical implications. Geochim. Cosmoch. Acta. 25, 1-13.

(3) Mason, B., (1966) The enstatite chondrites. Ibid., 30, 23-39.

(4) Skinner, B.J., (1971) Solid solutions of the type (Ca, Mg, Mn, Fe)S and their use as geothermometers for the enstatite chondrites. Amer. Mineral. 56, 1269-1296.

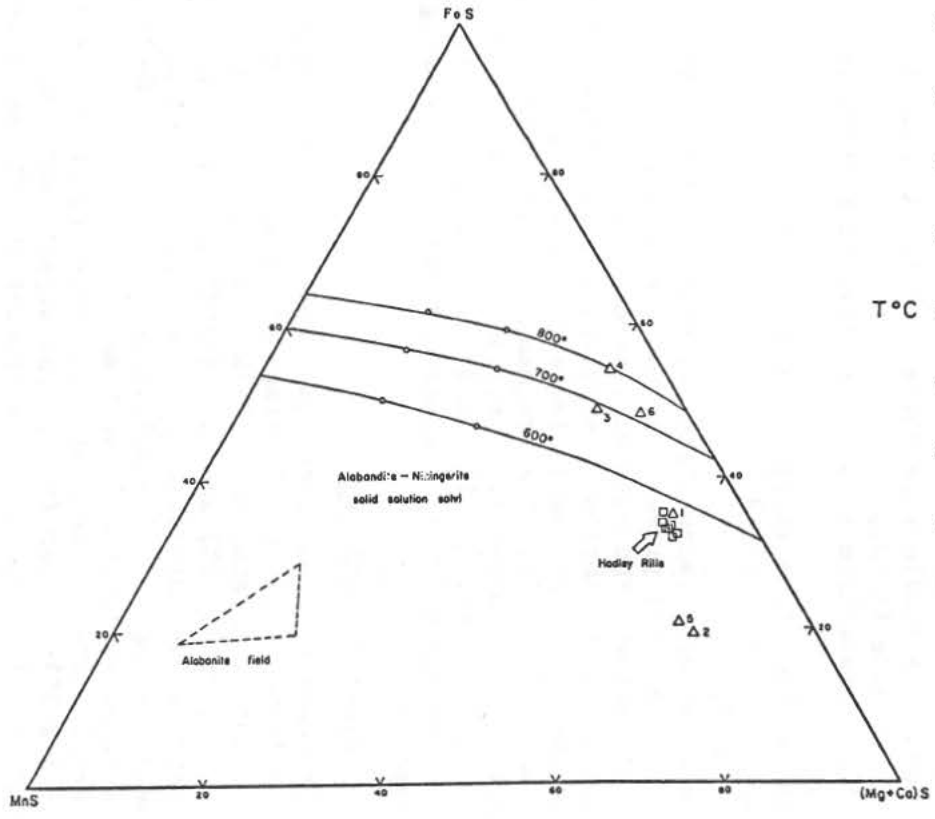

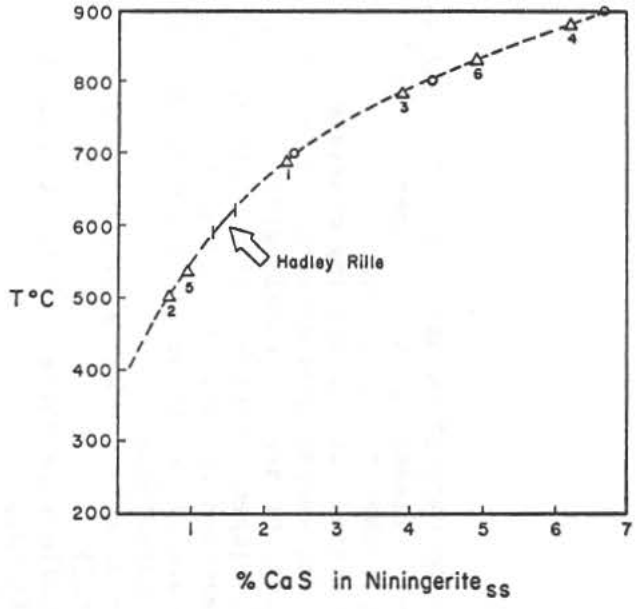

Fig. 2

Fig. 1: Niningerite$_{SS}$ in the Hadley Rille enstatite chondrite. The ternary is from Skinner and Luce (ref. 4). The O's represent compositions of experimental products, and the numbered Δ's are for N_{SS} (ref. 1) in Indach (1); Kota-Kota (2); Adhi-Kot (3); Abee (4); St. Mark's (5); and Saint Sauveur (6). The two latter meteorites are classified as "intermediate", and the remainder as Type 1 (ref. 1). The alabandite field is for Type 2.

Fig. 2: Diagram from Skinner and Luce (ref. 4), showing estimated minimum temperature of formation for N_{SS} in the Hadley Rille enstatite chondrite. Open circles are compositions of experimental products and Δ's are the same as those in Fig. 1.

THE MINERAL CHEMISTRY OF SOME DECOMPOSITION AND REACTION ASSEMBLAGES ASSOCIATED WITH Cr-Zr, Ca-Zr and Fe-Mg-Zr TITANATES. S. E. Haggerty, Geology Department, University of Massachusetts, Amherst, Mass. 01002.

A number of phase assemblages associated with Zr-bearing minerals have been identified in the lunar samples. The assemblages encountered in this study are present in complex intergrowths, or are in "fused" grain boundary contact; and are interpreted to have developed either by solid state decomposition of pre-existing phases, or by reaction of early formed minerals + liquid. The minerals in each assemblage are listed in decreasing order of abundance, with the sample number given in parentheses.

(a) ilmenite + rutile + chromite + zirkelite + baddeleyite (15102)
(b) Zr-armalcolite + ilmenite (15102)
(c) Zr-armalcolite + ilmenite + rutile + chromite + Phase Z1 (15102)
(d) Zr-Cr-armalcolite + ilmenite (15102)
(e) Zr-Cr-armalcolite + Zr-armalcolite + rutile + ilmenite ± chromite ± baddeleyite (61156)
(f) armalcolite (Zr, Nb) + ilmenite + rutile + chromite (14321)
(g) Zirkelite + ilmenite + Phase Z2 (14191)
(h) Zircon + ilmenite (14063)

Other Zr-bearing minerals reported are tranquillityite, Phase Y (?Zirkelite ref 1) and Phase β (2) but these are all present in discrete grains.

Within the context of this volume, the data will necessarily be restricted to those assemblages present in the Apollo 15 samples, and assemblages (a) through (d) only will be considered. These assemblages are present in three fragments in soil (1-2 mm) sample 15102,12. The fragments are laboratory numbered 4, 13 and 19. Fragment 4 is leucocratic, recrystallized and contains plagioclase, pyroxene, olivine, kamacite, troilite and assemblages (a), (b) and (c). Fragments 13 and 19 are maskelynite; fragment 13 contains assemblage (d) and fragment 19 assemblage (b).

Mineral Chemistry

Armalcolite: Two types of Zr-bearing armalcolites (and Phase Z1) are identified (Table 1). The first of these is present in fragments 4 and 19. ZrO_2 ranges from 2.1 to 4.5 wt % (mean of 12 analyses = 3.1%. FeO (14-17%), MgO (6-9%), Cr_2O_3 (≃1%), Al_2O_3 (≃1%), MnO (≃.1%) and SiO_2 (<.5%) are comparable to the ranges of compositions reported for armalcolite in the Apollo 11 samples. TiO_2 (≃68%) is noticeably less than Apollo 11 armalcolite (70-72%) and Nb_2O_5 (0.54%) and Y_2O_3 (0.48%) are reported for the first time.

The second Zr-bearing armalcolite is chemically distinctive; it is characterized by having less MgO (≃2.5%) and FeO (8-9%), and significantly more CaO (3.5%), Cr_2O_3 (7-11%) and ZrO_2 (4-6%). Nb_2O_5 is present (0.41%) but Y_2O_3 is below the detection limit of the electron microprobe. This phase appears to be similar to Phase X (1) and to the minerals reported by other investigators (3,4).

Zirconium-titanates

S. E. Haggerty

Phase Z1: This unidentified Zr-bearing non-silicate is present in assemblage (c). In spite of the relatively small grain size (≈10 μm) a good analytical summation was obtained (Table 1), although the oxide concentrations reported should only be regarded as semiquantitative. The mineral is opaque, dark gray and is of a lower reflectivity than the coexisting Zr-armalcolite. Chemically the mineral is a (Fe Mg)-Zr-titanate; MnO, CaO, Al_2O_3, Cr_2O_3, SiO_2 and Nb_2O_5 total 1.56%. The ratio $R^{+4}O_2/R^{+2}O \simeq 3:1$ and the tetravalent ions are in approximately 1:1 proportions, so that the mineral could be calculated on the basis of a modified armalcolite formula to read $(FeMg)ZrTiO_5$. It should be noted that this suggested formula differs from zirkelite only in the R^{+2} site. This phase and the two Zr-bearing (Zr and Zr-Cr) armalcolites may therefore be expressed in terms of a simplified quaternary system, $MgTi_2O_5$-$CaZrTiO_5$-FeO-Cr_2O_3(Fig. 1), with the following types of substitution: $Ca \rightarrow (FeMg)^{+2}$; $Zr^{+4} \rightarrow Ti^{+4}$; and $(FeCaMg)^{+2} + Ti^{+4} \rightarrow 2(CrAl)^{+3}$, which is similar to the coupled substitution ($Fe^{+2} + Ti \rightarrow 2Fe^{+3}$) that takes place in the terrestrial pseudobrookite ($Fe_2^{+3}TiO_5$-$Fe^{+2}Ti_2O_5$) series.

Zirkelite: This mineral is present in assemblage (a) and was identified only in fragment 4 in close association with baddeleyite. The zirkelite is similar in major element chemistry (Table 1) to the lunar zirkelites reported by Busche et al (5).

Baddeleyite: In common with zirkelite, baddeleyite is present only in fragment 4. This mineral is of a somewhat unusual composition (Table 1) with each of the oxides TiO_2, Y_2O_3 and FeO present in concentrations of >1%. Nb_2O_5 is present (0.6%), and the oxides of Ca, Mn, Mg, Cr, Al and Si were detected in concentrations of <.5%.

Rutile: TiO_2 is present in assemblages (a) and (c) in fragment 4; analyses were possible only in assemblage (a) where large irregular areas of TiO_2 are present. In assemblage (c) the rutile is "exsolved" from ilmenite and is present in <5 μm thick oriented lamellae. ZrO_2 (1.8%), Nb_2O_5 (0.7%), FeO (0.5%) and Cr_2O_3 (0.5%) are the major dilutants.

Ilmenite: A comparison of ilmenite compositions in assemblages (a) through (d) with coexisting discrete ilmenite shows that the ilmenite in the intergrowths generally have higher MgO (6-7%) contents, and also that ZrO_2 (0.1%) and Nb_2O_5 (0.3%) are present.

Chromite: Spinels, like rutile, are present in two modes and are in close association: (1) in thick oriented lamellae in ilmenite; and (2) in smaller irregular grains enclosed by, or in contact with, TiO_2 or Zr-armalcolite. Both spinel types are essentially similar in composition and may be classified as Mg-Ti-aluminian-chromite. $ZrO_2 + Nb_2O_5$ are present in concentrations of <.1%.

Conclusions

Detailed interpretation of the phase assemblages described in this report are difficult without the inclusion of data for assemblages (e) through (h) from Apollo 14 and 16. Critical differences are present in the partitioning of Zr and Nb and for this reason only preliminary conclusions applicable to the Apollo 15 assemblages follow.

Assemblage (a): The zirkelite-baddeleyite intergrowths are considered to be

Zirconium-titanates

S. E. Haggerty

partial decomposition products of Cr-Zr-armalcolite; Mg, Cr and Fe enter $FeTiO_3$-$MgTiO_3$ solid solution and excess TiO_2 + Cr_2O_3 "exsolve" from ilmenite-giekielite$_{ss}$ to form rutile + chromite.
Assemblage (b): Zr-armalcolite + liquid → $(FeTiO_3$-$MgTiO_3)_{ss}$
Assemblage (c): Partial decomposition of Zr-armalcolite → Zr-armalcolite (residual) + TiO_2(Zr) + Phase Z1 (FeMgZrTi) + (ilmenite-giekeilite)$_{ss}$; or alternative complete decomposition of Cr-Zr-armalcolite which is more likely because of the associated chromite.
Assemblage (d): Similar to assemblage (b).

References

(1) Peckett, A., Phillips, R., and Brown, G. M., (1972). New Zirconium-rich minerals from Apollo 14 and 15 lunar rocks. Nature 236, 215-217.

(2) Haines, E. L., Albee, A. L., Chodos, A. A., and Wasserburg, G. J., (1971) Uranium-bearing minerals of Lunar rock 12013. Earth and Planet. Sci. Lett. 12, 145-154.

(3) Christophe-Michel-Levy, M., Levy, C., and Pierrot, R., (1972) A new titanium and zirconium oxide from the Apollo 14 samples. Proc. 3rd Lunar Sci. Conf., Geochem. et Cosmoch. Acta (M.I.T. Press), in press.

(4) Steele, I. M., and Smith, J. V., (1972) Occurrence of diopside and Cr-Zr-armalcolite on the Moon. Nature Phys. Sci. 237, 105-106.

(5) Busche, F. D., Prinz, M., Keil, K., and Kurat, G., (1972) Lunar Zirkelite: A uranium-bearing phase. Ibid., in press.

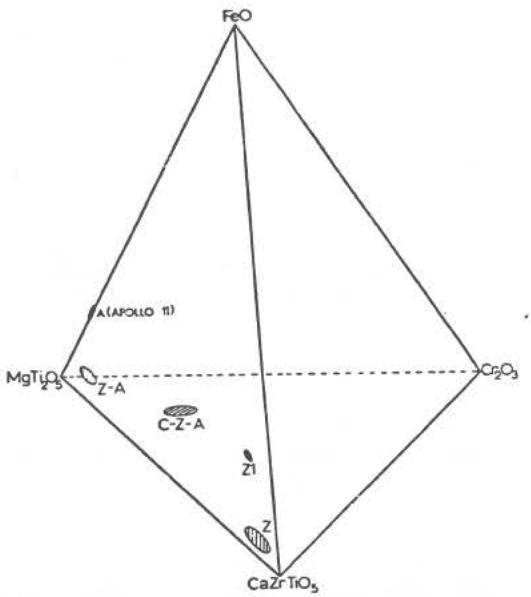

Fig. 1

Zr-bearing minerals in the system $MgTi_2O_5$ ("Karrooite")-$CaZrTiO_5$ (Zirkelite)-FeO-Cr_2O_3. A = armalcolite; C-Z-A = Cr-Zr-armalcolite; Z1 = a new mineral; Z = zirkelite.

Zirconium-titanates

S. E. Haggerty

Table 1 Zr-bearing Minerals

	1	2	3	4	5	6
FeO	16.09	9.33	22.02	5.63	1.22	0.47
MgO	7.06	2.31	4.33	0.89	0.09	0.15
MnO	0.11	0.13	0.30	0.15	0.17	0.01
CaO	0.63	3.40	0.32	7.32	0.12	0.28
Al_2O_3	1.62	1.49	0.15	0.80	0.10	0.10
Cr_2O_3	1.31	10.31	0.29	0.68	0.14	0.40
Y_2O_3	0.48	-	-	4.21	1.47	0.14
TiO_2	69.73	66.52	42.26	35.79	2.94	95.59
ZrO_2	2.06	6.01	30.17	41.25	93.49	1.82
SiO_2	0.32	0.23	0.24	0.28	0.29	0.20
Nb_2O_5	0.45	0.37	0.25	0.72	0.65	0.69
	99.86	100.10	100.33	97.72*	100.68	99.85

Atomic Proportions‡

Fe	0.486	0.286	0.755	0.206	0.021	0.005
Mg	0.380	0.126	0.265	0.058	0.003	0.003
Mn	0.003	0.004	0.009	0.005	0.003	0.000
Ca	0.024	0.134	0.010	0.343	0.003	0.004
Al	0.069	0.064	0.006	0.041	0.002	0.002
Cr	0.037	0.299	0.009	0.023	0.002	0.004
Y	0.009	-	-	0.098	0.016	0.001
Ti	1.892	1.834	1.331	1.176	0.045	0.973
Zr	0.036	0.108	0.623	0.879	0.918	0.012
Si	0.012	0.009	0.009	0.012	0.006	0.003
Nb	0.010	0.008	0.016	0.019	0.008	0.006
	2.958	2.872	3.033	2.860	1.027	1.013

(1) Zr-armalcolite; (2) Cr-Zr-armalcolite; (3) Phase Z1;
(4) Zirkelite; (5) Baddeleyite; (6) Rutile.
* REE detected in spectral scans.
‡ Analyses (1)-(4) calculated on basis of 5 oxygens;
analyses (5)-(6) on basis of 2 oxygens.

CHEMICAL CHARACTERISTICS OF SPINELS IN SOME APOLLO 15 BASALTS.

S. E. Haggerty, Geology Dept., Univ. of Mass., Amherst, Mass. 01002.

Abstract. Compositional data for spinels in the chromite-hercynite-ulvöspinel system from three large basalts (15058, 15535, 15555) and for spinels in 48 basalt particles (1-2 mm) in four soil samples (15032, 15042, 15102, 15602) show: (1) that the range of compositions are comparable to those of spinels in Apollo 12 basalts; (2) that the spinel series is complete between 0.75 $FeCr_2O_4$ 0.25 $FeAl_2O_4$ and Fe_2TiO_4; (3) that the Apollo 12 bimodal distribution is present insofar as chromite-rich and ulvöspinel-rich phases are more commonly present than compositions intermediate between these two end members; (4) well defined ionic relationships exist for those cations displaying high octahedral site preference energies in the spinel structure (viz. Cr vs Al and Ti vs Cr + Al); (5) cations displaying low site preference energies (Fe^{+2}, Mg) show poor correlation; and (6) the absence of a simple relationship between the divalent ions (Fe^{+2} and Mg), and the paucity (<10% of 356 analyses) of intermediate compositions suggests a strong dependence on the structural stability of intermediate members of a normal (hercynite, chromite) - inverse (ulvöspinel) solid solution series.

Spinel chemistry.

A representative selection of the 356 electron microprobe analyses determined in this study are listed in Table 1. Sample 15555 is among the few basalts that contain spinels whose compositions span the entire normal-inverse series (Fig. 1). In the two remaining large basalts 15058 contains only Cr-Al-ulvöspinel, whereas 15535 displays the typical bimodal ulvöspinel-rich and chromite-rich distribution (Fig. 2) but also contains a few spinels of intermediate composition. Of the 48 basaltic soil fragments, 16 contain only Cr-Al-ulvöspinel, 23 exhibit the 15535 pattern and the remaining 9 particles contain Al-chromian ulvöspinel plus Mg-aluminian-chromite. In the latter 9 fragments, the ulvöspinel-rich component contains the low intensity reduction assemblage ilmenite + Fe, and the trend towards intermediate compositions is therefore accomplished by solid-state reequilibration. In general the range of compositions, specifically the degree of solid solubility, relative Mg and Al enrichment factors and the crystallization trends (illustrated in the multicomponent spinel prisms Figs. 1 and 2) are in close agreement with spinels in basalts from the Apollo 12 site.

Substitutional relationships.

Projections for each of the two spinel prisms are illustrated in Figures 3a-b and 4a-b respectively. The five major oxides displayed in each of two projections show that the divalent (FeO/FeO + MgO) ratio as a function of the TAC ratio ($TiO_2/TiO_2 + Al_2O_3 + Cr_2O_3$) are comparable when sample 15555 is compared with the remaining data. The divalent-trivalent ($Cr_2O_3/Cr_2O_3 + Al_2O_3$) ratio relationship in contrast, is restricted in 15555 and the more typical Apollo 12 and 14 pattern is displayed by the soil fragments and the remaining large basalts.

Apollo 15 Spinels

S. E. Haggerty

Considering the trivalent and divalent ions separately we find (a) that in general there is a good positive correlation between Cr and Al; (b) that the Cr/Al ratios are limited to values between 2:1 and 3:1 (Fig. 5a-b); and (c) that with increasingly higher Ti contents the ratio of Cr/Al decreases dramatically from 2:1 to <1:1 for values of Cr <2 formula units. For the divalent (Fe vs Mg) relationship the correlation is poor to totally incoherent for the soil fragments and for 15058 and 15535 (Fig. 6a). The same holds true for sample 15555 but three distinct linear slopes do emerge if the Ti content of the spinels are also considered (Fig. 6b); the slopes decrease and the data become more scattered with decreasing Ti content. Superimposing the high and low Ti curves on the soil fragments (Fig. 6a) shows that there is a dependence on the Ti content and that this dependence increases with increasing crystallization, increasing Fe_2TiO_4 content and decreasing $FeCr_2O_4$ - $FeAl_2O_4$ contents.

The differences between the divalent and trivalent substitutional trends may be due, in part, to the site preference energies of Cr, Al, Fe^{+2}, and Mg. Cr and Al have high B site preference, whereas Fe^{+2} and Mg have relatively much lower site preference energies, with Fe^{+2} favoring B site coordination and Mg A site coordination respectively. Trivalent substitution is restricted therefore to 6-fold coordination whereas the divalent ions substitute in either 4 or 6 fold coordination. This and the fact that the character of the crystallizing spinel changes from all A site divalent ions in chromite-hercynite to A + B site divalent ions in ulvöspinel may account for the observed scatter.

The straight line shown in Figure 7 represents the theoretical concentrations present for these elements in the spinel structure and is extrapolated for intermediate members between ulvöspinel, with Ti = 8 ($^{IV}Fe_8{}^{VI}Fe_8{}^{VI}Ti_8O_{32}$) and chromite-hercynite, with Cr + Al = 16 ($^{IV}Fe_8{}^{VI}(Cr+Al)_{16}O_{32}$). The data in Fig. 7 correlate with the theoretical octahedral-line but <5% of the analyses are coincident; the majority show a negative displacement and <1% show a positive placement. In recalculating the atomic proportions it is assumed that titanium and chromium are in the Ti^{+4} and Cr^{+3} valency states respectively. If it is assumed that a significant part of each of these are in the Ti^{+3} and Cr^{+2} states, an even greater negative departure would result. Although we cannot conclude that Ti^{+3} and Cr^{+2} are absent, we can conclude that if these lower valency states are present, their respective concentrations must be very small.

Figure 7 illustrates a paucity of data for values of Cr + Al between 6 and 10 formula units and for values of Ti between 2 and 4 formula units. Less than 10% of the data occupy this intermediate compositional region and this is further illustrated in Figures 3 and 4 for the divalent-TAC relationship. The Apollo 12 compositional gap was defined on the basis of 109 published analyses from 10 laboratories as having TAC values between 0.31 and 0.49 (1). Within the present study 15 of 116 analyses in 15555, and 12 of 240 analyses in the remaining data, equivalent to 12.9 and 5.0% respectively, occupy the Apollo 12 gap. Of the 15 analyses in 15555, 10 data points were obtained at the grada-

tional contacts of two optically contrasting spinels (e.g. core-mantle overgrowths) which demonstrates that in most cases intermediate compositions develop as a result of the reaction of early formed chromite + liquid. The remaining 5 data points are for homogeneous grains and although no chromian spinel cores are visible in the plane of the analytical surface, the probability that these were once present is even too high.

Conclusions.

Spinels (chromite-hercynite-ulvöspinel series) in basalts at the Apollo 15 site are optically, texturally and compositionally comparable to spinels in basalts at the Apollo 12 site. The bimodal distribution of spinel compositions (ulvöspinel-rich and chromite rich) present at the Apollo 12 site and present in the majority of lunar basalts is reflected in the Apollo 15 data. Less than 10% of the 356 electron microprobe analyses determined in this study have compositions within the defined Apollo 12 miscibility gap.

Intermediate members of the spinel series may form by one of the three following processes: 1) primary precipitates (Apollo 11, and rare in Apollo 12 and 15); 2) incomplete reaction of early formed Mg-aluminian-chromite with liquid, resulting in intermediate compositions at the gradational interface of core (Cr-rich)-mantle (Ti-rich) boundaries (probably less common than generally believed because of the analytical uncertainties involved in an integrated and overlapping electron beam); and 3) reequilibration of Cr-Al-ulvöspinel by intense subsolidus reduction (rare - Apollo 14 only).

The low incidence of intermediate compositions may be due to a solvus below 1000°C for the join $FeCr_2O_4$ - Fe_2TiO_4. However, the strong correlations shown by cations in constant A site positions (Cr, Al, Ti) for all members of the series and the lack of correlation shown by the divalent ions, which evolve from all A site positions to A + B site positions during the course of crystallization, suggests that intermediate members, which have neither high normal nor high inverse coordination characteristics, are structurally metastable.

References

(1) Haggerty, S. E., (1971) Compositional variations in lunar spinels. Nature Phys. Sci. 233, 156-160.

Table 1 Caption

Analyses 1-20 are for spinels in sample 15555. Analyses 1-10 are discrete crystals ranging in color from dark-gray to tan. Analyses 11-15 are for a gradational core-mantle relationship, and 16-20 are for a crenulate boundary contact between bluish-gray Al-titanian-chromite and pink chromian-ulvöspinel. Analyses 21-30 are for discrete primary crystals in sample 15535. Analyses for each group are listed in increasing values of TAC ($TiO_2/TiO_2+Al_2O_3+Cr_2O_3$) and represent increasing degrees of crystallization.

Apollo 15 Spinels

S. E. Haggerty

OXIDES	1	2	3	4	5	6	7	8	9	10
TiO_2	4.10	4.58	6.10	10.01	13.01	18.12	21.10	26.40	28.14	31.56
Cr_2O_3	46.28	43.79	42.79	37.60	29.60	25.57	19.85	13.36	9.16	4.84
MnO	0.44	0.49	0.46	0.41	0.42	0.49	0.44	0.43	0.45	0.44
FeO	35.21	30.74	34.35	40.29	42.76	46.12	50.11	53.61	56.19	61.42
MgO	2.35	6.10	3.35	2.01	3.07	2.72	2.20	2.15	1.58	0.40
Al_2O_3	11.76	12.65	11.35	9.66	10.23	6.23	5.03	3.81	2.82	1.95
SiO_2	0.19	0.56	0.41	0.19	0.46	0.36	0.31	0.28	0.45	0.33
CaO	0.03	0.11	0.20	0.03	0.11	0.17	0.29	0.04	0.23	0.02
Total	100.37	99.01	99.01	100.30	99.65	99.87	99.32	99.97	99.02	100.95
	Atomic Proportions Based on 32 Oxygen Atoms									
Ti	0.854	0.937	1.275	2.108	2.735	3.875	4.598	5.709	6.210	6.925
Cr	10.103	9.417	9.402	8.343	6.540	5.748	4.538	3.037	2.125	1.116
Mn	0.103	0.113	0.108	0.097	0.099	0.118	0.108	0.105	0.112	0.109
Fe	8.153	6.993	7.985	9.435	9.995	10.968	12.019	12.891	13.790	14.987
Mg	0.970	2.473	1.388	0.839	1.279	1.153	0.948	0.921	0.691	0.174
Al	3.839	4.057	3.719	3.189	3.371	2.089	1.715	1.291	0.976	0.671
Si	0.053	0.152	0.114	0.053	0.129	0.102	0.090	0.081	0.132	0.096
Ca	0.009	0.032	0.060	0.009	0.033	0.052	0.090	0.012	0.072	0.006
Total	24.109	24.174	24.050	24.075	24.181	24.105	24.097	24.047	24.108	24.084
TAC	0.066	0.075	0.101	0.175	0.246	0.363	0.459	0.606	0.701	0.823

OXIDES	11	12	13	14	15	16	17	18	19	20
TiO_2	4.42	7.51	21.86	24.57	28.59	4.02	9.77	16.07	19.05	20.64
Cr_2O_3	44.96	39.80	19.24	15.10	8.06	46.09	38.40	26.95	23.83	21.18
MnO	0.41	0.40	0.41	0.37	0.41	0.44	0.44	0.44	0.38	0.40
FeO	38.11	42.62	53.02	56.13	59.49	34.63	39.57	44.52	46.49	48.15
MgO	0.78	0.66	0.63	0.60	0.56	3.13	2.91	2.77	2.82	2.71
Al_2O_3	11.29	10.41	4.19	3.33	2.49	11.95	9.69	6.97	5.94	5.92
SiO_2	0.19	0.19	0.19	0.21	0.21	0.22	0.33	0.31	0.35	0.40
CaO	0.03	0.02	0.02	0.02	0.02	0.01	0.13	0.18	0.14	0.10
Total	100.19	101.62	99.57	100.35	99.85	100.49	101.24	98.20	99.00	99.51
	Atomic Proportions Based on 32 Oxygen Atoms									
Ti	0.935	1.582	4.821	5.408	6.351	0.832	2.027	3.484	4.105	4.428
Cr	10.001	8.811	4.462	3.494	1.882	10.027	8.377	6.142	5.398	4.776
Mn	0.098	0.095	0.102	0.092	0.103	0.103	0.103	0.107	0.092	0.097
Fe	8.968	9.982	13.002	13.738	14.695	7.970	9.132	10.734	11.141	11.487
Mg	0.327	0.275	0.275	0.262	0.247	1.287	1.197	1.190	1.204	1.152
Al	3.745	3.437	1.448	1.149	0.867	3.874	3.152	2.369	2.007	1.991
Si	0.053	0.053	0.056	0.061	0.062	0.061	0.091	0.089	0.100	0.114
Ca	0.009	0.006	0.006	0.006	0.006	0.003	0.038	0.056	0.043	0.031
Total	24.138	24.241	24.172	24.210	24.213	24.156	24.117	24.171	24.090	24.076
TAC	0.073	0.130	0.483	0.571	0.730	0.065	0.169	0.321	0.390	0.432

OXIDES	21	22	23	24	25	26	27	28	29	30
TiO_2	3.85	4.46	8.01	13.85	21.65	24.04	25.25	27.40	29.96	31.47
Cr_2O_3	45.25	45.34	39.30	30.54	19.82	16.72	13.91	11.32	7.38	5.79
MnO	0.32	0.29	0.33	0.33	0.34	0.38	0.32	0.36	0.38	0.37
FeO	36.28	33.92	38.74	42.71	49.17	52.65	56.23	55.74	58.82	60.60
MgO	2.50	4.02	2.73	3.23	3.14	2.11	0.82	1.91	0.84	0.54
Al_2O_3	11.22	11.30	10.03	8.04	5.33	4.31	3.68	3.08	2.46	2.04
SiO_2	0.27	0.40	0.27	0.48	0.64	0.28	0.13	0.41	0.21	0.30
CaO	0.01	0.22	0.02	0.33	0.30	0.03	0.01	0.17	0.04	0.11
Total	99.70	99.95	99.43	99.51	100.39	100.52	100.35	100.39	100.09	101.22
	Atomic Proportions Based on 32 Oxygen Atoms									
Ti	0.617	0.925	1.695	2.961	4.603	5.180	5.536	5.904	6.668	6.865
Cr	10.100	9.880	8.744	6.864	4.430	3.787	3.206	2.564	1.671	1.328
Mn	0.077	0.068	0.079	0.079	0.081	0.092	0.079	0.087	0.092	0.091
Fe	8.330	7.819	9.119	9.917	11.626	12.615	13.709	13.596	14.328	14.700
Mg	1.052	1.651	1.145	1.369	1.323	0.901	0.356	0.816	0.359	0.232
Al	3.734	3.672	3.328	2.695	1.777	1.456	1.265	1.040	0.831	0.698
Si	0.076	0.110	0.076	0.136	0.181	0.080	0.038	0.117	0.060	0.087
Ca	0.003	0.065	0.006	0.101	0.091	0.009	0.003	0.052	0.012	0.034
Total	24.189	24.189	24.192	24.123	24.112	24.119	24.191	24.176	24.021	24.036
TAC	0.064	0.073	0.140	0.264	0.463	0.533	0.589	0.656	0.759	0.801

Apollo 15 Spinels

S. E. Haggerty

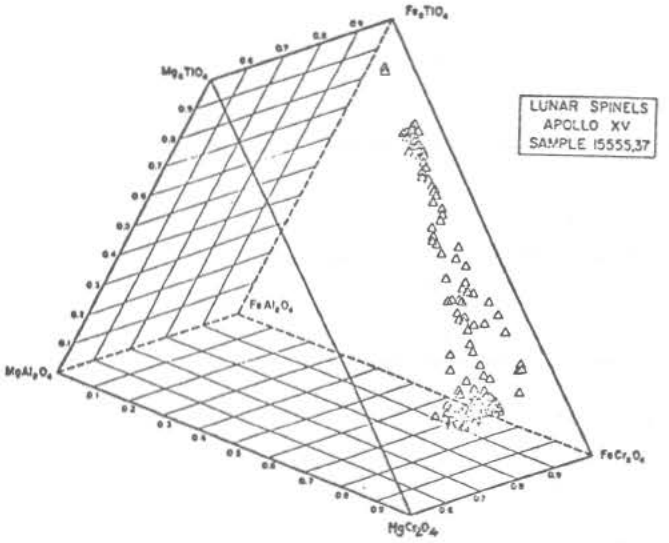

Fig 1

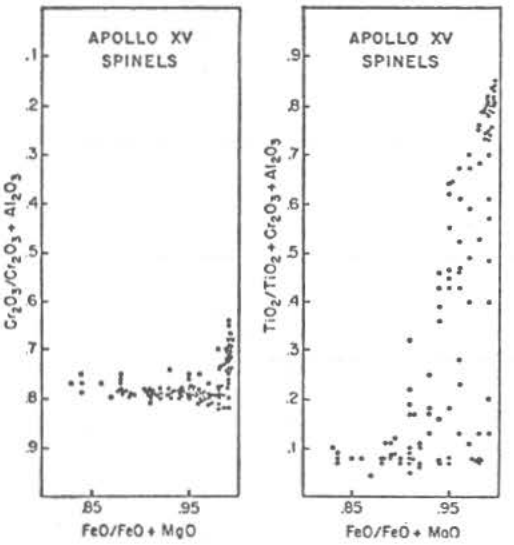

Fig 3a

Fig 3b

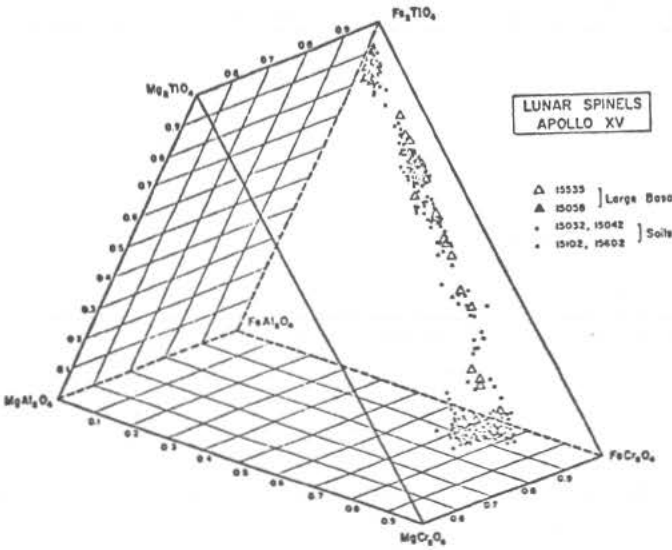

Fig 2

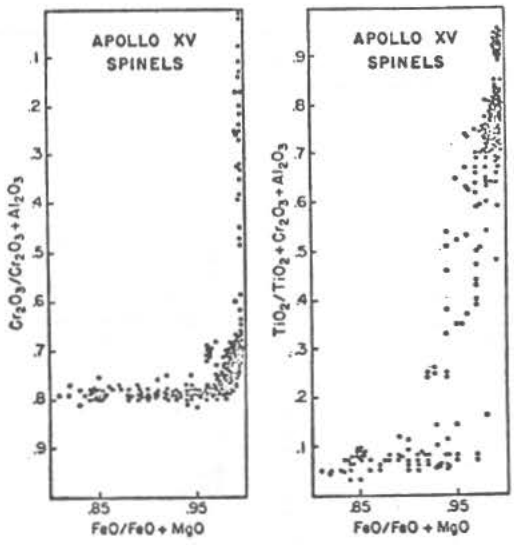

Fig 4a

Fig 4b

Apollo 15 Spinels

S. E. Haggerty

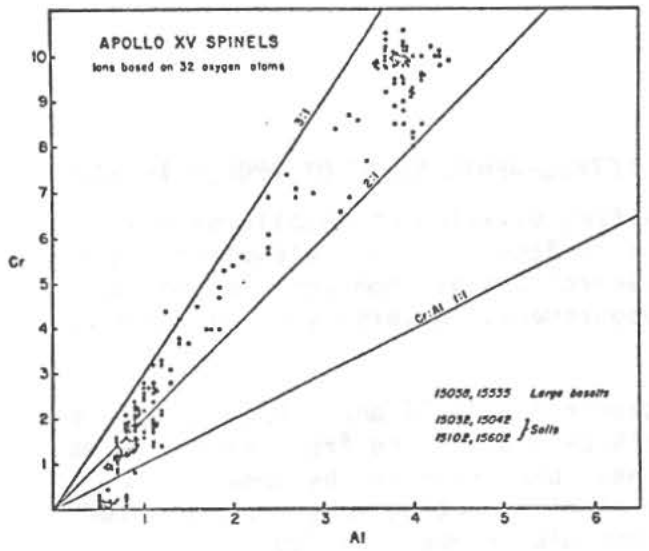

Fig 5a

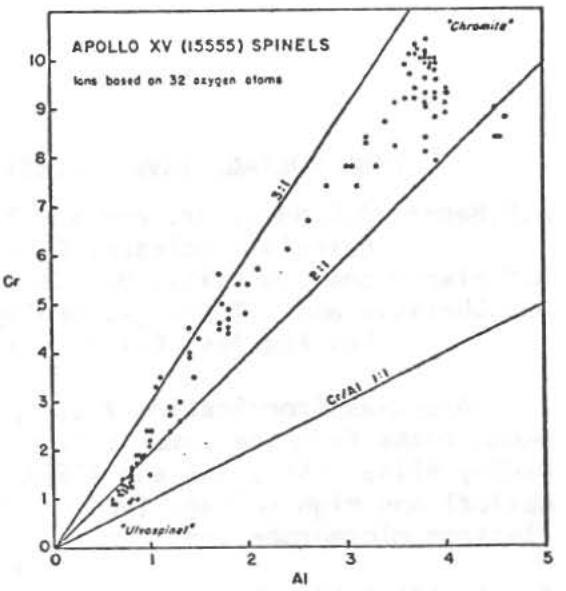

Fig 5b

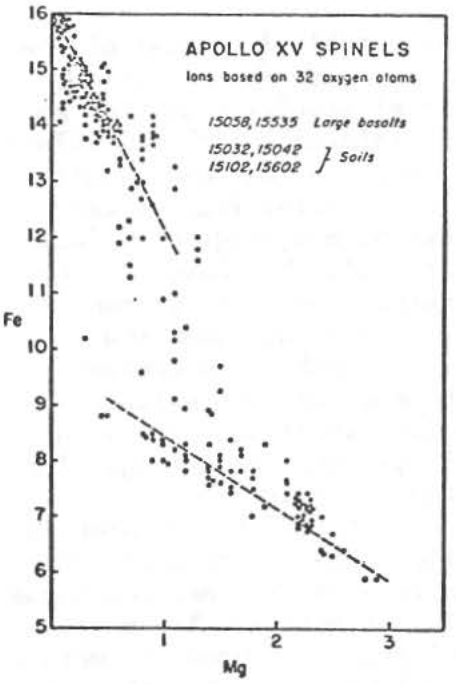

Fig 6a

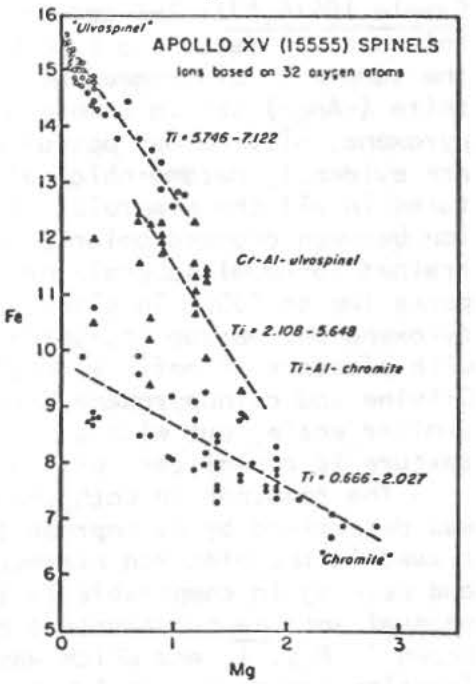

Fig 6b

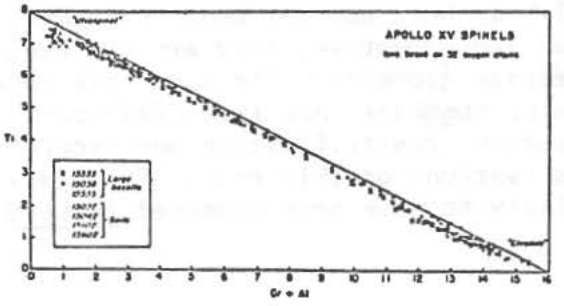

Fig 7

HIGH VOLTAGE (HVEM) ELECTRON PETROGRAPHIC STUDY OF APOLLO 15 ROCKS

A.H.Heuer, G.L.Nord, Jr. and S.V.Radcliffe, Division of Metallurgy and Materials Science, Case Western Reserve Univ., Cleveland, Ohio
R.M.Fisher and J.S.Lally, U.S.Steel Research Center, Monroeville, Penna.
J.M.Christie and D.T.Griggs, Geology Department, University of California, Los Angeles, California

Breccias from Station 7 at Spur Crater (15418,47 and 15455,13) and igneous rocks from the same station (15415,25 and 46) and from Station 9a at Hadley Rille (15555,163 and 15557,36) have been examined by comparative optical and high voltage (up to 1 Mev) electron petrography, supplemented by electron microprobe and scanning electron microscope techniques.

A. BRECCIAS

Sample 15418,47: The optical character differs considerably from that of the thin-section described by other investigators (1,2). At low magnification, the sample is of fragmental character, with large (1cm) angular clasts of anorthite (~An_{93}) set in a more heterogeneous matrix, containing anorthite, clinopyroxene, olivine and opaque minerals. At higher magnification the textures are evidently metamorphic, with extensive fine-scale recrystallization textures in all the minerals. The large anorthite areas have aggregate extinction between crossed polarizers, resembling single crystals, but have a fine-grained (5-20μm) subgrain or polycrystalline structure. They contain many pores (up to 100μm in size), commonly distributed in planes and some small pyroxene and opaque inclusions. The smaller areas of anorthite intermixed with clusters of mafic minerals in the groundmass have a similar texture. Olivine and clinopyroxene also show sub-grain or polycrystalline texture on a similar scale, but with a few larger single crystal pyroxenes remaining. The texture is reminiscent of that of a very fine-grained hornfels.

The feldspar in both the large "clasts" and the "matrix" of this breccia was determined by microprobe to be similar chemically. The substructures observed in the electron microscope within the anorthite were very heterogeneous and were again comparable in the large clasts and in the matrix. The most unusual and new substructure observed was a "spherulitic" or fibrous structure, shown in Fig. 1, and which was widely distributed. Although sufficient diffraction contrast experiments have not yet been performed to allow a rigorous characterization of these substructures, they are believed to be a devitrification product. Their presence (combined with a notable absence of glass, even at a sub-microscopic scale) suggests that these feldspars were glassy at some stage and underwent subsequent devitrification and recrystallization, consistent with the optical observations on this rock. The glass from which this product originated is likely to have been produced in situ by shock.

A second unusual feature in the anorthite was a high density of intracrystalline pores, ranging in size from ~25μm (visible optically) down to ~100Å. (These pores were also present in the other minerals in the matrix and are illustrated below.) They could have arisen from volatization of alkalis or other volatile species, or possibly as a result of the density difference between a glass and its devitrification product. As with virtually all plagioclases examined in the electron microscope, submicroscopic twins were abundant (Fig.2). The resorption of the twins shown is further evidence of extensive recovery (recrystallization). No regions of high dislocation density were found in the anorthite.

In contrast, the olivine showed extensive areas of very high dislocation density (Figs. 3 and 4). Evidence for recovery (Fig. 3) and primary recrystallization (Fig. 4) were abundant, as well as the submicroscopic porosity noted above. Recrystallization was also prevalent in the pyroxene; the recrystallized microstructure here was different from that in olivine, in that many new grains had nucleated (Fig. 5) rather than the growth of a few large grains as in olivine (Figs. 3 and 4). Pores and regions of heavy deformation were also abundant (Fig. 6).

Sample 15455,13: This "black and white" rock is seen in thin section to consist of a porous coarse-grained brecciated anorthosite fragment with ~10% orthopyroxene in contact with a dark non-porous fine-grained olivine-bearing annealed microbreccia. Some of the latter has penetrated the anorthosite fragment. Examination in reflected light shows a narrow zone of low porosity in the anorthosite fragment where it contacts the microbreccia. Our preliminary electron microscopy results indicate that the brecciated anorthosite clast is bonded with glass (Fig. 7) and that the narrow contact rim contains a higher proportion of glass, accounting for the reduced porosity there. Using a scanning electron microscope with a non-dispersive detector, no compositional difference was detected between the glass and the anorthite. In contrast, no glass has been seen to date in the dark microbreccia, the texture consisting of a mixture of submicron recrystallized grains and highly deformed grains, similar to the submicroscopic textures of the olivines and pyroxenes of 15418.

B. IGNEOUS ROCKS

Samples 15415,25 and 15415,46: Adequate optical characterization of this anorthosite has been given by other workers (3); chip 46 contains most of the features described in these reports. We have reported HVEM studies of the c-domain structure in the anorthite, as well as evidence for deformation and recovery (dense arrays of dislocations, subgrains, etc.)(4). This deformation structure was quite inhomogeneous, however.

Sample 15555,163: This sample is a coarse-grained olivine basalt with equigranular texture, consisting of approximately 20% olivine, 40% clinopyroxene, 35% plagioclase and 5% opaques and cristobalite. The olivine (~1mm) and strongly zoned pyroxene crystals (1-2mm) (pigeonite cores, augite rims) are poikilitically included in the large (2-5mm long) plagioclase, which showed little evidence of zoning. The rock is extensively fractured.

In the electron microscope, the olivine in this rock is generally devoid of substructure, with the exception of a modest dislocation density (Fig. 8). The dislocations appear to have formed during crystallization or cooling and are not indicative of shock deformation. Contrast experiments are consistent

with, but do not prove, a Burger's vector of a[100] for the dislocations shown in Fig. 8.

Exsolution on (100)(major) and (001)(minor) is present in all clinopyroxenes examined, but is quite heterogeneous. Within the pigeonite regions examined, the M-T APB's were ~700Å, somewhat larger than the APB's in pigeonite in 12038 (5). The scale of the exsolution lamellae was also slightly larger in this sample than in the Apollo 12 basalts.

The b-type domain structure in plagioclase is rather small, averaging 900Å. No unambiguous evidence of exsolution could be obtained.

Sample 15557,36: This is a finer-grained olivine basalt with intergranular texture. Relatively large (~1.5mm) anhedral olivine 15% and plagioclase 35% (0.5-1.5mm) are associated with small (0.1mm) anhedral clinopyroxenes and 10% opaque minerals.

Only pyroxene and plagioclase have been examined to date by HVEM in this sample. The plagioclase is zoned and displays a marked variation in the size of the b-domains with position in the crystal. Representative micrographs from a 30μm sequence illustrating this phenomenon are shown in Fig. 9; a systematic variation from 400Å to 20,000Å was found in this particular sequence.

The domain size is smallest in the central, more calcic region of the crystal, consistent with our original observations and interpretation (5) that the b-domains decrease in size with increasing calcium content in plagioclase. The reason for this variation is believed to be the decrease in the temperature of the ordering transformation with decreasing Ca content, which results in more difficult nucleation of the ordered domains and larger domain sizes. This again suggests the possible utility of the scale of the b-domains as an indicator of cooling rates, but also emphasizes the importance of knowing the local composition accurately when comparisons are made between different samples. The substructures of the pyroxenes in this sample were quite similar to those observed in 15555.

REFERENCES

1. Apollo 15 Prelim. Sci. Rpt. - NASA SP-289, p.6-12, (1972).
2. Lunar Samp. Int. Cat., Apollo 15, p.179-181 (1971).
3. James, O. B., Science 175, 432-5 (1972).
4. Lally, S., Fisher, R.M., Christie, J.M., Griggs, D.T., Heuer, A.H., Nord, G.L.,Jr., Radcliffe, S.V, Proc. 3rd Lunar Sci. Conf., (MIT Press), (1972). Heuer, A.H., Lally, J.S., Christie, J.M., Radcliffe, S.V., Phil. Mag., 26, 465 (1972). Heuer, A.H., Nord, G.L.Jr., Lally, J.S., Christie, J.M., Proc. NATO Conf. Feldspars, (1972).
5. Christie, J.M., Lally, J.S., Heuer, A.H., Fisher, R.M., Griggs, D.T., Radcliffe, S.V., Proc. 2nd Lunar Sci. Conf. Geochim. Cosmochim Acta, Suppl.2, Vol. 1, 69-89 (1971).

HIGH VOLTAGE ELECTRON PETROGRAPHIC

Heuer, et al.

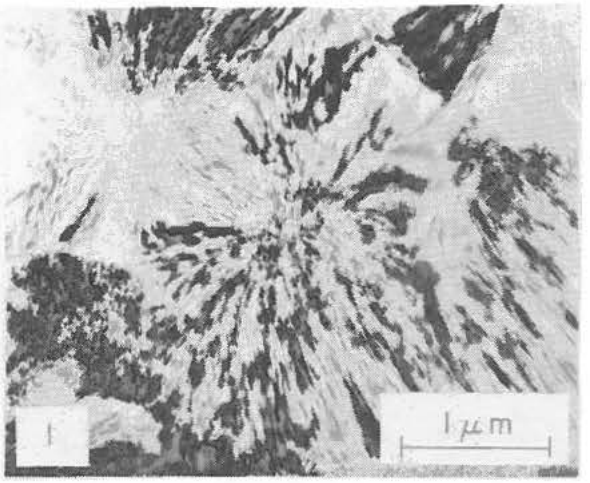

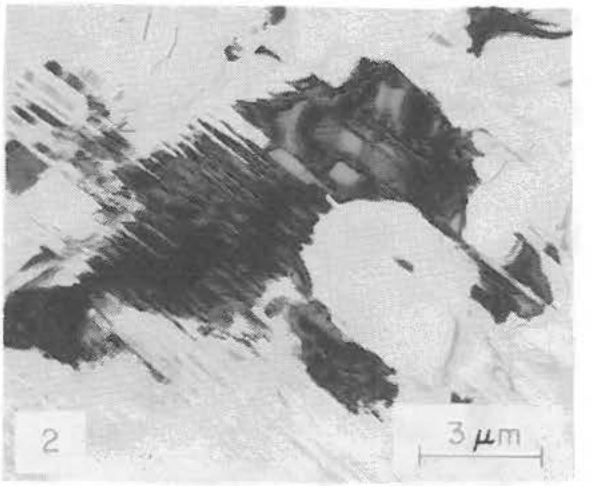

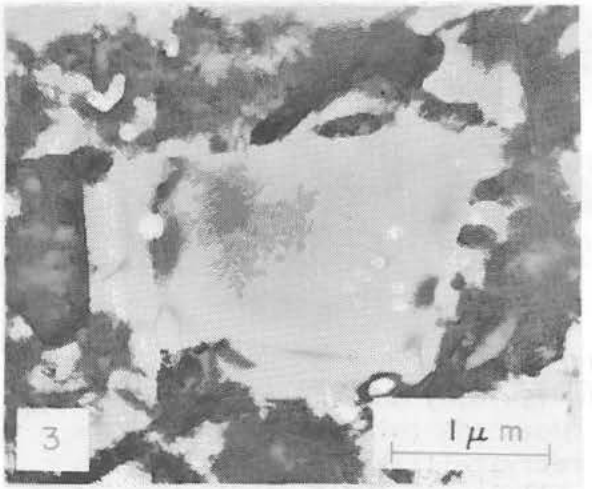

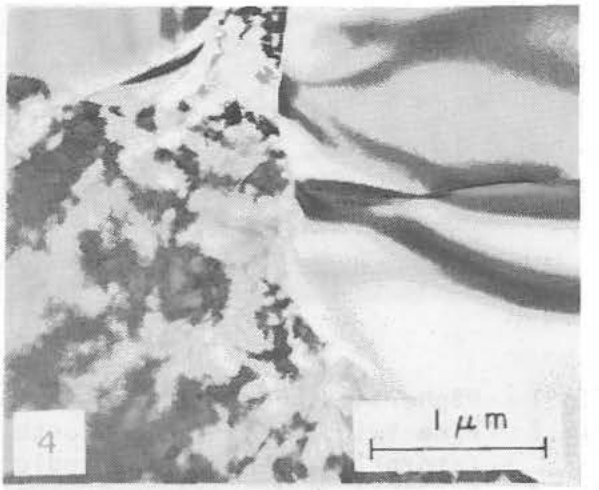

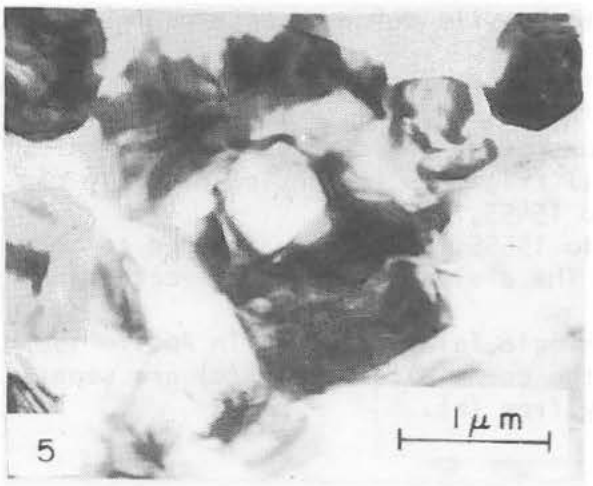

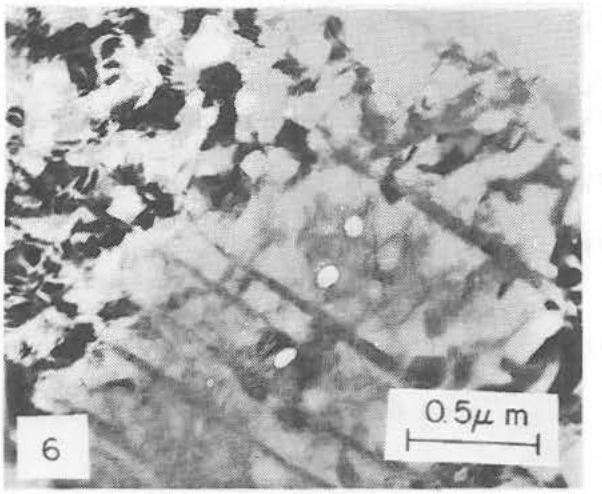

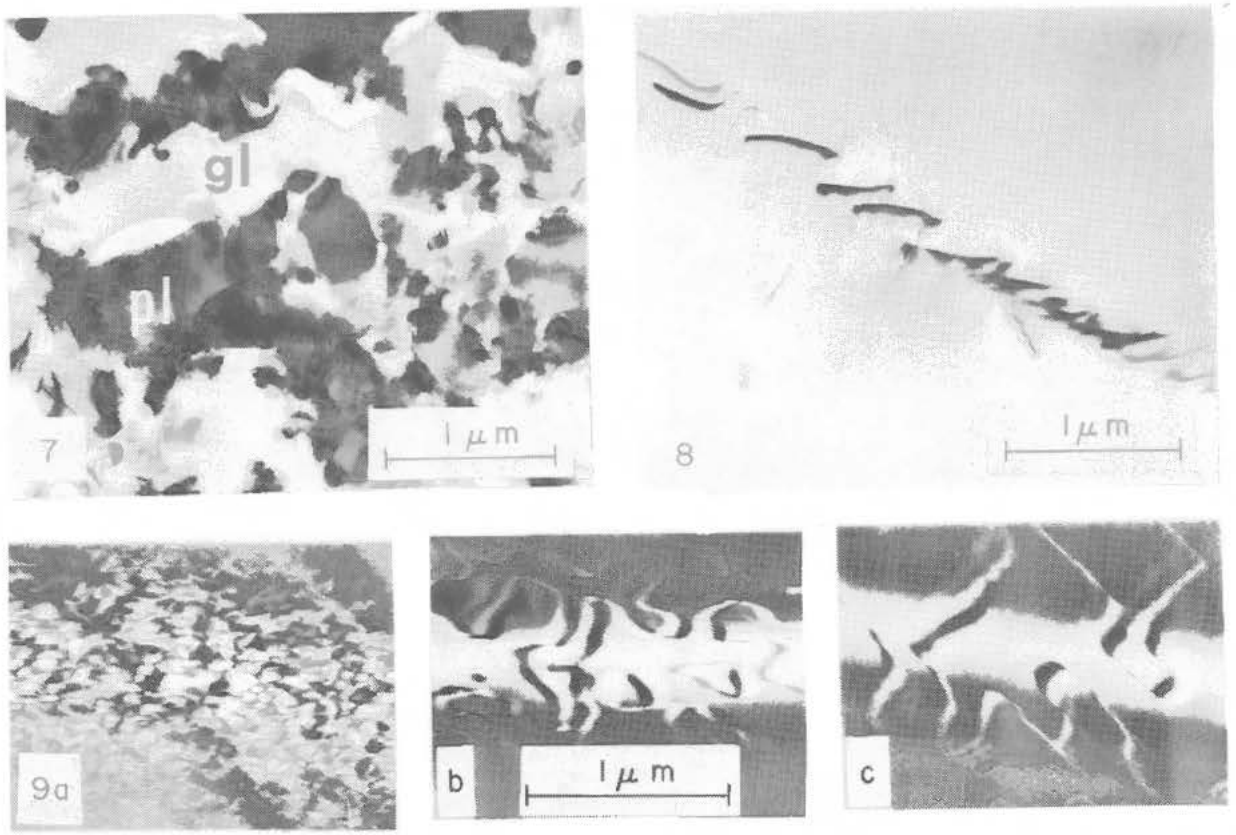

FIGURE CAPTIONS

Fig.1 "Spherulitic" or fibrous texture in 15418,47 anorthite.

Fig.2 Fine twins in 15418,47 anorthite. Note the twin-free grain, where resorption of the twins indicates recrystallization.

Fig.3 Variable dislocation structures in olivine in 15418, indicative of deformation followed by recovery. Note the fine scale pores.

Fig.4 Recrystallized olivine growing into heavily deformed olivine in 15418,47.

Fig.5 Recrystallization in pyroxene in 15418,47. Cf. Figure 4.

Fig.6 Heavily deformed pyroxene region in 15418,47. Note the fine-scale pores. The linear features are possible exsolution lamellae.

Fig.7 Glass (gl) bonding plagioclase (pl) fragments in the low porosity rim of the anorthosite clast in Apollo 15455,13.

Fig.8 Dislocations in olivine from Apollo 15555,163 have rearranged to form a low energy wall configuration. The dislocation Burgers vectors are consistent with a[100].

Fig.9 Type b antiphase domain within a single feldspar grain in Apollo 15557, 36. The smallest domains are in the core (a); (b) and (c) are separated by 10μm and 20μm respectively from (a).

PHASE EQUILIBRIA AND ORIGIN OF APOLLO 15 BASALTS ETC. D.J.Humphries, G.M. Biggar and M.J.O'Hara. Grant Institute of Geology, Edinburgh University.

Samples 15058, 15076, 15499 of types I and II show little or no olivine crystallization before pigeonite entry, olivine reacting out before anorthite entry, at which point the charges are substantially crystalline (fig. 1).

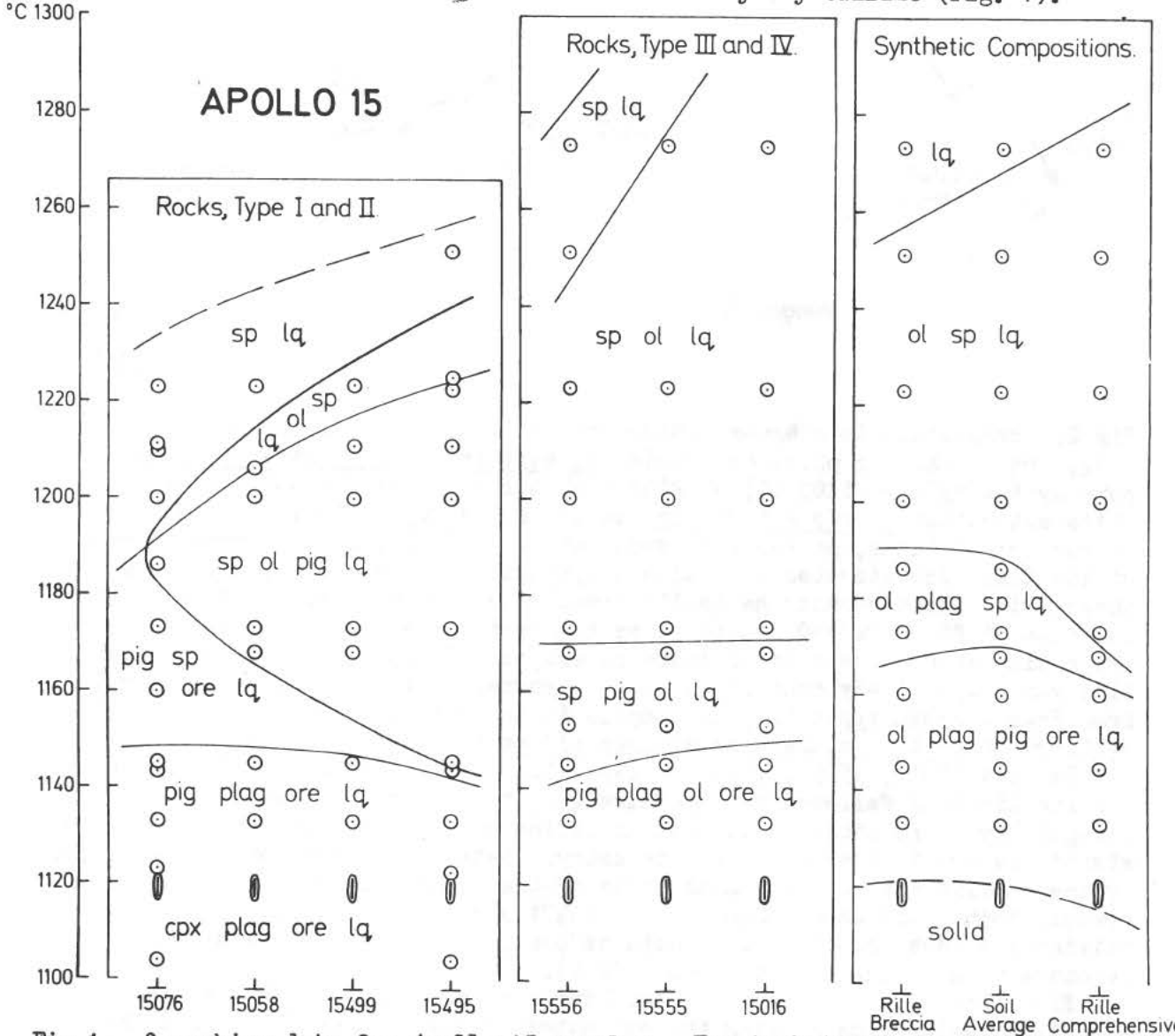

Fig 1. Quenching data for Apollo 15 samples. For techniques see (2,3); all refer to fO_2 = Fe/FeO equilibrium, temperature to IPTS 1968 scale. Abscissa has no scale significance.

PHASE EQUILIBRIA AND ORIGIN OF APOLLO 15 BASALTS ETC.

D.J. Humphries

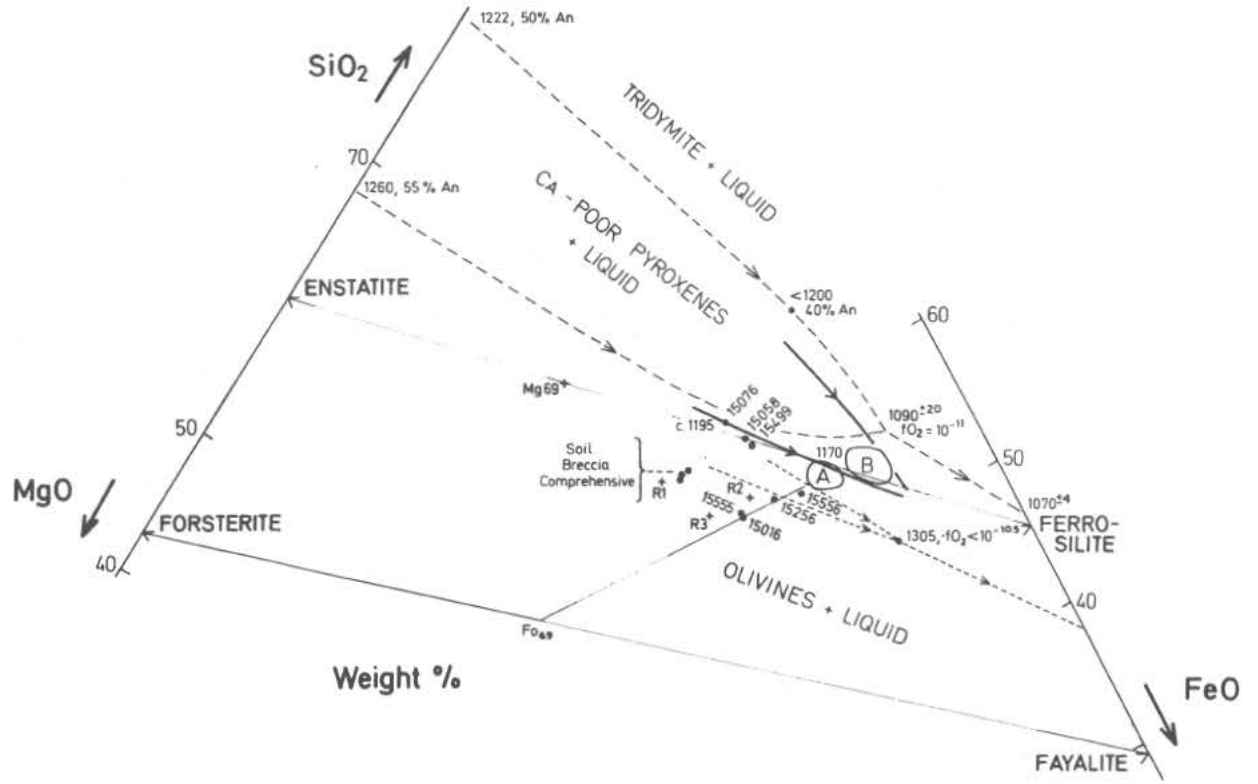

Fig 2. Projection into MgO-FeO-SiO_2 from albite, orthoclase, anorthite, $CaSiO_3$, TiO_2, Cr_2O_3, showing phase boundaries in equilibrium with metallic iron in pure system MgO-FeO-SiO_2 (5) as fine broken lines; phase boundaries at anorthite saturation at $fO_2 = 10^{-11}$atm. in MgO-FeO-Fe_2O_3-$CaAl_2Si_2O_8$-SiO_2 (6) as coarse broken lines, marked with temperatures and normative anorthite content of liquids. Investigated natural and synthetic Apollo 15 compositions are shown, with phase boundaries (solid lines) and temperatures consistent with our data at fO_2 = Fe/FeO, quite close to anorthite saturation. Fields A, B are estimates of liquid composition on eruption in types III, IV and types I, II lavas respectively consistent with petrography (1). An olivine control from Fo_{69} through types III, IV samples is indicated. The compositions of preferred mare-type glass compositions (7) at site shown by crosses.

Samples 15016, 15555, 15556 of types III and IV show high temperature olivine liquidus followed by pigeonite (fig 1). Types III and IV are related essentially by possible olivine accumulation or fractionation (4) and are substantially crystalline at anorthite entry. Data are also reported for 15495. Synthetic mixtures of the compositions of the Rille Comprehensive 15601, Rille breccia 15558, and an average of soil 15471 and 15501 samples (1) display olivine liquidus joined by anorthite before pigeonite, and at a higher temperature than in the lava samples (fig 1).

Fig 2 interprets these phase equilibria data in terms of Mg/Fe variation and silica saturation showing the estimated composition of the liquid phases in the lavas on eruption. Relative to bedrock, the comprehensive, breccia and soil appear enriched in an Mg-pyroxene bearing component.

PHASE EQUILIBRIA AND ORIGIN OF APOLLO 15 BASALTS ETC.

D.J. Humphries

Fig 3 interprets the same data in terms of variation in olivine, pigeonite and anorthite crystallization, again showing olivine control through types III, IV samples, and the estimated liquid composition in these lavas on eruption. Comprehensive, breccia and soil samples as well as the mare-type glasses are seen to be significantly enriched in anorthite relative to bedrock i.e. in a relatively magnesian norite or pyroxene-anorthosite component (see above).

All four lava types are samples of a consolidated mixture of dense phenocrysts (olivine, pigeonite) in liquids which were close in composition and

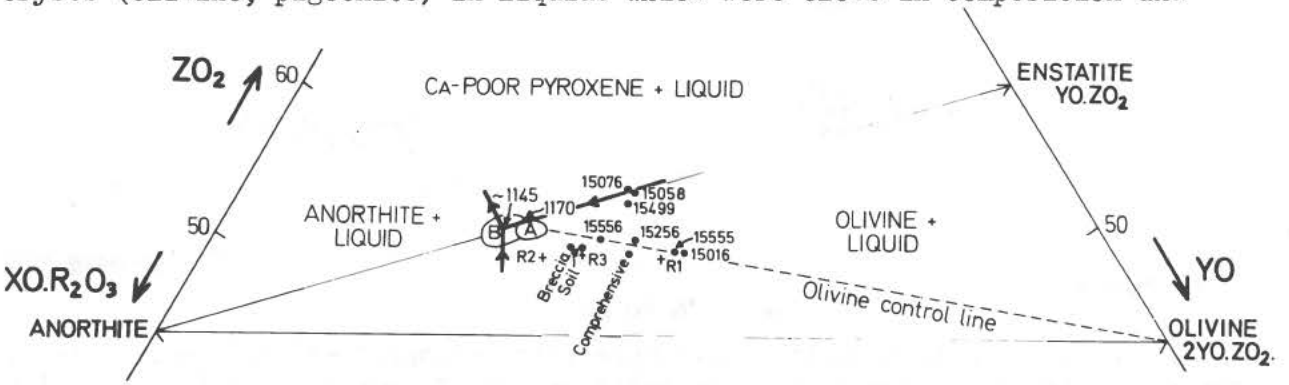

Fig 3. Projection from diopside into anorthite-olivine-silica (see 2) showing investigated samples, three preferred mare-type basalt compositions (7), and liquidus phase boundaries consistent with data of fig 1. Fields A,B as in fig 2.

temperature to those in cotectic equilibrium at low pressure with olivine, pigeonite and plagioclase. Phenocryst assemblages indicate eruption temperatures ~ 1170°C (types III,IV) and ~ 1150°C (types I,II) and far below the liquidus temperatures of many of the samples. At the Apollo 12 site, rock samples were markedly biased from the average magma compositions towards those of the dense phenocrysts (3,8). The same may prove true at the Apollo 15 site. If the average lava compositions are identical with those of the rock samples studied, a satisfactory explanation why the low viscosity magmas were erupted fully equilibrated to the low pressure cotectic and richly porphyritic, yet display only minor accumulation of the dense crystals is hard to devise. Crystal sinking could not have removed olivine without pyroxene from a parental magma common to all four lava types; at least two parental lava flows are required to explain the differences in phenocrysts, and eruption temperature between lava types I, II and types III, IV.

Fig 4 displays the same data as figs 2, 3 to show relationships between components other than olivine, which confirms the addition of an anorthite + pigeonite component to produce comprehensive, breccia and soil samples from bedrock, and combined with figs 2, 3 indicates that any relationship between types I and II lavas on the one hand, and types III, IV on the other must be dominated by pyroxene-liquid equilibria, with possible participation of olivine or silica.

One possible relationship is illustrated in figs 5,6. Parental magma A of types III, IV gave rise by essential anorthite + pigeonite fractionation at some slightly elevated pressure within the lava lake (broken phase boundaries apply) to parental magma B of types I, II. An escape of some of the liquid A

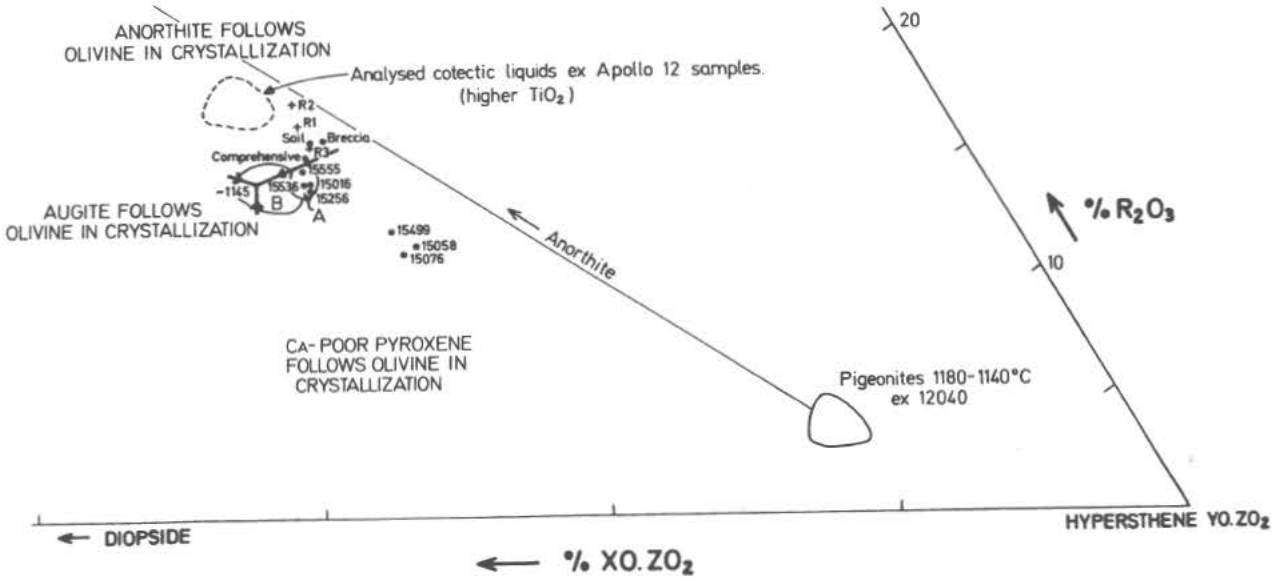

Fig 4. Projection from olivine into hypersthene-diopside-alumina etc. (see 2, fig 6) showing the investigated compositions, and fields A, B as in fig 2. Low pressure phase boundaries for Apollo 15 samples show small displacement relative to more TiO2 rich Apollo 12 results (see 2).

gave rise to the earlier, lower flow unit; expansion across composition A of the olivine liquidus volume because of the pressure release (solid phase boundaries apply) led to precipitation and local accumulation of olivine to yield samples such as 15016, 15555, 15556, in liquid fraction A'. On escape of liquid B, the olivine liquidus volume did not expand sufficiently to cover this composition, which precipitated pigeonite, yielding liquid B' as matrix to local accumulations of crystals, as in samples 15078, 15076, 15499.

A second interpretation involves fractionation at low pressure only. Fractionation and accumulation of crystals within parental magma A yields samples of types III, IV character until residual liquid A' is reached. Thereafter evolution is by pigeonite fractionation and accumulation only,

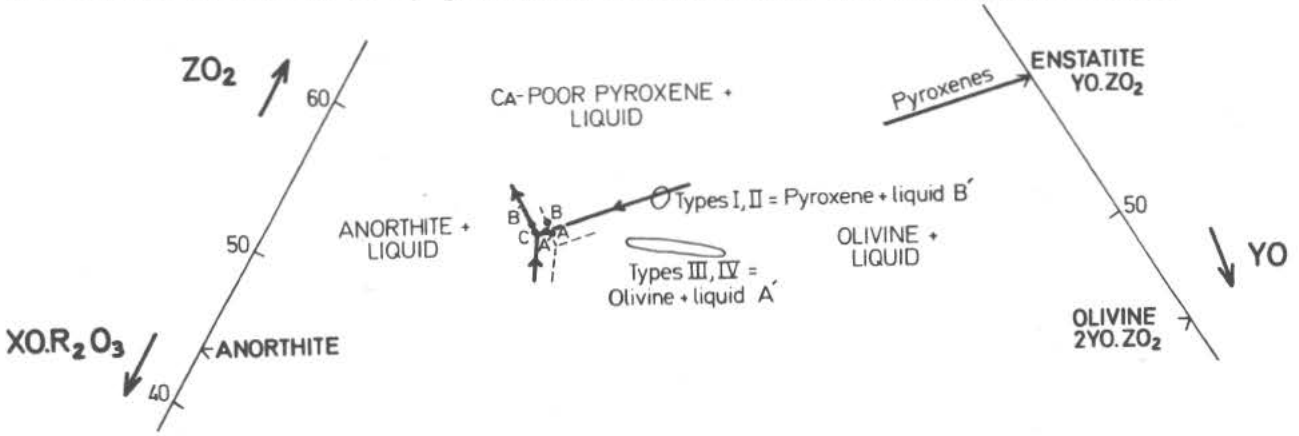

Fig 5. Diopside projection into anorthite-olivine-silica. See text.

PHASE EQUILIBRIA AND ORIGIN OF APOLLO 15 BASALTS ETC.

D.J. Humphries

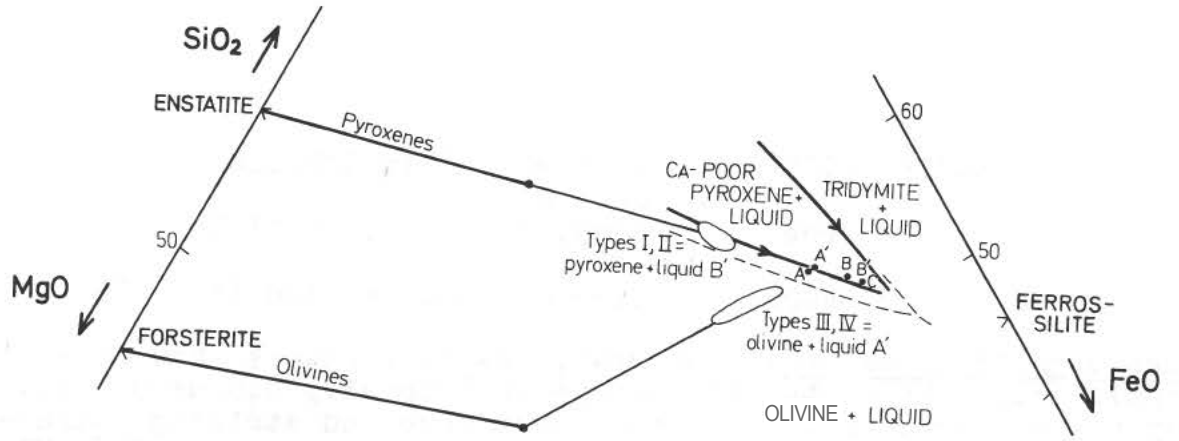

Fig 6. MgO-FeO-SiO2 projection. See text.

yielding types I, II samples, and residual liquid C. The process could scarcely have operated within a single lava flow, and requires the existence of at least a shallow-seated magma chamber.

Both explanations requires types III, IV to be stratigraphically older than types I, II, and both are apparently inconsistent with data of Brown et al. (this volume).

A third alternative, derivation of liquids C, A', A as progressive partial melts of a pyroxenite or olivine-pyroxenite source mantle predicts the reversed stratigraphic relationship, but still requires extensive post eruption crystal accumulation to explain the compositions.

Creation of primary magmas with the compositions of the investigated rock specimens by progressive partial melting of the same source mantle composition is impossible, even making allowances for pressure differences at the scenes of partial melting (Fe/Mg relations, see fig 5 especially).

References

(1) LSPET 1971. Lunar sample information catalog, Apollo 15. NASA Manned Spacecraft Center.

(2) Biggar, G.M., O'Hara, M.J., Peckett, A. and Humphries, D.J. 1971. Geochim. Cosmochim. Acta Suppl. 2 Proc. 2nd Lunar Sci. Conf. 1, 617-643.

(3) Biggar, G.M., O'Hara, M.J., Humphries, D.J. and Peckett, A. 1972. Maria lavas, mascons; layered complexes, achondrites and the lunar mantle. in The Moon ed. H.H. Urey, S.K.Runcorn I.A.U. (in press).

(4) O'Hara, M.J. and Biggar, G.M. A point of phase equilibria interpretation in connection with lavas from the Apollo 12 site. Earth Planet. Sci. Letters (in press).

(5) Bowen, N.L. and Schairer, J.F. 1935. Amer. J. Sci. 229, 151.

(6) Roeder, P.L. and Osborn, E.F. 1966. Amer. J. Sci. 264, 428-480.

(7) Reid, A.M., Warner, J., Ridley, W.I. and Brown, R.W. 1972. Major element composition of glasses in three Apollo 15 soils (preprint).

(8) Biggar, G.M., O'Hara, M.J., Humphries, D.J. and Peckett, A. 1972. in Lunar Science III 77-79 ed. C. Watkins Lunar Science Institute Contrib. 88.

MINERALOGICAL NOTES ON APOLLO 15 SAMPLES

J. Jedwab
Brussels Free University, Brussels, BELGIUM

Gabbro 15065 (Sample 15065,59 and LRL section 15065,81)

Micro-vugs in pyroxenes: Euhedral, Fe-Ca-pyroxenes show frequently under the photon microscope (PM) zonally disposed vugs. They are rather complex but their abundance and striking characters deserve a description. The following is based on SEM, EMP and PM observations: (a) The cavities contain a very small opaque mineral (ilm. or chrom.) and/or a K-felspar. (b) The walls are made up of pyroxene phenocrysts in crystallographic continuity with the host. (c) The vugs are very often surrounded by a scummy silicate deposit laying flat on the crystal face or along cleavage or twin planes of the host. Chemical compositions of these scums are not very different from that of the pyroxenes except for the Si, which is lower in the latter.

Ca-Fe-Phosphate: A high concentration of phosphates was found deposited on a free growing ilmenite crystal, by means of SEM and EMP. They consist of: (a) Hexagonal platelets interfering with the growth of ilmenite lamellae[1]; (b) rounded, partially facetted crystals forming linear rows; (c) a continuous layer stratified between the ilmenite and a late Ca-silicate. EMP-analyses indicate about 5% Fe and traces of Y and Ce. It was not yet possible to decide if it is apatite or whitlockite. Other finds of Ca-rich, Fe-poor phosphates, but with different morphologies, suggest a rather diverse phosphate-mineralogy in this rock.

Euhedral native iron: Facetted, isometric germs of native Fe of late deposition were observed by SEM and EMP on free-growing ilmenites from large vugs.

Comparison with previous studies: So far as can be said from a rather limited sampling, the afore-mentioned features were not observed in samples 10072,31 and 12036,2. On the other side, the silicate overgrowths which were so conspicuous in these rocks[1] are nearly absent in rock nr. 15065.

Basalt 15555,105

Blue rutile: A loose flat fragment of about 0.5mm, of ultramarine

colour, was observed in the sealed bag before opening it. XRD showed that it is a fine-grained rutile, and EMP confirmed the major Ti composition. Traces of Fe were also found; Zr, Nb, Ca, S, Si were looked for but not found. Under PM-transmitted light, the material is opaque but transparent on the edges. It is composed of an agglomerate of micron-sized, rounded grains massively coloured in blue. No matrix material was seen. Under PM-reflected light, the material is transparent with a very high dispersion.

The SEM allows to make the following observations: The overall shape of the platelet is that of an irregular fragment broken away from some larger body. The edges are grained and show a perpendicular parting. The faces are smoother, but pitted and striated. Thickness is about 40 microns; the faces are parallel, but the shape is undulated. Some layering parallel to the flattening is visible from the sides.

This puzzling object is privisionally considered as of lunar origin, due to: (a) Difficulties in synthetizing blue rutile[2], (b) unlikeliness of being contaminated by such an improbable compound at LRL and (c) probability of finding lower valencies of Ti (which could impart a blue colour to rutile) on the Moon[3].

Fines 15601,113

Molybdenite: An isolated crystal was noticed in a powder mount from a density concentrate. Under PM-reflected light, it has a strong metallic shine and crystalline faces. Brought under the EMP, it gave a definite Mo, S - composition. Morphologically it appears under the SEM as a stacking of very fine, flexible lamellae, which is consistent with a molybdenite determination.

Fines 15301,116

Hematite: Red, transparent, isolated crystals were repeatedly found in density concentrates. They have sometimes a scaly crystalline habit. XRD and EMP show that one has definitely to do with hematite.

ACKNOWLEDGEMENTS

I thank gratefully Cl. Frondel for fruitful discussion and encouragements.

REFERENCES

1) J. Jedwab, Proc., Sec. Lunar Sc. Conf. 1(1971)923.
2) GMELIN's Handbuch der/Am. Chemie. Titan. Weinheim (1951) 214, 244.
3) S.E. Haggerty et al.. Proc.Ap.11 Lun. Sc. Conf. 1(1970)527.

PETROLOGY AND CHEMISTRY OF SOME APOLLO 15 CRYSTALLINE ROCKS; V. C. Juan, J. C. Chen, C. K. Huang, P. Y. Chen and C. M. Wang Lee; Institute of Geology, National Taiwan University

Three polished thin sections 15058,14 (microgabbro); 15065,90 (basanite) and 15535,9 (olivine basalt) and 0.91 gm of 15065,48; 0.70 gm of 15535,2 and 0.49 gm of 15535,4 were received for petrographic and chemical studies.

15058,14 microgabbro was collected at about 30 m east northeast of the ALSEP central site 1. This gray porphyritic crystalline rock consists essentially of clinopyroxene (72 %) and plagioclase (22 %, An_{78}) with miror amounts of cristobalite (3 %), ilmenite (2 %) and troilite (< 1 %). The clinopyroxene is commonly zoned from a pigeonite core to a subcalcic augite rim. Noteworthy is that part of clinopyroxene exhibits shock-induced psendo-cleavages intersecting at 120°. The plagioclase is highly zoned and shows typical subophitic texture around clinopyroxene. It should be noted that many plagioclase laths contain elongate clinopyroxene cores along axes.

The coarse-grained equigranular basanite 15065,90 was collected at station 1. It is composed chiefly of plagioclase (27 %, An_{77}) and clinopyroxene (70 %) accompanied by ilmenite, spinel (2 %) and nepheline (< 1 %). Most plagioclase probably crystallized earlier than clinopyroxene, but some plagioclase show graphic texture with clinopyroxene suggesting contemporaneous precipitation. The subhedral to euhedral clinopyroxene is commonly zoned from colorless pigeonite cores ($2V_z=9°$) to pale brownish subcalcic augite rims ($2V_z=30°$). The largest clinopyroxene found in the rock is 5.6 x 2.0 mm in size. The occurrence of nepheline in the rock suggests that the parental magma from which the rock crystallized is deficient in silica and probably somewhat enriched in alkali elements.

The sample 15535,9, a porphyritic olivine basalt of mare type was collected at station 9a. It consists mainly of clinopyroxene (60 %), olivine (10 %, Fo_{76}) plagioclase (25 %, An_{83}) and opagues (4 % including ilmenite and ulvospinel) with minor amounts of cristobalite, zircon and pale brown glass (< 1 %). The clinopyroxene is commonly twinned with (100) as twin plane and zoned from a pigeonite core to a subcalcic augite rim. Many plagioclase laths are fractured and some show wavy extinction and bending of twin lamellae which might be due to shock effects. The subhedral pale green olivine (0.3-2 mm across) occurs as phenocrysts in the rock. Some olivines contain inclusions of clinopyroxene and ilmenite. It should be mentioned that clinopyroxene is followed by olivine then by plagioclase in the order of crystallization.

15065,48; 15535,4 have been chemically analyzed by means of AAS and colorimetric techniques, using USGS rock standards and artificial

PETROLOGY AND CHEMISTRY OF SOME APOLLO 15 CRYSTALLINE ROCKS

V. C. Juan, J. C. Chen, C. K. Huang, P. Y. Chen and C. M. Wang Lee

standards to construct the working curves. The results of the chemical analyses together with chemical data of Apollo 12, 14 and Lunar 16 and terrestrial rocks are listed in Table 1. The normative compositions of 15065,48; 15535,2 and 15535,4 are presented in Table 2. The chemical compositions of 15535,2 and 15535,4 are similar to those of mare basalts returned by Apollo 12 mission. 15535,2 and 15535,4 have lower TiO_2 content than Apollo 11 Type A and Type B rocks reported by compston et al[8] . That they are lower in Si, Al, K, Rb, Li and Ni but higher in Fe and Cr than non-mare crystalline basalt 14310,197 analyzed by Juan et al[5]. suggests that the former could not have been derived from the latter by partial melting. It should be noted that the Apollo 15 mare basalts have a Al/Ca ratio lower than that of chondritic meteorite and a Fe/Ni ratio of generally greater than 1000; while these two ratios in Apollo 14 non-mare basalt 14310,197 are significantly higher.

The high chromium content found in 15535,2 and 15535,4 suggests that large scale fractional crystallization is limited during their petrologic history because extensive fractional crystallization of ore minerals and clinopyroxene would cause drastic decrease in chromium abundance leading to the effective removal of the element from the liquid[9]. On the other hand, the chromium abundance is readily explainable in term of partition coefficient if Apollo 15 basalt 15535,2 and 15535,4 had formed by direct partial melting from parental material possessing approximately the chondritic abundances (Cr=3500 ppm).

15065,48 shows nepheline molecule in the norm and has major element composition similar to that of crystalline rock of Lunar 16, terrestrial Hawaiian basanitoid[6] and nepheline basanite[7]. When this is viewed togather with 15065,90 where modal nepheline has been found, 15065 would represent an earlier differentiate of a basaltic magma somewhat rich in alkalines. Barth[10] suggested that terrestrial basanite could be formed by gravitational differentiation from a parental magma of olivine basalt composition. However, the parental magma of 15065 may be chemically different from that of 15535 and may represent an independent magma type.

As mentioned before the chemical difference between the mare (15535) and non-mare (14310) basalts is apparent. This difference might be resulted from difference in the composition of the source region, differentiation process, degree of contamination with previously differentiated materials or the combination of all these factors[11]. It is clear that simple fractionation from a homogeneous source is not adequate to explain the chemical difference among lunar basalts.

Reference

[1] I. R. 36 (1971) Interagency Report 36: Preliminary description of Apollo 15 sample environments, 219 p.

[2] Engel, A. E. J., C. G. Engel, A. L. Sutton and A. T. Myers (1971) Composition of five Apollo 11 and Apollo 12 rocks and one Apollo 11 soil and some petrogenic considerations: Proc. 2nd Lunar Sci.

Conf. 1, 439-448. Pergamon Press.

[3] Biggar, G. M., M. J. O'Hara, A. Peckett and D. J. Humphries (1971) Lunar lavas and the achondrites: Petrogenesis of protohypersthene basalts in the maria lava lakes: Proc. 2nd Lunar Sci. Conf. 617-643.

[4] Vinogradov, A. P. (1971) Preliminary data on lunar ground brought to Earth by automatic probe "Luna-16" Proc. 2nd Lunar Sci. Conf. 1, 1-16. Pergamon Press.

[5] Juan, V. C., J. C. Chen, C. K. Huang, P. Y. Chen and C. M. Wang Lee Petrology and chemistry of some Apollo 14 lunar samples: Proc. 3rd Lunar Sci. Conf. MIT Press (in press).

[6] MacDonald, G. A. and T. Katsura (1964) Chemical composition of Hawaiian lavas. J. Petrology 5, 82-133.

[7] Johannsen A. (1938) A descriptive petrography: 4, 235, The University of Chicago Press.

[8] Compston, W., B. W. Chappel, P. A. Arriens and M. J. Vernon (1970) The chemistry and age of Apollo 11 lunar material. Proc. Apollo 11 Lunar Sci. Conf. 2, 1007-1027. Pergamon Press.

[9] Ringwood, A. E. (1970) Petrogenesis of Apollo 11 basalts and implications for lunar origin. JGR 75, 6453-6479.

[10] Barth T. F. W. (1952) Theoritical Petrology, John wiley and Sons. 387 p.

[11] Murthy, V. R., N. M. Evensen, B. M. John, M. P. Coscio, J. C. Dragon and R. O. Pepin (1972) Rubidium-strontium and potassium-argon age of sample 15555, Sci. 175, 419-421.

Table 1 Chemical compositions of Apollo 15 crystalline rocks as compared with Apollo 12, 14, Luna 16 and terrestrial rocks

	15065,48[a]	15535,2[b]	15535,4[b]	12021,51[c]	12075,16[c]	12064,38[d]
% SiO_2	43.30	45.50	44.73	47.05	45.06	46.41
% TiO_2	1.88	2.51	2.83	3.74	2.84	4.14
% Al_2O_3	10.10	9.70	9.55	10.97	8.92	10.50
% Cr_2O_3	0.804	0.602	0.571	0.351	0.687	0.38
% ΣFeO	19.20	21.70	22.15	19.04	20.23	19.95
% MnO	0.300	0.290	0.285	0.25	0.26	0.27
% MgO	11.50	10.34	10.34	7.08	13.32	6.38
% CaO	12.12	9.30	8.92	11.34	8.64	11.71
% Na_2O	0.715	0.195	0.195	0.29	0.30	0.30
% K_2O	0.068	0.041	0.046	0.08	0.05	0.07
ppm Ag	0.545	0.032	0.026	n.d.	n.d.	n.d.
ppb Au	4	4	2	n.d.	n.d.	n.d.
ppm Co	70	77	59	22	40	n.d.
ppm Cu	56	3	7	11	6	n.d.
ppm Ga	24	<10	<10	n.d.	n.d.	n.d.
ppm Li	7	8	7	7	6	n.d.
ppm Ni	147	92	76	3	63	n.d.
ppm Rb	n.d.	3.8	3.8	n.d.	n.d.	n.d.
ppm Sr	214	201	184	130	95	n.d.
ppm Zn	38	12	17	n.d.	n.d.	n.d.
MgO/ΣFeO	0.60	0.48	0.47	0.37	0.66	0.32
Na_2O/K_2O	10.51	4.76	4.24	3.63	6.00	4.29
K/Rb	n.d.	90	100	n.d.	n.d.	n.d.
Fe/Ni	1015	1833	2265	49333	2496	n.d.
Rb/Sr	n.d.	0.019	0.021	n.d.	n.d.	n.d.

(a) Basanite, This report, analyst J.C. Chen
(b) Porphyritic basalt of mare type, this report, analyst J.C. Chen
(c) Porphyritic basalt, [2]
(d) Microgabbro, [3]

Table 1 (Continued)
Chemical compositions of Apollo 15 crystalline rocks as compared with Apollo 12, 14, Luna 16 and terrestrial rocks

	Luna 16[e]	14310,197[f]	Hawaiian basanitoid[g]	Nepheline-Basanite[h]
% SiO_2	43.80	48.33	43.12	43.80
% TiO_2	4.90	1.26	2.11	1.88
% Al_2O_3	13.65	20.45	13.36	12.71
% Cr_2O_3	0.28	0.16	n.d.	0.10
% ΣFeO	19.35	8.40	12.74*	10.91*
% MnO	0.20	0.13	0.19	0.22
% MgO	7.05	8.00	13.07	13.54
% CaO	10.40	11.70	11.02	12.92
% Na_2O	0.38	0.628	2.55	2.83
% K_2O	0.15	0.520	0.60	1.08
ppm Ag	n.d.	0.04	n.d.	n.d.
ppb Au	n.d.	8	n.d.	n.d.
ppm Co	29	45	n.d.	n.d.
ppm Cu	13	16	n.d.	n.d.
ppm Ga	11	10	n.d.	n.d.
ppm Li	n.d.	25	n.d.	n.d.
ppm Ni	147	205	n.d.	n.d.
ppm Rb	n.d.	16	n.d.	n.d.
ppm Sr	445	258	n.d.	n.d.
ppm Zn	n.d.	13	n.d.	n.d.
MgO/ΣFeO	0.36	0.95	1.03	1.24
Na_2O/K_2O	2.53	1.21	4.25	2.62
K/Rb	n.d.	270	n.d.	n.d.
Fe/Ni	1023	318	n.d.	n.d.
Rb/Sr	n.d.	0.062	n.d.	n.d.

(e) Crystalline basalt of Sea of Plenty, [4]
(f) Non-mare crystalline basalt, [5]
(g) Hawaiian basanitoid, [6]
(h) Nepheline basanite [7], volatile free basis
* Recalculated to ΣFeO

Table 2 Normative compositions of 15065,48, 15535,2 and 15535,4 as compared with Luna 16 and terrestrial rocks (chemical data from Table 1).

		15065,48	15535,2	15535,4	Luna 16	Hawaiian basanitoid	Nepheline basanite
Chromite		1.12	0.90	0.90	0.45	-	0.22
Ilmenite		3.65	5.02	5.32	9.27	3.95	3.65
Orthoclase		0.39	0.28	0.28	1.11	3.34	3.89
Albite		7.86	1.57	1.57	3.14	10.48	-
Anorthite		22.80	25.30	25.02	35.03	23.35	18.63
Diopside	Ca	15.54	8.70	8.00	6.96	11.83	19.02
	Mg	7.30	3.70	3.40	2.70	7.70	7.30
	Fe	8.05	5.02	4.62	4.36	3.30	4.09
Hypersthene	En	-	17.40	17.10	13.50	-	-
	Fs	-	24.02	23.76	21.12	-	-
Olivine	Fo	14.28	3.36	3.78	0.98	17.50	14.42
	Fa	18.56	5.10	5.92	1.63	8.46	2.45
Nepheline		0.28	-	-	-	5.96	18.58
Leucite		-	-	-	-	-	2.18
Magnetite		-	-	-	-	3.48	5.80

PETROLOGY AND CHEMISTRY OF SOME APOLLO 15 REGOLITHS; V. C. Juan, J. C. Chen, C. K. Huang, P. Y. Chen and C. M. Wang Lee; Institute of Geology, National Taiwan University

Two microbreccias 15299,106 and 15565,93 and ten fines 15231,65; 15232,8; 15291,30; 15291,31; 15291,51; 15292,6; 15301,113; 15302,19; 15601,95 and 15602,25 have been petrographically and chemically studied. 15299,106 consists essentially of subangular to subrounded lithic clasts (12 %, including microgabbro, mare and non-mare basaltic rocks, pre-existing microbreccia and anorthosite); mineral clasts (11 %, including bytownite, clinopyroxene, orthopyroxene, olivine, spinel and other opaques); glass fragments (3 %) and glass spherules (4 %) set in a fine-grained (< 0.1 mm) glassy matrix (70 %). It should be noted that the pre-existing regoliths, crystalline lithic fragments and basaltic fragments in the rock commonly show strain effects such as fractures, distorted form, stress-induced twin lamellae, wavy extinction and bent twin lamellae. 15565,93 is composed chiefly of lithic clast (20 % including mare and non-mare basaltic rocks and pre-existing breccias); mineral clasts (19 %, including bytownite, pigeonite, olivine, ilmenite and ulvospinel), glass fragments (10 %) and glass spherules (1 %) set in a fine-grained glassy matrix (50 %).

Textural evidences suggest that the two microbreccias may be classified as welded breccia of McKay and Morrison[1]. The occurrence of pre-existing breccias, crystalline lithic fragments and basaltic rock with varying Px/Pc ratios may have resulted from cratering events with thick hot ejecta blankets. The minor amounts of anorthositic rock fragment found in 15299,106 may have originated from the Highland. That the mechanism of base surge deposition may be the best hypothesis to produce thermal sintering in the welded breccias.

The modal compositions of the fines were determined by pointcounting under petrographic microscope with at least 200 points on the grain mount. The results are presented in Table 1. Six components were recognized in the fines i.e. (1) agglutinates (2) glass fragments (3) glass spherules (4) mineral grains including plagioclase and pyroxenes (5) basaltic fragments and (6) anorthositic fragments. Many of the mineral grains and glass fragments in the fines show conspicuous strain effects such as fractures, broken spherules, wavy extinction, bending of twin lamellae, etc. The mean grain size of the fines generally decreases as the glass spherule content increases which may be due to the increase of the duration of the residence time in the active surface layer. The chemical compositions of 15299,13 and the ten fines determined by AAS and colorimetric methods are listed in Table 2. Fig. 1 shows the FeO vs Al_2O_3 plot for Apollo 15 regoliths we have analyzed. 15535,2; 15535,4 (porphyritic mare basalt) and 14310,197 (non-mare crystalline basalt) are also plotted for comparison. The negative

PETROLOGY AND CHEMISTRY OF SOME APOLLO 15 REGOLITHS

V. C. Juan, J. C. Chen, C. K. Huang, P. Y. Chen and C. M. Wang Lee

correlation between FeO and Al_2O_3 is apparent and is nearly linear between 8 and 20 % Al_2O_3 and 8 and 22 % FeO. In addition, TiO_2, Cr_2O_3, MnO, Na_2O and K_2O also show regular variations with Al_2O_3. It is suggested that two-end-member mixing of 15535 (Fe-rich mare basalt) and 14310 (Al-rich non-mare basalt) might be reponsible for the near-linear correlations (see Table 3). The most striking difference between the chemical compositions of Apollo 15 basalts and fines we studied is the relative enrichment in Al, Ni and alkali in the fines probably due to the admixture with premare basalt rich in those elements.

Reference

[1] McKay, D. S. and D. A. Morrison (1971) Lunar breccia: JGR 76, 5658-5669.

[2] Frondel, C., C. Klein Jr. and J. Ito (1971) Mineralogical and chemical data on Apollo 12 Lunar fines: Proc. 2nd Lunar Sci. Conf. 719-726.

[3] Keller, W. D. and W. H. Huang (1971) Response of Apollo 12 lunar dust to reagents simulative of those in the weathering environment of Earth: Proc. 2nd Lunar Sci. Conf. 973-981.

[4] Juan, V. C., J. C. Chen, C. K. Huang, P. Y. Chen and C. M. Wang Lee Petrology and chemistry of some Apollo 14 lunar samples: Proc. 3rd Lunar Sci. Conf. (in press).

Table 1 Modal compositions of Apollo 15 fines

		Station No.	agglutinate	glass fragments	glass spherules	pyroxene	plagioclase	basaltic fragments	anorthositic fragments
	100-200 mesh		53	6	1	19	18	3	-
15231,65		2							
	200-325 mesh		34	5	1	27	33	-	-
	100-200 mesh		56	4.5	0.5	11	19	-	8
15232,8		2							
	200-325 mesh		46	5	1	18	30	-	-
	100-200 mesh		38	2	-	45	13	2	-
15601,95		9A							
	200-325 mesh		37	3	2	42	15	1	-
	100-200 mesh		29	2.5	-	26	15	27.5	-
15602,25		9A							
	200-325 mesh		29.5	2	-	37.5	20	11	-
	100-200 mesh		65	5	2	15	13	-	-
15291,30		6							
	200-325 mesh		54	6	5	20	15	-	-
	100-200 mesh		63	5	2	16	13	1	-
15291,31		6							
	200-325 mesh		54	6	2	20	17	1	-
	100-200 mesh		54	9	3	17	14	3	-
15291,51		6							
	200-325 mesh		48	11	1	19	21	-	-
	100-200 mesh		40	12	-	16	27	5	-
15292,6		6							
	200-325 mesh		35	5	-	12	48	-	-
	100-200 mesh		52	19	12	7	8	2	-
15301,113		7							
	200-325 mesh		44	19	4	13	18	2	-
	100-200 mesh		58	8	5	10	19	-	-
15302,19		7							
	200-325 mesh		50	6	2	18	24	-	-

Table 2 Chemical compositions of Apollo 15 fines and microbreccia as compared with Apollo 12 fines, 15535 and 14310

	15231,65[a]	15232,8[a]	15291,30[a]	15291,31[a]	15291,51[a]	15292,6[a]	15301,113[a]
% SiO_2	47.48	47.45	47.60	47.30	47.40	47.33	46.65
% TiO_2	1.44	1.46	1.58	1.65	1.54	1.71	1.37
% Al_2O_3	18.50	18.98	16.30	17.20	16.51	17.57	14.70
% Cr_2O_3	0.285	0.297	0.330	0.339	0.317	0.316	0.386
% ΣFeO	11.35	10.65	12.25	12.80	12.50	12.80	14.50
% MnO	0.153	0.143	0.160	0.156	0.160	0.164	0.188
% MgO	9.82	10.54	10.14	10.24	10.14	10.02	11.08
% CaO	10.64	9.40	11.18	9.48	10.88	9.70	10.44
% Na_2O	0.390	0.455	0.450	0.450	0.410	0.505	0.355
% K_2O	0.195	0.223	0.238	0.133	0.236	0.264	0.170
ppm Ag	0.056	0.051	0.056	0.032	0.032	0.051	0.026
ppb Au	5	3	6	6	5	4	5
ppm Co	71	62	73	64	71	54	64
ppm Cu	5	3	8	5	3	3	3
ppm Ga	<10	<10	<10	<10	<10	<10	<10
ppm Li	13	16	15	15	15	18	12
ppm Ni	292	175	252	248	264	200	236
ppm Rb	5.0	6.6	5.0	6.2	6.2	8.4	2.4
ppm Sr	243	208	268	255	268	213	223
ppm Zn	30	33	34	34	30	24	40
MgO/ΣFeO	0.87	0.99	0.83	0.80	0.81	0.78	0.76
Na_2O/K_2O	2.00	2.04	1.89	3.38	1.74	1.91	2.09
K/Rb	324	280	395	178	316	261	588
Fe/Ni	302	473	378	401	368	497	477
Rb/Sr	0.021	0.032	0.019	0.024	0.023	0.039	0.011

Table 2 (Continued)
Chemical compositions of Apollo 15 fines and microbreccia
as compared with Apollo 12 fines, 15535 and 14310

	15302,19[a]	15601,95[a]	15602,25[a]	15299,13[a]	12001[b]	12070,128[c]	15535,2[a]
% SiO_2	47.25	46.23	46.65	45.90	45.60	45.90	45.50
% TiO_2	1.58	2.16	2.46	1.49	3.00	2.77	2.51
% Al_2O_3	15.80	10.86	11.02	18.50	13.90	13.00	9.70
% Cr_2O_3	0.286	0.485	0.514	0.342	0.30	0.40	0.602
% ΣFeO	14.00	19.00	20.15	11.65	16.20	16.40	21.70
% MnO	0.147	0.246	0.250	0.153	0.21	0.22	0.290
% MgO	9.82	10.56	9.70	10.08	10.20	10.70	10.34
% CaO	10.32	10.08	9.26	10.90	10.25	10.40	9.30
% Na_2O	0.405	0.315	0.270	0.430	0.45	0.50	0.195
% K_2O	0.171	0.091	0.086	0.224	0.23	0.23	0.041
ppm Ag	0.057	0.050	0.044	0.038	n.d.	n.d.	0.032
ppb Au	4	4	3	6	n.d.	n.d.	4
ppm Co	62	74	77	71	n.d.	n.d.	77
ppm Cu	7	10	7	3	n.d.	n.d.	3
ppm Ga	<10	<10	<10	10	n.d.	n.d.	10
ppm Li	14	10	10	15	n.d.	n.d.	8
ppm Ni	227	189	175	244	n.d.	n.d.	92
ppm Rb	3.2	2.4	3.2	5.0	n.d.	n.d.	3.8
ppm Sr	213	223	199	265	n.d.	n.d.	201
ppm Zn	36	27	19	35	n.d.	n.d.	12
MgO/ΣFeO	0.70	0.56	0.48	0.87	0.63	0.65	0.48
Na_2O/K_2O	2.37	3.46	3.14	1.92	1.96	2.17	4.76
K/Rb	444	315	223	392	n.d.	n.d.	90
Fe/Ni	479	781	895	371	n.d.	n.d.	1833
Rb/Sr	0.015	0.011	0.016	0.019	n.d.	n.d.	0.019

(a) This report (analyst J. C. Chen)
(b) Ref. [2]
(c) Ref. [3]

Table 2 (Continued)
Chemical compositions of Apollo 15 fines and microbreccia as compared with Apollo 12 fines, 15535 and 14310

	15535,4[a]	14310,197[d]
% SiO_2	44.73	48.33
% TiO_2	2.83	1.26
% Al_2O_3	9.55	20.45
% Cr_2O_3	0.571	0.16
% ΣFeO	22.15	8.40
% MnO	0.285	0.13
% MgO	10.34	8.00
% CaO	8.92	11.70
% Na_2O	0.195	0.628
% K_2O	0.046	0.520
ppm Ag	0.026	0.04
ppb Au	2	8
ppm Co	59	45
ppm Cu	7	16
ppm Ga	10	10
ppm Li	7	25
ppm Ni	76	205
ppm Rb	3.8	16
ppm Sr	184	258
ppm Zn	17	13
MgO/ΣFeO	0.47	0.95
Na_2O/K_2O	4.24	1.21
K/Rb	100	270
Fe/Ni	2265	318
Rb/Sr	0.021	0.062

(d) Ref. [4]

Table 3
Proportions of Two-end-member mixing for Apollo 15 fines

	14310	15535*
	(%)	
15602, 25	13	87
15601, 95	18	82
15301,113	51	49
15302, 19	58	42
15291, 51	67	33
15291, 30	67	33
15291, 31	68	32
15292, 6	70	30
15231, 65	79	21
15232, 8	84	16

* Average of 15535,4 and 15535,2

PETROLOGY AND CHEMISTRY OF SOME APOLLO 15 REGOLITHS

V. C. Juan, J. C. Chen, C. K. Huang, P. Y. Chen and C. M. Wang Lee

FIG. 1. Al_2O_3 VS FeO FOR APOLLO 15 FINES

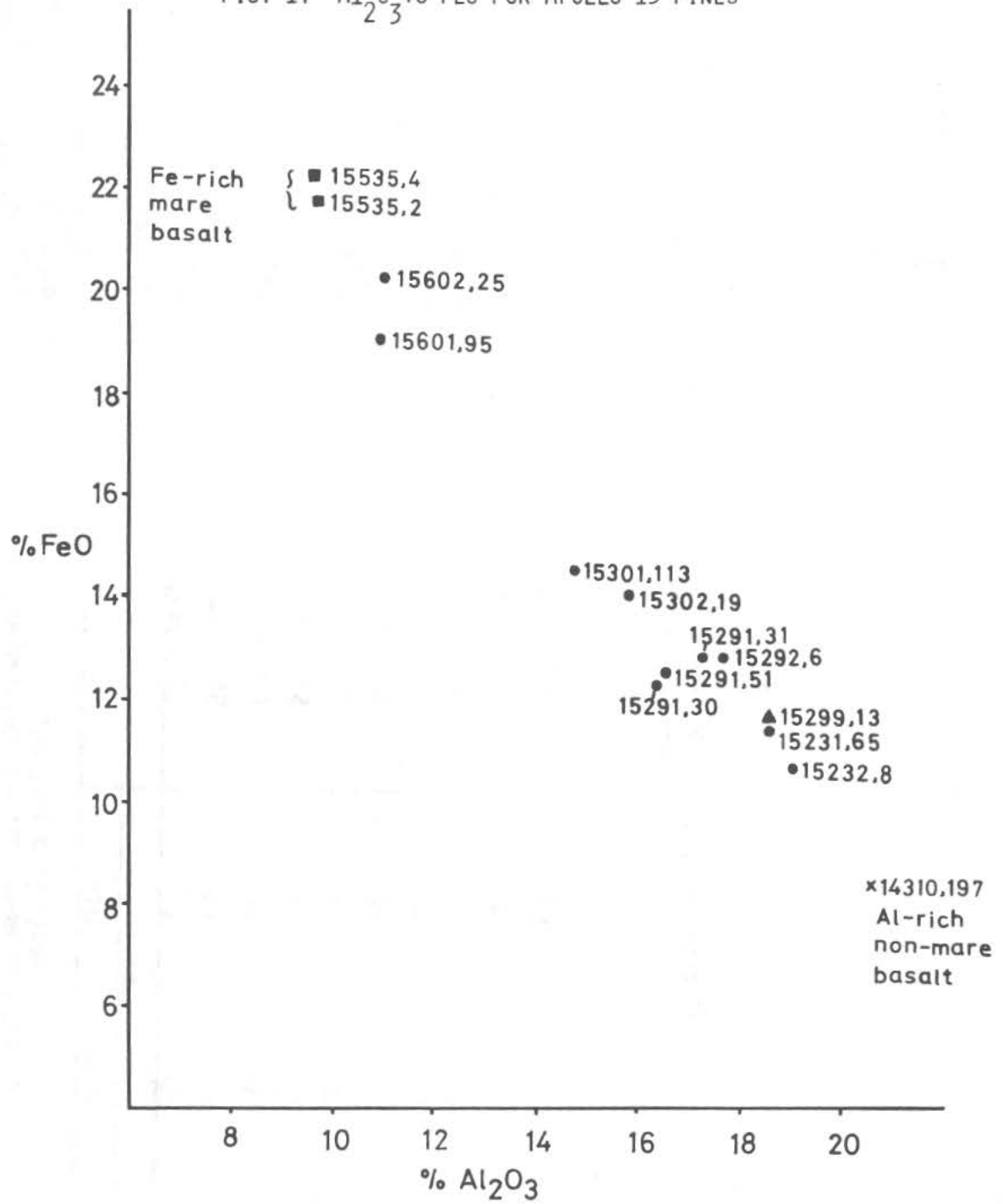

GLASS COMPOSITIONS IN BRECCIAS 15028 AND 15059; Stephen J. Kridelbaugh, Richard A. F. Grieve, and Daniel F. Weill, Center for Volcanology, University of Oregon, Eugene, Oregon, 97405.

15028 and 15059 are glass coated breccias recovered from the LM and ALSEP sites, respectively. They contain lithic fragments of basalt, pre-existing microbreccia, glass clasts of various shapes and colors, and monomineralic fragments set in a cryptocrystalline matrix. Also present are cross-cutting veinlets of highly vesicular brown glass. Texturally, the two breccias differ. 15028 shows a preferred orientation defined by elongate glass shards and the vesicular glass veinlets. Normal to the preferred orientation of 15028 lies a set of micro-faults. The micro-faults truncate all components of the breccia except the glass veinlets. 15059 does not have a preferred orientation or micro-faults. This paper reports principally on a compositional study of the glass fragments of breccias 15028 and 15059.

General Petrology

The breccias contain two types of lithic fragments; basalt clasts and clasts of a pre-existing microbreccia. Based upon the mafic mineral components, the basalt clasts can be subdivided into two groups. In 15028 the basalt is a porphyritic olivine basalt. Olivine is the major mafic component and is normally zoned from Fa_{32}-Fa_{66}, and the pyroxenes are composite grains with pigeonitic cores and augitic rims. The basalts in 15059 are ophitic pyroxene basalts, containing no olivine. The pyroxenes in 15059 are similar in composition to those found in 15028. Calcium-rich plagioclase (An_{87}-An_{92}) is the other major mineral present in all basalt clasts. Other minerals in the basalt clasts are ilmenite, Ti-chromite spinels, iron metal, troilite and residual phases. Clasts of microbreccia are subordinate in amount to basalt clasts. Microbreccia clasts are well rounded and noritic in mineralogy; the dominant minerals are orthopyroxene and plagioclase (An_{90}-An_{96}), with minor amounts of high-calcium pyroxene, ilmenite, olivine, and whitlockite.

The mineralogy of the crystal fragments includes: low-calcium pyroxene (orthopyroxene and pigeonite); augitic pyroxene; plagioclase (An_{76}-An_{95}); olivine (Fa_{11}-Fa_{56}); ilmenite (0.0-5.0 weight percent Mg); iron metal (1.5 - 14.0 weight percent Ni); troilite; and Ti-chromite spinel.

The grain size of both breccias ranges from greater than two millimeters for the basalt clasts to submicroscopic in the matrix. The average composition of six areas of the matrix in 15028 is given in Table 1 and plotted in Fig. 1.

Glass Composition in Breccias

Stephen J. Kridelbaugh

Glasses

Glass fragments constitute approximately thirty percent by volume in 15028 and twenty percent by volume in 15059. Fifty-five glass fragments were analyzed for ten elements by electron microprobe. A thirty-micron beam was used and several spots were analyzed on each fragment to determine homogeneity. The glasses are homogeneous with respect to their major element concentrations and the same preferred compositions recognized in the Apollo 15 soils (1) are also present in the breccias. The majority of the glasses show no sign of devitrification, but a few contain crystal inclusions.

Following the nomenclature of Ried, et al., (1) the dominant glass compositions correspond to mare basalts, Fra Mauro basalts and "green glasses" (2). The mare type basalt glasses occur in a variety of forms from spheres to angular fragments. They are colored in shades of brown, reddish-brown, and yellow. Compositionally, they are characterized by high iron contents and low aluminum contents (FeO ranging from 14.0 to 23.0 weight percent, and Al_2O_3 varying from 7.5 to 13.0 weight percent). On the basis of composition, glasses representative of all the subgroups of the mare type basalts, as defined by the Apollo 15 soil survey, can be recognized (Table 1, Fig. 1). It is also possible to discriminate between the mare subgroups on the basis of color. Bright yellow glasses correspond to the mare-2 type basalts and have a TiO_2 content from two to four percent, while the reddish-brown glasses conform to the mare- 4 type basalts and have a high TiO_2 content (12.0 to 14.0 weight percent). Mare-1 and mare-3 basalt types appear as brown glasses and cannot be discriminated on the basis of color.

The Fra Mauro (KREEP) basalt glasses are the most abundant type in 15028 and second only to the mare basalt glasses in abundance in 15059. They occur in colorless or light brown spherules, droplets and elongate shards, which show slight flow banding and may be subdivided in order of decreasing abundance into high potassium (1.0-1.6 K_2O), intermediate potassium (0.4-0.7 K_2O), and low potassium (0.0-0.2 K_2O) varieties. Analyses of the Fra Mauro basalt glasses are given in Table 1 and plotted in Fig. 1. Phosphorus, the other diagnostic KREEP element analyzed, is variable in content (0.26-2.19 P_2O_5). It is the Fra Mauro glass shards which define the preferred orientation in 15028.

The other major glass component is the distinctive "green glasses" (2), which are characterized by a high iron content (20.0 percent FeO) and high magnesium content (16.5 weight percent MgO), Table 1 and Fig. 1. They occur as glass spherules or as fragments of glass spheres. The color of the "green glass" in thin section varies from a light brown, few in number, to a very pale, yellow green.

Other glass compositions recognized were highland basalt (one fragment) and several glass fragments having a composition of Ca-rich plagioclase. The glass veinlets although showing flow banding are compositionally homogeneous and similar in composition to the matrix (Table 1, Fig. 1). The

Table 1. Average compositions and norms of glasses in breccias 15028 and 15059

	Glass		Mare Basalts				Fra Mauro Basalts			Green	Highland
	Matrix	Vein	M-1	M-2	M-3	M-4	Low K	Int K	High K	Glass	Basalt
SiO_2	47.98	46.47	47.16	43.84	43.84	37.03	49.38	50.49	52.74	45.36	44.49
TiO_2	1.75	1.60	2.15	3.76	3.72	13.33	0.57	1.76	1.94	0.39	1.02
Al_2O_3	14.66	16.49	13.98	10.03	8.21	7.97	19.46	16.18	15.97	7.55	23.20
Cr_2O_3	0.23	0.14	0.31	0.38	0.51	0.57	0.30	0.16	0.09	0.54	0.15
FeO	14.10	13.72	12.62	20.59	22.20	21.50	6.85	10.12	10.52	20.30	7.67
MgO	8.73	8.56	11.55	10.50	12.37	10.36	10.96	8.05	5.29	16.60	7.58
CaO	10.30	10.69	10.12	9.71	8.60	8.20	11.32	10.43	10.06	8.69	13.49
K_2O	0.41	0.36	0.23	0.09	0.08	0.15	0.06	0.52	1.15	0.02	0.15
Na_2O	0.59	0.64	0.59	0.33	0.39	0.56	0.43	0.80	1.00	0.09	0.66
P_2O_5	0.30	0.37	0.27	0.07	0.05	0.04	0.02	0.66	0.71	0.01	0.09
TOTAL	99.05	99.04	98.98	99.30	99.97	99.71	99.35	99.17	99.47	99.55	98.50
Rel Abundance*			7	14	9	7	5	17	22	17	2
Apatite	0.65	0.80	0.58	0.15	0.11	0.09	0.04	1.41	1.53	0.02	
Ilmenite	2.52	2.29	3.06	5.50	5.39	19.97	0.79	2.51	2.79	0.55	
Orthoclase	2.50	2.20	1.39	0.56	0.49	0.95	0.35	3.15	7.02	0.12	
Albite	5.47	5.91	5.41	3.11	3.64	5.41	3.86	7.36	9.27	0.82	
Anorthite	37.34	42.26	35.55	26.89	21.23	20.21	50.94	39.97	36.86	20.47	
Quartz	1.11	0.0	0.0	0.0	0.0	0.0	1.87	5.79	9.42	0.0	
Wollastonite	5.37	3.94	5.56	9.28	9.12	9.30	2.01	3.45	3.96	9.32	
Enstatite	24.90	21.35	29.64	21.97	22.37	23.43	30.22	22.76	15.08	23.76	
Ferrosilite	19.87	17.09	15.18	19.99	18.89	11.73	9.59	13.43	13.97	15.81	
Fosterite	0.0	2.23	2.18	6.34	9.86	5.50	0.0	0.0	0.0	17.12	
Fayalite	0.0	1.78	1.12	5.77	8.32	2.75	0.0	0.0	0.0	11.40	
Chromite	.26	.16	.35	.44	.58	.67	.33	.18	.10	.60	

*Relative Abundance not based on statistical survey.

Glass Compositions in Breccias

Stephen J. Kridelbaugh

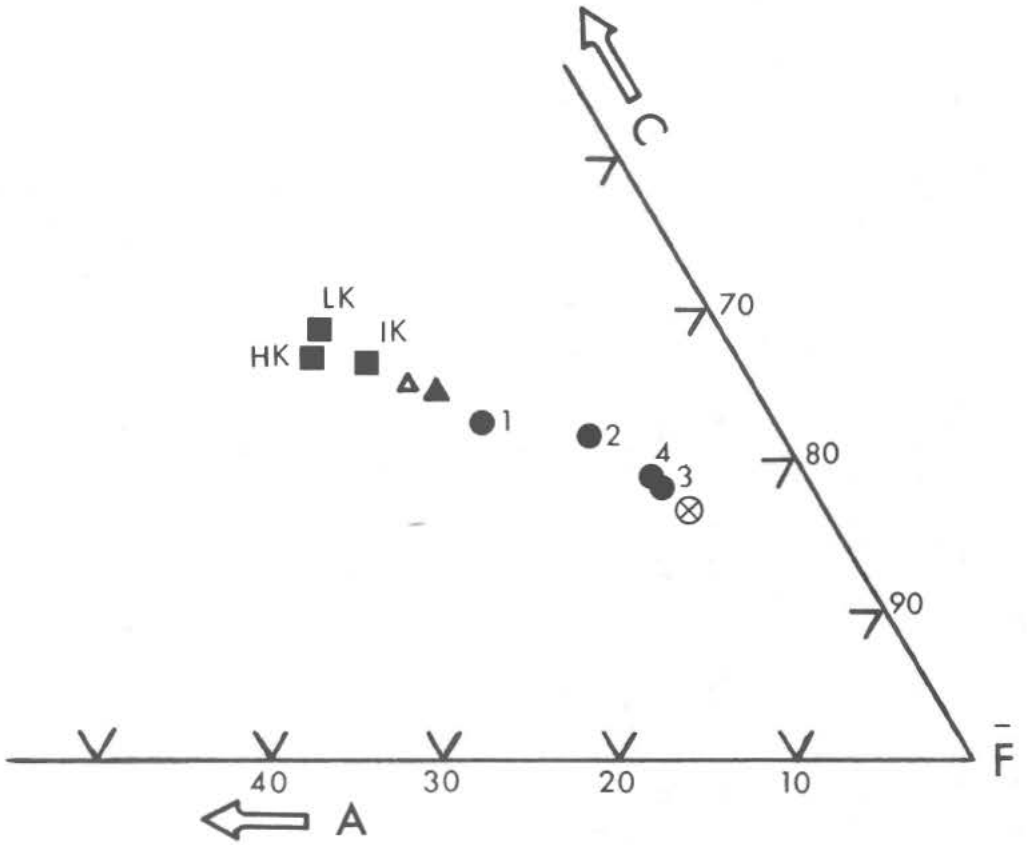

Fig. 1. ACF diagram of averaged glass compositions and matrix from Table 1. ■ represents Fra Mauro basalts; ● represents mare basalts; ⊗ is the green glass. The solid triangle is the matrix, and the open triangle is the vein.

glass vein and matrix should be a mixture of the major components, and, as shown in Fig. 1, the matrix and veinlet are intermediate between the Fra Mauro and mare basalts. Five glass particles could not be identified according to the compositional subdivisions in the Apollo 15 soil survey (1). Although a relatively small percentage of the glass population in the breccias was sampled, the volume distribution of the major compositional groups is similar to that found in the LM soil, 15021,113 (1). Most abundant are the mare and Fra Mauro (high K_2O) basalts, followed by "green glasses."

Summary

The LM and ALSEP sites are located on a possible ray from either the crater Aristillus or Autolycus. The dominance of KREEP in the LM soil (1) in contrast to the soil samples from the Apennine Front and Hadley Rille

Glass Compositions in Breccias

Stephen J. Kridelbaugh

has been equated with this ray. KREEP, especially in microbreccia 15028, is a dominant component, suggesting a common origin for both the soil and breccias. The breccias may represent a lithified portion of the ejecta from either the crater Aristillus or Autolycus.

Both microbreccias are unrecrystallized and exhibit evidence for a multi-event formation. They contain portions of an earlier ejecta blanket, as evidenced by the rounded clasts of noritic microbreccia. Following lithification as an ejecta blanket, both breccias have been subjected to similar postformational histories. Both breccias are glass coated and have glass veinlets. The close compositional similarity between the glass veinlets and the matrix suggest that the veinlets represent remobilized matrix. The local melting of the matrix to produce the glass veinlet and coating probably took place during excavation. 15028, unlike 15059, contains microfaults which truncate all components of the breccia except the glass veinlets and points to a period of mechanical disruption prior to or during excavation.

References

1. Reid, A. M., Warner, J. L., Ridley, W. I, and Brown, R. W.; Major element composition of glasses in three Apollo soils, 1972 (in press).

2. Ridley, W.I., Reid, A.M., Warner, J.L., and Brown, R.W.; Apollo 15 Green Glasses (in press) 1972, Science.

PETROLOGY OF SOME APOLLO 15 MARE BASALTS. I. Kushiro, Geophysical Laboratory, Washington, D. C., 20008.

Melting experiments and microprobe analysis have been carried out on a crystalline rock 15016(11, 51, 143). The rock is a coarse-grained basalt or dolerite with many vesicles, consisting of zoned olivine (Fo_{72}-Fo_{7}), pigeonite-ferropigeonite ($Ca_7Mg_{60}Fe_{33}$-$Ca_{11}Mg_{37}Fe_{52}$), subcalcic augite-subcalcic ferroaugite (e.g., $Ca_{25}Mg_{49}Fe_{26}$-$Ca_{19}Mg_{14}Fe_{67}$), hedenbergitic clinopyroxene (e.g., $Ca_{39}Mg_3Fe_{58}$), plagioclase ($An_{94}Ab_6Or_{0.1}$-$An_{80.7}Ab_{15.7}Or_{3.6}$), ilmenite, chromite solid solution, chromian ulvö spinel, cristobalite and minor constituent minerals. The amount of mafic minerals exceeds 70 vol.% of the rock. The bulk composition of the rock determined by conventional rock analysis method is as follows: SiO_2 43.78, TiO_2 2.28, Al_2O_3 8.17, FeO 22.50, MnO 0.33, MgO 11.58, CaO 9.06, Na_2O 0.24, K_2O 0.04, P_2O_5 0.25, Cr_2O_3 1.10, S 0.19, Total 99.52 (Analyst, H. Haramura). The FeO/MgO ratio is near the middle of the range of the Apollo 12 crystalline rocks, although its composition does not lie on the olivine control trends of the Apollo 12 crystalline rocks.

The results of the melting experiments are shown in Fig. 1. The oxygen fugacity of the runs which were made with graphite capsules was that for the stability of wüstite. Olivine is liquidus or near liquidus phase up to about 11 kb. Its composition is Fo_{72} near the liquidus (1290°C) at 6 kb, becoming less magnesian with lowering temperature (Fo_{70} at 1240°C). Spinel is a solid solution of spinel, chromite and ulvöspinel (e.g., 24, 67 and 9 mol.%, respectively at 1275°C at 10 kb). Pigeonitic clinopyroxene is the third mineral to crystallize up to about 11 kb, but may be on the liquidus above 15 kb. The composition is about $Ca_6Mg_{69}Fe_{25}$, $Ca_{10}Mg_{63}Fe_{27}$ and $Ca_7Mg_{67}Fe_{26}$ at 1275°-10 kb, 1250°-10 kb and 1240°-6 kb, respectively. Plagioclase crystallizes at lower temperatures and at pressures lower than 10 kb. Above 10 kb plagioclase is absent and olivine and spinel bearing pyroxenite assemblage is stable at subsolidus temperatures. The experimental results indicate that the melt of 15016 rock composition is in equilibrium with olivine up to about 7 kb and with olivine and spinel up to 11 kb(~200 km). The rock is relatively rich in olivine, but it is small in grain size and does not appear to be cumulate olivine. If the magma of this

PETROLOGY OF APOLLO 15 MARE BASALT

I. Kushiro

rock composition was formed in the lunar interior (<200km) by partial or complete melting, the source material must have contained olivine. The experimental results indicate that the

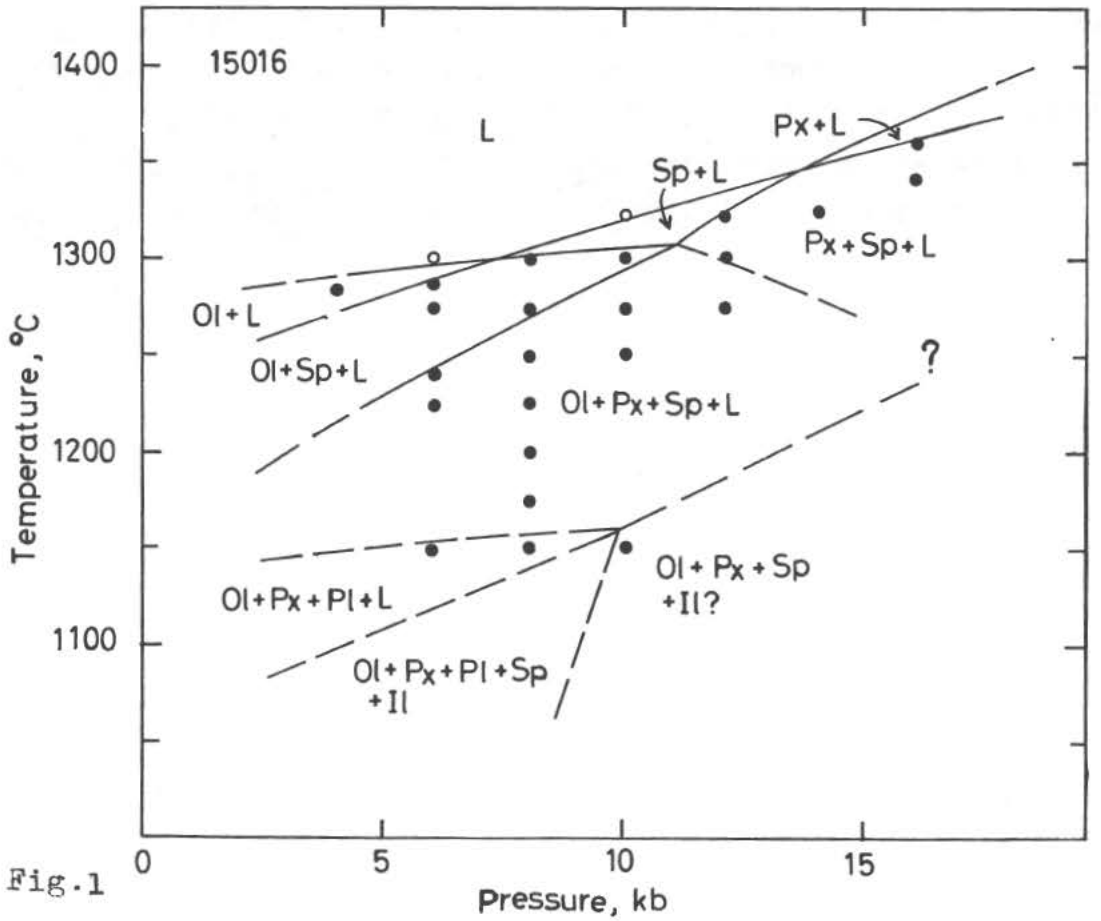

Fig.1

composition of olivine in equilibrium with this magma is Fo_{72} at about 6 kb (~110 km). Olivine of such composition is much more Fe-rich than those of the earth's upper mantle material such as peridotite inclusions in kimberlite. The Apollo 14 rocks (e.g., 14310) suggest, however, that the lunar interior has the Fe/Mg ratio similar to those of the earth's upper mantle materials. The discrepancy may be due to the heterogeneity of the lunar interior at least in Fe/Mg ratio, or the magma of 15016 as well as those of many other iron-rich basalts is a product of advanced fractional crystallization of a primitive magma with or without subsequent remelting.

Preliminary microprobe analysis has been also made on porphyritic pigeonite basalt 15476(32) and olivine basalt 15545 (2). The rock 15476, consisting of large euhedral pigeonite phenocryst and groundmass with variolitic texture, was clearly formed by rapid quenching of magma containing pigeonite crystals. The

PETROLOGY OF APOLLO 15 MARE BASALT

I. Kushiro

porphyritic pigeonite with low-Ca core ($Ca_5Mg_{69}Fe_{26}$-$Ca_9Mg_{61}Fe_{30}$) is rimmed by zoned augite-subcalcic ferroaugite (e.g., $Ca_{33}Mg_{45}Fe_{22}$-$Ca_{28}Mg_2Fe_{70}$) or is zoned to ferropigeonite and subcalcic ferroaugite ($Ca_{21}Mg_{23}Fe_{56}$). Plagioclase has composition $An_{94}Ab_6$-$An_{87}Ab_{13}Or_{0.1}$. The rock 15545 contains zoned olivine (Fo_{56}-Fo_{17}), pigeonite-ferropigeonite ($Ca_{11}Mg_{54}Fe_{35}$-$Ca_{12}Mg_{39}Fe_{49}$-$Ca_{15}Mg_{16}Fe_{59}$), augite-ferroaugite ($Ca_{31}Mg_{41}Fe_{28}$-$Ca_{22}Mg_{11}Fe_{67}$), subcalcic augite and ferroaugite and plagioclase ($An_{91}Ab_{8.5}Or_{0.5}$-$An_{79}Ab_{18}Or_3$).

PETROLOGY OF MARE/RILLE BASALTS 15555 AND 15065. John Longhi, David Walker, Edward N. Stolper, Timothy L. Grove and James Fred Hays, Department of Geological Sciences, Hoffman Laboratory, Harvard University, Cambridge, Mass. 02138

Lunar samples 15555 and 15065 are mare/rille type basaltic rocks. 15555, an olivine-phyric variety, has been extensively studied by LSPET and others (1); 15065 is a relatively coarse grained quartz-normative rock from the rim of Elbow Crater. We now report the results of petrographic and electron microprobe studies of sections of these rocks (15555,246 and 15065,86) and of melting and phase equilibrium experiments on rock powders (15555,225 and 15065,29).

Rock 15555 is medium grained (<1.5 mm) with zoned subrounded crystals of olivine (Fa29-41) and pigeonite poikilitically included in anhedral zoned plagioclase (An94-78). Cr-ulvöspinel and Ti-chrome spinel crystallized early and are included within the pyroxene grains as are many small olivine crystals. Ilmenite occurs only in the Fe-rich pyroxene rims and in the residuum with fayalite, cristobalite and glass. Cores of Mg-pigeonite zone to low calcium augite and then either toward ferrohedenbergite or ferrosilite. Ti/Al zoning in pyroxene shows a three-stage pattern: 1) increasing Ti and Al; 2) increasing Ti, constant Al; 3) decreasing Ti and Al. If the change from 1) to 2) corresponds to the onset of plagioclase crystallization and the change from 2) to 3) to the onset of ilmenite crystallization, then we infer that the rock was about 45% crystalline prior to the appearance of plagioclase and more than 90% crystalline prior to the appearance of ilmenite. This interpretation is supported by the Ti-Al contents of synthetic pyroxenes equilibrated at various temperatures (Fig. 1). Comparison of natural and synthetic pyroxenes shows that the high Ti/Al ratio of the natural pyroxenes precludes crystallization at a depth greater than 200 km.

Plagioclase grains have homogeneous cores (An94-91); Fe/Mg = .5) surrounded by strongly and continuously zoned rims (An91 to An78; Fe/Mg = .6 to .9). Rim crystallization apparently occurred simultaneously with the crystallization of pyroxene rims and the mesostasis. There is no evidence of alkali loss during crystallization.

Petrology of Mare/Rille Basalts

John Longhi

Rock 15065 is a relatively coarse grained (1-5 mm) rock with euhedral zoned pigeonite partially included within zoned plagioclase crystals (An91-80). A few pigeonite grains show an unusual intergrowth with plagioclase on their outer margins: parts of the pyroxene crystals appear poikilitically included in plagioclase but are optically continuous with the larger pyroxenes. This texture is interpreted as the result of slow late stage crystallization of these two phases.

Plagioclase zoning is similar to that in 15555. A few ragged anhedral olivine crystals (Fa_{48-50}) occur as inclusions in pyroxene. As in 15555, Cr-ulvöspinel and Ti-chrome spinel are included within the pyroxene while ilmenite is concentrated at the margins of zoned pyroxene grains and bordering the mesostasis. This mesostasis consists of euhedral fayalite (Fa_{98}), cristobalite and tridymite, native iron, and glass. Native iron also occurs within the outer margins of pyroxene grains in 15065 in contrast to 15555 where it occurs only in the mesostasis or with ilmenite. The smooth outlines of these grains of native iron suggest primary crystallization, and contrast with the ragged products of subsolidus reduction in Apollo 14 rocks (2).

Results of phase equilibrium experiments on these rock compositions are shown in Figs. 2 and 3. The low pressure crystallization sequence in each case matches the sequence inferred for the natural rock, except that we have not been able to crystallize ilmenite and other late-stage natural phases near the solidus. Compositions of synthetic ferromagnesian phases are more magnesian than those of the natural phases due to iron-loss during the experimental runs (3). After 10% correction for iron loss the liquidus olivine in 15555 has composition Fa_{31}. This is close to the prediction of Chappell *et al* (4); we find, however, in contrast to Chappell *et al*, that the cores of natural olivine in our section are also close to this composition, hence their argument for copious addition of cumulus olivine to this rock is weakened. We do find, however, that even after correction for iron loss, synthetic pyroxenes from both rocks are significantly more magnesian (*e.g.* $En_{76}Fs_{20}Wo_4$) than their natural equivalents (*e.g.* $En_{62}Fs_{30}Wo_8$). Thus addition of cumulus pyroxene to both rocks seems likely.

Note that plagioclase appears late in the crystallization sequence of both rocks from both textural and experimental evidence. This implies that schemes for relating compositional trends or explaining Eu anomalies that rely on fractionation of plagioclase crystals are suspect (5).

Petrology of Mare/Rille Basalts

John Longhi

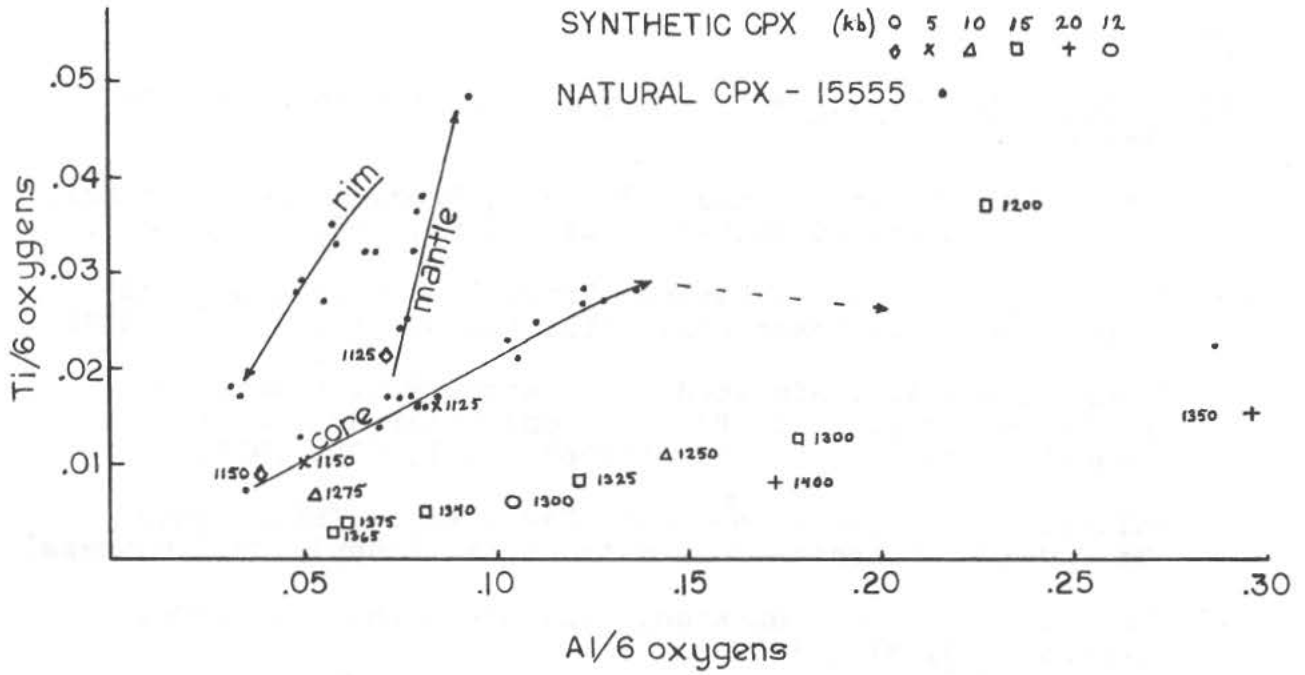

FIG. 1

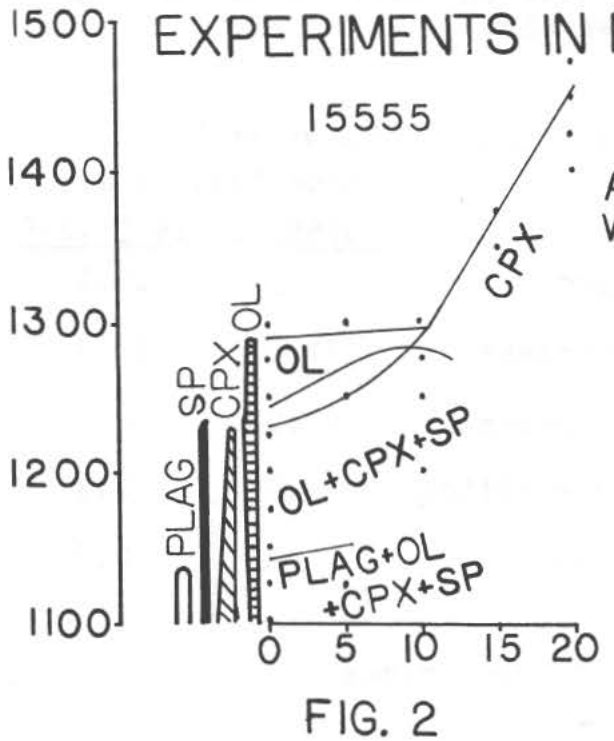

FIG. 2

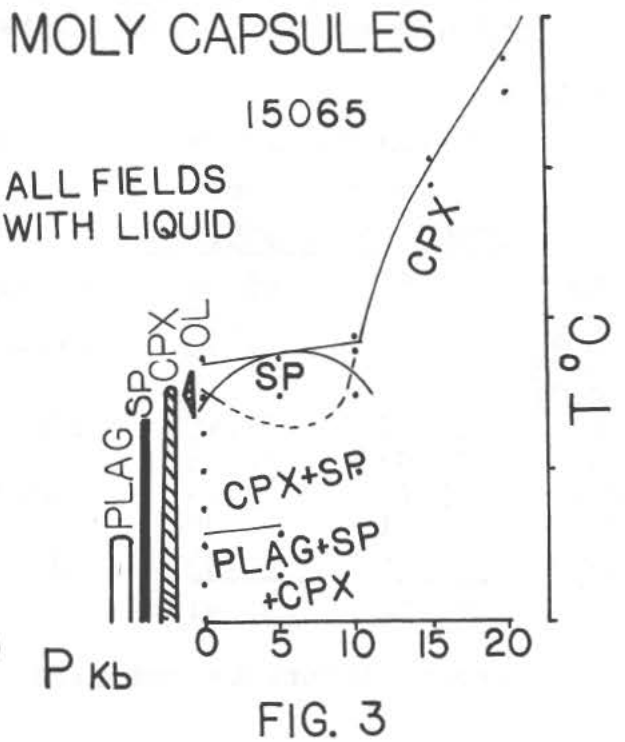

FIG. 3

Petrology of Mare/Rille Basalts

John Longhi

REFERENCES

(1) LSPET, Science 175, 363, 1972; and other papers in this issue.

(2) Longhi, J., D. Walker and J.F. Hays, Proc. Third Lunar Sci. Conf., Geochim. Cosmochim. Acta. (Suppl. 3), (in press).

(3) Ringwood, A.E. and E. Essene, Proc. Apollo 11 Lunar Sci. Conf., Geochim. Cosmochim. Acta, (Suppl. 1), 1, 769, 1970.

Green, D.H., A.E. Ringwood, N.G. Ware, W.O. Hibberson, A. Major and E. Kiss, Proc. Second Lunar Sci. Conf., Geochim. Cosmochim. Acta, (Suppl. 2) 1, 605, 1971.

Walker, D., J. Longhi and J.F. Hays, Proc. Third Lunar Sci. Conf., Geochim. Cosmochim. Acta, (Suppl. 3),(in press).

(4) Chappell, B.W., W. Compston, D.H. Green and N.G. Ware, Science 175, 415, 1972.

(5) Schnetzler, C.C., J.A. Philpotts, D.F. Nava, S. Schulmann and H.H. Thomas, Science 175, 426, 1972.

(6) This work supported by NASA grants NGR 22-007-175 and NGR 22-007-199 and the Committee on Experimental Geology and Geophysics, Harvard University.

TABLE 1

Major Element and Model Analyses of Lunar Samples

	Wt.% oxides*			Mode (Volume %)	
	15065,29	15555,225		15065,86	15555,246
SiO_2	48.66	45.86	olivine	1.3	12.1
TiO_2	1.55	2.40			
Al_2O_3	9.17	8.29	plagioclase	31.6	30.4
Cr_2O_3	.82	.69			
FeO	19.07	23.45	clinopyroxene	63.0	52.4
MgO	10.57	11.55			
CaO	9.70	9.24	glass + silica	1.9	2.3
K_2O	.11	.09			
Na_2O	.36	.34	opaques	2.2	2.7
	100.02	101.91			

*Electron microprobe analyses of fused rocks

MINERALOGY AND PETROLOGY OF LUNAR SAMPLES 15264,19, 15274,12, AND 15314,59 Brian Mason, Smithsonian Institution, Washington, D.C.

In the allocation of Apollo 15 coarse fines (4-10 mm) three fragments were received for investigation, as follows:
15264,19: 0.026 g; from trench at Station 6, base of Hadley Delta (Apennine Front).
15274,12: 0.037 g; from surface at Station 6, base of Hadley Delta.
15314,59: 0.169 g; from surface at Station 7, rim of Spur Crater of lower slope of Hadley Delta.

Sample 15264,19 is an anorthosite fragment, consisting of more than 90% plagioclase (An_{90-99}, average An_{96}, by microprobe analysis), with a little orthopyroxene (average composition $Wo_3Fs_{25}En_{72}$), and trace amounts of opaques (three small grains of metallic iron and one grain of chromite). The fragment has a cataclastic texture, the size of the plagioclase grains ranging from a few microns up to 0.5 mm. The rock is quite indurated, evidently by shock compaction, since there is no glassy interstitial matter welding the grains together.

Sample 15274,12 is a breccia consisting largely (~80%) of pale brown glass, which encloses angular fragments of plagioclase (An_{83-99}, average An_{91}) up to 0.3 mm across and occasional feldspathic basalt fragments (largely remelted and assimilated); a minute amount of opaque material, identified as micron-sized particles of metallic iron, is also present. The brown glass was analysed (10 spots) with the microprobe, with the following results (weight percent, range and average): SiO_2 44.9-48.8, 46.7; TiO_2 0.11-0.38, 0.23; Al_2O_3 25.3-31.4, 27.4; FeO 1.0-7.3, 3.9; MnO 0.02-0.10, 0.06; MgO 0.6-7.0, 3.9; CaO 15.5-19.0, 16.9; Na_2O 0.36-0.46, 0.41; K_2O 0.01-0.08, 0.05. The norm calculated from the average analysis is (weight percent): an 72.6, ab 3.7, di 6.9, hy 13.0, il 0.4, Q 1.9. This composition corresponds to an anorthositic gabbro, and is similar to rock 15418 from Station 7 analysed by LSPET (1). The structure and composition of this fragment suggests it may be a shock-melted sample of highland regolith.

Sample 15314,59 has gabbroic composition, consisting of plagioclase (60%), pyroxene (25%), olivine (10%), and ilmenite (5%). Plagioclase compositions range from An_{82} to An_{95}, with a mean of

MINERALOGY AND PETROLOGY OF LUNAR SAMPLES

Brian Mason

An_{90}; some of the grains are weakly zoned with An content diminishing somewhat from core to margin. Most of the pyroxene grains are composite, with colorless pigeonite cores (average $Wo_7Fs_{24}En_{69}$) rimmed by pale brown subcalcic augite (average $Wo_{27}Fs_{19}En_{54}$). Olivine grains are rather uniform in composition, averaging Fa_{32}. The fragment has a cataclastic structure with porphyroclasts of plagioclase up to 0.5 mm across in a finer-grained groundmass of plagioclase, pyroxene, olivine, and ilmenite. The groundmass has a granular or hornfelsic texture, suggesting it may have been somewhat annealed or recrystallized after the cataclastic event. Recrystallization is also indicated by the compositional relationship between olivine and pigeonite; the olivine has a somewhat higher Fe/Fe+Mg ratio than the pigeonite, consistent with equilibrium crystallization rather than sequential crystallization typical of magmatic conditions.

This work has been supported by grant NGR 09-015-146 from the National Aeronautics and Space Administration. I am indebted to Mr. J. Nelen for assistance with the microprobe analyses.

(1) LSPET (1972). The Apollo 15 lunar samples: a preliminary description. Science, 175, 363-375.

MINERALOGY AND PETROLOGY OF POLYMICT BRECCIA 15498

Brian Mason, Smithsonian Institution, Washington, D.C. 20560

Rock 15498 was a 2339.8 g specimen approximately 18 x 14 x 12 cm, collected at Station 4 on the south rim of Dune Crater. A 1.5 cm thick slab, weighing approximately 250 g, was cut from this rock, and portions of this slab distributed to a consortium for a variety of investigations. The present author is responsible for the mineralogical and petrographic description.

The cut surface of the slab was roughly rectangular, with maximum dimensions 9 x 7 cm; several fissures coated with dark vesicular glass transected the slab. The cut surface was medium gray in color, and numerous irregular-shaped rock clasts ranging up to about 1 cm in maximum dimension were prominent. All the clasts were lighter in color than the matrix, ranging from white to pale gray. A rough estimate of 10% of clasts larger than 0.5 cm in maximum dimension was made by visual inspection.

Most of the material examined microscopically was taken from a column 1.5 cm square cut from the slab. The LRL subnumbers for the specimens examined are 34, 38, 48, 49, 50, 52; in addition a polished thin section 15498,101 was provided.

The breccia is a well indurated rock, and tends to break through mineral grains and rock fragments. Porosity is very low, but the rock is cut by macroscopic and microscopic fissures, which show subparallel orientation in thin sections. The following components can be identified: rock fragments; mineral fragments; glass fragments, spherules, and fissure fillings; and interstitial glass welding these components together. The specific gravity of a small but representative fragment is 3.02.

The rock fragments make up about 20% of the rock. In a thin section most of them range from 0.5-2 mm across. They are mainly mare basalts, closely resembling those described from Dune Crater (1), and are presumably locally derived; some of these fragments show shock effects such as partial crushing and grain deformation. One fragment of a non-mare, KREEP - type basalt, 0.6 mm across, consisting of dominant plagioclase, orthopyroxene, and interstitial glass, was noted. Plagioclase-rich fragments, many of which showed partial granulation, are not uncommon, and are prominent among the larger clasts. One of these (15498,38) was sectioned and found to consist of 90% plagioclase (An_{85}-An_{95}),

MINERALOGY AND PETROLOGY OF POLYMICT BRECCIA 15498

Brian Mason

with minor amounts of olivine (Fa_{35}) and pyroxene (average $Wo_{15}Fs_{47}En_{38}$). One large rock clast (15498,52), about 10 mm in maximum dimension, proved to be a fine-grained (0.05-1 mm) pyroxenite, with interstitial plagioclase, chromite, and ilmenite. The pyroxene ranged in composition from pigeonite to subcalcic augite, the range being from $Wo_8Fs_{30}En_{62}$ to $Wo_{24}Fs_{46}En_{30}$ and the average $Wo_{15}Fs_{38}En_{47}$. Some small fragments of microbreccia, presumably from an earlier generation, were also noted.

The mineral fragments make up about 50% or possibly more of the breccia; since they range in size from about 0.5 mm down to the limit of microscopic resolution it is difficult to make a precise estimate. They consist of pyroxenes ($\sim$50%), plagioclase ($\sim$30%), olivine ($\sim$15%), and opaques ($\sim$5%). The pyroxenes are almost entirely pigeonite and subcalcic augite, and show a wide range in composition, from $Wo_6Fs_{28}En_{66}$ to $Wo_{26}Fs_{59}En_{15}$; the average is $Wo_{16}Fs_{40}En_{44}$. One grain of magnesium-rich orthopyroxene, $Wo_3Fs_{16}En_{81}$, was analysed. The olivine ranges in composition from Fa_{26} to Fa_{51}, with an average of Fa_{39}. Plagioclase ranges in composition from An_{75} to An_{98}, with an average of An_{85}. The proportions of these minerals and their composition ranges closely resemble those in the fines at this locality (1).

Glass fragments, spherules, and fissure fillings make up about 10% of the breccia. Spherules are rare, small (usually $<$ 0.1 mm diameter), commonly red-brown in color, and sometimes show devitrification. Glass fragments tend to be larger (up to 0.3 mm long), may be pale brown, pale green, or colorless, and frequently show devitrification. Fissure fillings consist of highly vesicular glass, gray-green and isotropic in thin section; a microprobe analysis gave the following results (weight percent): SiO_2 47.4, TiO_2 1.9, Al_2O_3 12.8, FeO 16.8, MnO 0.22, MgO 10.5, CaO 9.8, Na_2O 0.41, K_2O 0.11, sum 99.9. This analysis is very similar to the analysis of the fines from this locality (1).

The interstitial glass which welds the breccia together amounts to about 20% of the rock, and is pale to dark brown in color. It is turbid from the presence of minute included mineral grains and possible beginning devitrification.

The mineralogical and petrographic evidence supports the hypothesis that this breccia represents lithified regolith at the Dune Crater locality. Chemical and mineralogical composition is comparable with that of the fines at this locality. Most of the material in the breccia was ultimately derived from local mare basalts, with the addition of a minor amount of foreign material presumably derived from the Apennine Front. This foreign

MINERALOGY AND PETROLOGY OF POLYMICT BRECCIA 15498

Brian Mason

material was rich in calcic plagioclase, and probably consisted largely of anorthosite and anorthositic gabbro. Lithification has taken place largely by the welding action of interstitial glass. Whether lithification was caused by impact compaction or by a base-surge process is not entirely clear; however, the presence of subparallel microfractures suggests consolidation by impact events on the regolith.

This work has been supported by grant NGR 09-015-146 from the National Aeronautics and Space Administration.

(1) Mason, B., Jarosewich, E., Melson, W.G., and Thompson, G. (1972). Mineralogy, petrology, and chemical composition of lunar samples 15085, 15256, 15271, 15471, 15475, 15476, 15535, 15555, and 15556. Proc. Third Lunar Science Conference, in press.

CRYSTAL CHEMISTRY OF ZONED CLINOPYROXENES FROM LUNAR ROCK 15058; Anne Morawski, Dept. of Geology, Wellesley College, Wellesley, Mass. 02181, David J. Vaughan and Roger G. Burns, Dept. of Earth and Planetary Sciences, Massachusetts Institute of Technology, Cambridge, Mass. 02139.

Rock 15058 is a porphyritic basalt containing zoned acicular clinopyroxene phenocrysts up to 1 cm. in length. A 0.82 gm. sample of this rock was disintegrated with gentle crushing in an ultrasonic vibrator, and phenocrysts were separated by hand under a binocular microscope. The separated mineral fractions included pale yellow-green pigeonite "cores" and pale red-brown subcalcic augite "mantles", together with an opaque mineral fraction and a feldspar fraction containing pyroxene inclusions. We summarize here data on the crystal chemistry of the clinopyroxene fractions derived from microprobe analyses and measurements of the Mossbauer spectra and polarized absorption spectra of the pigeonite "cores" and subcalcic augite "mantles".

The Mossbauer spectra of ^{57}Fe in the pigeonite "cores" and subcalcic augite "mantles" are shown in figures 1 and 2, respectively. Computer fitting of the spectra indicates that Fe^{2+} ions occur in both M1 and M2 sites of the pyroxene structure in each fraction. However, the site populations estimated from the areas under component doublets differ significantly. In the "cores" the ratio of Fe^{2+} ions in M1:M2 is 0.601:1, compared to 0.316:1 for the iron-rich "mantles". No Fe^{3+} doublet could be resolved in the spectra. No evidence for Ti^{3+} ions could be obtained from the polarized absorption spectral measurements of single crystals in contrast to pyroxenes from Apollo 11 rocks.(1)

Electron microprobe analyses indicate that the pyroxene phenocrysts are compositionally zoned. The "cores" are magnesian pigeonite containing some iron and small amounts of Cr,Ti and Al. Assuming that (1) Ca occupies M2 positions only; (2) Cr and Ti occur in M1 positions; and (3) the deficiency of silicon is made up entirely by Al^{3+} ions, the site populations and oxidation states of the cations in the pigeonite "cores" may be expressed by the formula

$$(Ca^{2+}_{0.09}Fe^{2+}_{0.24}Mg^{2+}_{0.67})(Fe^{2+}_{0.15}Mg^{2+}_{0.82}Cr^{3+}_{0.02}Ti^{4+}_{0.01})(Si^{4+}_{1.96}Al^{3+}_{0.04})O_6$$

M2 M1

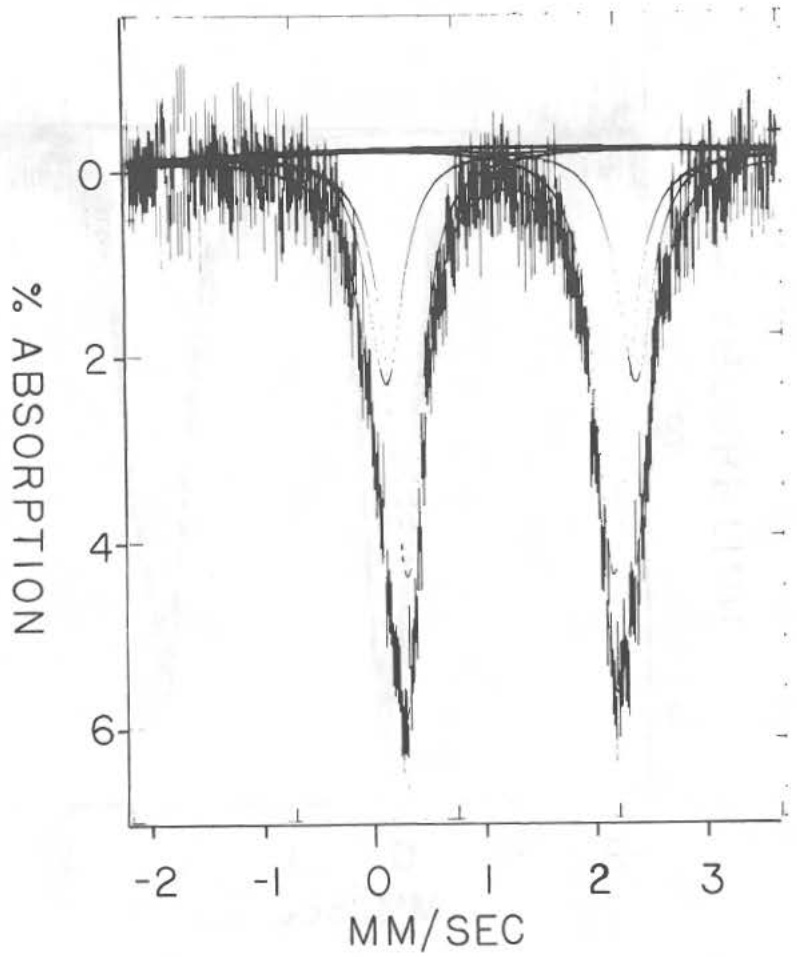

Figure 1. Mossbauer spectrum of ^{57}Fe in the pigeonite "cores" of clinopyroxene phenocrysts from lunar rock 15058. The spectrum was obtained at room temperature and the zero of the velocity scale is the center of the spectrum of iron at room temperature.

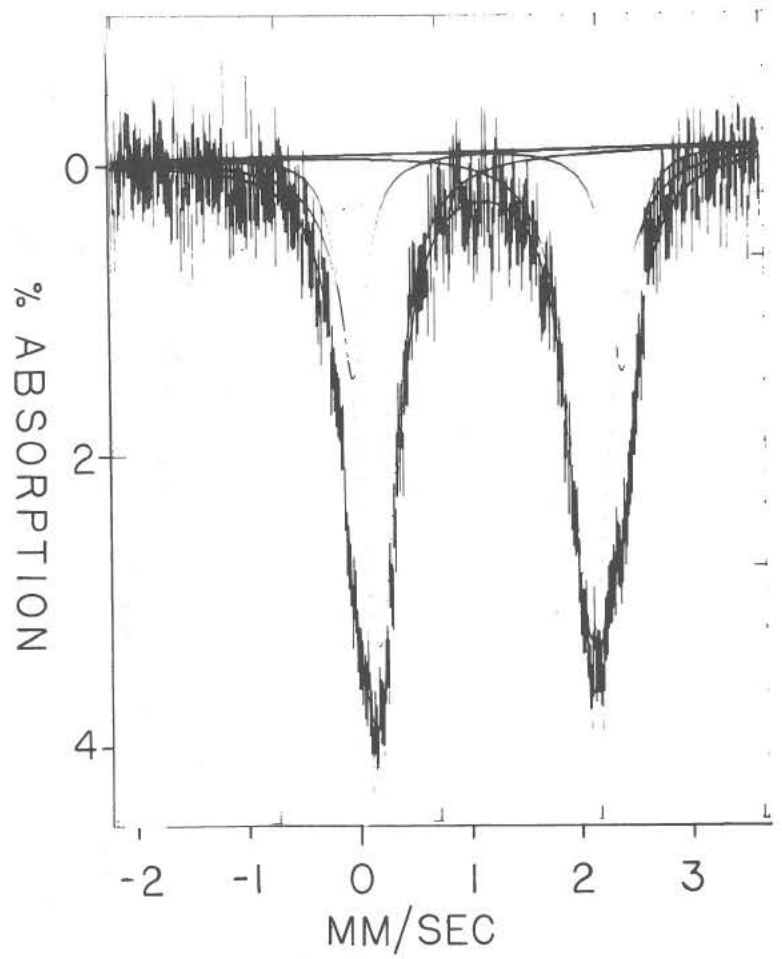

Figure 2. Mossbauer spectrum of ^{57}Fe in the subcalcic augite "mantles" of clinopyroxene phenocrysts from lunar rock 15058. The spectrum was obtained at room temperature and the zero of the velocity scale is the center of the spectrum of iron at room temperature.

Similarly, the "mantles" of subcalcic augite approximate the formula

$$(Ca^{2+}_{0.29}Fe^{2+}_{0.50}Mg^{2+}_{0.21})(Fe^{2+}_{0.16}Mg^{2+}_{0.81}Cr^{3+}_{0.01}Ti^{4+}_{0.02})(Si^{4+}_{1.95}Al^{3+}_{0.05})O_6$$

M2 M1

The research is supported by NASA Grant No. NGR 22-009-551.

Reference Cited

(1) R.G. Burns, R.M. Abu-Eid and F.E. Huggins, Proc. 3rd Lunar Sci. Conf., Geochim. Cosmochim. Acta, Suppl., vol. 1 (1972).

SUBSOLIDUS RELATIONS OF PYROXENES FROM APOLLO 15 BASALTS; J. J. Papike, A. E. Bence, and M. A. Ward, State Univ. of New York, Stony Brook, N. Y. 11790

Pyroxenes from Apollo 15 basalts 15499, 15058, 15016, and 15555 have been studied by a combination of single crystal X-ray diffraction and microprobe techniques. Individual crystals were first studied by X-ray diffraction to elucidate the exsolution relationships including the relative orientation of host and lamellae, symmetry of exsolved phases and the degree of subsolidus phase separation. These crystals were subsequently analyzed by microprobe techniques so that correlations between the chemical and crystallographic data could be made in defining subsolidus cooling histories.

A previous study[1] suggested that Apollo 15 rocks 15499 and 15058 could have come from the top and interior, respectively, of one lava flow. These conclusions were based on bulk chemistry, textural arguments, and the chemical zoning trends in the pyroxenes. The present study provides one test of this hypothesis. Rock 15499 contains composite pyroxenes with pigeonite cores and augite rims set in a fine-grained variolitic groundmass containing abundant vesicles. Major and minor element zoning trends of the phenocrysts indicate a continuous buildup of Al (figure 1, increasing Al indicated by size of triangles) to the augite rim at which time plagioclase and iron pyroxene coprecipitated in a fine-grained variolitic aggregate that includes abundant glass. No calcium discontinuity is observed in the major element trends. The phenocrysts are well-developed and show little evidence of resorption. All of these features suggest a rapid, late-stage quench. Rock 15058, on the other hand, contains composite pyroxenes phenocrysts set in a medium-grained subophitic groundmass. Vesicles are rare and interstitial glass is absent. Major and minor element zoning trends (figure 2) reveal only minor buildup of Al and a very pronounced Ca-discontinuity in the augite trend. This discontinuity correlates texturally with the appearance of plagioclase in the paragenetic sequence.[1] The pyroxene phenocrysts have poor form development and appear extensively resorbed.

Single-crystal X-ray diffraction studies of both pigeonite and augite from the 15499 phenocrysts indicate that virtually no exsolution has taken place; an observation consistent with rapid cooling (figure 3). Pyroxenes from 15058 with iron contents > Fs_{40} and calcium contents > Wo_{10} have significant exsolution and phase separation between the $\underline{P}2_1/\underline{c}$ pigeonites and $\underline{C}2/\underline{c}$ augites (figure 4) suggesting slow subsolidus cooling relative to 15499. One measure of this phase separation is the crystallographic parameter $\Delta\beta = \beta_{pigeonite} - \beta_{augite}$.[2] A mean $\Delta\beta$ for the 15058 pyroxene crystals studied is 2.9^{o} (Table 1). This is virtually identical to pyroxenes from rock 12021 which we previously concluded had a slow subsolidus cooling history. One important difference between pyroxenes from 15058 and 12021 is that pigeonites from 12021 have augites exsolved on (100) and (001), while pigeonites from 15058 show no exsolved augite (figure 4). The very low calcium content of the

Pyroxene Subsolidus

J. J. Papike

15058 pigeonites may account for the lack of exsolution. On cooling, these pigeonites, if sufficiently low in Ca, could intersect the solvus at a temperature where exsolution is inhibited.

Another pair of Apollo 15 rocks, 15016 and 15555, also display very similar bulk compositions but distinctly different textures. Basalt 15016 is a highly vesicular basalt containing weakly-zoned composite clinopyroxene phenocrysts in a matrix with an intersertal to subophitic texture. Olivine is abundant and ilmenite plates line the vesicles. Basalt 15555 also contains composite clinopyroxene as well as olivine phenocrysts in a matrix dominated by poikilitic plagioclase crystals enclosing small euhedral augites and olivines. Both interstitial glass and vesicles are absent. We previously suggested that 15016 could have come from a shallower and 15555 a deeper portion of the same lava flow. Although our crystallographic data is not complete on these rocks, there is an indication that 15016 cooled somewhat more quickly than 15555. The mean $\Delta\beta$ for five crystals from 15555 (figure 5) is 2.1^{o}, while the $\Delta\beta$ for 1 crystal from 15016 is 1.5^{o}. The abundance of vesicles in 15016, the only slightly smaller $\Delta\beta$ than 15555, and the identical chemistries of these two rocks are all consistent with their being derived from the top and interior of the same sill.

If $\Delta\beta$ is a valid measure of subsolidus cooling history, our results for the four Apollo 15 basalts studied indicate that the order from fastest to slowest cooling is 15499 > 15016 > 15555 > 15058.

An additional observation on the orientation of epitaxial augite on pigeonite is that the common plane is (100) which confirms our earlier observation for pyroxenes from Apollo 12 rock 12052.[2]

References

(1) Bence, A. E. and J. J. Papike, 1972, Pyroxenes as recorders of lunar basalt petrogenesis: Chemical trends due to crystal-liquid interaction. Proc. Third Lunar Sci. Conf., Geochim. Cosmochim. Acta, in press.

(2) Papike, J. J., A. E. Bence, G. E. Brown, C. T. Prewitt and C. H. Wu, 1971, Apollo 12 clinopyroxenes: Exsolution and epitaxy, Earth and Planetary Sci. Letters 10, pp. 307-315.

Pyroxene Subsolidus

J. J. Papike

Table 1

Sample number	Crystal number	Pyroxenes	a(Å)	b(Å)	c(Å)	β	V(Å^3)	Space group
15058	A-1	Pigeonite	9.78	9.03	5.27	108.6	442	$P2_1/c$
		(001) Augite	9.78	9.03	5.26	106.0	447	$C2/c$
15058	A-2	Pigeonite	9.73	8.99	5.28	108.8	437	$P2_1/c$
		(001) Augite	9.73	8.99	5.32	106.0	447	$C2/c$
15058	P-1	Pigeonite	9.69	8.90	5.22	108.8	426	$P2_1/c$
15058	P-2	Pigeonite	9.69	8.90	5.22	108.6	427	$P2_1/c$
15058	P-3	Pigeonite	9.69	8.90	5.22	108.5	427	$P2_1/c$
15058	1	Pigeonite	9.77	8.99	5.26	108.7	438	$P2_1/c$
		(001) Augite	9.77	8.99	5.20	106.0	440	$C2/c$
15058	2	Pigeonite	9.73	9.03	5.26	108.6	439	$P2_1/c$
		(001) Augite	9.73	9.03	5.25	105.7	444	$C2/c$
15058	3	Pigeonite	9.78	9.04	5.26	108.3	441	$P2_1/c$
		(001) Augite	9.78	9.04	5.26	105.8	448	$C2/c$
15058	4	Pigeonite	9.69	8.96	5.24	108.7	430	$P2_1/c$
		(001) Augite	9.69	8.96	5.25	106.0	438	$C2/c$
15499	1	Pigeonite	9.70	8.91	5.23	108.8	430	$P2_1/c$
15499	3	Augite	9.72	8.91	5.26	107.0	436	$C2/c$
15499	4	Pigeonite	9.70	8.89	5.23	108.7	427	$P2_1/c$
15499	5	Augite	9.75	8.91	5.28	107.2	438	$C2/c$
15499	6	Pigeonite	9.67	8.91	5.23	108.4	428	$P2_1/c$
15499	7	Pigeonite	9.66	8.90	5.22	108.6	426	$P2_1/c$
		(100) Augite	9.73	8.90	5.22	106.8	433	$C2/c$
15555	1	Pigeonite	9.71	8.90	5.23	108.6	428	$P2_1/c$
		(001) Augite	9.73	8.90	5.25	106.5	436	$C2/c$
15555	2	Pigeonite	9.75	8.95	5.25	108.6	434	$P2_1/c$
		(001) Augite	9.74	8.95	5.24	106.8	437	$C2/c$
15555	3	Pigeonite	9.75	8.96	5.25	108.6	435	$P2_1/c$
		(001) Augite	9.75	8.96	5.27	106.5	441	$C2/c$
15555	4	Pigeonite	9.75	8.97	5.22	108.8	432	$P2_1/c$
		(001) Augite	9.75	8.97	5.24	106.3	440	$C2/c$
15555	33	Pigeonite	9.73	8.94	5.29	108.9	435	$P2_1/c$
		(001) Augite	9.70	8.94	5.24	106.7	435	$C2/c$
15016	32-1	Pigeonite	9.68	8.93	5.24	108.5	434	$P2_1/c$
		(001) Augite	9.68	8.93	5.25	107.0	430	$C2/c$

Pyroxene Subsolidus
J. J. Papike

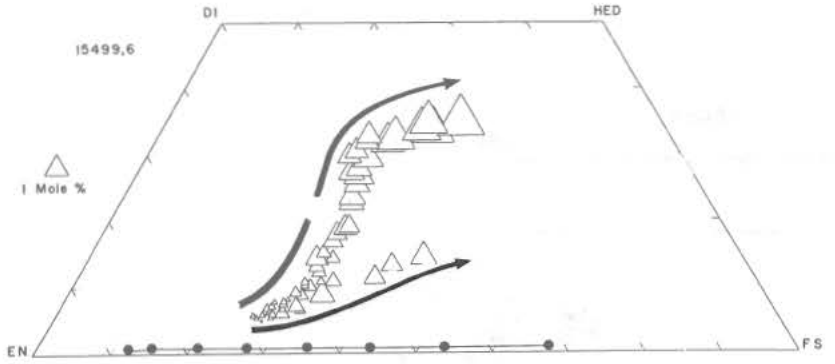

Fig. 1

Courtesy of MIT Press.

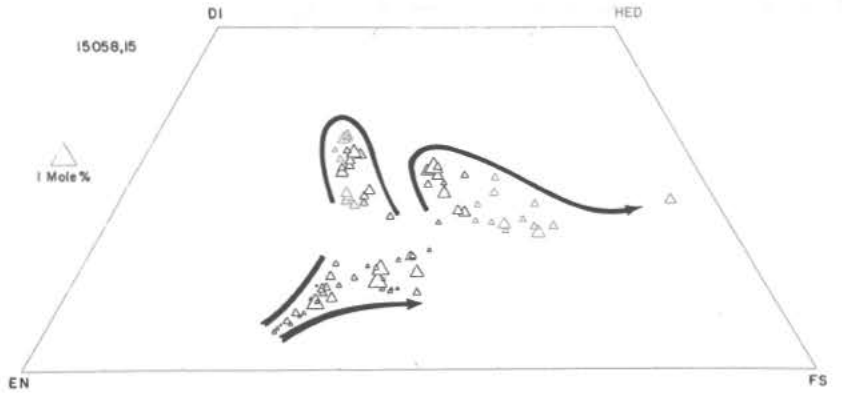

Fig. 2

Courtesy of MIT Press.

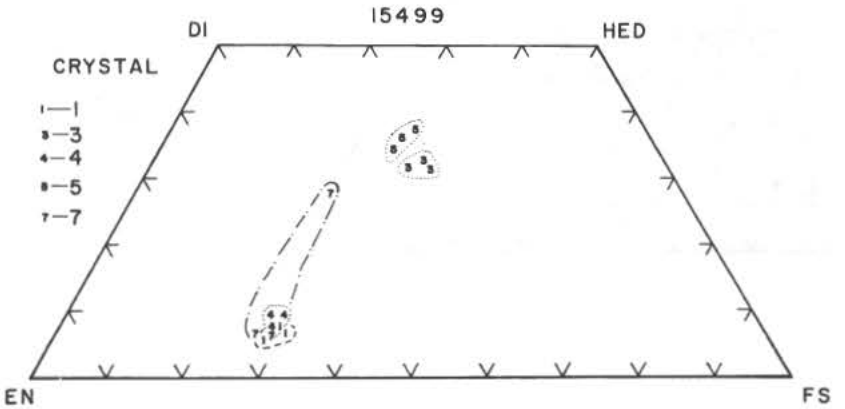

Fig. 3

Pyroxene Subsolidus

J. J. Papike

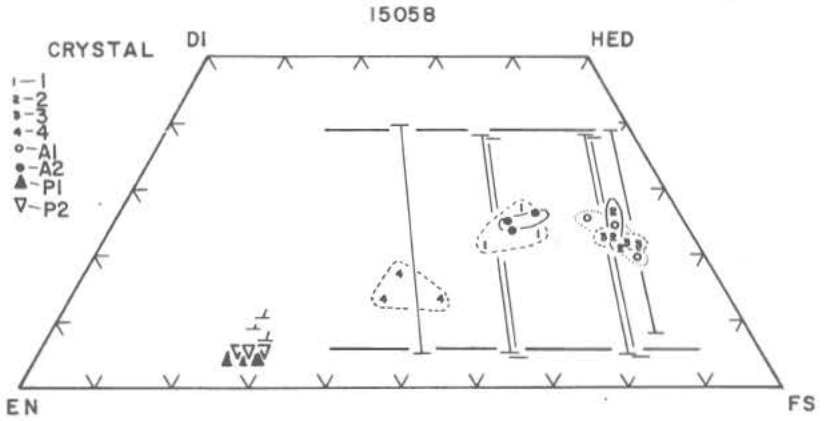

Fig. 4

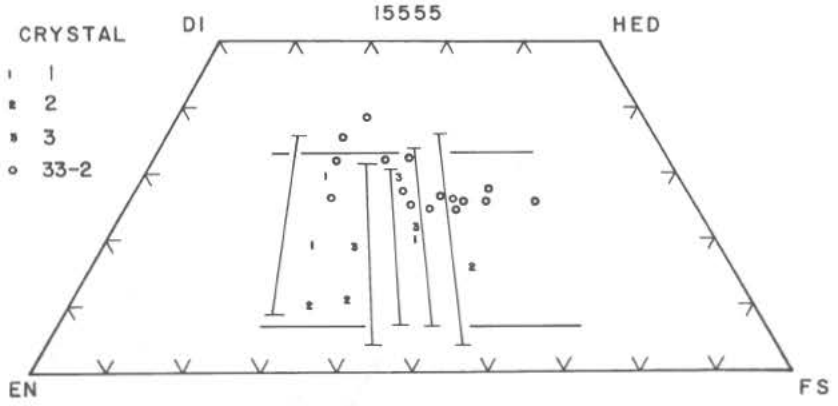

Fig. 5

CLASSIFICATION AND DISTRIBUTION OF ROCK TYPES AT SPUR CRATER. W. C. Phinney, J. L. Warner, NASA-MSC, Houston, Texas, C. H. Simonds, Lunar Sci. Institute and G. E. Lofgren, NASA-MSC.

Because Spur Crater is a fresh crater on a fresh slope which is relatively devoid of craters it is assumed that samples collected on the rim are ejecta from this crater and represent Apennine Front material. All samples (rocks, rakes and 4-10 mm fragments from soils) collected at Spur Crater on the Apennine Front were described and classified with the binocular microscope. In addition, thin sections from 95 of these samples were studied, and about 1500 microprobe analyses were performed. Table 1 sets out rock type populations for the Spur Crater samples. 15304, 15314, and 15414 are 4-10 mm fragments from soils and 15434 contains 4-10 mm fragments from the "pedestal" on which the anorthosite, 15415, occurred. These data show a distinct difference between the "pedestal" and the remaining samples.

Brown-glass-matrix breccia makes up from 50 to 85% of each population except that of the "pedestal" in which it is totally absent. These breccias contain 40 to 50% matrix, most of which is brown glass. Proportions of clast type vary from one fragment to another but always include green glass spheres, recrystallized breccias, anorthositic rocks, orange-brown glass, plagioclase, pyroxene, and devitrified glass. In a few cases basaltic textures occur in clasts. Microbreccias of green glass spheres occur in rock, rake, and coarse fine populations but are not present in the "pedestal". Study of rocks and thin sections make it clear that the source of the green glass in this area is a material consisting of over 90% green glass spheres and fragments of spheres. This material occurs as clasts in breccias whose matrices contain numerous green glass spheres. Soils from this area contain high percentages of these spheres in their fine fractions (1). Microprobe analyses of the green glass spheres in the brown-glass-matrix breccia (Table 2) agree with those previously published (2).

Over 50% of the "pedestal" fragments consist of KREEP basalt, flow-banded glass breccia and dark green glass, the latter two being of KREEP major-element composition whereas these fragment-types are nearly absent in the remaining populations, although it would appear that 15314 has a small amount of the "pedestal" material mixed with it. Unique properties of the "pedestal" material include a large number of clods (32 were separated from the sample before sieving) and a strongly adhering dust coating on all the 4-10 mm fragments. The dust appears to be welded to the surfaces suggesting that the "pedestal" is a poorly consolidated breccia rather than a soil.

Recrystallized breccias are distributed throughout all populations except the large rocks. Because these occur as clasts in nearly all breccias it is suggested that their occurrence in only the smaller fragment sizes is a result of their origination as clasts in breccias. A few mare basalts as well as a few fragments of orange-brown glass having mare basalt compositions (15434,48, Table 1) and containing tiny dendritic olivine crystals occur in the rake, soil, and "pedestal" samples. However, these types do not occur among the large rocks suggesting that such basalts are exotic materials at Spur Crater.

The populations, combined with the microprobe analyses, suggest the following hypotheses concerning the history of some rock types.

A. The major rock type in the debris underlying the Apennine Front in the vicinity

Classification & Distribution of Rock Types at Spur Crater

W. C. Phinney

of Spur Crater (and also station 6 from observations of thin sections) is a brown-glass-matrix breccia. Broadbeam microprobe analyses of the matrix of 15414,9 produces consistent results from one matrix area to another and shows a major element composition similar to that of KREEP from other sites (5), except for a significantly lower K_2O content (Table 2). This analysis is very similar to a whole rock analysis of a brown-glass-matrix breccia, 15265, from station 6 (Table 2). The remaining rock types (including all of the "pedestal" as a single breccia type) are erratics which are thought to be randomly scattered through the underlying material and were therefore carried into the Hadley Delta area as second generation breccias.

B. The KREEP fragments of the "pedestal" range from subophitic basalt texture with phenocrysts of orthopyroxene mantled by clinopyroxene and 20-30% cryptocrystalline mesostasis, through various stages of glass development. Analyses of the mesostasis of the basalt and the various glasses indicate a partial melting sequence commencing with the mesostasis and continuing through almost complete melting. Following the initial melting of mesostasis (15434,37) adjacent clinopyroxene and plagioclase melt to develop the glass of 15434,40. The rapid increase in FeO, P_2O_5, and TiO_2 is the result of melting the Fe-rich outer margins of clinopyroxene which contain abundant apatite inclusions and intergrown ilmenite. K_2O is diluted by the addition of melted plagioclase and clinopyroxene. Further development of these trends can be seen in 15434,56 and 15434,38 where the TiO_2 and P_2O_5 begin to decrease after the apatite and ilmenite have been melted and further melting is primarily of plagioclase and clinopyroxene. The triangular-diagrams for pyroxene and plagioclase of these rocks (Figure 1) agree with the sequence outlined above. In 15434,37 the most complete trend of pyroxene and plagioclase occurs. In 15434,40 the triangular-diagrams show a decrease in the extent of the Fe enrichment trend in the pyroxene and thin sections show a significant glass development. 15434,56 and 15434,38 show further decreases in the extent of the Fe and Na enrichment trends of pyroxenes and plagioclase respectively, which is accompanied in thin section by glass which fills fractures in the crystals and resembles the matrix of a breccia. 15434,45 is a flow-banded glass similar in color to the previously described samples and contains 10-20% clasts of pyroxene and plagioclase. The composition of this glass along with a dark green glass (Table 2) show the continued dilutions of K_2O, P_2O_5, FeO, and TiO_2 with concomitant increases in MgO, CaO, and Al_2O_3 as further melting of plagioclase and pyroxene occurs. These glasses approach the bulk composition of rake fragment 15382 (3), which is a basalt with chemistry similar to KREEP. Total melting of this material would be expected to further lower FeO and increase MgO in the glasses as Mg-rich orthopyroxene cores begin to melt. Regardless of the origin of these series of glasses the source of the "pedestal" was predominantly KREEP with only a few percent anorthosite mixed in. It should be noted that the anorthosites from the "pedestal" are not identical to the other anorthositic fragments which contain more mafic material, including olivine, in highly crushed aggregates as in the black and white breccias, 15445 and 15455, in contrast to the few scattered pyroxenes of the "pedestal" anorthosites.

C. The recrystallized breccias display a range of grain sizes and extent of development of a poikilitic texture, indicating varying degrees of recrystallization. They also have a wide range of bulk compositions from nearly 75% mafic minerals to 75% plagioclase. Clasts generally show a greater range of composition than their respective matrix minerals and those fragments interpreted as having undergone a higher degree of recrystallization (15314,38; 15314,42; 15304,16 and 15304,17) show a slightly higher Mg content in their pyroxenes than do less recrystallized fragments (15434,55 and 15314,43) (Figure 1). The pyroxene compositions in these rocks are quite similar to those of the anorthositic

Classification & Distribution of Rock Types at Spur Crater

W. C. Phinney

TABLE 1. ROCK TYPE POPULATIONS AT SPUR CRATER

	Large Rocks[a]	Rake Fragments[b]	4-10 mm Coarse Fines			
			15304	15314	15414	"Pedestal" 15434[c]
Brown glass matrix breccia[d]	7	46	20	20	7	0
Microbreccia of green glass spheres	3[e]	13	0	3	0	0
Recrystallized breccia	0	5	2	7	2	8
Mare basalt	0	7	0	6	0	3
Brecciated anorthosite	1	3[f]	0	2[f]	0	1[g]
Flow-banded glass breccia	0	0	0	3	0	33
Dark gray matrix breccia	0	0	0	1	0	28
KREEP basalt	0	1	1	1	0	15[h]
Orange-brown glass	0	0	0	0	0	11
Dark green glass	0	0	0	1	0	8
Brownish-gray devitrified glass	0	0	0	0	0	5
Green glass matrix breccia	0	2	0	0	0	0
Black and white breccia	2	0	0	0	0	0
Hollow green glass sphere	0	1	0	0	0	0
Totals	13	79	23	43	9	112

[a]Because the anorthosite, 15415, was a large clast in the breccia forming the "pedestal" material of 15434, it is not listed in this column.

[b]Due to lack of thin sections for some of the more ambiguous fragments, 3 of the samples from this group of 82 were not classified.

[c]Due to lack of thin sections for some of the more ambiguous fine-grained fragments, 10 of the samples from this group of 122 were not classified.

[d]From 15 to 30% of these usually occur as agglutinates or with partial glass coatings.

[e]Although these are separate rocks they were collected within a few centimeters of each other and probably represent one very friable original fragment which broke into several smaller fragments.

[f]These anorthositic rocks are much more similar texturally and mineralogically to the white parts of the black and white breccias than to the anorthosites from the pedestal including 15415.

[g]Two more fragments of anorthosite were removed from this sample and given separate rock numbers (15436 and 15437).

[h]Three of these (,38,40,56) contain significant amounts of orange glass.

Classification & Distribution of Rock Types at Spur Crater

W. C. Phinney

rocks (Figure 1, 15314,51 and 15434,50) in contrast to those of the KREEP rocks. However, the plagioclase is generally between An85 and An95 which is intermediate to the composition of anorthosite and KREEP basalt plagioclases. Some of the recrystallized breccias show unusual features. 15414,11 has a recrystallized texture similar to the 15314,38 group but shows no gap in pyroxene compositions and contains no mafic clasts and quite Ca-rich plagioclase. 15314,39 contains no olivine in its matrix yet every clast is a zoned olivine crystal. Its pyroxene compositions are quite distinct from the other breccias (Figure 1) and its texture is much coarser. The source material of the recrystallized breccias is uncertain but their occurrence in the brown-glass-matrix breccias as well as the "pedestal" breccia added to their occurrences at all previous landing sites plus the Apollo 16 site makes it clear that thermal metamorphism was widespread.

In summary, our data suggest the following model: 1. The debris which moved downslope and underlies Spur Crater represents Apennine Front material which consists predominantly of a brown-glass-matrix breccia having a major element chemistry similar to KREEP except for a significantly lower K_2O content. The same conclusion was reached in a study of the soils from this site (6). 2. The "pedestal" is dominated by fragments of KREEP composition including both glasses and basalts. 3. Microbreccias of green glass spheres and their derivatives, the "pedestal" and its associated anorthosite, recrystallized microbreccias, mare basalts, and the black and white breccias are considered as exotic on the Apennine Front and each makes up only a very small percentage of the regolith.

Table 2. Analyses of Glasses and Rocks

	Green Glass Spheres 15414,9	*Brown Glass Matrix 15414,9	Brown Glass[4] Matrix Breccia from Sta 6 15265	KREEP Mesostasis 15434,37	Glass in KREEP 15434,40	Glass in KREEP 15434,56	Glass in KREEP 15434,38	Flow-banded orange glass 15434,45	Flow-banded dark green glass 15314,41	**KREEP[3] Basalt 15382,9	Orange-Brown Glass 15434,48
SiO_2	45.33	46.99	46.94	68.84	41.52	47.82	47.59	49.81	48.41	NA	42.64
TiO_2	.41	1.18	1.40	0.97	7.12	4.60	5.27	1.36	1.04	2.17	3.50
Al_2O_3	7.17	17.42	16.41	11.34	7.49	9.66	9.84	16.81	18.04	14.93	9.28
Cr_2O_3	NA	NA	0.33	0.00	0.17	0.09	0.18	NA	NA	NA	NA
FeO	19.83	11.00	11.18	6.15	21.18	18.59	16.30	9.32	9.71	9.17	21.03
MgO	17.71	8.95	9.95	0.13	4.25	4.18	4.31	8.63	8.33	7.38	10.26
CaO	8.26	11.66	11.19	2.45	10.23	10.27	9.43	10.67	11.86	7.35	9.24
Na_2O	0.17	0.57	0.51	0.90	0.46	0.44	0.57	0.75	0.68	0.85	0.74
K_2O	0.00	0.19	0.25	5.81	0.83	1.20	1.25	0.48	0.42	0.64	0.14
P_2O_5	0.05	0.40	0.25	.81	3.33	2.68	1.82	0.39	0.18	NA	0.43
ZrO_2	NA	NA	0.06	.54	0.63	0.42	0.45	NA	NA	NA	NA
Total	98.93	98.36		97.94	97.21	99.95	97.11	98.21	98.68		97.25

NA = Not Analyzed

*Values in this analysis were increased by 10% to account for porosity in glass matrix.

**This analysis was from a 17 mg fragment and may not be representative of the whole rock but it is the only analysis of a KREEP composition with basalt texture that we know of.

References

1) Apollo 15 Lunar Sample Information Catalog, NASA-MSC Doc. 03209 (1971).
2) Ridley, W. I. et al., Physics of the Earth & Planetary Interiors, in press (1972).
3) Hubbard, personal comm. (1972).
4) Apollo 15 Preliminary Examination Team, Science 175, 363 (1972).
5) Meyer, C., Jr. et al., Proc. Second Lunar Sci. Conf., 1, 393-411 (1971).
6) Reid, A. M. et al., Meteoritics, in press (1972).

Figure 1. Mineral Compositions of Various Rocks

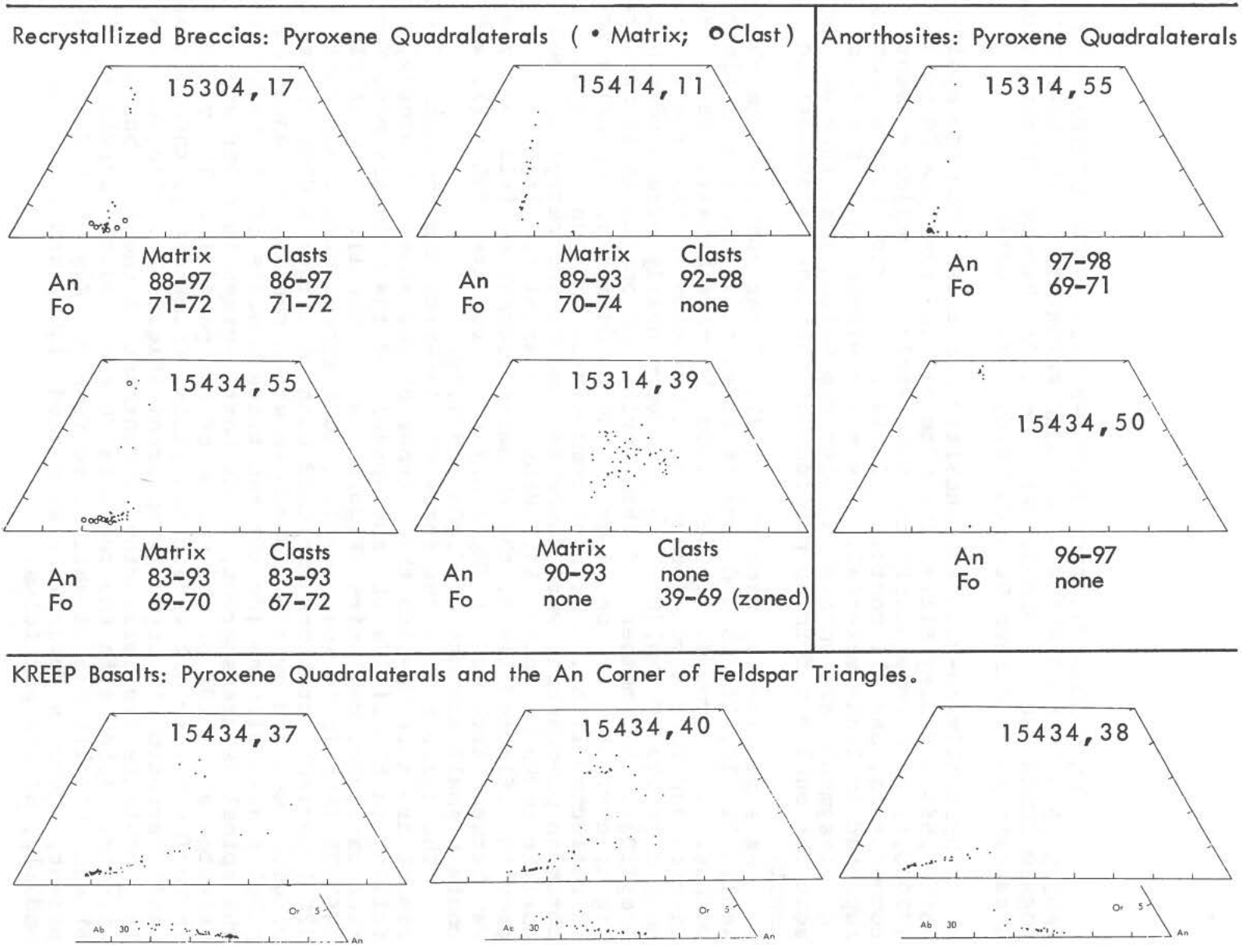

OLIVINE-RICH, TRUE SPINEL-BEARING ANORTHOSITES FROM APOLLO 15 & LUNA 20 SOILS - POSSIBLE FRAGMENTS OF THE EARLIEST FORMED LUNAR CRUST; John B. Reid, Jr., Smithsonian Astrophysical Observatory, 60 Garden St., Cambridge, Mass.02140.

Three olivine-rich anorthositic particles from the Apollo 15 soil (15602, Hadley Rille rim, site 9a) and the Luna 20 soil (22003,1) have very nearly the same whole rock major element composition, and all contain spinels of a composition as yet unreported in lunar material. The major element data for these rock fragments are consistent with the notion that they may represent the earliest forming portions of the lunar anorthositic crust.

As summarized by Haggerty (1971), lunar spinels from the Apollo 11, 12, 14, 15 and Luna 16 sites fall into two distinct compositional groups. Spinels from the mare basalts are Cr- and Ti-rich and form a continuous solid solution series from aluminous chromite $(Fe,Mg)(Cr,Al)_2O_4$ to very nearly pure ulvöspinel (Fe_2TiO_4). All members of this series are opaque to transmitted light; chromites are pearl gray, and ulvöspinels, a pinkish tan in reflected light. A second compositional group of spinels, the chromian pleonastes, were found in some of the recrystallized noritic rocks of Apollo 14. Pink in transmitted light, and light grey in reflected light, the chromian pleonastes fall nearly midway between true spinel ($MgAl_2O_4$) and hercynite ($FeAl_2O_4$), and contain small amounts of Cr_2O_3 and TiO_2.

The spinels from the three olivine-rich anorthosites of this report are more Mg-rich than either of the above two groups, falling in the fields of true spinel and the slightly more Fe-rich category, ceylonite (Figure 1 and Table 1). In particle (451-7) (Apollo 15 soil sample 15602) spinel occurs as small (20μ) perfect octahedra enclosed both by larger (100μ) clasts of plagioclase, and by the groundmass which consists of annealed plagioclase, olivine (Fo 80) and trace amounts of low-Ca pyroxene. The spinel is transparent, light bottle-green in color and constitutes about 10% of the volume of the particle. The variation in Fe/(Fe+Mg) is nil within analytical uncertainty, though some small variation in Cr_2O_3 is apparent (Figure 1). The very low TiO_2 contents are noteworthy in contrast to the mare basalt spinels. Spinels in the two Luna 20 anorthositic particles (514-6) and (514-21) are slightly more Fe-rich (Fig. 1) and are transparent, amber in color in transmitted light, and form about 5%, modally, of the particles.

Olivine-,True Spinel-Anorthosites

J. B. Reid, Jr.

The formation of spinel with compositions near $MgAl_2O_4$ (in these anorthositic particles) is a reflection of the unusual composition of the particles themselves. By defocussed beam analysis, the three fragments have very similar compositions which are noteworthy mainly because of their high contents of MgO, CaO and Al_2O_3 and their low contents of K_2O and P_2O_5 (Table 2). It is to be emphasized that this material contains Al_2O_3 in excess of the amount that can be accomodated by plagioclase, hence the formation of spinel. On a triangular plot showing the relative amounts of normative plagioclase, normative mafics + oxides, and normative orthoclase + apatite (Fig. 2), the three fragments fall at the plagioclase-poor, mafic-rich end of the anorthosite group. (This plot is used to separate the three groups of lunar rock types according to their notable mineralogic and chemical features, namely: anorthosites are plagioclase-rich, norites are KREEP-rich (high Or + Ap in the norm), while mare basalts are relatively poor in KREEP component and plagioclase content and relatively enriched in mafic silicates + oxides). If the three particles are, in fact, members of the anorthosite clan of rocks, and if lunar anorthosites in general represent the floated fraction of an early moonwide magma system, the Mg-rich, olivine-rich character of these three particles implies that they represent the earliest crystallizing portion of such a system.

From the petrography, the order of appearance of the phases is (1) spinel, (2) plagioclase, (3) olivine, (4) pyroxene. Walker et al. (1972) show a low-p pseudoternary liquidus diagram for the system Ol-An-Silica at $Fe/(Fe+Mg) \simeq 0.3$ on which a crystallization sequence consistent with the rocks' textures, can be traced. A liquid initially in the primary phase volume for spinel and richer in normative An than Ol will begin crystallization with spinel, then spinel + plagioclase, then plagioclase + olivine, and finally traces of pyroxene with additional plagioclase.

References: Haggerty, S. E. (1971)."Compositional Variations in Lunar Spinels," NATURE PHYSICAL SCIENCE, Vol.233, Oct. 1971.

Walker, D., J. Longhi and J. F. Hays. "Experimental petrology and origin of Fra Mauro rocks and soils." LUNAR SCIENCE III, Lunar Science Institute, Contrib. 88, 1972. pp. 770-772.

Olivine, True Spinel Anorthosites

J. B. Reid

Table 1: Average Major Element Compositions of Mg-, Al-rich spinels from three olivine anorthosites.

	(451-7)(A15) (15 analyses)	(514-6)(L20) (6 analyses)	(514-21)(L20) (4 analyses)
TiO_2	0.05	0.14	0.12
Al_2O_3	66.79	67.91	65.63
Cr_2O_3	1.94	1.83	1.51
FeO	5.55	8.99	10.55
MgO	23.54	22.46	20.74
	97.87	101.33	98.55
Fe/(Fe+Mg)	.115	.182	.221
Cr(Cr+Al)	.020	.018	.015

Table 2: Whole-particle major element compositions of three olivine-anorthosites by electron-probe defocused beam analysis.

	451-7(A15)	514-6(L20)	514-21(L20)
SiO_2	41.83	44.84	44.60
TiO_2	.30	.20	.11
Al_2O_3	23.90	24.09	28.61
Cr_2O_3	.11	.14	.07
FeO	5.98	4.86	4.07
MnO	.08	.10	.07
MgO	12.47	14.40	10.83
CaO	12.87	12.86	14.29
Na_2O	.37	.39	.47
K_2O	.08	.01	.02
P_2O_5	.14	.14	.10
SO_3	.07	.08	.02
NiO	.02	.00	.02
BaO	.00	.00	.04
	98.22	102.11	103.32
Fe/(Fe+Mg)	0.211	0.158	0.173
Or	0.47	0.06	0.12
Ab	2.67	2.78	3.85
An	62.93	63.80	70.24
Wo	0.00	0.00	0.00
En	2.13	7.24	4.93
Fs	.73	1.80	1.35
Fo	20.27	20.06	15.44
Fa	7.61	5.49	4.67
Cr	.16	.21	.10
Il	.57	.38	.21
Ap	.30	.20	.20
Co	.23	.16	2.10
	98.1	102.2	103.2

Olivine, True Spinel Anorthosites

J. B. Reid

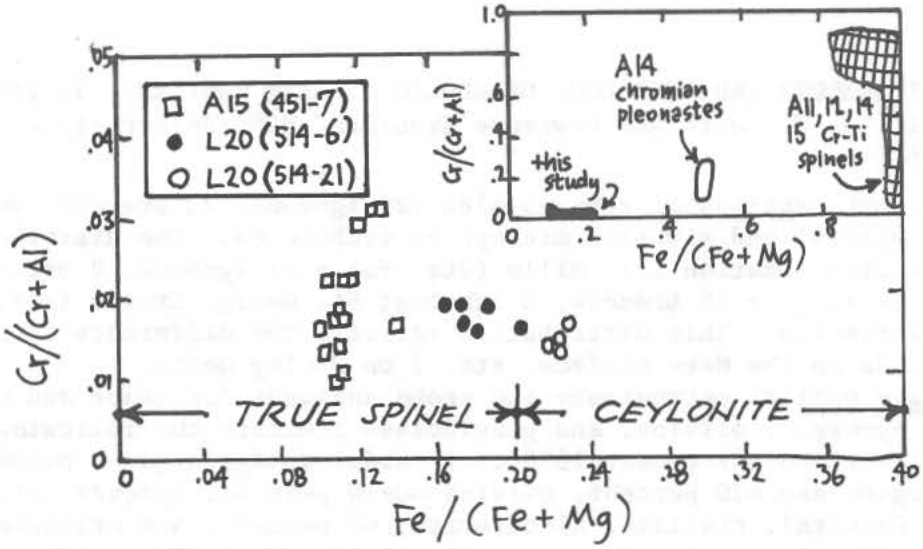

Figure 1. Cr/(Cr+Al) vs. Fe/(Fe+Mg) for Mg-, Al-rich spinels in 3 olivine anorthosites from the Apollo 15 and Luna 20 soils.

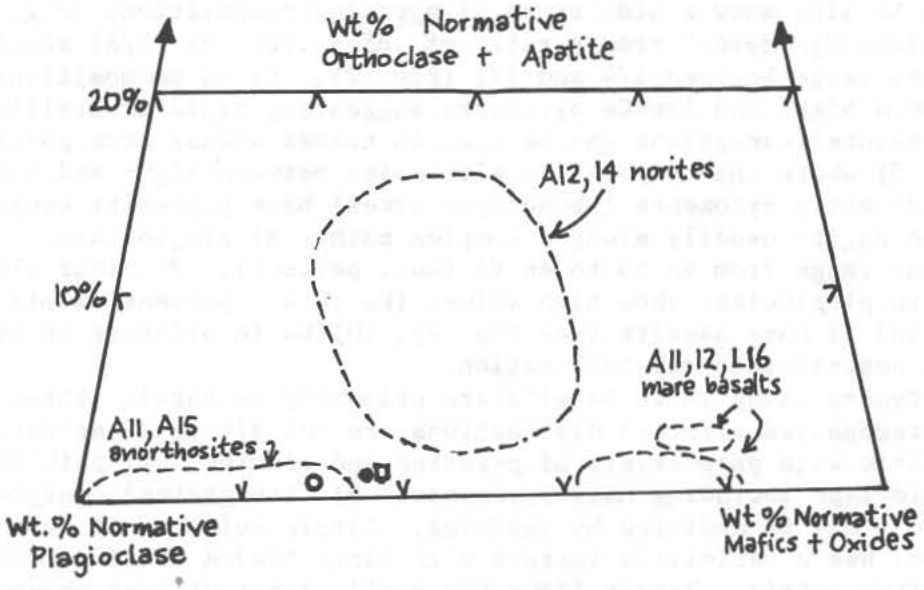

Figure 2. Normative compositions of 3 olivine anorthosites. Fields for the three major lunar rock types are shown in dashed lines. Symbols as in Figure 1.

MINERALOGY AND PETROLOGY OF APOLLO 15 RAKE SAMPLES: I. BASALTS

Ian M. Steele, J. V. Smith and Lawrence Grossman, HGS, University of Chicago, 60637.

Forty-eight sections of rake samples (26 igneous, 22 breccia) were examined by optical and electron microprobe techniques. The distribution of sample types with location is: Rille (sta. 9a) - 21 igneous, 2 breccia; Spur crater (sta. 7) - 18 breccia, 3 igneous; St. George Crater (sta. 2) - 2 igneous, 2 breccia. This distribution reflects the difference in sampled areas - sta. 9a on the Mare surface, sta. 7 on Hadley Delta.

Basalts - Optical petrography and probe analyses for major and minor elements in pyroxene, olivine, and plagioclase indicate the following similarities between all except 15386: 1) modal analyses give: pyroxene ~65 percent, plagioclase ~20 percent, olivine ~0-10 percent, opaques (ilmenite, ulvöspinel, Fe-metal, troilite, Al-chromite) ~5 percent, and cristobalite ~1 percent; 2) all contain olivine except 15117 and 15638 - olivine was not detected in 15117 and 15638 but the sections were small: 15667 shows no olivine and has an unusual texture; 3) average grain size of the matrix is ~.2mm indicating rapid cooling: some phenocrysts range up to 3mm; 4) typical basalts show a wide range of pyroxene compositions (e.g. Fig. 1) with a maximum Mg/(Mg+Fe) atomic ratio of .65 - .70; 5) Ti/Al atomic ratios of pyroxenes range between 1/4 and 1/2 (Fig. 2); 6) no compositional gap is shown between high- and low-Ca pyroxenes suggesting rapid crystallization at high temperature (exceptions can be seen in traces across some phenocrysts (e.g. Fig. 3) where the composition alternates between high- and low-Ca values); 7) early pyroxenes (phenocryst cores) have pigeonite compositions and zone to augite usually along a complex path; 8) plagioclase compositions range from An 85 to An 93 (mol. percent); 9) minor elements (Fe,K,Mg) in plagioclase show high values (Fe .4 wt. percent) similar to Apollo 11 and 12 Mare basalts (see Fig. 4); 10) Ca in olivines is high suggesting near-surface crystallization.

Differences among these basalts are primarily textural. Three types have been recognized although distinctions are not always clear-cut: 1) porphyritic with phenocrysts of pyroxene and olivine; 2) poikilitic with large plagioclase including many pyroxenes; 3) fine-grained equigranular. Types 1 and 3 may be modified by vesicles. Little evidence of shock is seen. Basalt 15667 has a variolitic texture with large bladed zoned pyroxenes set in a very fine matrix. Basalt 15608 has small equant olivine phenocrysts plus a fine variolitic assemblage of skeletal Mg-rich pyroxenes set in a finer matrix of Fe-rich pyroxenes and plagioclase: devitrification is indicated.

The above characteristics indicate that the majority of igneous rocks from the three sampled areas have Mare basalt characteristics i.e. near-surface, rapid crystallization of an Fe-rich, Al-poor liquid. Some textures indicate two-stage cooling histories.

MINERALOGY AND PETROLOGY OF APOLLO 15. I.

Ian M. Steele

One igneous rock from Sta. 7 (15386) is distinctly different: 1) it contains ~35 percent lath-shaped plagioclase, ~50 percent interstitial pyroxene, ~10 percent cristobalite, ~3 percent ilmenite in plates with serrated surfaces, minor phosphate, iron and sulfide; 2) its pyroxenes have a large composition range extending to an Mg/(Mg+Fe) atom ratio of .85 which is as high as for any lunar basalt (Fig. 5); 3) plagioclase is Na-rich relative to other basalts (15-30 mol. percent Ab); 4) minor elements in plagioclase are low and do not fall on the mare-basalt trend; 6) Mg-rich-pyroxenes have Ti/Al ratios of 1/10. The range of pyroxene compositions is similar to that for the controversial 14310 basalt, (Ridley et al. 1972) but the plagioclase is more sodic. Neither basalt contains olivine, and both have a relatively high modal content of plagioclase.

The similarity of most of the basalts to those from earlier Apollo and Luna missions confirms the ubiquity of the Mare-type basalts on the lunar near-side surface. The dominant igneous activity at the Apollo 15 site apparently involved Mare-type basalts. The breccias (paper II) contain no clasts of mare-type basalts, and their mineral fragments show a quite different chemistry.

The unusual features of the 15386 basalt suggest that it is related to the Front (highland?) material rather than Mare basalts. One breccia sample (15344) contains a clast of this basalt type, but this rock type does not appear to be common in the breccia samples.

Ridley et al., Abstracts - 3rd Lunar Science Conference (1972).

We acknowledge NASA Grant NGL 14-001-171.

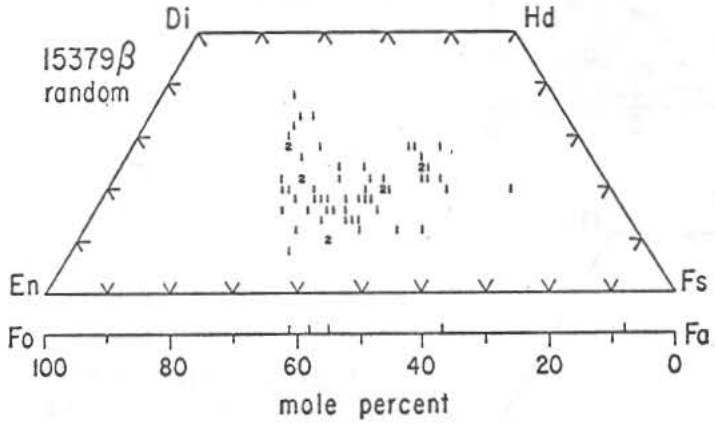

Fig. 1 - Typical pyroxene-olivine range in Apollo 15 basalt.

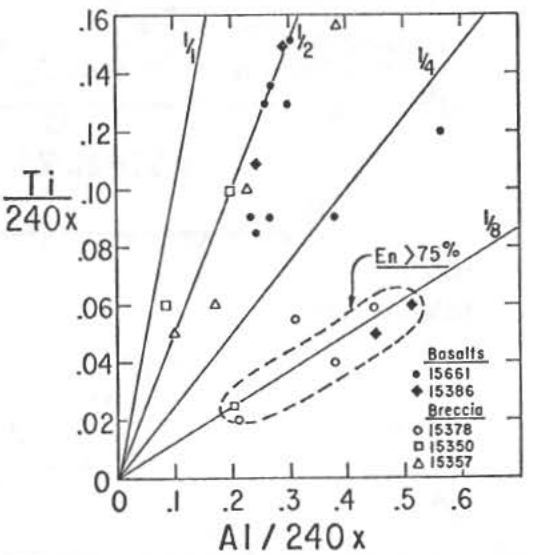

Fig. 2 - Ti vs. Al for pyroxene in Apollo 15 breccia and basalts.

MINERALOGY AND PETROLOGY OF APOLLO 15. I.

Ian M. Steele

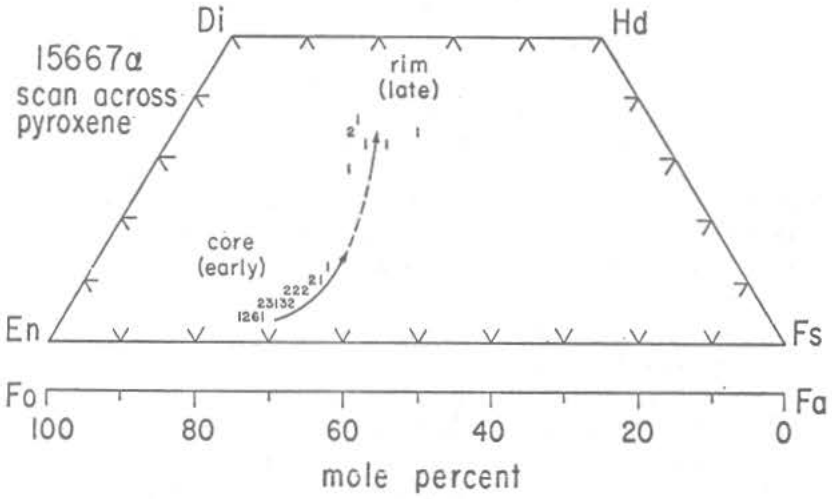

Fig. 3 - Zoning in pyroxene phenocrysts (15667).

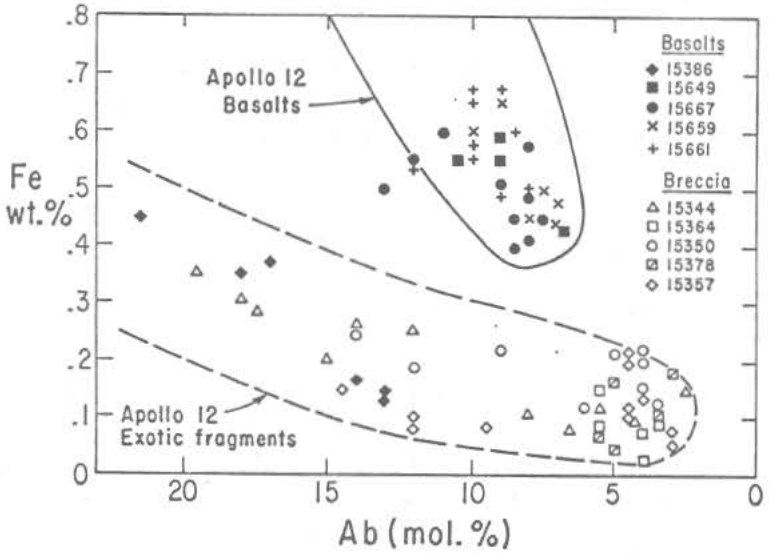

Fig. 4 - Fe in plagioclase from Apollo 15 basalts and breccia.

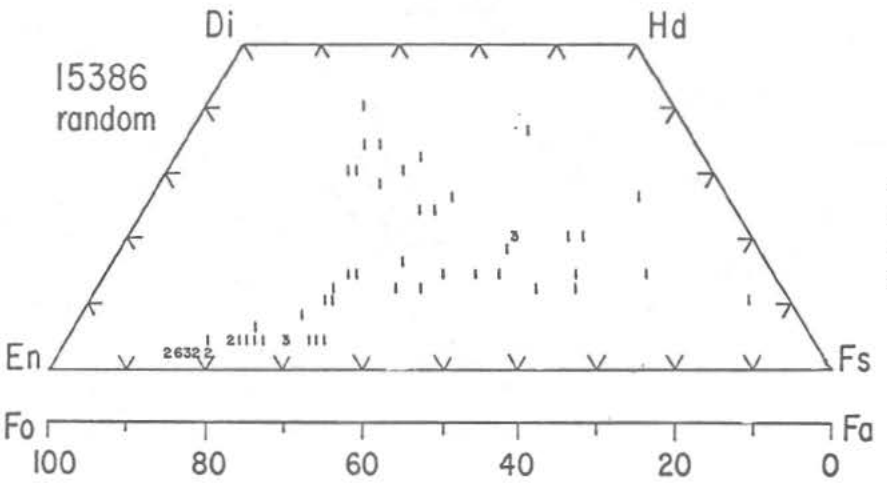

Fig. 5 - Pyroxene composition plot for unique basalt 15386. No olivine was found.

MINERALOGY AND PETROLOGY OF APOLLO 15 RAKE SAMPLES: II. BRECCIAS.
Ian M. Steele, J. V. Smith and Lawrence Grossman, HGS, University of Chicago, 60637.

Twenty-two breccias from three locations have been studied. Distribution and locations are: Rille (sta. 9a) - 2 breccias; Spur Crater (sta. 7) - 18 breccias; St. George Crater - 2 breccias. The larger proportion of breccias at sta. 7 probably reflects the dominant rock type of Hadley Delta.

The breccias are friable, requiring impregnation before preparation of thin sections. Each thin section was characterized with a detailed petrographic description as well as random microprobe analyses of pyroxenes and olivines for major elements (Mg,Fe,Ca,Al) which were automatically plotted on compositional diagrams. About eight sections have such a high percentage of glass and/or fine-grained dark matrix that few crystalline grains could be found. Detailed microprobe analyses were made on interesting sections or clasts.

Glass spheres and shards are present in all breccia sections except one. Percent glass ranges from 100 percent to 0 percent. Sample 15366 is composed of ~100 percent glass spheres or shards with essentially identical compositions: SiO_2 46.4 percent, FeO 20.3, MgO 18.1, Al_2O_3 7.50, CaO 8.10, TiO_2 .40, Na_2O .10, K_2O .07, Cr_2O_3 .51. This glass type was recognized or analyzed in nearly all breccias which contain appreciable glass. Because this glass type was not recognized in Apollo 14 material (Apollo Soil Survey, 1972) but is widespread at the 15 site, its formation is connected with the origin of the Apollo 15 breccias. Other glass types occur in the breccias and most have higher CaO and Al_2O_3 values (i.e. higher plagioclase content in norm). Because nearly all glass is not devitrified, these rocks have not been metamorphosed as were the Apollo 14 breccias (Warner, 1972). Thus these rocks were not part of a hot, thick ejecta blanket.

Of the crystalline material, mineral grains are most common and form a large part of the matrix of these breccias. Dominant mineralogy includes plagioclase and low-Ca pyroxene with minor olivine, spinels, ilmenite and metal. The range of ferromagnesian compositions typical of most breccia is shown in Figs. 1 and 2. The main feature is the high percentage of high-Mg, low-Ca pyroxenes which is outside the range for Mare-type basalts. Olivine is a minor component but analyses with high Mg/(Mg+Fe) atomic ratios (0.8-0.9) are almost always present, again distinct from the Fe-rich compositions for Mare basalts. Two breccias 15331 and 15316 contain unattached grains of olivine (~Fo 87) and pink spinel: they bring to mind the spinel-olivine-anorthite fragment described by Steele (1972).

Plagioclase analyses are uniformly high in Ca(An 85-An 97 and low in minor elements (Fe $<$ .4 wt. percent), similar to exotic fragments from Apollo 11, 12 and breccia from 14. The absence of plagioclase with high contents of minor elements (Fig. 4 of paper I) implies either that Mare-type basalts did not

MINERALOGY AND PETROLOGY OF APOLLO 15 RAKE SAMPLES: II.

Ian M. Steele

contribute plagioclase to the breccia, or that recrystallization occurred. No clasts resembling Mare-type basalts were found in the breccias. Hence the breccias formed from a region free of Mare-type basalt, perhaps because the latter had not yet appeared on the Moon, or perhaps because Mare-type basalts have a restricted spatial distribution.

One breccia (15357) is unique because it is holocrystalline and contains one dominant pyroxene composition (En 71, Fs 26, Wo 3): see Fig. 3. This composition is similar to that for Apollo 14 annealed breccia, and rock 15357 has been found to be high in KREEP (Haskin, pers. comm.).

Lithic clasts are contained in every breccia and are igneous or breccia in origin. Both types are dominated by plagioclase and pyroxene, with grain-size varying from less than .1mm to several mm. Principal types include: 1) polycrystalline plagioclase igneous fragments (anorthosite); 2) fine-grained plagioclase-low-Ca pyroxene basalts (feldspathic basalts); 3) coarse-grained (1mm) pyroxene-plagioclase fragments; 4) several olivine-plagioclase assemblages (one is unique with euhedral plagioclase (An 96) surrounded by olivine (Fo 71) and pyroxene); 5) high-Mg pyroxene basalt clast (similar to 15386); 6) "annealed" breccia fragments similar to 15357 and other Apollo 14 KREEP rocks. Fig. 4 shows pyroxene and olivine analyses from various igneous clasts. The mafic minerals from these clasts closely correspond to the range seen in the matrix of typical Apollo 15 breccia.

Principal conclusions are:

1) Low-Ca pyroxene and plagioclase occur commonly in the mineral grains and clasts of all the breccias.
2) The rare clasts imply the presence of several rock types varying from ultrabasic to basic compositions, and distinct from Mare-type basalts.
3) The overall compositions of the breccias are consistent with the Al/Si X-ray determinations by Adler et al. (1972) in the Apennine mountain region.

The high content of undevitrified glass implies that the breccias did not form in a thick ejecta blanket and are unlikely to represent the initial products of the Imbrian impact. Possibly local impacts on debris from major impacts produces the breccia. The high-Mg and Ca compositions would be consistent with early products of extensive igneous differentiation, perhaps representing a thick lunar crust.

Fig. 5 compares the pyroxene compositions from the different rock types, and raises the implied question about possible relationships by igneous differentiation including partial melting and crystal-liquid separation.

The relation of the igneous clasts to common glass compositions found by the Soil Survey and others is important, but cannot be answered fully at this time.

Adler et al. NASA SP-289. Paper 17 (1972).
Apollo Soil Survey EPSL, 12, 49-54 (1971).
Steele, I. M. EPSL 14 190-194 (1972).
Warner, J. L. Abstracts - 3 ed Lunar Science Conference. P.782-784 (1972).

We acknowledge NASA Grant NGL 14-001-171.

MINERALOGY AND PETROLOGY OF APOLLO 15. II.

Ian M. Steele

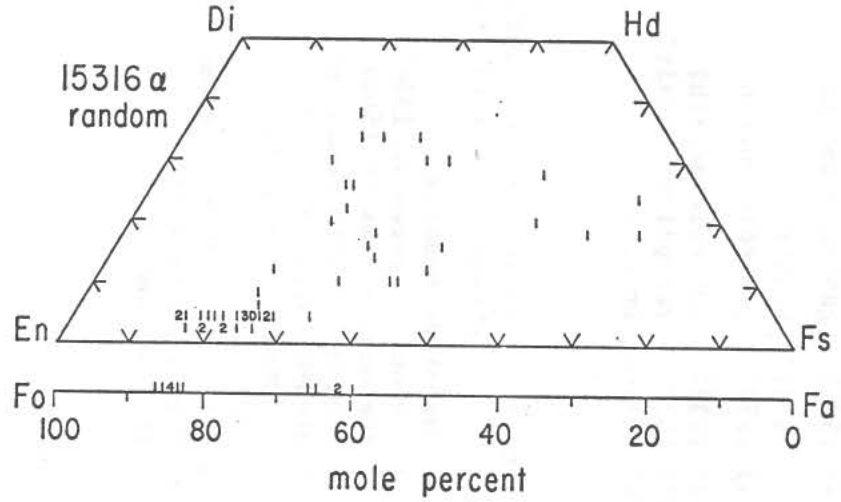

Fig. 1 - Pyroxenes and olivines in low-glass breccia 15316. (D = 13)

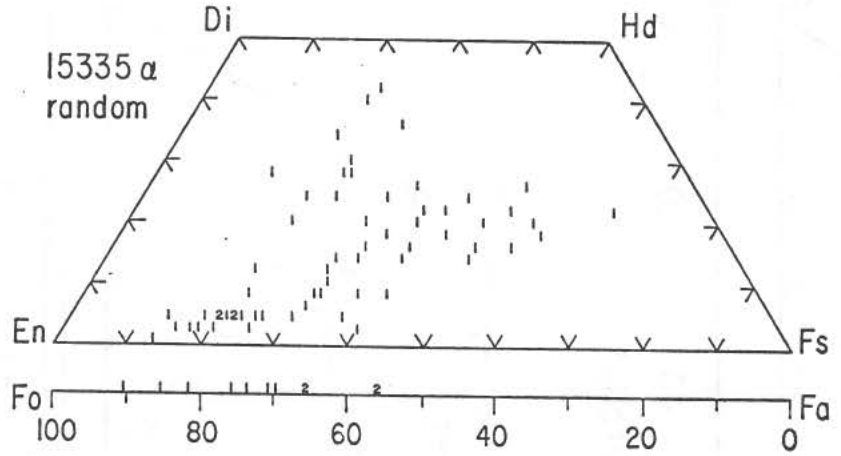

Fig. 2 - Pyroxenes and olivines in high-glass breccia 15335.

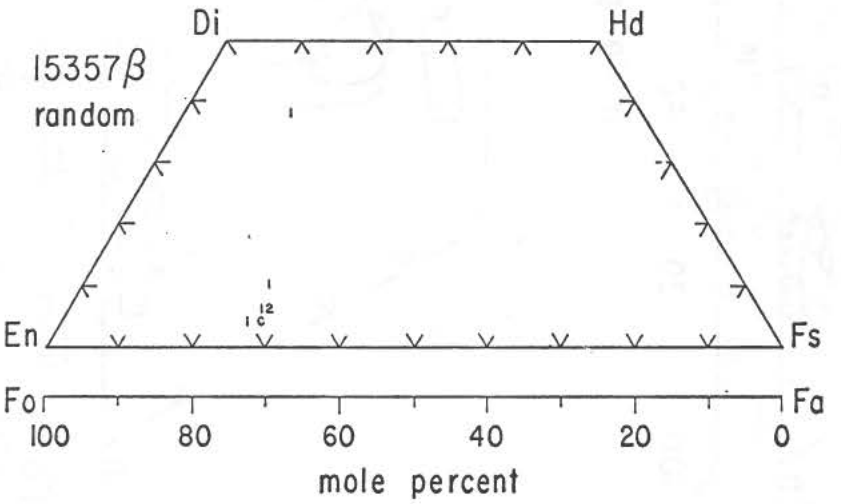

Fig. 3 - Pyroxenes in 15357 KREEP breccia. (C = 12)

Fig. 4 - Pyroxene and olivines in igneous clasts.

1) 15146 - coarse pyroxenite?
2) 15364 - euhedral plag in pyx-ol matrix
3) 15335 - pyx-plag basalt
4) 15335 - troctolite
5) 15316 - gabbroic anorth.
6) 15347 - pyx-plag basalt
7) 15347 - pyx-plag basalt
8) 15347 - plag-pyx basalt
9) 15331 - gabbroic anorth.
10) 15331 - basalt
11) 15331 - gabbroic anorth.
12) 15322 - gabbroic anorth?
13) 15322 - variolitic basalt?
14) typical breccia - 15331

Fig. 5 - Pyroxenes and olivines in various rock types.

1) Mare-type basalts
2) phenocryst cores in 15667
3) phenocryst rims in 15667
4) high-Mg breccia component
5) high-Mg olivines in several ultrabasic fragments and breccia
6) olivines in Mare-type basalts
7) pyroxenes in Apollo 15 and 16 anorthosites.

ANORTHOSITIC LITHIC FRAGMENTS IN APOLLO 15 SOILS AND FRACTIONAL CRYSTALLIZATION IN THE EARLY LUNAR CRUST, G. J. Taylor, Smithsonian Astrophysical Observatory, Cambridge, Mass., 02138

Sixty-three anorthositic (>60% plagioclase) particles have been studied in six 1–2 mm Apollo 15 soil samples. The highest proportions of anorthosites are found in samples collected on the Apennine Front: 15102 (9.5%), 15302 (5.4%), and 15272 (4.7%). A sample obtained on the mare near Dune Crater (15472) has as high a proportion of anorthosite (5.2%) as those from the Front, but three other mare samples (15602, 15042, and 15032) contain few anorthositic particles (2.4, 0.3, and 0.0, respectively).

Textures. All but one of the anorthositic fragments can be classified into four main categories. Of the 63 particles studied, 20 are "Type B breccias"[1]: relatively coarse-grained, unrecrystallized, shocked, and brecciated rocks. The mineral clasts in them are highly fractured, have undulatory extinction, and frequently have shock-produced twins or shock-isotropized plagioclase; there is no discernible intergrowth of the clasts with the matrix. Nineteen particles are similar to Type B breccias, but they are perceptibly recrystallized and the shock features are largely absent, presumably removed by annealing; these can be termed "slightly recrystallized breccias." Another 18 particles are more intensely recrystallized. The clasts and matrices are intimately intergrown, and some fragments have a granulitic texture with no observable clasts. These are "recrystallized breccias" and are the Type A breccias of Marvin et al.[1] There are gradations among all these categories but particularly between the latter two. Five particles comprise a fourth textural type and are similar to rock 15415: large, fractured plagioclase grains containing inclusions of smaller pyroxenes. A silica polymorph, which is present in 15415,[2] is also present in at least two of these particles. The one anorthositic fragment not belonging to any of these categories has been remelted. All these textures have been observed among the anorthositic particles in the Apollo 11 soils,[1, 3] save for the 15415 type.

Chemistry and Mineralogy. Defocused-beam microprobe analysis of 21 particles shows that anorthosites are characterized by high Al_2O_3 (26–36%) and CaO (13–21%), by low TiO_2 (<0.3%) and K_2O (<0.05%), and by generally low but variable FeO (0–6%) and MgO (0.2–7%). The atomic ratio Fe/(Fe+Mg) ranges from 0.10–0.54, although in 2/3 of the particles this ratio is <0.30. There are no systematic chemical differences among the main textural types.

Modal analyses were made on 51 particles. Ilmenite is present in very small amounts (absent to 0.5 vol.%); noritic rocks, such as those from Apollo 14, contain measurably greater quantities of opaque oxides. Modal plagioclase contents (converted to wt.%) are shown in Fig. 1, where they are compared to plagioclase contents in Apollo 11 anorthositic particles.[4] Although the Apollo 15 rocks have the same range of values as those from Apollo 11, the former are, on the average, more feldspar-rich.

ANORTHOSITIC LITHIC FRAGMENTS IN APOLLO 15 SOILS ----------

G. J. Taylor

Approximately 2/3 of the Apollo 15 fragments have more than 85% plagioclase, whereas 2/3 of the Apollo 15 fragments contain between 70 and 85% plagioclase.

Almost all the plagioclase contains >90 mol % An and <0.1% K_2O; this is similar to plagioclase in Apollo 11 anorthosites. Olivine is far less abundant than in Apollo 11. It is present in 4 of the 14 particles on which microprobe analyses were made; in contrast, almost all the Apollo 11 anorthosites contain olivine. The olivines are very uniform in composition in a given fragment (range of <6 mol % Fa), but there is considerable particle-to-particle variation (Fa_{14} to Fa_{47}). The olivines contain <0.1% TiO_2 and Cr_2O_3. Representative pyroxene analyses from each textural class are plotted in Fig. 2. The pyroxenes are quite homogeneous within a given particle; zonation within a single crystal is very slight, rarely more than ~0.5 mol % En. There are often coexisting low- and high-Ca pyroxenes. The range of compositions (Fig. 2) suggests a common fractionation trend among the Apollo 15 anorthosites. The existence of such a trend is also indicated in Figs. 3 and 4, where Cr_2O_3 and TiO_2, respectively, are plotted against the Fe/(Fe+Mg) ratio for anorthosite pyroxenes from Apollo 11 and 15 and Luna 20. In the light of the exceedingly complex history of brecciation and recrystallization that these rocks have suffered, it is remarkable that such smooth, well-defined trends of decreasing Cr_2O_3 and TiO_2 with increasing Fe/(Fe+Mg) should be apparent.

Fractional Crystallization in the Primitive Lunar Crust. Decreasing Cr_2O_3 of pyroxenes with increasing Fe/(Fe+Mg) is normal for magmas undergoing fractional crystallization (e.g., lunar basalts). However, in low-Ti systems (anorthosites contain <0.3% TiO_2), during fractional crystallization, the TiO_2 content in pyroxenes increases with increasing Fe/(Fe+Mg) as crystallization proceeds, which is opposite to the trend observed for lunar anorthosite pyroxenes (Fig. 4). On the other hand, in high-Ti systems such as Apollo 11 and Luna 16 basalts, early crystallizing ilmenite depletes the melt in TiO_2 and causes pyroxenes to show decreasing TiO_2 as crystallization proceeds (and as Fe/(Fe+Mg) increases). But ilmenite is never sufficiently abundant in the anorthosites to have caused the depletion in magma TiO_2 content that is reflected in the pyroxene compositional trend. This apparent paradox can be resolved by proposing that the anorthosites formed by crystal fractionation (plagioclase flotation)[5, 6] in an early Moon-wide magma system in which ilmenite crystallized early and sank, thus depleting the system in TiO_2 as crystallization proceeded. This interpretation requires that the hypothetical ocean of magma contained far more TiO_2 than is implied by the compositions of lunar anorthosites. The model also implies either a Ti-rich layer at depth in the Moon, or a gradual increase in Ti with depth in the outer layers of the Moon.

References

[1]Marvin, U. B., Wood, J. A., Taylor, G. J., Reid, J. B., Jr., Powell, B. N., Dickey, J. S., Jr. and Bower, J. F. (1971) Proc. Second Lunar Sci. Conf., Geochim. Cosmochim. Acta, Suppl. 2, vol. 1, 679-699.

[2]James, O. B. (1972) Science 175, 432-436.

[3]Taylor, G. J., Marvin, U. B., Reid, J. B., Jr., Bower, J. F., and Wood, J. A. (1972) Smithsonian Astrophysical Observatory Spec. Rep., in press.

ANORTHOSITIC LITHIC FRAGMENTS IN APOLLO 15 SOILS ----------

G. J. Taylor

[4]Taylor, G. J. (1972) Earth Planet. Sci. Lett., in press.

[5]Wood, J. A., Dickey, J. S., Jr., Marvin, U. B., and Powell, B. N. (1970) Science 167, 602-604.

[6]Wood, J. A., Dickey, J. S., Jr., Marvin, U. B., and Powell, B. N. (1970) Proc. First Lunar Sci. Conf., Geochim. Cosmochim. Acta 34, Suppl. 1, 965-988.

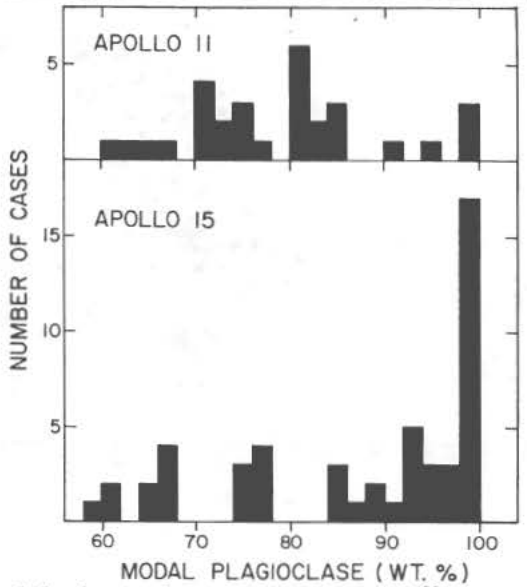

Fig. 1. Histogram of modal plagioclase contents (wt. %) in anorthositic lithic fragments from Apollo 15 and Apollo 11[(4)] soils.

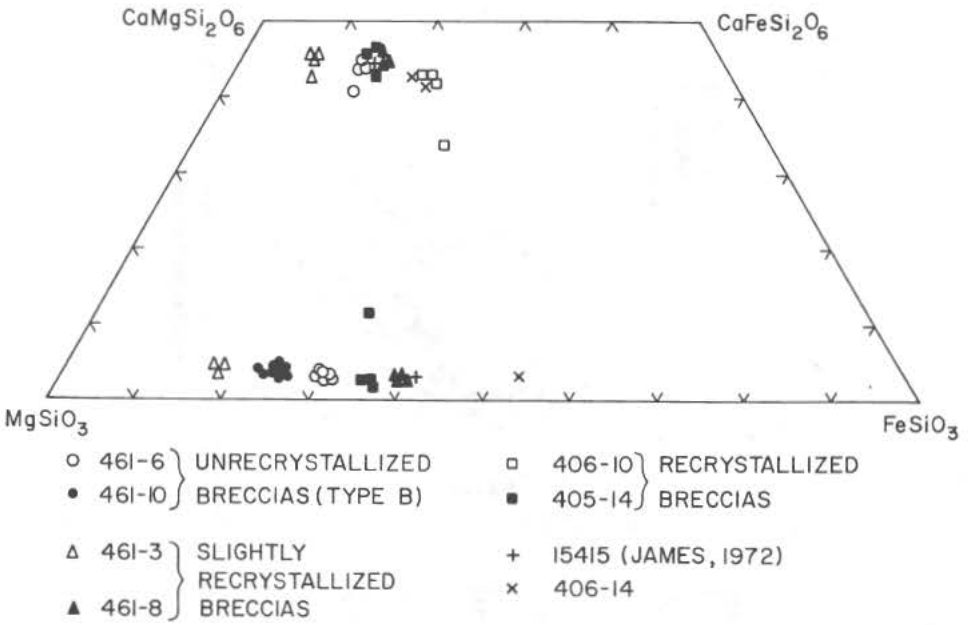

Fig. 2. Compositions of pyroxenes in representative Apollo 15 anorthosites, in terms of their relative content (mole %) of ideal pyroxene end members.

ANORTHOSITIC LITHIC FRAGMENTS IN APOLLO 15 SOILS -------

G. J. Taylor

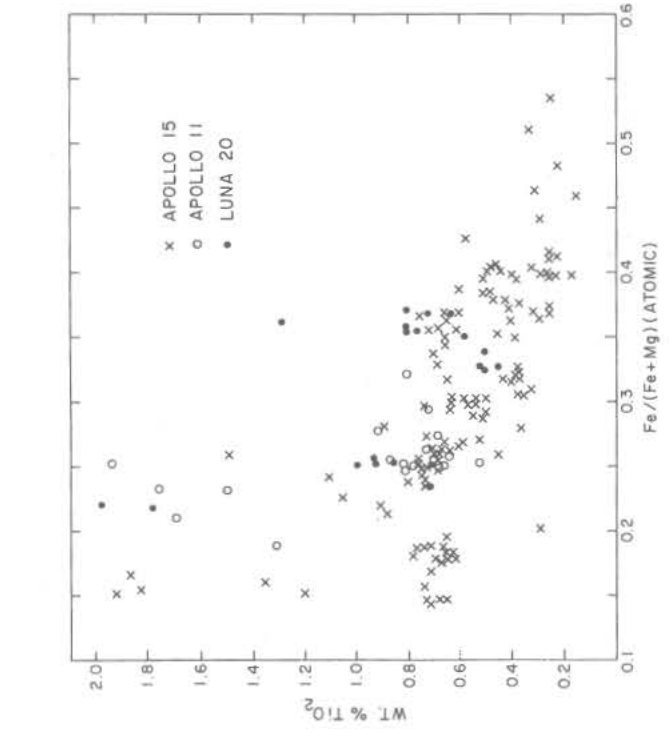

Fig. 4. TiO_2 vs. Fe/(Fe+Mg) for pyroxenes in Apollo 11 (ref. 6 and new data by the author), Apollo 15, and Luna 20 anorthositic lithic fragments.

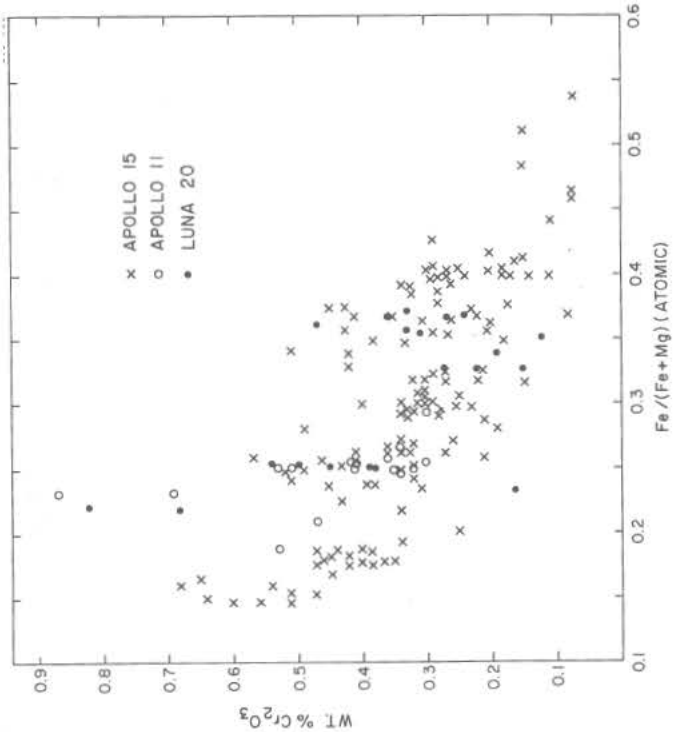

Fig. 3. Cr_2O_3 vs. Fe/(Fe+Mg) for pyroxenes in Apollo 11 (ref. 6 and new data by the author), Apollo 15, and Luna 20 anorthositic lithic fragments.

OPAQUE MINERALOGY OF APOLLO 15 ROCKS: EXPERIMENTAL INVESTIGATIONS OF ELEMENTAL PARTITIONINGS AND SUBSOLIDUS REDUCTION, L. A. Taylor and R. H. McCallister, Dept. of Geosciences, Purdue University, Lafayette, Indiana 47907.

The opaque mineralogies of lunar rocks are distinctive and have been investigated in detail by several groups. However, elemental distributions between coexisting phases have received relatively little study, and although the existence of ulvöspinel reduction to ilmenite + native iron and ilmenite reduction to rutile + native iron have been reported [e.g. 1,2], only sparce experimental data are available with which to interpret these findings. This paper concerns these two areas: 1) elemental partitionings and 2) subsolidus reduction. Expanded versions of portions of these discussions are presented by Taylor et al. [3], McCallister and Taylor [4] and Taylor and McCallister [5].

PARTITIONING STUDIES Ilmenites and chromian ulvöspinels in Apollo 11 thru 15 rocks contain notable amounts of zirconium - up to 0.42 and 0.23 wt%, respectively. These are the highest Zr values reported for these minerals, and the partitioning of Zr between coexisting ilmenite and ulvöspinel is always in favor of ilmenite.

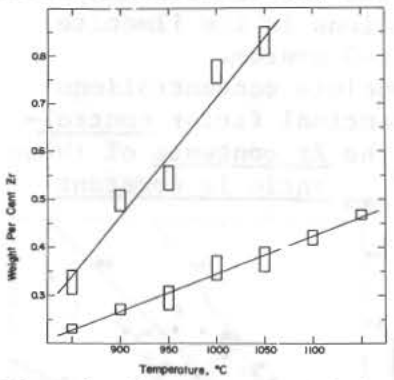

Fig. 1. Upper curve is for ilmenite; lower is for ulvöspinel.

It has been noted [6] that certain lunar rocks (e.g. 14310) contain relatively abundant baddeleyite (ZrO_2). In light of this fact, Taylor and McCallister [5] considered the assemblage $FeTiO_3$ + Fe_2TiO_4 + ZrO_2 + Fe + V to represent univariant equilibria in the Fe-Ti-Zr-O system. They determined the Zr contents of coexisting $FeTiO_3$ + Fe_2TiO_4, in the presence of ZrO_2 + Fe, as a function of temperature (Fig. 1). Effectively, the reaction Zr_{il} = Zr_{usp} was assumed to be an ideal dilute solution, and therefore, log Zr_{il} / Zr_{usp} should be a linear function of 1/T (^oK) as presented in Figure 2. It can be seen that the partitioning of Zr between ilmenite and ulvöspinel is strongly temperature dependent.

In as much as these experiments were at subsolidus conditions in the Fe-Ti-Zr-O system where the Zr activity was fixed by the presence of baddeleyite, certain assumptions must be made before applying these data to lunar mineral assemblages. At a given temperature, there are two important factors which can influence the absolute Zr concentrations in ilmenite and ulvöspinel - the activities of Zr and Ti. If the Zr activity in the melt is less than that necessary to crystallize baddeleyite, the absolute concentrations of Zr in ilmenite and ulvöspinel will be something less than the

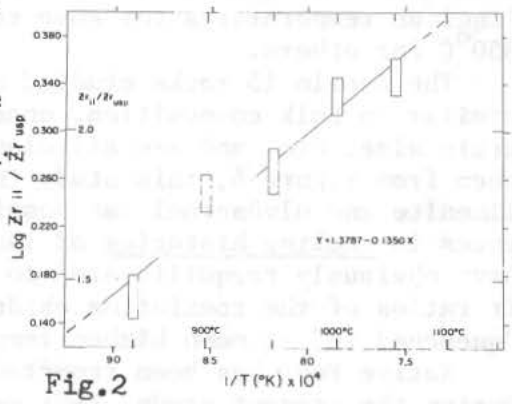

Fig.2

OPAQUES: EXPERIMENTAL STUDIES

TAYLOR

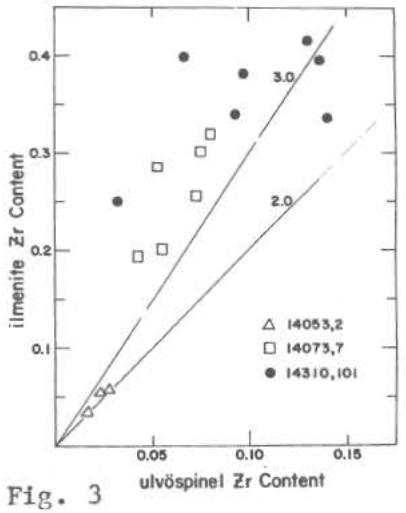

Fig. 3

maximum when baddeleyite is present. However, these lesser activities, from a_{Zr} = 1 in baddeleyite, should not affect the partitioning coefficient of Zr.

Based on crystal chemistry, Zr^{+4} should substitute only for Ti^{+4} within the ulvöspinel. Therefore, if an ulvöspinel contains other substituting elements - e.g. $2Cr^{+3} + Fe^{+2}$ for $2Ti^{+4}$ as in lunar chromian ulvöspinels - the Ti activity will be less than that in stoichiometric Fe_2TiO_4, and this will decrease the absolute Zr concentration. The assumption is made that the partitioning coefficient will be unaffected in such a system undersaturated in Ti.

As discussed in several papers [e.g. 6,7], the Ti content, and hence the Ti activity, in chromian ulvöspinels crystallizing from a lunar melt, increases as crystallization proceeds. Likewise, the Zr activity of the melt increases in the same direction. In general, the early-formed ulvöspinels in Apollo 14 and 15 rocks contain the lowest amounts of Zr, and the latest to crystallize (those occurring in the mesostasis) contain the highest Zr concentrations. Although the a_{Zr} in the melt may reach a value where ZrO_2 is precipitated, the composition of the ulvöspinel only approaches, but does not become, pure Fe_2TiO_4. Therefore, the conditions of the experiments are never really attained in lunar rocks, and the Zr concentrations in the ilmenite and ulvöspinel are always less than in the pure Fe-Ti-Zr-O system.

Although the activities of Ti and Zr control the absolute concentrations of Zr in ilmenite and ulvöspinel, temperature is the principal factor controlling the Zr partitioning. As shown in Figures 3 and 4, the Zr contents of these phases vary within a given rock; however, the Zr_{il} / Zr_{usp} ratio is constant within small limits.

The Apollo 14 and 15 rocks investigated have coexisting ilmenites and ulvöspinels with Zr ratios from 1.5 to over 3. Extrapolation of the data in Fig. 2 to a ratio of 3 gives a temperature of 1225°C. Thus it is obvious that the Zr partitionings between these coexisting phases in lunar rocks (Figs. 3 & 4) are indicative of equilibration temperatures from near liquidus temperatures for some rocks to less than 850°C for others.

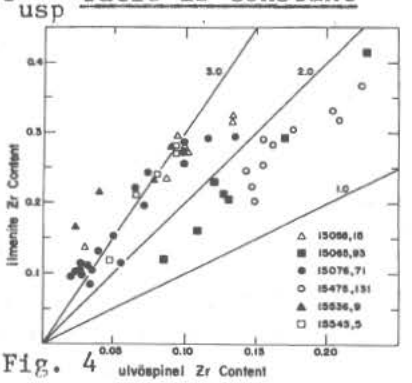

Fig. 4

The Apollo 15 rocks studied are not greatly dissimilar in bulk composition, opaque mineralogies, grain size, etc. and are all classed as crystalline igneous rocks. However, as seen from Figure 4, this study indicates that Zr partitionings of coexisting ilmenite and ulvöspinel can possibly be used as sensitive indicators of differences in cooling histories of lunar rocks. For example, rocks 15065 and 15475 have obviously reequilibrated to subsolidus temperatures of ~850°C whereas the Zr ratios of the coexisting oxides in the other rocks have apparently been "quenched in" at much higher temperatures.

Native FeNi has been reported [e.g. 1, 7, 8] to contain traces of Cr. During the present study, FeNi metals coexisting with chromites and chromian

OPAQUES: EXPERIMENTAL STUDIES

TAYLOR

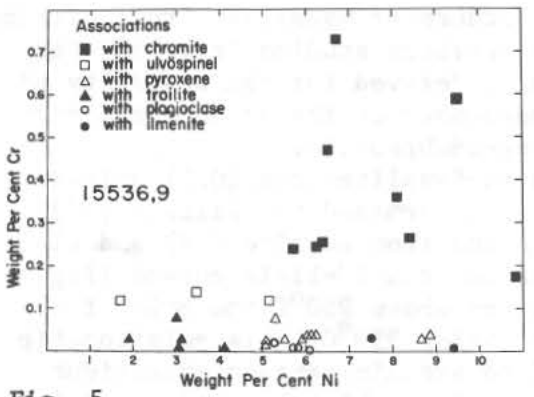

Fig. 5

ulvöspinels in several samples were probed for Cr content. Many of these metal grains gave detectable Cr counts; however, optical examination of these grains using a high power oil-immersion objective showed that the poor polishing behavior of the FeNi metal lends itself to contamination by minute particles of the coexisting spinel. Therefore, it is imperative that the metal grains be carefully inspected prior to analyses.

Of the several samples studied, only the FeNi metal grains in 15536,9 (Fig. 5) appear to show a correlation between Cr content and association. This Cr partitioning between the metal phase and coexisting spinel is relatively consistent. The significance of these findings are currently under investigation and the results will be published elsewhere.

Ti has been reported [1, 6, 7] to be present in minor amounts in troilite associated with ilmenite and/or ulvöspinel and contents of up to 0.8 wt% Ti have been measured. However, the majority of the Ti contents measured are less than 0.3 wt%, and there does not appear to be much consistency within a given rock. Preliminary experimental study of the univariant assemblage Fe + FeS + $FeTiO_3$ + Fe_2TiO_4 + V shows that FeS in this assemblage contains ~0.85 wt% Ti at 900°C. The relatively rapid reaction rates of troilite are well known to the sulfide experimentalist. In as much as the Ti contents of less than 0.3 wt% represent equilibration temperatures of less than 700°C, it is suspected that most troilites have reequilibrated to these low temperatures and little meaningful information can be gained from their Ti contents other than the cooling history of this sulfide phase.

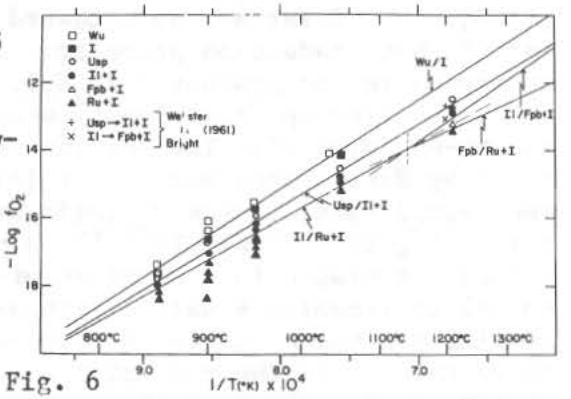

Fig. 6

SUBSOLIDUS REDUCTION Ilmenite and ulvöspinel (the latter actually solid solution members of the ulvöspinel-chromite series) are primary minerals in the lunar rocks. However, evidence can be found for subsolidus reduction to rutile + native Fe [6] and ilmenite + native Fe [1, 2, 6, etc.] resp. It is toward an understanding of these univariant reactions, namely $FeTiO_3 = TiO_2 + Fe + 1/2\ O_2$ and $Fe_2TiO_4 = FeTiO_3 + Fe + 1/2\ O_2$ that a portion of our study was directed. The univariant curves associated with the stabilities of these phases were determined using C-O-H-N gas-flow apparatus with f_{O_2} measured by a solid ceramic (calcia-zirconia) oxygen electrolyte cell and the details of this study as well as the thermodynamic calculations are presented in detail by Taylor et al. [3]. The curves determined are shown in Figure 6. The following equations best fit the experimental data - for the ilmenite curve, $1/2 \log f_{O_2} = -\frac{11,250}{T} + 0.98$ from 850-1050°C, and for the ulvöspinel curve, $1/2 \log f_{O_2} = -\frac{12,170}{T} + 1.93$ from 850-1210°C. These ilmenite and ulvöspinel curves are located at considerably higher oxygen fugacities (i.e.,

OPAQUES: EXPERIMENTAL STUDIES

TAYLOR

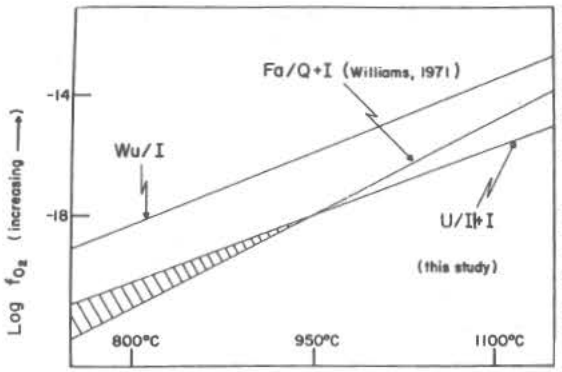

Fig. 7

3/4 and 1/4 orders of magnitude, resp.) than reported by previous studies [e.g. 9]. New data were also derived for the stability of the iron end-member of the armalcolite series - ferropseudobrookite.

The quartz-fayalite-iron (QFI) univariant curve as determined by Williams [10] lies between the iron-wustite (IW) and ulvöspinel-ilmenite-iron (U-Il-I) curves (Fig.7) at temperatures above 950°C and below the U-Ul-I curve below 950°C. This relationship can be used to explain certain subsolidus reduction reactions which have occurred in Apollo 14 rocks. Rocks 14053 and 14072 [3,11] contain fayalite which has broken down by subsolidus reduction to silica (tridymite) + native Fe. They also contain highly reduced ulvöspinels. Many lunar rocks contain apparently stable late-stage fayalite whereas the ulvöspinels commonly show evidence for reduction. Prior to this study by Taylor et al. [3], the U-Il-I curve was located below and approximately parallel to the QFI curve. Thus, it was difficult to explain why the ulvöspinels in many rocks were reduced whereas the fayalite appeared stable. However, based on our new data, as shown in Fig.7, values of f_{O_2} within the shaded region below 950°C would allow for the reduction of ulvöspinel without the concurrent breakdown of fayalite. The breakdown of fayalite is direct evidence for more reducing conditions than those necessary for ulvöspinel reduction.

Subsolidus reduction of chromian ulvöspinel results in the development of various textures [2, 6]. As a first approach toward an understanding of these reduction processes, a kinetic study was conducted on synthetic Fe_2TiO_4 [4].

Controlled f_{O_2} experiments were performed using $CO-CO_2$ mixtures. The details are given in the paper by McCallister and Taylor [4]. A series of isothermal rate studies was made at 900°C and $f_{O_2} = 10^{-17.5}$, $10^{-17.4}$ and $10^{-17.2}$. A pellet of ulvöspinel was placed in a platinum wire basket, and the percent reduction of ulvöspinel to ilmenite + native iron was obtained by the weight loss method. The results are shown in Fig. 8. Two points are worth mentioning in comparing the three curves. 1) The rate of reduction increases as f_{O_2} decreases. This is analogous to the effect that an increasing of supersaturation has on increasing the rate of exsolution when the operative mechanism is the continuous mode. 2) The rate of reaction appears to decelerate continuously from t_o. This suggests that the incubation period or time needed for stable nuclei to form is short compared to the overall transformation time. Optical examination of partially reduced pellets also suggests a nucleation and growth mechanism. In the case of the most reducing conditions (900°C and $f_{O_2} = 10^{-17.2}$), the transformation is initiated on grain boundaries and cracks within the grains, and the development of ilmenite lamellae in the ulvöspinel is not extensive. Under the least reducing conditions (900°C and $f_{O_2} = 10^{-17.5}$), however, the iron coales-

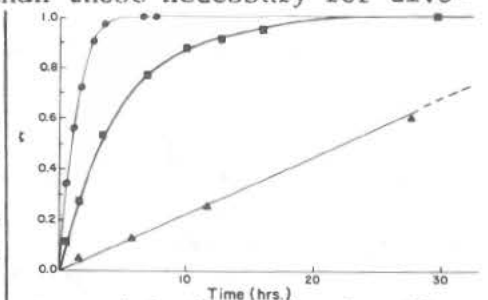

Fig. 8 Ordinate is fractional approach to equilibrium.

OPAQUES: EXPERIMENTAL STUDIES

TAYLOR

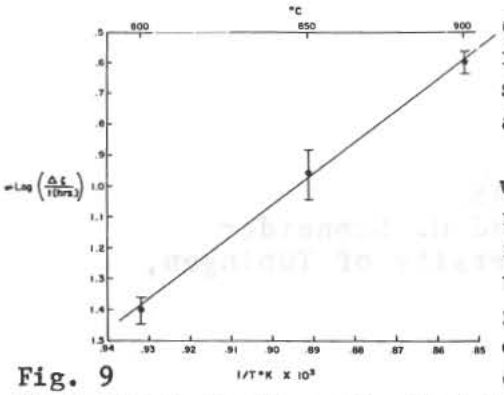

Fig. 9

ces to form large grains and the development of ilmenite lamellae parallel to [111] of the ulvöspinel is pronounced. Many of the textures formed are idential to those observed in lunar rocks.

In order to obtain additional information with respect to the mechanism of reduction, theoretical analysis of the rate data was performed for runs made at 900°C and $f_{O_2} = 10^{-17.4}$. The reasons for selecting this set of experiments are given by McCallister and Taylor [4]. Appropriate equations for: 1) Product growth controlled by diffusion of reactants thru the product layer, 2) Product growth controlled by reaction at the interface, and 3) Product growth controlled by product nucleation at active sites were employed in the analysis. The data do not indicate that growth is controlled at the interface. But, there is agreement with 3), and excluding the result for the least transformed fraction, 1) is also a possible explanation. Due to the fact that nucleation centers do not appear to be continuously forming as evidenced from optical observations, we tentatively propose that the mechanism is one of nucleation and growth where the growth stage may be controlled by reactant diffusing thru the product layer. It is interesting to note that the extrapolated value of results for the diffusion-controlled growth gives a non-zero intercept on the time axis. This suggests that there is a finite incubation period.

In order to obtain an activation energy for the growth stage of the process, pellets were annealed at 900°C and $f_{O_2} = 10^{-17.4}$ for one hour to saturate the active reduction sites. A value for the $f_{O_2} = 10^{-17.4}$ at 900°C is 0.5 log units below the ulvöspinel breakdown curve to ilmenite + Fe as determined by Taylor et al. [3] (see Fig. 6). This Δf_{O_2} value was kept constant for other prenucleated pellets which were subsequently annealed at 850° and 800°C. The rate as a function of 1/T is shown in Fig. 9, and the activation energy for the reaction as determined from an Ahrrenius plot is 46 ± 4 Kcal/mole.

This activation energy for ulvöspinel reduction is to be compared with 64 ±6Kcal/mole for the breakdown of ilmenite to rutile + Fe [12]. This explains the experimental observation that ulvöspinel placed at an f_{O_2} below the ilmenite reduction curve first breaks down to ilmenite + Fe and then, however, more slowly, the ilmenite breaks down to rutile + Fe. Thus the presence of ulvöspinel and the absence of ilmenite reduction in lunar rocks does not indicate that oxygen fugacities were necessarily between the two univariant curves as suggested by Haggerty [2]. The univariant curves only give upper limits of f_{O_2} since the "complete" breakdown of ulvöspinel to rutile + Fe is a stepwise process.

REFERENCES: [1] El Goresy, A. et al., 1971, 2nd Lunar Sci. Conf.: [2] Haggerty S.E., 1971, Nature; [3] Taylor, L.A. et al., 1972, EPSL; [4] McCallister, R.H. and Taylor, L.A., 1972, EPSL; [5] Taylor, L.A. and McCallister, R.H.,1972, EPSL [6] El Goresy et al., 1972, LSI Contr. 88; [7] Taylor, L.A. et al., 1971, 2nd Lunar Sci. Conf.; [8] Melson, W.G. et al., 1972, LSI Contr. 88; [9] Taylor,R.W. and Schmalzried, H., 1964, J. Phys. Chem.; [10] Williams, R.J., 1971, AJS; [11] El Goresy et al., 1971, EPSL; [12] El-Guindy, M.I. and Davenport, 1970, AIME.

APOLLO 15 REGOLITH AND BRECCIAS.

W. v. Engelhardt, J. Arndt, and H. Schneider
Mineralogical Institute, University of Tübingen,
Germany (BRD)

(I) Petrography

(a) Regolith and regolith breccia samples derived predominantly from local mare basalts have been investigated from the following sites: Hadley Rille edge (regolith sample 15601, regolith breccia 15505), Dune Crater (regolith sample 15471), Elbow Crater (regolith breccia 15086). The regolith contains about 8 % crystalline rocks. Predominant are pyroxene-rich mare type basalts (ophitic, intersertal) and dark olivine-bearing vitrophyres. Intersertal basalts contain orthopyroxene rimmed by clinopyroxene. Fragmental rocks (see under (b)) are much rarer. The contents of regolith breccia fragments and glassy agglomerates (average 36 %) and that of glasses (average 11 %, fragments and spherules) are relatively low. The dominant chemical composition of the colorless, yellow and brown glasses corresponds to group II of Table 1. The regolith shows high pyroxene + olivine/plagioclase ratios (≈ 2), indicating that the underlying rocks are rich in pyroxene. Median diameters (15601: 77 μ, 15471: 63 μ) are relatively large.

Breccias 15505 and 15086 are regolith breccias with a fragmental, perhaps a little glassy matrix. They are similar in composition to the regolith samples.

(b) Regolith, regolith breccia and rock samples derived predominantly from Apennine material with an admixture of mare basalt material have been investigated from station 6 (regolith sample 15291, regolith breccia 15285, fragmental rock 15256) and from St.George Crater (regolith sample 15221). The regolith samples and regolith breccia 15285 contain few (< 3 %) mare type fragments as described under (a). Predominant rock fragments are:

(1) Plagioclase-rich rocks (breccias with orthopyroxene and/or clinopyroxene, pure plagioclase breccias, anorthosites).
(2) Several types of fragmental rocks containing plagioclase and less pyroxene fragments in a fine-grained pyroxene-plagioclase-ilmenite matrix).
(3) Cumulates of plagioclase, orthopyroxene and clinopyroxene.

APOLLO 15 REGOLITH AND BRECCIAS

W.v.Engelhardt

Regolith breccia fragments and glassy agglomerates amount to about 45 % of the regolith samples. Glass contents of the regolith samples and breccia 15285 are high (average in the regolith 18 %). Characteristic are green glass spherules and fragments (average in the regolith 8 %) the chemical composition of which corresponds to group V, Table 1.

In accordance to the abundance of feldspar-rich fragments at these stations the pyroxene + olivine/plagioclase ratio is about 1 in regolith samples and breccia 15285. Median diameters of the regolith samples are low (15221: 51 µ; 15291: 40 µ). The regolith 15291 contains more mare material than 15221.

Rock 15256 contains in a matrix of much clinopyroxene with plagioclase and ilmenite of varying crystal sizes and fluidal texture, various basaltic fragments (light colored ophitic, olivine-bearing, dark, coarse- and fine-grained and vitrophyric rocks), single olivine crystals, clinopyroxene fragments and a few devitrified glass particles. An impact origin of this rock seems probable.

(c) Regolith and regolith breccia samples from the ALSEP-LM-area (regolith sample 15031, collected from the bottom of a trench, approximately 0,33 m below the surface; regolith sample 15041: same locality, taken from the top of the trench; regolith breccia 15565) are mixtures of mare basalt materials and components of the Apennine Front regolith. Regolith samples contain similar amounts of regolith breccia fragments and glassy agglomerates (average 50 %) as those from the Apennine Front but less glasses of different colors (average 14 %). The chemical composition of the glasses may correspond predominantly to group I, Table 1. Crystalline rocks of the regolith (average 4 %) are predominantly ophitic basalts, of regolith breccia 15565 intersertal orthopyroxene-bearing basalts. Less frequent are in the regolith and breccia 15565 noritic rocks and fragmental rocks with crystalline matrices as described under (b). Pyroxene + olivine/plagioclase ratio in the regolith is high (average 1,7).

Regolith sample from the bottom of the trench (15031) is richer in rock, glass and mineral fragments but poorer in regolith breccia fragments and glassy agglomerates than that from the top (15041). The difference in median diameters (15031: 41 µ; 15041: 56 µ) indicates that in the surface regolith (15041) a large part of fine particles has been incorporated into breccias and agglomerates.

(II) Shock effects

Shock effects in minerals and small rock fragments (diaplectic plagioclase glass, shock lamellae in pyroxene and

APOLLO 15 REGOLITH AND BRECCIAS

W.v.Engelhardt

olivine) have been observed in all regolith and regolith breccia fragments. They are rare in all samples, but more abundant near Hadley Rille than at the Apennine Front.

(III) Chemical composition of glasses

Glasses have been analyzed by microprobe from soil samples 15601 and 15602 (Hadley Rille), 15471 (Dune Crater), 15221 (St.George Crater), 15291 (station 6), 15041 (ALSEP) and all regolith breccias mentioned in paragraphs (1) - (3), above. Results are presented in Table 1. Five main types can be distinguished, which are supposed to have been produced by shock melting of the following rock-types: Anorthositic rocks (I), local low alkali mare basalts (II), high alkali basalts and/or regolith (III), high Ti- low Si-basalts (IV), Ti-poor "pyroxenitic" rocks (V). Some glasses contain Fe-Ni-spherules, which may represent meteoritical material.

(IV) Thermal expansion of glasses

The linear thermal expansion coefficient and the glass transition temperature measured on a black glass sphere from 15032,9 (fraction > 0,5 mm) are $\alpha_{20}^{600} \approx 10 \times 10^{-6}/^{o}C$ and T_g = 685 °C, respectively.

(V) Conclusions

(a) Differences in texture, modal and chemical composition of basalts and basaltic glasses in regolith and breccia samples derived from mare material show that the mare plane is underlain by different basaltic flow units (olivine-bearing vitrophyres, basalts of extremely low and higher alkali contents, Ti-rich basalts).

(b) The coarse grain sizes and modal composition (high content in rock fragments, low contents in agglomerates, regolith breccias and glasses) of regolith samples from Hadley Rille and Dune Crater suggest a young age of these soils.

(c) Apennine Front material is predominantly of anorthositic-noritic composition. Absence of larger rocks and intense brecciation of all small fragments indicate that the Apennine mountains at their exposed front are composed of a more or less solidified debris which, due to the scarcity of strong shock effects and of shock melted glasses of anorthositic composition, represents a weakly shocked impact breccia produced by the Imbrium and/or Serenitatis impact.

(d) Green glass spheres and fragments, most abundant at Apennine Front stations, are supposed to be products of shock

APOLLO 15 REGOLITH AND BRECCIAS

W.v.Engelhardt

melting of a particular pyroxene-rich rock, as yet unknown from the lunar surface. We suggest that their source may be a strongly shocked breccia layer produced from deep seated mafic rocks by the Imbrium impact and deposited at higher levels of the Apennine mountains. The mafic rocks may represent differentiation products underlying the plagioclase-rich cumulates which constitute the upper layers of the pre-Imbrian lunar crust.

Table 1: Electron microprobe analyses of 44 glass fragments and spherules (wt.%)

Group	I		II		III		IV		V	
Color	colorless		yellow to brownish		colorless to slightly colored		red-brown		green and slightly colored, colorless	
Number	2		6		15		5		16	
	range	av.	range	av.	range	av.	range	av.	range	av.
SiO_2	43,7 - 46,2	44,9	42,8 - 45,6	43,6	45,8 - 54,4	49,3	35,6 - 37,7	37,1	42,7 - 46,7	45,7
TiO_2	1,17 - 1,48	1,33	3,15 - 4,13	3,49	0,36 - 2,25	1,43	10,4 - 13,3	11,6	0,34 - 0,44	0,38
Al_2O_3	20,1 - 22,2	21,2	7,7 - 10,0	8,7	14,0 - 18,0	16,2	6,6 - 7,7	7,3	6,7 - 7,9	7,2
FeO	7,0 - 9,9	8,5	19,1 - 22,3	21,3	9,1 - 12,8	10,3	20,7 - 22,3	21,7	19,3 - 20,8	20,1
MgO	8,3 - 11,7	10,0	10,0 - 13,7	12,2	6,5 - 12,7	9,6	10,1 - 11,9	10,9	16,7 - 19,2	18,0
CaO	11,5 - 14,3	12,9	8,1 - 10,7	9,0	9,8 - 12,1	10,9	7,4 - 8,4	8,1	7,8 - 9,0	8,3
Na_2O	0,23 - 0,37	0,30	0,19 - 0,50	0,41	0,15 - 1,05	0,64	0,43 - 0,66	0,57	0,11 - 0,20	0,16
K_2O	0,02 - 0,06	0,04	0,00 - 0,03	0,01	0,05 - 0,88	0,37	0,05 - 0,11	0,08	0,00 - 0,01	0,00

APOLLO 15 GLASSES AND THE DISTRIBUTION OF NON-MARE CRUSTAL ROCK TYPES. Jeff Warner, NASA-MSC, Houston, Texas; W. I. Ridley, Lunar Science Inst.; A. M. Reid, NASA-MSC; and Roy W. Brown, Lockheed Electronics.

Over 600 nine element electron microprobe analyses of glasses from five Apollo 15 soils (15021, 15101, 15261, 15301, 15601) and one breccia (15427) have been completed (1, 2). The data have been grouped using a cluster analysis procedure (3); average compositions of the various lithologic types are set out in Table 1. In contrast to our previous work, anorthositic glasses have been combined with the Highland basalt (anorthositic gabbro) glasses. Aluminous basaltic glasses (Al_2O_3 = 14-21 wt. %), called Fra Mauro basalt by us (1, 3) and KREEP by other workers (4), have been subdivided into 3 varieties based on their K content: high-, moderate-, and low-K. Although the terminology of these rock types is in desperate need of revision, we use the Fra Mauro basalt and KREEP names as equivalents here. Four types of Mare basaltic glasses are recognized. From these data, combined with Apollo 15 site geology, we have concluded (1, 2):

1. Moderate- and high-K Fra Mauro basaltic glass (KREEP) is an "exotic" component at the LM site. KREEP is identified as the major component of the ray from Aristillus and/or Autolycus.
2. Low-K Fra Mauro basaltic glass (low-K KREEP) is a major rock type in Hadley δ Mountain, and thus in the Apennine Front.
3. Highland basalts (anorthositic gabbro) and anorthosite are not abundant at the Apollo 15 site.
4. Green glass is preferentially found in the Hadley δ Mountain samples, and probably represents a lunar mantle composition.
5. Various types of Fe-rich basaltic glass are present in all the soils. One type (Mare 2, Table 1) is compositionally equivalent to the Apollo 15 basaltic rocks. The other types of mare basalt may be derived from nearby maria such as Imbrium and Serenitatis.
6. Granitic glasses are rare.

The correlation of moderate- and high-K Fra Mauro basaltic glasses at the Apollo 15 site with the Aristillus and/or Autolycus ray is analogous to the correlation of Apollo 12 KREEP with a ray from Copernicus (4). Aristillus, Autolycus, and Copernicus are all large, Copernican-age craters that penetrated through mare basalts at the edge of the Imbrium Basin. This suggests that the material directly beneath the later mare basalts consists of KREEP. The Apollo 14 Fra Mauro breccias, which are essentially KREEP, represent the edge of the Imbrium basin ejecta blanket. Hence, the upper part of the crust in the Imbrium basin region prior to the Imbrium event consisted predominantly of KREEP.

Although the geochemical significance of low-K Fra Mauro basalt is uncertain (parent of KREEP or a parallel origin of KREEP), both its chemistry and abundance in the Apennine Front suggests that it is of non-mare origin. Regardless of the origin of Hadley δ Mountain (ejecta or upthrust block), its mass must originate at a depth of at least several kilometers. Thus, low-K Fra Mauro basalt must be representative of a moderately deep part of the Pre-Imbrium crust. Low-K Fra Mauro basaltic glasses

from Hadley δ Mountain may be the first samples of the deep Pre-Imbrium crust recognized to date in the Apollo program.

It has been suggested by many workers that the highlands consist of an anorthositic suite of rock types (e.g. 3, 5). The predominance of Highland basalt (anorthositic gabbro) compositions has been confirmed by the Apollo 16 (6), Luna 20 (7), and orbital X-ray fluorescence (8) data. However, Highland basaltic and anorthositic glasses are rare at the Apollo 15 site, indicating that the Apennine Mountains are not chemically representative highlands.

The (KREEP plus low-K KREEP)/(Highland basalt plus anorthosite) ratios for the various Apollo and Luna sites do not show a continuum of values. Apollo 11 and 16 and Luna 16 and 20 are all Highland-basalt-rich whereas Apollo 12, 14 and 15 are Highland-basalt-poor (Table 2). These data suggest that there are lateral inhomogeneities in the upper lunar crust: the Imbrium-Procellarum region has a KREEP plus low-K KREEP upper crust and the Tranquillitatis-Fecunditatis-Central Highlands region has an anorthositic upper crust. In addition to these lateral variations, vertical variations must also exist.

Green glass, which occurs as spheres and fragments of spheres, defines an extremely tight compositional cluster (see standard deviations in Table 1) that is ultramafic. The spheres are commonly clear emerald green, but some spheres and/or parts of spheres are devitrified to a light-brown, cryptocrystalline aggregate. Clear spheres commonly contain crystallites of olivine (Fo-76). Green glass is most abundant in Hadley δ Mountain samples, suggesting that the Apennine Front is the immediate locus for green glass. However, since green glass and green glass clods occur in low-K KREEP breccias, green glass must be considered a second generation rock type in the Front. The green glass, and other ultra-mafic glasses described from the Apollo 14 site (9), may ultimately be derived from deep seated ultra-mafic rocks that are the source region for mare basalts, i.e. the lunar mantle. However, the low Mg/Fe ratio of green glass is not compatible with the magnesian pigeonites found in some mare basalts.

References

1. Reid, A. M. et al. (1972) Meteoritics, in press.
2. Ridley, W. I. et al. (1972) Physics of the Earth and Planetary Interiors, in press.
3. Reid, A. M. et al. (1972) Proc. Third Lunar Sci. Conf., 1, 363-378.
4. Meyer, C., Jr. et al. (1971) Proc. Second Lunar Sci. Conf., 1, 393-411.
5. Wood, J. A. et al. (1970) Proc. Apollo 11 Lunar Sci. Conf., 1, 965-988.
6. LSPET (1972) Apollo 16 report, Science, in preparation.
7. Warner, J. et al. (1972) Abstract, Geol. Soc. Am. Ann. Meeting, in press.
8. Adler, I. et al. (1972) Science, 175, 436-440.
9. Marvin, U. B. et al. (1972) Lunar Science III, 507-509.

Table 2. (Fra Mauro basaltic glass) : (Highland basaltic glass) ratios for lunar landing sites.

Landing Site:	Luna 16	Apollo 11	Luna 20	Apollo 16	Apollo 12	Apollo 14	Apollo 15
Ratio:	.1	.2	.2	<.3	1.6	2.0	5.7

A-15 Glasses & Distribution of Non-Mare Crustal Rock Types

Jeff Warner

Table 1. Average composition of glass types in Apollo 15 soils.

		MARE BASALT			
	Green Glass	Mare 1	Mare 2	Mare 3	Mare 4
SiO_2	45.43(.63)	45.70(2.01)	44.55(1.94)	43.95(1.89)	37.64(2.27)
TiO_2	.42(.06)	1.60(.43)	3.79(.98)	2.79(.93)	12.04(2.00)
Al_2O_3	7.72(.33)	13.29(1.96)	11.77(1.88)	8.96(1.20)	8.46(1.07)
Cr_2O_3	.43(.03)	.33(.07)	.26(.06)	.46(.11)	.48(.10)
FeO	19.61(.84)	15.83(2.16)	18.83(2.14)	21.10(1.46)	19.93(1.76)
MgO	17.49(.54)	11.72(1.60)	8.84(1.88)	12.30(1.60)	10.49(1.58)
CaO	8.34(.41)	10.41(.80)	10.46(.94)	9.02(.70)	8.81(1.40)
Na_2O	.12(.05)	.30(.14)	.34(.20)	.27(.12)	.54(.17)
K_2O	.01(.02)	.10(.07)	.13(.11)	.05(.03)	.13(.05)
Total	99.57	99.28	98.97	98.90	98.52
CaO/Al_2O_3	1.080	.783	.889	1.007	1.041
$Mg/Mg+Fe^{atomic}$	.614	.569	.456	.510	.484
No. of analyses	187	67	21	26	6
Percentage of total analyses	34.2	12.2	3.8	4.8	1.1

	Highland Basalt plus Anorthosite	Low K	Moderate K	High K	'Granite' 1	'Granite' 2
SiO_2	44.35(2.38)	46.56(1.78)	49.58(1.43)	53.35(2.82)	73.13(1.36)	62.54
TiO_2	.43(.37)	1.25(.45)	1.43(.30)	2.08(.56)	.50(.71)	1.18
Al_2O_3	27.96(3.67)	18.83(1.85)	17.60(1.54)	15.57(1.65)	12.37(.87)	15.73
Cr_2O_3	.08(.04)	.20(.05)	.17(.03)	.12(.06)	.35(.49)	.03
FeO	5.05(2.28)	9.67(1.88)	9.52(1.31)	10.25(1.09)	3.49(3.16)	6.67
MgO	6.86(2.92)	11.04(1.61)	8.94(1.24)	5.77(1.61)	.13(.10)	2.51
CaO	15.64(1.63)	11.60(.93)	10.79(.69)	9.57(.77)	1.27(.62)	6.86
Na_2O	.19(.23)	.37(.14)	.74(.14)	1.01(.42)	.64(.16)	.98
K_2O	.01(.03)	.12(.07)	.47(.17)	1.11(.40)	5.97(.27)	3.20
Total	100.92	99.66	99.24	98.83	97.85	99.70
CaO/Al_2O_3	.559	.616	.613	.615	.103	.203
$Mg/Mg+Fe^{atomic}$	.708	.670	.626	.501	.062	.401
No. of analyses	36	82	90	29	2	1
Percentage of total analyses	6.6	15.0	16.5	5.3	.4	.2

(Numbers in brackets are one standard deviation.)

FERROMAGNETIC AND PARAMAGNETIC RESONANCE OF MAGNETIC PHASES AND Fe^{3+} IN APOLLO 15 SAMPLES: A COMPARISON*

R. A. Weeks
Solid State Division, Oak Ridge National Laboratory
Oak Ridge, Tennessee

Electron magnetic resonance spectra of samples of lunar fines (< 1 mm) from A-11, A-12, and A-14 exhibited a ferromagnetic component > 100 times more intense than any other component.[1][2][3][4][5] The spectra of crystalline rock samples from these collections have ferromagnetic components, none of which are similar to the component in the spectra of samples of fines. This component is observed in breccias which are poorly consolidated and apparently decreases with increasing consolidation and recrystallization.[5] Its line width, ΔH, and the temperature dependence of ΔH do appear to be a function of the site from which samples are collected. Hence ΔH data from A-15 fines will be additional evidence in determining if there is a site dependence. A site dependence may indicate that processes of formation of the ferromagnetic phase or phases differed at each site. Variations in distribution of particle sizes and shapes and variation of chemical composition of the ferromagnetic phase or phases from site to site will produce variations in the resonance spectra.

Spectral components attributable to paramagnetic states of Fe^{3+}, Ti^{3+}, and Mn^{2+} are observed in the spectra of crystalline rock samples. Spectral components attributable to Fe^{3+}, Ti^{3+}, and Mn^{2+} have been observed in the spectra of plagioclases from other Apollo collections.[1][3][5] Hence, the plagioclases from A-15 crystalline rocks are expected to contain paramagnetic Fe^{3+}, Ti^{3+}, and Mn^{2+}. The valence states of Fe and Ti are determined by the oxygen partial pressure in the liquid from which the plagioclases crystallized and by the valence state of all other impurity ions present in the plagioclase crystallites. Assuming that the lunar plagioclases have approximately constant concentrations of Fe, Ti, and other impurity ions, then a variation in intensity of the Fe^{3+} and Ti^{3+} spectral components would be indicative of a variation in oxygen partial pressure in the liquids from which they crystallized.

Measurements were made on samples from specimens 15271,68, 15601,80, 15475,22, 15475,24, and 15555,109. Samples of fines were prepared by removing all particles > 0.1 mm and then encapsulating $\sim$ 5 mg in a quartz tube (Varian Associates sample tubes). Mineral separates of crystalline rocks were prepared by separating fractions of the abundant large crystallite yellow-green mineral (presumed to be a pyroxene), the abundant large crystallite brown mineral (also presumed to be pyroxene) and colorless plagioclase intermingled with brown pyroxene. On the basis of microscopic observations the brown and

*Research sponsored by the U. S. Atomic Energy Commission under contract with Union Carbide Corporation and NASA contract No. MSC-T-74658.

FERROMAGNETIC AND PARAMAGNETIC RESONANCE OF MAGNETIC PHASES AND Fe^{3+}

R. A. Weeks

yellow-green pyroxene fractions were > 0.95, while the plagioclase fractions were > 0.75 of the samples. Measurements were made at 9 and 35 GHz and in some cases at temperatures ranging from ∿ 120K to 300K.

A summary of the data on ΔH and intensity, I, of the ferromagnetic spectral component observed in the spectra of Apollo fines is given in Table I. Various types of particles were also separated from the fines, and data on these are also included.

In the spectra of neither the yellow-green nor the brown pyroxene fractions were components detectable which could be attributed to Fe^{3+} or Ti^{3+}. On the basis of relative sample weights and estimated purity of the fractions, the concentrations of these two ions in the yellow-green and brown pyroxenes are at least an order of magnitude smaller than in those plagioclase fractions in which both Fe^{3+} and Ti^{3+} components have been detected.[1][3][5] Data on the relative concentrations of Fe^{3+} and Ti^{3+} in various plagioclase fractions are given in Table II. It has been noted that Fe^{3+} occupies at least two crystallographically distinct sites in lunar and terrestrial plagioclases.[6] The data in Table II on the resonance properties of Fe^{3+} are for only one of the sites.

On the basis of the limited number of samples upon which measurements have been made, it is evident from data in Table I that line width is a function of the site from which samples were collected, while I is not. A-11 samples have a spectral component with the greatest width, while the spectral component of A-14 samples has the smallest widths. The range in ΔH for any one of the Apollo sites is less than the difference between the widths of the resonance of samples from different sites. Magnetic fractions have slightly greater widths than the average of samples in which particles > 0.1 mm have been excluded. The ferromagnetic resonance component of selected particles, with one exception, have much smaller widths. A glassy layer from a sample of rock 14318 has the smallest width yet observed. Intensities for all of these samples of fines fall within the range 4.5 to 26, with one exception. One of the A-12 samples had an intensity of 1.5. An extensive discussion of the A-12 samples has been given elsewhere.[4] Selected particles from A-14 and A-15 fines have intensities < 1, with the exception of the grey-yellow glasses from 14003,60 and the glassy layer from a sample of rock 14318.

The plagioclase fractions from A-15 crystalline rocks all have significantly higher intensities of the Fe^{3+} component than do fractions from two A-14 rocks (Table II). Although the Ti^{3+} component was well resolved in the fractions from A-14 samples, it was not detected in any of the fractions from A-15 samples. This difference can be tentatively attributed to an oxygen partial pressure in the liquid (or gas) from which the A-15 plagioclases crystallized which was higher than that in the liquid (or gas) from which the A-14 plagioclases crystallized. (There is some evidence from the morphology of the plagioclase crystallites in the A-15 samples that they may have grown via vapor deposition.)

Radiation damage processes can alter the valence of impurity ions in some crystalline compounds.[7] It is possible that radiation damage processes have changed Fe^{2+} to Fe^{3+} and Ti^{4+} to Ti^{3+} during the time a rock was exposed on the lunar surface. If this process has occurred, then the concentration of Fe^{3+} ions in a sample would be a function of its distance from the surface.

FERROMAGNETIC AND PARAMAGNETIC RESONANCE OF MAGNETIC PHASES AND Fe^{3+}

R. A. Weeks

Two samples from the same crystalline rock, 15475, one from within 1 cm of the top of the parent rock and one from its bottom, ∿ 8 cm below its surface, had the same concentration of Fe^{3+} ions within experimental error (Table II). On the basis of these data, radiation damage processes have not generated Fe^{3+} nor Ti^{3+}. This conclusion is supported by the results of irradiating lunar plagioclases with ^{137}Cs gamma rays. Within experimental error, no increase in the intensity of the Fe^{3+} spectral component was observed.[8] Spectral components due to Mn^{2+} were observed in the spectra of all plagioclase fractions. They have not been observed in any of the pyroxene fractions.

References

(1) R. A. Weeks, J. L. Kolopus, A. Chatelain, D. Kline, and J. G. Castle, Science 167, 704 (1970). (2) R. A. Weeks, J. L. Kolopus, D. Kline, and A. Chatelain, Proc. Apollo 11 L.S.Conf., Geochim et Cosmochim Acta, Suppl. 1, Vol. 3, 2467 (1970). (3) J. L. Kolopus, D. Kline, A. Chatelain, and R. A. Weeks, Proc. 2nd L.S.Conf., Geochim et Cosmochim Acta, Suppl. 2, Vol. 3, 2501-2514 (1971). (4) R. A. Weeks, J. L. Kolopus, and S. Arafa, The Moon 4, 271 (1972). (5) R. A. Weeks, Proc. 3rd L.S.Conf., Geochim et Cosmochim Acta, Suppl. 3, to be published. (6) R. A. Weeks, unpublished data; J. M. Gaite and J. Michoulier, Bull. Soc. fr. Min. Crystall. 93, 341-356 (1970). (7) R. A. Weeks and J. L. Kolopus, "Paramagnetic Resonance of Some Silicate Minerals," Semiannual Progress Report for period ending June 30, 1968, ORNL CF No. 68-8-38. (8) R. A. Weeks and A. Chatelain, unpublished data.

FERROMAGNETIC AND PARAMAGNETIC RESONANCE OF MAGNETIC PHASES AND Fe^{3+}

R. A. Weeks

Table I
Intensities and Line Width of a Ferromagnetic Resonance Characteristic of Lunar Soils

Sample (comments)	Line Width ΔH (gauss)[4]	Relative Intensity[4] $I(mg^{-1})$
A-11	950	
A-12 (average of 4 samples)	750-768-785	1.5 - 26
A-12 (magnetic fraction[1])	791	18
A-14 (average of 5 samples)	600-613-634	8 - 18
A-14 (magnetic fraction average of 4 samples[1])	692-710-724	90 - 18
15271,68	670	5.0
15601,80	734	4.5
15271,68 (dark red spheroid[3])	600	0.7
15271,68 (30 green spheroids[3])	467	$\sim$ 0.3
14003,60 (6 spheroids[3])	568	$\sim$ 0.1
14003,60 (plagioclase-rich fragments[3])	510	$\sim$ 0.1
14003,60 (grey and yellow glasses[3])	750	3.4
14318,36 (glassy layer[3])	417	1.5

(1) The magnetic separation was made with a small alnico horseshoe magnet. The magnet was placed on the outside of a petri dish and the sample was distributed uniformly over the bottom of the dish. The particles were attracted by the magnet from a distance of $\sim$ 1 cm. Hence they were strongly ferromagnetic. Lustrous metallic particles were observed in the samples. (2) The first value is the minimum, and the third the maximum observed, the second value is the average of all values. (3) These samples were washed in ethanol to remove dust adhering to their surfaces. Some dust was observed on the surface of most particles after washing. (4) The intensity of the absorption was found from the relation $I = \Delta H^2 A/W$, with $\Delta H = H_{max} - H_{min}$ and A = amplitude of the dI/dH curve between the field, H_{max}, at which the maximum amplitude of the curve occurs and the field, H_{min}, at which the minimum amplitude occurs, and W is the sample weight in mg. The magnetic field modulation amplitude was constant for all these measurements. These values have all been normalized to a constant amplifier setting.

FERROMAGNETIC AND PARAMAGNETIC RESONANCE OF MAGNETIC PHASES AND Fe^{3+}

R. A. Weeks

Table II
Relative Intensities of the Resonance of Fe^{3+} and Ti^{3+}
in Several Lunar Plagioclases

Sample (comments)	W (mg)	ΔH (gauss)	$I^{(1)}$ (mg^{-1})
	Fe^{3+}		
14053,47 (> 99%)	54.2	28.3	1.3 ± 0.3
14321,166 (99%)	32.9	27	1.0 ± 0.3
15475,22 (surface, top, ∿ 75%)	15.7	40	6 ± 2
15475,24 (surface, bottom, ∿ 75%)	12.4	23.4	8 ± 3
15555,109 (∿ 1.5 cm from top)	12.8	20	3 ± 1
	Ti^{3+} / ΔH	$A^{(4)}$	
14053,47	100	20	(2)
14321,166	100	19	
15475,22, 15475,24, 15555,109	ND(3)		

(1) $I = \Delta H^2 A/W$ and normalized for amplifier gain. See footnote 4, Table I. (2) Because of the asymmetry of this spectral component, the relation used to calculate I for Fe^{3+} is not applicable. (3) ND = not detected. A signal with an amplitude, A, one-fourth A for 14053,47 would have been resolved. (4) A ≡ amplitude of dI/dH curve for this spectral component. This component and the Fe^{3+} component can be resolved from other components on basis of the Boltzmann dependence of A on temperature.

PETROLOGY OF PYROXENE VITROPHYRE 15597: P.W. Weigand, Dept. Geol. Geophys. Sci., Princeton Univ., Princeton, N.J. 08540

Apollo 15 pyroxene vitrophyre 15597 was collected at Station 9A (Rille Station) perhaps 8 m east of the rim of Hadley Rille in the area of the "bedrock" samples 15595 and 15596. Acicular pyroxene phenocrysts, commonly with a glass core, contribute up to 60 modal % by volume of this rock and are ~0.5-1.5 mm long and ~0.04-0.15 mm across. Length/width ratios range up to 25. One large, roughly equant phenocryst occurs in one of the four slides we studied and has a cross-sectional area of ~0.3 mm^2, approximately an order of magnitude greater than the other phenocrysts. Chrome spinel grains and native iron globules occur in minor amounts. Skeletal pyroxene crystals, microlite sheafs, and feather-shaped crystals are common between the pyroxene phenocrysts in the brown quench-glass. Vesicles constitute ~2.5 area % of the rock and range in size from a few tens to 500 microns across.

The pyroxenes are composed of pigeonite epitaxially rimmed by augite. The inner part of the pigeonites is unusually Mg-rich and Ca-poor, $Wo_4En_{70}Fs_{26}$, which zones outwards to ~$Wo_{15}En_{52}Fs_{33}$. The latter is in contact with augite of ~$Wo_{30}En_{40}Fs_{30}$ which itself zones to a Mg-poor pyroxene of ~$Wo_{32}En_{10}Fs_{58}$. Al_2O_3 and TiO_2 contents increase to extreme levels in the augite rims and are among the highest yet reported for lunar augites. The bulk of the large phenocryst is homogeneous; only the outer ~20% shows a change from a composition similar to the inner portions of the majority of smaller crystals. The skeletal pyroxene crystals in the glass matrix are nearly identical in composition to the phenocryst augite rims.

The chromite grains are distributed irregularly in the rock and constitute perhaps ~0.05 to ~1.0 modal %. They have a bimodal size distribution; a large group averages ~100μ across while a smaller group averages ~25μ across. The larger grains are euhedral, are commonly partially enclosed by the pyroxene phenocrysts and often occur in clusters. The smaller grains are euhedral to subhedral and are found completely or partially enclosed in pyroxenes and in the glass matrix. Wherever in contact with the glass the chromites have a thin rim of ulvospinel. The larger chromites are higher in Cr_2O_3 than the smaller ones,

Petrology of Pyroxene Vitrophyre 15597

P.W. Weigand

and are higher than any other lunar chromite reported to date. Grains of both groups show slight chemical zonation, with Cr and Mg decreasing and Al, Ti, and Fe increasing toward grain edges. On the other hand, whereas vanadium increases with decreasing Cr in the large chromites, it decreases with decreasing Cr in the small chromites.

Based on textural and mineralogical evidence, the following crystallization is inferred for sample 15597: 1) crystallization of native iron and the large chromites followed by crystallization of the smaller chromites, possibly in a different physical or chemical environment; 2) nucleation of pigeonite, probably after nucleation of the small chromites and possibly after they ceased crystallization, followed by 3) epitaxial over-growth by augite; 4) overgrowth of ulvospinel on chromite during, or after augite crystallization; and 5) growth of skeletal augites in the groundmass as final quenching took place. Much evidence in this rock suggests to us that eruption onto the lunar surface occured prior to pyroxene nucleation while the magma was essentially entirely liquid.

Table 1. Electron microprobe analyses of phases from 15597

	1	2	3	4	5	6	7	8	9
SiO_2	53.31	50.31	48.41	41.18	48.62	.19	.16	.27	.22
TiO_2	.30	.68	1.27	3.01	2.33	1.71	2.42	4.46	4.93
Al_2O_3	1.18	2.86	4.54	11.92	16.05	10.64	11.75	12.67	14.06
Cr_2O_3	.96	1.22	1.16	.04	.01	54.87	51.81	46.34	42.61
V_2O_3	-	-	-	-	-	1.33	1.76	1.69	1.45
FeO	16.32	19.58	16.87	26.92	21.26	24.38	25.66	29.44	31.54
MnO	.28	.32	.32	.36	.20	.27	.29	.25	.24
MgO	25.62	18.52	11.80	3.40	.43	7.23	6.92	5.65	4.86
CaO	2.47	6.25	14.73	12.09	9.29	.05	.12	.19	.28
Na_2O	.01	.02	.03	.06	.75	-	-	-	-
K_2O	-	-	-	-	.13	-	-	-	-
SUM	100.45	99.76	99.13	98.98	99.07	100.66	100.89	100.96	100.19

1. Average Mg-rich pigeonites in crystal centers (n = 15).
2. Average pigeonite at compositional break (n = 16).
3. Average augite in contact with (2) (n = 15).
4. Average augite at crystal edges (n = 16).
5. Average glass matrix from a 60μ traverse.
6.) 7.) Range in a large chromite grain (23-1).
8.) 9.) Range in a small chromite grain (16-11).

ON BYTOWNITE 15085,36 ; E. Wenk, A. Glauser and H. Schwander, University Basel, Switzerland

This sample contains plagioclases well suited for a combined optic and chemical study. From loose crystals several oriented thin sections were made. Most of them showed only albite twins. One crystal, though, was twinned in direct contact according to the albite and Roc Tourné laws, giving by combination also the Carlsbad law. The construction of the planes of symmetry between the 3 indicatrices produced an almost perfect, rectangular crystallographical coordinate system XYZ from which reliable Euler angles were deduced: Φ 25.5° ± 0.5°, Θ 36.1° ± 0.9°, Ψ -1.7° ± 0.4°. If compared with the Φ Ψ diagram of our earlier paper on lunar plagioclases, these data do not show the strange scatter of lunar anorthites and they fit optic curves derived from terrestrial feldspars. The results are similar to the mean values of a zoned crystal An 87.7 (An 82 - 92) of sample 14053,11 (Φ 25.8°, Θ 38.5°, Ψ -2.5°). For 15085,36 on high temperature curves an An-content 81 - 83 is read, on low curves An 85 - 88. The Ca-content determined by microprobe analysis is in favour of the second interpretation.

A more and more evident lunar feldspar enigma hampering interpretation is presented by the non-stochiometric composition. Careful microprobe analysis (16 point analyses each) of our crystal gave the following results:

	mean value and range in weight %	calculated corresponding An in mol %
SiO_2	45.8 (44 - 47.3)	89
Al_2O_3	33.4 (32.5 - 34.0)	80
Fe_2O_3	0.7	
MgO	0.6	
CaO	17.6 (17.1 - 17.8)	87
Na_2O	1.3 (1.1 - 1.4)	89
K_2O	0.1	

$\frac{An}{Ab + An}$ = 88 mol % (irrespective of Si and Al)

Icelandic volcanic bytownites with almost identical Ca-content measured simultaneously with the same apparatus and standards, did not show these deficiencies in Al and in minor amounts Na and Si, if referring to the given Ca-content.

On Bytownite 15085,36

E. Wenk

Reference:

Wenk, E., Glauser A., Schwander, H. and Trommsdorff, V., "Twin Laws, Optic Orientation, and Composition of Plagioclases from Rocks 12051, 14053, and 14310", Proceedings of the Third Lunar Science Conference, Geochim. Cosmochim. Acta, Suppl. 3, vol. 1, M.I.T. Press, 1972

SECONDARY ION ANALYSIS OF PYROXENES FROM TWO PORPHYRITIC LUNAR BASALTS; A. E. Bence, State Univ. of New York, Stony Brook, N. Y. 11790 and B. Autier, Cameca Instruments, Elmsford, N. Y.

The distributions of selected major, minor, and trace elements have been studied in clinopyroxenes from two porphyritic basalts using techniques of secondary ion mass analysis in conjunction with electron microprobe analyses. A previous study[1] has shown that the complex textural and compositional relationships in the lunar pyroxenes are permanent records of the physical, chemical, and kinetic variants among the various host basalts. Much of this work was based upon electron microprobe studies of the distribution patterns of major and minor elements. High limits of detectability precluded a similar study of the trace elements.

The secondary ion mass analyzer can determine trace element distributions through selected-area analysis with detectability limits in the ppb and ppm ranges depending upon the element. In addition, providing mass interferences can be corrected for or are not present, it can determine the isotopic composition of these same trace elements. The major drawback in the technique is that, because the mechanisms of secondary ion production are not yet fully understood, and because crystal orientation can affect sputtering rates and subsequent ionization efficiencies, neither theoretical nor empirical methods for obtaining accurate quantitative trace element analyses have been fully developed. One approach that has been used[2] utilizes the Saha-Eggert equation for ionized gases. However, until quantitative techniques are developed, semi-quantitative distribution patterns for trace elements within a single crystal can be determined by comparing ion intensities along a traverse. This approach, which eliminates or greatly reduces the problems of matrix and crystal structure effects, has been followed in the present investigation.

The compositions of pyroxenes in polished thin sections of 15499,12 and 12033,76 were first determined by the electron microprobe. The quadrilateral trends for single traverses are shown in Figures 1a and 2a. The major distinction between the two trends is the uninterrupted buildup of Al (indicated by the size of the triangles) in 15499 pyroxenes and the absence of a Ca-discontinuity. The 12033 pyroxene growth trend is interrupted by discontinuities in both Al and Ca--a phenomenon that correlates texturally with the first appearance of plagioclase. Selected area secondary ion analyses were determined for 10 micron spots along traverses superimposed on the microprobe traverses. The ions measured include $^{7}Li^{+}$, $^{23}Na^{+}$, $^{24}Mg^{+}$, $^{27}Al^{+}$, $^{39}K^{+}$, $^{40}Ca^{++}$, $^{47}Ti^{+}$, $^{55}Mn^{+}$, and $^{138}Ba^{+}$. Analyses were obtained on a Cameca ion analyzer using a primary beam of negative oxygens accelerated at 15 Kv and a primary beam current of 30 nanoamps. The sample was coated with a thin gold film for the traverses and a gold grid for imaging. The results of these traverses are shown in Figures 1b and 2b. In 15499, sodium is low in the pigeonite, increases markedly in the first-formed augite, drops off slightly as the iron content increases, and finally increases markedly near the augite periphery.

Secondary Ion Analysis

A. E. Bence

Lithium, on the other hand, is relatively evenly distributed between the pigeonite and augite although in the most iron-rich augites, there is an intensity decrease followed by a pronounced increase thus following the behavior of sodium. The spikes of Ca, Ti, Al, Li, K, Na, and Ba in the pigeonite are due to small fractures that were filled by late-stage melt subsequently quenched to glass. Spikes for Li, Na, K, and Ba also occur at the pigeonite-augite epitaxial surface (Figure 1b). Both the Ba and K concentrations are, as expected, very low in both pyroxenes. Approximately 40 microns from the crystal rim, the Ba and K concentrations increase slightly. Manganese, preferentially incorporated in the pigeonites, increases as the pigeonite becomes more iron-rich then drops off markedly when augite precipitates. Ion images (Figure 1c) of a 250 micron diameter circle of the traversed region reveal that the high signals for Li, Na, and K at the epitaxial surface are due to local concentrations of these elements rather than a uniform buildup all along the surface. These local concentrations are probably the result of material (probably melt) trapped in defects created by the mismatch of the two structures. As the pigeonite grew, elements incompatible with its structure were concentrated at the melt-crystal interface and were subsequently trapped when defects developed.

Pyroxenes from 12033,76 exhibit trace element patterns similar to those from 15499, i.e., Li and K buildup at the pigeonite-augite interface and concentration of sodium in the augite (Figure 2b). In addition, lithium shows a steady increase starting 60 microns from the epitaxial surface to a value 4 times that in the interior of the crystal. The $^{7}Li^{+}$ signal in the augite is twice that in the pigeonite. These observations suggest a uniformly higher lithium concentration in the melt surrounding the 12033 pyroxene than in the 15499 melt. The major difference in the crystallizations histories of 15499 and 12033 is that plagioclase and pyroxene coprecipitated relatively slowly in the late stages of the latter, whereas the former was quenched.[1,3]. The effects of plagioclase-pyroxene coprecipitation in 12033 are readily apparent in the trace element profiles (Figure 2b). Decreases in Ca, Al, Na, Li, and K in the late-stage iron augites (Figure 2a) are quite pronounced. This is due to the preference of these elements for the anorthite structure. A similar trend is anticipated for barium. Ion images (250 micron diameter) of the matrix reveal that K and Ba are concentrated in late-stage materials in the interstitial regions. Titanium is concentrated in the calcic pyroxenes and a silica polymorph (presumably cristobalite).

References

(1) Bence, A. E. and J. J. Papike, 1972, Pyroxenes as recorders of lunar basalt petrogenesis: Chemical trends due to crystal-liquid interaction. Proc. Third Lunar Sci. Conf., Geochim. Cosmochim. Acta, in press.

(2) Andersen, C. A. and J. R. Hinthorne, CARISMA, A quantitative correction. Procedure for the Ion Microprobe Mass Analyzer, Proceedings Seventh National Conference on Electron Probe Analysis, San Francisco, p. 39, 1972.

(3) Papike, J. J., A. E. Bence, and M. A. Ward, 1972, Subsolidus relations of pyroxenes from Apollo 15 basalts. "The Apollo 15 Lunar Samples" ed. J. W. Chamberlain and C. Watkins (Houston: Lunar Science Institute).

Secondary Ion Analysis

A. E. Bence

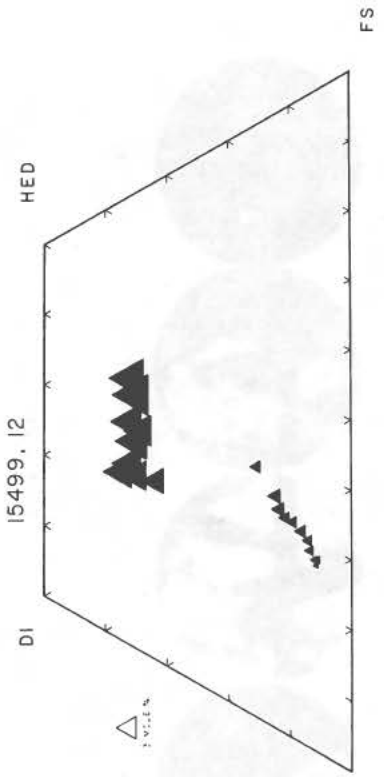

Fig. 1a

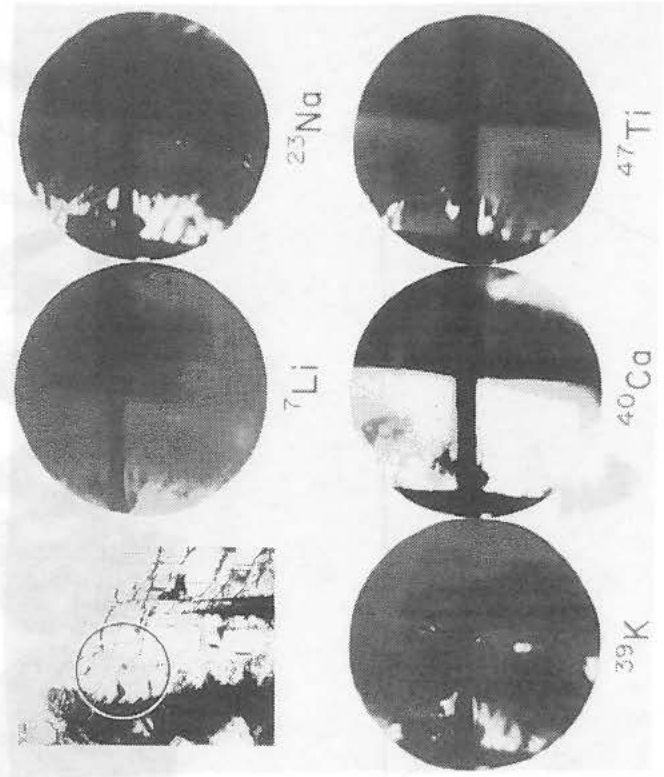

Fig. 1c

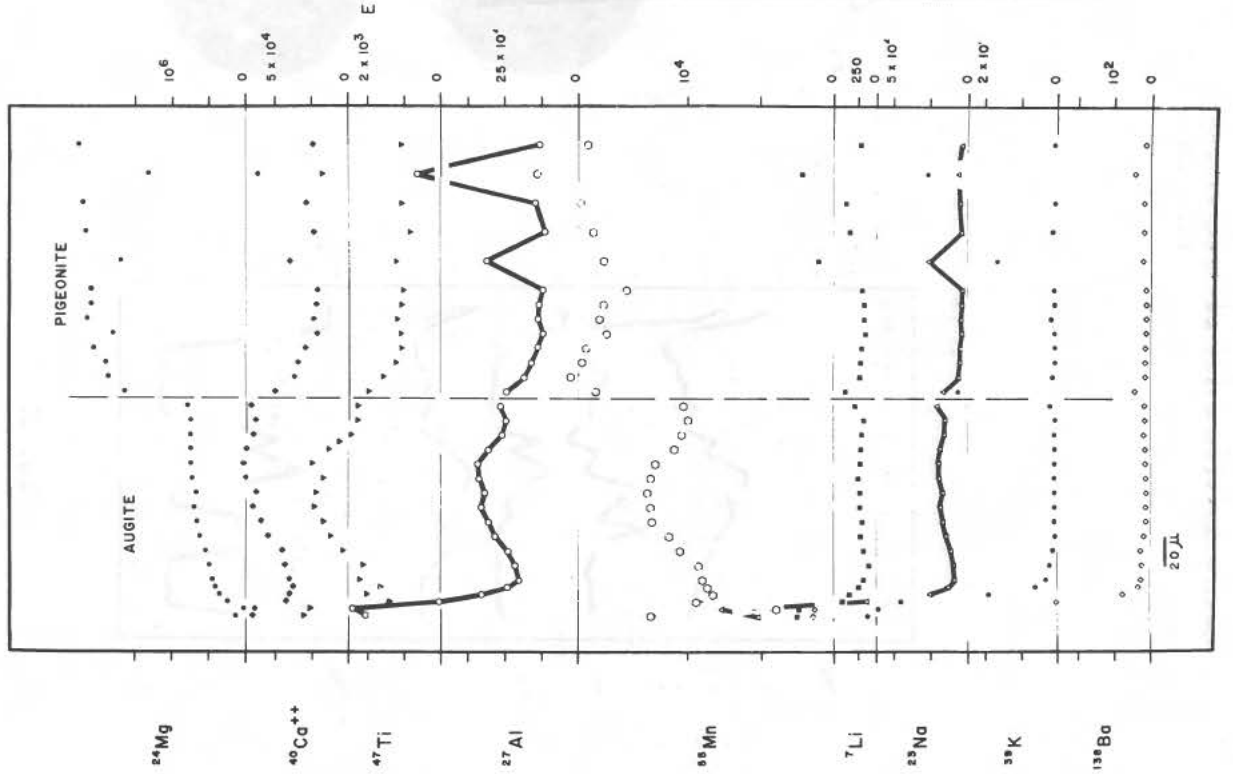

Fig. 1b

Secondary Ion Analysis

A. E. Bence

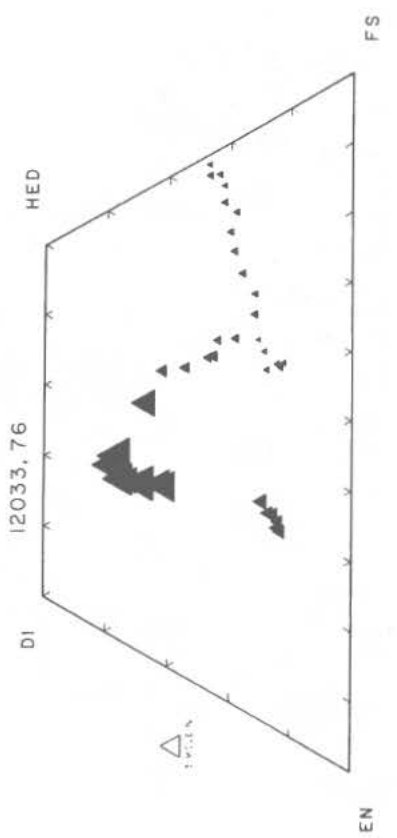

Fig. 2a

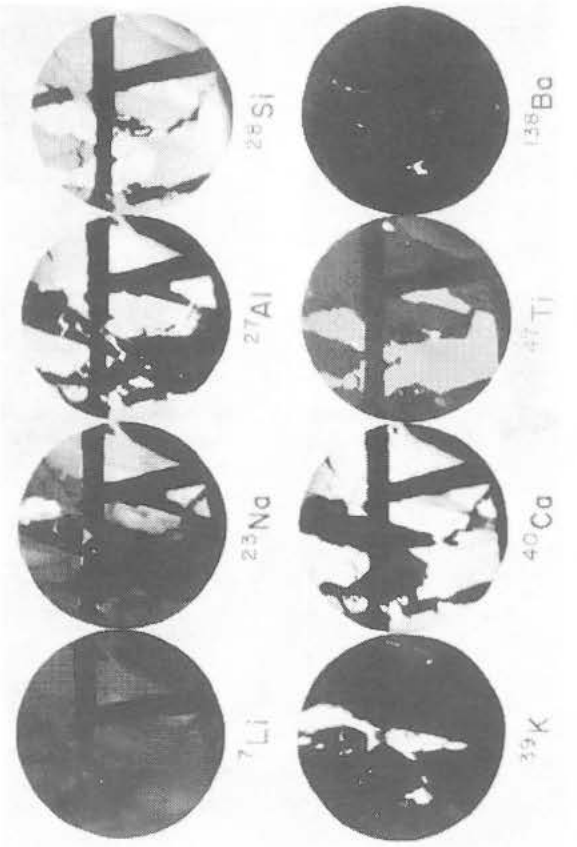

Fig. 2c

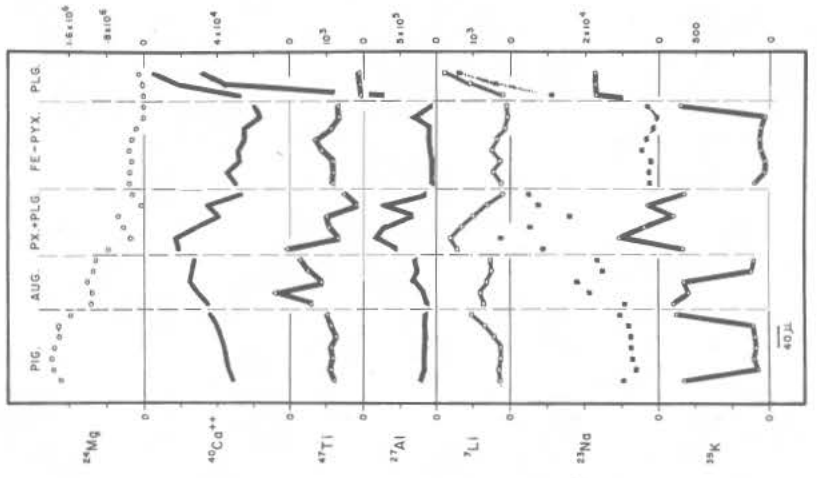

Fig. 2b

ELEMENTAL COMPOSITION OF APOLLO 15 SAMPLES, A.O.Brunfelt*, K.S. Heier*, B. Nilssen*, E. Steinnes** and B. Sundvoll*,
*Mineralogical-Geological Museum, University of Oslo,
**Institutt for Atomenergi, Kjeller.

The abundances of 40 elements have been determined by neutron activation analysis in nine lunar samples returned by the Apollo 15 mission (Table 1).

Three basaltic rocks were received: 1.1g of 15476 (a porphyritic basalt with brown pyroxene phenocrysts from STA 4 on the south rim of Dune Crater, 9.9g of 15555 (very vuggy, coarse-grained basalt) from STA 9A collected approximately 12 m north of the rim of Hadley Rille and 5.1g of 15556 (highly vesicular fine-grained basalt) also from STA 9A but collected approximately 60 m northeast of the rim. Data on elemental abundances for sample 15555 have previously been reported by Morgan (1) and Schnetzler (2). Rocks 15555 and 15556 are depleted in volatile and siderophile elements compared to the Apollo 12 mare basalts. Chondritic normalized REE patterns of the three basaltic rocks are shown in Fig. 1. Both samples exhibit a small negative Eu anomaly. Compared with the two STA 9A basalts the STA 4 basalt 15476 is enriched about 20% in Na and Ca and by about a factor of 10 for Rb and Cs; Fe, Cr, Co and Ni are depleted and the abundances of other elements are very much the same.

Two breccias were analyzed from STA 6 on the Apeninne Front: Soil breccia 15245 (1.2g) which was collected from the floor of a 1-m diameter crater and breccia 15299 (5.0g) which was collected from the surface. The compositions of these samples are nearly identical, except for Rb and Cs which are somewhat higher in the soil breccia. In Fig. 1 chondritic normalized REE patterns for these two samples are shown.

Four soil samples were analyzed. Three of these were from STA 6: soil 15261 (1.1g) collected from the bottom of a trench near the south rim of a 12-m crater, soil 15251 (1.1g) from the east rim of the same crater (this sample was described as "very fine light grey material") and soil 15291 (1.1g) which was collected about 30 m upslope from the 12-m crater. These three soil samples exhibit a nearly identical elemental composition. A soil, sample 15601 (1.0g) from STA 9A collected by rake approximately 20 m from the rim of Hadley Rille was found, however, to be depleted in Na, Al, Ca, Rb, Ba, REE, Hf, Ta, W, Th, and U and enriched in Ti, V, Mn, Fe and Se relative to the soils from STA 6. This difference in elemental composition

ELEMENTAL COMPOSITION

A.O. Brunfelt

indicates that the soils from STA 6 are enriched in plagioclase compared to the soil from STA 9. The STA 6 soils are very similar to the elemental composition found for the two STA 6 breccias 15245 and 15299.

In Fig. 2 chondritic normalized REE patterns of soil samples 15251 and 15601 are shown compared to soils from the Apollo 11, Apollo 12 and Apollo 14 missions.

In Fig. 3 a diagram comparing the compositions of Apollo 15 basaltic rocks with Apollo 15 soil is shown.

Analyses of separated minerals from 15555, 15556, 15299 and 15601 are in progress and will be reported later.

REFERENCES

(1) MORGAN J.W., KRAHENBUHL U., GANAPATHY R. and ANDERS E. (1972) in Lunar Science -III (ed. C. Watkin) Lunar Science Institute Contribution no. 88, page 555-557.

(2) SCHNETZLER C.C., PHILPOTTS J.A., NAVA D.F., SCHUMANN S. and THOMAS H. (1972) Science 175, 426-428.

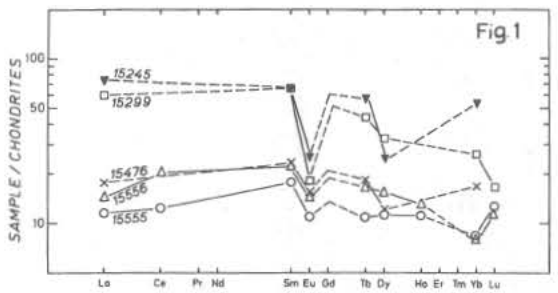

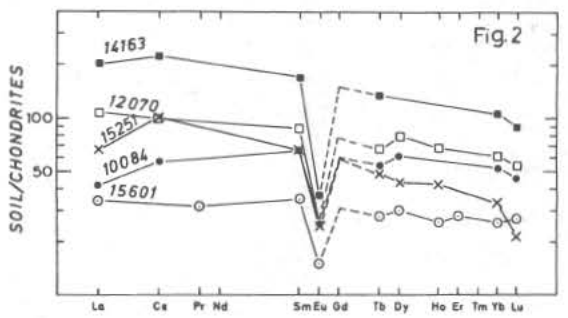

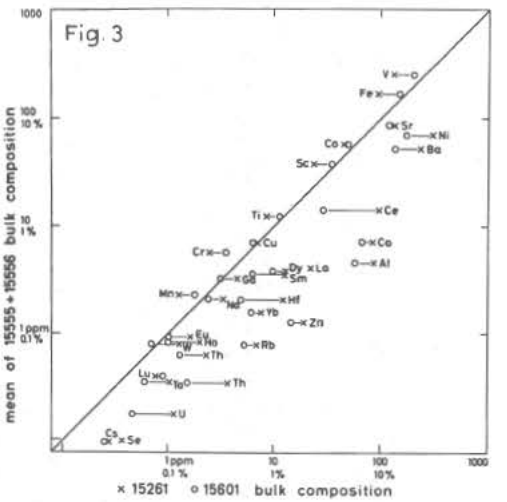

ELEMENTAL COMPOSITION

A.O. Brunfelt

Elemental composition of Apollo 15 rocks and soils.

	15245,17 breccia	15299,18 breccia	15476,11 basalt	15555,149 basalt	15556,59 basalt	15251,50 regolith	15261,67 regolith	15291,33 regolith	15601,75 regolith
Na %	0.34	0.35	0.26	0.21	0.21	0.34	0.33	0.33	0.24
Mg %	6.0	-	5.0	-	-	-	-	-	6.9
Al %	8.35	8.72	4.85	4.45	4.89	8.51	8.52	8.52	5.83
Ca %	7.0	7.7	9.9	7.4	7.1	8.5	8.5	8.5	6.8
Sc ppm	21.9	22.2	40.6	38.4	43.1	23.0	23.3	22.3	35.1
Ti %	0.74	0.73	1.14	1.22	1.23	0.84	0.84	0.81	1.18
V ppm	76	104	220	244	266	111	131	140	200
Cr %	0.225	0.229	0.328	0.482	0.472	0.243	0.245	0.233	0.351
Mn %	0.131	0.122	0.218	0.230	0.231	0.125	0.126	0.118	0.196
Fe %	9.3	9.1	15.1	17.2	16.6	9.3	9.4	8.9	14.6
Co ppm	38.8	39.3	34.4	61.8	50.3	43.6	44.6	39.2	48.9
Ni ppm	180	230	20	90	50	320	300	220	170
Cu ppm	-	5.5	-	6.6	7.1	7.4	7.0	6.8	6.4
Zn ppm	-	14	-	1.3	1.2	16	19	20	9.8
Ga ppm	-	4.3	-	2.9	3.7	4.3	4.5	4.4	3.1
As ppm	-	0.17	-	<0.05	<0.05	0.06	0.16	<0.05	<0.005
Se ppm	-	0.33	-	0.085	0.106	0.30	0.37	0.36	-
Rb ppm	6.3	4.5	6.0	0.75	0.84	6.1	6.9	6.3	5.3
Sr ppm	115	100	114	84	88	108	131	131	120
Ag ppm	-	0.019	-	<0.007	<0.007	0.021	0.045	0.065	-
In ppm	-	0.004	-	0.002	<0.002	0.008	0.039	0.023	-
Cs ppm	0.49	0.22	0.31	0.026	0.032	0.26	0.27	0.26	0.30
Ba ppm	210	221	54	47	59	236	231	241	135
La ppm	25	20	5.9	3.5	4.8	22	22	23	11.3
Ce ppm	-	78	-	10	18	84	92	84	29
Sm ppm	12.1	12.2	4.3	3.2	4.0	11.9	12.8	12.2	6.3
Eu ppm	1.80	1.21	1.13	0.75	1.00	1.69	1.60	1.73	1.01
Tb ppm	2.71	2.09	0.88	0.51	0.77	2.28	2.30	2.33	1.33
Dy ppm	10.0	12.2	3.5	3.2	4.4	12.6	12.7	12.4	9.7
Ho ppm	-	2.3	-	0.78	0.91	3.1	2.0	2.8	1.0
Er ppm	-	8.4	-	2.7	3.3	10	7	9	5.7
Yb ppm	10.7	7.3	3.4	1.64	1.59	7.4	2.5	6.7	5.2
Lu ppm	-	0.73	-	0.43	0.39	0.87	0.76	0.84	0.9
Hf ppm	10.5	9.8	3.6	2.1	3.1	13.0	12.2	12.4	4.9
Ta ppm	1.25	1.08	0.40	0.29	0.40	1.13	1.02	1.09	0.60
W ppm	-	0.91	-	1.2	0.43	1.0	1.3	1.8	0.66
Au ppb	-	3.9	-	0.48	0.85	4.8	5.5	6.8	-
Ir ppb	-	6.0	-	<0.1	<0.1	7.1	7.4	6.4	-
Th ppm	3.98	3.5	0.52	0.30	0.40	3.7	3.6	3.7	1.52
U ppm	1.02	0.97	0.21	0.14	0.21	1.16	1.14	1.13	0.46

ELEMENTAL ANALYSES OF LUNAR SOIL SAMPLES FROM APOLLO 15 MISSION*

by

M.K. Carron, C.S. Annell, R.P. Christian, Frank Cuttitta, E.J. Dwornik

D.T. Ligon, Jr. and H.J. Rose, Jr.

U.S. Geological Survey

Washington, D.C. 20242

Seven lunar soil samples collected at the Hadley Rille site by the Apollo 15 Mission were analyzed for major-, minor- and trace-element composition by semi-micro chemical, X-ray fluorescence, and d-c arc spectrographic techniques previously described[1,2,3]. Five soil samples collected at the base of the Apennine Front, Station 2,[4] have a high green-glass content, clinopyroxene grains, granular basalt fragments, vitric and recrystallized microbreccia fragments and agglutinates (plus brown aggregates). Two soil samples collected at Station 6, the LM area, contain basalt fragments of varied textures, recrystallized microbreccias, clinopyroxene and agglutinates. The main difference compared to Station 2 soils is the lower amount of green-glass content in soils from Station 6. Sample 15291,32, collected at Station 6 is one of the soils representative of the local regolith.[5]

The analytical data for lunar soils of Station 2 and 6 are given in Table 1. Comparison of both sets of soils shows that the major- and minor-element compositions are similar except for slight variations in some constituents. Compared to Station 6 soils, Station 2 soils are higher in alumina but lower in SiO_2, Na_2O, P_2O_5, Cr_2O_3, Zn, Cu, La, Y, and Yb. The trace-element abundances of all seven soils show variations consistent with those expected for geographically related soil samples.

In Table 2, the average composition[2,6] of lunar soils returned from the maria and highland areas by the Apollo 11, 12, 14, and 15 Missions are compared. The average major-element composition of the Apollo 15 soils with the exception of SiO_2 is more like that from the highland area (the Fra Mauro Formation) sampled by the Apollo 14 Mission. Greater similarity of composition of Apollo 15 average soil to that of Apollo 14 is to be expected because mineral assemblages and their proportions which characterize the lowland (maria) Apollo 11 and 12 regoliths are different from those of the highland Fra Mauro and Hadley Rille sites. Soils from Apollo 14 and 15 Missions are higher in

*Publication authorized by the Director, U.S. Geological Survey.

Elemental Analyses of Lunar Soil Samples from Apollo 15 Mission

M.K. Carron

alumina and, to a lesser degree, in silica than the Apollo 11 and 12 soils, but notably lower in ferrous oxide. Some minor-element abundances of the Apollo 15 soils, such as alkalies and phosphorus, are close to those of Apollo 11 soils. In contrast, other minor constituents of Apollo 15 soils, such as TiO_2, MnO and Cr_2O_3 have values closer to those of Apollo 14. Generally, the trace-element abundances of Apollo 11, 12, 14, and 15 soils show no significant trends relating them. While the major-element composition of the Apollo 15 soils is closest to that of Apollo 14, their trace-element contents are generally lower, with some elements being closer to those of Apollo 11 and 12 soils. Compared to Apollo 14 soils, some trace elements in Apollo 15 samples are markedly lower, the most significant being Cu, Li, Ba, Nb, La, Y and Zr.

Similar to the lunar soils returned by previous Apollo missions, each of the Apollo 15 soils has a greater reducing capacity (tables 1 and 2) than can be accounted for by its FeO content. As previously reported, this suggests an oxygen deficiency in the element-oxygen stoichiometry normally assumed for terrestrial geologic materials, or the presence of an element other than iron capable of existing in more than one valence state as a result of the highly reducing environment existing on the Moon. Studies are presently underway that may resolve this problem.

REFERENCES

1. Annell, C.S., and Helz, A.W., 1970b. Emission spectrographic determination of trace elements in lunar samples from Apollo 11. Proc. Apollo 11 Lunar Sci. Conf., Geochim. Cosmochim. Acta, Suppl. 1, vol. 2, pp. 991-994. Pergamon.
2. Cuttitta, F., Rose, H.J., Jr., Annell, C.S., Carron, M.K., Christian, R.P., Dwornik, E.J., Greenland, L.P., Helz, A.W., and Ligon, D.T., Jr. (1971). Elemental Composition of Some Apollo 12 Lunar Rocks and Soils. Proc. Second Lunar Sci. Conf., Geochim. Cosmochim. Acta, Suppl. 2, vol. 2, pp. 1217-1229. MIT Press.
3. Rose, H.J., Jr., Cuttitta, F., Annell, C.S., Carron, M.K., Christian, R.P., Dwornik. E.J., Helz, A.W., and Ligon, D.T., Jr. (1971). Semimicro analysis of Apollo 12 lunar samples. U.S. Geological Survey Prof. Paper 750-C, p. C182-C184.
4. Apollo 15 Preliminary Science Report (1972) NASA SP-289. 5-16.
5. Apollo 15 Preliminary Science Report (1972) NASA SP-289. 5-87.
6. Rose, H.J., Jr., Cuttitta, F., Annell, C.S., Carron, M.K., Christian, R.P., Dwornik, E.J., Greenland, L.P., and Ligon, D.T., Jr. (1972). Compositional data for twenty-one Fra Mauro Lunar materials. Proc. of the Third Lunar Sci. Conf., Geochim. Cosmochim. Acta, Suppl. 3, vol. 2, in press. MIT Press.

Elemental Analyses of Lunar Soil Samples from Apollo 15 Mission

M. K. Carron

Table 1. Composition of some Apollo 15 igneous rocks (oxides in weight percent, elements in ppm[1])

Sample No. Rock Type (Sta. No.)	15016,37 Basalt (3)	15065,8[2] Gabbro (1)	15065,31 Gabbro (1)	15076,24 Gabbro (1)	15117,8 Basalt (2)	15379,2 Basalt (7)	15495,3 Gabbro (4)	15555,27[2] Basalt (9a)	15557,27[2] Basalt (9a)	15607,3 Basalt (9a)	15643,5 Basalt (9a)	15659,4 Basalt (9a)	15672,4 Basalt (9a)	15676,6 Basalt (9a)
Constituent														
SiO_2	44.30	47.95	48.47	48.82	47.80	44.60	47.98	45.21	45.74	45.55	44.80	45.33	44.80	44.10
Al_2O_3	8.39	5.33	9.26	8.31	9.89	8.27	8.97	10.32	8.88	8.55	9.08	8.17	8.62	8.76
Fe_2O_3	0.00	0.00	0.00	0.00	0.00	0.00	0.00	0.00	0.00	0.00	0.00	0.00	0.00	0.00
FeO	22.95	23.60	19.18	20.45	20.41	22.92	20.74	20.16	22.35	22.33	21.28	22.17	21.78	23.03
MgO	11.65	10.15	10.58	9.43	8.02	10.75	8.96	11.20	9.43	9.96	12.20	12.27	11.98	9.82
CaO	9.20	9.30	9.94	10.30	10.98	9.55	10.26	9.96	10.29	10.10	9.48	8.98	9.44	10.10
Na_2O	.32	.25	.34	.40	.33	.27	.31	.35	.27	.35	.27	.27	.28	.31
K_2O	.05	.07	.05	.08	.07	.06	.07	.05	.05	.05	.05	.06	.06	.06
TiO_2	2.27	2.30	1.48	1.83	2.09	2.51	2.00	1.73	2.55	2.51	2.01	2.25	2.16	2.66
P_2O_5	.06	.09	.05	.05	.11	.12	.08	.05	.07	.08	.09	.12	.12	.11
MnO	.29	.31	.26	.29	.29	.29	.29	.25	.28	.29	.28	.26	.27	.28
Cr_2O_3	.66	.50	.53	.31	.28	.64	.29	.66	.45	.50	.49	.50	.47	.47
Total	100.14	99.85	100.14	100.27	100.27	99.98	99.95	99.94	100.36	100.27	100.03	100.38	99.98	99.70
ΔRC[3]	0.00	0.00	+1.28	+0.18	0.00	+0.58	+0.11	0.00	+0.30	+0.17	+0.12	+0.33	+0.12	+0.12
Cu	11	14	64	9.1	12	17	12	13	14	20	8.6	32	11	25
Ga	4.6	5.3	4.1	4.1	3.8	4.7	4.2	4.6	4.9	4.7	4.1	3.8	4.5	3.6
Li	4.6	6.3	5.9	5.6	5.2	6.9	6.4	5.5	6.9	6.3	4.7	5.4	5.6	7.7
Rb	<1	1.0	<1	1.2	1.0	<1	1.3	1.1	<1	<1	<1	1.0	1.2	<1
Co	65	66	52	42	38	67	44	87	60	60	74	66	66	60
Ni	86	54	151	32	30	120	26	96	49	51	145	87	69	63
Ba	30	75	50	58	100	70	92	30	40	50	43	62	56	56
Sr	80	100	110	98	150	130	105	93	105	125	140	130	120	130
V	200	178	158	135	188	250	152	240	185	185	156	215	180	190
Be	1.0	<1	--	1.2	1.4	<1	<1	-	-	-	<1	-	-	<1
Nb	<10	<10	12	<10	<10	12	10	17	12	<10	<10	<10	<10	<10
Sc	32	53	38	40	43	38	36	40	37	44	32	37	31	37
La	<10	22	<10	10	12	<10	10	-	22	15	<10	38	<10	12
Y	21	39	23	26	26	28	33	23	37	44	23	25	24	27
Yb	4.2	6.6	3.8	3.7	4.3	4.3	4.6	4.2	4.4	4.6	3.9	3.7	4.0	3.9
Zr	69	103	63	64	90	74	100	58	63	75	59	67	59	70

1. Trace elements listed in order of decreasing volatility.

2. Sample 15065,8 contains 32 ppm B; 15555,27 contains < 2 ppm Pb and 0.2 ppm Ag; 15557,27 contains 2.2 ppm Ag. The following elements were looked for but not detected in the analyzed samples. If present they would be in concentrations below those (in ppm) indicated in parenthesis: As(4), Au(0.2), Bi(1), Cd(8), Ce(100), Cs(1), Tl(1), U(500), W(200) and Zn(4).

3. ΔRC = Total reducing capacity measured for the lunar samples less the reducing capacity attributable to the FeO content of the lunar samples.

ERRATUM TO "THE APOLLO 15 LUNAR SAMPLES"

Please replace Table 1, Page 200, with this Table 1.

Elemental Analyses of Lunar Soil Samples from Apollo 15 Mission
M. K. Carron

TABLE 1. Composition of Some Apollo 15 Soils (oxides in weight percent, elements in ppm).

Constituent	15091,38 Station 2	15101,87 Station 2	15211,20 Station 2	15221,40 Station 2	15231,50 Station 2	15251,48 Station 6	15291,32 Station 6
SiO_2	46.47	46.29	46.35	46.56	46.40	47.02	47.21
Al_2O_3	17.47	17.70	17.73	17.54	17.14	16.28	16.40
Fe_2O_3	.00	.00	.00	.00	.00	.00	.00
FeO	11.57	11.53	11.66	11.32	11.53	12.00	11.75
MgO	10.50	10.55	10.48	10.69	10.47	10.31	10.25
CaO	11.77	11.54	11.68	11.87	11.88	11.25	11.47
Na_2O	.41	.41	.44	.45	.41	.54	.53
K_2O	.18	.19	.19	.19	.19	.22	.21
TiO_2	1.31	1.31	1.34	1.27	1.35	1.49	1.44
P_2O_5	.16	.16	.19	.16	.15	.24	.25
MnO	.17	.16	.16	.15	.16	.16	.17
Cr_2O_3	.24	.22	.23	.23	.23	.30	.29
TOTAL	100.25	100.06	100.45	100.43	99.91	99.81	99.97
Δ RC	+2.53	+1.97	+1.49	+2.18	+1.87	+2.35	+2.15
Pb	2.7	3.1	2.3	2.3	2.5	2.9	4.0
Zn	16	16	16	17	18	24	22
Cu	7.9	9.4	7.5	8.5	7.8	12	12
Ca	3.0	3.4	3.0	3.4	2.9	3.7	3.7
Li	8.0	9.7	8.5	8.4	11	9.0	9.5
Rb	5.4	5.6	5.0	4.9	5.0	5.4	6.0
Co	39	44	40	44	42	46	46
Ni	365	295	325	320	315	405	300
Ba	295	350	315	300	290	340	350
Sr	155	170	150	160	155	160	160
V	80	94	80	84	82	85	103
Be	3.2	3.2	3.2	2.6	1.7	3.6	4.0
Nb	18	12	14	18	12	23	18
Sc	21	21	22	20	22	24	24
La	32	28	32	24	28	40	42
Y	70	76	83	70	69	96	94
Yb	7.7	9.4	7.7	7.2	6.8	11	12
Zr	240	300	270	320	270	350	340

1. ΔRC - Total reducing capacity measured for the lunar samples less the reducing capacity attributable to the FeO content of the lunar samples.

Elemental Analyses of Lunar Soil Samples from Apollo 15 Mission

M. K. Carron

TABLE 2. Comparison of average composition of Apollo 11, 12, 14 and 15 lunar soil samples (oxides in weight percent, elements in p.p.m.)

Constituent	Apollo 11	Apollo 12	Apollo 14	Apollo 15
SiO_2	42.04	46.40	47.93	46.61
Al_2O_3	13.92	13.50	17.60	17.18
Fe_2O_3	.00	.00	.00	.00
FeO	15.74	15.50	10.37	11.62
MgO	7.90	9.73	9.24	10.46
CaO	12.01	10.50	11.19	11.64
Na_2O	.44	.59	.68	.46
K_2O	.14	.32	.55	.20
TiO_2	7.48	2.66	1.74	1.36
P_2O_5	.12	.40	.53	.19
MnO	.21	.21	.14	.16
Cr_2O_3	.30	.40	.25	.25
TOTAL	100.30	100.21	100.22	100.13
Δ RC[1]	+4.1	+1.3	+2.8	+2.1
Pb	<2	< 2	10	2.8
Zn	19.0	6.7	24.9	18.4
Cu	10.0	10.6	17.9	9.3
Ga	3.8	4.9	5.5	3.3
Rb	2.7	8.2	13.0	5.3
Li	11.0	18.0	23.0	9.2
Co	24.0	58.0	35.0	43.0
Ni	185	195	370	332
Ba	210	563	1030	320
Sr	130	131	189	159
V	50.0	107	55.6	86.9
Be	1.6	5.2	6.6	3.1
Nb	18.0	38.0	55.3	16.4
Sc	56.0	40.0	26.7	22.0
La	16.0	54.0	74.0	32.3
Y	81.0	164	276	79.7
Zr	273	548	813	299
Yb	-	-	-	8.8

1. Δ RC - Total reducing capacity less the reducing capacity attributable to the FeO content of the soil sample, in % i ?.

GEOCHEMISTRY OF GREEN GLASS SPHERES FROM APOLLO 15 SAMPLES.

G.Cavarretta,* R.Funiciello,* H.Giles,** G.D.Nicholls,** A.Taddeucci,* and J.Zussman.**

The occurrence of glass fragments and spheres in the lunar regolith raises conjecture as to their mode(s) of origin. A distinction has been drawn (1) between glasses which have solidified from liquid melts produced by fusion of pre-exisitng rocks or minerals, diaplectic glasses which are amorphous phases formed by shock waves in a subsolidus reaction and glasses formed by condensation of silicate vapour resulting from the vapourization of pre-exisitng basic rocks by intense shock metamorphism. A feature of several Apollo 15 soil samples is the presence of abundant spheres of green glass of distinctive composition (2) and remarkable chemical homogeneity. Similar green glass spheres have been reported from other lunar locations (3)(4), but elsewhere they have not been encountered in such abundance. We have examined green glass spheres from samples 15401 and 15301. Major element analyses of spheres from 15401 are virtually identical to those presented by other workers for spheres from other localities (table I). The glass composition does not correspond to any likely mineral and an equivalent crystalline rock would carry 45% pyroxene, 30% olivine, 20% plagioclase feldspar and minor ilmenite and chromite. Such a rock would differ from the lunar rocks so far obtained and examined, though it might represent more basic rock from the source region for mare basalts. The major element chemistry is similar to that suggested (5) for the outer lunar mantle and it is possible that the green glass has been derived from material upthrust from a depth of several kilometers. Fusion of multimineralic crystalline rocks would be expected to produce liquid droplets (yielding glass spheres) of varying composition, unless the volume of fused material was large compared with the grain size of the rock and mixing was effective. Diaplectic glasses produced from such rocks would also be expected to be heterogeneous. It appears more likely that the green glass spheres were produced by fusion of pre-existing glassy material or by condensation from a vapour phase. Our studies on the trace element geochemistry of Apollo 15 green glass spheres have been designed to discriminate between these two possibilities.

* University of Rome, ** University of Manchester.

GEOCHEMISTRY OF GREEN GLASS SPHERES

G. Cavarretta

Spheres of different sizes from sample 15401 were analyzed separately (table II). The contents of some elements (B, F, Rb, Cs) fall as the sphere size decreases but for other elements the variation in spheres of different sizes is not so systematic. However, for some elements (Sc, Ga, Sr, Y, Ba, Pb) there is a tendency for the contents to fall as the sphere size decreases, but V, Co, Zn and Ge do not show this effect. Variation in trace element geochemistry contrasts with major element homogeneity and is greater than would be expected in material produced by fusion of pre-existing glass. It is more readily understood in terms of the condensation hypothesis-occlusion from a vapour state by droplets of condensing silicate liquid of those trace elements whose contents fall in the smaller spheres, the smaller spheres occluding less than the larger.

Differences in trace element geochemistry exist between spheres of similar size from different samples, indicating that the trace element contents of the glass spheres are not simply functions of sphere size. 6 green glass spheres from sample 15301 have the trace element contents given in table III col. 1 (compare with table II col. 1). Sample 15301, like the other samples rich in green glass, contains some particles of a cloudy green glass, possibly representing the green glass displaying incipient devitrification. During such devitrification loss of occluded elements would be expected to occur. Analysis of 8 of the cloudy green particles (table III col. 2) shows that this glass is indeed relatively impoverished in B, F, Sc, Ga, Rb, Y, Cs, Ba and Pb compared with the associated green glass spheres. The elements V, Co, Zn and Ge do not display this impoverishment.

The variation in trace element contents between different samples of green glass from Apollo 15 locations, though much greater than major element variation, is small compared with the differences in trace element geochemistry between this distinctive green glass and other glasses from Apollo 14 samples which we have studied. Although trace element contents in the green glass do show significant variation, the overall chemical similarity of these green glass spheres is one of their more remarkable features and we attribute this to their mode of origin by condensation from a vapour phase rather than fusion of a pre-existing solid.

Geochemistry of Green Glass Spheres.

G. Cavarretta.

Table I. Major element composition of Apollo 15 green glasses.

Sample	15401	15301	15101	15427
SiO_2	45.20	45.27	45.21	45.38
TiO_2	0.42	0.47	0.43	0.39
Al_2O_3	7.58	7.45	7.63	7.34
Cr_2O_3	0.4	0.39	0.43	0.44
FeO	19.66	19.60	19.73	19.44
MgO	17.67	17.80	17.89	17.29
CaO	8.27	8.32	8.14	8.49
Na_2O	0.12	0.13	0.13	0.13
K_2O	0.00	0.02	0.00	0.02
P_2O_5	0.03			
Total	99.35	99.45	99.59	"99.42"
Number of analyses	5		28	11

15401 from Carusi et al.[6]; other data from Ridley et al.[5]

Table II. Trace element contents in green glass spheres from sample 15401. (in p. p. m. atomic).

	1 4 spheres av. diam. 0.33 mm.	2 12 spheres av. diam. 0.22 mm.	3 59 spheres av. diam. 0.16 mm.
B	2.7	2.2	1.4
F	17.4	12.3	9.8
Sc	1.3	0.32	0.47
V	8.9	10.5	3.5
Ce	6.1	9.5	8.1
Zn	35	105	100
Ga	13.5	2.2	2.2
Ge	0.33	0.60	0.30
Rb	8.8	1.1	0.81
Sr	9.3	1.2	1.6
Y	0.36	0.13	0.18
Cs	2.0	0.12	0.037
Ba	6.7		1.8
Pb	5.3	0.66	1.8

Geochemistry of Green Glass Spheres.
G. Cavarretta.

Table III. Trace element contents in green glass spheres from sample 15301. (in p. p. m. atomic).

	1 6 spheres green glass av. diam. 0.39 mm.	2 8 spheres cloudy green glass varying diam.
B	4.2	0.71
F	47	8.3
Sc	1.2	0.52
V	9.1	12
Ce	6.8	11
Zn	64	77
Ga	33	1.6
Ge	1.6	1.4
Rb	5.4	1.0
Sr	5.7	19
Y	1.4	0.29
Cs	1.8	0.19
Ba	37	4.0
Pb	3.2	1.2

References

1. Von Engelhardt, W., Arndt, J., Müller, W.F. and Stöffler, D. Proc. Apollo 11 Lunar Sci. Conf., Geochim. Cosmochim Acta, Suppl. 1, vol. 1., pp. 363-384, Pergamon, 1970.
2. Apollo 15 Preliminary Examination Team; Science 175; 363-375, 1972.
3. Chao, E.C.T., James O.B., Minkin, J.A.; and Boreman, J.A. Proc. Apollo 11 Lunar Sci. Conf., Geochim. Cosmochim Acta, Suppl. 1, vol. 1, 287-314, 1970.
   Fredriksson, K.; Nelen, J. and Melson, W.G.; ibid., 419-432.
   Lovering, J.F. and Ware, N.W.; ibid., 633-654.
   Winchell, H. and Skinner, B.J.: ibid., 957-964.
4. Brown, R.W., Reid, A.M., Ridley, W.I., Warner, J.L., Jakes, P., Butler, P., Williams, R.J. and Anderson, D.H.: NASA Technical Memorandum TMX-58080 (1971) Reid, A.M., Ridley, W.I., Jakes, P. and Warner, J.L.; NASA Technical Memorandum TMX-58081 (1971).
5. Ridley, W.I., Reid, A.M., Warner, J.L. and Brown, R.W., NASA Technical Memorandum (1972) - quoting Gast, P.W., "The Moon"; in press (1972).
6. Carusi, A., Cavarretta, G., Cinotti, F., Civitelli, G., Caradini, A., Funicello, R., Fulchignoni, M. and Taddeucci, A. Geol. Romana. 11, 137-151

CHEMICAL COMPOSITION OF SOME APOLLO 15 IGNEOUS ROCKS*

Ralph P. Christian, Charles S. Annell, Maxwell K. Carron, Frank Cuttitta, Edward J. Dwornik, Dennis T. Ligon, Jr. and Harry J. Rose, Jr., U. S. Geological Survey, Washington, D. C. 20242.

The major, minor and trace element composition of thirteen Apollo 15 igneous rocks has been determined by a combined technique of x-ray fluorescence, semi-micro chemical, and optical emission spectrographic analysis. Details of the analytical procedures and accuracy have been described previously.[1,2,3]

The Apollo 15 rocks fall into two general types: vesicular, porphyritic basalts and vuggy medium-grained gabbros.[4,5] They are characterized by the highest refractory and the lowest volatile element content of any returned lunar rocks to date. The ranges of the major element composition in weight percent are: SiO_2 (44-49), Al_2O_3 (5-10), FeO (19-23), MgO (8-12), CaO (9-11), Na_2O (.3-.4), K_2O (.05-.08), TiO_2 (1-3), P_2O_5 (.05-.12), MnO (.25-.31), Cr_2O_3 (.3-.7).

Fourteen samples of igneous rocks were analyzed. The composition, rock type and station number are given in Table 1. Two splits of rock 15065 were received; 15065,8 was labeled as fragments and 15065,31 was a homogenized powder that had been ground at the Lunar Receiving Laboratory. It is our opinion that the high values of 64 ppm Cu (15065,31) and 32 ppm B (15065,8) are likely due to contamination prior to receipt of the sample. These values probably should be discarded in any geochemical interpretation.

A comparison of the average composition of the Apollo 15 rocks reported in this paper with those returned from the Apollo 11, 12, and 14, missions is given in Table 2.[6] Compared to the igneous rocks returned from previous missions, the Apollo 15 basalt average is higher in FeO, MgO, MnO, and Cr_2O_3 and is lower in CaO, Na_2O, K_2O and P_2O_5. The average trace element content is high in Cu and V, and low in Rb, Ba, Be, Nb, Y, Yb, and Zr. The Apollo 15 elemental ratios derived from the average values are as follows: Si/Al 4.8, Ca/Si .33, Mg/Fe .37, Fe/Ni 2200, Cr/Ni 43,

*Publication authorized by the Director, U.S. Geological Survey

Chemical Composition of Some Apollo 15 Igneous Rocks

Ralph P. Christian

Ni/Co 1.3, Al/Ti 3.6, K/Ba 9.2, Ba/V .32, Ba/Sr .49, Cr/V 18. The Si/Al ratio is the highest, while the Ca/Si and Ba/Sr ratios are the lowest when compared to data from previous flights.[6] All the other ratios given above approximate the ratios found for the Apollo 12 samples.[6]

References

1). Annell, C.S. and Helz, A.W. (1970) Emission spectrographic determination of trace elements in lunar samples from Apollo 11. Proc. Apollo 11 Lunar Sci. Conf., Geochim. Cosmochim. Acta Suppl. 1, Vol. 2, pp. 991-994. Pergamon.

2). Cuttitta, F., Rose, H.J., Jr., Annell, C.S., Carron, M.K., Christian, R.P., Dwornik, E.J., Greenland, L.P., Helz, A.W., and Ligon, D.T., Jr. (1971) Elemental Composition of some Apollo 12 lunar rocks and soils. Proc. Second Lunar Sci. Conf., Geochim. Cosmochim. Acta Suppl. 2, Vol. 2, pp. 1217-1229. MIT Press.

3). Rose, H.J., Jr., Cuttitta, F., Annell, C.S., Carron, M.K., Christian, R.P., Dwornik, E.J., Helz, A.W., and Ligon, D.T., Jr. (1971) Semimicro analysis of Apollo 12 lunar samples. U.S. Geological Survey Prof. Paper 750-C, pp. 182-184.

4). LRL (Lunar Sample Information Catalog Apollo 15), MSC 03209, Nov., 1971.

5). Apollo 15 Preliminary Science Report (1972) NASA SP-289, 5-1-5-112, 6-1-6-25.

6). Rose, H.J., Jr., Cuttitta, F., Annell, C.S., Carron, M.K., Christian, R.P., Dwornik, E.J., Greenland, L.P., and Ligon, D.T., Jr. (1972). Compositional data for twenty-one Fra Mauro lunar materials. Proc. of the Third Lunar Sci. Conf., Geochim. Cosmochim. Acta Suppl. 3, Vol. 2, MIT Press (In press).

Table 1. Composition of some Apollo 15 igneous rocks (oxides in weight percent, elements in ppm[1])

Sample No. Rock Type (Sta. No.)	15016,37 Basalt (3)	15065,8[2] Gabbro (1)	15065,31 Gabbro (1)	15076,24 Gabbro (1)	15117,8 Basalt (2)	15379,2 Basalt (7)	15495,23 Gabbro (4)	15555,27[2] Basalt (9a)	15557,27[2] Basalt (9a)	15607,3 Basalt (9a)	15643,5 Basalt (9a)	15659,4 Basalt (9a)	15672,4 Basalt (9a)	15676,6 Basalt (9a)
Constituent														
SiO_2	44.30	47.95	48.47	48.82	47.80	44.60	47.98	45.21	45.74	45.55	44.80	45.33	44.80	44.10
Al_2O_3	8.39	5.33	9.26	8.31	9.89	8.27	8.97	10.32	8.88	8.55	9.08	8.17	8.62	8.76
Fe_2O_3	0.00	0.00	0.00	0.00	0.00	0.00	0.00	0.00	0.00	0.00	0.00	0.00	0.00	0.00
FeO	22.95	23.60	19.18	20.45	20.41	22.9	20.74	20.16	22.35	22.33	21.28	22.17	21.78	23.03
MgO	11.65	10.15	10.58	9.43	8.02	10.75	8.96	11.20	9.43	9.96	12.20	12.27	11.98	9.82
CaO	9.20	9.30	9.94	10.30	10.98	9.55	10.26	9.96	10.29	10.10	9.48	8.98	9.44	10.10
Na_2O	.32	.25	.34	.40	.33	.27	.31	.35	.27	.35	.27	.27	.28	.31
K_2O	.05	.07	.05	.08	.07	.06	.07	.05	.05	.05	.05	.06	.06	.06
TiO_2	2.27	2.30	1.48	1.83	2.09	2.51	2.00	1.73	2.55	2.51	2.01	2.25	2.16	2.66
P_2O_5	.06	.09	.05	.05	.11	.12	.08	.05	.07	.08	.09	.12	.12	.11
MnO	.29	.31	.26	.29	.29	.29	.29	.25	.28	.29	.28	.26	.27	.28
Cr_2O_3	.66	.50	.53	.31	.28	.64	.29	.66	.45	.50	.49	.50	.47	.47
Total	100.14	99.85	100.14	100.27	100.27	99.98	99.95	99.94	100.36	100.27	100.03	100.38	99.98	99.70
ΔRC[3]	0.00	0.00	+1.28	+0.18	0.00	+0.58	+0.11	0.00	+0.30	+0.17	+0.12	+0.33	+0.12	+0.12
Cu	11	14	64	9.1	12	17	12	13	14	20	8.6	32	11	25
Ga	4.6	5.3	4.1	4.1	3.8	4.7	4.2	4.6	4.9	4.7	4.1	3.8	4.5	3.6
Li	4.6	6.3	5.9	5.6	5.2	6.9	6.4	5.5	6.9	6.3	4.7	5.4	5.6	7.7
Rb	<1	1.0	<1	1.2	1.0	<1	1.3	1.1	<1	<1	<1	1.0	1.2	<1
Co	65	66	52	42	38	67	44	87	60	60	74	66	66	60
Ni	86	54	151	32	30	120	26	96	49	51	145	87	69	63
Be	30	75	50	58	100	70	92	30	40	50	43	62	56	56
Sr	80	100	110	98	130	130	105	93	105	125	140	130	120	130
V	200	178	158	135	188	250	152	240	185	185	156	215	180	190
Sn	1.0	<1	--	1.2	1.4	<1	<1	-	-	-	<1	-	-	<1
Nb	<10	<10	12	<10	<10	12	10	17	12	<10	<10	<10	<10	<10
Sc	32	53	38	40	43	38	36	40	37	44	32	37	31	37
La	<10	22	<10	10	12	<10	10	-	22	15	<10	38	<10	12
Y	21	39	23	26	26	28	33	23	37	44	23	25	24	27
Yb	4.2	6.6	3.8	3.7	4.3	4.3	4.6	4.2	4.4	4.6	3.9	3.7	4.0	3.9
Zr	69	103	63	64	90	74	100	58	63	75	59	67	59	70

1. Trace elements listed in order of decreasing volatility.

2. Sample 15065,8 contains 32 ppm B; 15555,27 contains < 2 ppm Pb and 0.2 ppm Ag; 15557,27 contains 2.2 ppm Ag. The following elements were looked for but not detected in the analyzed samples. If present they would be in concentrations below those (in ppm) indicated in parenthesis: As(4), Au(0.2), Bi(1), Cd(8), Ce(100), Cs(1), Ge(1), Hf(20), Hg(8), In(1), Mo(2), Nd(100), Pb(1), Pt(3), Re(30), Sb(100), Sm(10), Ta(100), Te(300), Th(100), Tl(1), U(500), W(200) and Zn(4).

3. ΔRC = Total reducing capacity measured for the lunar samples less the reducing capacity attributable to the FeO content of the lunar samples.

Chemical Composition of Some Apollo 15 Igneous Rocks

Ralph P. Christian

Table 2. Comparison of average composition of Apollo 11, 12, 14, and 15 igneous rocks (oxides in weight percent, elements in ppm).

Constituent	Apollo 11	Apollo 12	Apollo 14	Apollo 15[1]
SiO_2	40.10	47.10	47.70	46.10
Al_2O_3	8.60	12.80	21.44	8.63
Fe_2O_3	0.00	0.00	0.00	0.00
FeO	18.90	17.40	7.78	21.67
MgO	7.74	6.80	7.29	10.46
CaO	10.70	11.40	13.05	9.85
Na_2O	.46	.64	.70	.31
K_2O	.30	.07	.48	.06
TiO_2	12.20	3.17	1.16	2.17
P_2O_5	<0.2	.17	.42	.09
MnO	0.25	.24	.11	.28
Cr_2O_3	0.37	.31	.25	.48
Total	99.82	100.10	100.38	100.10
ΔRC[2]	+2.1	+0.37	+0.32	+0.24
Pb	<2	<2	11	<2
Cu	8.8	11	9.0	15[3]
Ga	4.8	4.9	3.7	4.4
Li	17	5.9	22	5.9
Rb	5.1	1.4	14	<1
Co	31	64	13	61
Ni	6.6	70	116	76
Ba	440	63	740	58
Sr	135	64	170	115
V	73	160	38	187
Be	3.1	1.4	4.1	<1
Nb	24	13	31	<10
Sc	97	40	23	38
La	26	<20	59	<20
Y	162	39	192	29
Yb	20	5.2	16	4.3
Zr	594	110	615	72

[1] The Apollo 15 averages are only of the rocks in this paper.

[2] ΔRC = Total reducing capacity less the reducing capacity attributable to the FeO content of the sample in % FeO.

[3] Rock 15065,31 value of 64 ppm Cu is not included in this average. This value is probably a result of contamination prior to receipt of the samples.

THE DISTRIBUTION OF K, Ti, Zr, U AND Hf IN APOLLO 14 AND 15 MATERIALS. S. E. Church, NASA Manned Spacecraft Center, Houston, Texas 77058; B.M. Bansal and H. Wiesmann, Lockheed Electronics Corp., Houston, Texas 77058.

The concentrations of K, Ti, Zr, U and Hf have been determined in a number of lunar samples by isotope dilution mass spectrometry. Several groups of lunar materials can be characterized on the basis of the abundance and various ratios of these elements. The Apennine Front suite from the Spur crater area is uniquely characterized by low Zr abundances, low Zr/U values of about 250 (see Figure 1) and variable Ti/Zr, Ti/K, and K/U values. Further chemical parameters characteristics of this suite are given by Nyquist et al. (1).

KREEP materials from the Apollo 14 and 15 sites have high Zr abundances (near 1000 ppm or greater), high Zr/Hf values, near 40, and low Zr/U values between 250-350. The Zr/U value for Apollo 15 crystalline KREEP however, may be higher than KREEP as a whole having Zr/U of 330±20. K/U is low having a consistent value of 1350±100. Ti/K and Ti/Zr are also rather consistent having values of 2±.4 and 9±2.

Basalts from all of the sampled mare regions on the moon differ from these materials. Apollo 12 mare basalts have Zr/U values of about 400 whereas the mare basalts from all other landing sites have ratios above 500. The Apollo 11 low-K basalts have the highest Zr/U value of all groups of lunar rocks studied to date having ratios greater than 1000. The Zr/Hf value for all mare basalts is similar to that found in meteorites and appears to be somewhat lower than that for KREEP rocks. Rhodes (3) has recognized two chemical groups among the Apollo 15 basalts. The quartz normative group has lower Ti/Zr and Ti/K values than the olivine normative variety. These ratios simply reflect the differing Ti abundances of the two groups, but otherwise the Apollo 15 mare basalts cannot be separated on the basis of any of the other element ratios discussed here. These data support the point of view that soils from these sites are basically simple mixtures of the three fundamental lunar rock types (i.e. mare basalt, KREEP, and gabbroic anorthosite).

Little data are available on the behavior of highly charged ionic species during partial melting. The Zr/Hf value in lunar rocks has been investigated to see if these particular elements fractionate during partial melting. In Figure 1, the value obtained for carbonaceous chondrites by Ehmann and Rebagay (4) and that determined during this study is dashed in for reference. The evidence, within the limits of experimental error, does not support fractionation of these two elements except for the small Zr enrichment in KREEP liquids. All available data on Zr/Hf values in Zr-rich phases (5) indicate a Zr/Hf value of about 50. If KREEP is a residual liquid, the Zr/Hf systematics require that no Zr-rich phase has crystallized and been separated from the melt. If KREEP is the result of a small degree of partial melting, then partial melting must have taken place in equilibrium with a Zr-rich phase. Because of the tendency of Zr/Hf to decrease in the liquid with increased differentiation (2) we view

KREEP as a partial melt rather than a residual liquid. In this respect, we also note that the Apollo 11 basalts are distinctly different from the Apollo 12 and 15 mare basalts and would suggest that this may reflect the influence of spinel in the source material (6) during partial melting. Erlank et al.(7) have studied the distribution of Zr and Nb in lunar materials and have shown that the Zr/Nb value is constant at about 15 in lunar rocks. Thus, it is apparent that, of the highly charged trace elements studied in detail to date, only U (and probably Th) are significantly enriched in the liquid relative to Zr during partial melting. Apparently, U and Th are rapidly partitioned into the melt similar to Rb and increasing degree of partial melting will only dilute the concentrations of U and Th present (e.g. the mare basalts).

Erlank et al., (7) have also pointed out that the K/Zr weight ratio (i.e., a volatile versus a refractory element) is remarkably constant (4.5) in lunar materials. Our data on KREEP and mare basalts from the Apollo 14 and 15 sites and from the Luna 20 site are in concurrence with this observations. However, we observe that the Apollo 11 low-K basalts are unique with respect to these elements having low K/Zr values near 2. Further work needs to be done on these samples to verify this observation and to offer an explanation for this unique suite. We note from the data summary in Figure 6 of Gast et al. (6) that all alkalies and U are strongly depleted in these rocks whereas the high-K Apollo 11 basalts do not show this characteristic. Vaporization processes during extrusion are excluded on the basis that the nonvolatile element U is also very depleted in these samples. Zr, relative to other elements discussed here, appears to have been concentrated in the low-K basalts. We would suggest that one possible explanation for the low alkali abundance, low K/Zr and the high Zr/U value for the Apollo 11 low-K basalts may be through differentiation processes involving the crystallization of some Ti-Zr bearing phases (e.g. armalcolite, 8).

References:

1. L.E. Nyquist et al., this volume.
2. J.R. Butler and A.J. Thompson, Geochim. Cosmochim. Acta 29 (1965), 167.
3. J.M. Rhodes, this volume.
4. W.D. Ehmann and T.V. Rebagay, Geochim. Cosmochim. Acta 34 (1970), 649.
5. L.H. Fuchs, Earth Planet. Sci. Lett. 12 (1971) 1970, has observed a Zr/Hf ratio of 50 in zircon from 14163; we have observed a calculated Zr/Hf ratio of 45-50 for an Apollo 16 soil which contains anomalously high concentrations of Zr, Hf and U.
6. P.W. Gast et al., Proceedings of the Apollo 11 Lunar Science Conference 2 (1970) 1143.
7. A.J. Erlank et al., Lunar Science III (1972) 239.
8. A.T. Anderson et al., Proceedings of the Apollo 11 Lunar Science Conference 1 (1970) 55.

Table 1

Analytical Results

Sample	Rock Type	K	Ti	Zr	Hf	U	K/U	Zr/U	Zr/Hf	Ti/Zr	Ti/K
Leedey	L-6	920	---	5.65	.19	.0164	56,100	345	29.74	---	---
Allende (8185)	C-3	300	---	6.75	.23	.0186	16,130	363	29.35	---	---
14053,50	nonmare basalt	912	16300	215[1]	(6.5)[2]	.600	1520	358	22.4	75.8	17.9
14152,2,102	KREEP basalt	4100	7010	893	23.3	3.24	1264	275	38.33	7.9	1.7
14161,35,7	breccia fragment	3730	6700	955	23.7	2.80	1333	341	40.30	7.0	1.8
14162,22	soil	5702	10500	1117	28.7	4.19	1361	267	38.92	9.4	1.8
14163,65,EG	soil	5300	9500	974	25.1	3.64	1456	268	38.80	9.8	2.0
15001,32	soil	2500	10370	600	17.8	1.69	1480	355	34.3	17.3	4.1
15015,15,2B	breccia clast	2070	6200	445	12.9	1.42	1458	313	34.50	13.9	3.0
15015,15,11	breccia clast	1950	10200	387	11.2	1.33	1466	291	34.55	26.4	5.2
15021,113	soil	1700	7560[1]	410[1]	---	1.29	1318	318	---	18.4	4.4
15023,2,5	KREEP basalt	4110	12740	---	---	3.09	1330	---	---	---	3.0
15076,21	mare basalt	411	11400	97[1]	---	.149	2758	653	---	117	27.7
15101,90	soil	1400	7600	298	9.6	.970	1443	307	31.04	25.5	5.4
15256,22	mare basalt	316	14750	89[1]	---	.139	2273	643	---	162	46.7
15271,66	soil	1700	8820	382[1]	---	1.22	1393	313	---	23.1	5.2
15273,4,2	spinel troctolite	690	2600	106	2.8	.408	1691	259	37.86	24.5	3.8
15273,4,3	metabasalt	2126	3200	422	13.35	1.48	1437	285	31.61	7.6	1.5
15273,4,9	KREEP basalt	4767	12260	1173	30.7	3.39	1406	346	38.21	10.5	2.6
15273,4,10	KREEP basalt	5304	12700	1293	35.5	3.92	1353	330	36.42	9.8	2.4
15301,76	soil	1400	7020[1]	260[1]	---	.875	1602	297	---	27.0	5.0
15303,3,7	glass	558	4950	63	2.1	.254	2196	248	30.0	78.6	8.9
15303,GC	---	143	2400	21.5	.7	.088	1625	245	30.7	136.4	16.8
15379,5	mare basalt	411	13700	86.3	2.2	.133	3090	649	39.23	159	33.3
15382,9,1	KREEP basalt	5272	13020	1170	32.7	3.73	1413	313.7	35.78	11.1	2.5
15415,11	anorthosite	125	---	---	---	.0125	10,000	---	---	---	---
15418,51	breccia	92	1570	17.6	.5	.045	2044	391	35.2	89.2	17.1
15445,9,1	breccia clast	122	920	35.5	<1	.151	808	235	>35	25.9	7.6
15445,17	breccia clast	582	840	115	4.1	.539	1080	213.4	28.05	7.3	1.4
15445,25	breccia matrix	1372	8900	315	10.5	.800	1715	393.8	30.0	28.3	6.5
15459,98	breccia matrix	1273	5460	215	5.4	.771	1651	278.9	39.82	25.4	4.3
15475,35	mare basalt	347	9900	84	2.7	.108	3213	777.8	31.11	118	28.5
15545,13	mare basalt	387	14100	96	3.0	.132	2932	727.3	32.0	147	36.4
15682,4	mare basalt	568	13500	110	2.9	.213	2667	516.4	37.9	123	23.8

[1] Personal communication, J. M. Rhodes (1972).

[2] Helmke and Haskin (1972) (estimated from data by correcting thru 14310).

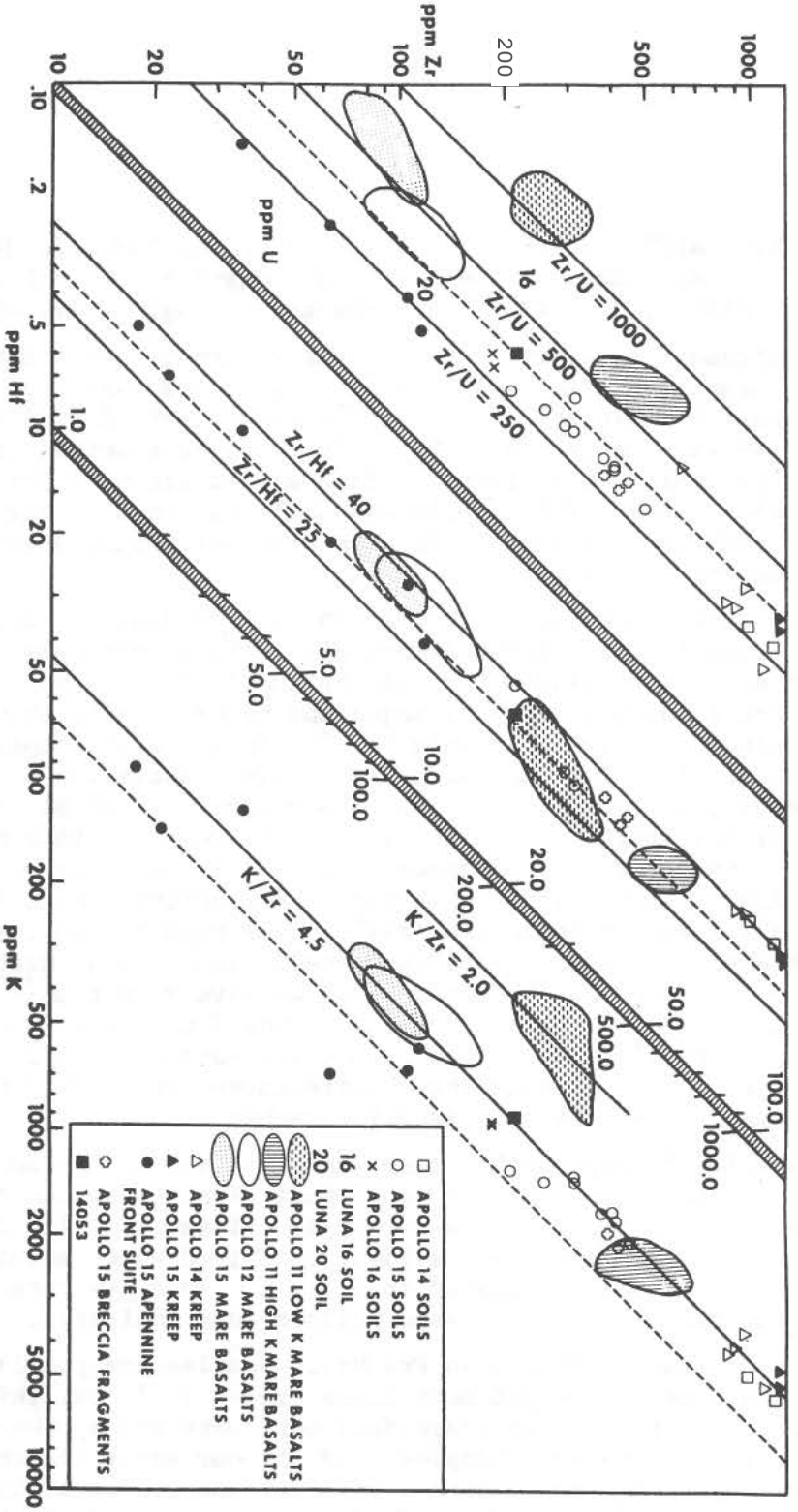

Figure 1. Log-log plot of Zr versus U, Hf and K for all lunar rocks to show the systematics for these elements. Comparisons of the Apollo 15 soils and breccias are made with the various lunar rock groups as well as soils from the Luna 16 and 20 sites and the Apollo 14 and 16 sites.

ELEMENTAL ABUNDANCE STUDIES OF APOLLO 15 AND SOME FRA MAURO FORMATION LUNAR SAMPLES, William D. Ehmann, Morteza Janghorbani and David E.Gillum, Department of Chemistry, University of Kentucky, Lexington, Ky. 40506

Elemental abundances reported in this paper have all been determined by instrumental neutron activation analysis[1]. Major elements are determined by 14 MeV neutron activation[2,3], minor elements by use of a ^{252}Cf isotopic neutron source and trace elements by high flux nuclear reactor irradiations. A total of 5 to 10 replicate analyses on each sample are used for the O and Si determinations and typically 3 replicate analyses are used for each of the remaining major and minor elements. Samples were split into 3 to 5 aliquants for the trace element analyses.

Only a brief discussion of the Apollo 15 data obtained to date will be presented here. Additional determinations are still in progress. Individual sample data and a complete discussion will be submitted for publication at a later time. A preliminary summary of major and minor element abundances in our Apollo 15 samples is given in Table 1. The four basalt samples exhibit a rather narrow range of composition with the greatest variation being that for Mg and to a lesser extent for Fe and Ti. The range of O and Si abundances reported here for the Apollo 15 basalts is almost identical to that we found for the Apollo 12 mare basalts. However, O and Si are not strongly correlated among the four Apollo 15 basalts. This might be expected considering the complex geologic setting of these samples[4]. The high Fe and low Al and Na contents of the Apollo 15 basalts are characteristic of other mare basalts we have studied and contrast sharply with values we have reported[3] for samples from the Fra Mauro region (see also Table 2). One factor that does distinquish the Apollo 15 basalts as a group from other mare basalts is their distinctly lower Ti content. Some of these differences are clearly delineated in Table 3 and will be discussed in detail elsewhere.

The four Apollo 15 soil samples also exhibited relatively small compositional variations based on our major and minor element abundance studies to date. The greatest variations observed were for Ti and for Al. Samples of two clasts and the matrix from breccia 15459 exhibited wide variations in composition and only ranges are listed in Table 1. In a few cases analyses are incomplete and the range may be even greater than indicated.

The data presented in Table 2 on Fra Mauro samples are published for the first time in this paper and supplement those presented in our Third Lunar Science Conference paper[3]. All these data were obtained by thermal neutron activation of splits of the same samples used for our major element studies. The Fe data are in good agreement with our 14 MeV neutron activation data. Standards used for these trace element determinations were 2 splits of standard rock W-1 and 3 splits of standard rock BCR-1. The compilation values of Flanagan[5] were used in the calculations. The similarity of samples 14053,42

and breccia clast 14321,225B which was noted previously for major elements, also extends to the trace element analyses reported here.

Acknowledgements: This work was supported by NASA Grant NGR 18-001-058. The assistance of M. Ma, C. L. Sya, M. Miller, and G. Gowdy is gratefully acknowleged.

References:

(1) W. D. Ehmann, Fortschr. der chem. Forschung, 14, 49-91 (1970).
(2) J. W. Morgan and W. D. Ehmann, Anal. Chim, Acta, 49, 287-299 (1970).
(3) W. D. Ehmann, D. E. Gillum and J. W. Morgan, Proc. Third Lunar Sci. Conf. Geochim. Cosmochim. Acta, Suppl. 3, MIT Press, In press, (1972).
(4) Apollo Lunar Geology Investigation Team, Science, 175, 407-415 (1972).
(5) F. J. Flanagan, Geochim. Cosmochim. Acta, 33, 81-120 (1969).
(6) LSPET, Science, 175, 363-375 (1972).

Table 1. Preliminary summary of major element abundances in Apollo 15 rocks and soils.†

Determined	Soils (Av. of 4)	Basalts (Av. of 4)	Breccia Components (Range, 3 samples)
O	43.0 ± 1.3%	39.3 ± 1.8%	42.6 - 46.1%
Si	22.6 ± 0.3	20.9 ± 0.7	21.4 - 23.9
Fe	12.8 ± 1.3	16.3 ± 1.1	8.5 - 15.4
Al	7.1 ± 1.0	4.7 ± 0.3	2.8 - 11.0
Mg	6.4 ± 0.4	6.2 ± 1.1	7.1 - >8.8
Ca*	~7.4	~6.9	~5.4 - 8.9
Ti	1.0 ± 0.4	1.6 ± 0.2	1.2 - 1.3
Na	0.28 ± 0.02	0.30 ± 0.02	0.26 - >0.28
Mn	0.16 ± 0.02	0.21 ± 0.01	0.09 - 0.20

† Soils included 15021,108; 15301,87; 15471,31 and 15601,73. Basalts included 15058,76; 15555,134; 15555,148; and 15016,31. Breccia components were derived from 15459. All abundances are in units of weight percent.

Statistical limits indicated for the group averages are simply the population standard deviations and are not a measure of the precision of the individual determinations.

* Calcium determinations listed here are derived from LSPET(6), or unpublished data circulated by NASA/MSC.

Table 2. Additional data on elemental abundances in Apollo 14 rocks.*

Element	Basalt 14053,42 (3 splits)	Basalt 14310,113** (3 splits)	Breccia Clast 14321,225B (5 splits)	Breccia 14321,171B (3 splits)
Fe (%)	12.9 ± 0.1	6.4 ± 0.1	11.9 ± 0.1	7.6 ± 0.5
Na "	0.339 ± 0.004	0.576 ± 0.003	0.442 ± 0.003	0.64 ± 0.04
Cr (ppm)	2650 ± 55	1030 ± 2	2660 ± 50	1375 ± 210
Ce "	53 ± 1	95 ± 1	69 ± 2	105 ± 2
Sc "	50 ± 1	16.6 ± 0.1	53 ± 1	23 ± 2
Co "	28.2 ± 0.2	16 ± 1	31.3 ± 0.3	25 ± 1
La "	16 ± 1	56 ± 3	25 ± 1	57 ± 1
Hf "	4.3 ± 0.3	15.1 ± 0.3	7.1 ± 0.2	16 ± 1
Th "	2.8†	9.6 ± 0.5	2.7 ± 0.3	9.6 ± 0.2
Eu "	1.3 ± 0.1	2.24 ± 0.03	1.5 ± 0.1	3.1 ± 0.3
Tb "	1.1 ± 0.1	3.7 ± 0.2	1.6 ± 0.1	3.6 ± 0.1
Lu "	0.90 ± 0.02	2.38 ± 0.05	1.4 ± 0.2	2.43 ± 0.04

* Splits were crushed, but not finely powdered aliquants of 0.2 to 0.4 g each. The error limits are the standard deviations of the mean based on the analyses of the three to five splits.

** Analyses on material as received. Data not corrected for any dilution during cutting.

† Only one split analyzed.

Table 3. Element weight ratios for basalts from various Apollo landing sites.*

Site	O/Si	Fe/Si	Al/Si	Ti/Si
Apollo 11	2.09	0.795	0.254	0.362
Apollo 12	1.89	0.725	0.223	0.126
Apollo 14	1.90	0.586	0.306	0.086
Apollo 15	1.88	0.779	0.225	0.076

* Based largely on data obtained in this laboratory.

RARE EARTHS AND OTHER TRACE ELEMENTS IN APOLLO 15 SAMPLES

by Philip A. Helmke and Larry A. Haskin, Chemistry Dept., University of Wisconsin, Madison 53706

The concentrations of the REE and other trace elements have been determined by neutron activation analysis in materials from the Apollo 15 mission. The materials include 4 samples of fines, 7 of large igneous rocks, and 11 peanuts (fragments from 4 to 10 mm coarse fines). Mineral separates of plagioclase, clinopyroxene, and pigeonite from 15085 were also analyzed. Representative results of the analyses are given in Table 1.

The concentrations of the REE in the crystalline rocks are among the lowest reported for lunar basalts. Of our samples of basalt, walnut 15535 has the lowest concentrations of the REE and walnut 15688 has the highest. Rock 15085 and walnut 15647 are representative of the majority of our samples. All of the basalt samples have nearly the same relative concentrations of the REE. The ratio of concentration of Sm to Eu varies only from 3.5 to 4.5. The range of REE concentrations found for the basalts overlaps slightly the range found for the Apollo 12 crystalline rocks. Rock 14072 also has REE concentrations low enough to fall within the range found for the Apollo 15 basalts. The concentrations of Cr in the Apollo 15 basalts are among the highest reported for lunar samples and are similar to those reported for some of the samples from Apollo 12 and for sample 14072.

The Apollo 15 basalts were collected from locations separated by several kilometers. The samples are believed to include materials that came from even greater distances. Their very similar concentrations of trace elements suggest that they might have been produced from a single source, perhaps by a single event or a series of very similar events. Unless these samples somehow represent material from only one small location, they are characteristic of the general region of the moon from which they were collected.

The fines samples returned by Apollo 15 have concentrations of the REE that are lower than those reported for any other lunar mission. The concentrations of the REE in the fines, however, are greater than those of the basalts. Apparently, like other regions of the moon sampled so far, the area around Hadley Rille is "contaminated" with KREEP. The concentrations of the REE in fines sample 15471 can be produced from a mixture of about 9% KREEP, as represented by sample 15404, and 91% basalt, as represented by the average concentration of the REE found for our samples of basalt. The concentrations of the REE in fines sample 15601 are about 8% greater than those reported for sample 15531 (1). The concentrations of the REE in fines samples 15471 and 15301 are approximately the same and are about 10% greater than those of 15601. Fines sample 15041, from the trench at the ALSEP site, has concentrations of the REE that are about 10% lower than those reported for the deep drill core (2) but about 25% greater than those of samples 15471 and 15301. The samples of fines with the lowest concentrations

RARE EARTHS AND OTHER TRACE ELEMENTS IN APOLLO 15 SAMPLES

Philip A. Helmke

of the REE were obtained from near Hadley Rille. Perhaps the KREEP component is less concentrated in the fines near the rille because some of it was lost into the rille during the turnover of the soil by meteorite impact or gravity slumping. Alternatively, the various soils from the Apollo 15 site may contain different amounts of ray material or materials from different rays.

In one of the walnut samples, 15357,3, a breccia, the concentrations of the REE are about 80 times those of chondrites. Of the 11 peanut sized samples 15024,13, 15404,18, 15434,17 have high concentrations of the REE, ranging from 130 to 190 times those of chondrites. Apparently, these samples are KREEP or are breccias that contain a large amount of KREEP.

Sample 15085 is unusually coarse grained. From this rock we handpicked 22 mg of plagioclase, 16 mg of clinopyroxene, and 7 mg of pigeonite. The concentrations of the REE, Co, Sc, and Hf in these mineral separates are given in Table 1. The relative abundances of the REE in the plagioclase are typical of those found for lunar and terrestrial samples. Pigeonite has a REE distribution very similar to that commonly found for orthopyroxenes. The relatively high concentrations of the light REE in the separate of clinopyroxene indicate that a significant portion of the sample that was analyzed was material that crystallized late. The relatively high concentration of Hf in the sample supports this interpretation.

REFERENCES:

1. Schnetzler et. al., Science 175 426-428 (1972)

2. Philpotts J. A., Personal Communication

TABLE 1. Trace element concentrations in ppm.

Element	15647,4*	15085,21	15668,2	15535,6	15601,74 Fines	15471,34 Fines
La	4.83±0.10	4.92	6.62	3.49	12.5	13.9
Ce	13.3±0.1	13.2	17.6	9.7	30.7	34.4
Nd	10.6±0.5	10.2	13.3	6.7	24	26
Sm	3.54±0.02	3.86	4.45	2.6	6.62	7.12
Eu	0.92±0.01	0.84	0.99	0.69	0.96	1.05
Gd	5.0±0.2	4.9	5.7	3.6	8.2	8.7
Tb	0.83±0.01	0.90	0.95	0.59	1.39	1.53
Dy	5.64±0.03	5.79	6.2	4.07	9.0	10.0
Ho	0.93±0.04	1.16	1.14	0.73	1.8	2.1
Er	3.0±0.3	-	2.08	-	4.9	5.4
Yb	2.27±0.04	2.63	2.90	1.69	4.5	5.07
Lu	0.327±0.003	0.393	0.394	0.236	0.660	0.710
Co	53±3	-	54	-	49.3	45.5
Sc	46.1±0.3	-	39.5	-	37.1	30.2
Hf	6.5±0.7	-	7	-	10.6	12
Zn	-	-	<5	-	16	19
Cr	4000±100	-	4200	-	5500	5200
Ga	3.5±0.1	-	3.7	-	4.9	4.8

TABLE 1 (Continued)

Element	15024,13	15404,18	15085 Plagioclase	15085 CPX	15085 Pigeonite
La	69	93	0.5±0.1	13.8	0.19
Ce	164	210	1.3±0.1	37.6	1.2
Nd	117	138	-	30	-
Sm	31.8	43.9	0.196±0.002	9.28	0.171
Eu	2.53	2.92	1.67±0.01	0.95	0.030
Gd	35	49	-	13.1	0.7
Tb	6.16	8.7	0.06±0.01	2.33	0.09
Dy	42.6	59.7	0.21±0.01	14.1	0.47
Ho	8.6	13	0.06±0.02	3.3	0.09
Er	23	32	-	9	-
Yb	21.1	30.4	0.14±0.03	6.8	0.3
Lu	3.14	4.51	0.014±0.002	1.01	0.054
Co	-	-	2.4±0.1	55	70
Sc	-	-	3.05±0.02	71	33.7
Hf	-	-	0.45±0.04	16	3.2
Zn	-	-	-	-	-
Cr	-	-	-	-	-
Ga	-	-	-	-	-

* Reported uncertainties are based mainly on counting statistics. When converted to percents, the uncertainties given for 15647 correspond approximately to those for the other whole-rock samples. Similarly, the uncertainties given for the plagioclase separates from 15085 correspond to those for the other mineral separates.

BULK AND REE ABUNDANCES IN ANORTHOSITES AND NORITIC FRAGMENTS. J.C. Laul, H. Wakita* and R.A. Schmitt. Dept. of Chemistry and the Radiation Center, Oregon State Univ., Corvallis, OR, 97331.

Elemental abundances of twenty-one major, minor and trace elements have been determined by sequential instrumental neutron activation analysis (INAA) in Ap. 15 anorthositic rake sample 15362, an anorthositic gabbroic breccia 15418 (sawdust) and in two noritic fragments separated from two Ap. 12 soils 12033 and 12037. The results are shown in Table 1. For comparison, elemental abundances are also listed for high K and low K type anorthosites[1,2] and the average elemental abundances and ranges of ten KREEP-noritic materials.[4-6]

Anorthosites: Anorthosites 10085[2] and 15362 and the anorthositic gabbro 15418 fall in the low K group. Based on their bulk composition, 15362 has 97% pl; 10085, 92% pl; and 15418, 72% pl. Other minerals in these anorthosites are very likely ol, opy and cpx, as observed in the low K type 14161 anorthosite.[1] Abundances of the pairs V-Cr_2O_3, Sc-FeO, MnO-FeO and K_2O-Hf fall on the correlation plots that were observed previously.[6] A high enrichment of Co at 77 ppm has been found in 15418, which consists of a maximum of 28% mafic minerals. We[7] also observed 63 ppm Co in separated cpx from an igneous gabbroic rock 15495. This suggests that a large fraction of Co may reside in ol, opx or the metallic phase of 15418.

Chondritic normalized REE abundances of these samples are plotted in Fig. 1. We have also included anorthosites[1] 15415, 14161 and 12033 and an Ap. 16 plagioclase separate of 68501,46 soil[8]. The high K type anorthosite 12033 has much higher REE abundances compared to the low K type anorthosites. Normalized Eu abundances for all low K type anorthosites essentially coincide at 10-12. This suggests the same Eu abundance in the magma sources for all low K anorthosites. The 15415 anorthosite with >98% pl has the lowest REE abundances observed to date.[1] As the plagioclase content decreases from >98% to 92%, the REE contents increase by a factor of ∿12. Two types of lunar anorthosites have been proposed;[1] e.g. 12033 anorthosites may be derived from non-mare KREEP basaltic magma and the low K anorthosites, from non-mare low K basaltic magma. If we assume that the low K anorthosites are all genetically related and that 15415 represents the prime anorthosite, the enhancement of REE abundances in mafic minerals such as cpx, ol and px in 15362, 14161, 10085 and 68501 is ruled out by known REE partition coefficients for both terrestrial and lunar matter. It has been suggested[9] that variable amounts of whitlockite, with their high REE contents,[10] may be responsible for the enriched REE abundances in these low K anorthosites relative to 15415. Also, since the degree of REE enrichment is roughly proportional to the mafic (non pl) content of these anorthosites, the ratio of whitlockite to mafic minerals appears nearly constant in these low K anorthosites.

An alternate explanation is to contaminate the low K anorthosites with

---

*Dept. of Chemistry, The University of Tokyo, Bunkyo-Ku, Tokyo.

BULK AND REE ABUNDANCES IN ANORTHOSITES AND NORITIC FRAGMENTS

J. C. Laul, H. Wakita and R. A. Schmitt

KREEP. If 15415 is assumed to be pure anorthosite, it can be shown that 15362 and 10085 anorthosites would have 0.2% and 1.3% KREEP, respectively. Hence, assuming 15415, 10085, 14161 and 15362 anorthosites originated from cratering events in the lunar highlands, we conclude that small amounts of KREEP-norite have been sprinkled onto the lunar highlands (Some Ap. 16 soils contain ∿13% KREEP component.[11] and that subsequent cratering events may conceivably mix KREEP with older highland material.

The similarity in bulk composition between the anorthositic gabbroic breccia 15418[12,7] and glasses in lunar soils with >21% Al_2O_3,[13] suggests that 15418 was ejected from the lunar highlands. However, if 15418 was ejected from Spur crater, then the Apennine front bedrock has a composition similar to highland material. We propose that the REE abundances in the highlands will range from those observed in 15415 to 10085. Additions of whitlockite or small (∿1%) quantities of KREEP could account for the REE pattern in 68501, pl.

Noritic fragments: Our mass balance calculations indicate that 12033-norite is composed of ∿70% average KREEP-norite and ∿30% high K type anorthositic plagioclase. A similar two component model for 12037-norite fragments suggest a combination of ∿40% average KREEP-norite and ∿60% anorthositic plagioclase. Our conclusion seems to be in good agreement with the microscopic observations[14] which indicate that these two noritic fragments contain more plagioclase than average lunar KREEP-norite.

Acknowledgements. This study was supported by NASA grants NGL38-002-039 and NGL38-002-020.

References.

1. Hubbard N.J., Gast P.W., Meyer C., Nyquist L.E. and Shih C. (1971), Earth Planet. Sci. Lett. 13, 71-75.
2. Wakita H. and Schmitt R.A. (1970), Science 170, 969-974.
3. Hubbard N.J. and Gast P.W. (1971), Proc. Sec. Lunar Sci. Conf., Geochim. Cosmochim. Acta Suppl. 2, Vol. 2, pp. 999-1020. M.I.T. Press.
4. Schnetzler C.C., Philpotts J.A. and Bottino M.L. (1970), Earth Planet. Sci. Lett. 13, 185-192.
5. Wakita H. and Schmitt R.A. (1970), Earth Planet. Sci. Lett. 13, 169-176.
6. Laul J.C., Wakita H., Showalter D.L., Boynton W.V. and Schmitt R.A. (1972), Proc. Third Lunar Sci. Conf. Geochim. Cosmochim. Acta, Suppl. 3, Vol. 2, in press, M.I.T. Press.
7. Laul J.C. and Schmitt R.A. (1972), To be published.
8. Taylor S.R., Gorton M.P., Muir P., Nance W., Rudowski R. and Ware N. (1972), Trace elements geochemistry of Apollo 16 soil 68501 from the Descartes region, lunar highlands. Pre-print.
9. Gast P.W. (1972), private communication.
10. Keil K., Prinz M. and Bunch T.E. (1971), Proc. Second Lunar Sci. Conf., Geochim. Cosmochim. Acta, Suppl. 2, Vol. 1, pp. 319-341, M.I.T. Press.
11. Laul J.C. and Schmitt R.A. (1972), "The Apollo 15 Lunar Samples", ed. J.W. Chamberlain and C. Watkins (Houston: Lunar Science Institute).
12. Lunar Sample Preliminary Examination Team (1972), Science 175, 363-375.
13. Reid A.M., Ridley W.I., Harmon R.S., Warner J., Brett R., Jakeš P. and Brown R.W. (1971), Feldspathic basalts in lunar soils and the nature of the lunar highlands, submitted for publication.
14. Wood,J.A., (1972), private communication.

Table 1. Elemental abundances of anorthosites and an anorthosite gabbro, two noritic fragments and KREEP-noritic materials.

	Anorthosite[a]		Anorthosites			Noritic Frag.[a]		KREEP-norite[c]	
Element	15362,2 56 mg	gabbro 15418 sawdust 147 mg	High K[b] 12033, 97,7	Low K 10085[d]	Low K 15415,[b] 11	12033, 71 24 mg	12037, 40 80 mg	Avg.	Range
TiO_2(%)	0.17	0.37		0.36		1.2	0.8	1.6	1.3-2.9
Al_2O_3	35.4	26.4		33.8		20.6	20.9	19	15-21
FeO	0.57	7.5		3.0		7.9	8.5	9	9-12
CaO	18.4	15.8	16.1	19.6		11	14	10.5	10-11
Na_2O	0.347	0.282		0.38		1.10	0.63	1.0	0.8-1.0
K_2O	<0.02	0.011	0.25	<0.02	0.015	0.63	0.34	0.9	0.5-1.1
MnO	0.014	0.086		0.037		0.114	0.132	0.18	0.16-0.22
Cr_2O_3	0.012	0.280		0.058		0.168	0.184	0.19	0.17-0.21
Sc(ppm)	1.6	12.7		5.5		17	22	25	
V	28	42				46	40	50	
Co	1.4	77		6.4		36	21	35	
Hf	0.1	0.8				20	12	36	
Th						10	5.7	19	
Ba		70	356	33	6.3	1080	400	1100	600-1600
La	0.33	1.2		1.6	0.12	81	48	110	93-134
Ce			12.8	3.5	0.33			297	243-374
Sm	0.12	0.69	1.14	0.69	0.048	34.6	21.4	49	38-62
Eu	0.79	0.73	2.63	0.89	0.807	4.8	2.5	3.2	2.6-3.7
Tb	<0.04	0.18		0.15				10	
Dy	0.20	1.2	0.96	0.80	0.052			60	
Yb	0.25	0.81		0.47	0.043	27	16.6	39	36-47
Lu	0.03	0.12	.068	0.074	0.003	4.0	2.5	5.7	4.7-7.0

a. One standard deviations are approximately ±2-3% for Al_2O_3, Na_2O, MnO and Cr_2O_3; ±5% for TiO_2, FeO, CaO, Sc, Co, La, Sm, Eu, Yb and Lu; ±10% for K_2O and Hf; ±15% for V, Th and Ba.

b. Hubbard *et al.* (1).

c. Values for TiO_2, Al_2O_3, FeO, CaO, Na_2O and K_2O are taken from Hubbard and Gast.[3] All other values from MnO to Lu are taken from six analyses by Hubbard and Gast,[3] three analyses by Schnetzler *et al.*[4] and one by Wakita and Schmitt.[2]

d. Wakita and Schmitt.[2]

BULK AND REE ABUNDANCES IN ANORTHOSITES AND NORITIC FRAGMENTS

J. C. Laul, H. Wakita and R. A. Schmitt

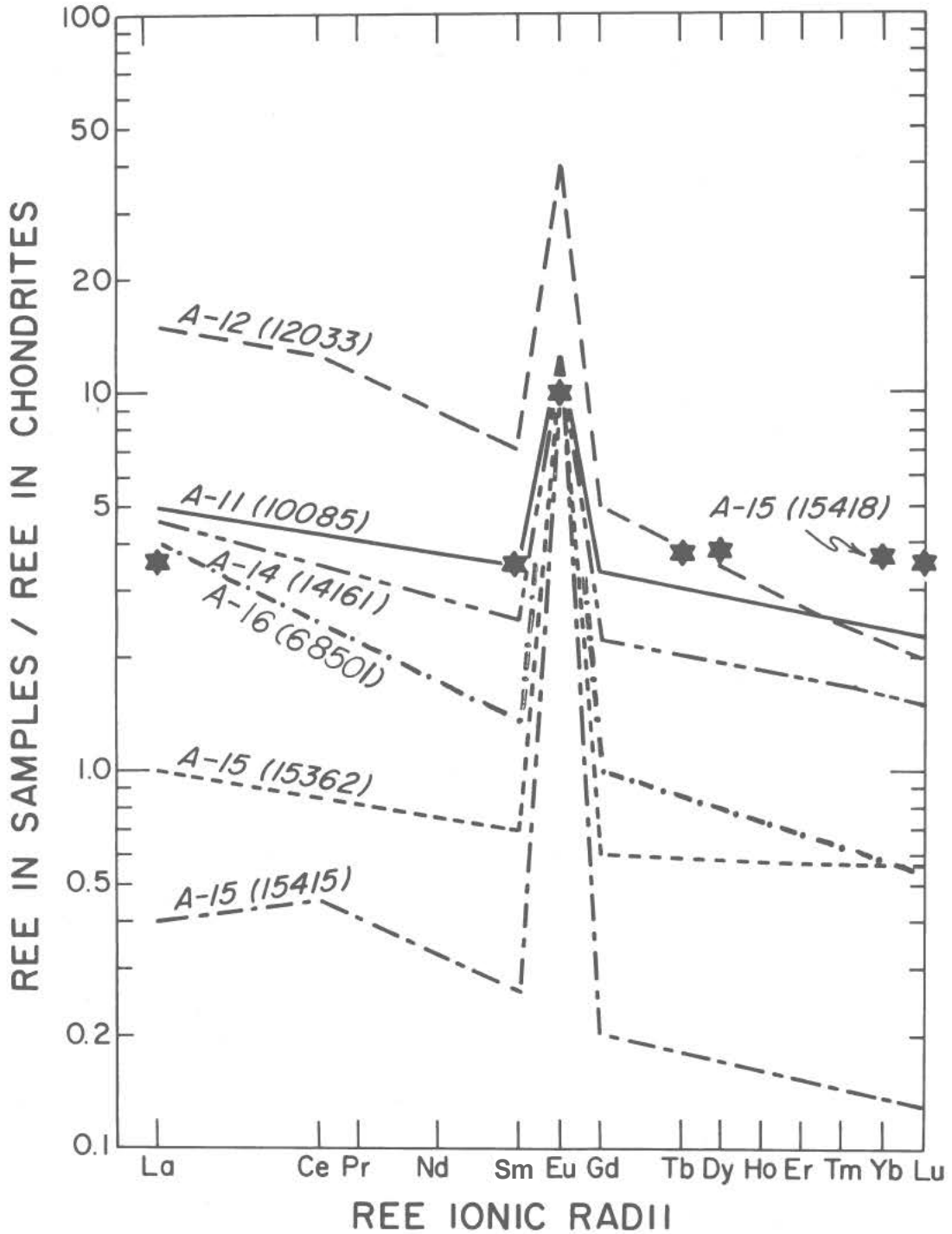

Fig. 1. Chondritic normalized REE. 10085 anorthosite (92% Pl) data are taken from Wakita and Schmitt;[2] 12033 (>99% Pl), 14161 (90% Pl) and 15415 (>98% Pl) anorthosites, from Hubbard et al.;[1] and 15362 (97% Pl) anorthosite and 15418 (72% Pl) anorthositic gabbroic breccia, from this work. 68501 is a pl separate from Ap. 16 soil of Taylor et al.[8]

BULK AND REE ABUNDANCES IN THREE APOLLO 15 IGNEOUS ROCKS AND SIX BASALTIC RAKE SAMPLES. J. C. Laul and R. A. Schmitt. Dept. of Chemistry and the Radiation Center, Oregon State Univ., Corvallis, OR 97331.

Elemental abundances of major (TiO_2, Al_2O_3, FeO, MgO and CaO) and minor and trace elements (Na_2O, K_2O, MnO, Cr_2O_3, Sc, V, Co, Zr, Hf, Ba, La, Sm, Eu, Tb, Dy, Yb, Lu and Ta) have been determined by sequential instrumental neutron activation analysis (INAA) in Ap. 15 three igneous rocks and six basaltic rake samples. The chondritic normalized REE patterns of these samples are plotted in Fig. 1. Data for basalt 15555[1] is also included for comparison. The bulk chemical composition of these Ap. 15 basaltic samples and the age of 15555[2] match closely the composition and ages of Ap. 12 mare basalts. REE abundances of Ap. 12 basalts are in general higher than Ap. 15 basalts of our study. Ap. 15 basalts, unlike Ap. 12, are more diversified in complexity, i.e., most of the basalts show a negative Eu anomaly except two rake basalts which show a positive Eu anomaly. REE studies suggest at least six lava flows.

Igneous rocks: Rocks, 15016 (STA 3) and 15659 (STA 9a), though picked up about 2 km apart, are essentially identical in composition with a Sm/Eu ratio of 4.2. This suggests a common flow for these two basalts. By local cratering events on the Rille, rock 15016 could have been thrown to STA 3. Rock 15495 (STA 4) is a gabbro from Dune Crater. The elemental composition of 15495 has lower TiO_2, MgO, Cr_2O_3 and Co and higher CaO, K_2O and Sc contents compared to rocks 15016 and 15659. The REE pattern of 15495, with a Sm/Eu ratio of 5.4, is higher than patterns of 15016 and 15659 and all the other rake samples. Rock 15495 seems to be derived from different flow.

Clinopyroxene separates of this gabbro show depletions in TiO_2, Al_2O_3, Na_2O, K_2O and Cr_2O_3 and enrichments in MgO, Sc, V and Co contents relative to the whole rock. Chondritic normalized REE abundances in 15495 cpx, that contain 9.8% CaO, are similar to those observed in Ap. 12 lunar pigeonites[3]; the REE in cpx constitute 20-30% REE of the whole rock.

Rake samples: These basalts are of various types and all may not necessarily come from the Ap. 15 site. Basalts 15607, 643, 672 and 676 were collected at STA 9a, near Hadly Rille. The bulk compositions and the REE contents of 15607 and 15676 are nearly identical with a Sm/Eu ratio of 3.5 and probably originated from the same common lava flow as did 15016 and 15659. Rock 15672 is slightly higher in MgO and Cr_2O_3 and lower in CaO, Na_2O, K_2O and REE contents as compared to 15607 and 15676. However, the Sm/Eu ratio for 15672 is the same at 3.5. This basaltic sample could have been derived from the same flow as were 15607 and 15676.

The porphyritic basalt 15643, also from Hadly Rille, is a unique rake sample. It is lower in TiO_2, K_2O, Cr_2O_3, Sc, V, Hf and REE contents and higher in MgO than the Ap. 15 mare basalts. Rock 15643 has the mare basaltic FeO and Al_2O_3 abundances of 24% and 10%, respectively, and is a low K-type (0.018% K_2O) basalt, and has a positive Eu anomaly with a Sm/Eu ratio of 2.2. The chondritic normalized Eu abundance coincides with the anorthositic rock 15362

BULK AND REE ABUNDANCES IN THREE APOLLO 15 IGNEOUS ROCKS -----

J. C. Laul and R. A. Schmitt

and other anorthosites[4]. The amount of plagioclase (≈27%) in 15643 is about the same as found in five other rake samples.

Another coarse basalt, 15388 (STA 7) picked up from the Apennine front also shows a positive Eu anomaly with a Sm/Eu ratio of 1.35 and has ≈42% Pl. Rock 15388 is lower in FeO (15.1%), MnO, Cr_2O_3, Co, Hf and REE and higher in Al_2O_3 (15.4%) and CaO when compared to 15643 and common mare basalts. Both 15643 and 15388 apparently derived from two different lava flows. Since the FeO and Al_2O_3 contents of 15643 classify it as a mare type basalt, this rock was probably derived by a higher degree of partial melting, involving a larger fraction of plagioclase melting in the source rock, than postulated for 15555. On the other hand, 15388 could have been ejected from either the highlands or could be a basaltic fragment from the Apennine front, whose composition may be similar to highland matter, as evidenced by the study of 15418 sawdust[4].

15379 (STA 7), a fine-grained basalt, matches closely to the fine-grained 15676 (STA 9a) basalt and 15607 (STA 9a) basalt and has a similar Sm/Eu ratio of 3.9. This implies a common lava flow for these basalts. Although 15379 was picked up on the Apennine front, it could have been ejected on the front by mare cratering events.

In a highly differentiated body like the Moon, the pairs MnO-FeO, V-Cr_2O_3, Sc-FeO and Hf-K_2O correlate strongly for igneous basalts, breccias and soils, sampled from all Apollo and Luna 16 sites. A strong correlation between MnO-FeO (Fig. 2) implies no fractionation between these elements in lunar magmatic processes. Anorthosites 10085[5] and 15362[4] also fall on the line. We suggest that any primary source matter, from which lunar crustalrocks were derived, must have a FeO/MnO ratio of ≈80[6].

Acknowledgements: This work was supported by NASA grants NGL-38-002-039 and NGL-38-002-020.

References

1. Schnetzler C.C., Philpotts J.A., Nava F.D., Schuhmann S. and Thomas H.H. (1972), Science 175, 426-428.
2. Podosek F.A., Huneke J.C. and Wasserburg G.J. (1972), Science 175, 423-425.
3. Schnetzler C.C. and Philpotts J.A. (1971), Proc. Second Lunar Sci. Conf., Geochim. Cosmochim. Acta, Suppl. 2, Vol. 2, pp. 1101-1122, M.I.T. Press.
4. Laul J.C., Wakita H. and Schmitt R.A. (1972), "The Apollo 15 Lunar Samples", ed. J.W. Chamberlain and C. Watkins (Houston: Lunar Science Institute).
5. Wakita H. and Schmitt R.A. (1972), Earth Planet. Sci. Lett. 13, 169-176.
6. Laul J.C., Wakita H., Showalter D.L., Boynton W.V. and Schmitt R.A. (1972), Proc. Third Lunar Sci. Conf. Geochim. Cosmochim. Acta, Suppl. 3, Vol. 2, in press, M.I.T. Press.

BULK AND REE ABUNDANCES IN THREE APOLLO 15 IGNEOUS ROCKS -----

J. C. Laul and R. A. Schmitt

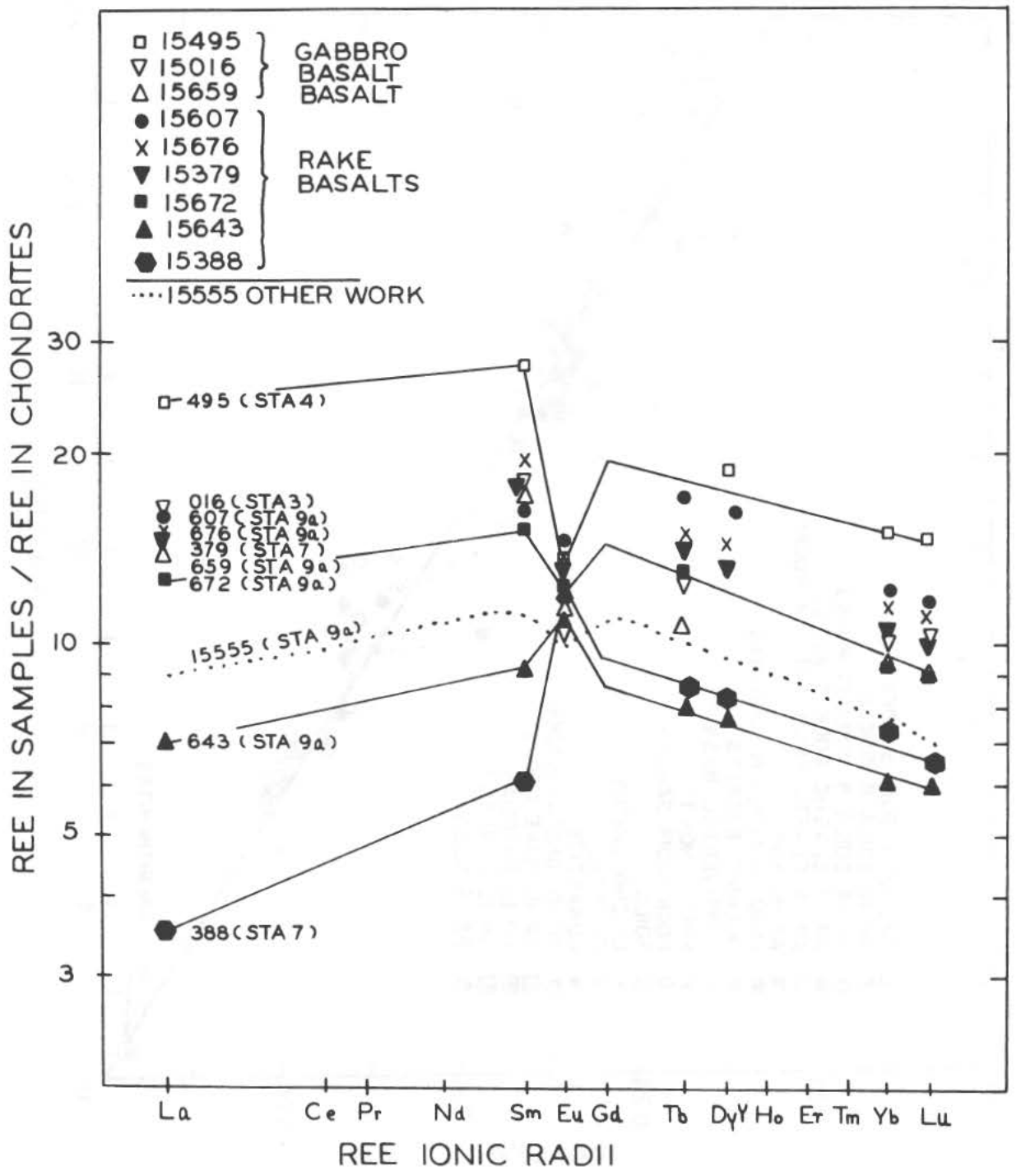

Figure 1. Chondritic normalized abundances of REE. Data for 15555 igneous basalt are taken from Schnetzler et al.[1] Open symbols represent igneous basalts and a gabbro 15495 and closed symbols represent igneous rake samples.

BULK AND REE ABUNDANCES IN THREE APOLLO 15 IGNEOUS ROCKS -----

J. C. Laul and R. A. Schmitt

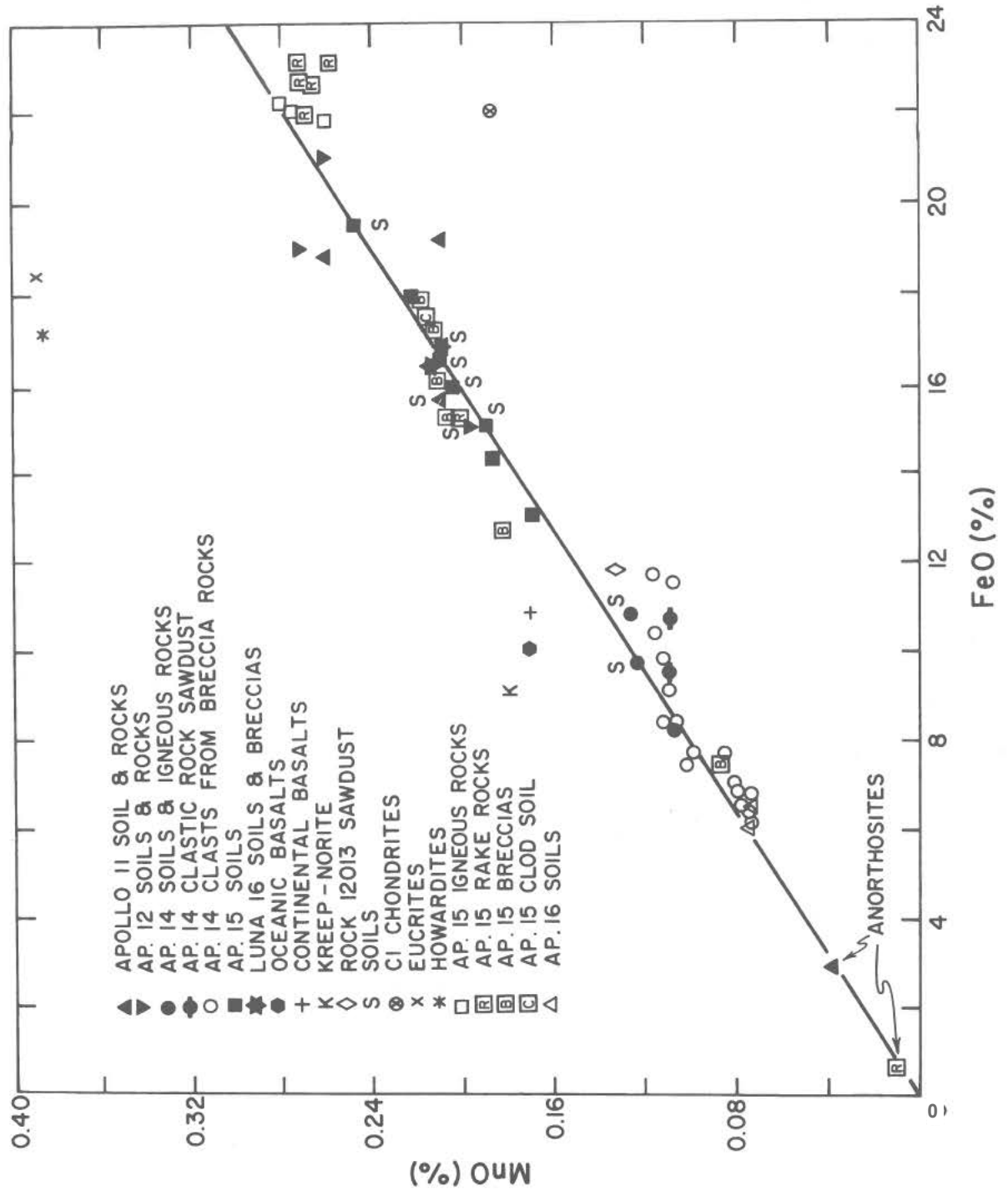

Figure 2. Abundances of FeO and MnO in lunar, meteoritic and terrestrial matter. This figure is taken from Laul *et al.*[6] Additional data on Ap. 15 and Ap. 16 also fall on the line.

ELEMENTAL ABUNDANCES OF APOLLO 15 FOUR SOILS, A CLOD AND FIVE BRECCIA ROCKS AND TWO SOILS OF APOLLO 16. J.C. Laul, D. L. Showalter,* and R.A. Schmitt. Dept. of Chemistry and the Radiation Center, Oregon State Univ., Corvallis, OR 97331.

Elemental abundances of major (TiO_2, Al_2O_3, FeO, MgO and CaO) and minor and trace elements (Na_2O, K_2O, MnO, Cr_2O_3, Sc, V, Co, Ni, Zr, Hf, Th, U, Ba, La, Ce, Nd, Sm, Eu, Tb, Dy, Yb, Lu and Ta) have been determined by sequential instrumental neutron activation analysis (INAA) in Ap. 15 four soils, a clod and five breccia rocks and two Ap. 16 soil samples. The bulk composition of Ap. 15 soils and breccias fall in a narrow range and overlap the Ap. 12 soil range. Meteoritic influx, based on our Ni data in four soils, shows an average meteoritic component (without the small indigenous correction) on Palus Putredinis site of 1.9% Cl type like material, which is similar to Ap. 12 site.[1]

The chondritic normalized REE patterns are plotted in Fig. 1. All soils and breccias show a negative Eu anomaly. The REE range for Ap. 15 basalts is also indicated. KREEP-norite is a component in the REE patterns of the soils as shown in Fig. 1. In order to explain the derivation of soil in terms of a simple two component mixing model of pulverized basalt and KREEP, we will neglect the meteoritic and anorthositic[2] contributions which additionally add $\sim$2% and $\lesssim$5%, respectively, to Ap. 15 and 16 soils. Average Sm and Eu values of KREEP[3] and average Sm and Eu abundances of six basalts[4] are taken for mass-balance calculations for the soil.

Soils: 15021 (LM), 15031 (bottom trench, STA 8) and 15041 (top trench, STA 8) soils are identical in their overall chemical composition. The REE patterns of these soils are essentially the same. This suggests soil homogeneity near the LM and trench area at the ALSEP. The Sm/Eu ratio for these soils is 9.8. The KREEP component in these soils is 21%. 15411 (STA 7, Apennine front) soil is similar in bulk chemical composition as compared to the other three soils except for a low REE content in 15411, which in turn reflects low KREEP content in this soil. The Sm/Eu ratio is 8.4 and the KREEP contribution is about 12% for 15411 soil. The ratio, Th/U = 3.0, is constant for Ap. 15 soils. Data for 15471 (STA 4), 15501 (STA 9) and 15531 (STA 9a) soils are already reported[3] and the REE patterns of these soils are also shown in Fig. 1. The KREEP-norite contributions for these soils are 13%, 18%, and 5%, respectively.

15933 (STA 4, Dune Crater) is "rock-soil" residue from a bag containing 15485 and 15486 basalts. This powdered residue, if relics of basalts, should have a similar chemical composition to basalts such as 15495 (STA 4).[4] However, the 15933 chemical data, including the REE (Fig. 1) are between the basaltic range and 15498 (STA 4) breccia range. This breccia is presumably derived from soil compaction. Mass-balance calculations indicate that the powdered residue largely consists of soil, resulting from mechanical shaking and loss of adhering soil to the rocks.

*Dept. of Chemistry, Wisconsin State University, Stevens Pt., Wisconsin.

ELEMENTAL ABUNDANCES OF APOLLO 15 FOUR SOILS

J. C. Laul, D. L. Showalter and R. A. Schmitt

The chemical composition of the clod 15515 (STA 9) is essentially identical to the chemical composition of soil 15501 (STA 9).[3] The REE patterns of 15515 and 15501 are essentially the same. This seems to confirm that 15515 is merely a compacted soil.

KREEP-norite contribution in Ap. 15 soils are very low as compared to KREEP-norite in Ap. 12 and 14 soils. Even though the Ap. 15 site is on the eastern edge of Mare Imbrium, the presumed source of ejected KREEP matter, the low KREEP content in Ap. 15 soils indicates that basaltic components dominate the soil constituency. This suggests that the Palus Putredinis mare basalts (3.2 AE), perhaps derived by melting processes at depths >200 km, have covered the older (3.9 AE) Mare Imbrium basin with many lava flows of considerable thicknesses.

Breccias 15015 (LM): The elemental abundances of this breccia are identical to the contingency soil 15021 (LM). In Fig. 1, the open symbols represent breccias and the closed symbols represent soils. Such a close similarity between soil and breccia compositions indicates that 15015 breccia is a compacted soil. Likewise, breccia 15505 (STA 9) is similar to soil 15501 (STA 9) and the clod soil 15515 (STA 9) in elemental composition. This implies that 15015 is also a compacted soil.

Breccia 15405 is described as a coherent dark-gray matrix and thoroughly coated with greenish-gray soil. Our analysis for the breccia sawdust indicates generally lower TiO_2, FeO, MnO, Cr_2O_3, Sc, V and Co and higher MgO, Na_2O, K_2O, Hf, Th, U, Ba and REE as compared to breccias and soils. Unusually high K_2O, REE and other refractories suggest KREEP contamination, which is calculated to be 41%.

15498 (STA 4) (B. Mason consortium): Two clastic fragments of this breccia were analyzed. The bulk composition of both clasts are identical. REE patterns are the same with Sm/Eu ratios of 9.2. The KREEP-norite contribution in these clasts is 9%.

Ap. 16 soils (66041 and 66081): These soils were sampled in a typical highland terrain. Based on our analyses, these highland soils are characterized by high Al_2O_3 (27%) and CaO (17%) and low TiO_2 (0.75%), MgO (6.4%), MnO (0.073%), K_2O (0.11%), FeO (6.3%), Cr_2O_3 (0.120%), V (25 ppm) and Sc (11 ppm) as compared to Ap. 11, 12 and 15 and Luna 16 mare soils. These high abundances of Al_2O_3 and CaO indicate a high plagioclase content of 73%, which is suggestive of Eu enrichments. However, the Ap. 16 soils do show negative Eu anomalies and this suggests that considerable KREEP-norite is present in the lunar highlands. Both 66041 and 66081 soils are identical in chemical composition. The REE patterns (Fig. 1) match closely the 15471 (STA 4) soil. We[2] have suggested that breccias like 15418 are representative of highland material. In terms of a two-component model, the Ap. 16 soil composition can be explained by 13% KREEP-norite and 87% 15418 breccia like matter. Only three elements, Cr_2O_3, V and Co disagree with the above simple mass-balance calculations.

The pairs MnO-FeO, V-Cr_2O_3, Sc-FeO and Hf-K_2O correlate strongly[3] for igneous basalts, breccias and soil samples from all Apollo and Luna 16 sites. The ratio Cr_2O_3/V = 30 is essentially constant. The lithophilic pair V-Cr_2O_3 does not support the fission hypothesis for the origin of the moon. The points for Cl and howardites tend to eliminate these two as primary lunar matter.

ELEMENTAL ABUNDANCES OF APOLLO 15 FOUR SOILS

J. C. Laul, D. L. Showalter and R. A. Schmitt

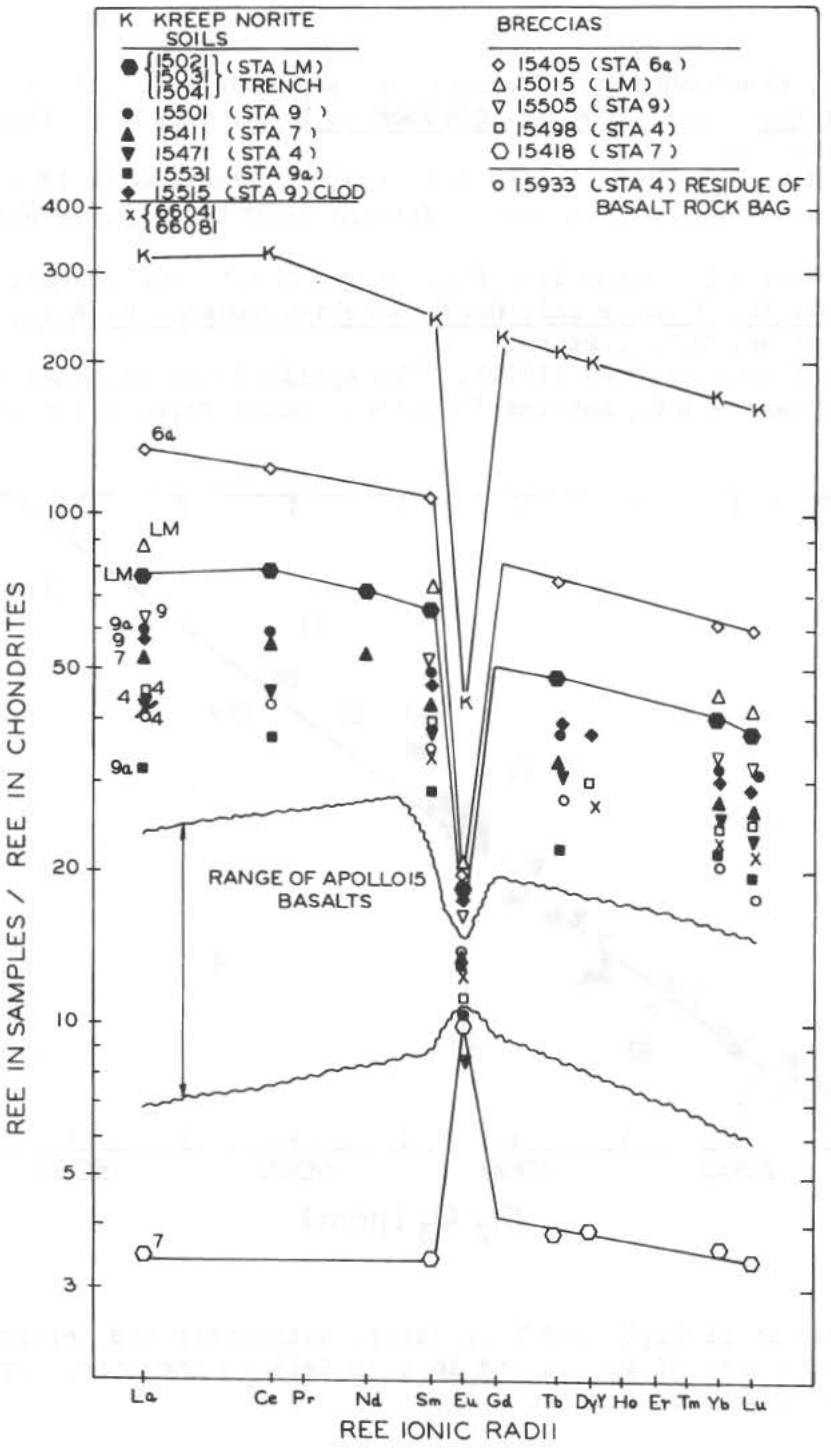

Figure 1. Chondritic normalized abundances of REE. Data for 15501, 15471 and 15531 are taken from Laul et al.[3] Open symbols represent breccias and residue of basalt rock and closed symbols represent soils. K is KREEP-norite.

ELEMENTAL ABUNDANCES OF APOLLO 15 FOUR SOILS

J. C. Laul, D. L. Showalter and R. A. Schmitt

Acknowledgements: This study was supported by NASA grants NGL-38-002-039 and 38-002-020.

References

1. Morgan J.W., Krähenbühl U., Ganapathy R. and Anders E. (1972), Proc. Third Lunar Sci. Conf. Geochim. Cosmochim. Acta, Suppl. 3, Vol. 2 in press, M.I.T. Press.
2. Laul J.C., Wakita H. and Schmitt R.A. (1972), "The Apollo 15 Lunar Samples", ed. J.W. Chamberlain and C. Watkins (Houston: Lunar Science Institute).
3. Laul J.C., Wakita H., Showalter D.L., Boynton W.V. and Schmitt R.A. (1972), Proc. Third Lunar Sci. Conf. Geochim. Cosmochim. Acta, Suppl. 3, Vol. 2, in press, M.I.T. Press.
4. Laul J.C. and Schmitt R.A. (1972), "The Apollo 15 Lunar Samples", ed. J.W. Chamberlain and C. Watkins (Houston: Lunar Science Institute).

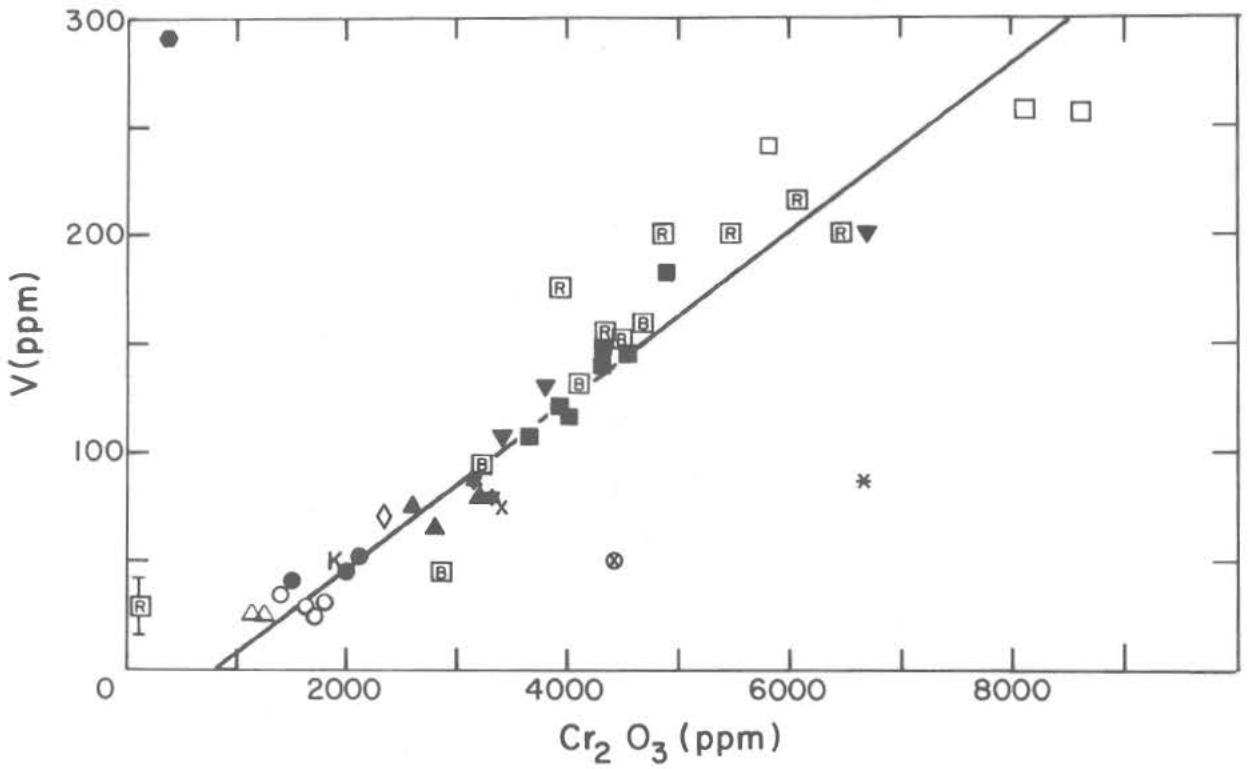

Figure 2. Abundances of Cr_2O_3 and V in lunar, meteoritic and terrestrial matter.[3] Additional data of Ap. 15 and 16 also fall on the line. Symbols are the same as those from Fig. 2 of ref. 4.

CHEMICAL COMPOSITION OF SOME APOLLO 15 LUNAR SAMPLES

J.A. Maxwell and J.-L. Bouvier
Geological Survey of Canada
Ottawa, Ontario, K1A 0E8, Canada

and

H.B. Wiik
Finnish Research Council for Sciences
Helsinki, Finland

Abstract

Major, minor and trace element data are given for Apollo 15 samples 15271, 15545, 15555 and 15557, with brief details of the procedures used. These samples are characterised by high FeO and Cr_2O_3 contents; values obtained for Al_2O_3, Na_2O, K_2O and P_2O_5 are much lower than those found for Apollo 14 rocks, and resemble more those found in Apollo 12 material.

1. INTRODUCTION

In this fourth brief report of analytical data obtained on samples from the Apollo missions which were distributed to Maxwell and Wiik[1,2,3] the results of the analytical work are again presented jointly, to facilitate their use by others.

The specimens represented here are samples of three rocks, and one sample of the regolith[4], Sample 15271,53 (Maxwell) is a portion of the < 1mm fraction of material collected from Apennine Front on the north-facing slope of Hadley Delta. Sample 15545,35 (Wiik) is a slightly vuggy, fine to medium-grained basalt taken from the north rim of a moderately-fresh small crater near the rim of Hadley Rille. Samples 15555,153 and 15557,40 (Maxwell) are also basalts which were collected adjacent to the rille rim; 15555 is very vuggy and coarse-grained in appearance.

The samples were sieved, crushed and ground, as required, in the individual laboratories.

Chem. compn. of some Apollo 15 lunar samples

Maxwell, J.A.

2. ANALYTICAL TECHNIQUES

(a) At the Geological Survey of Canada (JAM, JLB)

The conventional rock analysis methods used to determine Si, Fe (II), Fe (III) and H_2O^- (JAM) are those described by Maxwell[5]. The other constituents were determined (JLB) by the revised and improved composite scheme, involving a lithium metaborate-hydrofluoric acid decomposition followed by atomic absorption spectroscopy supplemented with colorimetry[P] which was used for the analysis of lunar samples from previous missions[6,7]. Total C and Total S, and also Fe (II), were determined titrimetrically, using an automatic burette and procedures developed in the GSC laboratories[8]. A measurement of the reducing capacity of the samples, other than that due to Fe (II), was made during the potentiometric determination of Fe (II) and total Fe, using the Fe (III) addition described previously[1]. A significant value was obtained only for the regolith sample 15271,53, as follows:

Reducing capacity (wt. %) of Apollo 15 material

Sample	
15271,53	≡ + 0.95

It is assumed that this value represents chiefly the small amount of metallic material known to be present in the sample.

A reference basalt, USGS-BCR-1, was analyzed at the same time and by the same procedures as the lunar samples, to provide a means for evaluating the accuracy of the analytical data. The results of the chemical analyses are given in Table 1.

The determination of selected trace elements was done by optical emission spectrography, using an air-jet controlled d.c. arc and a Jarrell-Ash 3.4 metre grating spectrograph. The data for the lunar samples, and for BCR-1, are given in Table 2.

(b) At the Geological Survey of Finland (HBW)

Conventional gravimetric, titrimetric and colorimetric methods were used to determine Si, Al, Mg, Ca, H_2O^-, Fe, Ti, and P in 15545,35. Neutron activation was used to determine Na and K, fluorine was done by specific ion electrode[9], and Mn and Cr by atomic absorption spectroscopy. Metallic Fe was determined titrimetrically, following extraction by $HgCl_2$ in an argon atmosphere. The results are given in Table 1.

Optical emission spectroscopy was used to determine Be, Co,

Cu, Ni, Sc, Sr, V and Y, instrumental neutron activation analysis for the determination of Ba, Cs, Hf, La, rare earths, Rb, Ta, Th, U and Zr, and atomic absorption spectroscopy for Zn. The results are given in Table 2.

3. SUMMARY

While readily admitting the superficiality of attempting a comparison between the composition of these few samples from the Apollo 15 mission and of those from preceding missions, it appears that the analytical data presented in this paper resemble more those obtained for the Apollo 12 samples[2] than for those from Apollo 14[3]. Si, Al, Na, K and P contents are lower for Apollo 15 than for Apollo 14, and Ti, Cr and, especially, Fe (II) are higher; among the trace constituents V and Sc are higher, while Sr, Y, Zr, Hf, Ba, rare earths, Th and U are lower. These differences are particularly notable in the rocks, and less so in the regolith sample. The very high Cu content (370 ppm) of 15545,35 must be attributed to contamination. The contents of Ca, Mg and S do not differ much from those found for samples from previous missions which were analyzed by us.

4. ACKNOWLEDGEMENTS

We sincerely thank our colleagues at the two Geological Surveys for their co-operation and contributions to these analyses: at the Geological Survey of Canada, G.A. Bender, D.A. Brown, and K.A. Church; at the Geological Survey of Finland, P. Ojanperä, M. Taug, M. Hynönen, A. Löfgren and A. Savola; P. Kauranen, Radiochemical Institute, University of Helsinki; R. Rosenberg, Reactor Laboratory, Technical University of Helsinki.

5. REFERENCES

(1) Maxwell, J.A., Peck, L.C., and Wiik, H.B. (1970). Chemical composition of Apollo 11 lunar samples 10017, 10020, 10072 and 10084. Geochim. Cosmochim. Acta Suppl. 1, Vol. 2 p. 1369-1374.

and

(2) Maxwell, J.A. & Wiik, H.B. (1971). Chemical composition of Apollo 12 lunar samples 12004, 12033, 12051, 12052 and 12065. Earth and Plan. Sci. Letters 10 285-288.

(3) Wiik, H.B., Maxwell, J.A., and Bouvier, J.-L. (in press). Chemical composition of some Apollo 14 lunar samples. Earth and Plan. Sci. Letters.

(4) National Aeronautics and Space Administration (1972). Apollo 15 Preliminary Science Report, NASA SP-289, pp. 5-1 to 5-112.

(5) Maxwell, J.A. (1968). Rock and Mineral Analysis, John Wiley and Sons, Ltd., New York, 258 pp.

(6) Abbey, Sydney (1970). Analysis of rocks and minerals by atomic absorption spectroscopy; Part 3, A lithium-fluoborate scheme for seven major elements. Geol. Survey Canada Paper 70-23, 20 pp.

(7) Abbey, Sydney and Lee, N.J. (in preparation). Analysis of rocks and minerals using an atomic absorption spectrophotometer. Part 5, Further applications of the lithium-fluoborate system. Geol. Survey Canada Paper.

(8) Bouvier, J.-L., Sen Gupta, J.G., and Abbey, Sydney (1972, in press). Use of an 'automatic sulphur titrator' in rock and mineral analysis: Determination of sulphur, total carbon, carbonate and ferrous iron. Geol. Survey Canada Paper, 72-30.

(9) Ingram, B.L. (1970). Determination of fluoride in silicate rocks, without separation of aluminum, using a specific ion electrode. Anal. Chem., 42, 1825-1827.

CHEMICAL COMPOSITION OF SOME APOLLO 15 LUNAR SAMPLES

J. A. Maxwell and J. L. Bouvier and H. B. Wiik

Table 1. Chemical analyses (wt. %) of Apollo 15 material

Constituent	15271,53	15545,35	15555,153	15557,40	USGS BCR (80,26)
SiO_2	46.73	45.72	44.22	45.06	54.47
TiO_2	1.42	2.40	2.36	2.43	2.26
Al_2O_3	16.19	8.3	7.54	8.82	13.50
Fe_2O_3	0.00	0.00	0.00	0.00	3.55
Cr_2O_3	0.58	0.63	0.73	0.67	0.00
FeO	12.19	21.99	24.24	22.50	8.82
MnO	0.17	0.30	0.29	0.29	0.19
MgO	10.48	10.39	11.11	9.52	3.44
CaO	11.23	9.62	9.18	10.05	6.92
Na_2O	0.53	0.28	0.29	0.34	3.32
K_2O	0.19	0.04	0.04	0.04	1.65
H_2O^+	ND	ND	ND	ND	0.66
H_2O^-	0.02	0.00	0.00	0.00	0.64
P_2O_5	0.21	0.11	0.06	0.07	0.37
S (total)	0.07	ND	0.07	0.065	0.04
F	ND	0.00	ND	ND	ND
Fe (metal)	ND	0.00	ND	ND	ND
Sub-total	100.01	99.7_8	100.13	99.86	99.83
Less O≡S	0.03	-	0.03	0.03	0.02
Total	99.98	99.7_8	100.10	99.83	99.81

15271,53; 15555,153; 15557,40: Geological Survey of Canada; analysts, J.A. Maxwell and J.-L. Bouvier. 15545,35: Geological Survey of Finland; analysts, H.B. Wiik, P. Ojanperä, M. Hynönen, P. Kauranen and R. Rosenberg

ND - not determined

CHEMICAL COMPOSITION OF SOME APOLLO 15 LUNAR SAMPLES

J. A. Maxwell, J. L. Bouvier, and H. B. Wiik

Table 2. Minor and trace elements (ppm) in Apollo 15 material

Constituents	15271,53	15545,35	15555,153	15557,40	USGS BCR (80,26)
Be	ND	< 5	ND	ND	ND
Sc	31	42	49	48	36
V	110	168	240	240	430
Co	39	21	59	54	34
Ni	240	69	86	65	NF
Cu	10	370	21	13	34
Zn	ND	23	ND	ND	ND
Sr	130	70	84	94	310
Y	88	33	25	25	36
Zr	470	190	140	140	240
Cs	ND	0.08	ND	ND	ND
Ba	260	81	48	49	670
La	ND	4.8	ND	ND	ND
Ce	ND	8.9	ND	ND	ND
Nd	ND	7.6	ND	ND	ND
Sm	ND	3.3	ND	ND	ND
Eu	ND	0.74	ND	ND	ND
Gd	ND	4.5	ND	ND	ND
Tb	ND	0.65	ND	ND	ND
Dy	ND	5.2	ND	ND	ND
Yb	10	1.4	4.3	4.6	5.1
Lu	ND	0.31	ND	ND	ND
Hf	ND	2.2	ND	ND	ND
Ta	ND	0.38	ND	ND	ND
Th	ND	0.2	ND	ND	ND
U	ND	0.12	ND	ND	ND

NF - not found; ND - not determined

15271,53; 15555,153 and 15557,40: Geological Survey of Canada, analysts G. A. Bender, D. A. Brown, K. A. Church, by optical emission spectroscopy.
15545,35: Geological Survey of Finland, analysts A. Löfgren and A. Savola (opt. emission spectroscopy), M. Taug (AAS), R. Rosenberg (inst. neutron activation anal.)

TRACE ELEMENTS IN APOLLO 15 SAMPLES: IMPLICATIONS FOR METEORITE INFLUX AND VOLATILE DEPLETION ON THE MOON.* John W. Morgan, Urs Krähenbühl, R. Ganapathy, and Edward Anders, Enrico Fermi Institute and Department of Chemistry, University of Chicago, Chicago, Illinois 60637.

Five Apollo 15 soils and 4 rocks were analyzed by neutron activation analysis for Ag, Au, Bi, Br, Cd, Co, Cs, Ge, In, Ir, Ni, Sb, Se, Rb, Re, Te, Tl, and Zn. Elbow Crater soil 15081, collected 65 m from the rim, contains a meteoritic component equivalent to 1.72% Cl material, similar to that at other lunar sites. Other soils are lower, owing to dilution by fresh bedrock, or talus from the Apennine Front. A component rich in Rb, Cs, Cd, and Zn (KREEP?) seems to be present in all soils, but though the abundance of these elements is highest in soil 15431 from the Front, it does not decrease regularly with distance from the Front. Hence the Front may not be the only or even the principal source of KREEP.

Anorthosite 15415 is outstandingly low in the above elements. Apollo 11 anorthosites, on the other hand, contain a sizeable meteoritic component, similar to that in Apollo 14 dark norites. This component may represent debris of the Imbrian or Serenitatis projectiles, or mixed planetesimal debris from the Pre-Imbrium regolith.

---

*This is the abstract of a paper which is being published in full in the Proceedings of the Third Annual Lunar Science Conference.

Courtesy of MIT Press.

ALKALI AND ALKALINE EARTH ELEMENTS, LA AND U IN APOLLO 14 AND APOLLO 15 SAMPLES.

O. Müller, Max-Planck-Institut für Kernphysik, 69 Heidelberg, Germany

Elemental concentrations of Li, Na, K, Rb, Cs, Mg, Ca, Sr, Ba, La and U have been determined in Apollo 14 fines 14003,24 and clastic (fragmental) rock 14303,13, and in Apollo 15 fines 15021,94, 15101,59, 15601,63 and the two basalts 15016,33 and 15556,25. Li, Mg and Ca have been analyzed by atomic absorption spectrophotometry, all other elements by destructive neutron activation analysis.

The Apollo 14 samples, collected from the FRA MAURO region of the moon, were the first lunar highland specimens returned to earth. Fines 14003,24 analyzed in this work belong to the contingency samples collected near the lunar module during the first extra-vehicular activity (EVA) and is one of the seven soil samples returned by Apollo 14. Sample 14303,13 is part of a clastic rock the location of which was not well established by photography or comments of the astronauts. It seems likely that this sample was collected during the first EVA. The comprehensive sample is the most reasonable place in which to include rock 14303.

The three Apollo 15 fines derive from different sites of the Hadley-Apennine sampling area. 15021 belongs to the contingency samples and was collected near the lunar module. 15101 comes from station 2 near St.George crater and is a comprehensive soil sample. 15601 was sampled at station 9A at the edge of Hadley rille and was collected with the comprehensive samples. Sample 15016 is a highly vesicular rock of fine-grained basalt and was sampled at station 3 (seat belt station). 15556 is also a highly vesicular, fine-grained basalt collected at station 9A.

For analysis the bulk fines as delivered by NASA, grain size $<$ 1mm, were used. From the rock samples, we obtained several grams for investigation. Several small chips of each rock sample with a total weight of about 1 gr were ground to a grain size below 60 μm and the powder was used for analysis. Neutron irradiations of lunar samples, rock standard diabase W-1 and monitors were performed both in the FR2 reactor, Karlsruhe-production of ^{24}Na, ^{42}K, ^{86}Rb, ^{134}Cs, and in the TRIGA reactor, Heidelberg - production of ^{87m}Sr, ^{139}Ba, ^{140}La, ^{239}U. After radiochemical separation the γ-activities of these nuclides were measured with 3x3" NaI scintillation solid and well counters. For the AAS-analysis of Li, Mg and Ca the Perkin-Elmer-Model 403 was used.

The results of the alkali, alkaline earths, La and U concentrations in Apollo 14 and Apollo 15 samples are given in table 1. Averaged data on replicate analyses of standard diabase W-1, analyzed along with the lunar samples, are shown in table 2, and compared with recommended values (1). The numbers agree well for most elements; in this work, Li is slightly higher, Ba and La somewhat lower compared to the recommended values.

Apollo 14 Samples. Apollo 14 fines are characterized by significant en-

ALKALI AND ALKALINE EARTH ELEMENTS, LA AND U

O. Müller

richments of Li, K, Rb, Cs, Ba, La and U and other elements, especially rare earths, relative to Apollo 11, 12, 15 and Luna 16 fines. Elemental abundances of fines 14003 are rather similar to those found in different Apollo 14 fines by other authors (2,3,4,5). The averaged data of whole rock samples and soils (6,7) resemble the Apollo 14 soil compositions. There exist, however, non-uniform elemental differences between clastic rocks and fines. This is obvious when comparing elemental ratios of 14303 with 14003 in table 3. The heavier alkali elements K, Rb and Cs are more enriched in the clastic rock than the elements Li, Na, Ba, La and U. Consequently, the K/U ratios in 14303 and 14003 are distinctly different, 1870 and 1320, respectively.

Apollo 15 Samples. Contrary to Apollo 14 fines the three soil samples of Apollo 15 analyzed in this work differ significantly among each other in chemical composition. Li, Na, K, Ba, La and U concentrations decrease in the sequence 15021 (lunar module), 15101 (near St.George crater), 15601 (Hadley-rille). Moreover, the compositions of Apollo 15 fines are systematically different from the compositions of the igneous rocks, e.g. 15016, 15556. Most of the elements shown in table 1 have higher contents in the fines than in the basalt samples. Therefore, the soils are probably mixtures of local basalt and a foreign component as was the case for Apollo 12 samples. The most likely candidate for the admixed material is KREEP (a material high in K, Rb, Cs, Ba, U, rare earth elements, and phosphorus). In how far plagioclase from the nearby Apennine mountains and highlands was added to the soils can be estimated from the Sr contents relative to those of the igneous rocks. There appears to be only little or no admixture of plagioclase to fines 15601, whereas soils 15101 and 15021 might contain a few per cent plagioclase as foreign component (table 1). The rille soil 15601 contains distinctly less KREEP elements than the fines from most of the other locations at Hadley base. Its chemical composition appears to be rather similar to that of fines 15531 (station 9A) for which Schnetzler et al. (8) have found the lowest concentrations of K, Sr, Ba, REE and Zr of any lunar soil material yet reported. This depletion is possibly due to impact erosion the effect of which is greater at the edge of the rille than on horizontal terrains (9).

The two mare-type basalts 15016 (station 3) and 15556 (station 9A) show for most elements analyzed similar concentrations. Mg and Ca contents of the two basalts, however, differ distinctly. The chemical composition resembles to that of the Apollo 11 low-potassium basalts and the Apollo 12 mare basalts. The trace element levels of basalts 15016 and 15556 are somewhat higher compared to basalt 15555 (station 9A) which appears to be the least differentiated material yet returned from the moon (8). Whether this also applies to samples 15016 and 15556, depends on the pattern of the rare earth elements, especially the extent of the europium anomaly.

To illustrate the large compositional differences, mainly due to the KREEP component, the concentrations found for fines 15101 are plotted versus those of basalt 15556 in Fig.1. Cs and U which are even stronger enriched in 15101 than other KREEP elements, and Mg and Ca are not included in this graph. Fig.2 is a similar plot demonstrating the great abundance of the KREEP component in fragmental rock 14303 relative to fines 15101 (Cs, Mg and Ca not plotted). Noteworthy is the strong enrichment of Li in 14303 (and in 14003) which was found to a similar extent in the Apollo 14 soils 14141 and 14259 by Eugster (10).

ALKALI AND ALKALINF EARTH ELEMENTS, LA AND U

O. Müller

Acknowledgments. We thank the National Aeronautics and Space Administration for providing the lunar samples. Valuable discussions with Prof. W. Gentner and Dr. T. Kirsten are appreciated. The collaboration of Mrs. S. Hasse, Mr. D. Kaether and Mr. V. Cercasov is gratefully acknowledged. We are thankful to the crews of the FR2 reactor, Karlsruhe, and the TRIGA reactor, Heidelberg, for the neutron irradiations.

References.

1) M. Fleischer, Geochim. Cosmochim. Acta 33, 65 (1969).
2) C. C. Schnetzler and D. F. Nava, Earth Planet. Sci. Lett. 11, 345 (1971).
3) A. O. Brunfelt, K. S. Heier, E. Steinnes and B. Sundvoll, Earth Planet. Sci. Lett. 11, 351 (1971).
4) H. Wakita, D. L. Showalter and R. A. Schmitt, in Lunar Science-III (ed. C. Watkins), p. 767, Lunar Science Institute, Contr. No. 88 (1972).
5) H. Wänke, H. Baddenhausen, A. Balacescu, F. Teschke, B. Spettel, G. Dreibus, M. Quijano, H. Kruse, F. Wlotzka and F. Begemann, ibid. p. 779.
6) H. J. Rose, Jr., F. Cuttitta, C. S. Annell, M. K. Carron, R. P. Christian, E. J. Dwornik and D. T. Ligon, Jr., ibid. p. 660.
7) S. R. Taylor, P. Muir, W. Nance, R. Rudowski and M. Kaye, ibid. p. 744.
8) C. C. Schnetzler, J. A. Philpotts, D. F. Nava, S. Schuhmann and H. H. Thomas, Science 175, 426 (1972).
9) G. D. O'Kelley, J. S. Eldridge, E. Schonfeld and K. J. Northcutt, Science 175, 440 (1972).
10) O. Eugster, in Lunar Science-III (ed. C. Watkins), p. 247, Lunar Science Institute, Contr. No. 88 (1972).

Elements ppm, %	Fragm. rock	Fines				Basalt	
	14303	14003	15021	15101	15601	15016	15556
Li	38.0	32.7	14.6	13.0	9.6	7.5	8.0
Na	5980	5350	5290	3120	2360	3100	3450
K	7460	4360	1760	1430	820	340	390
Rb	24.7	14.6	4.4	4.6	2.5	1.0	0.85
Cs	1.15	0.63	0.18	0.20	0.11	0.04	0.03
Mg %	5.88	5.51	6.29	6.16	6.78	6.71	4.94
Ca %	7.10	7.92	7.56	8.40	6.99	6.47	7.74
Sr	166	188	127	135	99	90	103
Ba	999	825	291	216	132	53	53
La	76	69	27	19	13	5.2	5.5
U	4.0	3.3	1.2	0.91	0.51	0.15	0.15

Table 1. Elemental concentrations of Apollo 14 and Apollo 15 lunar samples (in ppm;Mg and Ca in wt.%). Most of the analyses are single determinations, but replicate analyses of diabase W-1 (table 2) yielded errors of smaller than ± 4%. Complete sample numbers are given in the text.

Elements ppm, %	This work	Recommended values (Fleischer, 1969)
Li	13.0	12
Na %	1.63	1.60
K	5320	5300
Rb	21.8	22
Cs	1.04	1.0
Mg %	3.97	3.99
Ca %	7.64	7.83
Sr	188	180
Ba	153	180
La	10.5	12
U	0.55	0.5

Table 2. Elemental concentrations of USGS standard rock diabase W-1 (in ppm; Na,Mg and Ca in wt. %). Also the recommended values of (1) are listed.

ALKALI AND ALKALINE EARTH ELEMENTS, LA AND U

O. Müller

Elemental ratios of	Li	Na	K	Rb	Cs	Mg	Ca	Sr	Ba	La	U
14303/14003	1.16	1.12	1.71	1.69	1.83	1.07	0.90	0.88	1.21	1.10	1.21

Table 3. Elemental ratios of clastic rock 14303,13 and fines 14003,24.

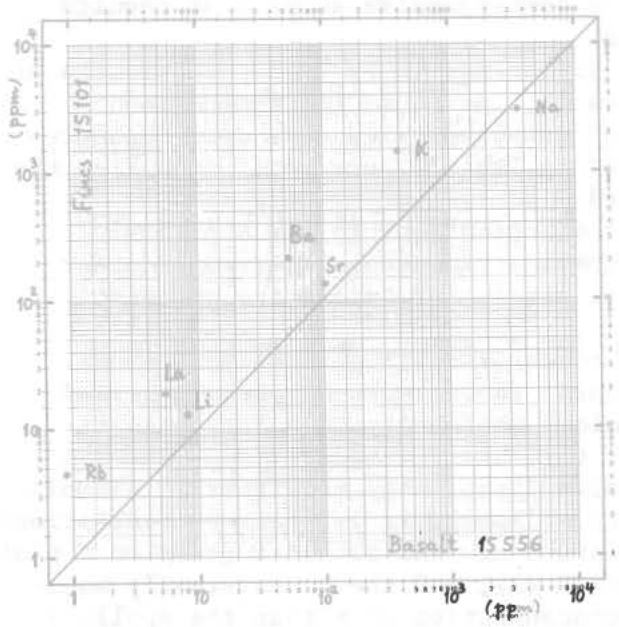

Fig. 1. Comparison of fines 15101,59 and basalt 15556,25 (concentrations in ppm).

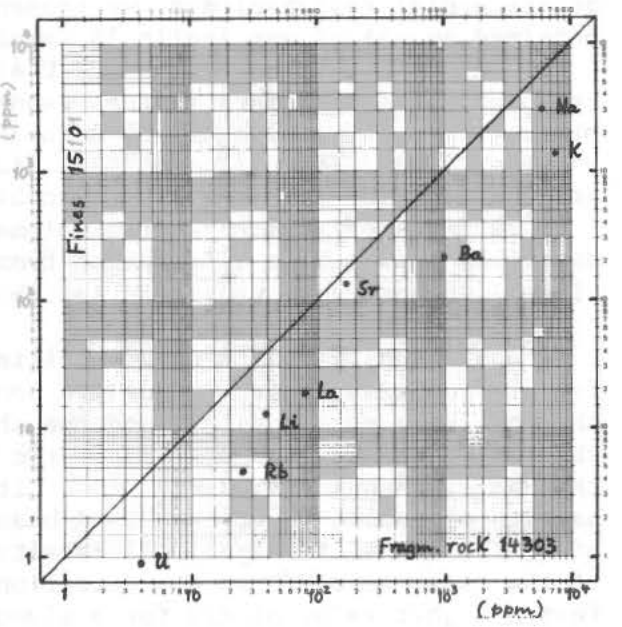

Fig. 2. Comparison of fines 15101,59 and fragmental rock 14303,13 (concentrations in ppm).

ABUNDANCES OF THE PRIMORDIAL RADIOELEMENTS K, Th, AND U IN APOLLO 15 SAMPLES, AS DETERMINED BY NONDESTRUCTIVE GAMMA-RAY SPECTROMETRY,* G. Davis O'Kelley, James S. Eldridge, and K. J. Northcutt, Oak Ridge National Laboratory, Oak Ridge, Tenn. 37830.

Since publication of our previous reports (1) on samples obtained early in the Apollo 15 mission, we have received 12 additional samples for study by nondestructive gamma-ray spectrometry. In this communication on concentrations of primordial radionuclides, we present a comprehensive summary of results obtained on all of our Apollo 15 samples.

Concentrations of K, Th, and U are summarized in Table 1. Abundances of cosmogenic radionuclides in these samples will be found in a companion paper (2). The equipment and methods of data reduction were described previously (1,3). The bulk densities listed in Table 1 were determined from the volumes of calibration replicas, combined with the sample weights.

Patterns of primordial radioelement distributions in the Apollo 15 materials show subtle differences from the distributions observed at other sites. The new data presented in Table 1 verify and extend the systematic trends observed earlier (1).

Our extensive suite of crystalline rocks is distinguished by its uniformity in primordial radionuclide content. These rocks may be classified chemically as mare basalts, and the chemical uniformity seen here suggests that these samples are characteristic of the basaltic flows which underlie the Hadley-Apennine landing site. Although these rocks most nearly resemble basalts of Apollo 12 or the low-K basalts of Apollo 11 in their concentrations of K, Th, and U, the Apollo 15 basalts form a new and distinct group on a plot of the mass ratio K/U vs concentration of K (1), and they consistently manifest a higher value of K/U for a given concentration of K than the Apollo 12 basalts. The range of K concentration for the Apollo 15 basalts lies between about 300 ppm (K/U = 2200) and 510 ppm (K/U = 3400).

The soils and breccias of Apollo 15 are much higher in primordial radioelement concentrations than the basalts from the same area. The data of Table 1 combined with other measurements show that these soils and breccias also lie in a hitherto unoccupied zone of the K/U systematics, intermediate between values for the Apollo 12 basalts and the zone corresponding to the soils and breccias of Apollo 12 and 14. It is apparent that a simple, two-component mixing model which produces Apollo 15 soils and breccias from mare basalt as one end member requires as the other end member a material very similar to the lunar material KREEP (4). Although KREEP is ubiquitous at the Apollo 15 site, it only varies from about 8 - 21%, much lower than the range of 60 - 85% estimated for clastic rocks and soil from the Fra Mauro site. The unique rake sample 15382 from the comprehensive sample of Station 7 has many of the properties expected for pure KREEP basalt, and is the subject of a separate report (5).

Abundances of K, Th, and U

G. Davis O'Kelley

Samples 15471, 15475, 15476, and 15495 were collected in a group 28 m south of the rim crest of Dune crater. The rocks are notable for their lack of filleting or burial. They are also similar to each other in their contents of K, Th, and U, which suggests that they were derived from the underlying basaltic flow. Although these rocks are of recent origin, they may not have all been ejected onto the surface at the same time (2). Rock 15498 is a recrystallized soil breccia collected near the large boulder on the rim of Dune crater. As shown in Table 1, soil 15471 resembles very closely the chemistry of 15498, indicating that both are typical of the recent regolith in this region of Station 4.

At Station 1 a three-part radial sample was taken along a line extending from the rim of Elbow crater. Basalts 15065 (4 m east) and 15076 (25 m east) are very similar in composition to the most distant sample of the series (6), 15085 (60 m east). All of these basaltic rocks are chemically similar and are probably representative of the material excavated by the Elbow crater event. However, the small fillets banked against these rocks suggest that they were recently moved to the collection site, and so their locations on the ejecta blanket may not be related to the depths in the crater from which they were derived.

References and Notes

*Research carried out under Union Carbide's contract with the U. S. Atomic Energy Commission through interagency agreements with the National Aeronautics and Space Administration.

1. G. D. O'Kelley, J. S. Eldridge, E. Schonfeld, K. J. Northcutt, Science 175, 440 (1972); paper to be published in "Proc. Third Lunar Sci. Conf.," Geochim. Cosmochim. Acta (Suppl. 3, Vol. 2), MIT Press, 1972.

2. J. S. Eldridge, G. D. O'Kelley, and K. J. Northcutt, Concentrations of Cosmogenic Radionuclides in Apollo 15 Rocks and Soil, in "The Apollo 15 Lunar Samples," ed. J. W. Chamberlain and C. Watkins (Houston: Lunar Science Institute), 1972.

3. G. D. O'Kelley, J. S. Eldridge, E. Schonfeld, and P. R. Bell, "Proc. Second Lunar Sci. Conf.," Geochim. Cosmochim. Acta (Suppl. 2, Vol. 2), p. 1159, MIT Press, 1971; ibid., p. 1747.

4. C. Meyer, Jr., R. Brett, N. J. Hubbard, D. A. Morrison, D. S. McKay, F. K. Aitken, H. Takeda, and E. Schonfeld, "Proc. Second Lunar Sci. Conf.," Geochim. Cosmochim. Acta (Suppl. 2, Vol. 1), p. 393, MIT Press, 1971.

5. E. Schonfeld, G. D. O'Kelley, J. S. Eldridge, and K. J. Northcutt, K, U, and Th Concentrations in Rake Sample 15382 by Nondestructive Gamma-Ray Spectrometry, in "The Apollo 15 Lunar Samples," ed. J. W. Chamberlain and C. Watkins (Houston: Lunar Science Institute), 1972.

6. J. E. Keith, R. S. Clark, and K. A. Richardson, paper to be published in "Proc. Third Lunar Sci. Conf.," Geochim. Cosmochim. Acta (Suppl. 3, Vol. 2), MIT Press, 1972.

Abundances of K, Th, and U

G. Davis O'Kelley

Table 1. Concentrations of K, Th, and U in Apollo 15 Lunar Samples.

Sample	Station	Density (g/cm^3)	K (ppm)	Th (ppm)	U (ppm)	K/U Mass Ratio
			Crystalline Rocks			
15016*	3	2.4	374 ± 20	0.52 ± 0.02	0.15 ± 0.01	2493 ± 213
15058	8	2.8	405 ± 20	0.52 ± 0.03	0.13 ± 0.01	3115 ± 285
15065	1	3.0	385 ± 20	0.51 ± 0.03	0.15 ± 0.02	2567 ± 367
15076	1	2.4	410 ± 25	0.45 ± 0.03	0.12 ± 0.01	3417 ± 288
15379	7	-	400 ± 40	0.49 ± 0.05	0.15 ± 0.02	2667 ± 444
15475*	4	2.9	354 ± 20	0.40 ± 0.02	0.12 ± 0.01	2950 ± 297
15476	4	2.8	412 ± 20	0.51 ± 0.03	0.14 ± 0.01	2943 ± 254
15486	4	2.2	510 ± 70	0.64 ± 0.05	0.15 ± 0.02	3400 ± 651
15495*	4	2.9	495 ± 25	0.60 ± 0.03	0.16 ± 0.01	3094 ± 249
15499	4	2.3	480 ± 25	0.59 ± 0.03	0.16 ± 0.01	3000 ± 244
15545	9a	3.0	340 ± 20	0.43 ± 0.02	0.13 ± 0.01	2615 ± 253
15557	9a	3.0	340 ± 17	0.45 ± 0.03	0.14 ± 0.01	2429 ± 212
15597	9a	3.1	440 ± 30	0.53 ± 0.04	0.14 ± 0.01	3143 ± 310
			Breccias			
15285*	6	2.4	1610 ± 80	3.4 ± 0.1	0.93 ± 0.05	1731 ± 127
15455*	7	-	900 ±150	2.0 ± 0.3	0.53 ± 0.08	1698 ± 382
15498	4	2.6	1140 ± 65	2.5 ± 0.2	0.65 ± 0.05	1754 ± 168
			Soils			
15031*	8	-	1860 ± 95	4.3 ± 0.2	1.10 ± 0.05	1691 ± 116
15041*	8	_	1740 ± 90	4.0 ± 0.2	1.10 ± 0.05	1582 ± 109
15101*	2	1.2	1484 ± 74	3.1 ± 0.3	0.86 ± 0.08	1726 ± 182
15471	4	-	1100 ± 55	2.4 ± 0.3	0.56 ± 0.05	1964 ± 201
15601*	9a	1.7	900 ± 45	1.8 ± 0.2	0.51 ± 0.05	1765 ± 194

*Preliminary analysis of this sample reported in Ref. (1).

TRACE ELEMENT COMPARISONS BETWEEN MARE AND APENNINE-FRONT NONMARE SAMPLES* G. W. Reed, Jr. and S. Jovanovic, Chemistry Division, Argonne National Laboratory, Argonne, Ill., 60439.

The halogens, Hg, Ru, Os, Li, U and Te contents in soil and rock samples representative of the nonmare and mare terrain at the Apollo 15 site are reported and the results are compared with those from earlier missions. The measurements were made by neutron activation analysis; hot water leaching and volatilization procedures were carried out as in previous studies[1]. Of the samples measured, nonmare end-members were the anorthosite clast 15415, the gabbroic anorthosite 15418, and breccias 15455 and 15265; at the mare end were basalts 15535 and 15557. Soils from station 2 (St. George) are described by LSPET as representative of the nonmare front samples while those from stations 6 at the front and 8 on the mare are considered to be a part of a ray from Aristillus or Autolycus. We, therefore, use our Apollo 11 and 12 mare results for comparison of the soils. All our Apollo 15 data are given in Table 1.

We have reported[1] that the non-leachable Cl concentrations in lunar samples correlate with the concentrations of the elements that comprise the KREEP component found mixed in soils and breccias from all sites, including soils from stations 2, 6 and 8 at the Apollo 15 site. Breccia 15265, which is almost entirely of nonmare origin (Wilshire and Brett, Apollo 15 sample catalogue), falls on the correlation line. The non-leachable Cl content of soils from stations 6 (front) and 8 (mare) is $\sim$20 ppm and is significantly different from the Cl in soils from station 2 (front) at $\sim$12 ppm. This may be chemical evidence, in addition to that reported by LSPET, for the presence of ray material at station 6 as well as at station 8. The lowest non-leachable Cl concentrations of all the lunar samples we measured so far, are 0.12 and 0.44 ppm in 15415,42 and 15418,30-08, respectively. Their Cl(ppm)/P_2O_5(%) ratios are 12 and 15. Mare basalts from the 11, 12 and 15 sites have 2-4 ppm non-leachable Cl and Cl/P_2O_5 ratios of $\sim$40. Two rocks appear to be exceptions. Rock 14310 has been described as being a remelted breccia; however its Cl/P_2O_5 ratio of $\sim$10 is very low. The dark part of 15455 is also classified as a breccia; its non-leachable Cl content (of $\sim$1 ppm) is low for a breccia and requires that if it is a typical breccia its P_2O_5 content must also be low ($\sim$0.01 wt%). Perhaps the pattern for 14310 and 15455-dark indicates that they were formed at a time prior to or at a site inaccessible to the introduction of the Cl-P_2O_5 bearing phase found in breccias and in soils. Low Br as well as Cl contents of 15455 also suggest that these elements were not available to the rock at the site or time of its formation.

In general, although total Cl in nonmare type rocks tends to be lower than in mare types (Ap 11, 12 and 15), the Br contents are similar. This is probably consistent with Br being a dispersed element. Total Cl and Br contents in soils at all sites tend to overlap.

*Work performed under the auspices of the USAEC and NASA.

TRACE ELEMENTS- APENNINE FRONT

G. W. Reed, Jr.

The results on I are particularly interesting. Because of the relatively high U contents (few tenths to several ppm) in all previously measured samples, including Ap 11 and 12 igneous rocks, we were able to detect natural I radioactivity only in the aqueous leach solutions which contain little of the fission product I radioactivities. A number of Ap 15 samples have U contents of a few hundredths ppm. Nevertheless natural I was detectable only in the leach solutions. This is strong support for the suggestion we have made that since the fraction of halogen that is water-leachable increases from F→Cl→Br then possibly all the I is available at surfaces. This is also borne out by the observation of Alexander et al.(2) that Xe^{128} produced from natural I is volatilized from samples at 80°C or less. Most I concentrations in 11, 12 and 14 samples fall between 10 and 100 ppb; most Ap 15 I values cluster around 2 ppb. If such low concentrations are typical of nonmare material the possibility of observing an I associated Xe^{129} anomoly appears to be small.

The 3.5 ppb Os in the anorthosite 15415,42 which is reported to be 99% anorthosite and 1% pyroxene and the 9.3 ppb Os in the gabbroic anorthosite 15418,30-08 are in good agreement with previously reported 4.5 ppb Os from anorthositic fractions from Ap 11 soil, 10084,75 and Ap 12 breccia 12073,34(3). This value (4.5 ppb) is also indicated by other Ap 11, 12 and 14 data(1). This is then not only evidence that an appreciable amount of the Os is lunar in origin but also that this Os is probably concentrated in the nonmare crust. The Os contents of the Ap 15 mare basalts and soils are similar to those from samples from other sites. This is also true for Ru in Ap 15 soils; the Ap 15 mare rocks have not been measured. The nonmare rocks 15415,42 and 15418,30-08 have lowest Ru observed so far.

In all non-mare samples and mare soils Li contents cluster ∿15 ppm. The mare rocks contain ∿6 ppm Li, similar to the concentrations found in Apollo 12 igneous rocks.

The concentrations of elements studied in Ap 15 breccias 15205,35 and 15206,17 bear striking resemblance to Ap 14 soils 14163,108 and 14259,96 as illustrated below:

Element Sample	Cl	Br	I	U	Li	Te
15205,35	67	0.41	1.1	3.2	22	nd
15206,17	66	0.51	2.9	4.9	21	nd
14163,108	51	1.3,0.29	9.2	1.8,4.1	19	0.34
14259,96	55	0.2	4.0	4.0,3.3	19	nd

Some conclusions about Hg in Ap 15 samples are: 1. Hg concentrations in soils and rocks are in the ppb range; 2. much of the Hg is labile at temperatures of 130°C or less; 3. as previously noted, unexposed (i.e., cold) surfaces contain higher concentrations of labile Hg; 4. as in the Ap 14 samples much more Hg was found in retentive sites (volatilized at ≳ 450°C) than in samples from the Ap 11 and 12 sites; 5. there is no evidence for a labile Hg concentration gradient associated with the diurnal thermal pulse in deep drill core samples, all of which are from depths greater than 40 cm; the labile Hg profile in these samples suggests a layering process with little or no mixing(4).

TRACE ELEMENTS - APENNINE FRONT

G. W. Reed, Jr.

Table 1. Halogens, ruthenium, osmium, mercury and other trace elements in Apollo 15 Samples. All data on a line are for a single aliquant.*

Station	Sample	Cl r† ppm	Cl l† ppm	Br r ppm	Br l ppm	I†† ppb	Ru ppb	Os ppb	$Hg_{\leq 130}$ ppb	Hg_{total} ppb	U ppm	Li ppm	Te ppb
	Soils												
2	15091,32**	11	7.3	0.42	0.29	2.1					0.97	16	~0
2	15091,32**						25	24	0.5	10			
2	15101,45>74 μm	11	2.8	0.20	0.06	35					0.86		
2	15101,45<74 μm	14	9.0	0.28	0.22	211					2.3	13	
2	15231,29**						16	14	7.8	11			
6	15251,28**	21	3.4	0.52	0.25	8.3					2.0	16	nd
8	15041,32**	20	-	0.29	0.28	2.8					1.7	15	nd
8	15041,32						-	18	0.39	5.5	1.1		
8	15031,27***						21	(6)	0.38	2.2	1.4		
	Deep Drill Core*												
8	15001,20						18	(10)	2.2	8.7	2.2		
8	15002,16							7.2	0.21	0.4	1.5		
8	15003,18						5	(22)	2.8	7.0	1.5		
8	15004,15							16	0.29	0.9	1.2		
8	15005,16						11	(38)	0.61	8.3	0.9		
8	15006,27							21	1.6	10.5	1.5		
	Rocks												
2	15205,35	58	9.4	0.38	0.03	1.1					3.2[b]	22	nd
2	15206,17	54	12	0.44	0.07	2.3					4.9	21	nd
6	15265,17	19	7.2	0.45	0.17	0.24					0.067	9.1	nd
7	15455,3 white	1.5	0.43	0.019	0.014	0.44					0.073	8.4	124
7	15455,3 dark	1.1	1.8	0.03	0.05	0.20					0.14	14	171
7	15418,30-08	0.44	0.67	0.023	0.029	1.6					0.01[c]	16	6.3
7	15418,30-08			0.022	0.017		3.4[a]	9.3			0.036[c]		
7	15415,42	0.12	0.48	0.021	0.036	1.1					0.0066	15	68
7	15415,42			0.006	0.091		≤0.5	3.5			0.031[d]		
9a	15535,31	2.2	0.59	0.010	0.007	2.0					0.11	7.1	1.4[e]
9a	15557,24	3.2	5.2	0.027	0.014	1.8					0.045	5.6	7.5[f]
9a	15557,24							≥0.24	0.03	5.4	≤0.18		
9a	15557,65							1.4	0.24	0.98	≤0.14		
9a	15557,66							0.21	0.11	1.4	≤0.25		

† r = residue after leaching, l = leach solution †† I detected in leach only
() Uncertain due to possible loss of some of the Os tracer prior to equilibration with carrier.
* The counting statistical errors are about 10% except for (a) $^{+0.2}_{-0.8}$, (b) $^{+0.7}_{-0.3}$, (c) $^{+0.004}_{-0.012}$, (d) $^{+0.003}_{-0.011}$, (e) ±1.4, (f) ±1.2.
** Reed et al. (1972) ***Jovanovic and Reed (1972) nd = not detected.

REFERENCES

(1) Reed G. W., Jr., Jovanovic S. and Fuchs L. H. (1972) Trace element relations between Apollo 14 and 15 and other lunar samples, and the implications of a moon-wide Cl-KREEP coherence and Pt-metal non-coherence. Proceedings of Third Lunar Science Conference, Supplement 3, Geochim Cosmochim Acta, MIT Press, in press.

(2) Alexander E. C., Jr., Davis P. K., Lewis R. S., and Reynolds J. H. (1972) Rare gas analyses on neutron irradiated lunar samples (abstract), Lunar Science III (Editor, C. Watkins) Lunar Science Institute Contr. No. 88, 12.

(3) Reed G. W., Jr., Jovanovic S. and Fuchs L. H. (1971) Fluorine and other trace elements in lunar plagioclase concentrates. Earth Planet. Sci. Lett. 11, 354-358.

(4) Jovanovic S. and Reed G. W., Jr. (1972) Trace element profiles, notably Hg, from a preliminary study of the Apollo 15 deep-drill core. Earth Planet. Sci. Lett. to be published.

MAJOR ELEMENT CHEMISTRY OF APOLLO 15 MARE BASALTS. J. M. Rhodes, Lockheed Electronics Co., Manned Spacecraft Center, Houston, Tx., 77058

Twelve samples of mare basalt from the Apollo 15 landing site have been analyzed for major and minor elements by X-ray fluorescence analysis. The preliminary chemical data[1] obtained for seven of these samples showed that the range in composition is "remarkably small," and that they are closely similar in bulk composition to Apollo 12 mare basalts, but with slightly lower concentrations of TiO_2, K_2O and P_2O_5. The additional analyses, taken in conjunction with the preliminary data, confirm this comparison, and permit recognition of two distinct basalt types at the Apollo 15 site (Table 1, Fig. 1).

One group is significantly higher in FeO and TiO_2 and correspondingly lower in SiO_2 than the other group. Basalts in the high iron-low silica group are all olivine normative, whereas those in the low iron-high silica group are all quartz normative. The olivine normative group shows a greater compositional range than the quartz normative group, but both are restricted in range compared with the Apollo 12 basalts.

These two chemically defined groups can be reconciled with the four textural varieties recognized during the preliminary petrographic examination of the Apollo 15 samples[1], in that the olivine normative group includes examples of both porphyritic olivine basalt and highly vesicular basalt, whereas the quartz normative group includes both porphyritic clinopyroxene basalt and porphyritic clinopyroxene vitrophyre.

Least squares calculations[2] show that, starting with an initial magma compositionally equivalent to the mean composition of the olivine normative basalts, all the rocks in this group can be derived from this magma either by addition or subtraction of small amounts of olivine. This is clearly illustrated in Fig. 1, where the composition of the analyzed rocks fall close to the straight line connecting the mean composition with a "best fit" olivine (Fo 72.9). Such calculations do not shed any light on the composition of the parental magma, nor do they determine whether the rocks in question are cumulates or derivative magmas. They merely demonstrate that, starting with a common parental magma, small amounts (about 12%) of high level crystal fractionation, involving olivine of realistic composition (±1% spinel), are capable of generating the chemical variation observed in these rocks.

Similar calculations for the quartz normative basalts show that the removal (or addition) of both pigeonite and minor olivine is necessary to account for the small chemical variation found in this rock type. As with the olivine normative basalts, the composition of the parental magma of these rocks is not known. However, the wide textural variation in conjunction with

MAJOR ELEMENTS IN MARE BASALTS

J. M. Rhodes

relative chemical homogeneity encourages the idea that the mean composition of this group cannot be far removed from that of the parental magma.

Further calculations show that neither basalt group can be derived from the other by high level crystal fractionation involving combinations of olivine, pigeonite or spinel, the most likely low pressure liquidus phases in rocks of these compositions. Only if plagioclase is introduced as an additional liquidus phase can one be derived from the other. However, this is a most unrealistic model since in Apollo 12 rocks of similar composition, plagioclase becomes the liquidus phase only after the magma is 50 to 60 percent crystallized[3].

It is suggested, therefore, that the chemical variation observed within each of the basalt types derives from a small amount of surface or near-surface crystal fractionation, whereas the difference in chemistry between groups results either from small variations in the amount of partial melting of lunar mantle, or from partial melting of a heterogeneous mantle source.

References:

1. Lunar Sample Preliminary Examination Team, Science 175, 363-375 (1972).

2. Bryan, W. B., Finger, L. W., and Chayes, F., Science 163, 926-927 (1969).

3. Green, D. H., Ringwood, A. E., Ware, N. G., Hibberson, W. O., Major, A., and Kiss, E., Proc. Apollo 12 Lunar Sci. Conf., 1, 601-615 (1971).

Table 1. Mean composition of Apollo 15 mare basalts.

Olivine normative basalts*				Quartz normative basalts†			
SiO_2	44.84	Quartz	-	SiO_2	47.83	Quartz	1.39
TiO_2	2.47	Orthoclase	0.20	TiO_2	1.89	Orthoclase	0.27
Al_2O_3	8.86	Albite	2.03	Al_2O_3	9.32	Albite	2.28
FeO	22.32	Anorthite	23.00	FeO	20.10	Anorthite	24.09
MnO	0.30	Diopside	22.12	MnO	0.29	Diopside	23.28
MgO	9.72	Hypersthene	35.86	MgO	8.51	Hypersthene	43.79
CaO	10.03	Olivine	10.57	CaO	10.53	Olivine	-
Na_2O	0.24	Ilmenite	4.69	Na_2O	0.27	Ilmenite	3.59
K_2O	0.03	Apatite	0.15	K_2O	0.04	Apatite	0.17
P_2O_5	0.07			P_2O_5	0.08		
S	0.07			S	0.07		
Total	98.69			Total	98.93		
100•MgO/ MgO+FeO	30.3			100•MgO/ MgO+FeO	29.7		

*Based on 15016,4; 15256,15; 15256,22; 15545,13; 15555,8; 15556,5; 15668,2.
†Based on 15058,5; 15076,21; 15475,35; 15499,2.

MAJOR ELEMENTS IN MARE BASALTS

J. M. Rhodes

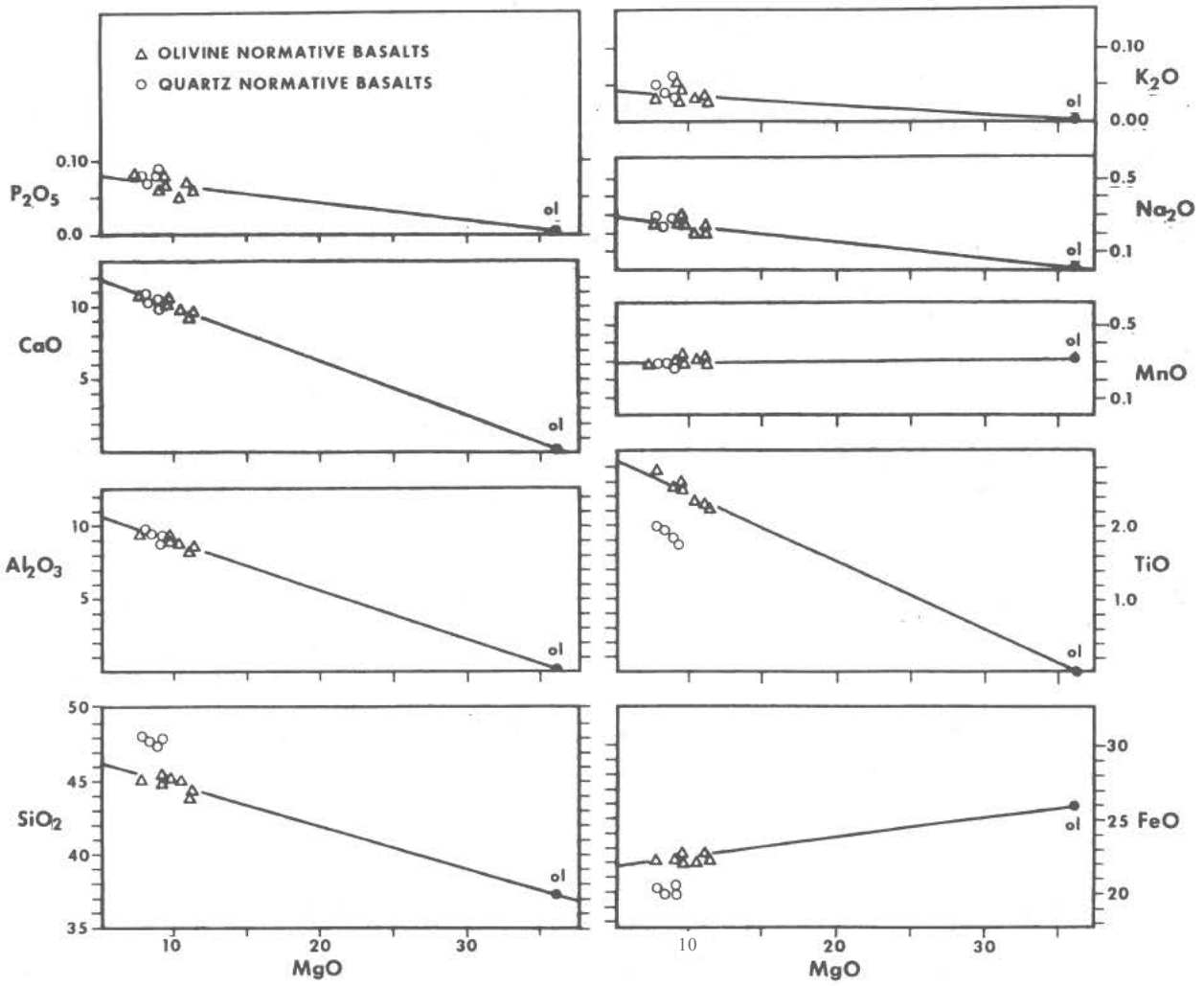

Fig. 1 MgO variation diagrams for major and minor element concentrations (weight percent) in Apollo 15 mare basalts.

K, U, AND Th CONCENTRATIONS IN RAKE SAMPLE 15382 BY NON-DESTRUCTIVE GAMMA-RAY SPECTROSCOPY. E. Schonfeld, NASA Manned Spacecraft Center, Houston, Texas 77058; G. D. O'Kelley, J. S. Eldridge, and K. J. Northcutt, Oak Ridge, National Laboratory, Oak Ridge, Tenn., 37830.

Basalt fragments with fresh subophitic textures and characteristic KREEP chemistry (1) have been found (2) in soil 15023. Thin sections of rake sample 15382 (total weight 3.2 g) have similar textures and mineralogy indicating that 15382 may be a KREEP basalt (3). The old formation age of KREEP of 4.4 billion years (3) and its rather wide distribution (4) make 15382 an interesting sample for the determination of the K, U, and Th concentrations.

The sample was studied first at the Manned Spacecraft Center (MSC) with a Ge(Li) detector. These measurements indicated much higher concentrations of K, U, and Th than those of mare basalts. Following the measurements at MSC, sample 15382 (2.24 g) was analyzed with the high-sensitivity, low-level gamma-ray detector at Oak Ridge National Laboratory (5,6,7). The results are shown in Table 1.

Table 1.

K, U, AND Th CONCENTRATIONS IN 15382, 14310, AND KREEP

Sample	K ppm	U ppm	Th ppm	K/U	^{26}Al dpm/Kg
15382	4900 ± 500	3.1 ± 0.4	10.5 ± 0.5	1610	74 ± 20
14310[a]	4250	3.06	10.8	1390	
KREEP[b]	5200	4.5	17.2	1160	

a) Tatsumoto et al. (10); Silver (11). b) Schonfeld and Meyer (3)

No other known lunar rock type has K, U, and Th concentrations similar to those of KREEP (3); consequently sample 15382 could be pure KREEP. Data collected from Apollo 12 and 14 samples (7,8,9) suggests that there is about a 30% variation in the K, U, and Th concentrations of KREEP, and sample 15382 is within that range. One possible source of variability is the amount of residual liquid in the crystalline KREEP (or granitic component(2)) has a higher K/U ratio of about 2500 and therefore an excess of residual liquid will tend to increase the K/U ratio. Of course, one cannot exclude the possibility that sample 15382 is a mixture, but if so the amount of contaminants should be small.

If in fact this sample represents original crystalline KREEP basalt it is

obviously an important sample for future study of the mineral isochron and bulk and mineral chemical composition.

References

1. C. Meyer, Jr., R. Brett, N.J. Hubbard, D.A. Morrison, D.S. McKay, F.K. Aitken, H. Takeda, and E. Schonfeld, Proc. Second Lunar Sci. Conf., Geochim. Cosmochim. Acta, Suppl. 2, Vol. 1, 393 (1971).
2. C. Meyer, Jr., Lunar Science III, Lunar Science Institute Contr. No. 88 page 542 (1972).
3. E. Schonfeld and C. Meyer, Jr., Proc. Third Lunar Sci. Conf., Geochim. Cosmochim. Acta (in press, 1972).
4. A.E. Metzger, J.I. Trombka, L.E. Peterson, R.C. Reedy, and J.R. Arnold, Lunar Science III, Lunar Science Institute Contr. No. 88, page 540 (1972).
5. G.D. O'Kelley, J.S. Eldridge, E. Schonfeld, and P.R. Bell, Proc. Apollo 11 Lunar Sci. Conf., Geochim. Cosmochim. Acta, Suppl. 1, Vol. 2, 1407 (1970).
6. G.D. O'Kelley, J.S. Eldridge, E. Schonfeld, and P.R. Bell, Proc. Second Lunar Sci. Conf., Geochim. Cosmochim. Acta, Suppl. 2, Vol. 2, 1159 (1971); ibid., p. 1747.
7. G.D. O'Kelley, J.S. Eldridge, E. Schonfeld, and K.J. Northcutt, Science 175, 440 (1972).
8. N.J. Hubbard and P.W. Gast, Proc. Second Lunar Sci. Conf., Geochim. Cosmochim. Acta, Suppl. 2, Vol. 2, 999 (1971).
9. N.J. Hubbard, P.W. Gast, M. Rhodes, and H. Wiesmann, Lunar Science III, Lunar Science Institute Contr. No. 88, page 407 (1972).
10. M. Tatsumoto, C.E. Hedge, B.R. Doe, and D. Unruh, Lunar Science III, Lunar Science Institute Contr. No. 88, page 741 (1972).
11. L.T. Silver, Lunar Science III, Lunar Science Institute Contr. No. 88, page 704 (1972).

CHEMICAL ANALYSIS OF LUNAR SAMPLES 15101,65 and 15211,6

J. H. Scoon, Department of Mineralogy and Petrology, University of Cambridge, Cambridge, England.

The composition of lunar samples 15101,65 and 15211,6 together with their C. I. P. W. norms are given in Table 1. Classical methods of chemical analysis were used, as described by Scoon[1], except that PbO was used as a flux in the Penfield method for the determination of total water in place of $PbCrO_4$. The total reducing capacity of these samples was estimated by carrying out the Pratt method for the determination of ferrous iron in the presence of a known excess of a ferric salt. The result was calculated as FeO. The total iron in the sample was also calculated as FeO. The difference between these two figures is shown as ΔRC in Table 1.

The two samples appear to be of almost identical composition. Iron is present entirely in the ferrous state. Na_2O, K_2O, TiO_2 and P_2O_5 are less abundant than in the Apollo 14 samples.

Reference

(1) Agrell, S. O. and Scoon, J. H. et al. (1970) Observations on the chemistry, mineralogy and petrology of some Apollo 11 lunar samples. Proceedings of the Apollo 11 Lunar Science Conference, Geochim. Cosmochim Acta, Supplement I, I. 93-128.

Chemical Analysis of Lunar Samples

J. H. Scoon

TABLE 1

Chemical Analyses (Wt%) of Lunar Rocks

	15101,65	15211,6
SiO_2	46.63	46.70
Al_2O_3	17.56	17.54
Fe_2O_3	nil	nil
FeO	11.74	11.77
MnO	0.16	0.16
MgO	10.06	10.08
CaO	11.73	11.63
Na_2O	0.43	0.46
K_2O	0.18	0.18
H_2O^+	nil	0.05
H_2O^-	0.01	nil
TiO_2	1.41	1.41
P_2O_5	0.17	0.16
Cr_2O_3	0.32	0.30
S	0.07	0.08
F	nil	nil
	100.47	100.52
less S ≡ O	0.02	0.02
	100.45	100.50
Total Iron as Fe_2O_3	12.71	12.79
Δ RC	0.74	0.76

C.I.P.W. Norms

	15101,65	15211,6
Q	-	-
Or	-	-
Ab	3.64	3.90
An	45.94	45.88
Di	10.00	9.78
En	2.79	2.71
Fs	2.12	2.10
Wo	5.09	4.98
Hy	31.51	31.60
En	17.88	17.82
Fs	13.63	13.78
Ol	5.63	6.00
Fo	3.06	3.24
Fa	2.57	2.76
Cm	0.47	-
Il	2.68	2.68
Ap	-	-
Pr	0.13	0.15

ANALYSIS OF LUNAR SAMPLES 15065, 15301 AND 15556, WITH ISOTOPIC DATA FOR $^{7}Li/^{6}Li$: A. Strasheim, J. H. J. Coetzee, P. F. S. Jackson, F. W. E. Strelow*, F. T. Wybenga, A. J. Gricius and M. L. Kokot, Natl. Phys. Res. Lab., (*Natl. Chem. Res. Lab.), C. S. I. R., P. O. Box 395, Pretoria, South Africa.

Abstract - The analytical results obtained for the macro and minor elements, including the rare earths, of the lunar samples 15054,32, 15301,75 and 15556,12 are presented.

Introduction

The three Apollo 15 samples received were 1.79g of a gabbro (15065,32), 2.1g of <1mm fines (15301,75) and 2.01g of a vesicular basalt (15556,12). These samples were comprehensively analyzed for major and minor elements and for lithium isotope ratios by analytical methods mentioned before[1].

Low voltage discharge spark mass spectrometers normally give weak mass lines for the rare elements. A new method using a cation exchange resin was accordingly developed.

Analysis of rare earths

The samples, weighing ±0.2 grams, were dissolved by heating them in a mixture of hydrofluoric, hydrochloric and perchloric acids and heating them to strong fumes for 20 mins. The wet salts were dissolved in 1 M HCl and any undissolved salts were treated with phosphoric acid and redissolved in 1 M HCl. These solutions were added onto cation exchange resins, and the elements Fe, Ca, Mg and Al were eluted with 1.75 M HCl. The rare earth group, together with Ba, Zr and Hf, were eluted with 4M HCl and the elutes were taken to incipient dryness. Concentrated HNO_3 was added to the salts and the solutions were heated to fumes to convert the salts to nitrates. The salts were then co-deposited onto graphite in an 80% acetone/20% water mixture, using Sn as an internal standard.

These graphite mixtures were analyzed by a spark mass spectrograph, using the intensities of Sn isotopes as internal standards, and a computer to deconvolute concurrent lines. A precision of better than ±5% was regularly achieved.

Results and Discussion

The results obtained by the different techniques, and their mean values, are given in Table 1. These results and those reported on Apollo 14 materials warrant the following conclusions:

1. The weak analysis lines for the rare earth elements where the material is directly analyzed by the spark mass spectrographs are overcome by using our extraction pre-concentration step. The 5% precision of this method seems very satisfactory. The direct and extraction methods can be compared for the elements

ANALYSIS OF LUNAR SAMPLES

A. Strasheim

Ba, Ce, and La. For Ba, by using equal intense lines in both methods, satisfactory comparative results were recorded. For the elements Ce and La the results of the extraction technique are preferred.

2. The samarium anomaly reported by Wakita[2] for the Apollo 14 is less significant for these three Apollo 15 samples.
3. The chemical results indicate that sample 15301,75 (fines) differ significantly from the gabbro (15065,32) and basalt (15556,12) samples. This fines sample's composition is similar to that of the three Apollo 14 samples analyzed by us.
4. The significant difference between the two groups of samples indicated in (3) above is that the elements Si, Al, K and Zr are present in lower concentrations in 15065 and 15556 than in the Apollo 14 materials and the fines sample 15301. The reverse is true for the elements Zr, Ba, Fe and Nb.
5. Using the $^{7}Li/^{6}Li$ relation the ages for the samples 15065,32 15301,75 and 15556,12 are, respectively, 3.30, 3.26 and 3.05 x 10^{9} years.

References

1. A. Strasheim, P. F. S. Jackson, J. H. J. Coetzee, F. W. E. Strelow, F. T. Wybenga, A. J. Gricius, M. L. Kokot, and R. H. Scott, "Analysis of lunar samples 14163, 14259, and 14321 with isotopic data for $^{7}Li/^{6}Li$," *Proceedings Third Lunar Science Conference, Vol. 2*, 1972.
2. H. Wakita, D. L. Showalter, and R. A. Schmitt, *Third Lunar Science Conference*, Houston, 1972.

TABLE 1: CHEMICAL ANALYSES OF LUNAR SAMPLES

	15065-32						15301-75						15556-12					
	CHEM	XRP	AA	XRF	MS	AVERAGE	CHEM	XRP	AA	XRF	MS	AVERAGE	CHEM	XRP	AA	XRF	MS	AVERAGE
MAJOR (%)																		
SiO_2	47.02	47.4		47.31		47.24	46.59	45.7		47.2		46.5	-	46.6	47.0	44.99		46.2
Al_2O_3	9.32	9.53		9.15		9.33	14.48			14.8		14.64	9.41	9.36		9.54		9.44
Fe	19.25	18.91		19.34		19.17	13.74	13.96	13.42	13.58		13.68	21.62	21.72		21.51		21.62
MgO	10.60	10.52		10.95		10.69	12.00	12.48		12.50		12.33	7.85	8.29		8.11		8.09
CaO	9.57	9.71		9.31	8.9	9.53	10.45	10.70	9.65	9.87		10.17	10.41	10.58	10.55	10.64	10.5	10.54
K_2O	0.042	0.05			0.06	0.05	0.151	0.14		0.11	0.12	0.13	0.043	0.05	0.06	0.08	0.05	.06
TiO_2	1.53	1.57		1.42	1.65	1.54	1.16	1.22		1.18	1.27	1.19	2.65	2.68		2.65	2.72	2.68
MnO	-	0.255	0.27	0.27	0.24	0.26	-	0.160	0.16	0.16	0.18	0.16	0.29	0.250	0.27	0.28	0.23	0.26
Cr_2O_3	-	0.68	0.57	-	0.68	0.64	-	0.35	0.34	-	0.35	0.35		0.64	0.61	-	0.63	0.63
P_2O_5	-	0.06	-	0.09	-	0.08	-	0.15	-	0.14	-	0.15	-	0.08	-	0.09	-	.08
Na_2O	0.26		0.19	-	-	0.23	0.34	-	0.24	-	-	0.29	0.26	-	0.18	-	-	.22
TOTAL (%)						98.76						99.59						99.82

	15065-32			15301-75				15556-12					15065-32	15301-75	15556-12
	XRP	MS	AVERAGE	CHEM	XRP	MS	AVERAGE	CHEM	XRP	MS	AVERAGE		MS*	MS*	MS*
Zr	68	90	79		225	229	227	67	75	114	85	Ce	30.0	42.0	16.0
V	180	190	185	61	84	83	76	270		240	255	Pr	3.7	5.7	2.6
Ni	76	80	78	205	199	165	190	72	40	60	57	Nd	20.0	24.7	10.8
Co	50	44	47	-	51	50	51	49	47	50	49	Sm	5.0	8.1	3.95
Y	29	29	29		65	65	65		31	32	32	Eu	1.05	1.19	1.1
Sr	86	110	98		104	110	107		88	104	96	Gd	5.6	8.05	4.5
Rb	8	3.0	5		4	1.6	3		6	0.3	3	Tb	0.86	1.60	0.85
Zn	< 5				24				< 5			Dy	6.8	9.90	5.3
Cu	43	53	48		15	20	17		3	15	9	Ho	1.25	2.22	1.3
Sc		88				34				35		Er	3.9	5.78	2.85
Nb	11	15	13		18	22	20		7	8	8	Tm	0.47	1.0	0.48
Ba	80	90	85		215	210	213		90	80	85	Yb	2.9	5.5	2.5
La		6.3				6.7				7		Lu	0.3	0.65	0.33
Ce		18.2				23.3				20		Ba	84	207	74
$^7Li/^6Li$		13.5				13.3				12.2		La	7.1	11.0	3.7

CHEM: Wet chemical; XRP: X-Ray powder; XRF: X-Ray fusion; AA: Atomic Absorption; MS: Mass spectrography

*Extraction procedure

CHEMISTRY OF PYROXENES FROM APOLLO SOIL 15501,53. H. C. Jim Taylor and James L. Carter, The University of Texas at Dallas, Geosciences Division, Dallas, Texas 75230. Contribution no. 221.

Delineation of the individual soil and rock types in a composite lunar soil sample can be achieved by electron microprobe studies of the mineral chemistry of a representative set of fragments from a soil sample. This should provide information on the rate of mixing of different soil types and permit identification of rock types not returned as hand specimens. Pyroxenes are ideally suited for this purpose because of their wide range of chemistry and abundance in most lunar types. In soil sample 15501,53, for example, pyroxene fragments are more abundant than plagioclase fragments by approximately 4 to 1.

Partial analyses of 64 pyroxene fragments from the less than 1 mm fraction of the comprehensive sample 15501,53 were obtained using an ARL scanning electron microprobe with an energy dispersive X-ray analyzer. Analyses for Si, Fe, Mg, Ca, Ti, and Al were made on fragments within the 75 to 150 micron fraction. These occurred primarily as individual grains, but also occurred as components within microcrystalline fragments, agglutinates, and microbreccias.

The pyroxene fragments analyzed cover a wide area of the pyroxene quadrilateral (Fig. 1), ranging from augites, subcalcic augites, and low-calcium, magnesium pyroxenes to ferroaugites, subcalcic ferroaugites, and pyroxferroites. No one type is dominant but the distribution is not random. Plots of the chemical components clarify the possible trends. For example, the plot of Al/Si versus Fe/Mg (Fig. 2) suggests two distinct trends; one of increasing alumina enrichment similar to the early trend of rock 15499 (1). The other is a very distinct trend of extreme iron enrichment which suggests the presence of a genetically separate group of pyroxene fragments in this soil sample. The plot of Ti versus Al (Fig. 3) is consistent with the conclusion that more than one genetic unit is represented by these pyroxenes.

The mixing of genetically unrelated fragments from different lunar localities could result in the observed variation of pyroxene chemistry. Such a process, based upon the efficiency of meteoritic impacts into the lunar regolith as a transport and mixing mechanism, may explain the extreme variations noted. The trends observed are consistent with the mixing of soils from the rill area and the ray trending through the LM site (2). Alternatively, a wide range of melt compositions combined with the partitioning of chemical components between the melt and crystalline phases could explain the variation in the observed pyroxene chemistry.

References

(1) Bence, A.E., Proc. 7 Nat. Conf. EPA, EPASA, 51A-51C, 1972.
(2) Apollo 15 Prel. Exam. Team, Sci. 175, 363-375, 1972.

CHEMISTRY OF PYROXENES

H.C. Jim Taylor

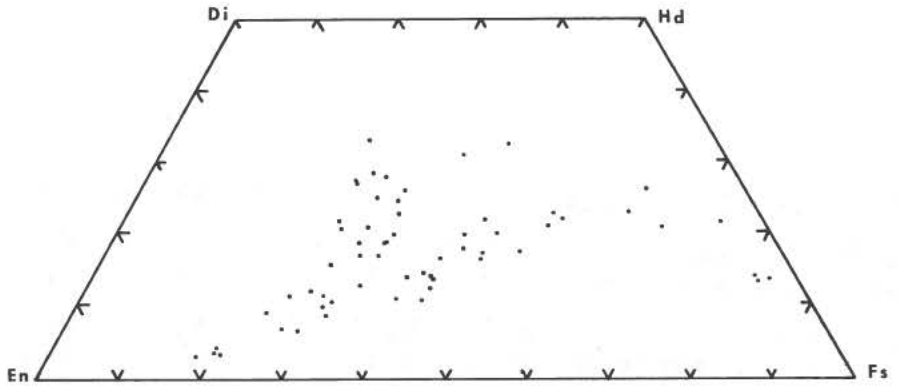

Fig. 1. Composition of pyroxenes.

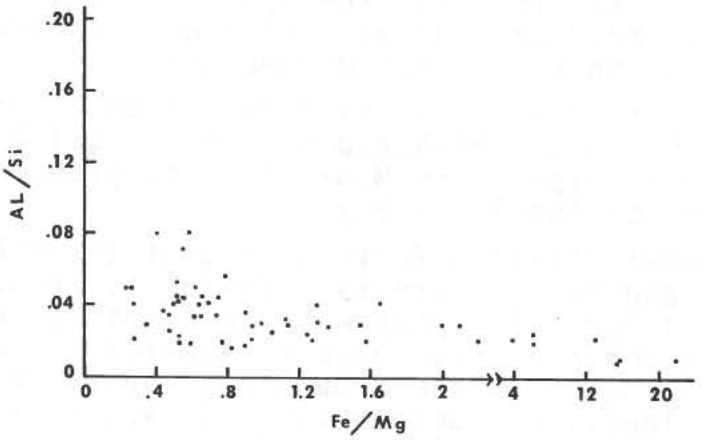

Fig. 2. Al/Si vs. Fe/Mg (atomic proportions, O = 6).

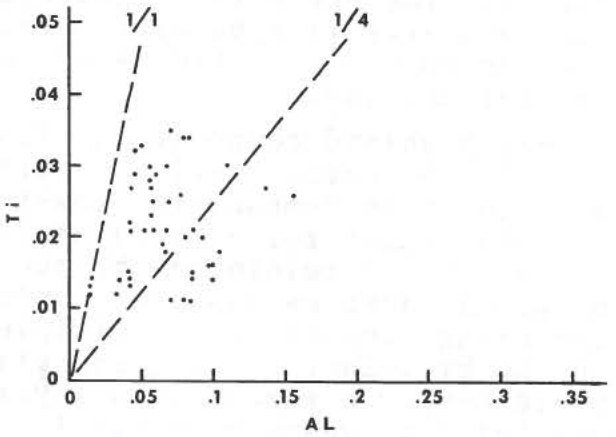

Fig. 3. Ti vs. Al (atomic proportions, O = 6).

COMPOSITION OF THE LUNAR HIGHLANDS II THE APENNINE FRONT

S.R.Taylor, M. Gorton, P.Muir, W.Nance, R.Rudowski and N. Ware
Dept.of Geophysics & Geochemistry,Australian National University.

Breccias: For many elements (REE, Th, Y, Zr, Hf, Nb, Ba),breccia compositions can be represented by a two component model (Fig.2) whose end members are highland basalt (15455 white)and low K Fra Mauro basalt (15455 black). Most Apollo 15 breccias contain more Cr, V, Sc, Co and less Sr and Eu, indicating that a third more basic component is present. The Apollo 16 soil 68501 composition fits a 58/42 mix for most elements, indicating a widespread distribution of the two components.

Soils: These consist of variable mixtures of mare, low-K Fra Mauro, high-K Fra Mauro and Highland basalts. Soil 15031 (L.M. Station 8) is rich in High K Fra Mauro basalt, probably derived from the Aristillus or Autolycus ray.

Green glass: The most striking feature is that the REE contents are low (Table 1) and the pattern is parallel to chondrites (Fig. 1). Only a slight Eu depletion is present ($Eu/Eu^{+}=0.86$). REE, Th, U, Zr, Ba contents fit those of howardites, but Cr, V, Sc, Co are higher. Glass is too abundant to be ray material and is considered lunar, not meteoritic. If so, it is the most primitive lunar composition yet analysed.

15016: This mare derived vesicular basalt has a small Eu depletion ($Eu/Eu^{+}=0.76$). The REE pattern resembles that of the green glass, but its chemistry is typically mare, and the glass has a more primitive composition. 15016 is probably derived by a high degree of partial melting.

Conclusions: The lunar highland compositions from the Apennine front (Apollo 15) and the Descartes region (Apollo 16) are probably dominated by two main components, low-K Fra Mauro and Highland basalts. This argues for a broad uniformity in highland composition, a conclusion reinforced by the orbital XRF data. Possible original layering has been destroyed by the intense highland cratering, resulting in multiple mixing of these components in the breccias. The green glass composition represents a probable deeper pyroxene rich layer and is a possible source material from which mare basalts could be derived by partial melting.

LUNAR HIGHLAND COMPOSITION

S.R. TAYLOR

Table 1

	Breccias white 15455	Breccias black 15455	Breccias 15459	Soils 15301	Soils 15271	Soils 15031	Apollo 16 68501	Glass 15426	Rock 15016
Station	7	7	7	7	6	8	8	7	3
Cs	-	0.16	0.15	.19	.22	.21	0.09	-	-
Rb	-	2.7	3.4	3.1	5.7	5.9	2.3	0.34	0.83
Ba	42	370	230	227	360	390	185	17	61
Pb	1.0	3.0	3.3	3.3	2.8	3.0	2.2	0.53	0.56
Sr	218	141	108	98	141	200	170	24	93
Sr/Eu	162	78	92	84	95	111	132	115	107
La	2.9	32	19	17.9	27	33	15.7	1.4	5.3
Ce	6.7	81	51	45	76	85	41.5	3.8	14.4
Pr	0.92	11.5	6.5	6.4	10	12.7	5.54	0.53	2.0
Nd	3.55	47	27	25.8	41.5	52	21.6	2.2	9.6
Sm	0.85	12.8	8.7	8.25	10.6	15.1	6.32	0.76	3.42
Eu	1.63	1.82	1.18	1.16	1.48	1.80	1.29	0.21	0.87
Gd	0.92	15.5	11.5	9.4	12.2	17	7.57	0.91	4.5
Tb	0.14	2.41	1.74	1.55	1.99	2.78	1.23	0.15	0.73
Dy	0.82	16	10.8	10.4	13.3	17.4	8.35	1.10	4.55
Ho	0.17	3.76	2.68	2.44	2.91	4.11	1.92	0.27	1.10
Er	0.44	10.7	7.7	6.83	9.2	11.6	5.45	0.80	2.86
Tm calc.	0.06	1.6	1.2	1.1	1.4	1.8	0.75	0.15	0.40
Yb	0.38	9.8	7.2	6.40	8.65	10.9	4.95	0.93	2.42
ΣREE	20	247	157	144	218	304	122	13.4	53
Eu/Eu^{+}	6.4	0.43	0.41	0.45	0.44	0.38	0.62	0.86	0.76
Y	4.8	93	63	51	86	105	49	7.2	26
Th	0.23	5.31	3.71	3.33	4.37	4.8	2.45	0.08	0.50
U	0.05	1.37	0.87	0.93	1.16	1.2	0.63	0.02	0.12
Th/U	4.2	3.9	4.3	3.6	3.8	3.7	3.9	4.0	4.1
Zr	42	480	294	251	390	540	220	22	94
Hf	0.17	9.8	6.2	5.7	7.1	10.6	4.0	0.42	2.04
Zr/Hf	247	49	51	44	55	51	55	51	46
Nb	0.95	33	19	16.3	24.5	33	14.9	1.5	6.2
Zr/Nb	44	14.5	15.5	15.4	15.9	16	14.8	15	15.1
Cr	440	1800	2150	3000	2400	2600	1000	2800	4100
V	16	39	96	125	76	86	27	150	140
Sc	-	13	23	17	19	14	6	43	25
Ni	12	184	232	197	220	222	420	170	74
Co	10	22	42	56	40	44	34	72	56
Cu	1.3	3.3	4.4	4.7	9	8	4.5	3.5	10

All data in p.p.m.(wt.). Analytical methods : Spark source mass spectrography except for Cr, V, Sc, Ni, Co, Cu (emission spectrography)

LUNAR HIGHLAND COMPOSITION

S.R. TAYLOR

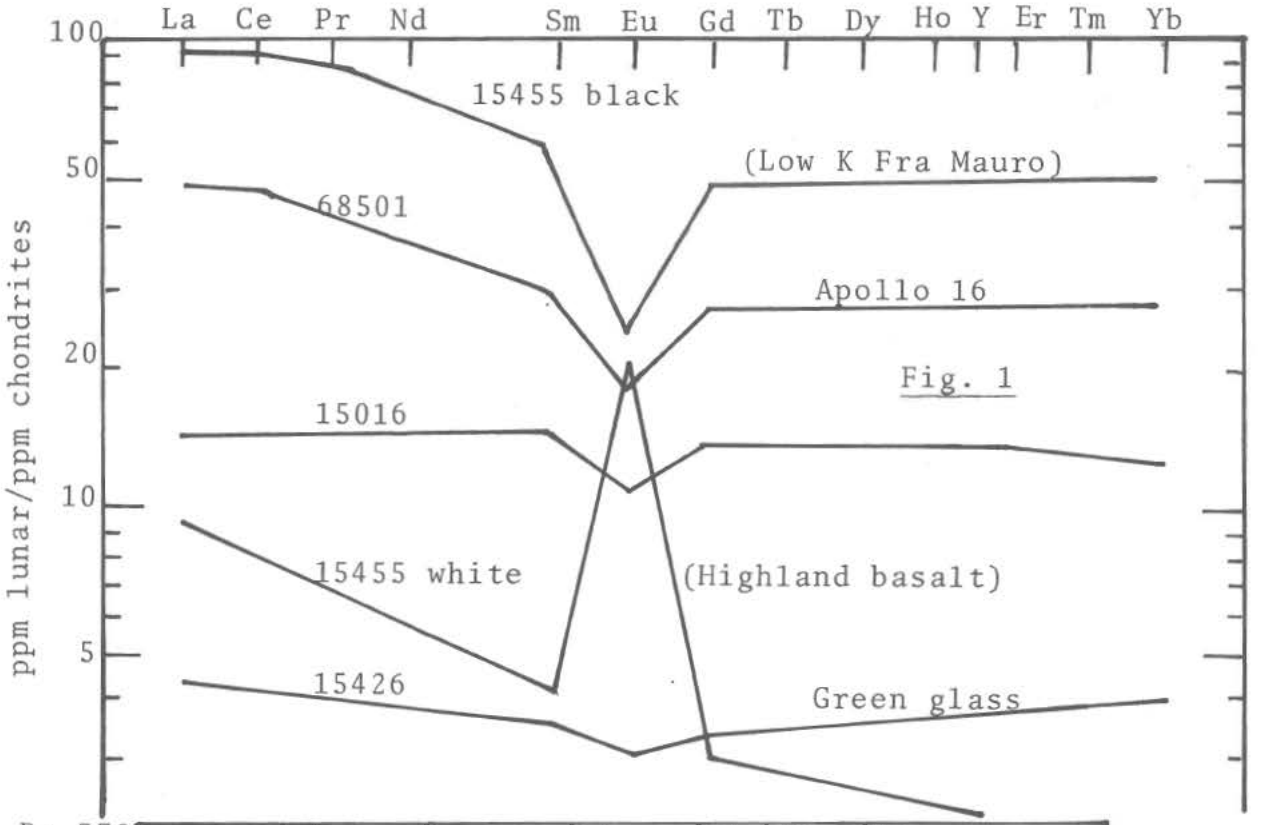

Fig. 1

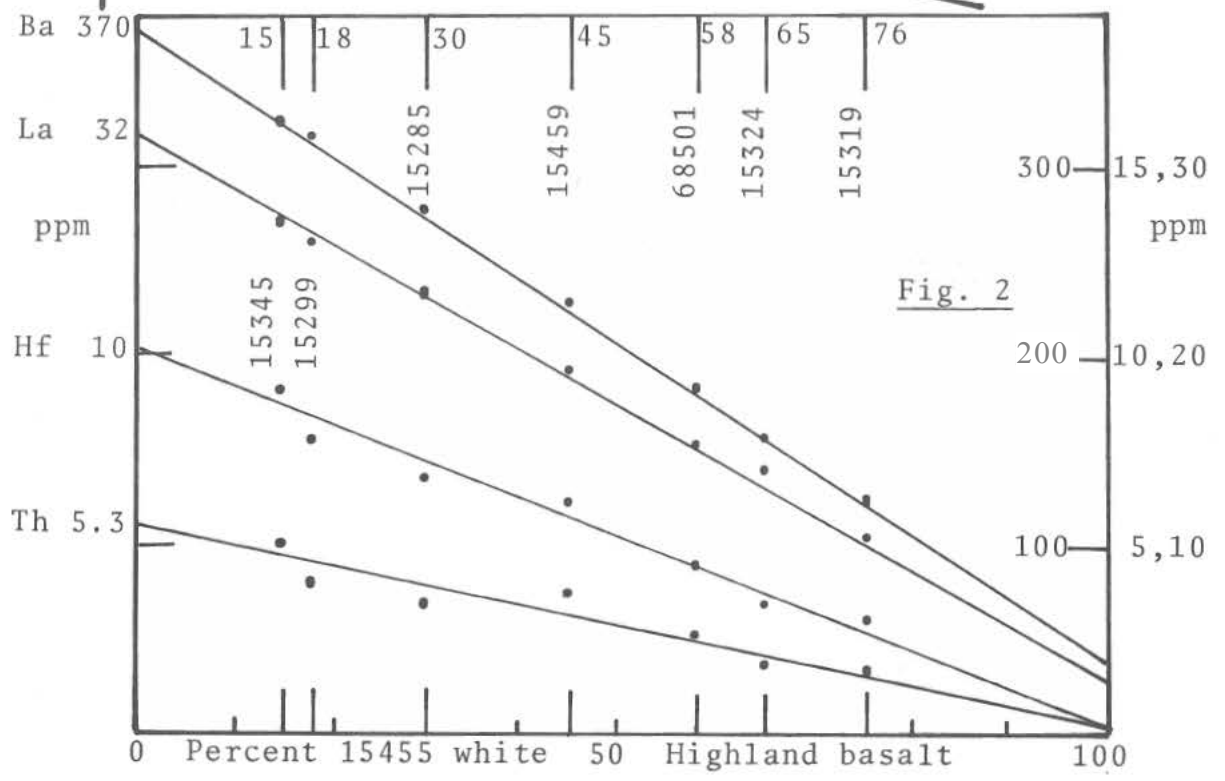

Fig. 2

MULTIELEMENT ANALYSES AND A COMPARISON OF THE DEGREE OF OXYDATION OF LUNAR AND METEORITIC MATTER

H. Wänke, H. Palme, B. Spettel, and F. Teschke
Max-Planck-Institut für Chemie (Otto-Hahn-Institut), Mainz, Germany

In the Figs. 1 to 4 we have plotted the elements U, Ba, K, and W against La. The nearly perfect linear correlation of U and La (Fig.1) for all lunar samples, terrestrial granite and basalt as well as for various meteorite classes over about three orders of magnitude indicates the geochemical similarity of the two elements. Similar correlations are observed for many other large ion lithophile elements, we only give as one further example Ba vs. La (Fig.2). Potassium another LIL element seems to be depleted in terrestrial samples compared to chondrites and is even more depleted for the lunar samples and some rare meteorite classes. The similar variation of the K/U-ratio has been discussed by many authors[2]. Here we only want to point out the constancy of the K/La-ratio for lunar samples, basaltic achondrites and the silicate phase of mesosiderites.(Fig. 3).

Surprisingly, the correlation to La holds for some other trace elements with medium ion radius also, e.g. for tantalum (Ta^{+5} R=0.684 A), hafnium (Hf^{+4} R=0.78 A), and tungsten (W^{+4} R=0.70 A).

We find the W-La-plot especially interesting. W shows the same linear correlation with La (Fig.4) both for the lunar samples and for the basaltic achondrites (the eucrites: Juvinas and Stannern. Howardite: Kapoeta). Terrestrial samples seem to have a somewhat different W/La-ratio, but the chondritic value is about a factor 17 off. Of course, tungsten will be found always highly concentrated in the metal phase. The distribution of W between metal and silicate depends on the degree of oxydation. Hence, we are forced to conclude that both the moon and the parent body of the eucrites have had an identical degree of oxydation. This finding is another indication that the fractionation of chondritic to eucritic (howarditic) matter occured prior to accretion as suggested previously by various authors[3,4,1]. Consequently, the moon or at least the outer 200 km of the moon was formed of eucritic matter.

Nine Apollo 15-samples (1 breccia and 8 soil samples) were analysed for all major and many minor and trace elements (24 elements altogether). All determinations given here in Table 1 were obtained by INAA only. For sample 15601 many other elements were analysed via RNAA (for data see[1]. Several samples were analysed prior to RNAA by Wasson and coworkers.

Multielement Analyses

H. Wänke

%	15021 -80 Fines LM	15080 - 3 Fines Stat.1	15091 -36 Fines Stat.2	15211-8 Fillet boulder Stat.2	15231-51 Soil ben. boulder Stat.2	15299 -14 Brecc. Stat.6	15471 -29 Fines Stat.4	15531 -46 Fines St.9a	15601 -45 Fines St.9a	%accuracy
O	43.8	42.6	43.8	43.7	43.9	42.8	42.7	41.1	41.8	1
Mg	6.32	6.72	6.29	6.49	6.38	6.64	6.99	6.84	6.77	4
Al	7.46	7.33	9.32	9.12	9.48	8.61	7.08	5.22	5.67	2
Si	20.0	22.5	21.9	21.8	22.0	21.7	22.6	21.7	21.8	1
Ca	6.5	8.0	7.9	8.0	8.0	8.4	7.1	6.7	6.7	10
Ti	1.1	0.9	0.6	0.7	0.6	0.9	0.7	1.3	0.9	20
Fe	11.6	12.6	8.9	8.8	8.9	9.2	12.8	15.9	15.0	3
ppm										
Na	2890	2680	2980	2930	2930	3280	2470	2110	2260	5
K	1650	1230	1380	1440	1430	1630	1000	720	870	5
Sc	26.6	31.6	21.0	21.1	21.0	23.2	31	39.9	36.3	5
Cr	2500	3040	2120	2070	2110	2290	2980	3810	3540	5
Mn	1420	1530	1160	1160	1120	1200	1560	1960	1880	5
Co	42	50	40,0	37.0	36.6	39.6	14.6	55	51	5
La	25	18.1	20.1	20.6	20.3	26.6	45	10.6	12.9	5
Nd	-	33	33	-	34	48	-	24	-	20
Sm	9.7	9.4	9.4	10.1	9.9	11.9	-	5.9	5.1	10
Eu	1.34	1.33	1.29	1.33	1.33	1.51	1.12	1.04	1.03	5
Tb	-	2.4	2.5	2.7	2.7	2.5	1.8	1.8	1.6	10
Dy	16.5	11.3	13.6	14.6	13.4	14.1	9.7	8.0	9.4	10
Ho	-	3.1	-	3.2	3.5	3.6	-	2.0	1.6	10
Yb	8.3	6.5	6.8	7.4	6.4	8.5	5.1	3.9	4.7	5
Lu	1.20	0.95	0.90	0.90	0.95	1.15	0.72	0.67	0.77	10
Hf	8.8	6.7	6.9	7.2	7.0	8.7	5.5	3.9	4.4	10
Ta	1.20	0.79	0.95	0.97	0.86	1.06	0.68	0.52	0.46	15
Σ %	99.5	101.5	99.4	99.4	99.9	99.1	100.8	99.8	99.6	

Mixing model calculation will be presented elsewhere. As can be seen from Table 1 the chemical composition of the various soil samples differs from station to station but is identical for different samples of the same station. One should note in particular the identity (within our errors) of the chemical composition of the three samples from station 2. Sample 15091 is a normal soil sample, 15231 was taken from beneath a large boulder and sample 15211 is the fillet next to another large boulder.

1) Wänke H., Baddenhausen H., Balacescu A., Teschke F., Spettel B., Dreibus G., Palme H., Quijano-Rico M., Kruse H., Wlotzka F., and Begemann F. (1972) Proc. Third Lunar Sci. Conf., Geochim. Cosmochim. Acta, in press.

Multielement Analyses

H. Wänke

2) LSPET (1969), Science 165, pp. 1211 - 1227.
3) Tera F., Eugster O., Burnett D. S., and Wasserburg G.J.(1970), Proc. Apollo 11 Lunar Sci.Conf., Geochim.Cosmochim.Acta Suppl.1, Vol.2, pp. 1637 - 1657.
4) Gast P.W. and McConnell R.K., Jr. (1972), Lunar Science-III (editor C.Watkins), pp.289-290, Lunar Science Institute Contr.No. 88.

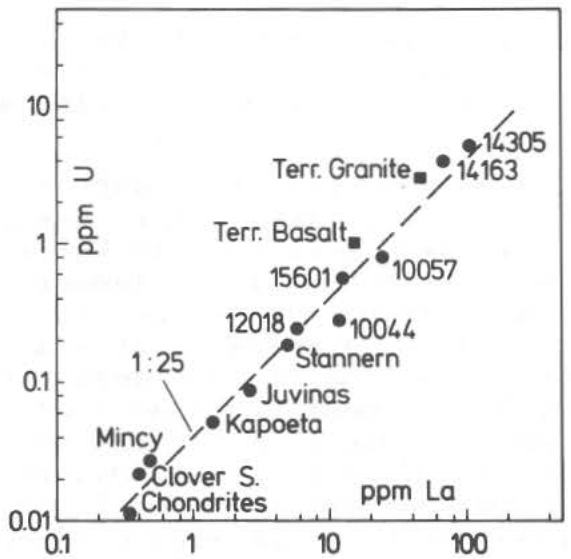

Fig. 1

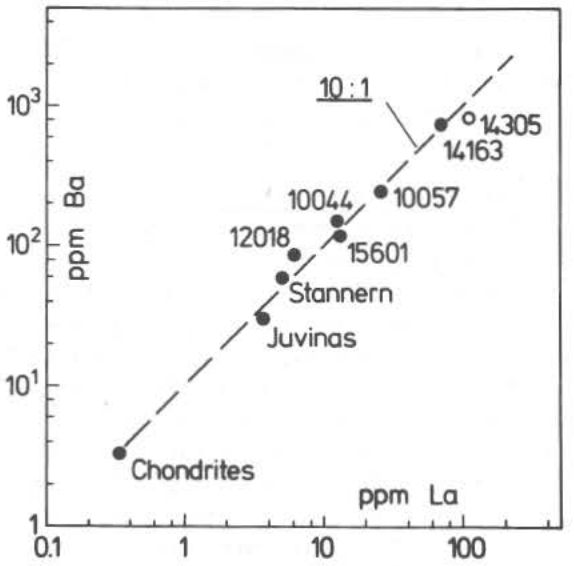

Fig. 2

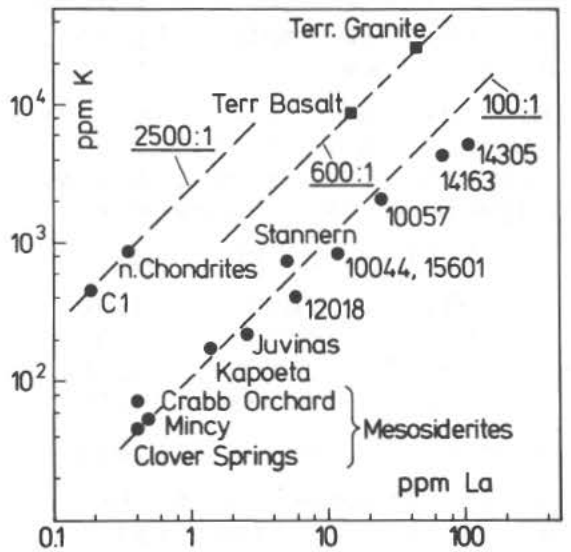

Fig. 3

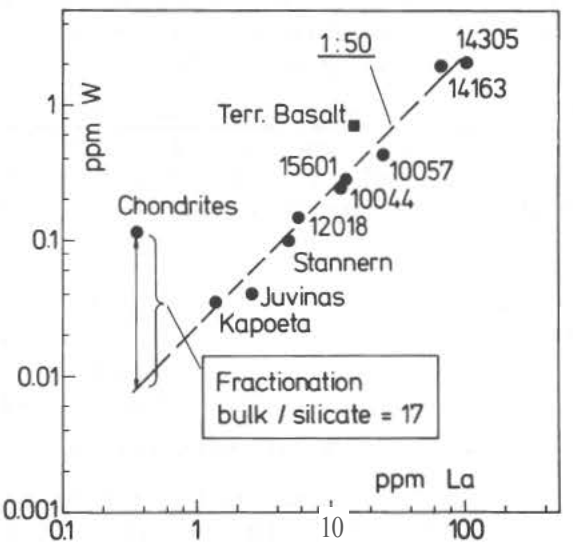

Fig. 4

GEOCHEMICAL FEATURES OF APOLLO 15 MATERIALS.

J.P.Willis, A.J.Erlank, J.J.Gurney and L.H.Ahrens, Department of Geochemistry, University of Cape Town, Rondebosch, South Africa.

Our major and trace element data, derived as before by X-ray fluorescence analysis, are presented in Table 1. We use these data, together with that which we have previously reported, including 15101,67 [1][2], to make the following observations.

1. Rocks and Fines. The data in Table 1 support the general conclusions presented by LSPET (1972)[3]. The high-Fe mare basalts are similar to the Apollo 11,12 and 14 low-K mare basalts but two (15058 and 15557) contain lower amounts of incompatible elements (K,Ba,Zr,Nb,Y) than any others we have analysed, due either to larger degrees of partial melting or smaller degrees of crystal fractionation during their formation. As at the other sites, the Apollo 15 soils have higher incompatible element abundances and lower Ca/Al ratios than the mare basalts, indicating the presence of varying amounts of KREEP type basalt and anorthositic material respectively. It is not yet possible to characterize exactly the KREEP basalt present in Apollo 15 fines although present evidence shows it to be very similar, with respect to incompatible elements, to that present in Apollo 14 fines. However, the rock-fines mixing lines shown in the Zr-Y plot (Fig.1) reveal subtle differences in the trace element character of KREEP materials at the different Apollo sites. Fractionation of Y is implied by the relative constancy of K/Zr and Zr/Nb at all sites.

2. Interelement relationships. Interelement ratios given in Table 1 confirm the close relationships we have previously observed [1][2][4] for some pairs of incompatible elements. Relevant statistics for all samples (20) analysed by us to date are:

	K/Ba	K/Zr	K/Nb	Zr/Nb	Zr/Ba
Median	6.10	4.23	67.1	16.0	1.40
Mean	6.09	4.22	68.5	16.3	1.45
s	0.74	0.46	9.17	1.60	0.20
c,%	12.1	11.0	13.4	9.83	13.2

(s = standard deviation, c = coefficient of variation)

There are no noticeable systematic differences in these ratios between the various sample sites. Involatile (refractory) element relationships (Zr/Nb, Zr/Ba) are closely similar to those observed by us in stony meteorites and this may also apply to Zr-Y if mare basalts (Fig.1) are more representative of the moon as a whole.

GEOCHEMICAL FEATURES OF APOLLO 15 MATERIALS

J.P. Willis.

TABLE 1 CHEMICAL ANALYSES OF APOLLO 15 SAMPLES

MAJOR ELEMENTS (%)

	15205,37 Breccia	15021,15 Fines	15411,18 Fines	15557,29 Rock	15495,58 Rock	15058,39 Rock
SiO_2	51.03	47.23	46.22	45.01	48.00	48.47
TiO_2	1.99	1.73	1.09	2.53	1.80	1.60
Al_2O_3	14.92	13.92	15.08	8.84	9.57	8.90
FeO*	11.28	15.11	13.36	22.68	20.07	19.75
MnO	0.159	0.196	0.176	0.284	0.261	0.274
MgO	8.23	10.30	11.74	9.38	8.42	9.56
CaO	9.94	10.57	10.91	9.99	10.43	10.23
Na_2O	0.73	0.37	0.36	0.25	---	0.28
K_2O	0.528	0.205	0.159	0.045	0.062	0.038
P_2O_5	0.557	0.230	0.167	0.071	0.090	0.049
Cr_2O_3	0.34	0.42	0.37	0.58	0.51	0.66
S	0.080	0.095	0.077	0.090	---	0.057
Subtotal	99.784	100.376	99.709	99.750	(99.213)	99.868
$O \equiv S$	0.040	0.048	0.039	0.045	---	0.029
Total	99.74	100.33	99.67	99.71	---	99.84

* Total Fe as FeO.

TRACE ELEMENTS (PPM)

Ba	673	289	200	55	---	49
Nb	59.4	25.3	17.4	6.1	7.7	4.9
Zr	979	402	275	88.4	126	70.9
Y	201	86.2	61.5	24.2	32.2	21.1
Sr	171	135	111	96.4	114	99.2
Rb	14.4	6.3	4.3	< 2	< 2	< 2

INTERELEMENT RATIOS

Ca/Al	0.90	1.03	0.98	1.53	1.47	1.55
K/Ba	6.51	5.89	6.60	6.80	---	6.43
K/Zr	4.48	4.23	4.80	4.23	4.09	4.44
K/Nb	73.8	67.3	75.9	61.3	66.9	64.3
Zr/Nb	16.5	15.9	15.8	14.5	16.4	14.5
Zr/Ba	1.45	1.39	1.38	1.60	---	1.45

GEOCHEMICAL FEATURES OF APOLLO 15 MATERIALS

J.P. Willis

Lack of selective fractionation of involatile elements between the moon and stony meteorites implies that the enrichment of these elements in KREEP materials is produced by fractionation processes within the moon. Volatile-involatile element relationships negate the suggestion that selective volatilization has been an important process in producing the low abundances of heavy alkali metals in lunar lavas. Furthermore, these relationships place restrictions on the manner in which the moon formed. It has been postulated[5][6] that the moon accreted as a heterogeneous body in which refractory elements are relatively enriched in the outer regions of the moon, with the older KREEP type basalts being derived from shallower depths than the mare basalts. The constancy of K/Ba,K/Zr and K/Nb in our samples implies a similar constancy for the separate source regions involved and this is in conflict with a simple volatility dependent heterogeneous accretion model.

(3) Breccia 15205 LSPET (1972)[3] noted that breccia 15206, which is from the same large boulder as 15205 (Station 2 on the Appenine Front),contained a higher K content (0.45%) than any other Apollo 15 sample analysed and was similar to Apollo 14 breccia samples. Table 1 confirms the high concentration of incompatible elements in 15205; in this respect 15205 is closely similar to 14259 soil. This is shown in Fig.1 which also suggests that 15205 is unrelated to other Apollo 15 materials, agreeing with the observation that 15205 is a recent arrival at Station 2[7]. It is unique amongst the Apollo 15 breccias[8] and its high SiO_2 content (7.0% normative quartz) is noteworthy. The nearest comparable major element analyses are for Type D Fra Mauro glasses which have 9% normative quartz[9]; however these contain more Al and less Mg. 15205 with its two types of non-mare basalt and lack of anorthosite clasts appears to contain a distinctive type of KREEP material and further study is recommended.

References:

1. J.P. Willis et al, Proc.2nd Lunar Sci. Conf. 2, 1123 (1971).
2. J.P. Willis et al, Proc.3rd Lunar Sci. Conf. In Press.
3. LSPET, Science, 175, 363 (1972).
4. A.J. Erlank et al, In Lunar Science - III, 239 (1972).
5. P.W. Gast and R.K. McConnell, Jr., In Lunar Science - III,289 (1972).
6. A.E. Ringwood, In Lunar Science - III, 651 (1972).
7. Apollo 15 Preliminary Science Report, NASA SP-289 (1972)
8. Apollo 15 Lunar Sample Information Catalogue,MSC 03209 (1971)
9. Apollo Soil Survey, Earth Planet. Sci.Lett. 12, 49 (1971).

GEOCHEMICAL FEATURES OF APOLLO 15 MATERIALS

J.P. Willis.

FIG. 1.

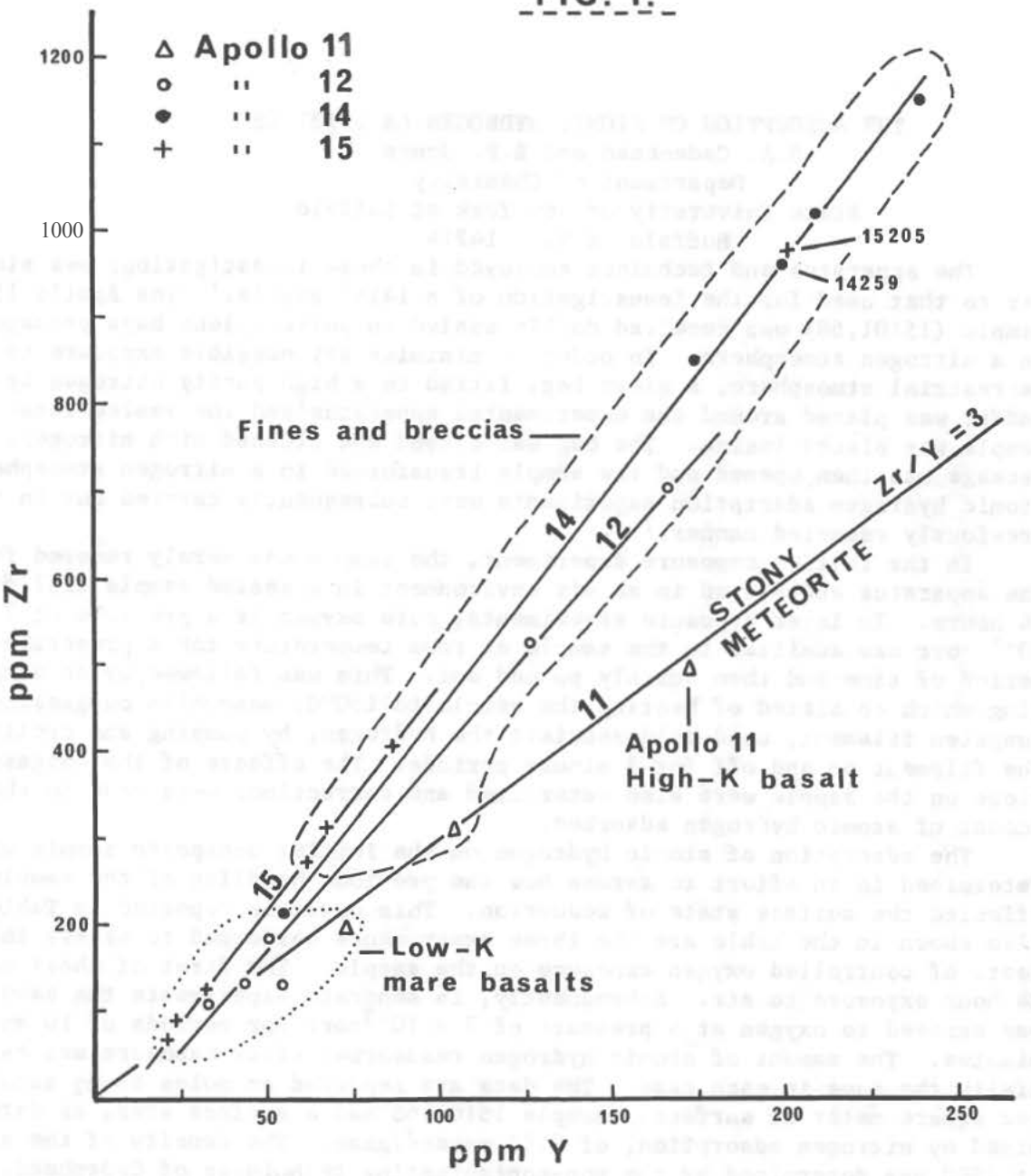

Acknowledgments: We thank Henri Fortuin for analytical assistance and the C.S.I.R., Pretoria, and UCT Staff Research fund for financial support.

THE ADSORPTION OF ATOMIC HYDROGEN ON 15101,68

D.A. Cadenhead and B.R. Jones
Department of Chemistry
State University of New York at Buffalo
Buffalo, N.Y. 14214

The apparatus and technique employed in these investigations was similar to that used for the investigation of a 14163 sample.[1] The Apollo 15 sample (15101,68) was received doubly sealed in polyethylene bags packaged in a nitrogen atmosphere. In order to minimize any possible exposure to a terrestrial atmosphere, a glove bag, fitted to a high purity nitrogen cylinder, was placed around the experimental apparatus[1] and the sealed lunar fine sample was placed inside. The bag was closed and flushed with nitrogen. The package was then opened and the sample transformed in a nitrogen atmosphere. Atomic hydrogen adsorption experiments were subsequently carried out in the previously reported manner.[1]

In the initial exposure experiment, the sample was merely removed from the apparatus and stored in an air environment in a sealed sample vial for 24 hours. In later exposure experiments, pure oxygen at a pressure of 7 x 10^{-3} torr was admitted to the sample at room temperature for a prescribed period of time and then quickly pumped out. This was followed by an outgassing which consisted of heating the sample to 150°C, meanwhile outgassing the tungsten filament, used to dissociate the hydrogen, by pumping and cycling the filament on and off for 3 minute periods. The effects of the outgassing alone on the sample were also determined and corrections were made to the amount of atomic hydrogen adsorbed.

The adsorption of atomic hydrogen on the initial unexposed sample was determined in an effort to assess how the previous handling of the sample had affected the surface state of reduction. This datum is reported in Table I. Also shown in the table are the three experiments performed to assess the effects of controlled oxygen exposure on the sample. The first of these was a 24 hour exposure to air. Subsequently, in separate experiments the sample was exposed to oxygen at a pressure of 7 x 10^{-3}torr for periods of 10 and 30 minutes. The amount of atomic hydrogen readsorbed after exposure was essentially the same in each case. The data are reported as moles of H_2 adsorbed per square meter of surface. Sample 15101,68 had a surface area, as determined by nitrogen adsorption, of 0.65 meter^2/gram. The density of the sample at 25°C was determined by the non-contaminating techniques of Cadenhead, et al[2] and found to be 3.1 g/cc. (Table I)

The results indicate that the sample, as initially received, was not in the fully reduced state one would expect for a surface lunar sample. The amount of atomic hydrogen adsorbed represents a surface coverage of 380 Å^2 per H atom. Further, the controlled exposure experiments show that partial rapid oxidation of the fully reduced surface is brought about by an exposure of less than 10 minutes to a low pressure of oxygen at room temperatures.

The Adsorption of Atomic Hydrogen on 15101,68

D.A. Cadenhead

It should be noted that the degree of oxidation was essentially the same after a 24 hour exposure to a much higher pressure of oxygen. The surface coverage in both these cases was 140 A^{o2}/atom.

In previous investigations carried out in this laboratory,[1] the surface reduction of another lunar sample 14163,111 was studied. This fine material had undergone extensive air exposure over a period of several months and, as received from N.A.S.A., adsorbed 12.0 x 10^{-7}moles/meter^2 of hydrogen expressed as H_2. After an 18 hour exposure to 7 x 10^{-3}torr of oxygen it readsorbed only 6.9 x 10^{-7}moles/meter^2. The surface coverages were, respectively, 50 A^{o2} and 120 A^{o2} per H atom. A detailed comparison of the Apollo 14 and 15 samples cannot be made because of their distinctly different composition. However, the closeness of the agreement of the amount of atomic hydrogen adsorbed after a brief (up to 24 hour) exposure to oxygen, suggests that they are behaving in a qualitatively similar manner. On this basis then, it would seem that the Apollo 15 sample was much less contaminated by collection and handling since it initially adsorbed only one-sixth as much atomic hydrogen. In addition, both samples appear to have undergone a rapid surface oxidation to approximately the same extent, readsorbing atomic hydrogen to a surface coverage of 120-140 A^{o2}/atom. There also appears to be a second, much slower, type of oxidation occuring as shown by the data for the Apollo 14 sample. The amount of atomic hydrogen adsorbed after months of exposure to air being approximately twice the adsorption after exposure of one day.

While more extensive studies may be required before the generality of these observations can be established, it would seem that the findings for 14163,111 may be considered atypical in that it suffered exceptional exposure and contaminating conditions. The results for 15101,68 probably indicate more typical exposure conditions. Thus, in addition to nitrogen, exposure to various gases from lunar module, astronaut and sample container atmospheres, as well as trace impurities in the nitrogen can all result in changes in the lunar sample surface composition. At this point in the study it would appear that in this latter sample we see a minimal exposure to contaminating gases. Further precautions might reduce this amount but would not completely eliminate all such effects.

Finally, the ability of atomic hydrogen to surface reduce lunar materials has important implications. Typically it provides a viable mechanism for the production of hydrocarbons and other materials.[3] It also suggests that all lunar samples should be fully reduced before studying interactions with other gases. This work was carried out with the support of N.A.S.A. grant N.G.R. 33-183-004.

The Adsorption of Atomic Hydrogen on 15101,68

D.A. Cadenhead

Table I

Treatment	Atomic Hydrogen adsorption moles/$m^2 x10^{-7}$	Surface coverage A^{o2}/atom
As received	2.2	380
24 hour air exposure	5.8	140
10 minute O_2 exposure at $7x10^{-3}$torr	5.8	140
30 minute O_2 exposure at $7x10^{-3}$torr	5.4	150

References

1. Cadenhead D.A. and Jones B.R. "The Surface Reduction of Lunar Fines 14163,111." Submitted to Science.
2. Cadenhead D.A., Wagner N.J., Jones B.R. and Stetter J.R. "Some Surface Characteristics of Apollo 14 Fines and Rock Fragments", Proceeding 3rd Lunar Science Conference, M.I.T. Press 1972.
3. Pillinger C.T., Cadogen P.H., Eglington G., Maxwell J.R., Mays B.J., Grant W.A., and Nobes M.J. "Simulated Study of Lunar Carbon Chemistry." Nature 235, 108 (1972).

ANALYSIS OF ORGANOGENIC COMPOUNDS IN APOLLO 15 SAMPLES. D.A. Flory, J. Oró, S. Wikstrom, D. Beaman, and D. Nooner. Department of Biophysical Sciences, University of Houston, Houston, Texas 77004.

In this work we have attempted to identify and quantitate by GC-MS the various volatile species released by acidolysis and thermal treatment of Apollo 15 samples. Acidolysis was performed with DCl in order to aid in distinguishing identified compounds present as such from those produced by reaction of the acid with active carbon species. One sample was also extracted with benzene-methanol and no extractable organics found at the 1 ppb (10^{-9}g/g) level. Samples analyzed include 15081, 15221, 15298, 15494 and 15601.

EXPERIMENTAL

The experimental equipment and techniques have been modified extensively since our previous work (1) in order to chromatographically separate all evolved gases and obtain improved quantification. The attached sketch gives a schematic diagram of the new apparatus. A and B show the gas handling system for thermal extraction and acidolysis, respectively. C is a detailed sketch of the acidolysis reactor. These units are designed so that the helium carrier gas used to sweep the volatiles into the gas chromatograph flows through the sample area rather than the flow-by technique used previously. The gas handling system is all metal with the exception of the quartz sample tube. Valves V_1, V_2 and V_3 are Nupro brass toggle valves. For thermal runs the lunar sample is placed in the quartz tube (a new tube is used for each sample) passing through the furnace, quartz wool plugs inserted in each end to hold the sample in place, and the quartz tube sealed into the system at points A and B using Swagelok fittings with teflon ferrules. The system is then evacuated to approximately 10^{-2} torr and the furnace heating controlled by a variable power transformer. The furnace is heated in steps to 250°, 500°, 800° and 1100°C. As each temperature is reached the valves are switched to divert the carrier gas flow from the by-pass line through the heated sample tube. Tests have shown that a four-minute sweep time will remove better than 90% of the volatiles in the tube (or reactor in the case of acidolysis). The volatiles are trapped on the front end of a 5m x 1.5mmI.D. Carbosieve (60/80 mesh) packed column held at -30°C. The column is then programmed at 12°C/min to 300°C. Hydrocarbons heavier than C_2 cannot be seen under these conditions. The column is interfaced to an LKB Mass Spectrometer as described previously (1).

The gas handling system is somewhat different when set up for acidolysis. The portion of the system between A and B in sketch B is composed of pyrex glass, teflon and Viton B O-rings to minimize damage by exposure to acid. V_1, V_2 and V_3 are Eck & Krebs glass high vacuum stopcocks (Cat. No. T9050) with teflon stems and O-ring seals on the stems. The inlet tube on the reactor is

also lined with a teflon cylinder. This teflon liner and the modified Swagelok fittings used to mount a silicone rubber septum on the end of the inlet tube are removable to allow the sample to be introduced. The sample rests on a glass fritted disc (fine porosity) and is evacuated to 10^{-2} torr after being loaded. The reactor plus valves V_1, V_2 and V_3 is sealed into the gas handling system at A and B as in the thermal extraction technique. (A new reactor is installed for each sample run by cracking off and resealing the glass at points C and D). The DCl is then introduced by inserting a Hamilton gas syringe through the septum and down into the teflon liner. This syringe has a very short needle and a glass body with teflon tipped plunger to minimize acid-metal contact. After allowing 15 minutes reaction time the gases released are swept out and analyzed, as in the thermal technique.

Multiple ion plots were constructed from mass spectral scans taken at short intervals during gas chromatographic peak elution as in our previous work. Blanks were run on the system prior to the analyses to insure against interference from artifacts. Calibration of the GC-MS was accomplished by injecting a calibration mixture of CO, CH_4, C_2H_4, C_2H_6, C_3H_8 and N_2. The CH_4 calibration was used for H_2O and the N_2 calibration for H_2.

RESULTS

The results of the analyses performed are summarized in the attached table. Treatment with DCl released H_2, N_2, CO, CH_4, C_2H_4, C_2H_6, and CO_2 in the quantities shown in the table. Small amounts of Ar and O_2 were also observed in every sample. The hydrocarbon values include all deuterated species as they are calculated from the gas chromatogram peak areas and the deuterated species are not resolved. Water was observed in all runs but is not reported because of its presence in the DCl. The crystalline rock 15495,57,2 released substantially less volatiles than the fines or breccia rock. The high N_2 reading for sample 15081,14,3 is partially due to an air leak since O_2 and Ar were observed as peaks in the gas chromatogram. It is not known what portion of the N_2 released is from terrestrial exposure, but the high amounts released by the fines in comparison to the crushed rocks indicate a surface correlation. The surface correlation is not necessarily due to terrestrial adsorption and may well be due to a solar wind origin for the nitrogen. Large amounts of CO_2 were released by each sample as was CO, with the exception of the crushed crystalline rock. In all cases CO_2 was released in larger quantities than CO. The amounts of CO_2 are much larger than previously noted (1,2,3). We cannot account for this difference at the present time. Methane and C_2 hydrocarbons were also released in quantities generally larger than in previous analyses. The CD_4/CH_4 ratios are also given and range from 2.2 to 3.7, similar to our values reported for Apollo 11, 12 and 14 lunar samples (1). All possible C_1 and C_2 deuterated species were observed in the multiple ion plots supporting our previous suggestion (1) that partially hydrogenated carbon species are present in the sample.

The results of the GC-MS analysis of the volatiles released by thermal treatment are also given in the table. Volatiles released included N_2, CO, CH_4, CO_2 and H_2O in the quantities shown for each of the temperature steps. Only CO_2 and H_2O were observed at the 250°C step. Any adsorbed nitrogen from

terrestrial exposure was apparently pumped away by the vacuum applied prior to beginning the heating. The only hydrocarbon found in greater than 0.1 ppm quantities was methane. The methane contents are similar to those reported (1) in some of our previous analyses and the maximum release temperature range (500-800°C) is also similar. CO_2 was the major carbon containing species at temperatures below 500°C for the fines and breccia while CO became the dominant species at the higher temperatures. In the crushed crystalline rock, however, more CO_2 than CO was released at 500, 800 and 1100°C. The total quantities of N_2 and H_2O released range from about 50-250 ppm and both are given off in significant amounts at temperatures greater than 500°C indicating the presence of either chemically bound or physically trapped (in vesicles) N_2 and H_2O.

If one converts the values for the various carbon containing compounds released by acid and thermal treatment to carbon content the values for total carbon are generally slightly larger than those reported by Moore et al (4) for similar samples from Apollo 11 and 12. It is also interesting to compare the proportion of carbon released as hydrocarbons in volatilization and acidolysis. The proportion of hydrocarbons is much higher in acidolysis than in volatilization. We feel that a more detailed comparative study of these two methods of analysis will eventually provide accurate information on the nature and source of the carbon compounds actually present in the lunar samples.

REFERENCES

1. FLORY D.A., WIKSTROM S., GUPTA S., GIBERT J.M. and ORÓ J. Analysis of Organogenic Compounds in Apollo 11, 12 and 14 Lunar Samples, Proceedings of the Third Lunar Science Conference, LSI (in press).
2. CADOGAN P.H., EGLINTON G., MAXWELL J.R. and PILLINGER C.T. (1971) Carbon Chemistry of the Lunar Surface, Nature 281, 29-31.
3. CHANG S., KVENHOLDEN K., LAWLESS J., PONNAMPERUMA C. and KAPLAN J.R., Carbon Carbides and Methane in an Apollo 12 Sample, Science 171, 474-477.
4. MOORE C.B., LEWIS C.F., LARIMER J.W., DELLES F.M., GOOLEY R.C. and NICHIPORUK W. (1971) Total Carbon and Nitrogen Abundances in Apollo 12 Lunar Samples, Proc. Second Lunar Sci. Conf., p. 1343-1350, MIT Press.

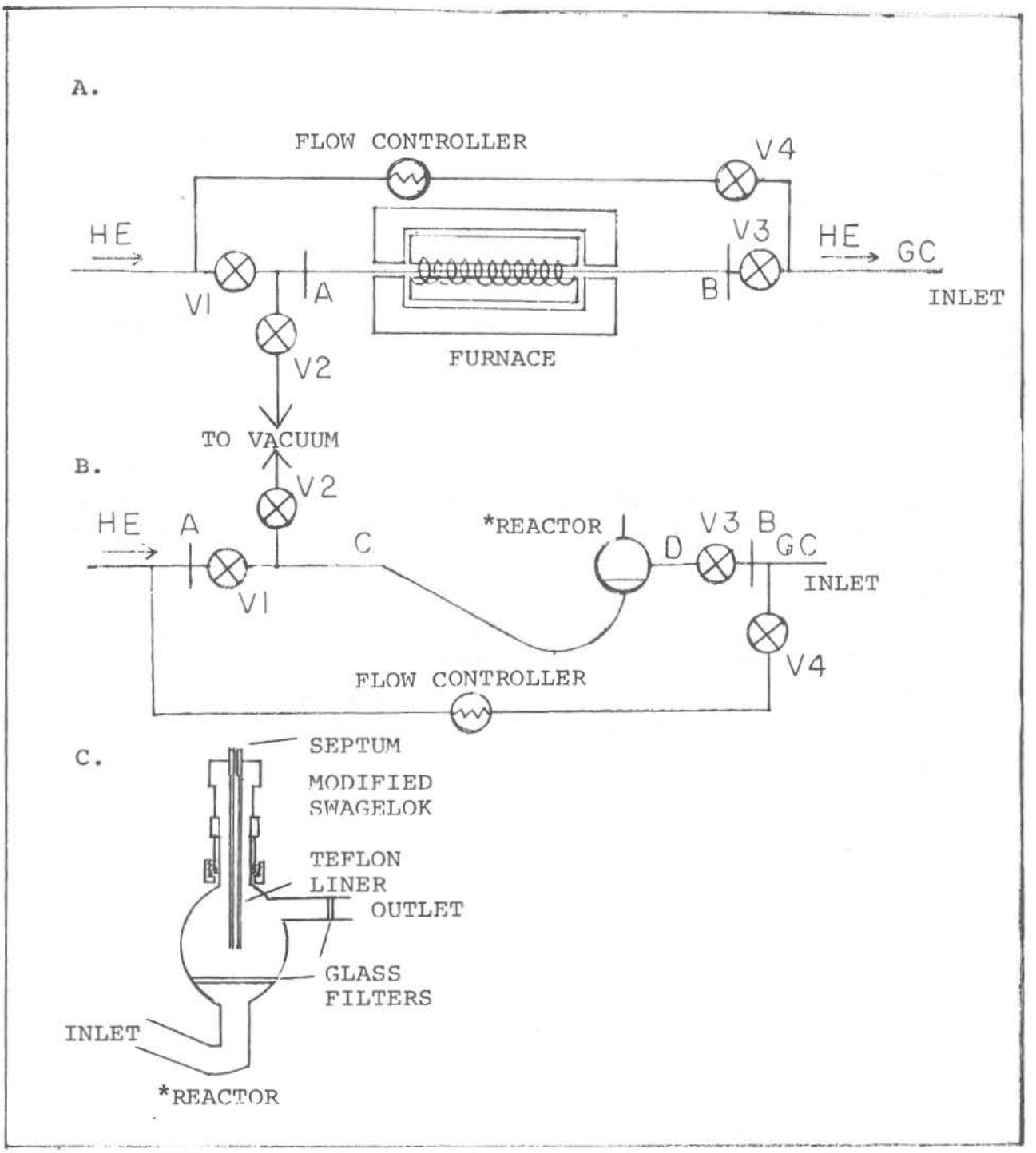
A.
FLOW CONTROLLER
V4
HE
V3
HE
GC
V1
A
B
INLET
FURNACE
V2
TO VACUUM
B.
V2
HE
A
*REACTOR
V3
B
GC
C
D
INLET
V1
V4
FLOW CONTROLLER
C.
SEPTUM
MODIFIED
SWAGELOK
TEFLON
LINER
OUTLET
GLASS
FILTERS
INLET
*REACTOR

SAMPLE INFORMATION				RESULTS (in PPM)													
				ACIDOLYSIS							VOLATILIZATION					
SAMPLE NO.	TYPE	ANAL	AMT	H_2	N_2	CO	CH_4	CO_2	C_2	CD_4/CH_4	°C	N_2	CO	CH_4	CO_2	H_2O
15081,14,3	Fines	Acid	0.45	850	3200	Tr.	81	460	21	2.8						
15081,14,4	Fines	Vol	0.49								250	Tr.	Tr.		Tr.	48
											500	8.1	1.3	3.7	22	24
											800	102	340	13	70	42
											1100	55	195		63	4.9
15221,22,3	Fines	Acid	0.58	260	1200	260	65	580	80	2.2						
15221,22,4	Fines	Vol	0.51								250					140
											500	2	11	Tr.	33	48
											800	100	140	5.2	56	89
											1100	110	280		63	83
15298,24,2	Crushed Breccia	Acid	1.17	310	8.8	70	45	1200	3.8	2.5						
15298,24,3	Crushed Breccia	Vol	0.86								250				59	74
											500	33	46	11	53	52
											800	130	200	7.6	100	40
											1100	130	390		37	55
15495,57,2	Crushed Crystal Rock	Acid	1.36	-	100	Tr.	Tr.	150	-	-						
15495,57,3	Crushed Crystal Rock	Vol	0.89								250	20	28		20	24
											500	8.9	9.7	2.0	140	48
											800	20	35		83	15
											1100	11	35		43	20
15601,23,2	Fines	Acid	0.70	640	450	240	53	360	32	3.7						
15601,23,3	Fines	Vol	0.62								250				70	39
											500				8.9	8.1
											800				9.9	6.7
											1100		17		22	2.4
15601,23,4	Fines	Extr.	5.00	No extractable organics at the ppb level												

INERT GASES IN FINES FROM THE HADLEY-APENNINE REGION, J. L. Jordan, S. Lakatos, and D. Heymann, Departments of Geology and Space Science, Rice University, Houston, Texas, 77001.

We have measured He, Ne, Ar, Kr, and Xe mass-spectrometrically in eight bulk fines and one sample of 2-4 mm fines (15603) from stations LM-ALSEP, 2, 6, 6a, 7, and 9a. For 15091 and 15601 we have also determined these gases in size fractions. The samples come from three of the major morphologic units of the landing site: the Front, the Mare, and the Rille.

1) The He^4 contents of the bulk fines range from 0.13 to 1.05 x 10^{-1} cm^3 STP/g. He^4 and the other trapped gases are inversely proportional to grain diameter in the size fractions of 15091 and 15601. More than 90% of the trapped gas is surface correlated; hence is probably directly implanted solar wind.

2) He^4/Ne^{20} ranges from about 20 to 60; Ne^{20}/Ar^{36} from 5 to 8; Ar^{36}/Kr^{84} from 2400 to 3200; and Kr^{84}/Xe^{132} from 3.2 to 7.3. The smallest He^4/Ne^{20} ratios occur in the Front fines which are rich in green glass spherules. The spherules themselves (Lakatos and Heymann, unpublished results) have very small He^4/Ne^{20} ratios, usually less than 10. The He^4/Ne^{20} ratio in bulk fines evidently reflects the amount of green glass present in them.

3) He^4/He^3 ranges from about 2100 to 2700; Ne^{20}/Ne^{21} from 12.7 to 13.2; Ne^{21}/Ne^{22} from 0.035 to 0.041; and Ar^{36}/Ar^{38} from 5.26 to 5.45.

4) The measured Ar^{40}/Ar^{36} ratios range from 0.757 to 3.56; however, when these ratios are corrected for radiogenic Ar^{40}, the range becomes 0.50 to 3.45. The largest ratios were found in the Front samples, especially from stations 6a and 7a at Spur Crater.

The concentrations of trapped inert gases in the bulk fines are the same within a factor of 3 across the area that was sampled (exception: 15421). The only salient trend is that the samples from near Spur Crater (station 6a and 7) are, on the average, slightly poorer in trapped gas than the others. Again, this may be due to an enrichment of green glass (up to $\sim$40%) in these samples. The green glass itself contains about 10 times less trapped gases than bulk fines poor in this glass (Lakatos and Heymann, unpublished results).

Ne^{21}_c radiation ages were calculated for all of the samples. The youngest ages, range from 50 to 90 m.y.; they occur at the LM-ALSEP station (15021), station 2 (15091), and station 6a (15401). Sample 15301 from station 7 gives an age of 120 m.y. The other samples are considerably older: 200 m.y. at stations 6 (15271) and 8 (15031); and about 240 m.y. at station 7 (15421). Apparently the various fines have been excavated and deposited in the top few inches of the regolith at widely different times, and seem to come from at least four distinct crater-forming impacts.

Perhaps our most interesting observation is that the corrected Ar^{40}/Ar^{36} ratios tend to be greater in the Front samples than in the Mare and Rille samples. This could be due to differences in exposure geometry between the slopes of the Front and the flat-lying Mare; the angle of incidence of atmospheric Ar^{40} is greater on the Front slopes than it is in the Mare terrain. Alternatively, it could be that the Front fines acquired their atmospheric Ar^{40} at a time when the concentration of neutral Ar^{40} in the lunar atmosphere was relatively high.

This work was supported by NASA grant NGR-44-006-(061).

TOTAL NITROGEN ABUNDANCES IN FIVE APOLLO-15 SAMPLES (HADLEY-APENNINE REGION) BY NEUTRON ACTIVATION ANALYSIS (B. K. Kothari and P. S. Goel, Dept. of Chemistry, Indian Institute of Technology, Kanpur, India).

Total nitrogen concentrations in several lunar samples consisting of three fines, one breccia and one basaltic rock have been determined by neutron activation analysis. The method which uses (n,p) reaction has been described earlier.[1,2]

The data are reported in Table 1. These have about ±10% error.

Table 1. Nitrogen contents of Apollo-15 samples

Sample No.	Classification	Description	Mass (mg)	Nitrogen**(ppm) Value	Weighted mean
15557,41	Basalt	Pieces	115.5,70.5	17.3,16.6	17
15299,17	Fine Breccia (medium grey-matrix)	Pieces	113,92	60.5,62.3	61
15271,84	Fines (Apennine Front)	-	51,57	86,93.5	90
15013,14	Fines (Apennine Front)	-	23,17.5	120*,120*	110
			30,15	106.5*,101*	
	SESC sample		39.2	107	
15012,11	Fines (ALSEP)	-	10.5,19	103*,95.5*	98
	SESC sample		16,21	90.5*,94*	
	'Exhaust-Contaminated'		22	105	

*Sample not exposed to atmospheric nitrogen
**Error ±10%

The total nitrogen contents of Apollo-15 samples range from 17 to 110 ppm as reported for samples from earlier missions. Fines are enriched in nitrogen compared to the basaltic rocks. The brecciated rock 15299 has a nitrogen of 61 ppm. It indicates that during breccia formation a large fraction of the excess nitrogen can be retained.

We were provided with two samples of fines from SESC (SURFACE Environmental Sample Container). Our aliquots were packed entirely in an atmosphere of helium at Berkeley. This avoided any contact with atmospheric nitrogen. These were opened in an oxygen atmosphere and were sealed in quartz vials after evacuation. Aliquots were also vacuum sealed after exposure to air to check the possibility of adsorption of nitrogen. The results from all such runs

NITROGEN ABUNDANCES

B. K. Kothari

were almost identical showing an absence of atmospheric adsorption. One of the SESC sample, 15013, was supposed to be 'exhaust-contaminated.' It has normal nitrogen.

References:

1. Goel, P. S. (1970) Determination of nitrogen in iron meteorites. *Geochim. Cosmochim. Acta 34*, 932-935.
2. Goel, P. S. and Kothari, B. K. (1972) Total nitrogen contents of some Apollo 14 lunar samples by neutron activation analysis. *Third Lunar Science Conference Proceedings* (in press).

INERT GASES IN GREEN GLASS FROM APOLLO 15, S. Lakatos and D. Heymann, Departments of Geology and Space Science, Rice University, Houston, Texas, 77001.

We have measured He, Ne, and Ar mass-spectrometrically in green glass spherules separated from samples 15091, 15271, 15301, 15421, 15426, and 15601. These samples come from stations 2, 6, 7, and 9a. Our measurements were done on grain size fractions as well as on single spherules. We have also determined the inert gas contents of the corresponding bulk fines (from which spherules have been extracted). The following are our salient results:

1) The glass has either lost substantial amounts of trapped He^4, or the gas that was trapped in it had already been strongly fractionated. Sixteen of the nineteen $(He^4/Ne^{20})_T$ ratios in the glasses are 10 or less; in bulk lunar fines this ratio is typically 50-100.

2) The $(Ne^{20}/Ar^{36})_T$ ratios, on the other hand, are greater in the glass than in typical fines. Sixteen of eighteen values are 10 or greater; the ratio in fines is usually around 6.

3) The absolute amounts of Ar^{36}_T in the 15426 and 15421 green glass are about 10^{-6} cm^3 STP/g; in the green glass from the remaining fines $\sim 10^{-5}$ cm^3 STP/g; in the bulk fines themselves about $\sim 10^{-4}$ cm^3 STP/g.

4) The trapped gas content in the green glass from the soil clod 15426 does not correlate with grain size.

5) The measured Ar^{40}/Ar^{36} ratios in the glass are nearly always greater than those seen in the bulk fines. This reflects the small content of trapped Ar^{36}_T as well as a possible large contribution from radiogenic Ar^{40}_R.

6) All but two of the eighteen measured He^4/He^3 ratios in the green glass are less than 1500, reflecting the presence of substantial amounts of cosmogenic He^3_c. Cosmogenic Ne^{21}_c is clearly present in 15426, because all of the measured Ne^{20}/Ne^{22} ratios in this glass are smaller than 10.

7) The mean Ne^{21}_c and Ar^{38}_c cosmic ray exposure ages are (in 10^6 years): 15426 (350, 370); 15301 (310, 330); 15421 (340, 350); 15271 (460, 480); 15091 (450-750, 360-510); 15601 (280, no Ar^{38}_c age could be computed). The He^3_c radiation ages are always at least three times younger, reflecting substantial He^3_c

INERT GASES IN GREEN GLASS FROM APOLLO 15

S. Lakatos and D. Heymann

losses. The Ne^{21}_c and Ar^{38}_c ages of the green glass are very similar to the ages of the bulk fines.

We have considered the following possible origins of the trapped gas. a) Solar wind implantation. b) Genuine primordial lunar gas. c) An ambient lunar atmosphere. d) Gas from projectile that produced the glass on impact. Case a) is somewhat weak because the interaction of solar wind with grain surfaces usually leads to $(Ne^{20}/Ar^{36})_T < 10$. If the trapped gas is primordial, albeit strongly fractionated, we can rule out the possibility that primordial lunar inert gas was similar in composition to that known in the overwhelming majority of carbonaceous chondrites. We can also rule out a composition similar to that of the Earth's atmosphere. The composition of primordial lunar gas must then have been similar either to the "solar" component in gas-rich chondrites, or to the trapped gas in the howardite Kapoeta. The ambient atmosphere could have, in part, consisted of primordial lunar gas. If the gas came from a projectile, the latter was almost certainly not a carbonaceous chondrite.

The soil "clod" 15426 was probably formed either by a primary, or secondary impact. The low trapped gas content of glass spherules from this "clod" indicates that they were essentially protected from solar wind implantation.

This work was supported by NASA grant NGR-44-006-(061).

APOLLO 15 LUNAR SAMPLES: LM EXHAUST PRODUCTS IN THE SESC 15013.

B. R. Simoneit, P. C. Wszolek and A. L. Burlingame, Space Sciences Laboratory, University of California, Berkeley 94720.

The LM exhaust contaminated sample was collected in a Special Environment Sample Container (SESC) from the lunar surface in an area disturbed by the DPS engine just north of the LM. The SESC was opened in the controlled atmosphere of a glove box under dry helium (1).

A sample of 15013,10 was subjected to pyrolysis-mass spectrometry as previously described (2,3). Ninety-six ppm of carbon was released as CO and CO_2 (2 ppm) and 78 ppm of nitrogen as N_2. Surface adsorbed species such as NO (1.6 ppm), H_2O (41 ppm) and HCN (0.2 ppm) were released in the temperature range of 100-220°C and the following species were released in the range of 300-900°C: H_2O (38 ppm), NO (0.2 ppm), HCN (8.8 ppm), NH_3 (4.5 ppm), CH_4 (3.6 ppm) and traces of benzene and SO_2.

Another portion of the sample (3.33 g) was extracted with 50 ml redistilled nanograde toluene and methanol (3:1 v/v) solution, using ultrasonication for 20 min, filtered through a fine fritted filter and then the extract was concentrated on a Büchi rotary evaporator. The residual solvent was removed under a stream of dry nitrogen before mass spectrometric analysis (4,5). A procedural blank was also analyzed and the mass spectrometric data are corrected for background and solvent contributions. The same mass spectrometric online conditions were used as reported earlier (4,5).

The concentrations of extractable compounds were low and are estimated from pyrolysis and acid dissolution data to be in the range of 2 ppm. The major species attributable to LM engine exhaust are listed in Table I (6,7). The compositions C_4H_9 (m/e 57) and $C_8H_5O_3$ (m/e 149) are listed in Table I to indicate the residual contamination levels due to hydrocarbons and phthalate esters after deletion of the blank contribution.

The DF dissolution results are found in Table II. The large amounts of CH_4, CD_4, ^{20}Ne and ^{36}Ar are indicative of a mature soil, and the yields of C_2 to C_5 deuterocarbons, HCN and DCN are significantly higher than previously observed for soils (3,8). The other volatile species released on dissolution and attributable to LM products are mainly NO and NO_2 with minor amounts of HCNO, NH_3, and CH_3CN.

LM Exhaust Products in the SESC 15013

B. R. Simoneit

Table I. Composition of the toluene-methanol extract of the SESC fines 15013,10, as determined by high-resolution mass spectrometry.

Nominal mass	Compositional species	15013,10*
17	$NH_3^{\dagger}$	400
27	$HCN^{\dagger}$	40
30	$NO^{\dagger}$	300
30	$CH_4N^{\dagger}$	120
42	$C_2H_4N^{\dagger}$	210
43	$HCNO^{\dagger}$	100
44	CO_2	5600
44	$C_2H_6N^{\dagger}$	430
45	$CH_3NO^{\dagger}$	1550
46	$CH_4NO^{\dagger}$	1100
46	$NO_2^{\dagger}$	90
57	$C_2H_3NO^{\dagger}$	20
57	C_4H_9	3800
58	$C_2H_4NO^{\dagger}$	75
59	$C_2H_5NO^{\dagger}$	60
72	$C_3H_6NO^{\dagger}$	360
85	$C_2H_3N_3O^{\dagger}$	550
86	$C_2H_4N_3O^{\dagger}$	100
149	$C_8H_5O_3$	3000

* Average ion current (relative)
† Composition attributable to LM engine exhaust (6,7)

LM Exhaust Products in the SESC 15013

B. R. Simoneit

Table II. Yields of the gaseous species released from the SESC fines 15013,10 on DF dissolution.

Nominal mass	Species	Yield (nanomoles/g)
16	CH_4	378
20	Ne	82
20	CD_4 + CHD_3	2110
27	HCN*	40
28	DCN	65
30	NO*	528†
30	C_2H_6	36
31	C_2HD_3	31
32	C_2D_4	82
34	H_2S	1160
36	C_2D_6	41
35 + 36	HDS + D_2S	5440
36	Ar	20
37	PD_3	137
41	CH_3CN*	0.8†
43	HCNO*	0.6†
46	NO_2*	8.8†
76	CS_2	2.5
	C_3 deuterocarbons	28
	C_4 deuterocarbons	5
	C_5 deuterocarbons	1
ratio	CD_4/CH_4	5.6:1

* Species correlatable to LM engine exhaust (6,7)
† The ionization efficiency of CH_4 was used to estimate the yields of these species

LM Exhaust Products in the SESC 15013

B. R. Simoneit

From these preliminary results it appears that the LM touchdown vicinity was heavily blanketed by LM engine exhaust products, especially the oxidizer, N_2O_5. The concentration of the nitrogenous compounds attributable to LM exhaust is in the range of 2 ppm. The major species observed by mass spectral analysis are: NO, NO_2, CH_3NO and CH_4NO, and since these are only mono-nitrogen compositions, it can be concluded that the exhaust contained an excess of oxidizer. Such overoxidation would result in the low concentrations of polynitrogenous species derived from the UDMH fuel. The fragment ions C_2H_6N and C_3H_6NO (cf. Table I) are possibly derived from dimethylformamide (7,10). All the nitrogenous species in Table I were found in the experimental LM exhaust analysis program (6,7) and in extracts from portions of Surveyor III (9,10). Species such as CH_4N_2O, $C_2H_6N_2O$, $>C_3$ nitriles, N_4 porphine-like and other polynitrogen moieties, which were found in the experimental LM (6,7) were not detected in this sample. No reaction products of LM exhaust with terrestrial hydrocarbons were detected (7,10).

The bimodal pyrolytic evolution pattern for the species NO, HCN and H_2O indicates an adsorption process for these gases evolved in the 100-220°C temperature range and a possible chemical reaction (bonding) process for these gases evolved from 300-900°C. This second possibility should be examined further.

Acknowledgements. We thank Miss R. Jackson and Dr. J. J. Chang for the high resolution mass spectrometry; the Apollo 15 crew, astronauts D. R. Scott, A. M. Worden and J. B. Irwin for collecting and returning the SESC; and NASA (Grant NGR 05-003-435) for financial support.

References

(1) B. R. Simoneit, J. T. Wilder and P. C. Wszolek, "UCB Space Sciences Laboratory Organic Clean Room and Lunar Material Transfer Facilities. The Transfer of Pristine Lunar Material from the Apollo 15 SESC 15012 and SESC 15013," University of California, Space Sciences Laboratory Report, Berkeley, June 10, 1972.

(2) P. T. Holland, B. R. Simoneit, P. C. Wszolek and A. L. Burlingame, Space Life Sciences, in press.

(3) P. T. Holland, B. R. Simoneit, P. C. Wszolek and A. L. Burlingame, Proc. Third Lunar Sci. Conf., D. Heymann, Ed., Geochim. Cosmochim. Acta, in press.

(4) A. L. Burlingame, M. Calvin, J. Han, W. Henderson, W. Reed and B. R. Simoneit, Proc. Apollo 11 Lunar Sci. Conf., Geochim. Cosmochim. Acta, Vol. 2, Suppl. 1, Pergamon, London, 1970, pp. 1779-1791 and references therein.

(5) W. Henderson, W. C. Kray, W. A. Newman, W. E. Reed, B. R. Simoneit and M. Calvin, Proc. Second Lunar Sci. Conf., Geochim. Cosmochim. Acta, Vol. 2, Suppl. 2, M.I.T., Cambridge, 1971, pp. 1901-1912.

(6) B. R. Simoneit, A. L. Burlingame, D. A. Flory and I. D. Smith, Science, 166, 733 (1969).

(7) D. A. Flory, B. R. Simoneit, A. L. Burlingame and I. D. Smith, "Experimental Determination of Potential Lunar Surface Organic Contamination in the Lunar Module Descent Engine Exhaust," NASA Technical Report R-389 (1972).

(8) P. T. Holland, B. R. Simoneit, P. C. Wszolek, W. H. McFadden and A. L. Burlingame, Nature, 235, 106 (1972).

(9) B. R. Simoneit and A. L. Burlingame, Nature, 234, 210 (1971).

(10) B. R. Simoneit and A. L. Burlingame, in Analysis of Surveyor 3 Material and Photographs Returned by Apollo 12, NASA SP-284, U.S. Government Printing Office, Washington, D.C., 1972, pp. 127-142.

CARBON, NITROGEN AND SULFUR RELEASED DURING PYROLYSIS OF BULK APOLLO 15 FINES. S. Chang[†], J. Smith [*#], H. Sakai[*], C. Petrowski[*], K. A. Kvenvolden[†], and I. R. Kaplan[*] ([†] NASA, Ames Research Center, Moffett Field, CA 94035; *University of California, Institute of Geophysics and Planetary Physics, Los Angeles, CA 90024; #Permanent address: Division of Minerology, C. S. I. R. O., North Ryde, NSW, Australia)

In a vacuum pyrolysis experiment performed by stepwise heating, we examined the abundance and isotopic composition of carbon, nitrogen and sulfur released as volatile gases and the amounts of hydrogen and helium from a 6.261g. bulk sample of 15012 fines. Details of the experimental method will be published elsewhere.

The sample was initially outgassed overnight at 200°C to remove adsorbed terrestrial contamination; after combustion of the resulting liquid nitrogen condensable gases, 3 ppm CO_2 was detected. At the end of the pyrolysis at 1170°C, the sample was combusted while raising the temperature to 1200° to remove the unpyrolyzed C, N and S. The identity and elemental abundances in ppm of the gases evolved at each pyrolysis step are summarized in Figure 1. The pattern of evolution of gases over the range 200°-1170°C is consistent with those previously reported for Apollo 11, 12, 14 and 15 samples of fines. Hydrogen, helium and methane, presumably all of solar wind origin are released almost entirely below 800°C, with maximum evolution at 400°-600°C. In this temperature range small quantities of CO, CO_2 and N_2 are also released. However, the major fraction of carbon and nitrogen are evolved as CO and N_2 at higher temperatures, apparently as a result of interaction between non-volatile carbon and nitrogen phases with minerals in the sample. Although H_2S and SO_2 were carefully sought, only traces of H_2S were detected between 400° and 600°C, comparable in quantity to blank levels in the analytical system. Combustion of the pyrolysed residue, in oxygen, however, liberated 556 ppm S with δS^{34}=+10 per mil. There is reason to believe that complete sulfur release was not accomplished.

Pyrolysis of Bulk Apollo 15 Fines

S. Chang

Isotopic measurements on the evolved gases are listed in the Table.

Table
δC^{13}_{PDB} (per mil)

	200°-400°C	400°-600°C	600°-800°C	800°-1000°C	1000°-1170°C	1200°C plus 0_2
CH_4		+31	+46			
CO	-22	+21	+29.0	+12.9	+15.3	
CO_2	+3.3	+18.7	+20.4	+9.8	+34.9	-6.3

Several features of the isotopic data appear to be of considerable interest.

1. Relatively low values of δC^{13}PDB for CO and CO_2 observed only in the 200°-400°C pyrolysate suggest that a small amount of terrestrial contamination is removed at this temperature range.

2. Ten ppm carbon represented by the CO_2 resulting from final combustion of the pyrolysis residue is also enriched in C^{12} relative to the bulk of the carbonaceous gas. This fraction may represent relatively unaltered primordial lunar carbon or meteoritic carbon or both.

3. The values of δC^{13}_{PDB} for lunar CH_4 are the highest recorded thus far for reduced carbon from any natural source.

4. The ^{13}C enrichment in CH_4 and in CO_2 and CO released below 600°C might well be the result of preferential removal of ^{12}C by solar wind "hydrogen stripping", whatever the source of the carbon.

5. CO evolved at 600°-800°C with δC^{13}_{PDB} = +29 °/oo. There is evidence that pyrolysis of graphite or solarwind carbon in a matrix of lunar fines does not produce CO at these temperatures, whereas meteoritic carbide does yield CO. If the observed CO is derived from carbide, the carbide must have been highly depleted in ^{12}C.

Pyrolysis of Bulk Apollo 15 Fines

S. Chang

6. Variations in isotopic compositions of CO and CO_2 released at different stages between 600° and 1170°C may reflect the existence of carbon phases with more than one range of isotopic values.

Preliminary data not listed in Table I indicate that the nitrogen evolved throughout the 200°-1170° C range is as much as 25 per mil enriched in ^{15}N relative to terrestrial atmospheric nitrogen. $\delta^{15}N$ values are not given at this stage until they can be confirmed.

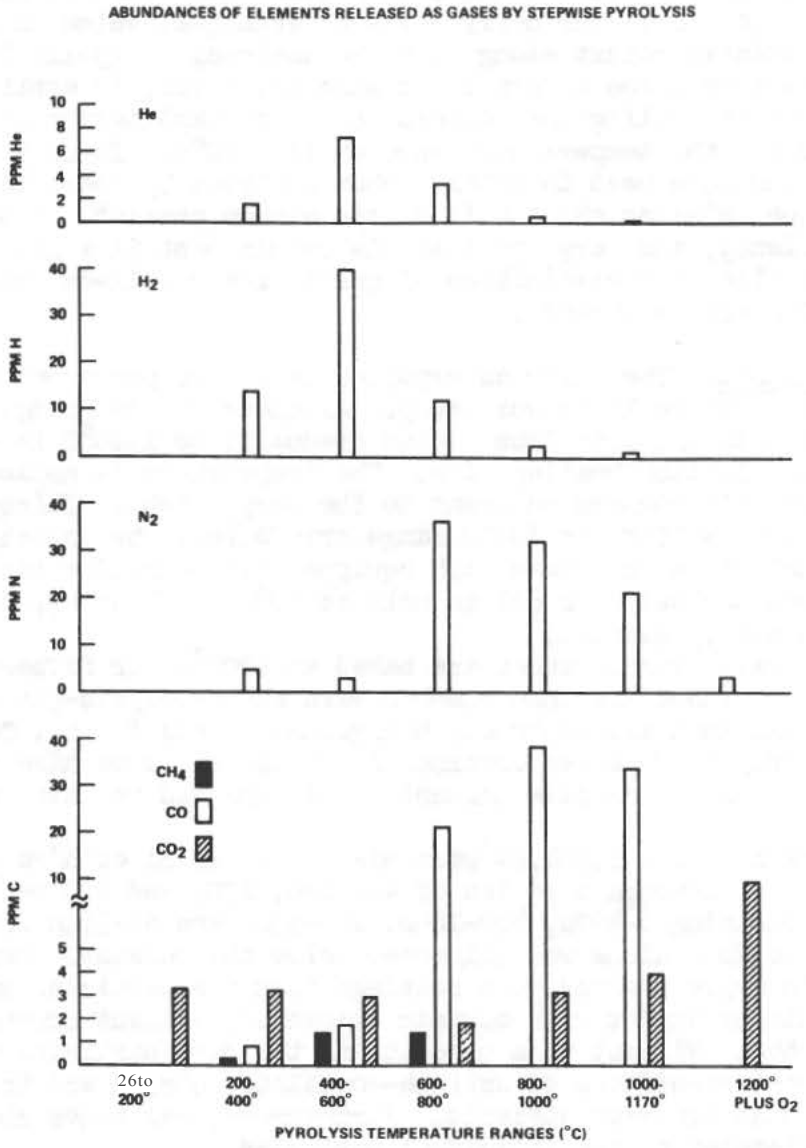

PYROLYSIS STUDY OF CARBON IN LUNAR FINES AND ROCKS

David J. DesMarais, J. M. Hayes, and W. G. Meinschein

Department of Geology, Indiana University, Bloomington, Indiana 47401

Many investigators have studied the carbon compounds released during the heating of lunar samples. Our newly devised technique, which is described in this preliminary report along with the analyses of Apollo 15 rocks, fillet fines, mature fines, and mature fines size fractions, is applicable to samples as small as a few milligrams, offers accurate quantitation of H_2, CH_4, CO, and CO_2, and covers the temperature range up to 1300°C. In comparison to the combustion technique used in total carbon analyses by Moore and Gibson, the present technique releases about half of the carbon present. Notwithstanding that deficiency, the very small sample requirement is a great advantage, and will allow the examination of particularly well-defined samples, for example, monomineralic separates.

Experimental Method. The analyses reported here were performed using the instrument described previously by our group[1]. Aliquots (10 to 30 mg) of lunar material are enclosed in a quartz tube heated gradually to 1300°C in an ohmic oven with 0.020 inch platinum heating wire. The temperature is monitored by a Pt - Pt13%Rh thermocouple mounted adjacent to the sample tube. Thirty minute periods of heating over a 150°C or 300°C range are followed by injection of any evolved gases into a gas chromatograph equipped with a helium ionization detector. A six foot Carbosieve B column held at 50°C resolves H_2, O_2, N_2, CO, CH_4, and CO_2 in twenty minutes.

Prior to use, quartz sample tubes are baked at 1200°C for fifteen hours with helium flow. The tubes are then checked with the pyrolysis-gas chromatograph system. For all analyses reported, background levels for H_2, CO, and CH_4 are below one percent of values obtained for lunar rocks we have analyzed, and CO_2 and N_2 levels are below five percent. All reported results are background corrected.

About 0.7 grams of fines 15301,24 were mixed with 20 ml of high purity liquid argon and poured through a series of 40, 140, 270, and 400 mesh stainless steel sieves[2], yielding >420μ, 420-105μ, 105-53μ, and 53-37 μ fractions respectively. The <37μ residue was collected below the screens. Repeated washings with liquid argon removed dust coatings from the particles nearly as well as ultrasonic treatment with organic solvents[3], without contaminating the sample with carbon. Without this precaution, the dust particles might contribute significant quantities of surface-correlated carbon and thus obscure the results of the size fraction analysis. Furthermore, the argon cleaning facilitates identification of the individual particles.

Pyrolysis Study of Lunar Carbons

D. J. DesMarais

Results and Discussion. We have analyzed three samples for which total carbon determinations have been made by the combustion technique developed by Moore. Table 1 shows that about half the total carbon is released by this

Table 1. Efficiency of Carbon Extraction

Sample	ppm C releated by pyrolysis as CH_4	CO	CO_2	total	Total C (combustion) ppm
15058	1.6	13	4.0	18	27 ± 5 (4)
15301	2.3	57	6.6	67	160 ± 10 (4)
	1.7	63	4.7	69	
	2.1	64	5.1	71	
61221	1.0	37	12	50	100 ± 10 (5)

pyrolysis technique. The efficiency of extraction is roughly independent of the time vs temperature profile, with an extra 30 min holding cycle at 1300°C increasing the yield by about 5% or less. Because all the samples are melted, we assume that the ultimate yield is also independent of grain size. Presumably the carbon which is not observed is simply partitioned into the melt. For some types of studies, notably of carbon distribution among mineral phases, this partial yield is worrisome, and we plan to investigate the use of O_2 and trapping (of CO_2) in order to obtain better extraction.

The best evidence for the quantitative reliability of the technique is furnished by the mass balance and parallel release patterns obtained from the sieving experiment discussed below. Replicate analyses of bulk fines samples (Table 1, Table 2) furnish both examples of remarkable reproducibility and of sharp disagreement. It seems only remotely possible that the occasional fluctuations are due to sampling, with peculiar carbon-rich grains being substantially more abundant in some 10 mg aliquots than in others. We are studying this problem carefully.

Duplicate pyrolysis experiments on 10 mg aliquots of each of five different fines samples provide some interesting comparisons. The samples examined and the results obtained are summarized in Table 2. Figures 1-3 show the gas release vs temperature curves for these samples. Very similar gas release curves have been observed for nearly all samples examined, including rocks, breccia, and fines. It seems remarkable that this should be true for samples having substantially different histories and mineral compositions. Many lunar samples are multi-component mixtures, and some smearing-out of gas evolution patterns can be expected due to the different gas release patterns of the components, but we suspect that the observed uniformity is at least in part an artefact of the pyrolytic release mechanism, and that the composition of the gases is strongly influenced by the analytical procedure itself. The temperature ranges in which the major portions of the various gases are released do not vary substantially: CH_4, 450-750°C; CO, 600-1300°C; and CO_2, 25-600°C, 750-1200°C. Within the carbon monoxide curve, separate stages of evolution can be observed in some samples, one fraction being released in the range

Pyrolysis Study of Lunar Carbons

D. J. DesMarais

600-1050°C, the other fraction being apparently associated with sample melting above 1100°C.

Table 2. Carbon Compounds Produced by Pyrolysis of Apollo 15 Fines Samples

Sample	Station & Remarks (6)	ppm C as CH_4	CO	CO_2
15221,36	2, Oldest Apennine Front, near Rille	4.2	151	22
		2.4	102	9.6
15231,37	2, as above, from beneath large boulder	3.0	117	5.5
		3.0	108	4.9
15250,4	6, Old Apennine Front	2.7	88	9.1
		3.7	114	10.
15301,24	7, Youngest Apennine Front, Spur Crater	1.7	63	4.7
		2.1	64	5.1
15401,13	6a, Very fresh fines from fillet (7)	0.9	19	4.9
		0.8	15	4.3

The results summarized in Table 2 show that freshly produced fines from the top of a fillet are still quite low in carbon and do not differ appreciably from rock samples which we have analyzed. Most of the solar wind and/or meteoritic carbon found in the older fines must be picked up in the regolith. Some further evidence of this is seen in the station 7 fines, which are somewhat lower in carbon than the station 6 and station 2 fines. Figure 3 shows clearly that the younger samples and the older sample from beneath a boulder share the characteristic of particularly low CO_2 abundance. We have speculated[8] that some of the CO_2 might be derived by reimplantation of lunar atmospheric species. It would be interesting to learn the relative ^{40}Ar contents of these samples.

Five sieve fractions (>420μ, 420-105μ, 105-53μ, 53-37μ, and <37μ) of mature fines 15301,24 were obtained as described above. Green glass comprised approximately one-third of each of the four larger fractions. Light colored grains (feldspar, anorthosite, colorless glass, etc.) were abundant in the 105-53μ and 53-37μ fractions but sparse in the 420-105μ and >420μ fractions. Black aggregates and/or basalt were abundant throughout and dominated the two coarse fractions. The <37μ fraction was too fine grained to examine.

A portion of each sieve fraction was pyrolyzed, and the carbon yields as CH_4, CO, and CO_2 were plotted against the inverse of the radius corresponding to the assumed average surface area for the particles of a given size fraction. We have not yet made a measurement[3] of the actual average grain diameters, and we must stress that the indicated diameters assume a flat distribution of mass versus grain size within each size fraction. Figure 4 suggests a correlation between surface area and content of CH_4, CO, and CO_2. In addition, the non-zero intercepts suggest that sizable fractions of the

gases are not surface-correlated. Further study requires the examination of specific particle types within the fines.

References:

1. D. J. DesMarais, et al, ASTM Symposium on Analytical Methods Developed for application to Lunar Sample Analysis, in press.

2. P. T. Holland, et al, p. 383 in "Lunar Science-III", ed. C. Watkins (Houston: Lunar Science Institute), 1972.

3. P. Eberhardt, et al, Proc. Apollo 11 Lunar Sci. Conf., Geochim Cosmochim Acta, Suppl. 1, Vol. 2, pp. 1037-70. Pergamon (1970).

4. Lunar Sample Information Catalog-Apollo 15, LRL-MSC 03209, November 1971.

5. E. K. Gibson, MSC, private communication, 1972.

6. Geologic Setting of the Apollo 15 Samples, Science 175, 407 (1972).

7. H. R. Hart, Jr., et al, p. 360 in "Lunar Science-III", ed. C. Watkins (Houston: Lunar Science Institute), 1972.

8. J. M. Hayes, Space Life Sciences, in press.

Pyrolysis Study of Carbon in Lunar Fines and Rocks

D. J. DesMarais

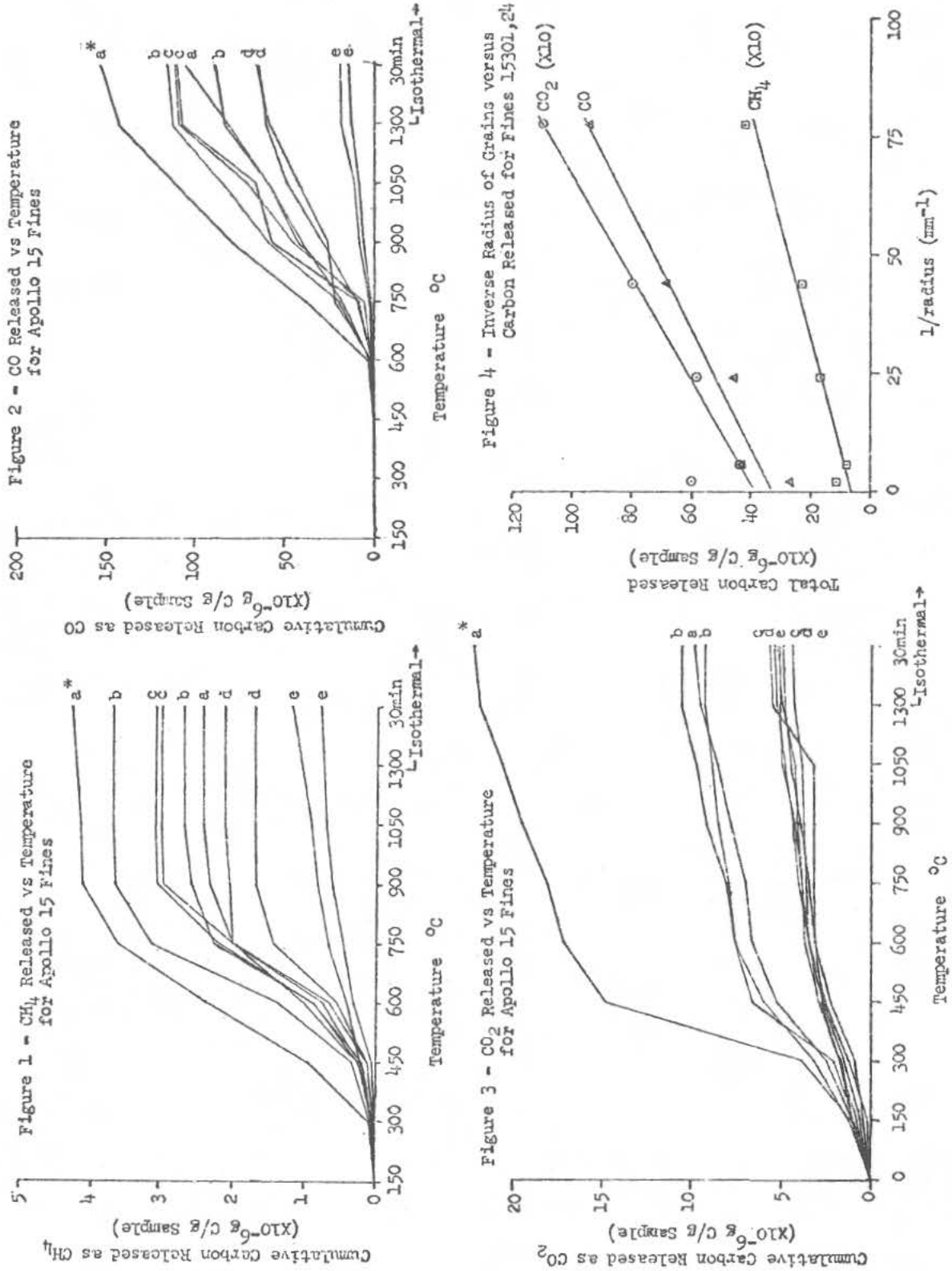

*Sample Identification: a - 15221, b - 15250, c - 15231, d - 15301, e - 15401.

ANALYSIS FOR AMINO ACID PRECURSORS OF A SAMPLE OF LUNAR SOIL SUBJECTED TO ROCKET EXHAUST ON APOLLO 15. Sidney W. Fox, Kaoru Harada, Institute for Molecular and Cellular Evolution, University of Miami, Coral Gables, FL 33134 and P. E. Hare, Geophysical Laboratory, Carnegie Institution of Washington, D.C. 20008.

Several α-amino acids have been found in hydrolyzates of hot aqueous extracts of lunar fines from seven collections from Apollo missions 11, 12, and 14[1]. By employing procedures of extraction, hydrolysis, and instrumental assay developed in these laboratories, other teams have verified these findings, in one case through an intralaboratory comparison of two methods of assay[1]. Since the two methods of instrumental assay used indicated the same amino acids in the same range of quantitative content, the essential balance sheet of amino acids first reported (by retention time on ion-exchange column) for Apollo 11 samples is confirmed.

The possibility that the amino acids found are obtained from oxidized rocket fuel on the lunar surface has been tested directly with a sample returned by Apollo 15. Sample 15013,5 was collected at the LM after exposure to the descent engine[2], and it has now been examined in the laboratory.

METHODS

Methods have been described[1].

RESULTS

Results are presented in Table I for three successive extractions of sample 15013,5. Three extractions were used as a check.

The ratio of sample value/blank value is 30/1, indicating once again almost total freedom from contamination during analysis.

DISCUSSION

The analysis of Table I reveals for the first extract a total of 0.15 nmole of total amino acids per g. of lunar soil. This corresponds, on a weight basis, to 12 ng/g. The lowest value found previously for the first extract of other samples is 19 ng/g., recorded for samples 12033 and 14003 both. The likely interpretation of this result is that no amino acid precursors were added to the lunar soil from the oxidized rocket fuel. The results, rather, are consistent with the view that the indigenous amino acid precursors are partially destroyed by the rocket blast, perhaps by a slight oxidation.

The use of a sample of soil subjected to a blast from rocket fuel constitutes the most direct way of answering the question of whether the oxidized fuel is a source of amino acids on hydrolysis. Experiments in the laboratory in oxidizing 1,1-dimethylhydrazine have been negative for amino acids[3]. A

Amino Acid Precursors

S. W. Fox

sample of fuel exhaust products supplied by Dr. A. L. Burlingame and Dr. D. Flory[4] showed only trace amounts of ninhydrin-positive material other than ammonia. These products were not supplied with a control, so correction for the amount found in that special sample cannot be made. The uncorrected amount found in that instance, however, was a fraction of the quantity of total amino acid identified in our controls tested by the laboratory analysis used in 1970[3]. Moreover, the Burlingame-Flory sample revealed a single definite peak, whereas all analyses performed during and since the sampling of Apollo 11 (eight collections) indicate several amino acids on hydrolysis[1]. The result with the Burlingame-Flory sample has been part of the evidence against the fuel as a source, although it was not alluded to as such at the time only the Apollo 11 analyses were available.

The analysis of the sample collected at the actual mission site (Table I), however, provides more rigorous evidence than that collected heretofore.

Table I

Amino Acids in Hydrolyzate of Aqueous Extract of Rocket Fuel-Blasted Sample from Apollo 15 (15013,5) in 10^{-2} nmole/g

Amino Acid	First Extract	Second Extract	Third Extract	Blank
Aspartic acid	0.3	0.3	-	<0.1
Threonine	0.3	0.1	-	-
Serine	1.0	0.3	0.3	0.1
Glutamic acid	0.5	0.5	0.5	<0.1
Glycine	11.0	3.0	1.3	0.1
Alanine	1.3	0.5	0.3	0.1
Isoleucine	0.3	0.3	-	-
Leucine	0.3	0.3	-	-

No other amino acids detected

Contamination by human products of astronauts[5], by rocket exhaust products, or by subsequent handling are thus essentially ruled out. The amino acid precursors are evidently indigenous to the Moon.

The small amounts found are consistent with the low carbon and nitrogen contents of the lunar soil[6-8]. The ratio of amino acid precursor to nitrogen and carbon content is more significant than the proportion of amino acid precursor to lunar soil.

Of special significance is the fact that the amino acids are found as precursors easily converted to amino acids by hydrolysis, instead of in the free state. Although amino acids are stabilized somewhat by their inner salt structure[9], they are easily converted to polymers by simple heating[10] at temperatures such as occur on the Earth or have evidently existed on the Moon. The availability of amino acids as evolutionary intermediates could, however, have resulted from their tendency to be generated continuously from precursors, by reaction with water. The nature of simulation experiments in the production of amino acids has been such as to obscure this dynamic relationship. Because of these facts, we may infer that lunar exploration has

revealed perspectives on molecular relationships that probably would not have been uncovered by laboratory experiments for some time.

The exact chemical nature of the precursors is being investigated.

REFERENCES

1. S. W. Fox, K. Harada, P. E. Hare, Proc. Third Lunar Sc. Conf. 2, in press (1972).

2. R. L. Sutton, M. H. Hait, K. B. Larson, G. A. Swann, V. S. Reed, G. G. Schaber, Interagency Report: Astrogeology 47 (April, 1972, preliminary; U.S. Geol. Survey), pp. 23, 24, 256.

3. S. W. Fox, K. Harada, P. E. Hare, G. Mueller, G. Hinsch, Science 167, 767 (1970).

4. P. E. Hare, K. Harada, S. W. Fox, Proc. Apollo 11 Lunar Sc. Conf. 2, 1799 (1970).

5. K. Harada, P. E. Hare, C. R. Windsor, S. W. Fox, Science 173, 433 (1971).

6. P. H. Cadogan, G. Eglinton, J.N.M. Firth, J. R. Maxwell, B. J. Mays, C. T. Pillinger, in Lunar Science--III (editor C. Watkins), pp. 113-115, Lunar Science Inst. Contr. no. 88.

7. C. B. Moore, C. F. Lewis, J. Cripe, W. R. Kelly, F. Delles, in Lunar Science--III (editor C. Watkins), pp. 550-551, Lunar Science Inst. Contr. no. 88.

8. C. Ponnamperuma, S. Chang, J. Lawless, K. Kvenvolden, I. R. Kaplan, in Lunar Science--III (editor C. Watkins), p. 612, Lunar Science Inst. Contr. no. 88.

9. S. W. Fox and J. F. Foster, Introduction to Protein Chemistry, John Wiley and Sons, Inc., New York, 1957.

10. S. W. Fox, Ann. N.Y. Acad. Sci. 194, 71 (1972).

ISOTOPIC COMPOSITION OF CARBON AND HYDROGEN IN SOME APOLLO 14 AND 15 SAMPLES* Irving Friedman, Kenneth G. Hardcastle, and Jim D. Gleason, U. S. Geological Survey, Denver, Colo. 80225

Abstract. A new combustion line was constructed that yielded low blanks for CO_2 and H_2. The results from combustion of fines and breccia from Apollo 14 and fines, breccia, and basalt from Apollo 15 were compared with data obtained by heating samples in a vacuum to over 1350°C. The two techniques gave similar results.

Total carbon in the fines ranged from 51 to 110 ppm with a δC^{13} from +12 to -8 permil PDB. The breccias have 22 to 50 ppm carbon with a δC^{13} of -21 to -25 permil. The crystalline rock (15555) has a carbon content of about 7 ppm and a δC^{13} of -28 permil.

The total hydrogen in the fines ranges from 66 to 120 ppm, with a D/H x 10^{-6} from 39 to 90. The breccias have 8 to 38 ppm H_2 with a D/H x 10^{-6} of 103 to 144. The crystalline rock contains about 2 ppm H_2 with a D/H x 10^{-6} of about 140.

Arguments are presented to show that the contamination by earth materials is not as serious a problem as has been proposed by previous authors.

INTRODUCTION. Although three separate groups of investigators have carried out δC^{13} and three groups have carried out D/H analysis of lunar material, there has been little agreement between the analysts on the carbon and hydrogen isotopic composition of lunar material. It has always been our belief, as expressed in the report of the First Lunar Science Conference (Friedman et al.(1)), that much of the apparent disagreement is a result of sample inhomogeneity.

By the time of the Second Lunar Science Conference we had not changed our belief. Our additional analyses gave a range of δC^{13} values from -3 to -25 permil for dust, breccia, and crystalline rocks. Epstein and Taylor(2) and Kaplan et al.(3) had determined a range in carbon values from +20 to -30 permil.

CARBON. In order to settle some of the points at issue, we have constructed a new combustion line made of glass and metal, with no organic materials of any kind.

Before a sample was combusted, it was heated in vacuo in the combustion tube for at least 16 hours at a temperature of 125°-150°C. Blanks were always run before moving the combustion boat from the 125°C section of the vycor combustion tube into the 950°C section. These blanks always resulted in an amount of gas condensable with liquid N_2 equivalent to less than 1 μg CO_2 and gas condensable at dry ice temperature equivalent to less than 0.5 μg H_2 as

---

*Publication authorized by the Director, U. S. Geological Survey.

ISOTOPIC COMPOSITION OF C AND H IN SOME APOLLO 14 AND 15 SAMPLES

Irving Friedman

H_2O. These are in contrast to the blanks of 205 μg CO_2 and 88 μg H_2 reported by Epstein and Taylor[4] and ∿5 μg C reported by Kaplan and Petrowski[5]. Combustions were carried out for 1 to 1 1/2 hours, and the reaction products were condensed in a trap cooled with liquid oxygen.

Reproducibility of the combustion apparatus was checked by use of small (∿2 mm diameter) disks that were punched out of filter paper. First a number of disks equivalent to 500 μg carbon were combusted, then one-half of a disk, equivalent to 48 μg carbon, was combusted. The large sample gave a δC^{13} of -24 5 permil and the small sample a δC^{13} of -24.6 permil. Our combustions, with the exceptions of the two residues from our pyrolysis, were made with carbon in amounts ranging from 8 to 108 μg.

From these analyses, we concluded that we could secure δC^{13} analysis by combustion on samples of ∿50 μg with a precision of ± 2 permil, and that our error on samples of ∿10 μg was probably not greater than ± 5 permil.

In order to check on the importance of exposure to air of our outgassed crucible, we built an apparatus that allowed us to completely outgas the equipment and crucible before dropping the outgassed sample into the platinum crucible.

In spite of these precautions, we found that the gases evolved from the two rocks processed consisted mostly of CO_2 and H_2O. The ratio of total CO_2 to CO (or CH_4) was about 5 to 10. The H_2O-H_2 ratio ranged from 3 to 40. The preponderance of oxidized species was found at temperatures of 200° to 600°C, and some were found at higher temperatures. These findings reinforce our previous conclusion that CO_2 is a primary constituent and not an artifact of our procedures. One sample (14305) showed a lower ratio of CO_2 to CO at the lower temperatures, thus it is possible that the lower CO_2-CO ratios found by Epstein and Taylor[6] were evolved at temperatures lower than they state. It is noteworthy that they used an induction heater for all of their heating and measured their temperatures with an optical pyrometer. They estimated temperatures below ∿600°C, and their temperatures below this may have been off by as much as 100°C.

At temperatures above about 700°C the reduced carbon species present in the sample (C, CO, CH_4) probably react with the iron oxides and silicates to produce a mixture of CO and CO_2. Any free hydrogen will also react to give H_2O. Therefore, we do not think that the proportions of oxidized versus reduced species of carbon and hydrogen evolved at elevated temperature has any relation to their original ratio in the unheated sample. In addition, all of the samples have been exposed to some atmospheric oxygen, and this contaminant may not be easily removed, especially on dust (soil) samples. Table 1 gives the results of our analyses.

Our experience with stepwise heating (pyrolysis) versus combustion for the determination of carbon content and δC^{13} is that the two techniques give essentially identical results (see Table 2).

Table 1. Results of heating and combustion.

Sample No.	Type	Wt. (g)	Temp. (°C)	Vacuum Heating H_2 ppm	δD	H_2O ppm H_2	δD	CO_2 ppm	δC^{13}	$CO + CH_4$ ppm	δC^{13}	Combustion H ppm	δD	C ppm	δC^{13}	Total H ppm	D/H x 10^6	δD	C ppm	δC^{13}
15271,29	dust	1.02	950									120	-510	105	-3.9	120	78	-510	105	-4
14422,13	dust	0.98	950									82	-434	110	-8.4	82	90	-434	110	-8
15100,3	fines	0.97	950									90	-554	99	+7.9	90	71	-554	99	+8
15459,30,37	breccia	0.34	950									8	-200	22	-25	8	126	-200	22	-25
15459,100	breccia	0.30	950									38	-346	50	-22	38	103	-346	50	-22
14305,57	breccia	0.74	950									20	-109	50	-21.9	20	141	-109	50	-22
15555,144	basalt	1.41	950									2.8	-130	7.3	-27.5	2.8	138	-130	7.3	-28
15100,3	dust	0.95	950									66	-617	74	+11.5	66	60	-617	74	+12
15555,144	basalt	3.49	180- 600	.22	-62	.46	-104	1.5	-28.0	0.3	-38									
			600- 1350	.09	--	.51	-5	4.0	-15.8	0.6	-43									
			combusted									.70	-160	1.3	-28.4	2.0	143	-93	7.7	-24
14305,57	breccia	2.49	180- 600	.33	-100	13.6	-88	11.3	+22.9	2.3	-24.7									
			600- 760	.04	--	3.1	-79	10.8	-24.6	0.5	-27.5									
			760- 1350	.02	--	.9	-99	17.8	-21.3	0.2	--									
			combusted									1.8	-128	1.9	-27.3	20	144	-90	45	-21
15100,3	dust	3.0	210- 415	5	-900	18	-598	--	--	--	--									
			415- 585	29	-826	18	-826	1.3	+7.3	--	--									
			585- 760	2.3	-567	10	-756	1.8	+14.3	combined $CO+CO_2$										
			760-1350	.1	-370	1.4	-619	43	+8.3	4	+10.3									
			combusted									1	-284	1	--	85	39	-756	51	+9

Concentrations = ± 20 percent of amount present.

D/H x 10^6 = ± 10 percent.

δC^{13} = ± 1 permil, except for samples of < 10 µg.

δD = ± 10 permil, except for samples of < 5 µg.

δC^{13} values are permil deviations from PDB.

δD values are permil deviations from SMOW.

D/H x 10^6 was calculated from δD.

SMOW values, using the relation D/H x 10^6 = 0.158 (1000 + δD permil).

ISOTOPIC COMPOSITION OF C AND H IN SOME APOLLO 14 AND 15 SAMPLES

Irving Friedman

Table 2. Comparison between pyrolysis and combustion techniques.

Sample No.	Sample wt. (g)	Procedure	Carbon ppm	Carbon δ	Hydrogen ppm	Hydrogen δ
14305,57	2.49	pyrolysis	45	-21	20	-90
	.74	combustion	50	-22	20	-109
15100,3	3.0	pyrolysis	50	+9	85	-760
	0.97	combustion	99	+8	90	-550
	0.95	combustion	74	+11	66	-620
15555,144	3.49	pyrolysis	7.7	-24	2.0	-90
	1.41	combustion	7.3	-27	2.8	-130

HYDROGEN. The total hydrogen, including molecular H_2, H_2O, and CH_4, ranges from 2 ppm ($\sim$ 143 x 10^{-6} D/H) for 15555 to 120 ppm (78 x 10^{-6} D/H) for 15271.

Although terrestrial contamination is always a possibility, as has been previously discussed (Friedman et al.[1]; Epstein and Taylor[6]), we believe that our experiments give an indication of the amount of this contamination. Dust samples that have been combusted at 900°C and then opened to laboratory air and recombusted show a maximum contamination of 5 ppm H_2. Samples that have been melted in vacuum at 1350°C and then exposed to laboratory air and combusted give an upper limit of 0.7 to 1.8 ppm H_2 contamination.

The exact molecular "species" that contains the hydrogen is uncertain, and to some extent a semantic problem. Certainly the extraction procedures used by us and by Epstein and Taylor cannot easily differentiate whether the H_2 present as atomic H in a radiation "hole" is bound loosely or tightly to oxygen in the silicate or oxide mineral. Hydrogen generated by spallation reactions will probably be more tightly bound than hydrogen "adsorbed" by lunar outgassing, while solar wind protons will probably have some intermediate stability in relation to the host lattice. Materials subject to a high degree of shock metamorphism before the introduction of protons may provide a stronger H-O bound than more perfect silicate (or oxide) lattices.

The range in total H_2 in the dust samples leads us to believe that contamination is not as serious a problem as indicated by Epstein and Taylor. It would appear that crystalline rocks contain about 2 to 9 ppm H_2 with a deuterium concentration of 130 to 210 ppm. This hydrogen is probably spallationogenic, plus hydrogen remaining after melting and partial outgassing of the rocks.

The dust and breccia contain an additional component of hydrogen that is partially of solar wind origin, partially captured meteoritic hydrogen, and partially captured lunar outgassing hydrogen.

ISOTOPIC COMPOSITION OF C AND H IN SOME APOLLO 14 AND 15 SAMPLES

Irving Friedman

The authors thank James R. O'Neil and Prof. H. Kranzenmeyer for their clever suggestions, help, and encouragement.

REFERENCES

(1) FRIEDMAN I., GLEASON J. D., and HARDCASTLE K. G. (1970) Water, hydrogen, deuterium, carbon and C^{13} content of selected lunar material. *Proc. Apollo 11 Lunar Sci. Conf., Geochim. Cosmochim. Acta*, Suppl. 1, Vol. 2, pp. 1103-1109.

(2) EPSTEIN S. and TAYLOR H. P., Jr. (1970) The concentration and isotopic composition of hydrogen, carbon and silicon in Apollo 11 lunar rocks and minerals. *Proc. Apollo 11 Lunar Sci. Conf., Geochim. Cosmochim. Acta*, Suppl. 1, Vol. 2, pp. 1085-1096.

(3) KAPLAN I. R., SMITH J. W., and RUTH E. (1970) Carbon and sulfur concentration and isotopic composition in Apollo 11 lunar samples. *Proc. Apollo 11 Lunar Sci. Conf., Geochim. Cosmochim. Acta*, Suppl. 1, Vol. 2, pp. 1317-1330.

(4) EPSTEIN S. and TAYLOR H. P., Jr. (1972) O^{18}/O^{16}, Si^{30}/Si^{28}, C^{13}/C^{12} and D/H studies of Apollo 14 and 15 samples. *Proc. Third Lunar Sci. Conf.* (in press).

(5) KAPLAN I. R. and PETROWSKI C. (1971) Carbon and sulfur isotope studies on Apollo 12 lunar samples. *Proc. Second Lunar Sci. Conf., Geochim. Cosmochim. Acta*, Suppl. 1, Vol. 2, pp. 1397-1406.

(6) EPSTEIN S. and TAYLOR H. P., Jr. (1971) O^{18}/O^{16}, Si^{30}/Si^{28}, D/H and C^{13}/C^{12} ratios in lunar samples. *Proc. Second Lunar Sci. Conf., Geochim. Cosmochim. Acta*, Suppl. 1, Vol. 2, pp. 1421-1441.

THERMAL ANALYSIS-INORGANIC GAS RELEASE STUDIES ON APOLLO 14, 15, AND 16 LUNAR SAMPLES. Everett K. Gibson, Jr., NASA Manned Spacecraft Center, Houston, TX 77058 and Gary W. Moore, Lockheed Electronics Corp., Houston, TX 77058

Two Apollo 14 soils, one Apollo 14 breccia, four Apollo 15 soils, two Apollo 15 basalts, and two Apollo 16 soils have been analyzed by thermal analysis-inorganic gas release techniques (1-3). Samples were heated at 6°C/min. to 1400°C under vacuum, and the released gaseous species, abundances, temperature ranges, and sequences of release were determined (Figures 1-11). Gases measured included H_2, He, H_2O, CO, N_2, HCN, O_2, H_2S, CO_2, SO_2, and CS_2.

The gas release pattern for the soil samples 14259,111, 15261,26, 15271,25, 15301,25, and 15601,31 are all similar (Figures 1-5). No major differences were noted for the samples taken from the bottom (15261,26) and top (15271,25) of the Apollo 15 trench. Soil samples 14259,111, 15301,25, and 15601,31 have almost identical gas release patterns to soil 14163,178 reported on previously (3). The only apparent difference is in the amount of gases (CO, N_2) released near the sample melting points arising from gases strongly bound or gases escaping from gas-rich inclusions from samples 14259,111 and 15601,31. Soil 14003,71 collected near the LM is apparently contaminated with exhaust products. The sample contains unusually large amounts of CO and CO_2 which are lost from the sample at temperatures below 150°C (Figure 6). Simoneit et al. (4) previously noted that these two gases are major components from the exhaust products of the LM fuels. The low-grade breccia 14301,48 has a gas release pattern almost identical with soils from the Apollo 14 site, but its weight-loss curve is distinctly different from those obtained with Apollo 14 soils (Fig. 7).

The gas release patterns from two Apollo 15 basalts (15058,72 and 15065,39) are similar (Figures 8 and 9). The absence of solar wind derived species (e.g. H_2 and CO_2) which are released below 700°C is apparent. The basalts contain less volatile components by a factor of 5 to 10 than lunar soils and low grade breccias.

Two Apollo 16 soil samples do not have the "normal" lunar soil gas release pattern. Subsurface soil 61221 is unusually rich in volatiles which are released between 175° and 350°C (Figure 10) and is distinctly different from any previously analyzed lunar soil. A weight loss of 0.03% occurs over the temperature ranges of greatest volatile release. A semi-quantitative analysis of the volatiles released between 175° and 350°C indicates: 40-50% H_2O, 15-20% CO_2, 5-10% H_2, 5-10% CH_4, 5-10% HCN, 1-5% other hydrocarbons and 2-5% CO and/or N_2. The low temperature released volatiles are different in their release profiles from terrestrially adsorbed components or solar wind derived gases. We have suggested (5) that the unusually volatile rich soil 61221 was derived from North Ray crater and possibly contains remanants of volatiles associated with the impacting projectile which may have been a comet.

Sample 66041 collected at Station 6 (the site of sample 66095 which apparently contains goethite (6)) contains trace amounts of water which is

released in the temperature ranges similar to the release of H_2O from terrestrial goethites. Sample 66041 (Figure 11) does not contain the unusually large quantities of CO_2, H_2, HCN, CH_4 or hydrocarbons found in sample 61221.

The gases derived from lunar samples are from several sources: (1) atmospheric contaminants or LM rocket exhaust products, (2) solar wind derived species, (3) chemical reaction products, (4) gases from vesicles and gas-rich inclusions and/or gases tightly bound which are released when the samples are molten, and (5) possible remanant components from volatile-rich projectiles. Deposition of ray material on the lunar surface followed by rapid burial may result in retention of selected volatiles at depth. The conclusions of this study support those previously advanced by Gibson and Johnson (1) and Gibson and Moore (3,5).

References

1. E.K. Gibson and S.M. Johnson, Proc. Second Lunar Sci. Conf. 2, 1351-1366 (1971).
2. E.K. Gibson, Thermochim. Acta (in press) 1972.
3. E. K. Gibson and G.W. Moore, Proc. Third Lunar Sci. Conf., in press (1972).
4. B.R. Simoneit et al., Science 166, 733-738 (1969).
5. E.K. Gibson and G.W. Moore, Science (submitted) (1972).
6. LSPET-Apollo 16, Science (in press) (1972).

Note: The gas release patterns vs temperature have been plotted so that each of the gases has been normalized to 100% amplitude in their region of greatest abundance. The arrow on the weight loss curve of each figure represents the initial melting point of the sample.

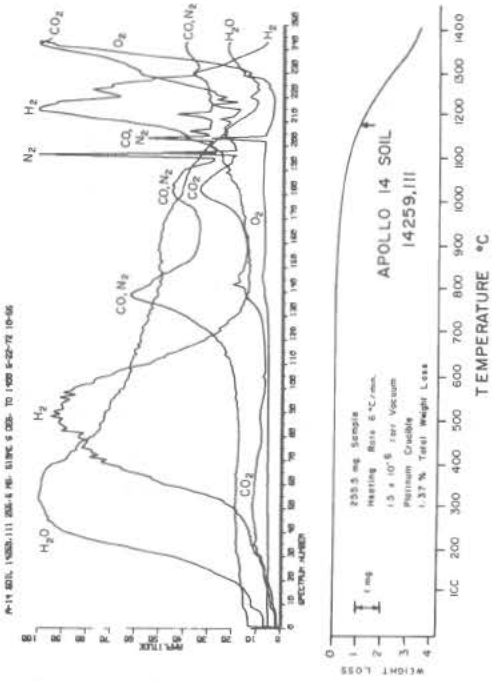

FIGURE 1

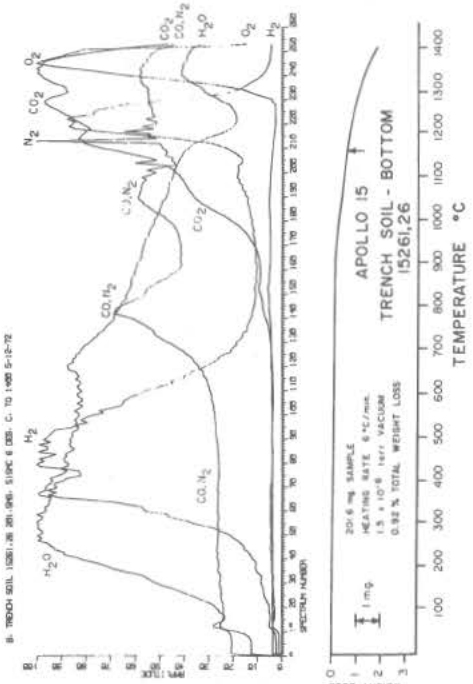

FIGURE 2

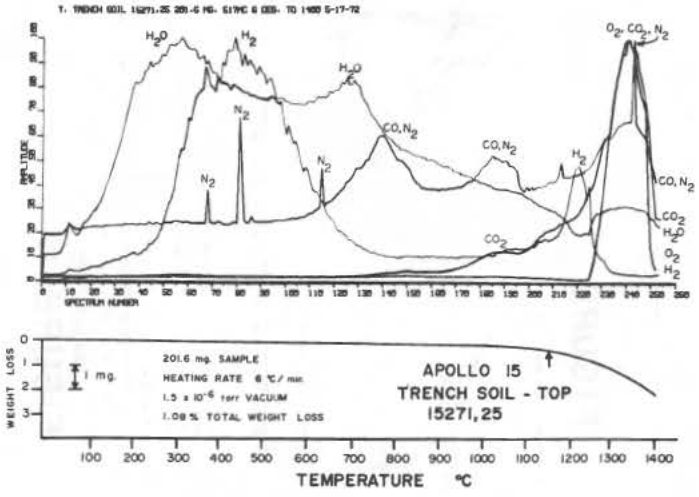

FIGURE 3

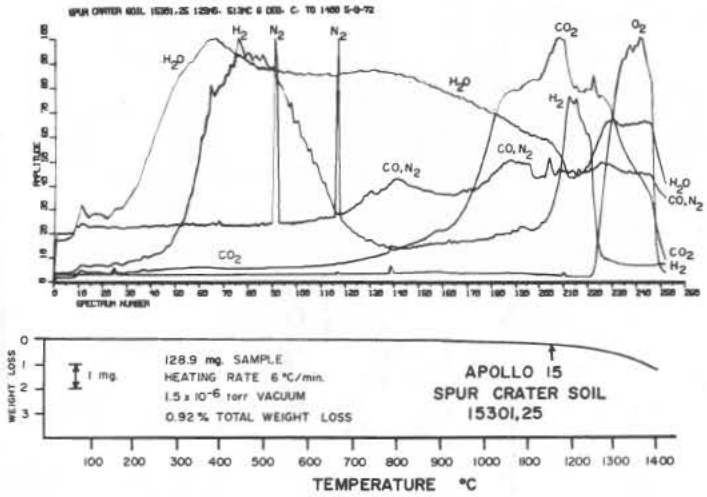

FIGURE 4

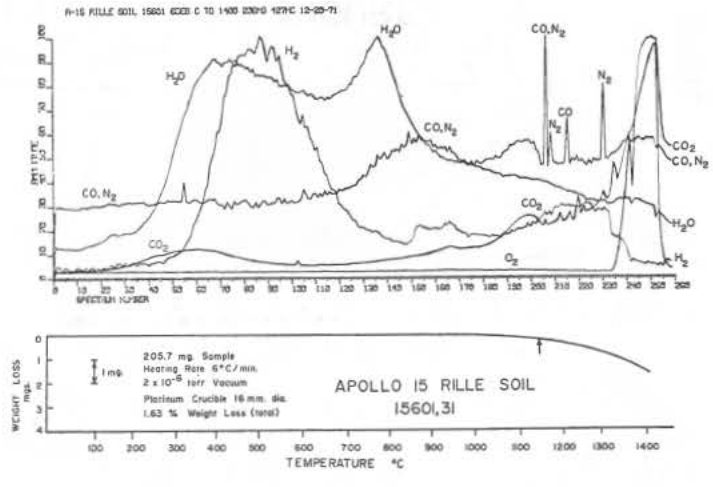

FIGURE 5

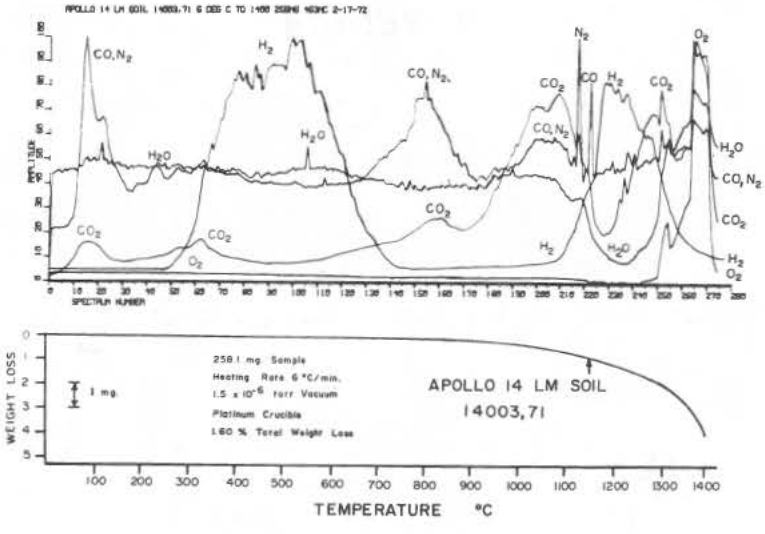

FIGURE 6

Thermal analysis-inorganic gas release studies ....
E. K. Gibson

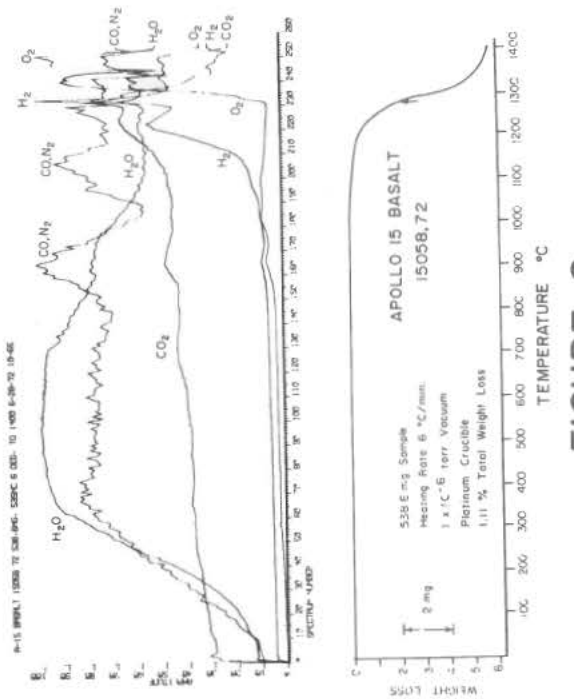

FIGURE 8

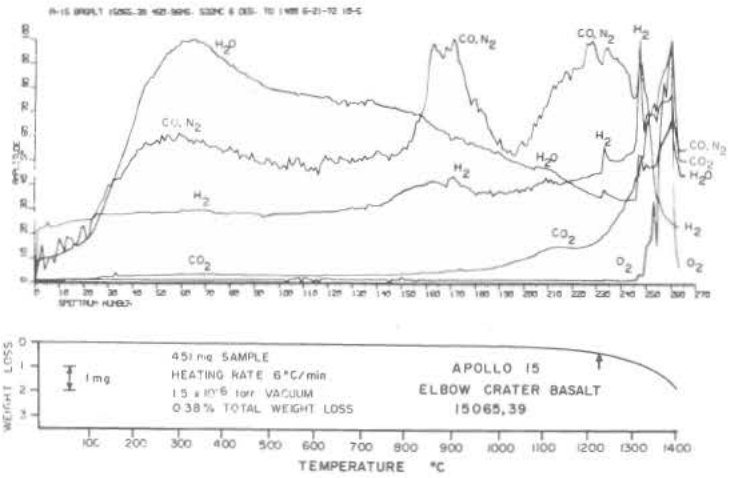

FIGURE 9

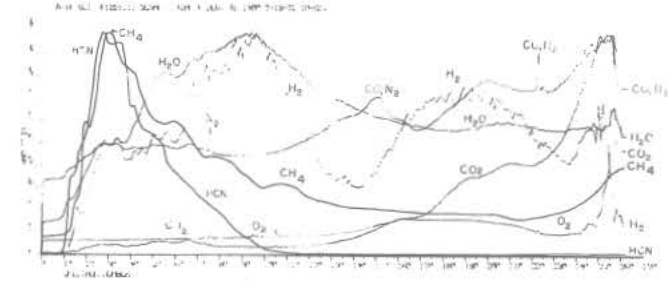

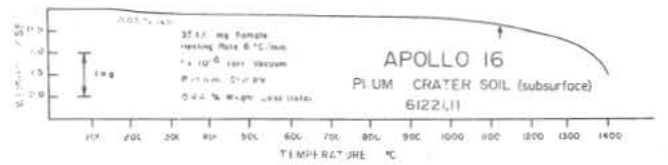

FIGURE 10

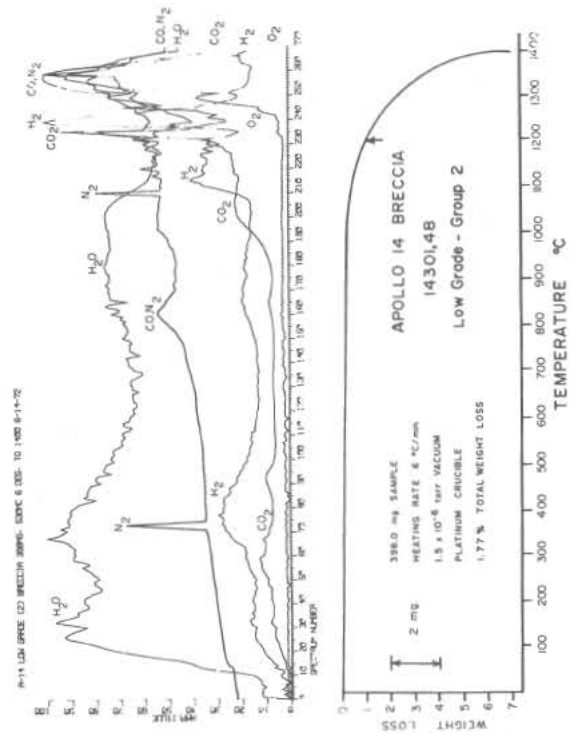

FIGURE 7

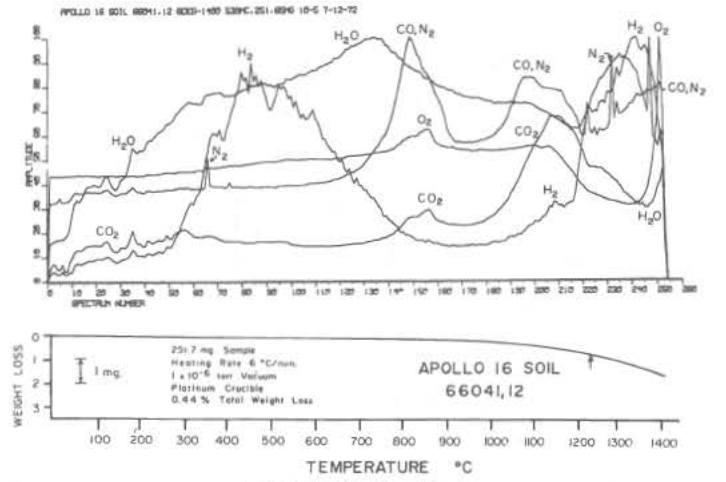

FIGURE 11

CARBON COMPOUNDS IN APOLLO 15 LUNAR SAMPLES

by

Judith E. Modzeleski, Vincent E. Modzeleski,
Lois A. Nagy and Bartholomew Nagy
The University of Arizona, Tucson, Ariz., 85721

Paul B. Hamilton
A. I. du Pont Institute, Wilmington, Del., 19899

William S. McEwan
Naval Weapons Center, China Lake, Cal., 93555

Harold C. Urey
The University of California at San Diego, La Jolla, Cal., 92037

Carbonaceous gases were determined by a combined vacuum pyrolysis mass spectrometric technique. The primary carbonaceous gases liberated were CO, CO_2 and CH_4. The Apollo 15 samples which were analyzed consisted of: six fines, one clod fines ("green-rock" sample 15426), five breccias, and nineteen samples from the "deep core", section 15005. The quantitative results of these analyses may be found in Tables I and II. Sample 15471 is described by NASA as being collected in an area which was previously disturbed by the activities of the astronauts; consequently this sample may contain a small percentage of "kicked over" material [1]. It is noteworthy that this particular sample yielded the highest total carbon content (100.5 ppm) of all the fines studied. Sample 15426 is unique in that it contained no CO. This is the first lunar sample analyzed in this laboratory which has been totally lacking CO. This particular sample also gave the lowest total carbon content of any of the Apollo 15 samples analyzed. The clod fines or "green-rock" sample is described as consisting of approximately 50% green glass. This glass has not been previously observed in lunar samples and is a unique glass with regard to its homogeneity and nonvesicular character [2]. Sample 15455 is a breccia which consists of approximately 50% white (norite) and 50% dark material [2]. The white material (15455,65) shows a total carbon content of over twice that in the dark portion (15455,66) of this rock. This increase is found primarily in the carbon from CO_2 and CH_4.

Carbon Compounds in Apollo 15 Lunar Samples

Judith E. Modzeleski

The nineteen core samples covered a depth of 14.4 cm in the second section of the deep drill core. The first section was reported to range from 32.9 - 39.9 cm in depth [3]. Based upon these values, the depth covered by the analysis of these nineteen samples ranged from approximately 33 cm to 47 cm beneath the lunar surface. This can be considered as a minimum estimate because of the somewhat uncertain depth range of the first core section (15006). The distribution of the carbon content from the three gases of these core samples is shown in Fig. 1. It is evident from this figure that the basic core profile is relatively constant for each gas. The notable exceptions are the large increase in the values at a depth of 10.0 - 10.5 cm (15005,155) and a somewhat lesser increase at the 12.0 - 12.5 cm depth (15005,165). In both of these cases all three gases showed increased values. At a depth of 13.0 - 13.5 cm, however, the CO shows a large increase whereas both CO_2 and CH_4 do not. The relative proportions of these gases may not represent their original distribution because of possible alterations in their ratios caused by the analytical procedure.

The Apollo 15 SESC sample was extracted by refluxing with hot water and then the extract was hydrolyzed with HCl. Some amino acids appeared in concentrations which were definitely above the procedure blank. The origin of amino acids in lunar samples is still not fully known.

References

1. Swann, G. A. et al. (1972), Preliminary Geologic Investigation of the Apollo 15 Landing Site in Apollo 15 Preliminary Science Report, NASA SP-289, p. 5-80.

2. The Lunar Sample Preliminary Examination Team (1972), Preliminary Examination of Lunar Samples in Apollo 15 Preliminary Science Report, NASA SP-289, pp. 6-12, 6-14, 6-16.

3. Mitchell, J. K. et al. (1972), Soil Mechanics Experiment in Apollo 15 Preliminary Science Report, NASA SP-289, p. 7-8.

Carbon Compounds in Apollo 15 Lunar Samples

Judith E. Modzeleski

Table I

Apollo 15 - Gas Analyses

Sample No.	Carbon in ppm from carbonaceous gases			
	CO	CO_2	CH_4	Total C
15071,10 (fines)	30.5	0.8	0.3	31.6
15091,21 (fines)	45.5	4.4	2.6	52.5
15091,25 (fines)	45.9	5.9	1.0	52.8
15100,8 (fines)	39.5	2.4	0.8	42.7
15240,1 (fines)	31.4	9.9	1.0	42.3
15471,13 (fines)	72.7	23.2	4.6	100.5
15426,33 (clod fines)*	-0-	2.4	0.1	2.5
15455,65 (rock-white portion)	1.6	6.6	0.8	9.0
15455,66 (rock-dark portion)	2.0	2.0	0.2	4.2
15466,3 (rock)	2.2	3.8	0.1	6.1
15498,32 (rock)	9.2	6.8	0.4	16.4
15505,22 (rock)	24.1	23.1	0.4	47.6

*Values are an average of two runs.

Carbon Compounds in Apollo 15 Lunar Samples

Judith Modzeleski

Table II

Apollo 15 - Gas Analyses - Deep Drill Core, Section 15005

Sample No.	Depth (cm)	Carbon in ppm from carbonaceous gases			
		CO	CO_2	CH_4	Total C
15005,131	3.0 - 3.5	25.6	13.0	0.3	38.9
15005,133	3.5 - 4.0	23.2	7.0	0.3	30.5
15005,134	4.0 - 4.5	24.3	8.4	0.3	33.0
15005,137	4.5 - 5.0	24.5	9.5	0.1	34.1
15005,139	5.0 - 5.6	28.7	5.8	0.3	34.8
15005,140	5.6 - 6.0	25.4	4.2	0.04	29.6
15005,141	6.0 - 6.5	27.5	6.1	0.3	33.9
15005,142	6.5 - 7.0	22.0	5.0	0.3	27.3
15005,150	8.5 - 9.0	27.2	8.0	0.3	35.5
15005,153	9.5 - 10.0	23.8	4.6	0.3	28.7
15005,155*	10.0 - 10.5	46.4	21.4	3.8	71.6
15005,158	10.5 - 11.0	26.2	9.0	0.2	35.4
15005,160	11.0 - 11.5	20.1	6.8	0.1	27.0
15005,163	11.5 - 12.0	22.6	10.2	0.3	33.1
15005,165	12.0 - 12.5	38.1	32.2	0.6	70.9
15005,167	12.5 - 13.0	24.9	9.9	0.4	35.2
15005,170*	13.0 - 13.5	45.7	9.8	0.3	55.8
15005,172	13.5 - 14.0	24.0	11.1	0.4	35.5
15005,175	14.0 - 14.4	32.5	13.4	0.3	46.2

*Values are averaged for two runs.

Carbon Compounds in Apollo 15 Lunar Samples

Judith E. Modzeleski

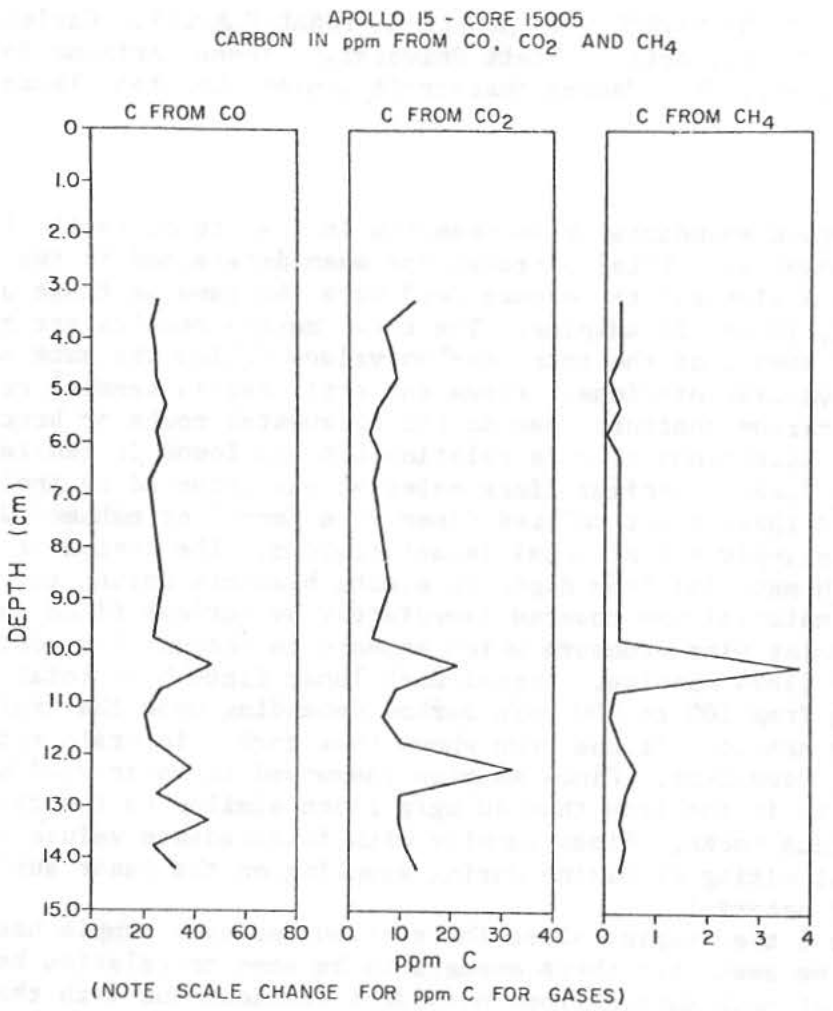

Figure 1

CARBON AND NITROGEN IN APOLLO 15 LUNAR SAMPLES. Carleton B. Moore and Charles F. Lewis, Arizona State University, Tempe, Arizona 85281 and Everett K. Gibson, Jr., NASA Manned Spacecraft Center, Houston, Texas 77058.

Total carbon abundances have been run in a suite of Apollo 15 fines, breccia and rock samples. Total nitrogen has been determined in two related fines samples. The analytical techniques used were the same as those utilized for the Apollo 11, 12 and 14 samples. The total carbon results are given in Table 1. It may be seen that the total carbon values follow the same pattern as those of the earlier missions. Fines and soil breccia samples generally have higher total carbon contents than do the fragmental rocks or breccias and igneous rocks. Exceptions to this relationship are found in samples of light colored lunar fines. Similar fines material was returned by Apollo 12. It was concluded that these light colored fines were formed or exhumed during the formation of relatively recent local impact craters. The cratering process removed regolith material from depth to ejecta blankets during the impact. Most of the fines material was covered immediately by surface fines and hence protected from solar wind exposure which appears to account for most of the excess carbon in the fines samples. Normal dark lunar fines have total carbon contents ranging from 100 to 200 μg/g carbon depending upon the grain size distribution in the sample. It has been shown that carbon is grain size, and hence surface area, dependent. Fines samples unexposed to solar wind have low total carbon contents in the less than 40 μg/g range similar to the carbon in igneous and meta-igneous rocks. Fines samples with intermediate values may indicate either natural mixing or mixing during sampling on the lunar surface of exposed and unexposed material.

In Table 1 the sample collection station for each sample has been indicated. It may be seen that there appears to be some correlation between the carbon contents of each sample from individual stations and with the sample environment. Normal high carbon samples were collected at stations 1, 2, 6, 8 and 9 and at the lunar module. This indicates that the fines in these areas were the product of a uniform evolution and gardening rate. Samples from stations 4, 6a, 7 and 9a show low carbon contents. The station 4 samples were taken from a single locality outside the rim of Dune Crater and the station 7 samples near the rim of Spur Crater. In this sense they are similar to the samples taken near the rims of Bench and Head Craters on Apollo 12. Stations 6a and 7 are both near the front of Hadley Delta, a site of potential instability. Station 6 showing normal mature fines is in the same region and illustrates the possible variations in local sampling. Station 9a close to the rim of Hadley Rille is also a site of potential instability.

C AND N IN APOLLO 15 LUNAR SAMPLES

Moore, Carleton B.

The overall total carbon results support earlier conclusions that the excess carbon in the fines samples is due to solar wind implantation of carbon atoms. Low carbon contents indicate sample shielding from solar wind.

Two samples from the SESC containers were analyzed for total nitrogen. Samples 15012,2 and 15012,12 had a total nitrogen content of 60 µg/g. SESC control samples 15013,13 and 15013,15 likewise had total nitrogen contents of 60 µg/g. Earlier work indicated that atmospheric nitrogen may account for 20 to 40 µg/g of the measured total nitrogen in lunar material. This leaves a residue of 20 to 40 µg/g of nitrogen in the lunar fines most likely added by solar wind.

Table 1. Carbon in Apollo 15 samples (µg/g)

Sample No.	Station	Sample Type	Total C µg/g
15012,2	6	fines, SESC	135
15012,12	6	fines, SESC	140
15013,13	6	fines, SESC lunar module	150
15013,15	6	fines, SESC lunar module	150
15021,4	LM	fines <1mm	160
15021,38	LM	fines <1mm	140
15031,15	8	fines, trench bottom <1mm	125
15031,31	8	fines, trench bottom	145
15041,15	8	fines, trench top <1mm	160
15041,34	8	fines, trench top	160
15058,4	8	porphyritic basalt	27
15071,19	1	fines <1mm	110
15076,3	1	gabbro	21
15080,6	1	fines, unsieved	115
15091,34	2	fines <1mm	120
15100,10	2	fines, unsieved	115
15101,2	2	fines <1mm	125
15101,2	2	fines <1mm	135
15221,32	2	fines <1mm	115
15231,38	2	fines <1mm	130
15240,3	6	fines, unsieved	100
15250,5	6	fines, unsieved	175
15261,33	6	fines <1mm	115
15271,15	6	fines <1mm	170
15271,30	6	fines <1mm	110
15291,27	6	fines <1mm	105
15298,2	6	microbreccia	160
15298,26	6	microbreccia	130
15301,1	7	fines <1mm	155
15301,30	7	fines <1mm	110
15401,14	6a	fines <1mm	29

C AND N IN APOLLO 15 LUNAR SAMPLES

Moore, Carleton B.

Table 1. (cont.)

Sample No.	Station	Sample Type	Total C µg/g
15411,13	7	fines <1mm	74
15418,5	7	breccia, vitreous matrix	11
15421,10	7	fines <1mm	35
15426,32	7	green and gray clod	21
15431,17	7	fines <1mm	73
15459,1	7	breccia	85
15471,2	4	fines <1mm	89
15471,18	4	fines <1mm	74
15501,1	9	fines <1mm	130
15501,12	9	fines <1mm	110
15556,4	9a	vesicular basalt	16
15558,2	9a	breccia	110
15600,8	9a	fines-comprehensive, unsieved	72
15601,3	9a	fines-comprehensive, <1mm	95

Underlined samples were analyzed during the preliminary examination.

Acknowledgments - This work was supported by NASA grants NGL-03-001-001 and NGR-03-001-057.

DISTRIBUTION OF CARBON AND SULFUR IN HYDROLYZED APOLLO 15 LUNAR FINES. H. Sakai*, S. Chang#, C. Petrowski*, J. Smith *† and I. R. Kaplan* (*University of California, Institute of Geophysics and Planetary Physics, Los Angeles, Ca. 90024; #NASA, Ames Research Center, Moffett Field, Ca. 94035; †Permanent Address: Division of Minerology, C. S. I. R. O., North Ryde, N. S. W., Australia)

CH_4, CO, CO_2, H_2S, H_2 and He have been released by acid treatment from bulk samples of 15012 and 15013 fines and from aliquots of size separated and magnetically separated 15012 fines. Data from analyses of bulk and sieved aliquots are listed in Table 1. The total CH_4 yields from bulk samples lie in the range measured previously for lunar fines. When indigenous methane (free) amounting to 3 ppm C with an average δC^{13} value of +38‰ is taken into account, the carbide derived CH_4 component in 15012 represents 10 ppm carbon with δC^{13} = +12 ‰. It is apparent that most of the CO and CO_2 detected cannot be terrestrial contamination because of their high ^{13}C enrichments. The H_2S released from the bulk fines amounts to about 710 ppm. The value of δS^{34} = + 9.85 ‰ represents the highest S^{34} enrichment measured thus far in bulk samples of fines. Using the value of 72 ppm solar wind H obtained by pyrolysis of sample 15012, and assuming that the remainder of the H is derived only from dissolution of metallic iron, an estimate of the metallic iron abundance and the FeS/Fe ratio can be obtained. These estimates are listed in parentheses in Table 1. Helium abundances in these experiments are consistent with the 14 ppm released during pyrolysis.

Data for various fractions of the sieved sample are depicted in the Figure. The concentrations of all gases appear to be surface correlated. However, the correlation for H_2 and H_2S does not appear to extend to the coarsest fragments. As solar wind H_2 is expected to be surface correlated, the excess H_2 from dissolution of metallic iron, and therefore the iron itself appears to be surface correlated.

The following isotopic data from Table 1 are particularly noteworthy. 1. The respective values of -8 ‰ and -7 ‰ for CO_2 and CH_4 released from the coarsest fraction are consistent with a contribution from either unaltered primordial lunar carbon or unaltered meteoritic

carbon. Terrestrial contamination is expected to be least in the coarsest size fraction because of its lower surface area and minimal handling. 2. In the finest size fraction, the H_2S, CO_2 and CH_4 are strongly enriched in S^{34} and C^{13} relative to the coarsest fraction; thus either the major contributing sources of C and S in these two fractions are isotopically different or fractionation processes leading to heavy isotope enrichment act most efficiently on the finest particles. Whatever, the surface process(es) responsible for these data (solar wind?), it (they) must account for the total C and S enrichment in the finest particles as well as the concommitant C^{13} and S^{34} enrichments.

An aliquot of sieved 15012 fines (<50 μm) was treated with 6 N H_2SO_4 at three different temperatures. In addition, a sieved aliquot (50 to 125 μm) was separated into a magnetic and a less magnetic fraction, and each fraction was hydrolyzed at three different temperatures. The resulting data are compiled in Table 2 and Table 3, respectively. Several features of the data are especially significant. 1. (Table 2) Isotopically light CO_2 was released only after heating to 100°C for 49 hours, suggesting an unaltered carbon source, either primordial lunar or meteoritic, that has been protected from surficial C^{12} depletion mechanisms. 2. (Table 2) Given a value of δC^{13} = +16.55 (from Table 1) for total CH_4 in this sieve fraction, an isotopic balance requires that the CH_4 released at -16° to -13°C be the most depleted in C^{12}, which would be consistent with a process preferentially depleting C^{12} on the surfaces of particles (solar wind?). 3. (Tables 2 and 3) In all instances, S^{32} enriched H_2S is first released at the lower temperatures. 4. Substantially more CH_4, CO_2, H_2S, and H_2 are released from the magnetic than from the less magnetic fraction. Thus carbide and sulfide phases are preferentially associated with magnetic phases. 5. (Table 3) Essentially equivalent amounts of He are released from magnetic and less magnetic fractions indicating equivalent exposure to solar wind. The fact that sulfide in the magnetic fraction is more enriched in S^{34} than the less magnetic fraction suggests that solar wind interaction with particle surfaces cannot be the only process responsible for depletion of S^{32} in the very fine sieve fractions. Similarly, more than one mechanism may be available for preferential depletion of C^{12}.

TABLE 1. PRODUCTS FROM 6N H_2SO_4 HYDROLYSIS OF BULK (15012 & 15013) AND SIEVED (15012) FINES

RECIPROCAL MEAN GRAIN RADIUS	$3\ mm^{-1}$		$11\ mm^{-1}$		$23\ mm^{-1}$		$80\ mm^{-1}$					
SIEVE FRACTION	>250 μm		125 TO 250 μm		50 TO 125 μm		<50 μm		15012 BULK		15013 BULK	
SAMPLE WEIGHT (g)	0.998		1.657		2.601		3.022		1.9398		1.793	
HYDROLYSIS TEMPERATURE (°C)	100		100				100		100		100	
PERIOD OF HYDROLYSIS (HR.)	124		144				48		72		336	
GASES RELEASED	ppm	%*	ppm	%*	ppm	%*	ppm	%*	ppm	%*	ppm	%*
CH_4	5.4 C	−7.0	5.8 C	+15	6.9 C		17.7 C	+16.55	13.0 C	+17.67	16.0 C	+17.66
CO_2	15.5 C	−8.0	16.4 C	−9.35	24 [1b] C		23.7 C	+6.44	8.0 C	+17.81	7.5 C	+5.18
CO	0		0.6 C								1.0 C	+6†
H_2S	5.82 S	+6.33	571 S	+8.05	584 S	+8.20	710 S	+10.60	711 S	+9.85	707 S	+9.2
H_2	163 H (4,570 Fe)		163 H (4,570 Fe)		208 H (5,830 Fe)		500 H (14,000 Fe)		278 H (5770 Fe)		380 H (8060 Fe)	
He	1.8 He		2.9 He		5.5 He		16.0 He		12.7 He		16.2 He	
(FeS/Fe)	(0.223)		(0.219)		(0.175)		(0.090)		(0.120)		(0.090)	

Carbon and Sulfur Distribution

H. Sakai

TABLE 2. PRODUCTS FROM 6N H_2SO_4 HYDROLYSIS OF 15012 FINES, < 50 μm SIEVE FRACTION.

	HYDROLYSIS TEMPERATURES AND TIMES							
	−16 to −13°C, 2 HOURS		+10°C, 3 HOURS		100°C, 49 HOURS			
GASES RELEASED	ppm	%*	ppm	%*	ppm	%*	TOTAL ppm	WEIGHTED AVERAGE %
CH_4	2.6 C		12.0 C	+12.6	5.5 C	+11.3	20.1 C	
CO_2	5.8 C	+5.0	5.6 C	+16	3.2 C	−6.05	14.6 C	+4.1
CO	0		0		0.6 C		0.6 C	
H_2S	252 S	+5.72	294 S	+15.67	168 S	+20	714 S	+13.2
H_2	54 H (1,510 Fe)		210 H (5,870 Fe)		108 H (3,020 Fe)		372 H (10,400 Fe)	
H_e	5.0 He		7.7 He		9.5 He		22.2 He	
(FeS/Fe)	(0.291)		(0.088)		(0.098)		(0.120)	

TABLE 3. PRODUCTS FROM 6N H_2SO_4 HYDROLYSIS OF MAGNETICALLY DIFFERENTIATED 15012 FINES (>50 TO 125 μm)

	(1) MAGNETIC FRACTION 1.3731g							(2) LESS MAGNETIC FRACTION 1.2278g						
EXTRACTION	1ST		2ND		3RD		TOTAL	1ST		2ND		3RD		TOTAL
TEMPERATURE OF HYDROLYSIS	−15 TO −20 C		+10 C		100 C			−18 TO −12 C		+10 C		100 C		
PERIOD OF HYDROLYSIS	2 HOURS		2 HOURS		55 HOURS			2 HOURS		2 HOURS		24 HOURS		
GASES RELEASED	ppm	%*	ppm	%*	ppm	%*	ppm	ppm	%*	ppm	%*	ppm	%*	ppm
CH_4	1.6 C		5.5 C	+10.4	1.4 C		8.5 C	2.0 C		1.6 C		1.3 C		5.0C
CO_2†●	(26 C)†●		(7 C)†●		(2 C)†●		(35 C)†●	5 C	−10.2	(5 C)†●		(2 C)†●		(12 C)
H_2S	184 S	+8.52	283 S	+9.24	235 S	+10.25	702 S	113 S	+3.80	150 S	+7.48	182 S	+8.25	445 S
H_2	28 H		153H		94 H		275 H	35 H		53 H		43 H		131 H
	(780 Fe)		(4,300 Fe)		(2,630 Fe)		(7,710 Fe)	(970 Fe)		(1,480 Fe)		(1,200 Fe)		(3,640 Fe)
He	1.3 He		2.2 He		2.2 He		5.7 He	0.9 He		1.9 He		2.5 He		5.3 He
FeS/Fe	(0.4)		(0.114)		(0.155)		(0.158)	(0.220)		(0.174)		(0.380)		(0.216)

●DATA FOR THIS FRACTION CONSIST OF WEIGHT AVERAGED VALUES OF ALL EXTRACTION FRACTIONS FROM TABLE 3.

†MEASURED BY ISOTOP DILUTION.

*δC^{13}_{PDB} OR δS^{34}

●THIS FRACTION CONTAINED VARIABLE AMOUNTS OF IMPURITIES, THEREFORE ACTUAL AMOUNTS OF C AS CO_2 RANGE FROM 10 TO 50% LOWER THAN INDICATED.

Carbon and Sulfur Distribution

H. Sakai

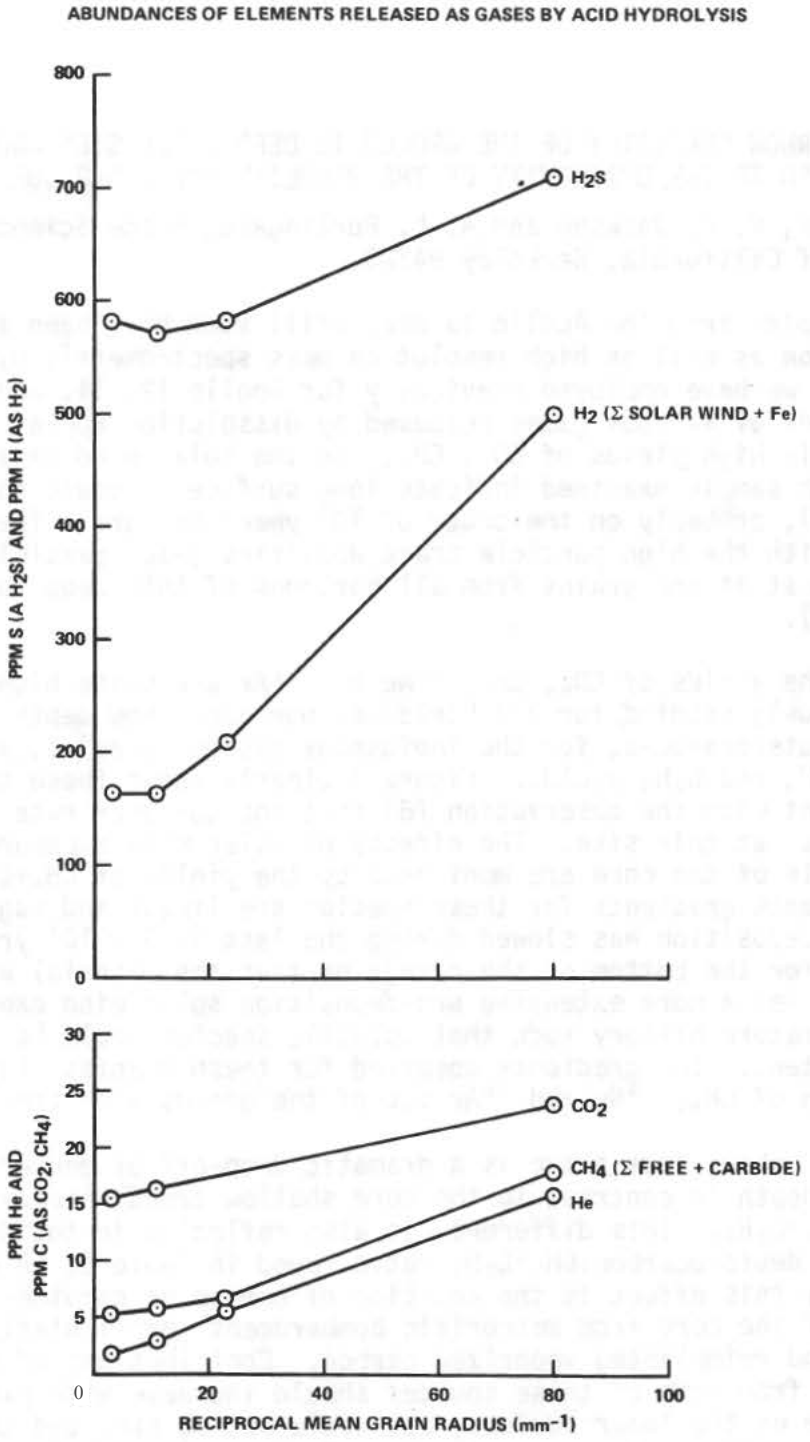

CARBON CHEMISTRY OF THE APOLLO 15 DEEP DRILL STEM AND A GLASS-RICH SAMPLE RELATED TO THE UNIFORMITY OF THE REGOLITH AND LUNAR SURFACE PROCESSES.

P. C. Wszolek, R. F. Jackson and A. L. Burlingame, Space Sciences Laboratory, University of California, Berkeley 94720.

Six samples from the Apollo 15 deep drill stem have been studied by the DF dissolution as well as high resolution mass spectrometric pyrolysis techniques which we have employed previously for Apollo 12, 14, and 15 samples (1-3). Yields of various gases released by dissolution appear in Table I. The relatively high yields of CD_4, CH_4, and the solar wind gases ^{20}Ne and ^{36}Ar for each sample examined indicate long surface exposure to solar wind radiation (3), probably on the order of 10^7 years or more. These data are compatible with the high particle track densities (>10^8 particles/cm^2) observed for most of the grains from all horizons of this deep core studied to date (4,5).

While the yields of CD_4, CH_4, ^{20}Ne and ^{36}Ar are quite high (compared to soils previously studied) for all horizons, our data show depth gradients for the total deuterocarbons, for the indigenous gaseous species, and for the sum of the CH_4 and C_2H_6 yields. Figure 1 clearly shows these trends which are consistent with the observation (6) that the turnover rate to 240 cm is $> 5 \times 10^8$ yrs. at this site. The effects of solar wind exposure on the various levels of the core are monitored by the yields of $CH_4+C_2H_6$, ^{20}Ne and ^{36}Ar. The depth gradients for these species are linear and suggest that: the rate of deposition has slowed during the last 5-10 $\times$ 10^8 yrs [the age deduced (6) for the bottom of the core]; or that the material at the top of the core has had a more extensive pre-deposition solar wind exposure; or a milder temperature history such that volatile species would be retained to a greater extent. The gradients observed for these species might also reflect the diffusion of CH_4, ^{20}Ne and ^{36}Ar out of the grains with time.

Figure 1 shows that there is a dramatic drop-off of deuterocarbon yields with depth in contrast to the more shallow trends observed for ^{20}Ne, ^{36}Ar, and $CH_4+C_2H_6$. This difference is also reflected in the decline with depth of the deuterocarbon:$CH_4+C_2H_6$ ratio found in Table I. A partial explanation for this effect is the addition of carbon or carbide-like material to the top of the core from meteoritic bombardment, particularly micrometeorites and reimplanted vaporized carbon. Contributions of carbon to the regolith from both of these sources should increase with exposure time of the sample on the lunar surface, but would not be expected to account for the large differences observed here. Another less likely possibility is that carbon has become more abundant with time in the solar wind relative

Wszolek, P. C.

Table I. Gases released on DF hydrolysis of Apollo 15 samples.

	Sample						
	15006, 178	15006, 135	15004, 182	15003, 10	15002, 306	15001, 10	15426, 30
Depth below surface (cm)	0	37	89	159	167	239	--
CD_4	1011	755	497	471	379	450	10
CH_4	244	139	142	161	119	131	25
^{20}Ne	56.9	65.7	31.9	40.2	29.3	17.9	7.4
^{36}Ar	9.2	7.9	8.3	7.3	6.4	4.5	1.4
C_2H_6	19	46	22	23	18	33	*
C_2D_2	32	*	5	*	16	*	*
C_2D_4	118	25	41	47	52	27	*
C_2D_6	56	32	42	15	45	29	*
C_3D_6	27	17	11	11	11	8	0.1
C_4D_8	4	2	2	2	2	*	*
total deutero-carbons	1248	831	598	549	505	514	10
$CH_4+C_2H_6$	263	185	164	184	137	164	25
ratio deutero-carbons: $CH_4+C_2H_6$	4.7	4.5	3.7	2.9	3.7	3.1	0.40
Total C(ppm)	62	36	43	92	29	29	7
Total N(ppm)	84	36	21	89	18	20	29

(nanomoles/g)

* not detected

CARBON CHEMISTRY OF APOLLO 15 DEEP DRILL STEM

Wszolek, P. C.

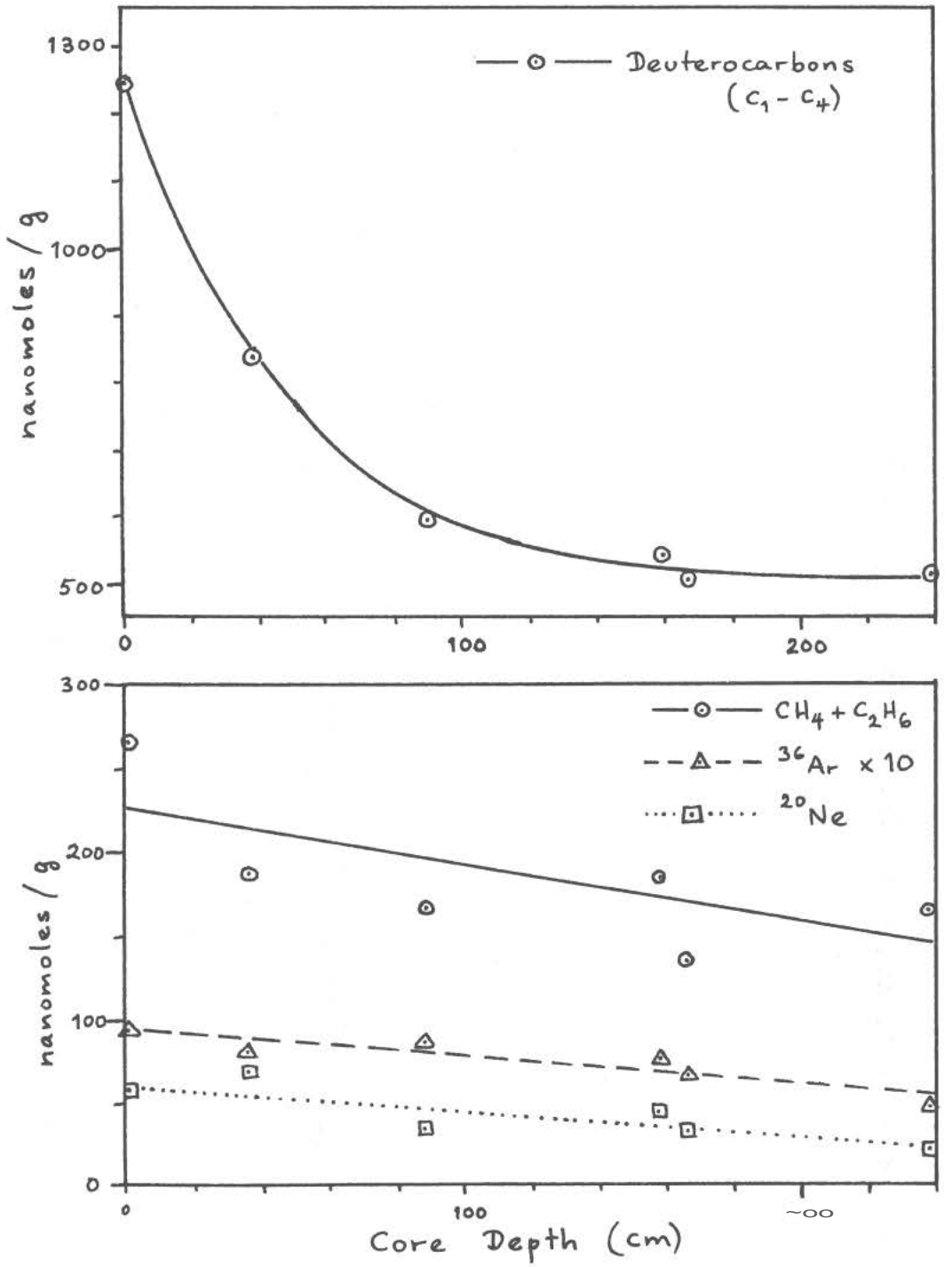

Figure 1. Yields of gases released by DF etch versus sample depth in the Apollo 15 deep drill stem.

CARBON CHEMISTRY OF APOLLO 15 DEEP DRILL STEM

Wszolek, P. C.

to hydrogen, ^{20}Ne and ^{36}Ar. The remarkable depth dependence of deuterocarbon yield may indicate, however, that a completely different mechanism is influencing the production of acid labile carbon in addition to surface exposure to the solar wind and meteoritic material. The bombardment of light nuclides such as ^{16}O and ^{14}N by energetic protons and neutrons from cosmic rays or indirectly from spallation could produce carbon and partially explain this depth dependence. Other workers have found a steep depth dependence for ^{14}C in rock 12053 (7) similar to that observed for the cosmogenic products ^{22}Na and ^{26}Al.

Our total carbon and total nitrogen numbers (in Table I), obtained from vacuum pyrolysis to 1300°C (1,3), appear to be low, considering the yields of C_1-C_4 hydrocarbons and deuterocarbons. With the exception of the relatively higher total C number for sample 15003,10, total C drops off with depth similar to the deuterocarbon yields.

Dissolution data for sample 15426,30 are also presented in Table I. This sample, taken from a friable breccia at the north rim of Spur Crater, is noteworthy for its unusually high MgO concentration and large proportion (>50%) of green glass spheres (8). The green glass component is expected to be important as a tracer in the study of the regolith at the Apollo 15 site since it is found in small amounts in most of the soils and is especially abundant in Spur Crater and Apennine Front soils (8).

Our data show that only very small amounts of CD_4, CH_4, ^{20}Ne and ^{36}Ar are evolved on DF dissolution of 15426. It is of considerable interest that the CD_4/CH_4 ratio is inverse of that of typical surface soils examined on other missions. Its dissolution behavior resembles that of the complex Apollo 14 breccias, 14310 and 14301 (3).

Vacuum pyrolysis of sample 15426 to 1300°C releases only 7 ppm C as CO (5 ppm) and CO_2 (2 ppm) and 29 ppm N. Instead of the typical bimodal evolution pattern for these species (1,9), there is only one peak at about 1200°C probably due to sample melting. The evolution peak at about 800°C is not observed, suggesting that there is little surface implanted carbon and nitrogen (1). Our data are consistent with the presumed origin for 15426 as material excavated from a depth of about 20 m when Spur Crater was formed (10). Even if any significant quantity of carbon were present in this sample prior to impact, this probably would be lost due to high temperatures associated with impact melting and formation of the green glass spheres.

Acknowledgements. We thank Dr. J. J. Chang for assistance in obtaining high resolution mass spectrometry data; the Apollo 15 crew, astronauts D. R. Scott, A. M. Worden and J. B. Irwin for drilling the core and returning this valuable sample; and NASA (Grant NGR 05-003-435) for financial support.

CARBON CHEMISTRY OF APOLLO 15 DEEP DRILL STEM

Wszolek, P. C.

References

(1) P. T. Holland, B. R. Simoneit, P. C. Wszolek and A. L. Burlingame, Space Life Sciences, in press.

(2) P. T. Holland, B. R. Simoneit, P. C. Wszolek, W. H. McFadden and A. L. Burlingame, Nature, 235, 106, (1972).

(3) P. T. Holland, B. R. Simoneit, P. C. Wszolek and A. L. Burlingame, Proc. Third Lunar Sci. Conf., D. Heymann, Ed., Geochim. Cosmochim. Acta, in press.

(4) G. Crozaz, R. Drozd, C. M. Hohenberg, H. P. Hoyt, Jr., D. Ragan, R. M. Walker and D. Yuhas, Lunar Science III, C. Watkins, Ed., LSI Contr. No. 88, 167 (1972).

(5) P. P. Phakey, I. D. Hutcheon, R. S. Rajan and P. B. Price, Lunar Science III, C. Watkins, Ed., LSI Contr. No. 88, 53 (1972).

(6) G. P. Russ, III, D. S. Burnett and G. J. Wasserburg, Earth Planet. Sci. Lett., 15, 172 (1972).

(7) F. Begemann, W. Born, H. Palme, E. Vilcsek and H. Wänke, Lunar Science III, C. Watkins, Ed., LSI Contr. No. 88, 53 (1972).

(8) Apollo 15 Preliminary Examination Team, Science, 175, 363 (1972).

(9) E. K. Gibson and S. M. Johnson, Proc. Second Lunar Sci. Conf., Geochim. Cosmochim. Acta, Vol. 2, Suppl. 2, 1351 (1971).

(10) G. A. Swann, M. H. Hait, G. G. Schaber, V. L. Freeman, G. E. Ulrich, E. W. Wolfe, V. S. Reed and R. L. Sutton, Interagency Report 36: Preliminary description of Apollo 15 samples environment, U.S.G.S., 141 (1971).

RARE GAS AND PARTICLE TRACK STUDIES OF APOLLO 15 SAMPLES: HADLEY RILLE AND SPECIAL SOILS*, C. Behrmann, G. Crozaz, R. Drozd, C. M. Hohenberg, C. Ralston, R. M. Walker and D. Yuhas, Washington Univ., St. Louis, Mo. 63130.

15595 is a Rille Station basalt chipped from a large protrusion (tentatively identified as outcropping bedrock (PET, 1971)) in the immediate vicinity of Hadley Rille. Cosmic-ray exposure ages for this rock were computed from accumulated cosmogenic rare gases using two different techniques to determine the production rates. Production rates were computed both from target element abundances and from the equilibrium abundance of Kr^{81}. In the first case the calculated exposure age represents the accumulation time at a "standard" production rate. The second case is the usual Kr^{81}-Kr exposure age with the production rate based upon the last few hundred thousand years of exposure, presumably at its highest (unshielded) value. Any partial shielding during the exposure history would result in an apparent Kr^{81}-Kr exposure age which underestimates this exposure history.

With the exception of the He^3 age, all cosmic-ray exposure ages are in remarkable agreement with the Kr^{81}-Kr method, suggesting a particularly simple exposure history for 15595 (Table 1). Moreover, the isotopic spectra of spallation Kr and Xe, which can be precisely determined for this rock (Table 1), show a fairly hard cosmic ray spectrum which suggests a single-step transition from a well shielded to an un-shielded location. The Kr^{81}-Kr exposure age is 110 my. Considering the close proximity of Hadley Rille, the massive size of the parent rock, and a similar exposure age for at least one other rock in the immediate area (Podosek et al., 1972; York et al., 1972; Marti and Lightner, 1972), one is led to interpret the exposure history with dynamics of the Rille itself, very possibly a major rock-slide that un-earthed this particular outcrop.

The uranium content, measured in an aliquot of 15595, was found to be 208 ± 29 ppb. There are 2.5×10^{-13} ccSTP/g of fission-produced Xe^{132} in the rock which is the amount expected from insitu uranium decay over 3.5 ± .3 billion years, in general agreement with age data for the Apollo 15 samples.

The track densities measured in the large pyroxene crystals of 15595 are highly zoned and anomalously low considering the 100 my. exposure age and implied simple history. The low density may mean that the boulder was chipped on the several cm scale relatively recently, or it may be that the thermal stability of tracks in pyroxene is not sufficient to insure their retention for 10^8 years. Track data on contiguous feldspar crystals, which is crucial to the correct interpretation, is ambiguous at this time due to experimental difficulties.

*We report here Apollo 15 data and interpretations in a necessarily brief form. A more complete treatment of the data will appear elsewhere.

HADLEY RILLE AND SPECIAL SOILS

Behrmann, C. et al.

Rock 15555 has a cosmic-ray track age of 34 my. - the longest yet found by us in lunar rocks. Comparing this number with the spallation age of roughly 85 my. (Podosek et al., 1972; York et al., 1972; Marti and Lightner, 1972), a rigorous upper limit of 1.3 ± .1 mm/my can be set for mass wastage type of erosion (as distinct from micro-erosion rates which are measured by solar flare track data (Crozaz et al., 1971)). In common with other lunar rocks, the depth dependence is flatter than would be expected from a simple exposure history. The calculated track density including erosion, varies a factor of 2.7 in going from 1 to 9 cm while the experimental factor is 1.8^{+3}_{-4}. Since solar flare tracks were not observed on the outer part of our sample 15555, it is possible that our sample was buried a few centimeters below the soil line. This would tend to further flatten the spectrum.

Track densities were measured in the feldspar fraction of seven different samples of fines. The results in Fig. 1 show that different soils range from heavily irradiated to lightly irradiated (see Crozaz et al. (1972) for a discussion of the distinction). The track data correlate very well with the geologic settings of the samples as given in the preliminary description of Apollo 15 sample environments (Swann et al., 1971). For example, soil sample 15231 described as a highly mature regolith (Swann et al., 1971) is found to have a very high average track density. In contrast, 15401 which is a fillet sample described by Swann et al. (1971) as "probably derived from the rock" is found to have a very low track density consistent with this interpretation. In contract, sample 15231 which was removed from the bottom of boulder 15200-15206 must represent soil that was already in place before the boulder arrived (this soil sample can thus be used to study the properties of solar wind and solar flares prior to the emplacement time). A further discussion of these results, including the implications for the emplacement time and rate of erosion of rock 15405 will be given in a later publication.

Bogard, D. D., Funkhouser, J. G., Schaeffer, O. A., Zahringer, J., Noble gas abundances in lunar material - cosmic ray spallation products and radiation ages from the Sea of Tranquility and the Ocean of Storms, J. Geophys. Res. 76, 2757-2779 (1971).

Crozaz, G., Walker, R., Woolum, D., Nuclear track studies of dynamic surface processes on the moon and the constancy of solar activity, Proc. Second Lunar Sci. Conf., Geochim. Cosmochim. Acta 3, Suppl. 2, 2543-2558, MIT Press (1971).

Crozaz, G., Drozd, R., Hohenberg, C. M., Hoyt, H. P. Jr., Ragan, D., Walker, R. M., Yuhas, D., Solar flare and galactic cosmic ray studies of Apollo 14 and 15 samples, Proc. Third Lunar Sci. Conf., Geochim. Cosmochim. Acta 3 (1972).

Marti, K., Lightner, B. D., Rare gas record in the largest Apollo 15 rock, Science 175, 421-422 (1972).

Preliminary Examination Team, A preliminary description of the Apollo 15 lunar samples, 1 November (1971).

Podosek, F. A., Huneke, J. C., Wasserburg, G. J., Gas-retention and cosmic-ray exposure ages of lunar rock 15555, Science 175, 423-425 (1972).

Swann, G. A., Hait, M. H., Schaber, G. C., Freeman, V. L., Ulrich, G. E., Wolfe, E. W., Reed, V. S., Sutton, R. L., Preliminary description of Apollo 15 sample environments, U.S.G.S., Interagency Report:36 (1971).

York, D., Kenyon, W. J., Doyle, R. I., ^{40}Ar-^{39}Ar ages of Apollo XIV and XV samples, Lunar Science III, (Ed. Carolyn Watkins), 822-824 (1972).

TABLE 1

	He^3	Ne^{21}	Ar^{38}	Kr^{81}-Kr
Prod. Rate ccSTP/my*	1.0×10^{-8} /g sample	5.6×10^{-9} /g Mg+Si	1.7×10^{-8} /g Ca	$P_{81}/P_{83} = .59$
Amount ccSTP/g	6.58×10^{-8}	1.66×10^{-7}	1.30×10^{-7}	
Exposure Age (my)†	6.5	112	105	110 ± 17

SPALLATION KRYPTON ($Kr^{83} \equiv 100$)

78	80	82	84
16.88 ± .84	48.7 ± 1.5	75.5 ± 2.2	51.3 ± 1.5

SPALLATION XENON ($Xe^{130} \equiv 100$)

124	126	128	129	131	132	134
54.8 ± .8	95.0 ± 1.5	146. ± 1.	167. ± 8.	506. ± 1.	93. ± 7.	7. ±2.

*Production rates, Bogard et al. (1971)

†Target element abundances were derived from the average of 15555 and 15556, both Rille Station basalts of similar composition (PET, 1971).

HADLEY RILLE AND SPECIAL SOILS

Behremann, C. et al.

FIGURE 1

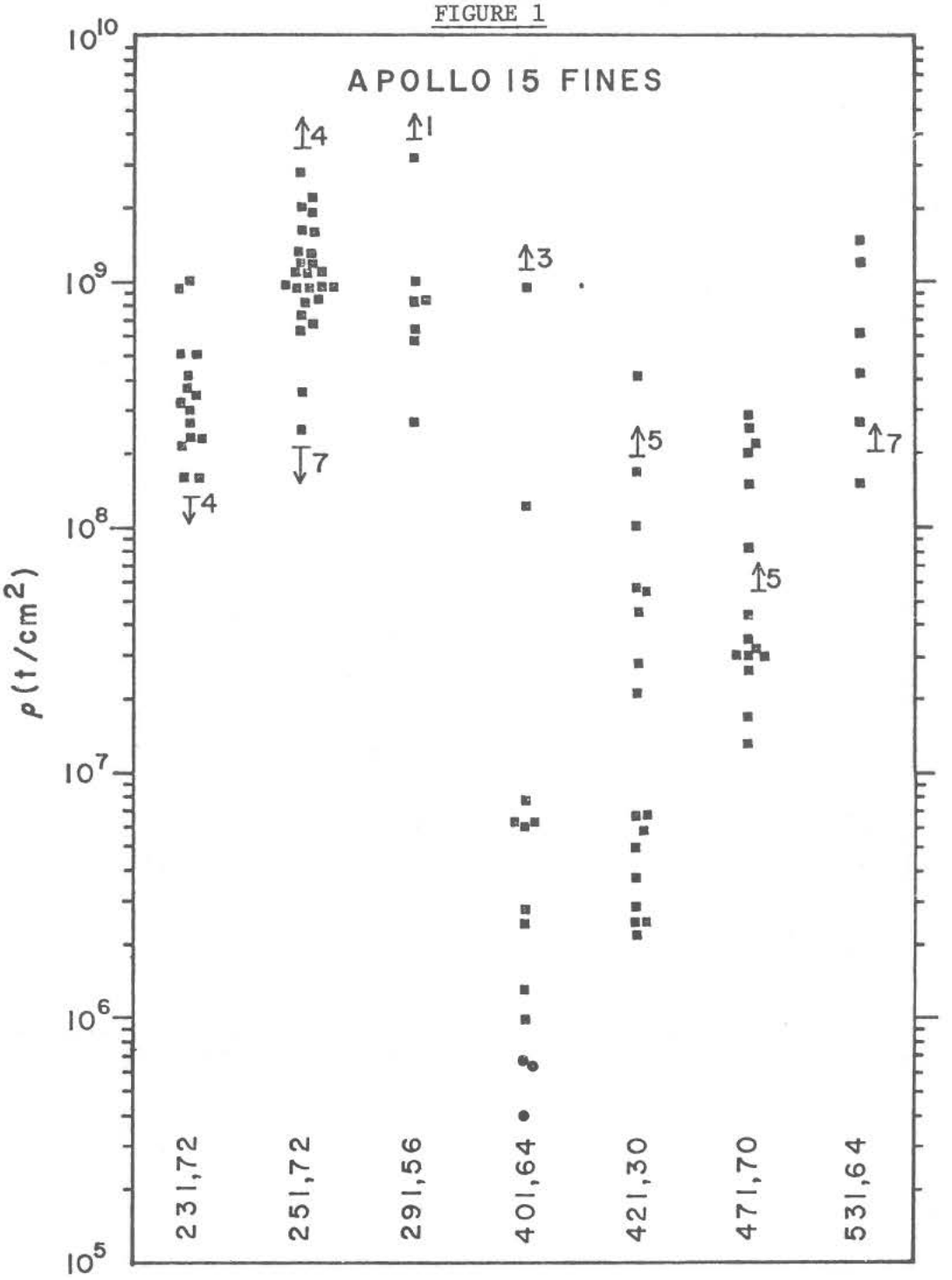

TRACK DENSITY DISTRIBUTIONS IN APOLLO 15 FINES

▪ Scanning electron microscope • Optical microscope

IRRADIATION STUDIES OF LUNAR SOILS : 15 100, LUNA 20, AND COMPACTED SOIL FROM BRECCIA 14 307

J.L. Berdot, G.C. Chétrit, J.C. Lorin, P. Pellas and G. Poupeau,
C.N.R.S. and Laboratoire de Minéralogie du Muséum, Paris, France.

Minimum track-density values have been measured in, respectively 43 and 48 anorthite fragments of soils 15 100,7 (station 2) and Luna 20 (16-27 cm depth in the core) (Fig. 1). From their high percentages of TRF (Track-Rich Fragments with minimum track-density $> 10^8/cm^2$) these two soils are numbered among the most VH-particles irradiated ones.

Soil 15 100 is outstanding by its high content (~ 50 %) of track-density gradients. However, only 1 out of 22 gradient-bearing-fragments gives evidence for a 4 π irradiation geometry. From Fig. 1 it is also clear that for a given soil, the larger the grain size the lower the minimum track-densities and the more frequent the track gradients, a fact already observed by Macdougall et al.[1].

Breccia 14 307 considered as a pre-irradiated compacted soil

This F2 coherent breccia [2] (a typical K-REEP rock) contains millimeter-sized white clasts set in a dark matrix. Both light fragments and dark matrix have large amounts of solar gases, the matrix being enriched in ^4He, ^{20}Ne and ^{36}Ar by a factor of about 2.4 compared to the white clasts (L. Schultz and P. Signer, personal communication, February 1972). Very small amounts of material (10^{-3} to less than 10^{-4} the original sampling weights) survived the batch etching treatment for track revelation. Track studies were mostly carried out on ortho and clinopyroxenes. The results are :

1) In four out of five matrix samples, the percentages of TRF ranges bet-

ween 90 and 100. In the remaining one, TRF amount only 21 %. In the last case, among 59 crystals non-TRF, 11 cluster at a track-density of $3.10^6/cm^2$, allowing a determination of the maximum surface residence time for 307 stone (Poupeau et al., this volume).

2) A white brecciated clast contains 100 % TRF.

3) Preliminary SEM studies on few TRF show that minimum track-densities range up to $1.2 \times 10^9/cm^2$ (Fig. 2 and 3).

The mean model age (T_{BABI}) for K-REEP material is about 4.4 b.y. [3]. If it is assumed that the compaction of breccia 307 resulted from the Imbrium event, dated at ~ 3.8 b.y. [4], then the available time budget (~ 0.6 b.y.) seems too short to produce the observed track-density pattern with the present solar flare activity. One way to circumvent the difficulty would be to postulate a significantly higher solar flare activity between ~ 4.6 and 3.8 b.y. Same conclusion had already been reached in trying to explain the high irradiation level observed in the anorthite crystals of Luna 16[5].

The dark matrix of 307 contains the largest absolute amount of "excess" ^{40}Ar (2.57×10^{-3} cc STP/g, after maximum radiogenic correction) ever measured in a lunar sample, with a $^{40}Ar_{exc}/^{36}Ar$ ratio of 4.8. It appears difficult to explain the large excess in ^{40}Ar by invoking K volatilization because of the high K/U ratio (1500)[6] on the one hand, and the presence of both large amounts of solar gases and cosmic-ray tracks on the other hand. In this context it would be enlightening to measure the K isotopic ratios in a few samplings of breccia 307.

REFERENCES

(1) Macdougall D. et al. (1972), Lunar Science III, p. 498.

(2) Jackson E. D. and Wilshire H. G. (1972), Lunar Science III, p. 418.

(3) Nyquist L.E. et al. (1972), Lunar Science III, p. 584.

(4) Wasserburg G. J. and Papanastassiou D.A. (1971), Earth Planet. Sci. Lett., 13, 97.

(5) Poupeau G. et al. (1972), submitted to Geochim. Cosmochim. Acta.

(6) Hubbard N.J. and Gast P.W. (1972), Lunar Science III, p. 407.

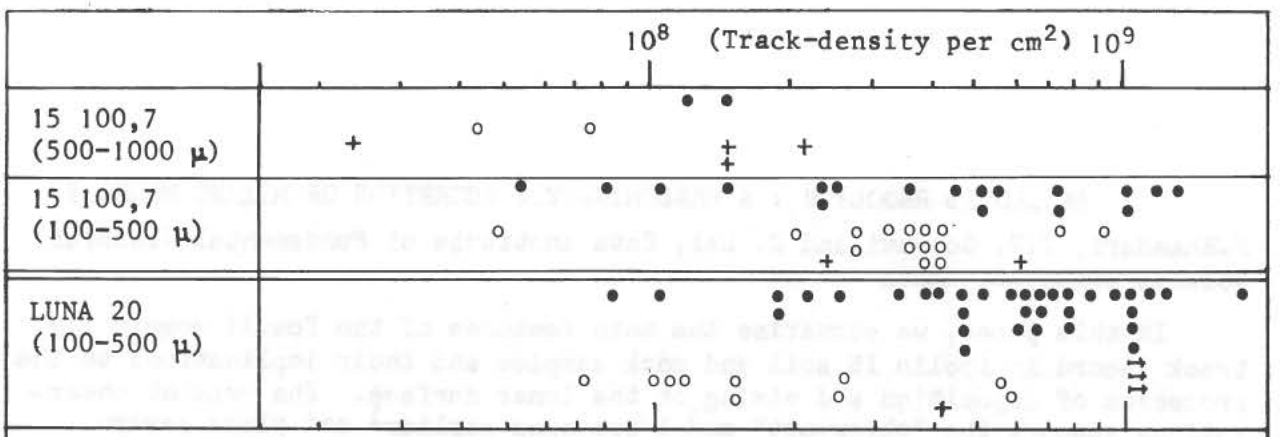

• : Fragment with no track gradient or track gradient < 3

o : Fragment with track gradient ~ 3 and < 10

+ : Fragment with track gradient > 10

Fig. 1.- Reported SEM track-densities in anorthite normalized to optical microscopy measurements (x by a factor of 0.5)

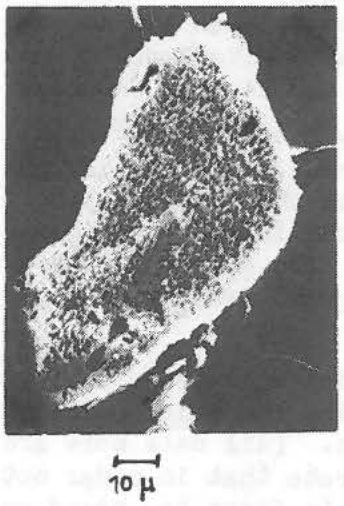

Fig. 2.- 14 307 breccia
cross section of track-rich clinopyroxene : the deterioration of the high track-density external surface can be observed (minimum track-density in the center : 1.6 x 10^8/cm^2).

(SEM picture, Laboratoire de Géologie du Muséum, Paris)

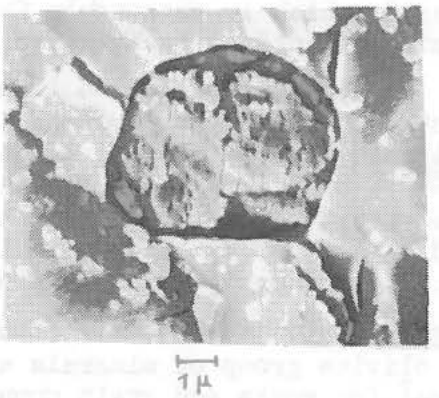

Fig. 3.- 14 307 breccia
Feldspar inclusion inside a pyroxene (track-density in feldspar is 1.2 x 10^9/cm^2).

(SEM picture, Laboratoire de Géologie du Muséum, Paris)

APOLLO 15 REGOLITH : A PREDOMINANTLY ACCRETION OR MIXING MODEL ?

N.Bhandari, J.N. Goswami and D. Lal, Tata Institute of Fundamental Research, Colaba, Bombay-5, India

In this paper, we summarise the main features of the fossil cosmic ray track record in Apollo 15 soil and rock samples and their implications to the processes of deposition and mixing on the lunar surface. The present observations support the "throw-out" model proposed earlier[1] and place severe constraints on mechanisms and rates of transport and mixing.

The earlier fossil track work of Arrhenius et al[1] led to the proposal that at the Apollo 12 site, regolith up to 70 cm depth primarily came about as a result of throw-out, i.e. discrete sedimentation. The deposited material was shown to be deep seated material which had previously not been irradiated to any significant extent. This layer by layer deposition model did not find any support from observations of Gd isotopic data[2,3] which showed that both Apollo 11 and 12 fines were well mixed - vertically. Similar inferences were also drawn by trackologists (c.f. Comstock et al[4]). Prior to analysis of Apollo 15 samples, the only support of the sedimentary model could be found in the work of McKay et al[5] who found a correlation between the amount of "glass", which is presumably formed due to micro-meteorite impacts, and the cosmic ray surface irradiation ages for Apollo 12 and 14 soil samples.

In the case of Apollo 15 core, the cosmic ray produced Mn^{53} profile is identical to that at production (Arnold, Priv. comm.). The Gd isotope data[6] in Apollo 15 core show existence of a maximum in the concentration of Gd^{158} at 250 $g.cm^{-2}$ implying that the rate of deposition/vertical mixing is less than 2 $g.cm^{-2}$ my^{-1}, for this depth interval. The present track data lead to a layer by layer deposition with an average sedimentation rate of $\lesssim 0.5$ $g.cm^{-2}$ my^{-1}, which is even smaller.

Experimental: We have measured fossil track densities in feldspar, pyroxene and olivine group of minerals and in glass following the thick section technique[7] for rocks and grain mount method[1] for fines. (All data here are based on optical microscopy). It is important to reiterate that in order not to introduce any bias, the track density frequencies in fines are based on measurements in all grains above a certain dimension (about 50 microns) as in earlier work[1].

Apollo 15 rock irradiation - cosmic ray record: In Table 1, are given all relevant data on the Apollo 15 rocks studied for fossil tracks. The patterns of track gradients have so far been studied in about 50 lunar rocks with a view to study the history of cosmic radiation as also the irradiation history of rocks (c.f. review by Lal[8]). Based on a detailed analysis of track data in rocks, Bhandari et al[9,10] determined the long-term averaged energy spectrum

APOLLO 15 REGOLITH : A PREDOMINANTLY ACCRETION OR MIXING MODEL ?

Bhandari et al.

of cosmic ray iron group nuclei up to kinetic energies of 500 MeV/n and introduced the concept of "sun-tan" and "sub-decimeter" track exposure ages based on the observation that in the case of rocks which were exposed on the lunar surface, the gradients in track densities at depths less than a few millimetres are usually similar but at greater depths they often deviated. The present results on Apollo 15 rocks (Fig.1) now support the validity of discussing separately the two track ages - sun-tan and sub-decimeter. As an illustration, in Fig.1b, we have plotted the best fit track profiles for several Apollo rocks; the hatched region shows the spread, rather a variable flattening of the track profile at depths exceeding 1 cm due to multiple exposures when the rock was either partly buried in the regolith or as a result of irradiation prior to fragmentation to its present size.

The sun-tan and burial ages are also given in Table 1. The Apollo 15 rocks are unique in as much they have usually very small sun-tan ages, less than 1 m.y. and this probably reflects their high fragility.

Apollo 15 soil irradiation - cosmic ray record: We have examined five surface samples 15091, 15101, 15211, 15221 and 15231 from around the boulder at Station 2. The similar track data in all these cases, including the sample collected from base of the boulder, clearly indicate appreciable irradiation of the "soil" prior to placement of the boulder. The radiation age of sample 15302 from the Spur Crater is 10 m.y.

In the case of Apollo 15 core, we have examined eleven samples, one each from the principal layers[11] of 15002, in detail.

The surface exposure of individual grains in soil is characterized[1] by two parameters. One of these is, N_H/N, the fraction of grains having either a steep track density gradient or a high track density ($> 10^8$ cm^{-2}). The other is the quartile track density, i.e. the value below which a quarter of the grains in a soil sample have lower track densities. The N_H/N values lie between 0.3-0.8 and the quartile values range between (5-75) x 10^6 cm^{-2}(Fig.2, Table 2). It was pointed out earlier[1] that the surface scoops and the double core at Apollo 12 site showed similar variations in these parameters and since the same situation holds for all Apollo 15 fines, it follows that the track density distribution at a given depth must be governed by accumulation of tracks when the samples were near the surface. It is quite obvious that such features cannot result by assuming that the entire soil layer was deposited quickly at some time and mixed later. We will therefore discuss further implications of the discrete deposition model[1].

1. We note that surface irradiation ages for the surface and 15002 core samples lie in the range 0-70 m.y., similar to Apollo 12 results[1]. The time duration for deposition of drill stem 15002 is $\sim$ 200 m.y. and it implies that the bottom of core 15001 was laid $\sim$ 1 B.Y. ago.

2. We consider it a significant observation that three of the layers of 15002 have surface exposure ages < 1 m.y. indicating their rapid episodic burial.

3. In the case of Apollo 15 core, we find an inverse correlation between

grain size and track density. This implies that smaller size grains are transported closer to surface regions during impact gardening, i.e. the larger grains are more sluggish. This observation leads us to think of an in-situ gradation process occurring on the lunar surface, due to impacts, leading to a stratification.

4. The observation[1,10] of large variation in surface irradiation ages of Apollo 12 and 14 scoop samples, separated by distances of the order of 100 meters, necessitates that the soil must be transported from short distances < 1 km (such large variations would not be expected if the material was transported from large distances). A local deposition model would also be required to explain the Gd data[6] for the Apollo 15 core. The calculated neutron fluences for the surface and deep regions both require that pre-irradiated material, i.e. from not too large depths, be deposited.

We therefore conclude that one of the fairly prominent features of the regolith dynamics at the four Apollo sites is the discrete deposition, layer by layer, of soil excavated from depths exceeding few decimeters. Subsequent to deposition, mixing[10] generally occurs up to depth of the order of 1 cm due to micro-meteorite impacts which results in preferential transport of lighter material and generates a stratification in-situ. The track data and Gd data require that the material be transported from local regions, of the order of 100 meters. The average rate of sedimentation at the Apollo 15 site, based on drill stem, 15002 is of the order of 0.4 $g.cm^{-2}.my^{-1}$.

We now intend to analyse other samples from 15001-6 to obtain a complete deposition and mixing history of this important core.

Acknowledgements: This paper is dedicated to Astronauts, D.R. Scott, J.B. Irwin and A.M. Worden for their extra-successful completion of the Apollo 15 mission. Thanks are due to NASA, Dr. Michael Duke and his colleagues for making the special lunar samples available to us.

References

1. G. Arrhenius et al., Proc. Second Lunar Sci. Conf. 3 (MIT Press) 2583 (1971).
2. O. Eugster et al., Earth Planet. Sci. Letters 8, 20 (1970).
3. D.S. Burnett et al., Proc. Second Sci. Conf. 2 (MIT Press) 1671 (1971).
4. G.M. Comstock et al., Proc. Second Lunar Sci. Conf. 3 (MIT Press) 2569 (1971).
5. David S. McKay et al., to be published in the Proc. Third Lunar Sci. Conf. 1 (1972).
6. G.P. Russ III et al., Earth Planet. Sci. Letters 15, 172 (1972).
7. N. Bhandari et al., Proc. Ind. Acad. Sci. LXXVI, No. 1, Sec. A 27 (1972).
8. D. Lal, Hard rock cosmic ray archaeology, to be published in Space Sci. Rev. (1972).
9. N. Bhandari et al., Proc. Second Lunar Sci. Conf. 3 (MIT Press) 2611 (1971).

APOLLO 15 REGOLITH : A PREDOMINANTLY ACCRETION OR MIXING MODEL ?

Bhandari et al.

10. N. Bhandari et al., Proc. Third Lunar Sci. Conf., to be published in Vol. 3 (1972).
11. G. Heiken and M. Duke, preprint (1972).

Caption to Fig. 1 Observed best fit track profiles in Apollo 15 rock slices (Fig. a), and in selected lunar rocks from Apollo missions 12, 14 and 15, normalised at 1 mm depth (Fig. b). The hatched region is a manifestation of multiple exposure history of rocks as partly "buried".

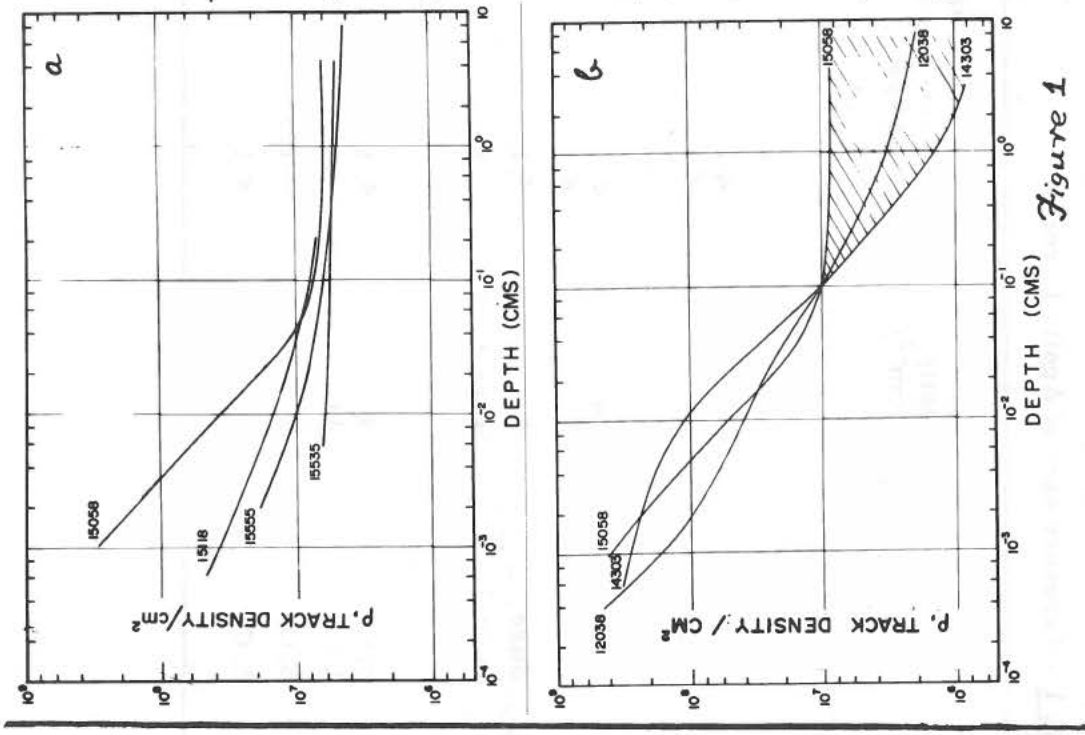

Figure 1

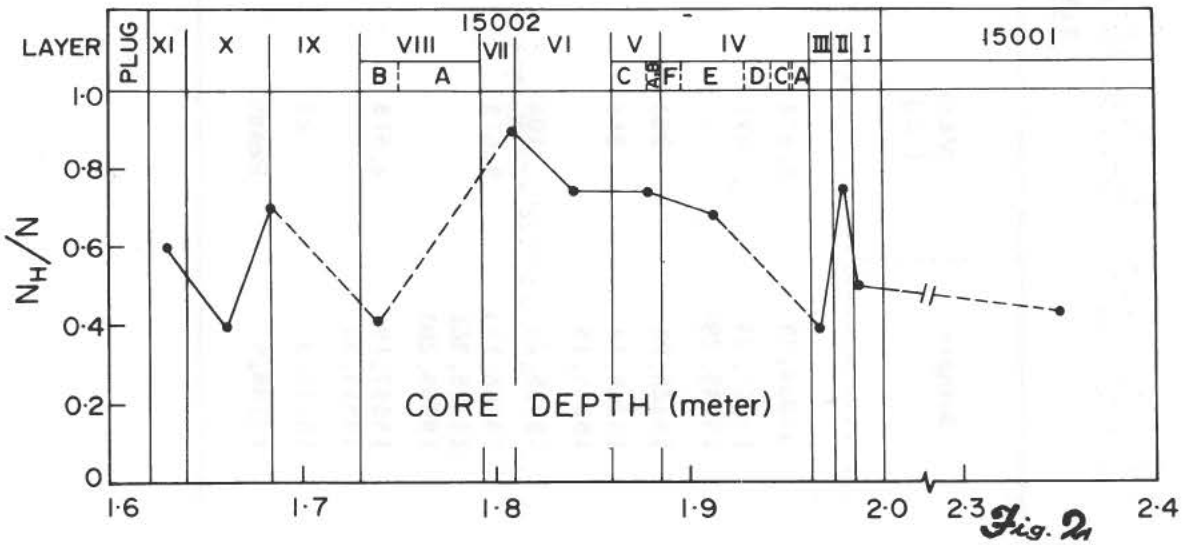

Fig. 2

Table 1 - Exposure ages of Apollo 15 rocks

Sample	Mass (gm)	Sample detail	Range of track density (10^6 cm^{-2})	Fossil track ages (m. y.)	
				Suntan age	Sub-decimeter age
15058,49	2,672	Slice	6-500	2	10
15085, 27	471	S. C.	6	< 1	-
15085, 29		S. C.	12	< 1	-
15426,75	223	I. C.	7	?	< 15
15265,14	314	S. C.	10	< 1	-
15265,15		S. C.	6	< 1	-
15535,25	404	Slice	5	< 1	< 10
15555,199 15555,201 15555,203	9,613	Slice	5-14	1	26
15557,19	2,518	S. C.	9	< 1	-
15557,37		I. C.	14		-
15118,3	27	S. C.	8-50	1.3	-
15388,5	Peanut	S. C.	5	< 1	-

Table 2 - Exposure ages of Apollo 15 core strata* and surface samples

Sample No.	Layer, thickness or location	Depth in core (meters)	N_H/N (No. of grains)	Quartile track density (10^6 cm^{-2})	Surface Irradiation age (m. y.)
Core Samples					
15002,121	XI, 1.8 cms	1.63	0.6 (53)	18	6
15002,111	X, 4.6 cms	1.66	0.4 (20)	18	23
15002,107	IX, 4.3 cms	1.684	0.7 (30)	64	35
15002,93	VIII B, 2 cms	1.74	0.41 (24)	11	~0.5
15002,79	VII, 1.7 cms	1.804	0.9 (21)	32	17
15002,72	VI, 4.8 cms	1.84	0.75 (32)	64	40
15002,63	V C, 2.0 cms	1.88	0.75 (36)	30	14
15002,55	IV E, 3.2 cms	1.912	0.69 (52)	45	28
15002,45	III, 1.3 cm	1.966	0.4 (20)	7	< 1
15002,43	II, 0.8 cm	1.98	0.75 (46)	45	18
15002,41	I, 1.5 cm	1.986	0.5 (43)	7	< 1
15001	?	2.33	0.4 (44)	5	-
Surface Samples					
15091,67	Station 2	0.03†	0.8 (27)	38	34
15101,131	Station 2	"	0.79 (34)	75	69
15211,49**	Base	"	0.79 (62)	19	17
15221,72**	N.W. Rim	"	0.74 (27)	27	23
15231,70**	S. Rim	"	0.58 (27)	40	35
15302,28	Spur crater	"	0.3 (21)	11	10
			0.17 (31 glass)	3.3	-

* Based on the model of Arrhenius et al.[1]

† Assumed scoop depth.

** The location of these samples is given with respect to the boulder or its crater.

NOBLE GASES IN THE APOLLO 15 DRILL CORES. D. D. Bogard and L. E. Nyquist, NASA Manned Spacecraft Center, Houston, Texas 77058

Noble gas isotopic abundance measurements have been made on lunar soil from all six sections of the Apollo 15 deep drill core (15001-006) and the top and bottom of a nearby trench (15041 and 15031). This core presents the first opportunity to directly measure characteristics of the deeper lunar regolith, and extends the sampling depth by a factor of three over previous cores. A portion of our noble gas results are presented in Table 1, along with the approximate depth of the sample beneath the lunar surface. A complete compilation of noble gas data obtained on these and other drill samples, along with a more detailed discussion of their significance, is presented elsewhere (Bogard and Nyquist, 1972). The more obvious and significant aspects of these noble gas data are discussed here.

Samples from different depths generally possess similar noble gas concentrations of a solar wind implantation origin, which are also similar to concentrations reported for various Apollo 15 surface soils (Lunar Sample Preliminary Examination Team, 1972). The ^{4}He and ^{22}Ne concentrations vary by a factor of two, but the $^{4}He/^{22}Ne$ ratio varies by only 14%. This clustering in $^{4}He/^{22}Ne$ values indicates an equilibrium concentration for both isotopes in these soils. The $^{22}Ne/^{36}Ar$ and $^{36}Ar/^{132}Xe$ ratios possess greater variations, with a tendency for higher ratios to occur for lower ^{132}Xe concentrations. There is evidence that ^{36}Ar and ^{132}Xe have not reached equilibrium concentrations in several depth samples (Bogard and Nyquist, 1972). The fact that similar noble gas concentrations exist throughout the 2.4 meter sampling depth demonstrates that these deeper layers have been exposed on the lunar surface for an appreciable length of time. Thus, even material as deep as 2.4 meters has experienced a prior upper regolith history, rather than being derived directly from deeper rock layers. This conclusion is consistent with the observation of high ionization track densities ($>10^{8}cm^{-1}$) in all six section of the drill string (Crozaz et al., 1972 and Phakey et al., 1972).

The $^{4}He/^{3}He$, $^{20}Ne/^{22}Ne$, and $^{36}Ar/^{38}Ar$ isotopic ratios measured for these depth samples exhibit only small variations and are similar to values determined for surface soils from previous missions. (The $^{22}Ne/^{21}Ne$ ratios reflect the presence of cosmic ray produced ^{21}Ne). Variations in measured $^{4}He/^{3}He$ most likely reflect different equilibrium values and the presence of spallogenic ^{3}He, but also may be due in part to variable $^{4}He/^{3}He$ ratios in the solar wind (Buehler et al., 1972). The $^{40}Ar/^{36}Ar$ ratios vary considerably among depth samples, as was also the case for Apollo 15 surface soils and breccia (LSPET, 1972). In addition to solar wind implanted ^{36}Ar, this ratio also reflects ^{40}Ar from <u>in situ</u> radioactive decay and ^{40}Ar from lunar atmosphere implanted gases. Apparently the mechanism of lunar atmosphere ion implantation has also occurred on ancient lunar regolith surfaces which now lie deeply buried.

There is no direct support in the data presented here for an appreciable

NOBLE GASES IN THE APOLLO 15 DRILL CORES

D. D. Bogard and L. E. Nyquist

variation in the solar wind composition with time. It has been suggested that the lunar regolith at the Apollo 15 deep drill site has remained relatively static to a depth of 2.4 meters for at least 400×10^6 yrs (Russ et al., 1972). In such a case, noble gases in the deeper portions of the drill core would represent solar wind ions implanted at least this long ago, and should reflect any differences in the ancient solar wind composition. If any such compositional variations exist in the Apollo 15 drill samples, they are smaller than those variations seen among surface fines and breccia.

Concentrations of cosmic ray produced ^{21}Ne, ^{80}Kr, and ^{126}Xe (Figure 1) have been calculated from measured data and an assumed two component mixture of trapped solar and spallation gases. Isotopic ratios taken for the trapped component were $^{22}Ne/^{21}Ne = 31$, $^{80}Kr/^{86}Kr = 0.0385$, and $^{126}Xe/^{136}Xe = 0.0144$. Typical Kr and Xe spectra contained about 80% spallogenic ^{80}Kr and ^{126}Xe, while typical Ne spectra contained about 15-25% spallogenic ^{21}Ne. Also plotted in Fig. 1 are the concentrations of solar wind trapped ^{22}Ne and ^{132}Xe (Table 1). Total variation in ^{21}Ne is less than a factor of two, while ^{126}Xe and ^{80}Kr vary by a factor of four. None of these cosmogenic nuclides show a concentration-depth pattern indicative of a single stage, in situ irradiation. Such an irradiation is expected to produce smooth concentration gradients with much lower relative concentrations for depths greater than 80 cm (Reedy and Arnold, 1972). Preliminary data on several depth samples from core 15005 indicates that the concentrations of cosmogenic ^{21}Ne and ^{126}Xe vary considerably even over small depth changes (dotted boxes of Fig. 1). It therefore appears that a substantial fraction of these cosmogenic nuclides in some samples were acquired in variable amounts in earlier irradiations, and before deposition as layers in the present regolith. Assuming cosmogenic ^{21}Ne and ^{126}Xe production rates measured on lunar rocks, all depth samples give minimum ^{21}Ne and ^{126}Xe exposure times of about 4×10^8 yrs., except for two ^{126}Xe values at $1\text{-}2 \times 10^8$ yrs. The recent shielding of these two samples (about 68 and 135 g/cm^2) is comparable to that estimated for a number of lunar rocks (Burnett et al., 1971). Gd isotopic measurements of the thermal neutron fluence as a function of depth in the drill core (Russ et al., 1972) implies a static core for the past 450×10^6 yrs., which also received an earlier and uniform neutron fluence. These results on Gd may not be in contradiction to the noble gas results. There exists absolute calibration uncertainties of the production rates of both cosmogenic noble gases and thermal neutrons. In addition, the cosmogenic production rates of noble gases are expected to decrease much more rapidly with depth than is the case for the thermal neutron flux, such that material which exhibits appreciable differences in cosmogenic noble gas isotopes could have received comparable neutron fluxes. It is hoped that additional measurements in progress of the cosmogenic noble gases in the drill core will permit more detailed comparisons.

References

Bogard, D.D. and Nyquist, L.E. (1972) Noble gases in the Apollo 15 and 16 drill cores, in preparation.

Buehler, R., Cerutti, H., Eberhardt, P., and Geiss, J. (1972) Results of the Apollo 14 and 15 solar wind composition experiments (abstract). Lunar Science III, Lunar Science Institute Contr. 88.

Burnett, D.S., Huneke, J.C., Podosek, F.A., Russ, G.P.III, and Wasserburg, G.J.

NOBLE GASES IN THE APOLLO 15 DRILL CORES

D. D. Bogard and L. E. Nyquist

(1971) The irradiation history of lunar samples. Proc. Second Lunar Sci. Conf., Geochim. Cosmochim. Acta Suppl. 2, 1671.

Crozaz, G., Drozd, R., Hohenberg, C.M., Hoyt, H.P., Rogan, D., and Walker, R. M. (1972) Solar flare and galactic cosmic ray studies of Apollo 14 samples (abstract). Lunar Science III, Lunar Sci. Inst. Contr. 88.

Lunar Sample Preliminary Examination Team (1972) The Apollo 15 lunar samples: A preliminary description, Science 175, 363-388.

Reedy, R.C. and Arnold, J.R. (1972).Interaction of solar and galactic cosmic-ray particles with the moon, J. Geophys. Res. 77, 537-555.

Russ III, G.P., Burnett, D.S., and Wasserburg, G.J. (1972) Lunar neutron stratigraphy, Earth Planet. Sci. Letters 15, 172-186.

Phakey, P.P., Hutcheon, D., Rajan, R.S., and Price P.B. (1972) Radiation damage in soils from five lunar missions (abstract). Lunar Science III, Lunar Sci. Inst. Contr. 88.

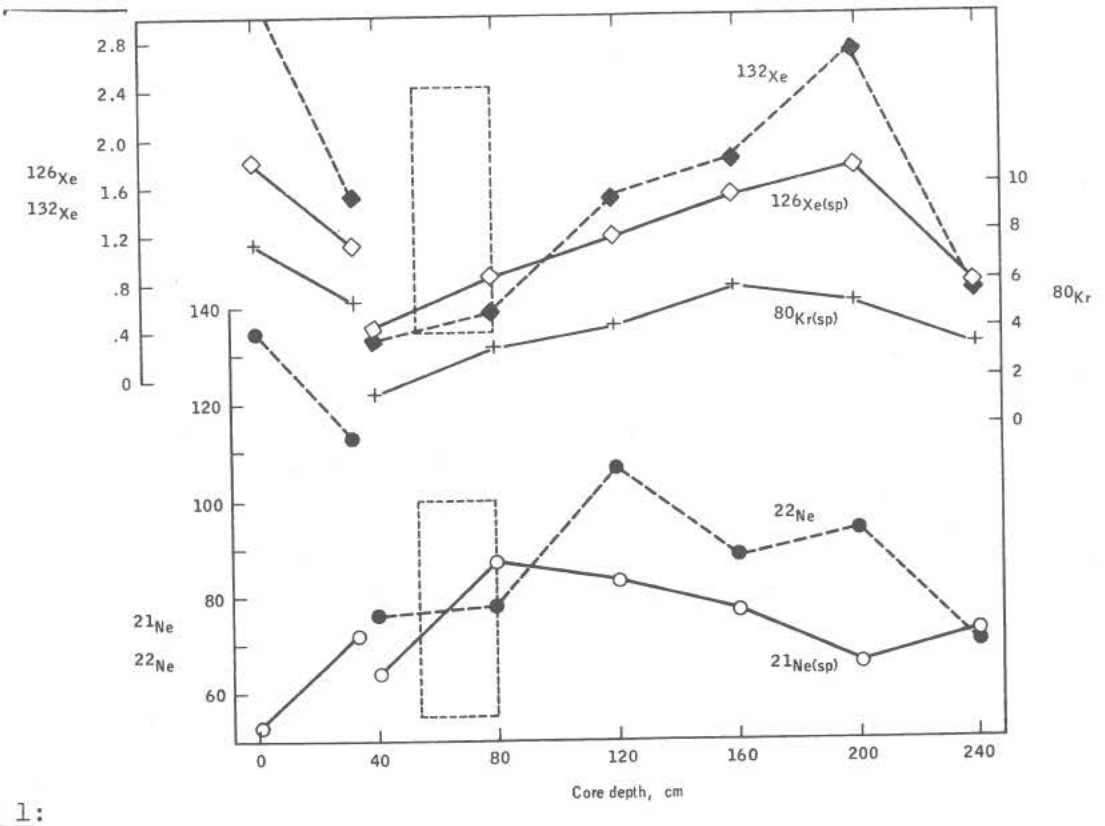

Figure 1:

Concentrations of cosmogenic ^{21}Ne (10^{-8} cm^3/g), ^{126}Xe (10^{-10} cm^3/g), and ^{80}Kr (10^{-10} cm^3/g) and trapped solar wind ^{22}Ne (10^{-6} cm^3/g) and ^{132}Xe (10^{-8} cm^3/g) as a function of depth in the Apollo 15 lunar regolith. Samples plotted at ∿2 and ∿35 cm. are top and bottom of the deep trench, and the remainder of the samples are from the deep drill core.

Noble Gas Concentrations in Apollo 15 Drill Cores

Sample	Depth cm	X 10^{-5} cm^3 STP/g ^{4}He	^{22}Ne	^{36}Ar	X 10^{-9} cm^3/g ^{84}Kr	^{132}Xe	^{4}He/^{3}He	^{20}Ne/^{22}Ne	^{22}Ne/^{21}Ne	^{36}Ar/^{38}Ar	^{40}Ar/^{36}Ar
15041,80	surface	9730	13.3	35.7	239	33.2	2585	12.57 ± .04	27.7 ± .1	5.33 ±.01	0.747
15031,70	~ 35	7790	11.3	23.7	136	15.2	2890	12.70 ± .03	28.6 ± .	5.41 ±.01	0.775
15006,20	40	5476	7.58	4.25	22.5	3.31	2295	12.63 ± .02	25.0 ± .5	5.37 ±.02	0.98
15005,19	80	5310	7.87	9.22	40.2	5.72	2275	12.59 ± .02	23.3 ± .2	5.39 ±.10	1.62
15004,20	120	8100	10.7	20.8	88	15.1	2875	12.63 ± .09	25.0 ± .2	5.36 ±.02	1.20
15003,22	160	6175	8.88	17.6	110	18.1	2495	12.62 ± .04	24.5 ± .3	5.32 ±.01	1.39
15002,20	200	7200	9.43	19.9	11.7	27.3	2565	12.66 ± .02	22.9 ± .2	5.32 ±.01	1.85
15001,24	240	4745	7.04	9.18	41.7	7.19	2390	12.60 ± .08	23.7 ± .3	5.38 ±.03	1.97

Abundance uncertainties based on spectrometer sensitivity variations are 5-10%. Uncertainties given for isotope ratios are one sigma of multiple measurements. Blank and mass discrimination corrections have been applied.

NOBLE GASES IN THE APOLLO 15 DRILL CORES

D. D. Bogard and L. E. Nyquist

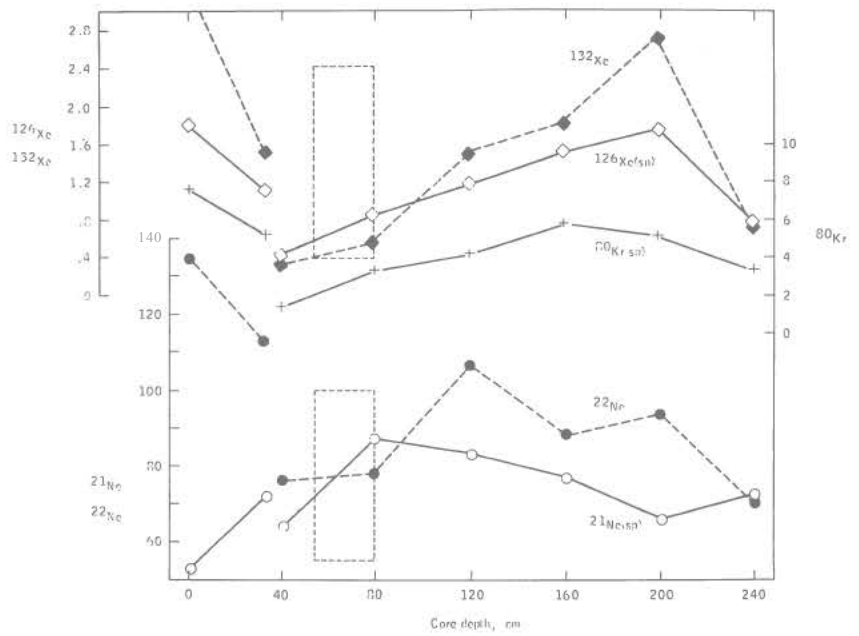

STRONTIUM ISOTOPE GEOCHEMISTRY OF APOLLO 15 BASALTS

W. Compston, J.R. de Laeter, M.J. Vernon
Dept. of Geophysics and Geochemistry
Australian National University.

We present here Rb,Sr and $^{87}Sr/^{86}Sr$ analyses for 10 Apollo 15 basalts (Table I) and 6 Apollo 15 soils (Table 2). Major- and trace-element analyses on aliquots of the identical (powdered) samples will be reported elsewhere (1). Isotope dilution (ID) and X-ray fluorescence (XRF) were used for the Rb,Sr concentration measurements. $^{87}Sr/^{86}Sr$ was calculated from the mixtures of sample plus ^{84}Sr tracer, and unspiked measurements were made for a number of samples also. The mass-spectrometer, calibrated measurement system, and standard analytical procedures were the same as for our Apollo 14 work (2). During the course of the Apollo 15 analyses, we obtained 0.71029±10 and 0.70800±10 respectively for the NBS SRM987 and the E. & A. strontium carbonate, and 0.70918±10 was obtained previously for the C.I.T. seawater. We have employed a new mixed spike of ^{85}Rb and ^{84}Sr calibrated using the NBS stoichiometric salts SRM984 and SRM987: The use of enriched ^{85}Rb instead of ^{87}Rb permits more confident correction for any Rb interference during Sr analysis. Processing blanks for the basalts were less than 1.5% for Rb and less than 0.1% for Sr.

The samples used for ID were aliquots of between 25 and 50mg taken from powdered chips of between 0.3 and 5.8g in weight. Sampling effects are evident in the duplicate analyses of 15016, 15499 and 15545 (Table I), which show correlated differences in $^{87}Rb/^{86}Sr$ and $^{87}Sr/^{86}Sr$ consistent with dispersion along their mineral isochrons of presumed 3.3 b.y. age. Consequently, the several unspiked $^{87}Sr/^{86}Sr$ analyses need not agree with the calculated $^{87}Sr/^{86}Sr$ for different aliquots, and for 15595 such a disagreement appears to exist. The Rb content is more affected by sampling than Sr, as expected from its very low abundance. If the original basalt fragments contained a few percent of lunar soil which at the Apollo 15 site (Table 2) is comparatively enriched in Rb, the Rb sampling effect could produce dispersion of the basalt analyses along an isochron older than 3.3 b.y., perhaps as old as 4.6 b.y., depending on the isochron parameters of the Rb-rich phases in the soil. The observed sampling effects do not discriminate between the above two possibilities.

Strontium isotope geochemistry of Apollo 15 basalts

W. Compston

The XRF results for Rb (1) have internal precision (2σ) of better than 2% of the concentrations for the soils, and better than 5% for the basalts except for 15545, for which 2σ is 12%. However, the values are systematically lower than the ID results by an apparently constant amount, about 0.2 ppm, which represents the kind of analytical bias expected in the XRF method at low elemental concentrations. The internal precision for Sr by XRF is better than 0.3%. Bias with respect to the ID results is less than 2%, although precise comparison is impossible owing to sampling fluctuations in the smaller ID samples.

Compared with Apollo 12, the Apollo 15 basalts form a single particularly coherent group on an isochron diagram, but with an internal alignment which more resembles 3.3 b.y. than 4.6 b.y. Some of this alignment will be due to sampling effects. No differences in initial $^{87}Sr/^{86}Sr$ can be seen (Table 3) (taking all ages as 3.3 b.y.), so the specimens cannot be separated here into the quartz-normative (15475,15499,15595,15597) and olivine-normative groups recognized by Chappell and Green (1). However, the Sr content of the quartz basalts is consistently higher (Table 1). The group evenly straddles the 4.6 b.y. reference isochron through the basaltic achondrite initial $^{87}Sr/^{86}Sr$, which is consistent with its single-stage production from a lunar mantle chemically-closed between ∿4.6 b.y. to 3.3 b.y. If $^{87}Sr/^{86}Sr$ in the magma(s) during partial melting at 3.3 b.y. equalled that in the mantle residue, then little or no change in Rb/Sr could have occurred during melting. Alternatively, if the melt(s) had a higher Rb/Sr than the residue, then its $^{87}Sr/^{86}Sr$ also must have been higher and unequilibrated with the bulk residue. In either case, no nett change in Rb/Sr occurred during any subsequent high-level crystal fractionation.

Our total-rock data reported previously for 15555,16 (3) are in satisfactory agreement with those for the second chip 15555,13 reported here, and also with the results of Wasserburg and Papanastassiou (4) after adjustment by 0.00010 for inter-laboratory bias in $^{87}Sr/^{86}Sr$ using the C.I.T. seawater reference. We cannot agree in initial $^{87}Sr/^{86}Sr$ for 15555 with Murthy et al. (5) despite the use of reference samples, a fact which Compston (6) suggested might indicate a variation in initial $^{87}Sr/^{86}Sr$ within this rock. However, the homogeneity of the Apollo 15 basalts as a group and the replication of the second chip from 15555 now make the latter rather unlikely.

The Apollo 15 soils, like the Apollo 12 and some of Apollo 14, show an abundance of Rb-bearing constituents relative to the mare basalts and they preserve old model ages in the range 4.5 to 4.6 b.y. We do not know whether these are the remains of a

single-stage 4.6 b.y. lunar crust or of a two-stage 4.4 b.y. igneous rock (7) or whether, in the light of the 4.6 b.y. model ages of the Apollo 15 basalts, no time significance should be attached to the bulk soil data.

References

1. B.W. Chappell and D.H. Green (1972) In preparation.
2. W. Compston, M.J.Vernon, H. Berry, R.Rudowski, C.M. Gray, N. Ware, B.W. Chappell and M. Kaye (1972). Proc. 3rd Lunar Science Conference. In Press.
3. B.W. Chappell, W. Compston, D.H. Green and N.G. Ware (1972) Science 175, 415-6.
4. G.J. Wasserburg and D.A. Papanastassiou (1971) Earth Planet. Sci. Letters, 13, 97-104.
5. V. Rama Murthy, N.M. Evensen, Bor-Ming Jahn, M.R. Coscio, J.C. Dragon and R.O. Pepin (1972) Science, 175,419-21.
6. W. Compston (1972) Transactions, Amer.Geophys.Union 53 538 (abstract).
7. E. Schonfeld (1972) Lunar ScienceIII 683-85, Lunar Sci. Inst. Contr. No. 88.

Table 1: Analytical data for Apollo 15 mare basalts. The experimental uncertainty (2σ) for $^{87}Rb/^{86}Sr$ is estimated as ±3%, and for $^{87}Sr/^{86}Sr$ as ±0.00010. Station numbers refer to the Apollo 15 traverse. All X-ray fluorescence data are from B.W. Chappell and M.J.Kaye (1).

Table 2: Preliminary analytical data for Apollo 15 soils. Owing to sampling fluctuations, uncertainty of the order ±5% must be assigned to combining $^{87}Rb/^{86}Sr$ calculated from XRF data with unspiked $^{87}Sr/^{86}Sr$ analyses made on separate aliquots.

Table 3: Initial $^{87}Sr/^{86}Sr$ for Apollo 15 basalts assuming 3.3 b.y. for their age. No differences above experimental error (2σ±0.00015) are detected.

Strontium isotope geochemistry of Apollo 15 basalts

W. Compston

Table 1

	Rb (ppm) ID	Rb (ppm) XRF	Sr (ppm) ID	Sr (ppm) XRF	$^{87}Rb/^{86}Sr$	$^{87}Sr/^{86}Sr$
15016,38	0.73		89.7		0.0233	0.70064±10
Station 3	0.81		91.4		0.0255	0.70083±10
		0.65		93.3		
15475,34	0.73		105.0		0.0201	0.70039±10
Station 4		0.58		106.8		0.70029*±10
15499,18	0.94		108.6		0.0248	0.70062±10
Station 4	1.05		108.2		0.0280	0.70092±25
		0.90		109.4		0.70077*±10
15545,15	0.84		96.9		0.0250	0.70074±10
Station 9A	0.73		96.1		0.0219	0.70051±10
		0.57		97.6		
15555,13	0.63		89.9		0.0203	0.70051±10
Station 9A		0.54		92.2		0.70048*±10
15595,16	0.90		99.4		0.0261	0.70074±10
Station 9A		0.72		103.8		0.70055*±10
15597,21	1.13		111.0		0.0294	0.70091±10
Station 9A		0.90		109.4		
15622,5	0.89		93,8		0.0274	0.70074±15
Station 9A		-		-		
15636,5	0.72		90.9		0.0229	0.70059±10
Station 9A		0.52		94.6		
15674,4	0.80		100.3		0.0231	0.70059±10
Station 9A		0.65		100.9		0.70056*±10

Table 2

15231,45	-		-			
Station 2		4.51		138.4	0.098[x]	0.70561*±10
15071,24	3.32		115.9		0.0827	0.70444±15
Station 1		3.17		118.9		
15081,19	-		-			
Station 1		3.75		122.4	0.093[x]	0.70507*±10
15271,62	5.88		139.2		0.1220	0.70725±15
Station 6		5.63		139.4		
15471,28	-		-			
Station 4		3.17		116.6	0.083[x]	0.70437*±10
15531,32	-		-			
Station 9A		2.11		98.9	0.067[x]	0.70335*±10

* Unspiked analysis of separate 25-50mg aliquot of powdered sample.

x Calculated from XRF data after removing bias of -0.2 ppm Rb.

Strontium isotope geochemistry of Apollo 15 basalts
W. Compston

Table 3

Quartz basalts		Olivine basalts	
15475	0.69945	15016	0.69954
15499	0.69945		0.69963
	0.6996±3	15545	0.69956
15595	0.69951		0.69948
15597	0.69953	15555	0.69956
		15622	0.69945
		15636	0.69951
		15674	0.69950

CHARGED-PARTICLE TRACK PARAMETERS OF APOLLO 15 LUNAR GLASSES

S. A. Durrani and H. A. Khan, Department of Physics, University of Birmingham, Birmingham B15 2TT, England

This paper describes preliminary results of measurements of charged-particle (primarily, fission-) track parameters, mainly in light brown and light green glasses picked out microscopically from fines samples 15301, 84 and 15261, 70. A majority of the glasses selected for examination were roughly spherical or ellipsoidal with diameters or major axes ranging from ~300 to 500 μm.

General Velocity of Etching, V_g The following procedure was used to measure the general, or bulk, velocity V_g in light brown ('1-b' for short) and light green ('1-g') glasses from sample 15301, 84. The 'spherules' were mounted individually in epoxy resin on plastic (Perspex) backing, and then slightly ground and polished to yield plain initial surfaces. They were then etched under identical conditions for 50 and 100 sec successively, using fresh 48.0 volume % HF at a temperature of $21.0 \pm 0.5^{\circ}C$, controlled to within $\pm 0.1^{\circ}C$. The thickness of the glass removed in 50 or 100 sec was measured with a ZEISS Photomicroscope (at 630 x), using a fiducial mark on the mounting. The results are shown in Table 1. The value of V_g in 1-g glasses is ~ 6 times that in 1-b glasses. (V_g was seen in Ref. 1 apparently to go up with the CaO content).

Table 1. General velocity of etching, V_g, in glasses from sample 15301, 84*

Colour	Spherule no.	V_g (μm/sec)	Colour	Spherule no.	V_g (μm/sec)
Light brown	15	0.131	Light green	18	0.760
" (1-b)	16	0.126	" (1-g)	19	0.813
"	17	0.127	"	20	0.753
	Mean $V_g = 0.128 \pm 0.002$			Mean $V_g = 0.776 \pm 0.014$	

* Etched in 48.0% HF at $21 \pm 0.5^{\circ}C$ for 50 and 100 sec.

Critical Angle of Etching, θ_c This important parameter was measured in sample 15301, 84 light brown and light green glasses by the 'comparison

method[1,2]: The lunar spherules - including two irregularly shaped 'chips' - as well as a piece of 'reference glass' (U-2) were first annealed (at 600°C for 60 min); the spherules were then mounted (9 1-b glasses on one backing and 5 1-g glasses on another), and ground and polished to yield plain surfaces. Next, the lunar glasses as well as the reference glass were exposed to a ^{252}Cf spontaneous-fission source in '2 π geometry' for the same length of time (30 sec). This was followed by simultaneous etching in HF under identical conditions (48.0%, at 21.0 $\pm$ 0.5°C for 30 sec). Since the critical angle for reference glass ($\theta_{c,r}$) has been previously measured by us[2], $\theta_{c,l}$ for the lunar glasses can be readily calculated from the relation

$$\rho(\text{lunar})/\rho(\text{ref}) = (1 - \sin\theta_{c,l})/(1 - \sin\theta_{c,r}) \quad \ldots 1,$$

where ρ is the track density per unit area in each case.

To accumulate enough statistics in the case of lunar glasses, repeated exposures (9 for 1-b and 15 for 1-g group) to the ^{252}Cf source were carried out, alternating with successive polishing stages to remove the previous etch pits (because of the high V_g in them, 1-g glasses were etched for only 10 sec each time.) This resulted in ~ 500 to 600 fission tracks being counted in each spherule. The values of θ_c calculated from eq. (1) are recorded in Table 2; the difference between the two colour groups is again noticeable.

Table 2. Critical angle of etching, θ_c, for glasses from sample 15301, 84 *

Light brown (1-b) spherules				Light green (1-g) sperules	
No.	θ_c	No.	θ_c	No.	θ_c
31	26°25'	32	24°16'	51	34°20'
33	24°18'	34	26°15'	52	35°06'
35	25°39'	36	31°45'	53	34°57'
37	32°41'	07 (chip)	27°00'	051 (chip)	35°48'
		08 "	26°06'	052 "	35°24'
Mean of 9 particles: 27°06' $\pm$ 0°57'				Mean of 5 particles: 34°58' $\pm$ 0°24'	

*Determined by the 'comparison method' using reference glass U-2 (θ_c = 31°45') and an external fission source)

Prolonged Etching Factor f(t), and Fission Fragment Range R The prolonged etching factor, f(t), has been defined by us[1] as

$$f(t) = \rho(t)/\rho(o) \quad \ldots 2,$$

Charged-Particle Track Parameters

S. A. Durrani

where $\rho(t)$ and $\rho(o)$ are the (internally produced) track densities, in a given material, for an etching time t and (by extrapolating backwards) for 'instantaneous etching' (t=o), respectively, under any specified etching conditions. Twenty 1-b and ten 1-g glasses from sample 15301, 84 were annealed, mounted on two backings, and ground and polished to yield plain initial surfaces. The two sets were then irradiated in a nuclear reactor (with fluences of 1.05×10^{15} and 4.95×10^{15} thermal neutrons/cm^2 for 1-b and 1-g glasses, respectively). After irradiation, the top ~ 20 μm were removed from all spherules by a second light polishing, in order to ensure constancy of track-forming geometry ('4π'). The two sets were then etched in 48.0 vol. % HF at $21.0 \pm 0.5^{\circ}$C - controlled to within $\pm 0.1^{\circ}$C - for times varying from 10 to 100 sec, and the resulting track densities measured as a function of time. Table 3 shows f(100) values. Note the markedly distinct f(t) values, reflecting the difference in chemical composition (and hence in the V_g values), for the 1-g and 1-b groups.

As explained in Ref. 1, the measured value of f(t) can be used to derive the average fission fragment range, R, in the material concerned. In '4π geometry' (as here), it is given by

$$R = V_g . t / (f(t) - 1 \ (1 + \sin \theta_c)) \qquad \ldots 3,$$

where all the parameters involved have been measured. The mean values of R for the 1-b and 1-g groups are recorded in Table 3 (the value for the 1-g group is less sensitive to measuring errors in f(t), since the latter is $\gg 1$).

Uranium Content, C_u The uranium content of light brown and light green glasses from sample 15301, 84 was determined by the 'auxiliary detector' method: In the reactor irradiation carried out for the measurement of f(t), a sheet of mica (annealed at 750°C for 60 min to remove fossil tracks) had been sandwiched between each set of lunar glasses and a section of reference glass (U-2). After irradiation, the mica detectors were etched in 48.0% HF at $21.0 \pm 0.5^{\circ}$C for 15 min, and fission etch pits counted on the two faces of each detector. Since the U-content in the reference glass is known[1] (43 ± 1 ppm by weight; but the U-235 isotope is depleted by a factor ≈ 2), the uranium content in the lunar glasses is readily found by comparing the track densities. (A total of 59;201; and 1392 tracks were produced by 1-b;1-g;and U-2 glasses) The calculated values of C_u in the two groups of lunar glasses are recorded in Table 3. In this table, we have collected together, for easy reference, the mean values of all the parameters of Apollo 15 lunar glasses measured by us.

Track Profile and Age One light brown spherule (No. 11 from the fines sample 15261, 70) was studied in great detail for charged-particle and fission

Charged-Particle Track Parameters

S. A. Durrani

Table 3. Parameters of Apollo 15 lunar glasses from sample 15301, 84

Colour	V_g(μm/sec)*	θ_c	R(μm)	f(100 sec)*	C_u (ppm)
Light brown Mean of:	0.128±0.002 (3 spherules)	27°06'±57' (9)	16.3±0.3 (10)	1.54 (10)	0.46 ± 0.06 (20)
Light green Mean of:	0.776±0.014 (3 spherules)	34°58'±24' (5)	15.2±0.3 (10)	4.26 (10)	0.67 ± 0.05 (10)

* V_g and f(t) measured for etching in 48.0 vol. % HF at 21.0 ± 0.5°C

track profiles. Starting with an arbitrary layer called A (see Fig. 1), ~41 μm below the top surface, successive polishings and etchings were carried out to reveal layers B-F. Etched track density ρ was measured at each of these layers. Known thicknesses of glass were then carefully removed by polishing, and the surviving etch pits at each stage counted. When none remained, the whole procedure was repeated. The relative track density ρ at layers A-F is plotted in Fig. 1 as an inset. The residual track density data as a function of glass thickness removed are plotted in Fig. 2: so are those using a ^{252}Cf source. The detailed analysis (to be published) indicated a probable orientation of the glass spherule on the moon. The results were compatible with the exposure of the spherule at the very top of the lunar surface in two successive orientations at an angle of ~90° with each other. Since sample 15261 is known to have come from the bottom of a trench ~20 cm deep and, in a companion paper in this volume[3] we find from thermoluminescence observations that sample 15261, 70 has remained in that environment for the last ~15000 years, it would appear that some mechanical phenomenon (a meteoritic impact?) prior to that period of time has buried it to the depth now observed.

It is also seen from Fig. 2 that the total track density goes through a broad minimum well inside the spherule. A comparison of the shape (and the apparent etch pit diameter distribution) of the lower half of the family of curves with that due to the ^{252}Cf fission fragment tracks suggests that there is a steady background of natural (U-238) fission in the spherule, upon which are superimposed (cf. the early part of the curves) what would appear to be tracks of external charged particles (solar wind, etc.). By using this minimum track density, and utilizing the values of C_u, R and θ_c given in Table 3, we obtain an age estimate of ~7.5×10^8 yr for the spherule. On correction for the α-decay of ^{238}U over this period, the age is reduced to ~7×10^8 yr. Effects of lunar temperature cycling on the thermal lowering of ages, as well as on tracks created in lunar and comparable materials by the laboratory bombardment of heavy ion beams of known charge and energy spectra, are now under investigation.

Charged-Particle Track Parameters
S. A. Durrani

References

1. Khan H. A. and Durrani S. A. (1972) Prolonged etching factor in solid state track detection and its applications. Rad. Effects 13, 257-266.
2. Khan H. A. and Durrani S. A. (1972) Efficiency calibration of solid state nuclear track detectors. Nucl. Instr. and Meth., 98, 229-236.
3. Durrani S. A. et al. (1972) Thermoluminescence of Apollo 15 lunar samples: (II) 20 to 550°C. (This volume.)

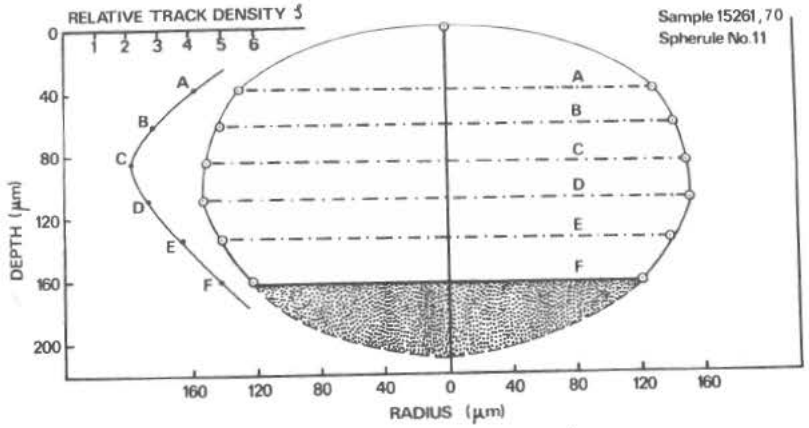

FIG. 1. Geometry of the layers A-F studied in a light brown spherule (No. 11, sample 15261, 70).

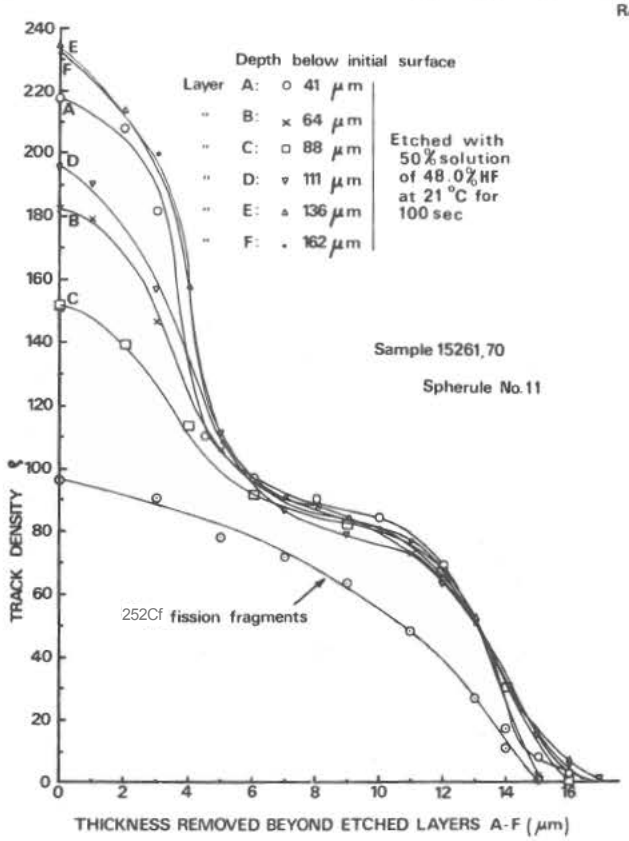

FIG. 2. Track desity profile in the spherule revealed by successive etching and polishing stages.

CONCENTRATIONS OF COSMOGENIC RADIONUCLIDES IN APOLLO 15 ROCKS AND SOIL,* James S. Eldridge, G. Davis O'Kelley, and K. J. Northcutt, Oak Ridge National Laboratory, Oak Ridge, Tenn. 37830.

The techniques of nondestructive gamma-ray spectrometry have made it possible to study in some detail the irradiation history of lunar samples by measuring the concentrations of radionucludes produced by solar and galactic cosmic-ray bombardment. A preliminary report (1) on data from several samples obtained early in the Apollo 15 mission stressed the information derived from determination of short-lived species such as ^{48}V and ^{56}Co. This note summarizes all of the information obtained on concentrations of cosmogenic radionuclides in our entire suite of Apollo 15 samples. Our latest results are mostly concerned with nuclides of long half-life, because the samples in question were measured rather long after they were collected. The abundances of K, Th, and U in these samples is the subject of a separate report (2).

Cosmogenic radionuclide concentrations determined by our group are given in Table 1. The general concentration patterns resemble those in our earlier paper (1), but because more data are now available a number of more detailed problems may be explored. Our suite of samples includes a large group of basaltic rocks with low concentrations (2) of K, Th, and U, and so the weak components of the gamma-ray spectra due to cosmogenic radionuclides can be determined in these samples with less interference than in lunar soils and breccias. Because target element concentrations have not been published for most of the samples reported here, detailed interpretations cannot be made in some cases. However, it is often possible to discern important trends in the data, and also to calculate quantitative results for some situations.

A set of radial samples was collected at Station 1 along a line extending east of Elbow crater. From these samples we measured 15065 (4 m east) and 15076 (25 m east); Keith, Clark, and Richardson (3) measured basalt 15085 and breccia 15086 (60 m east). The basalts appear to have been part of the ejecta from the Elbow crater event (2), but their positions relative to the crater rim may not reflect their original positions in the ejecta blanket if they have been extensively recycled. Although the major element chemistry of these rocks has not been determined, the ^{22}Na concentrations seem to have reached their equilibrium values. Estimates of the saturation value of the ratio $^{26}Al/^{22}Na$ derived from studies of samples from all Apollo missions show that 15065 and 15085 apparently contain equilibrium concentrations of ^{26}Al. The ^{26}Al content of 15076 seems marginal, but is consistent with a surface exposure of at least two million years. The ^{26}Al data for 15086 suggest that it was moved to the surface only within the last 0.2 - 0.5 million years (3). These results indicate that it may prove very difficult to relate the positions of these recycled samples directly to the stratigraphy of the Elbow crater event.

Cosmogenic Radionuclides

James S. Eldridge

Sample 15379 (58.6 g) is a small basaltic fragment collected with the rake as part of the comprehensive sample at Station 7 (Spur crater). This fragment is also a newcomer to the lunar surface, as its ^{26}Al content indicates that it was ejected from depth only 0.8 - 1.3 million years ago.

We have studied a group of samples consisting of soil 15471, and rocks 15475, 15476, and 15495, which were collected 28 m south of the rim crest of Dune crater (Station 4). The ^{22}Na and ^{26}Al data for 15471 are compatible with a mean sampling depth of about 2 cm, in good agreement with field geology predictions (4). The rocks are all fresh in appearance and when on the lunar surface were observed to lack either fillets or extensive burial (4). The ^{26}Al concentration of 15475 is below saturation, and indicates that it was ejected onto the lunar surface as recently as 0.7 - 1.1 million years ago. Similar considerations suggest that 15476 has resided on the surface for only 0.8 - 1.5 million years. The exposure of 15495 is difficult to assess; however, it apparently has lain exposed for a minimum of 2.5 million years.

Also at station 4, samples 15486 and 15499 were broken off a large macrovesicular basaltic boulder on the southern rim crest of Dune crater. Sample 15486 (45.6 g) was broken off a large vesicle, and 15499 (582 g) was broken off the top. We did not find the expected high concentrations of ^{22}Na and ^{26}Al characteristic of exposed, thin materials bombarded by solar-flare protons. Apparently, 15486 was partially shielded by overhanging rock; sample 15499 was a large piece of rock without much exposed surface area. Both of the boulder samples exhibit equilibrium concentrations of ^{26}Al and ^{22}Na, and so their exposure is too long to estimate by the simple $^{26}Al/^{22}Na$ method. A long exposure age for this boulder is consistent with the presence of a well-developed fillet against it and the apparent long exposure of breccia 15498, which was about 1/3 buried in the fillet.

References and Notes

*Research carried out under Union Carbide's contract with the U. S. Atomic Energy Commission through interagency agreements with the National Aeronautics and Space Administration.

1. G. D. O'Kelley, J. S. Eldridge, E. Schonfeld, K. J. Northcutt, Science 175, 440 (1972); paper to be published in "Proc. Third Lunar Sci. Conf.," Geochim. Cosmochim. Acta (Suppl. 3, Vol. 2), MIT Press, 1972.

2. G. D. O'Kelley, J. S. Eldridge, and K. J. Northcutt, Abundances of the Primordial Radioelements K, Th, and U in Apollo 15 Samples, as Determined by Nondestructive Gamma-Ray Spectrometry, in "The Apollo 15 Lunar Samples," ed. J. W. Chamberlain and C. Watkins (Houston: Lunar Science Institute), 1972.

3. J. E. Keith, R. S. Clark, and K. A. Richardson, paper to be published in "Proc. Third Lunar Sci. Conf.," Geochim. Cosmochim. Acta (Suppl. 3, Vol.2), MIT Press, 1972.

4. G. A. Swann, M. H. Hait, G. G. Schaber, V. L. Freeman, G. E. Ulrich, E. W. Wolfe, V. S. Reed, and R. L. Sutton, "Preliminary Description of Apollo 15 Sample Environments," U. S. Geological Survey Interagency Report 36, 1971.

Cosmogenic Radionuclides

James S. Eldridge

Table 1. Concentrations (dpm/kg) of Cosmogenic Radionuclides in Apollo 15 Samples. Decays Corrected to 1711 Hours GMT, 2 August 1971.

Sample	^{22}Na	^{26}Al	^{46}Sc	^{48}V	^{54}Mn	^{56}Co
			Crystalline Rocks			
15016,0*	29 ± 2	82 ± 4	3 ± 1	10 ± 2	31 ± 4	16 ± 3
15058,29	26 ± 3	62 ± 4			27 ± 4	
15065,0	23 ± 3	68 ± 6			25 ± 10	
15076,0	36 ± 4	69 ± 4	4 ± 2		22 ± 3	6 ± 4
15379,0	31 ± 4	42 ± 4			32 ± 5	
15475,0*	32 ± 3	40 ± 3	3 ± 2		23 ± 3	11 ± 5
15476,0	43 ± 3	62 ± 4	≤ 6		27 ± 5	20 ± 8
15486,0	40 ± 4	87 ± 7			45 ± 25	
15495,0*	29 ± 3	69 ± 3	3 ± 1		25 ± 2	11 ± 2
15499,9	37 ± 4	77 ± 5			30 ± 5	
15545,0	27 ± 3	69 ± 4			34 ± 12	
15557,0	24 ± 3	59 ± 6			30 ± 4	
15597,0	31 ± 4	88 ± 9			30 ± 6	
			Breccias			
15285,0*	50 ± 4	85 ± 4			30 ± 5	
15498,0	26 ± 6	60 ± 6			25 ± 5	15 ± 9
			Soils			
15031,86*	33 ± 3	49 ± 3			40 ± 10	
15041,100*	57 ± 4	99 ± 7	3 ± 2		33 ± 10	17 ± 5
15101,1*	44 ± 5	120 ± 12	≤ 4	9 ± 6	28 ± 8	11 ± 6
15471,3	58 ± 3	122 ± 3	≤ 7		26 ± 5	45 ± 16
15601,2*	55 ± 6	112 ± 11	≤ 4		32 ± 8	28 ± 9

*Preliminary analysis of this sample reported in Ref. (1).

LUNAR ACTINIDES: ^{236}U, ^{237}Np, ^{244}Pu, ^{239}Pu AND ^{238}Pu* P. R. Fields, H. Diamond, D. N. Metta and D. J. Rokop, Chemistry Division, Argonne National Laboratory, Argonne, Illinois, 60439.

Earlier papers[1] have reported the observation of 2.4×10^7 yr ^{236}U and 2.14×10^6 yr ^{237}Np in Apollo 12 and 14 samples. These nuclides as well as ^{238}Pu and ^{239}Pu could appear on the moon if they were produced by neutrons and charged particles from galactic and solar cosmic rays reacting with indigenous uranium. A less likely model would invoke the production of these nuclides (and perhaps ^{244}Pu) elsewhere, with subsequent accretion by the moon.

The reported[1] ^{236}U:^{238}U ratio of $(2.33 \pm 0.15) \times 10^{-7}$ in 12070,91, and $(1.1 \pm 0.3) \times 10^{-13}$ gm ^{237}Np per gram of the same sample, provided strong evidence for an intense, long, solar cosmic ray bombardment. This in turn suggested that the sun might have been more active 2-10 million years ago than it has been more recently. To develope this model, attempts were made to find ^{237}Np and ^{236}U in Apollo 15 samples, and in another sample of 12070.

Some estimate of the exposure of uranium to cosmic ray neutrons can now be made from the data.

EXPERIMENTAL

The ^{236}U:^{238}U determinations were made with the tandem magnetic mass spectrometer described[1] earlier. A reagent blank was run with 3.4 μg of uranium obtained from pitchblende (Great Bear Lake, Port Hope Refinery, Ontario). The ^{236}U content of this uranium had been determined[2] to be $(6.2 \pm 2.2) \times 10^{-10}$ of the ^{238}U. The small positive blank is not sufficient to interfere with conclusions derived from thy other data in Table 1. Sample 14259,132 was thoroughly mixed, and run in duplicate to test the reproduceability of the ^{236}U determination. The results in Table 1 show good agreement for the unexpectedly low ^{236}U content of the two portions of the sample.

The ^{237}Np was determined with the 100-inch mass spectrometer,[3] using ^{239}Np as an isotopic diluent. The abundance of uranium in lunar material can be a billion times that of neptunium. If this uranium is not sufficiently removed from the neptunium sample, ^{238}U can interfere with the measurement of ^{239}Np tracer. The reagent blank of 4.5×10^{-15} g ^{237}Np is lower than had been previously established, but as is seen in Table 3, it is close to the ^{237}Np observed in the lunar sample.

The sensitivity for ^{239}Pu and ^{244}Pu have been slightly improved through reduction of the amount of HF used in sample dissolution and larger lunar samples. The limit to ^{239}Pu sensitivity is now imposed by the 5% ^{239}Pu component in the ^{236}Pu used for isotopic dilution.

*Work was performed under NASA Contract No. T76536 and the auspices of the U. S. Atomic Energy Commission.

LUNAR ACTINIDES

P. R. Fields

RESULTS AND DISCUSSION

Uranium

The data in Table 1, coupled with earlier[1] measurements of the $^{236}U:^{238}U$ ratio in lunar samples now show that five (12013,10,42 and 14305,80 breccias; and 15021,79; 15271,51 and 14259,132 soils) of the 10 samples measured exhibit $^{236}U:^{238}U$ ratios of (4-10) x 10^{-9}. Such constancy is characteristic of neutron reactions since neutrons penetrate the moon deeply, whereas solar cosmic ray protons have an effect only within the top few cm. If we assume a ^{235}U capture cross section of 106 barns, a 5 x 10^{-9} ^{236}U content in uranium, and an infinitely long irradiation the neutron flux would be 6 neutrons/(sec. cm^2). This is consistent with calculations by Armstrong and Alsmiller,[4] and also with measurements of neutrons by gadolinium isotopes ratios[5] providing appropriate sample exposure ages are invoked.

As discussed in an earlier paper,[1] the very high ^{236}U (and ^{237}Np) content of 12070,91 cannot be explained by the neutron irradiation of ^{235}U. Solar cosmic ray protons still appear to be the only reasonable source for so much activation.

There should be about five times as much thermal neutron induced fission of ^{235}U as there is neutron capture by ^{235}U. Thus, in a sample where the $^{236}U:^{238}U$ is 5 x 10^{-9} and where the exposure to neutrons has been several times longer than 2.4 x 10^{7} years, the neutron induced fission rate for ^{235}U would be 10 times the spontaneous fission rate for ^{238}U. This relationship might be useful for the interior of rocks, where the sample history is not as confused as it is for lunar soils.

The ^{236}U in 12070,3 was less then half that in 12070,91. This will be discussed in the neptunium section.

The activity ratio for $^{238}U:^{234}U$ in 14259,132 was 1.02 ± .02 - again failing to repeat the anomalous ratio reported for 10084,75 uranium.[6]

Table 1. $^{236}U:^{238}U$ ratio in lunar samples

	$^{236}U:^{238}U$*
15021,79	$(7.6 \pm 1.0) \times 10^{-9}$
15271,51	$(7.4 \pm 1.0) \times 10^{-9}$
14259,132 I	$(4.2 \pm 0.4) \times 10^{-9}$
14259,132 II	$(3.6 \pm 0.4) \times 10^{-9}$
reagent blank (net)	$(1.3 \pm 0.7) \times 10^{-9}$

*Results do not include any correction for the blank.

LUNAR ACTINIDES

P. R. Fields

Plutonium

Another insight into the neutron flux comes from the limit to 2.439×10^4 yr ^{239}Pu in lunar samples. If one uses a 2.7 barn capture cross section for ^{238}U neutron capture the data in Table 2 sets limits of <56 neutrons/(cm^2sec) for 15271,51, and <102 neutrons/(cm^2sec) for 15021,79.

The limits to ^{244}Pu in Table 2 are the lowest yet achieved. The limit for 15271,51 is 30 times greater than the ^{244}Pu content reported for a terrestrial bastnesite.(7)

No alpha activity ascribable to ^{238}Pu was seen in the plutonium fraction of 14259,132. The limit is $<2 \times 10^{-16}$ gm ^{238}Pu/gm of sample.

Table 2. Upper limits* to ^{239}Pu and ^{244}Pu in lunar samples

Sample number	gm ^{239}Pu/gm sample	gm ^{244}Pu/gm sample
15271,51 (4 gm)	2×10^{-16}	3×10^{-17}
15021,79 (4 gm)	4×10^{-16}	6×10^{-17}

*A reagent and instrument blank gave $(1.5 \pm 0.5) \times 10^{-15}$ gm ^{239}Pu and $< 1.6 \times 10^{-16}$ ^{244}Pu.

Neptunium

The data in Table 2 are all quite close to the reagent blank, but each sample shows a positive indication of ^{237}Np. The neptunium in 12070,3 is at least 15-fold lower than the readily observed ^{237}Np in 12070,91. Although not precisely determined, the ^{236}U data also showed wide discrepancies between the two samples. These differences, perhaps re-enforce the earlier(1) observation of markedly less ^{236}U in the coarsest portion of 12070,91 than in the sample as a whole.

Table 3. ^{237}Np in lunar samples and blank

Sample number	gm ^{237}Np found	gm ^{237}Np/gm sample*
15271,51	$(7.6 \pm 0.8)\times10^{-15}$	$(1.2 \pm 0.3)\times10^{-14}$
15021,79	$(6.2 \pm 0.6)\times10^{-15}$	$(9.7 \pm 2.0)\times10^{-15}$
12070,3	$(6.9 \pm 2)\times10^{-15}$	$(7 \pm 2)\times10^{-15}$
blank	$(4.5 \pm 0.5)\times10^{-15}$	

*not corrected for blanks

LUNAR ACTINIDES

P. R. Fields

COMMENT

Further experimental work on the detection of ^{237}Np is now in progress. Studies of meteoritic samples and successive layers of a lunar rock that has been exposed to solar cosmic ray protons are planned. As more lunar samples analyses for ^{236}U and ^{237}Np are obtained one might hope for further insight into the intensity and time distribution of cosmic rays.

REFERENCES

(1) Proceedings of the Third Lunar Science Conferences (Supplement 3, Geochimica et Cosmochimica Acta) Vol. 2, pp. 0000-0000, The MIT Press, 1972 (contains references to earlier work).

(2) Rokop D. J., Metta D. N., and Stevens C. M. (1972) $^{236}U/^{238}U$ measurements for three terrestrial minerals and one processed ore. Int. J. Mass Spectroscopy and Ion Physics 8, 259-264.

(3) Moreland P. E. Jr., Stevens C. M., and Wahling D. B. (1967) Semiautomatic data-collection systems for the mass spectrometer. Rev. Sci. Inst. 38, 760-764.

(4) Armstrong T. W. and Alsmiller R. G. Jr. (1971) Calculation of cosmogenic radionuclides in the moon and comparison with Apollo measurements. Proc. Second Lunar Sci. Conf., Geochim. Cosmochim. Acta Suppl. 2, Vol. 2, pp. 1729-1745. MIT Press.

(5) Burnett D. S. Huneke J. C., Podosek F. A., Russ G. P. III and Wasserburg G. J. (1971) Irradiation history of lunar samples. Proc. Second Lunar Sci. Conf., Geochim. Cosmochim. Acta Suppl. 2, Vol. 2, pp. 1671-1679. MIT Press.

(6) Fields P. R., Diamond H., Metta D. N., Stevens C. M., Rokop D. J., and Moreland P. E. (1970) Isotopic abundances of actinide elements in lunar material. Proc. Apollo 11 Lunar Sci. Conf. Geochim. Cosmochim. Acta Suppl. 1, Vol. 2, pp. 1097-1102. Pergamon.

(7) Hoffman D. C., Lawrence F. O., Mewherter J. L., and Rourke F. M. (1971) Detection of Plutonium-244 in Nature, Science 234, 132-134.

DEPTH VARIATION OF Ar^{37} AND Ar^{39} IN LUNAR MATERIAL, E. L. Fireman, Smithsonian Astrophys. Obs., Cambridge, Mass. 02138

Solar flares and galactic cosmic rays are recorded in lunar materials by their production of radioactivities. Solar flares produce large, sudden increases in particle intensities, while galactic cosmic rays are relatively constant. For a long-lived radioactivity ($\geq \sim$ 1-yr half-life), the activity produced by solar flares can be separated from that produced by cosmic rays only by comparing the amounts at various depths with the amounts expected from cosmic rays. The expected amounts of activity are obtained by calculations. In Apollo 15 material, the depth variation of the Ar^{37} activity (35-day half-life) produced by cosmic rays can be measured directly since there were no significant solar flares for a long period (greater than 4 months) before the mission.

Table 1 gives our measurements of the Ar^{37} activities in samples with known depths from the Apollo 12, 14, 15, and 16 missions and the Ca contents as determined by other investigators. Figure 1 shows plots of the Ar^{37}/Ca ratio as a function of depth for the four missions. The top-surface sample of rock 15555, 0 to 2 g/cm^2 in depth, and soil sample 15271.17, which was scooped from the surface, had the lowest Ar^{37}/Ca ratios, 236 ± 42 and 264 ± 25 dpm/kg Ca, respectively. At large depths ($\geq$ 15 g/cm^2), the Ar^{37}/Ca ratios from the four missions were the same. At shallow depths ($\leq$ 10 g/cm^2), the Ar^{37}/Ca ratios for the Apollo 12, 14, and 16 samples were larger than for the Apollo 15 samples by different amounts. The Ar^{37}/Ca enhancements are attributed to the solar flares of November 2, 1969, January 24, 1971, and April 19, 1972, respectively. The intensities of these flares calculated with Ar^{37} production cross sections obtained from target measurements[1] are given in Table 2. According to these cross-section measurements in simulated lunar targets, Ar^{37} is produced in significant amounts only by protons with energies above 50 Mev.

Because the production rate[2] of Ar^{39} (270-yr half-life) from Ca is more than an order of magnitude smaller than that of Ar^{37} from Ca, and because a substantial amount of Ar^{39} can be produced from K by neutrons[3] in lunar material, Ar^{39} can be produced in similar amounts from four target elements: Fe, Ti, Ca, and K. The determination of the Ar^{39} produced in the separate elements as a function of depth could be obtained from the measurement of Ar^{39} in four samples from the same depth with different abundances of these target elements. Rock 14321 had a factor of 15 more K and our Apollo 16 samples had factors of 2 more Ca and 4 less Fe than our Apollo 15 samples; however, our Apollo 12 and 15 samples had similar chemical compositions. If the reasonable assumption is made that the Ar^{39} production in Ti is 4 times its production in Fe (based on preliminary cross-section measurements), then the Ar^{39} from the separate elements Fe, Ca, and K at depths of $\sim$ 1, $\sim$ 5, $\sim$ 15, and $\sim$ 30 g/cm^2 can be obtained from the Ar^{39} measurements. Table 3 gives the results. The Fe $\rightarrow$ Ar^{39} at all depths is approximately 20 dpm/kg Fe, which is twice the value expected from galactic cosmic rays.[4] If the excess Fe $\rightarrow$ Ar^{39} is attributed to solar flares, the (> 200 Mev) proton flux averaged over the past 1000 yr was 5×10^7/cm^2 yr. This result indicates that the 19th solar cycle (1950–1961), which had a number of very energetic solar flares, was more typical of the solar activity during the past 1000 yr than was the

Depth Variation of AR^{37} And Ar^{39} in Lunar Material

E. L. Fireman

20th solar cycle. The $Ca \rightarrow Ar^{39}$ decreases with increasing depth at less than 15 g/cm^2 and then increases at 30 g/cm^2, in a manner very similar to that observed for the Ar^{37}/Ca ratios in Apollo 12 and 14 samples. It appears that Ar^{37} and Ar^{39} in Ca arise from protons of similar energies and that the intensities of the solar-flare protons averaged over the past 1000 yr responsible for the Ar^{39} in Ca are equivalent to 5 flares per year of the January 24, 1971, intensity. The $K \rightarrow Ar^{39}$ depth dependence shows that the neutrons involved in the $K^{39}(n, p)Ar^{39}$ reaction have been moderated to such an extent that the solar-flare effect cannot be separated from the cosmic-ray effect.

Table 1. Ar^{37} activities, depths, and Ca contents.

Sample	Depth (g/cm^2)	Ar^{37} (dpm/kg)	Ca (%)	Ar^{37}/Ca (dpm/kg Ca)
60007,93,94,95	0–2.0	39.0 ± 2.2	11.4	352 ± 20
60007,96,97,98	5.0–7.0	47.9 ± 1.9	11.4	422 ± 17
60007,99,100,101	14.0–16.0	58.5 ± 2.4	11.4	513 ± 22
60007,102,103,104	25.3–27.3	68.1 ± 2.9	11.4	598 ± 25
15555,98	0–2.0	15.8 ± 2.8	6.7	236 ± 42
15555,80	~15	31.2 ± 3.3	6.7	465 ± 49
15555,77	~40	35.0 ± 6.5	6.7	520 ± 97
15271,17	~ 2	21.4 ± 2.0	8.1	264 ± 25
14321,81,83	0–1.5	38.5 ± 2.5	6.1	632 ± 39
14321,81,83	1.5–3.0	37.6 ± 2.5	6.1	618 ± 39
14321,81,83	3.0–4.5	35.0 ± 4.0	6.1	574 ± 63
14321,95	~35	34.0 ± 2.7	6.1	537 ± 42
12002,57	0–2.4	30.0 ± 4.0	5.4	556 ± 65
12002,57	2.5–9.0	25.0 ± 1.5	5.4	463 ± 28
12002,59	14.5–19.0	27.5 ± 2.5	5.4	510 ± 46

References

(1) D'Amico J., DeFelice J., Fireman E. L., Jones C., and Spannagel G. (1971), Proc. Second Lunar Sci. Conf., Geochim. Cosmochim. Acta Suppl. 2, Vol. 2, pp. 1825-1839, MIT Press.

(2) Stoenner R. W., Lyman W. J., and Davis R. Jr. (1970), Proc. Apollo 11 Lunar Sci. Conf., Geochim. Cosmochim. Acta Suppl. 1, Vol. 2, pp. 1029-1036, Pergamon Press.

(3) Begemann F., Vilcsek E., Rieder R., Born W., and Wänke H. (1970), Proc. Apollo 11 Lunar Sci. Conf., Geochim. Cosmochim. Acta Suppl. 1, Vol. 2, pp. 995-1007, Pergamon Press.

(4) Reedy R. C. and Arnold J. R. (1972), J. Geophys. Res. 77, 537-555.

(5) Bostrom C. (1971), Solar-Geophysical Data, U.S. Dept. of Commerce.

(6) Fireman E. L., D'Amico J., DeFelice J., and Spannagel G. (1972), Proc. Third Lunar Sci. Conf., Geochim. Cosmochim. Acta Suppl. 3, Vol. 2, MIT Press, in press.

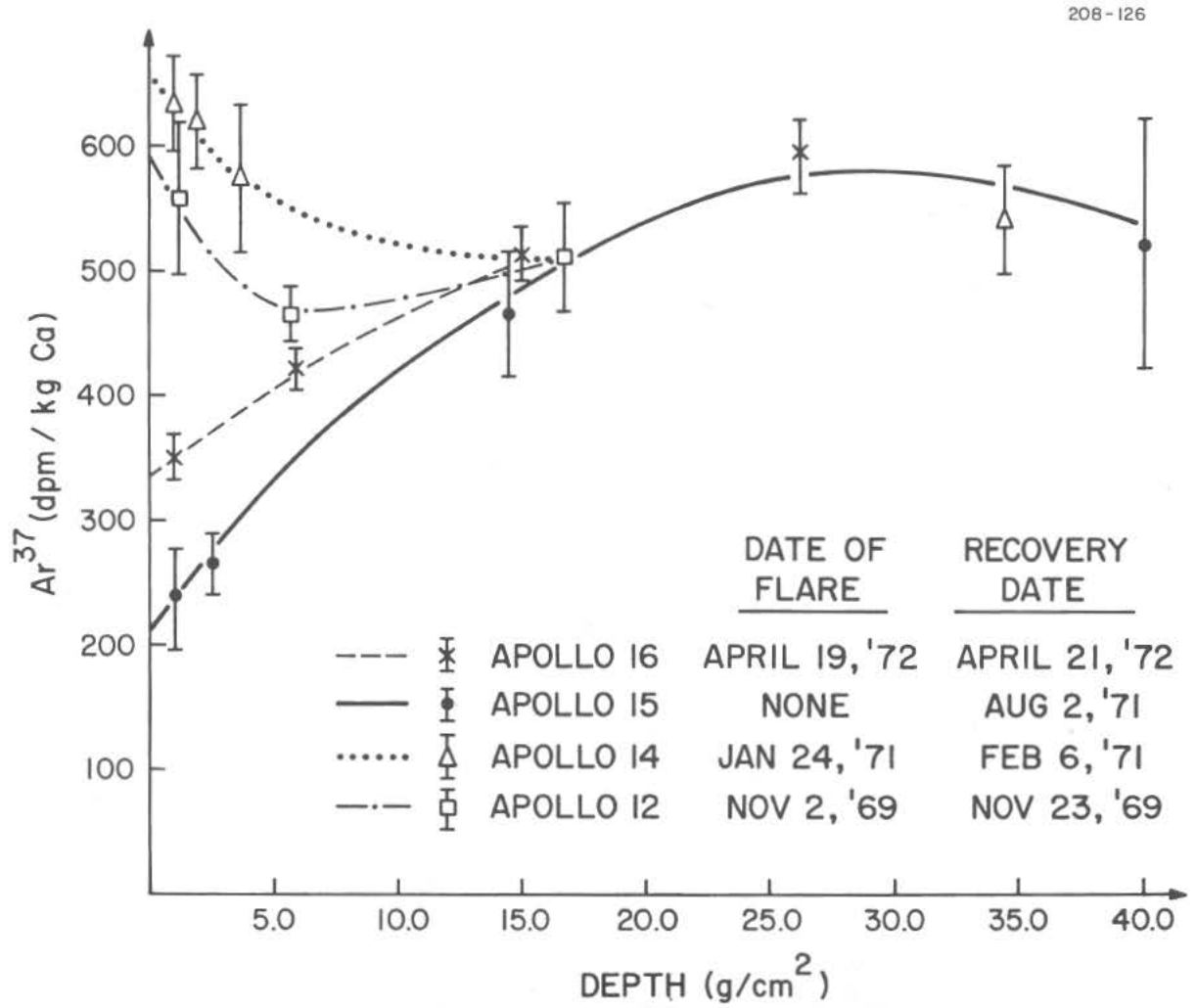

Figure 1. Ar^{37}/Ca versus depth.

Table 2. Solar-flare proton fluxes (≥50 Mev) from Ar^{37}/Ca and from satellite data.

Flare date	ΔAr^{37}/Ca (dpm/kg Ca)	Time before recovery (days)	$(\Delta Ar^{37}/Ca)^{*}_{cor.}$ (dpm/kg Ca)	Proton flux† ($10^7/cm^2$)	Proton flux‡ ($10^7/cm^2$)	Proton flux** ($10^7/cm^2$)
April 19, 1972	95 ± 35	2	98 ± 38	0.7 ± 0.3	–	–
January 24, 1971	370 ± 40	13	490 ± 52	3.7 ± 0.6	3.1 ± 0.6	2.9
November 2, 1969	300 ± 70	21	455 ± 105	3.4 ± 0.9	2.0 ± 0.4	2.0

*Corrected for elapsed time between flare and sample recovery.

†Integral flux (≥50 Mev) over 2π solid angle from ΔAr^{37}/Ca and cross sections from D'Amico et al.[1]

‡Integral flux (>55 Mev) over 2π solid angle (private communication from J. Van Allen, 1971).

**Integral flux (>60 Mev) over 2π solid angle.[5]

Table 3. Ar^{39} produced* in Fe, Ca, and K versus depth in the moon.

Depth (g/cm^2)	Fe → Ar^{39} (dpm/kg Fe)	Ca → Ar^{39} (dpm/kg Ca)	K → Ar^{39} (dpm/kg K)
1.0	20 ± 4	60 ± 7	700 ± 200
~ 5.0	22 ± 3	50 ± 8	1000 ± 300
15.0	21 ± 4	35 ± 7	2000 ± 300
~30.0	22 ± 4	62 ± 12	2200 ± 300

*Ar^{39} production in Ti is assumed to be 4 times that in Fe; calculated from Ar^{39} data given in Fireman et al.[6] and preliminary data for Apollo 16.

PARTICLE TRACK RECORD OF APOLLO 15 GREEN SOIL AND ROCK, R. L. Fleischer and H. R. Hart, Jr., General Electric Research and Development Center, Schenectady, New York 12301.

Some of the most unusual and fascinating of the sets of lunar materials are the green soils and rock from near the Apennine Front that were sampled on Apollo 15 at stations 6a and 7. The green color arises from the abundance of clear, green glass in the form of spheres, ellipsoids, and other figures of revolution in this material. We have measured track densities (Figure 1), track stability (Figure 2), and uranium contents (Table I) in samples of a soil fillet (15401) from the top of a boulder at station 6a, a piece of that boulder (15405,17) and a chunk or clod of friable green material from nearby station 7 (15426,74). Sample 15426, although classified as a rock, contains the same major minerals as the soil 15401, including the abundant green glass spherules. This green glass appears to be rather homogeneous in its track registration properties but non-uniform in its uranium content, specific gravity, and bulk etching rate. The major components of a soil sample, 15401, are found to be unusually young (5×10^5 yrs) and to have been stirred at least once during its lifetime. A nearby soil clod, 15426, appears to have been formed of the same material in the same event. 15405, the rock upon which 15401 was perched, has recorded deformation features and track densities compatible with its surface residence having begun at the same time.

Table I: Uranium Content of Lunar Glasses

Sample Type	Sample #	Specific Gravity	Uranium Content [wt fraction x 10^9] ($\pm 2\sigma$)
Green Glass	15426,74,2,2	<2.6	5.1 ($\pm$ 1.5)
Green Glass	15401,63,2,15	<2.6	69.3 ($\pm$ 5.0)
Green Glass	15401,63,4,2,2	>2.6	32.8 ($\pm$ 2.7)
Green Glass	15401,63,1,13	>2.6	244 ($\pm$ 19)
Amber Glass	15401,63,2,4	<2.6	1840 ($\pm$ 120)

GREEN SOIL AND ROCK

Robert L. Fleischer

Figure 1:

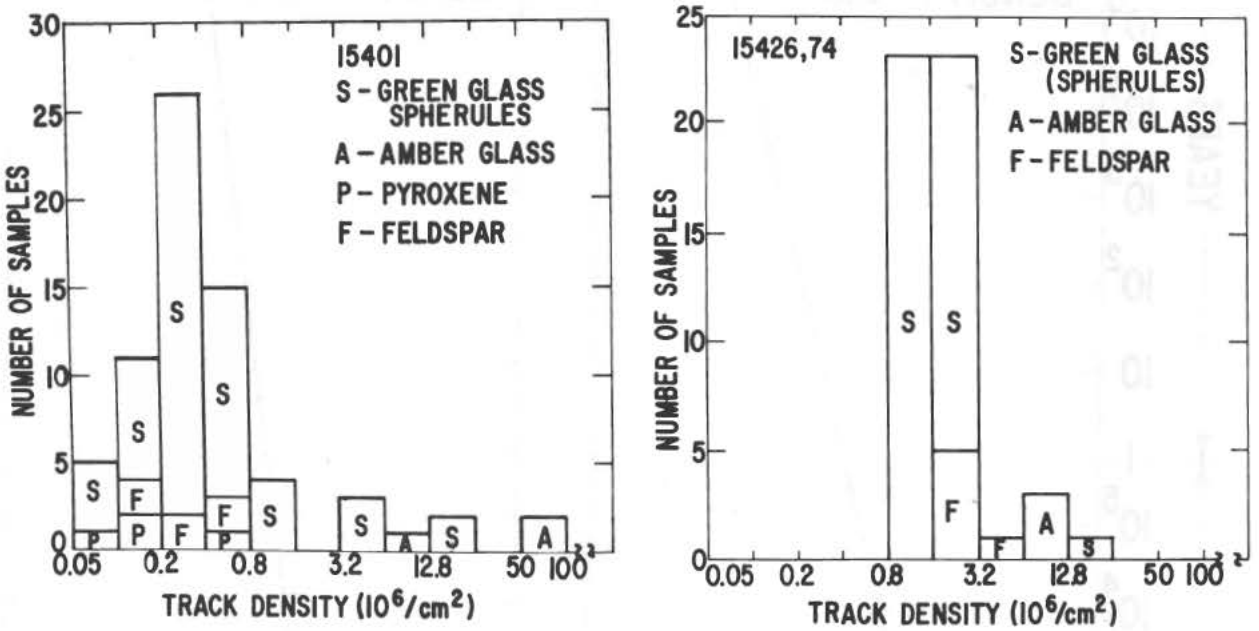

Histogram of Track Densities Observed in Soil 15401 and Soil Clod 15426,74. The green glass is corrected for an etching efficiency of 0.19; amber glass, 0.14; and pyroxene, 0.7. All 69 grains had track densities $<10^8/cm^2$.

Figure 2

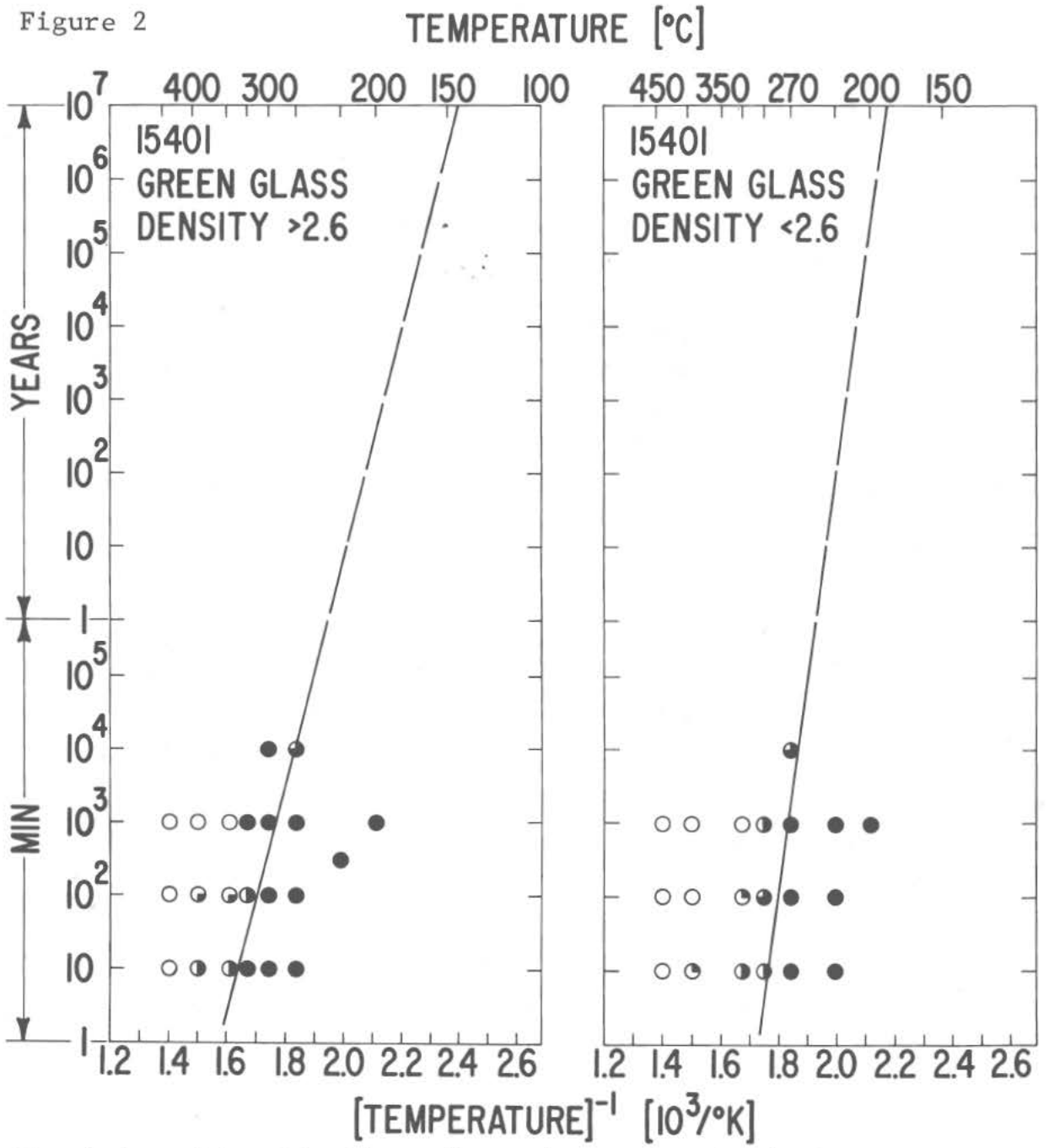

Track Annealing Kinetics of cosmic ray tracks in two fractions of Green Glass 15401. Open circles indicate fading; solid dots retention; partially filled circles, partial fading. Extrapolations indicate full retention at all normal lunar temperatures, even for the worst case lines drawn.

PARTICLE TRACK RECORD IN APOLLO 15 DEEP CORE FROM 54 TO 80 CM DEPTHS, R. L. Fleischer and H. R. Hart, Jr., General Electric Research and Development Center, Schenectady, New York 12301.

Lunar soil columns present unique opportunities for observing the results of various long term processes that act on the moon. In particular the 2.4 m Apollo 15 core revealed an extensive stratigraphy that should allow the complicated processes of soil excavation, redistribution, and mixing to be traced into the past. Since cosmic ray tracks are produced only in surface or near surface exposure of track recording crystals and glasses, they are appropriate tools for deriving parts of this complicated history.

Figure 1 records our results on >500 grains from thirteen samples in the depth range 54 to 80 cm in Apollo 15 core sample 15005, and Figure 2 compares various measures of these distributions - median, 25th percentile density, and minimum track density - with the visual stratigraphy of the core.

Certain inferences follow clearly from these data:

(1) The exposure histories of individual grains (Figure 1) are widely varied at each depth, representing therefore mixed material with different surface exposure histories prior to deposition.

(2) The near surface exposure prior to deposition is most of the total near surface exposure, since no systematic overall decrease in track density with depth is visible.

(3) The existence of similar details in all 3 curves in Figure 2 support the idea[1] that the minimum track densities do give a physically meaningful measure of surface exposure that is not strongly affected by extraneous effects.

(4) There is stratigraphic information on a finer scale than indicated by the visual layering. For example the ascending track densities with depth for the three depths in layer V-E are incompatible with its having been a single static layer or it having been homogenized by gardening prior to being covered over.

Two less obvious inferences that we will document in greater detail are that the layers from 40 to 80 cm depths were laid down in less than 80 million years at an average rate of $\gtrsim 0.5$ cm/m.y.

The Luna 20 sample, which comes from a geologically similar site to that of Apollo 15, has a track density distribution similar to those of our typical Apollo 15 layers.

(1) Fleischer, R.L., G.M. Comstock, and H.R. Hart, Jr., (1972), J. Geophys. Res. 77, September 10.

APOLLO 15 DEEP CORE

Robert L. Fleischer

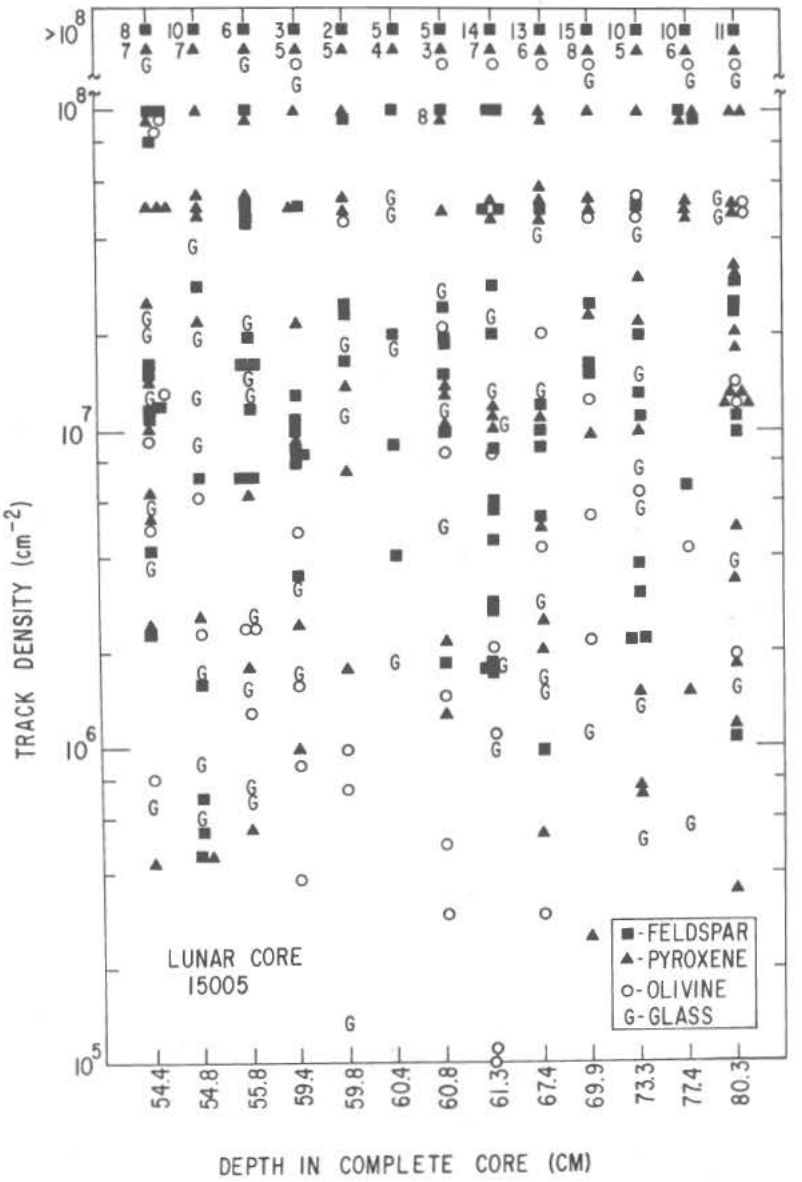

Figure 1: Track densities observed in four mineral types from thirteen samples at different depths in core 15005. The numbers to the left of the symbols indicate the numbers of samples measured when multiple samples are involved. Pyroxenes and glass samples are corrected for etching efficiencies of 0.7 and 0.2 respectively.

APOLLO 15 DEEP CORE

Robert L. Fleischer

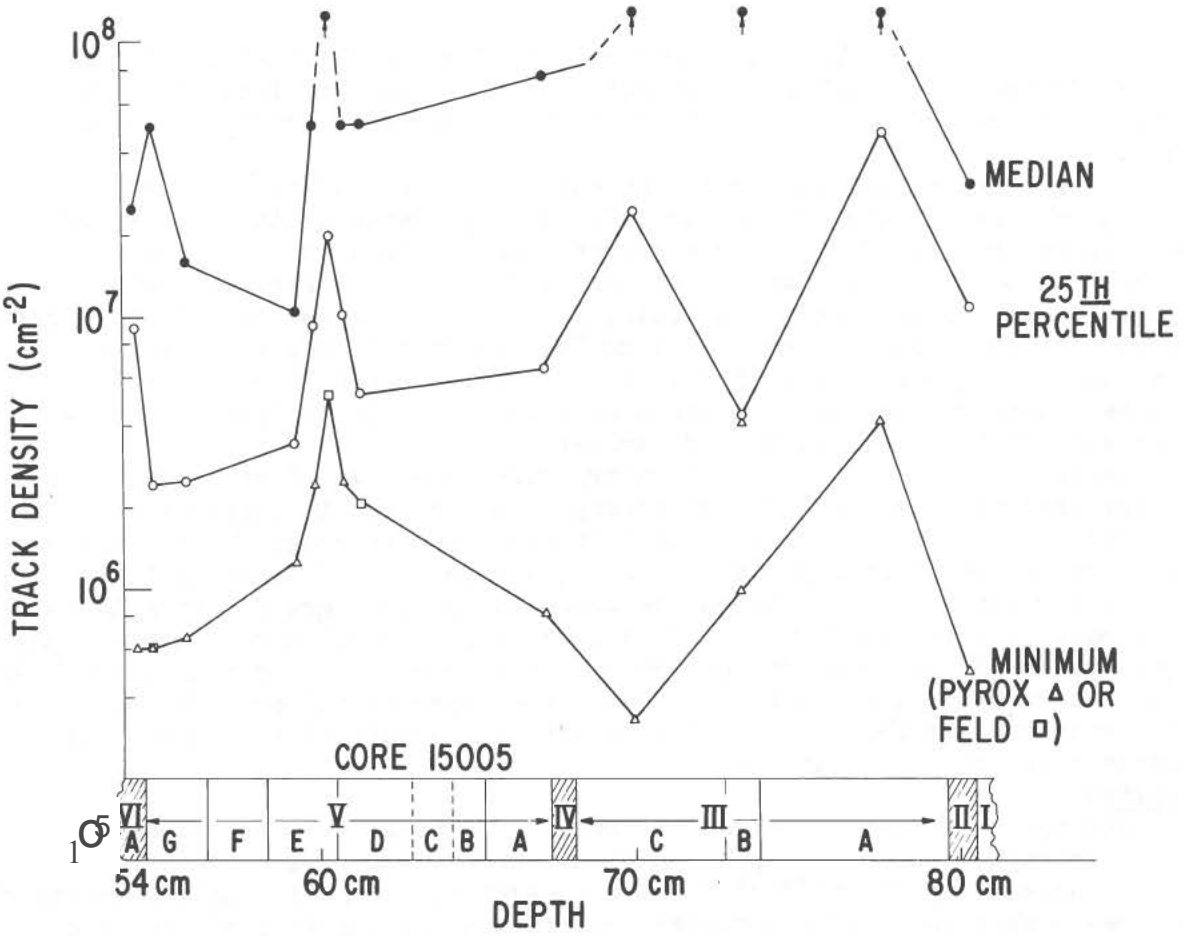

Figure 2: Measures of the track density distributions given in Figure 1 compared with the visual stratigraphy of the core. In deciding the minimum track densities, glasses and olivines were neglected because of possible track fading.

THE ^{40}Ar - ^{39}Ar AND COSMIC RAY EXPOSURE AGES OF APOLLO 15 CRYSTALLINE ROCKS, BRECCIAS AND GLASSES. Liaquat Husain, Department of Earth and Space Sciences, State University of New York, Stony Brook, N.Y. 11790.

The gas retention and cosmic ray exposure ages have been determined for a suite of lunar samples from Sta 2 (St. George crater), Sta 3 (Rhysling), Sta 4 (Dune crater), Sta 6 (the Apennine Front), Sta 7 (Spur crater), Sta 8 (ALSEP) and Sta 9A (the edge of the Hadley Rille). The samples analysed include large crystalline rocks 15016, 15058, 15415, 15499 and 15555, eight walnut size samples, thirteen 2 - 4 mm "coarse fines" fragments, a breccia 15465 and the "green clod", 15426. In addition trapped $^{40}Ar/^{36}Ar$ ratios have also been measured for brown glass microbreccias. The analyses of a few of these samples have been published earlier. [1, 2]

Samples received in this laboratory were generally first described and photographed under a binocular microscope. All fragments larger than 10 mg were split into two parts: One for this work and the other for a polished thin section for mineralogic and petrologic studies.[3] This makes it possible to look for correlations between the ages and the petrographic rock types. The samples I have analysed include all major petrographic rock types found among Apollo 15 samples. The gas retention ages were determined by the ^{40}Ar -^{39}Ar method using incremental heating. The experimental procedure used has been described earlier.[2] Following is a brief summary of the results of various types of lunar material.

Basalts:

The ages have been obtained for twenty two basalts. The K-concentration on the average is about 300 ppm. Most of the samples give well-defined plateau ages i.e.; $^{40}Ar^*/^{39}Ar^*$ ratio increases as a function of gas released to a reasonably well-defined plateau and then stays constant within experimental uncertainties. It should be pointed out, however, that due to relatively low K-concentrations and younger ages and small size samples (as low as 10 mg) some plateau ages uncertainties are as high as 0.1 Gy (1Gy = 10^9yr). About a third of the sample, however, show the characteristic decrease of the $^{40}Ar^*/^{39}Ar$ ratios at high temperatures observed for the Fra Mauro material.[2,4] The radiogenic argon, $^{40}Ar^*$, losses for the large rocks are as follows: 15016, 19%; 15058, 9%; 15415, 4%; 15499, 0.8%; and 15555, 24%. The "coarse-fines" fragments and walnut size igneous rocks show from negligible $^{40}Ar^*$ loss to as high as 40%. The loss of cosmogenic ^{38}Ar($^{38}Ar_{sp}$) is not always possible to determine. In lunar samples $^{38}Ar_{sp}$ is predominantly produced from galactic cosmic ray protons interactions with calcium, and to a small extent with titanium and iron. To complicate further ^{38}Ar is also produced during neutron irradiation via $^{37}Cl(n,\gamma)$ ^{38}Cl β^- $\rightarrow$ ^{38}Ar. In favorable cases, however, it is possible to determine the loss of $^{38}Ar_{sp}$. For example, the fragment 15473,3,15 has lost 24.6% of its $^{40}Ar^*$ but practically none of

The ^{40}Ar - ^{39}Ar and Cosmic Ray Exposure Ages

Liaquat Husain

its $^{38}Ar_{sp}$. The cosmic ray exposure age of this fragment is 656 ±43 m.y. The gas release pattern of $^{40}Ar^*$ and $^{38}Ar_{sp}$ are quite different, 48% of the K-derived argon is released by 750°C, and 10% of $^{38}Ar_{sp}$. If solar heating causes the loss of $^{40}Ar^*$ on the lunar surface, measurable loss of $^{38}Ar_{sp}$ would be quite probable.

The gas retention ages for all of the basalts analysed in this work lie in the range of 3.3 ± 0.1 Gy, except 15668, a 15.1 g Apollo 11 intersertal type basalt has an age of 3.15 ± 0.06Gy. The age spread is shown in Fig. 1. Within the experimental uncertainties, no correlation between the age and the petrographic rock type is observed. If more than one flow unit of basalts was sampled [5], the flows occurred within 100 m.y. No sample younger than 3.1 Gy was found. Thus, no evidence for volcanic activity since 3.1 Gy has been found in the lunar material studied so far. The ages of Apollo 15 basalts then are very similar to those from Ocean of Storms. [6,7] The volcanic activity in the Marsh of Decay, Ocean of Storms and Sea of Fertility occurred about the same time and about 200-300 m.y. after that in Sea of Tranquility and about 400-500 m.y. after the excavation of the Imbrium basin, about 3.8 Gy ago. [8,9]

Breccias:

Twenty two brown glass microbreccias from St. George crater, the Apennine Front and the Hadley Rille were analysed for rare gases. All of these microbreccias contain large amount of trapped atmospheric ^{40}Ar and solar wind $^{36}Ar[^{40}Ar/^{36}Ar) \geq 0.9]$. The presence of the non radiogenic ^{40}Ar make the age measurements difficult if not impossible. One of these microbreccia 15603,12,1 was neutron irradiated and gas release pattern studied. Fig. 2 shows a plot of $^{40}Ar/^{36}Ar_{sw}$ vs $^{39}Ar^*/^{36}Ar_{sw}$. $^{36}Ar_{sw}$ is obtained by taking solar wind $^{36}Ar/^{38}Ar$ ratio as 5.35 and cosmogenic $^{36}Ar/^{38}Ar = 0.54$ measured for 600 MeV proton interactions with calcium.[10] From Fig. 2 one obtains$(^{40}Ar/^{36}Ar)_{trapped} = 0.5$. Using this ratio to correct for trapped ^{40}Ar, an approximate age of 3.2 to 3.45 Gy is obtained. An accurate ^{40}Ar-^{39}Ar age is not obtained because the trapped ^{40}Ar and $^{36}Ar_{sw}$ do not have similar release pattern. ^{40}Ar is released at earlier temperatures than $^{36}Ar_{sw}$.

Two breccia fragments, 15263,4,1 and 15263,4,7 contain, however, very little trapped ^{40}Ar and ^{36}Ar, and age determination was possible. The fragment 15263,4,1 is a recrystallized breccia and contains very little trapped gases, in contrast to the microbreccia with abundant glass.[3] It has lost very little of its radiogenic argon, and $^{38}Ar_{sp}$. It has an age of 3.98 ± 0.05 Gy and cosmic ray exposure age of 595 ± 40 m.y. The other breccia 15263,4,7, is a recrystallized fragment containing some glass.[3] It has a complex thermal history as indicated by its gas release pattern. $^{40}Ar^*/^{39}Ar^*$ ratio rises in early temperatures and then giving a plateau corresponding to 3.79 ± 0.04 Gy and again rising in the highest temperatures to 3.95 Gy. This breccia fragment was probably thermally metamorphosed at the time of Imbrium event. The 3.79 ± 0.04 Gy plateau is completely consistent with the age of the Imbrium event. [7,8] A whole K-Ar (minimum) age of 3.91 ± 0.05 Gy and an exposure age of 216 ± 15 m.y. is obtained. In contrast to the Apollo 15 Basalts these breccia fragments have lost very little of their $^{40}Ar^*$.

THE ^{40}Ar - ^{39}Ar & COSMIC RAY EXPOSURE AGES

Liaquat Husain

Glasses:

Splash glass fragment 15286,10 and surface glass from breccia 15465 gave complex gas release patterns and minimum ages of 0.99 ± 0.25 and 1.09 ± 0.14 Gy, respectively. This may be the age of the Aristillus and/or Autolycus cratering events. The mafic green glass spherules of unique chemical composition from the "green clod" 15426 have also been analysed. The K-concentration of these spherules is 120 ppm, and $^{40}Ar/^{36}Ar_{sw}$ ratio, 13.86 ± 0.48. An ^{40}Ar - ^{39}Ar age of 3.79 ± 0.08 Gy is obtained. This mafic green glass is compositionally similar to the meteorite type Howardites, which suggests that material of Howardites composition served as a source for the lunar green glasses.[11] These glasses were probably formed as a result of the Imbrium event and due to the proximity of the Apollo 15 site to Imbrium basin probably came from a depth of a few kilometers or more. The 3.79 Gy age is completely consistent with the age of Imbrium event based on the ages of Fra Mauro samples.[8,9]

References:

1. L. Husain, O. A. Schaeffer and J. F. Sutter, Science 175, 428 (1972)
2. L. Husain, O. A. Schaeffer, J. Funkhouser, and J. F. Sutter, Proceedings of the Third Lunar Conference, Vol. 2, M.I.T. Press (1972)
3. K. L. Cameron, J. W. Delano, A. E. Bence and J. J. Papike, "The Apollo 15 Lunar Samples", Ed. J. W. Chamberlain and C. Watkins (Houston: Lunar Science Institute)
4. G. Turner, J. C. Huneke, F. A. Podosek and G. J. Wasserburg, Earth & Planet. Science Letters, 12, 19 (1971)
5. Apollo Lunar Geology Investigation Team Report, Science 1975, 407 (1972)
6. G. Turner, Earth Planet. Science Letters, 11, 169 (1971)
7. D. A. Papanastassiou and G. J. Wasserburg, Earth & Planet. Science Letters, 11, 37 (1971)
8. J. F. Sutter, L. Husain and O. A. Schaeffer, Earth & Planet. Science Letters, 11, 249 (1971)
9. L. Husain, J. F. Sutter and O. A. Schaeffer, Science 173, 1235 (1971)
10. J. Barber and O. A. Schaeffer, Private Communication
11. U. B. Marvin, J. B. Reid, Jr., G. J. Taylor and J. A. Wood, Lunar Science - III, Revised Abstracts, Third Lunar Science Conference, Houston, Texas (1972).

The ^{40}Ar - ^{39}Ar and Cosmic Ray Exposure Ages

Liaquat Husain

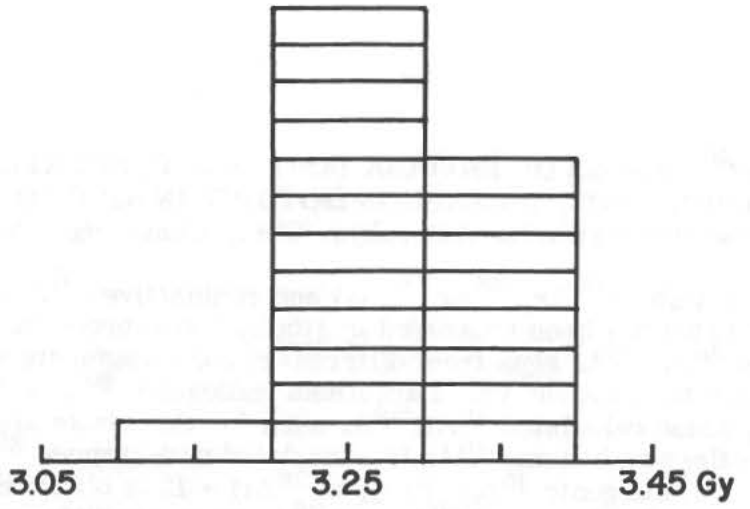

Fig. 1 ^{40}Ar - ^{39}Ar Ages of Apollo 15 Basalts

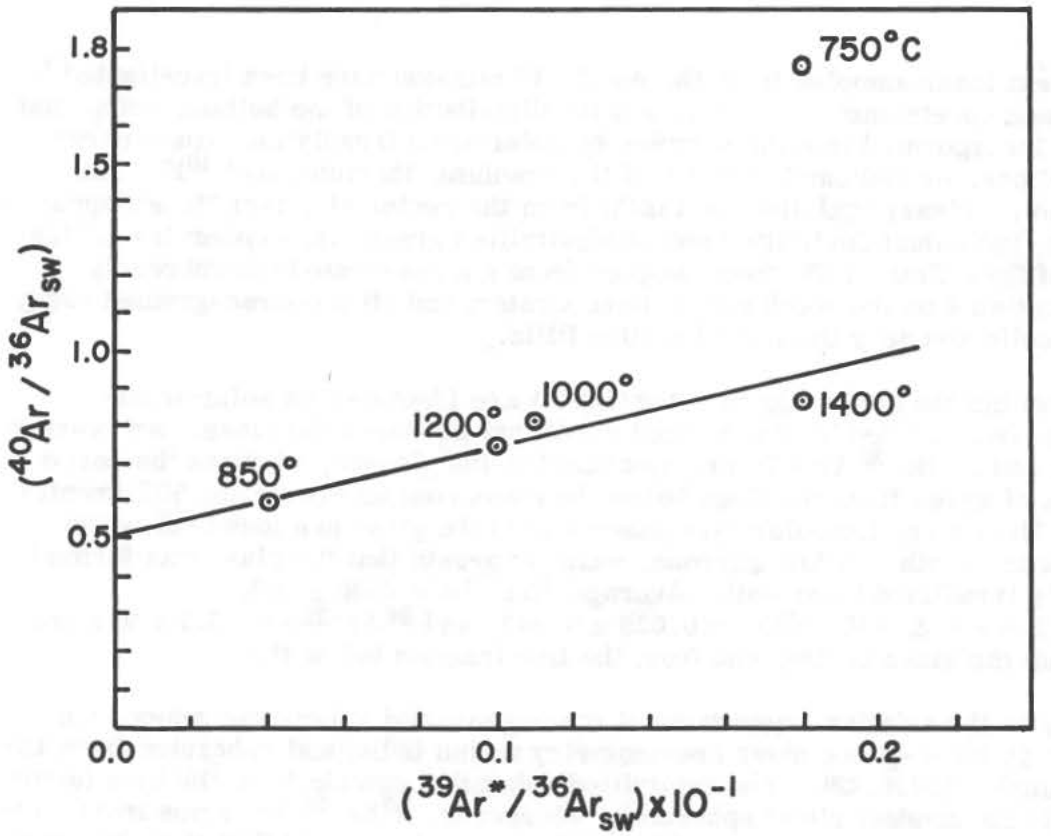

Fig. 2 A plot of $^{40}Ar/^{36}Ar_{sw}$ vs $^{39}Ar^{*}/^{36}Ar_{sw}$ for sample 15603,12,1

IN SITU $^{40}Ar/^{39}Ar$ AGES OF BRECCIA 14301, AND CONCENTRATION GRADIENTS OF HELIUM, NEON, AND ARGON ISOTOPES IN APOLLO 15 SAMPLES, G. H. Megrue, Smithsonian Institution Astrophys. Obs., Cambridge, Mass. 02138.

The distribution of stable (^{36}Ar, ^{38}Ar, ^{40}Ar) and radioactive (^{37}Ar, ^{39}Ar) isotopes within lunar breccia 14301 has been measured in situ by laser-probe mass spectrometry. The calculated $^{40}Ar/^{39}Ar$ ages from different clastic fragments within the breccia range from 2.0 to 4.1×10^9 yr. Parentless radiogenic ^{40}Ar exists within the fine-grained matrix, since calculated $^{40}Ar/^{39}Ar$ ages for this phase are $> 6 \times 10^9$ yr; moreover, this parentless radiogenic ^{40}Ar is correlated with trapped ^{36}Ar and ^{38}Ar ($^{36}Ar/^{38}Ar \sim 5.2$). A (radiogenic ^{40}Ar)/(trapped ^{36}Ar) = 12 is observed for a five-fold variation in absolute abundances of ^{40}Ar and ^{36}Ar from six different regions of the fine-grained matrix. These observations suggest that an ambient gas phase or an atmosphere was incorporated into the breccia sometime during the past. The remobilization and homogenization of radiogenic and solar argon were most likely caused by an impact event.

Four different lunar samples from the Apollo 15 mission have been investigated by laser-probe mass spectrometry to ascertain the distribution of the helium, neon, and argon isotopes incorporated into the samples by solar-wind irradiation, cosmic-ray spallation reactions, or radioactive decay of the uranium, thorium, and ^{40}K. The samples include (1) glassy agglutinates (15245) from the center of a 1-m "fresh-appearing" crater; (2) individual devitrified and nondevitrified green glass spherules (15426) from the rim of Spur Crater; (3) four samples from a glass-coated microbreccia (15498) from station 4 on the south rim of Dune Crater; and (4) a coarse-grained vuggy basalt (15555) collected near the rim of Hadley Rille.

The gases within the glassy agglutinates (15245) are identified as solar-wind-implanted gases fractionated by the thermal event that produced the glass. An average $^4He/^{20}Ne = 23$ and a $^4He/^{36}Ar = 71$ are measured in the glasses, whereas the corresponding ratios of gases from the fines below the glass coating are 23 and 50% greater, respectively. Moreover, the solar-type gases within the glass are found below the normal penetration depth of a few microns, which suggests that the glass was formed from previously irradiated lunar soil. Average $^4He/^3He = 2500 \pm 100$, $^{20}Ne/^{22}Ne = 12.5 \pm 0.2$, $^{21}Ne/^{22}Ne = 0.038 \pm 0.002$, and $^{36}Ar/^{38}Ar = 5.2 \pm 0.1$ are measured within the glass coating and from the fine fraction below it.

Differences in the relative abundances of cosmogenic and solar-type gases have been measured by laser-probe mass spectrometry within individual spherules from the green glass sample (15426, 43). The devitrified spherules contain less ^4He by a factor of 2 to 4 than do the nondevitrified spherules. Moreover, $^{20}Ne/^{36}Ar$ varies from 10 to 20 between individual glass spherules. This ratio is consistently higher than the corresponding one from soil samples of Apollo 12 and 14. The cosmogenic ^{21}Ne from the devitrified green spherules is 5 times as abundant as the concentration of cosmogenic

gas within the nondevitrified spherules. A sample of this material was dated by the Stony Brook group as having a $^{40}Ar/^{39}Ar$ age of 3.9×10^9 yr.

The distribution and relative abundances of the helium, neon, and argon isotopes from four different samples of 15498 are highly variable. In particular, the $^4He/^{20}Ne$ from different glass coatings within and on the sample varies from 5 to 26, whereas the $^4He/^{36}Ar$ ranges from 250 to 400. The variations within these ratios are attributed to mass fractionation during the melting of lunar soil previously irradiated by solar wind. Previously solar-irradiated fine-grained material from below the glass coating of 15498, 55 has a $^4He/^{20}Ne = 47$ and $^4He/^{36}Ar = 100$. The distribution of the solar gases within 15498 indicates that this sample is a consolidated lunar soil.

Rb-Sr SYSTEMATICS FOR CHEMICALLY DEFINED APOLLO 15 MATERIALS. L. E. Nyquist, P. W. Gast, S. E. Church, NASA Manned Spacecraft Center, Houston, TX 77058; H. Wiesmann and B. Bansal, Lockheed Electronics Corp., Houston, TX 77058

We have chemically and isotopically analyzed several specimens of each of three major rock groups found at the Hadley-Apennine site. Several bulk soil samples, breccia clasts, and breccia matrices were also analyzed. The three major groups which are distinguished are (a) KREEP basalts, (b) mare basalts, and (c) a suite herein referred to as the Apennine Front Suite. Chemical analyses (1,2) show that the KREEP basalts (from stations 6 and 7) have the chemical characteristics defined for Apollo 12 KREEP glasses (3) and Apollo 14 KREEP breccias (4), but have igneous textures (5,6). The mare basalts are from stations 1, 4, 6, 7 and 9A. Of these, 15256 and 15103,3,4 are described as shock melted (7,6). The other samples are typical mare basalts (8). The suite of breccia clasts and lithic fragments, which we call the Apennine Front Suite, are all from the vicinity of Spur Crater (i.e., stations 6 and 7 (7)). They are non-mare materials based on their trace element distributions (2). For example, Zr/U ~250 clearly resolves them from mare basalts which have Zr/U ~500-800 (9). The anorthosite 15415 and the gabbroic anorthosite 15418 are also included in this group. The reader is referred to Table 1 of the paper by Church et al. (9) for further characterization of the individual samples.

Analytical procedures were similar to those previously reported (10), except that a mixed Rb-Sr spike was used to reduce the relative Rb/Sr errors. The spike was calibrated with NBS standard salts 984 (RbCl) and 987 ($SrCO_3$). Four new analyses of the C.I.T. seawater standard and one analysis of NBS 987 show that our analyses are biased with respect to those of the C.I.T. group by (+0.00012±0.00007) as previously reported (10). Model ages are thus calculated using a "BABI" value of 0.69910. The analytical results are presented in Table 1 and Figure 1.

The whole rock Rb-Sr systematics of the KREEP basalts 15023,2,5 and 15382,9,1 are identical to Apollo 14 KREEP basalts 14073 and 14001,7,3 (11). A whole rock isochron for nine Apollo 14 and 15 crystalline KREEP samples yields an apparent age of $4.15\pm0.11\times10^9$y and an initial $^{87}Sr/^{86}Sr=0.69965\pm32$(0.69953 corrected for our bias). The average $^{87}Rb/^{86}Sr$ and $^{87}Sr/^{86}Sr$ values of the four Apollo 15 crystalline KREEP basalts are 0.237 and 0.7138, respectively, in good agreement with averages of 0.239 and 0.7141 for 30 KREEP materials previously recognized (see Schonfeld and Meyer (12) for a summary). However, a systematic tendency towards lower model ages of crystalline KREEP samples (Apollo 14 and 15) than for KREEP glasses and breccias (Apollo 11, 12, and 14) does appear to exist. Whether the apparent 100 m.y. difference has time significance or is a result of volatilization loss of Rb from the glass and breccia samples is presently unclear. It is worth noting that model ages for KREEP-rich Apollo 14 soils range from 4.36-4.72 AE (11) and that some Apollo 14 KREEP breccias show definite evidence of Rb loss (10,13).

Most members of the Apennine Front Suite fall on a 4.61±.09 AE whole rock

isochron with an initial intercept of 0.69910±3; equal to the BABI value corrected for our bias. (At the present time the uncertainty in $^{87}Sr/^{86}Sr$ is best considered as a measure of the internal consistency of the data, as we have not yet demonstrated our long-term precision to this level.) The green glass samples are exceptions, as might be expected. Inclusion of 15415 and 15418 in this suite is responsible for making the whole rock age equal to the model age and raises the possibility that the above result may simply reflect the tendency of lunar rocks to have model ages near 4.6 AE. On the other hand, their inclusion is a natural one and the resultant age is not necessarily in conflict with the $^{39}Ar/^{40}Ar$ age of 15415 which may be only a lower limit to the crystallization age of this rock (14).

Because of the low abundance of Rb and the small spread in the Rb-Sr systematics for the Apollo 15 mare basalts which we received, the age and calculated initial $^{87}Sr/^{86}Sr$ values for these materials as determined by the whole rock method are subject to relatively large errors. The mineral isochron age of 15555 is 3.32 AE (15,16). Assuming that this age is typical of mare basalts, our calculated initial value for these Apollo 15 mare basalts range from .69938 -.69951 excluding the shock-metamorphased samples described earlier. These values are .00028 to .00041 higher than the $^{87}Sr/^{86}Sr$ initial intercept for the Apennine Front Suite.

The data for soils lie along a line, interpreted as a mixing line, from which individual data points diverge by only slightly more than the analytical uncertainties. The mixing line passes through the crystalline KREEP basalt data identifying them as the radiogenic end member in the soil mix. As shown in Figure 1, the two groups of non-radiogenic materials which we analyzed do not lie on the lower extension of this mixing line. Thus the Rb-Sr systematics of these soils cannot be duplicated by mixing the rocks we have analyzed from this site; at least one additional component is required. The properties of this component should be such that it either lies along the 4.6 AE reference line in Figure 1, yielding 4.6 AE model ages in the absence of crystalline KREEP, or that it lies along and perhaps slightly above the lower extension of the mixing line. The first alternative is the "magic component" hypothesis; an interesting candidate not previously considered is the low-K KREEP basalt suite postulated by Reid et al. (17) who have found that glasses of this chemical composition are abundant in the Front soils. Alternatively, the magic component could be brecciated KREEP which has lost Rb through repeated metamorphism during impact events, shifting the model ages toward 4.6 AE. The high intersection of the soil mixing line and the 4.6 AE reference line could also be due to the presence of a component with low Rb/Sr and an initial $^{87}Sr/^{86}Sr$ greater than BABI; we note two possibilities. The mixing line could be a sampling artifact arising from a mechanical enrichment of plagioclase relative to the more radiogenic components. This alternative is improbable as it requires an *ad hoc* mechanism to produce the segregation and further requires that the KREEP component be present in the correct proportion to yield model ages which seldom exceed 4.6 AE. A more likely possibility would be the presence of a plagioclase rich member of a differentiated rock suite which formed significantly later than 4.6 AE ago from a trace element rich melt. Preliminary data from Apollo 16 soils support this alternative. In any case, the spectrum of Apollo 15 soil model ages from 4.36 to 4.62 AE appears to result from admixing crystal-

line KREEP with a material (itself a mixture) whose model age is approximately 4.6 AE.

Rb analyses by N. J. Hubbard and discussions with E. Schonfeld are acknowledged.

References:

1. Hubbard, N.J., et al., Proc Third Lunar Sci. Conf., Geochim. Cosmochim. Acta, Suppl. 3 (1972) in press.
2. Hubbard, N.J., unpublished data.
3. Hubbard, N.J., et al., Earth Planet. Sci. Lett. 10 (1971) 341.
4. Hubbard, N.J., et al., Lunar Sci. III, Lunar Sci. Inst. Contr. 88 (1972) 407.
5. Meyer, C., Lunar Science III, Lunar Sci. Inst. Contr. 88 (1972) 542.
6. Meyer, C., personal communication.
7. LSPET, Science 175 (1972) 363.
8. Rhodes, J.M., this volume.
9. Church, S.E. et al., this volume.
10. Nyquist, L.E., et al., Proc. Third Lunar Sci. Conf., Geochim. Cosmochim. Acta, Suppl. 3 (1972) in press.
11. Papanastassiou, D.A. and Wasserburg, G.J., Earth Planet. Sci. Lett. 12 (1971) 36.
12. Schonfeld, E. and Meyer, C., Proc. Third Lunar Sci. Conf., Geochim. Cosmochim. Acta, Suppl. 3 (1972) in press.
13. Gibson, E. K. and Hubbard, N. J., Proc. Third Lunar Sci. Conf., Geochim. Cosmochim. Acta, Suppl. 3 (1972) in press.
14. Turner, G., Earth Planet. Sci. Lett. 14 (1972) 169.
15. Wasserburg, G.J. and Papanastassiou, D.A., Earth Planet. Sci. Lett. 13 (1971) 97.
16. Murthy,V.R., et al., Science 175 (1972) 419.
17. Reid, A.M., et al., Meteoritics (1972) in press.
18. Papanastassiou, D.A. and Wasserburg, G.J., personal communication.

Table 1. Rb and Sr Analytical Results for Apollo 15 Materials

Sample	wt (mg)	Rb (ppm)	Sr (ppm)	$^{87}Rb/^{86}Sr$ [a]	$^{87}Sr/^{86}Sr$ [b]	T_M [c]
I. KREEP basalts						
15023,2,5	5.25	13.05	177.4	0.213 ± 4	0.71208 ± 7	4.26 ± .10
15273,4,9	9.82	14.64	191.2	0.221 ± 2	0.71291 ± 5	4.35 ± .07
15382,9,1	11.99	16.12	194.8	0.240 ± 3	0.71383 ± 6	4.29 ± .06
15273,4,10	16.02	17.12	188.6	0.263 ± 2	0.71532 ± 5	4.31 ± .04
II. Mare basalts						
15076,21	61.06	0.924	111.8	0.0237 ± 4	0.70051 ± 7	4.15 ± .26
15256,22	60.16	0.680	99.9	0.0197 ± 5	0.70042 ± 7	4.67 ± .32
15379,5 [d]	33.51	0.827	98.5	0.0243 ± 7	0.70057 ± 11	4.23 ± .26
15379,5 [d,e]	107.3	0.836	97.4	0.02486 ± 10	0.70048 ± 5	4.21 ± .14
15475,35	51.9	0.688	110.7	0.0180 ± 5	0.70037 ± 6	4.90 ± .35
15545,13	50.0	0.750	103.9	0.0209 ± 6	0.70041 ± 4	4.37 ± .26
15682,4 [d]	37.71	1.143	129.8	0.0255 ± 6	0.70071 ± 8	4.40 ± .33
15682,4 [d,e]	128.8	1.145	128.7	0.02576 ± 10	0.70048 ± 5	4.06 ± .14
15103,3,4	22.75	1.00	113.7	0.0254 ± 10	0.70081 ± 12	4.68 ± .50
III. Apennine Front Suite						
15415 II	90.90	0.142	172.2	0.0024 ± 2	0.69926 ± 5	--
15415 I [f]	53.25	0.17	177	0.0028 ± 3	0.69938 ± 18	
15415-A [g]	1.0	0.196	240	0.0024	0.69926 ± 12	
15415-B [g]	3.7	0.145	173	0.0024	0.69917 ± 12	
					0.69914 ± 5	
15418,51	55.8	0.162	140.1	0.0034 ± 3	0.69934 ± 5	--
15303,3,7	23.22	1.227	169.7	0.0209 ± 7	0.70044 ± 7	4.47 ± .38
15459,38	24.77	1.69	205.3	0.0239 ± 5	0.70067 ± 5	4.58 ± .24
15273,4,2	14.69	1.36	139.0	0.0283 ± 12	0.70100 ± 7	4.67 ± .38
15445,17	51.00	1.426	129.9	0.0318 ± 4	0.70122 ± 4	4.64 ± .15
15445,9 [h]	4.72	0.80	42.6	0.054 ± 12	0.70238 ± 44	4.2 ± 1.6
15301,GG [h]	16.78	0.253	28.6	0.026 ± 5	0.70069 ± 31	4 ± 2
15303,GC [h]	87.42	0.329	27.8	0.0343 ± 10	0.70111 ± 7	4.10 ± .25
IV Soils						
15021,13 [i]	59.4	5.91	132.2	0.129 ± 1	0.70755 ± 13	4.55 ± .12
15101,90 [f]	9.59	4.58	141.6	0.0936 ± 20	0.70524 ± 8	4.57 ± .15
15101,90	53.7	4.52	144	0.0908 ± 10	0.70514 ± 31	4.62 ± .30
15271,66	50.9	5.70	140.3	0.118 ± 1	0.70660 ± 60	4.44 ± .38
15301,76	45.3	4.03	114.8	0.102 ± 1	0.70585 ± 11	4.59 ± .14
15001,32	10.79	8.10	136.3	0.172 ± 3	0.70935 ± 5	4.36 ± .10
15002,28	8.75	7.17	136.8	0.1517 ± 26	0.70872 ± 8	4.42 ± .11
15003,30	9.3	6.11	134.1	0.1318 ± 24	0.70738 ± 17	4.38 ± .16
15004,28	7.68	5.89	131.7	0.1293 ± 29	0.70721 ± 9	4.38 ± .14
15005,27	8.95	6.39	136.4	0.1356 ± 25	0.70762 ± 9	4.38 ± .13
15006,28	7.63	5.94	126.9	0.1353 ± 31	0.70783 ± 10	4.50 ± .15
22001,6(Luna 20)	18.81	1.602	140.8	0.0329 ± 9	0.70125 ± 7	4.55 ± .28
V. Miscellaneous						
15273,4,3	13.35	6.54	149.4	0.127 ± 2	0.70711 ± 4	4.41 ± .10
15445,25	57.66	3.56	160.3	0.0643 ± 7	0.70322 ± 6	4.47 ± .11
15459,31	28.02	0.697	54.9	0.0367 ± 16	0.70109 ± 6	3.80 ± .27
15459,98	62.54	3.76	129.5	0.084 ± 10	0.70437 ± 14	4.37 ± .16
Sr Isotopic Standards						
CIT Seawater	4/10/72				0.70912 ± 4	
	5/ 2/72				0.70918 ± 8	
	7/28/72				0.70926 ± 10	
	8/ 7/72				0.70923 ± 5	
NBS 987	8/ 8/72				0.71025 ± 8	

a. Uncertainties correspond to last figures.
b. Uncertainties correspond to last figures and represent $2\sigma_{mean}$.
c. Model age assuming I=0.69910 (BABI plus our bias).
d. Aliquots of the same dissolutions supplied through the courtesy of D.A. Papanastassiou.
e. Papanastassiou and Wasserburg (18).
f. Earlier analysis - Nyquist et al. (1972).
g. Wasserburg and Papanastassiou (15).
h. Green glass.
i. Simplified column chemistry for Rb and Sr only.

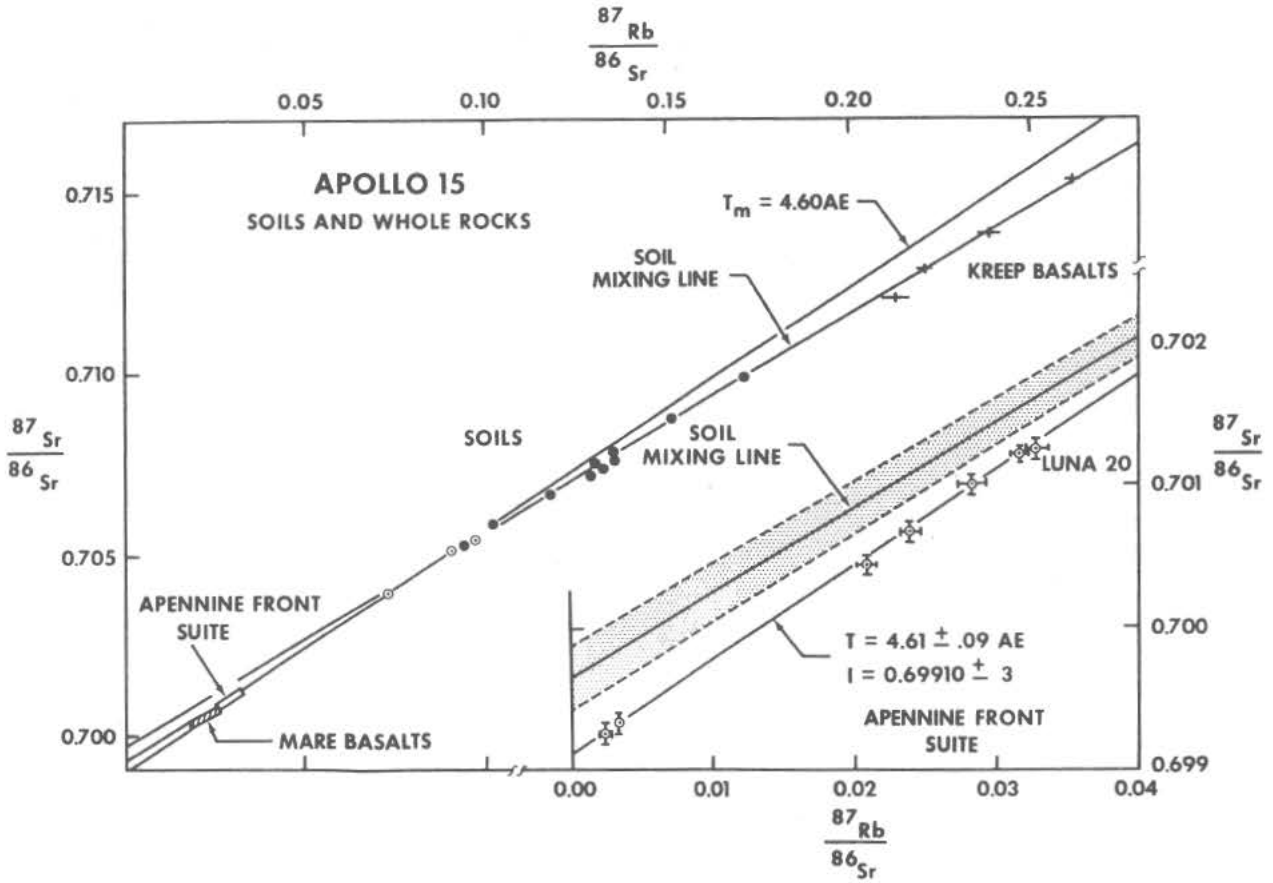

Fig. 1. Rb-Sr systematics for Apollo 15 soils and whole rocks. Open circles represent soils 15081, 15221, and 15601 (15). The mixing line is a least squares fit to the soil data only, the shaded area in the insert shows its uncertainty (2σ).

TRACK ANALYSIS OF ROCKS 15 058, 15 555, 15 641 AND 14 307

G. Poupeau, P. Pellas, J.C. Lorin, G.C. Chétrit and J.L. Berdot,
C.N.R.S. and Laboratoire de Minéralogie du Muséum, Paris, France.

15 058,32 (Station 8) : We studied a 7.8 cm slab sawn in the inner part of the rock and extending from bottom (B) to top (T) surfaces (LRL coordinates). The track-density profile in feldspars is shown in Fig. 1. The rather large error bars report the actual uncertainties in track-densities and not the mere statistical errors. They reflect the poor quality of the detectors. Face B shows clear solar flare irradiation whereas no such an irradiation was found on T. This observation agrees with the fact that few zap pits were observed on B while none were found on T[(1)]. The highest track-density measured on different locations of B does not exceed $6.10^7/cm^2$, a rather low value. The track-density profiles in the first mm away from B differ widely in nearby locations (either due to attrition losses or to "vug" effects).

In the galactic region the profile is rather flat and track-densities vary by only a factor of 1.7 ± 0.1 between 1 and 7.8 cm depth. Nothing warrants that this profile is the steepest one. Taken at face value it would indicate that the major fraction of tracks was registered under unknown shielding.

From the flux of solar flare VH particles recorded at 1 mm depth in Surveyor glass[(2)], and assuming a long term average flux half of that reported, the surface exposure of face B is estimated to be 1 m.y. within a factor of 2.

15 555,167, 177, 189 (Station 9A) : We were provided with numerous fragments coming from a disrupted slab extending from the approximate center to the North surface. The lack of knowledge of the relative distances between the fragments prevents to draw a track-density profile. The track-density values are : 1)near the center, $2.4 \pm 0.4 \times 10^6/cm^2$; 2)midway between center and N, $2.7 \pm 0.4 \times 10^6/cm^2$; 3)at the extreme North, $10 \pm 0.1 \times 10^6/cm^2$.

In the latter location a solar flare irradiation is not excluded but diffi-

cult to appreciate because of shock effects in feldspars. The maximum surface exposure age, derived from the minimum track-density value of $2.4 \times 10^6/cm^2$ at a mean depth of 8 cm, is 26 ± 5 m.y. This age is shorter than the ^{81}Kr-Kr exposure age of 81^{+17}_{-7} m.y. [3], implying that the rock has undergone a subsurface irradiation history as pointed out by Marti and Lightner [3].

Rake rock 15 641,0 (station 9A) : The basaltic fragment (2 x 1.5 x 1.45 cm) was investigated in 25 surface locations using feldspars. Solar flare irradiation was found to correlate with rounded dust-coated pitted surfaces. Track-densities range between 0.7 and > $20 \times 10^7/cm^2$. The steepest track-density profile was found across the LRL cross-sectioned surface. In this profile the track-densities vary from 10 to $3.5 \times 10^7/cm^2$ in the first outer mm, and decrease to $0.7 \times 10^7/cm^2$ at a depth of 5.8. mm. The extreme friability of the rock prevented any sawing in view to obtain a steeper slope. The above result confirms, if need be, that the depth affected by solar flare VH particles extends at least down to 6 mm, a fact already recognized by Crozaz et al. [4] for rocks 10 017 and 10 057.

14 307,30 (station G) : This breccia highly enriched in solar gases is in fact a pre-irradiated compacted soil (Berdot et al., this volume). In one location the well determined minimum track-density is $3 \pm 0.25 \times 10^6/cm^2$ as measured in 11 pyroxenes. Such a low track-density in a small rock (~ 150 g) sets an upper limit of 5 m.y. for the surface residence time of the rock in its present shape. This result agrees with the fact that no zap pits have been observed. It agrees also with the low maximum surface ages reported by Hart et al. [5] for a number of F1 and F2 rocks, according to the Jackson and Wilshire classification [6]. Such a short surface exposure cannot account for the large concentrations of spallation isotopes reported by Bogard and Nyquist [7]. These authors suggest that 307 has been brought up near the surface by an older cratering event than that of Cone Crater. Our track data do not support this interpretation but rather points to a rather recent exhumation of the rock (Cone Crater event being not exluded if the rock comes from a larger boulder). In this perspective the larger part of the spallation products are likely to have been built up together with the implantation of solar gases and solar

TRACK ANALYSIS ...

G. Poupeau

flare tracks, probably prior the Imbrium event. From this standpoint, an overall "spallation age" of the order of 10^8 y. for this compacted soil is rather low by lunar regolith standards. It remains to explain how 307 "should exhibit considerable evidence of low energy neutron flux" from the $^{131}Xe/^{126}Xe$ ratio (7).

REFERENCES

(1) Lunar Sampl. Inform. Catalog, LRL, NASA-MSC 03209, Nov. 1971.

(2) Crozaz and Walker (1971), Science, 171, 1237 ; Fleischer et al. (1971), ibid, 1240 ; Barber et al. (1971), Proc. Second Lunar Sci. Conf., 3, 2705.

(3) Marti and Lightner (1972), Science, 175, 421.

(4) Crozaz et al.(1970), Proc. First Lunar Sci. Conf., 3, 2051.

(5) Hart et al. (1972), Proc. Third Lunar Sci. Conf., to be published.

(6) Jackson and Wilshire (1972), Lunar Science III, p. 584.

(7) Bogard and Nyquist (1972), Lunar Science III, p. 89.

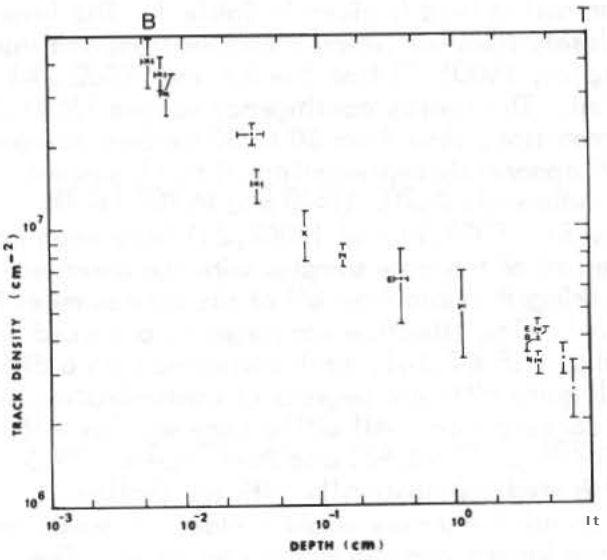

Fig. 1.- 15 058

Track-density profile from bottom to top (LRL coordinates). E, B and N are for east, bottom and north, and refer to measurements made in different orientations. In the first millimeters two sets of measurements (crosses and dots) made in near-by locations show appreciable differences (attrition ?, vug effect ?).

URANIUM-THORIUM-LEAD ISOTOPES AND THE NATURE OF THE MARE SURFACE DEBRIS AT HADLEY-APENNINE. Leon T. Silver, Div. of Geological and Planetary Sciences, California Institute of Technology, Pasadena, Calif. 91109

Samples of the regolith on the mare surface, including segments of the drill core at ALSEP, have been analyzed for U, Th and Pb by isotope dilution and mass spectrometry (Table 1). The concentration levels and lead isotope compositions are in sharp contrast to comparable parameters observed in the local mare basalts. The regolith contains a remarkably homogeneous set of daughter-parent isotope systems suggesting a common non-mare derivation for the samples reported here.

Eight aliquots of deep drill core, including samples from the bit and the lower junctions of the five higher core tubes, have been analyzed, representing nominal depths from 239 to 39 cm. Surface soil 15021 is the contingency sample collected 75 meters to the southeast at the LM. Sample 15471 is from the south side of Dune crater at station 4, 3.3 km SSE. Samples 15501 and 15515 are a soil and soil clod from a very young crater rim at station 9, 1.8 km to the west of the LM-ALSEP area (1).

The drill core samples show very constant U and Th levels averaging 1.32 ± 0.04 and 5.00 ± 0.12 ppm for the upper 176 cm which then increase to 1.75 and 6.58 ppm in the bit at 239 cm. The Th/U ratio is remarkably constant at $3.78 \pm .03$ throughout the entire core. In contrast the lead abundances are extremely variable in the analyzed samples. This variation can be attributed to massive terrestrial lead contamination of the samples, particularly at the joints. Post-mission analyses of spare flight hardware have identified the probable sources and composition of the contaminating lead in the core tubes. The measured isotopic composition of the contamination lead is given in Table 1. The levels of contamination can be estimated rather closely from the isotopic compositions and the parent-daughter systematics. Two core samples, 15001,11 from the bit and 15002,241 from 176 cm, show slight to no contamination. The nearby contingency sample 15021,8 is similar. The other six core samples, by comparison, show from 50 to 80 percent contamination in total lead with the observed Pb^{204} apparently representing 70 to 98 percent contamination. Accordingly, to study the radiogenic Pb^{206}/U^{238} and Pb^{207}/U^{235} systematics, non-radiogenic lead corrections for 15001,11 and 15002,241 have been made with a primitive meteorite lead, and for the rest of the core samples with the observed contamination lead. This simple procedure brings the data from all of the core samples into nearly uniform agreement as shown in Figure 1. The effective convergence produced by the corrections is seen for segments 15002,8 and 15002,241, each corrected with a different lead. Samples 15005,8 and 15005,231 with quite different degrees of contamination and the same type of correction show excellent convergence. All of the core samples fall within a 3 x 5 percent ellipse centered at $Pb^{206}/U^{238} = 0.985$ and $Pb^{207}/U^{235} = 79.5$. Within this ellipse the core samples are distributed systematically with the shallower samples being slightly more discordant and containing a very slightly older composite lead. The highest core sample 15006,9, requires the largest contamination correction. The resultant daughter-parent ratios are within 2 percent of the values observed in the nearby surface soil 15021,8, which shows little obvious contamination. Selected "best" values for the deeper core (15001-15003) are: $Pb^{206}/U^{238} = 1.02 \pm 0.01$ (4575 m.y.); $Pb^{207}/U^{235} = 81.0 \pm 1.0$ (4535 m.y.); the corresponding model Pb^{207}/Pb^{206} age is 4515 m.y.

U-Th-Pb Isotopes in Regolith

Leon T. Silver

The surface soil samples show greater variation in uranium and thorium levels, probably reflecting the 5 km spread of the three principal sampling sites. It is noteworthy that 15021 is nearly identical to the upper core material, and that the levels are distinctly lower at stations 4 and 9. The average Th/U ratio of the four surface soils is 3.77 ± 0.12, similar to the core. The observed lead isotopic compositions, corrected for chemistry blanks, are quite radiogenic reflecting little contamination, if any. The U^{238}/Pb^{204} ratios vary from 160 to 240, typical of much lunar regolith material.

Daughter-parent ratios for the surface samples, corrected with a primitive lead for the non-radiogenic component, are also shown in Figure 1. Samples 15021, 15501 and 15515 are slightly discordant and are narrowly confined to the region occupied by the upper drill core samples. Sample 15471 from the south side of Dune crater has about 10 percent higher daughter-parent ratios than the other surficial samples, but has nearly the same lead isotopic composition. The strong similarity of these daughter-parent ratios to those found throughout the drill core suggests that all regolith samples we report here have a close genetic relation. They occur in a region of the "concordia" diagram unoccupied by any other analyzed Apollo or Luna regolith samples.

U-Th-Pb isotopic data on Apollo 15 mare basalts have not been published. Preliminary results on three basalts analyzed in our laboratory show them to occupy the patterned region shown in Figure 1, clearly different from the regolith materials. All of the available U and Th concentration data for the Hadley mare basalts are in the range 0.12-0.25 and 0.45-0.90 ppm, respectively. Other large lithophile ions show corresponding depleted levels in the basalts when compared to the regolith samples(2). The bulk chemistry of Apollo 15 mare soils and basalts also shows strong contrasts(2). Macroscopically, fragments of the distinctive Apollo 15 basalts are subordinate constituents in the regolith, except in soils at the rille edge which we have not analyzed. One must conclude that the U-Th-Pb isotope systems and the bulk chemistry of the mare regolith are dominated by materials other than the local mare basalts. The deeper part of the drill core is most strongly influenced by this exotic component and has not penetrated beyond it. Our current mineralogical and isotopic studies indicate that the principal immediate rock sources for these comminuted regolithic materials are the abundant, partially vitrified blocks of breccia (e.g. 15015, 15505, 15558) found on the mare surface. This is supported by other bulk and trace element chemistry data (2, table VI-4), (3). These breccias lack fragments of the local basalt. Swann et al. (1) suggest the fresh 15 m crater at station 9 penetrated into a layer of dark, angular glassy blocks at 1.5 m depth. This type of block concentration elsewhere may be the local sources of the numerous Apollo 15 breccias with fragile, dark glassy fracture coatings. Their ultimate source is still not defined.

It has been proposed that the mare surface may be partly mantled by ray material from the crater Aristillus and/or Autolycus. If this blanket, characterized by unique isotopic and chemical characteristics, is indeed derived from those impacts it is far more extensive than anticipated. Work now in progress indicates that similar exotic material is prominent at stations 6 and 7 on the Apennine Front, both as blocks and in the fines. This position is downrange from the secondary crater cluster attributed to a ray origin. A Front source must also be considered despite the lack of an obvious transport mechanism.

Preliminary studies of the volatile lead components in the soils suggest a very young time ($\lesssim 10^9$ m.y.) of accumulation of the regolith blanket on the mare surface.

References: (1) Swann, G. A. and others (1972), Preliminary Geologic Investigation of the Apollo 15 Landing Site. Preliminary Science Report, NASA SP-289, p. 5-1. (2) LSPET (1972), Preliminary Examination of Lunar Samples. NASA SP-289, p. 6-1. (3) Schonfeld, E. (1972), Lunar Science III, LSI Contr. 88, p. 683.

U-Th-Pb Isotopes in Regolith

Leon T. Silver

Table 1

Sample	Depth (cm)	Expt No.	Pb Isotope Composition			Concentrations (ppm)				
			206/204	207/204	208/204	Total Pb	Contam. Pb (2)	U	Th	Th/U
15001,11	239 (B)	1	361.2	212.5	372.9	4.22	<0.3	1.75	6.58	3.77
15002,8	199 (J)	1,2	43.71	30.06	62.62	8.27	4.8	1.54	5.80	3.76
15002,241	176	1	197.7	117.2	205.9	3.32	<0.5	1.32	4.96	3.75
15003,11	159 (J)	1	45.79	31.16	(1)	5.88	3.0	1.26	4.85	3.84
15004,8	119 (J)	1	34.47	24.87	(1)	7.99	5.0	1.33	5.00	3.75
15005,8	79 (J)	1	39.56	27.99	(1)	7.06	4.0	1.37	5.16	3.77
15005,231	54	1	56.26	37.50	(1)	5.16	2.0	1.38	5.21	3.77
15006,9	39 (J)	1	26.29	20.23	(1)	12.19	9.5	1.27	4.84	3.80
Core Tube Contamination			18.60	15.69	38.55					
15021,8	Surface	3	232.3	141.4	238.8	2.77	--	1.26	4.73	3.77
15471,8	Surface	1	177.9	113.1	186.7	1.59	--	0.62	2.28	3.67
15501,21	Surface	1,3	353.6	214.8	371.6	1.88	--	0.88	3.49	3.94
15515,97	Clod	1	314.3	193.7	313.6	1.99	--	0.85	3.15	3.71

(B) = drill bit; (J) = lower joint; (1) Spiked with Pb^{208}; (2) Values are ± 0.3 ppm.

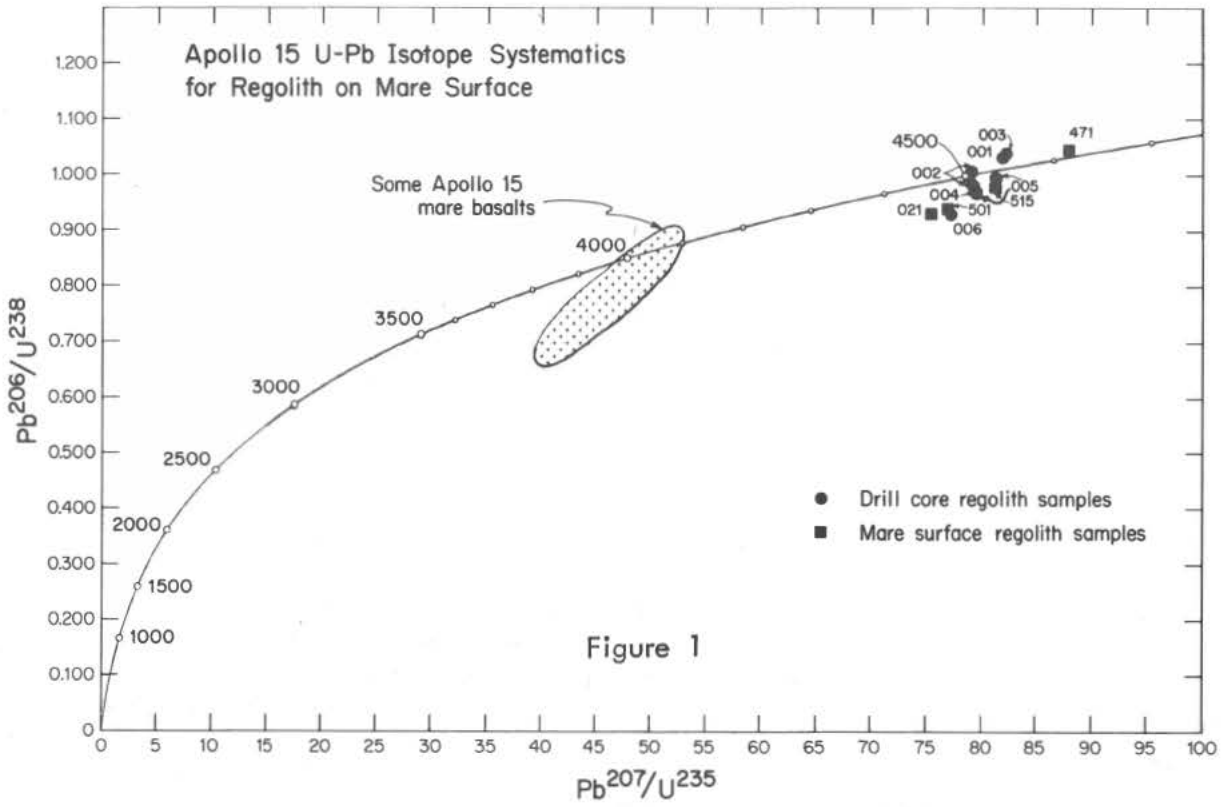

Figure 1

U-Th-Pb, Rb-Sr, AND K MEASUREMENTS ON SOME APOLLO 15 AND APOLLO 16 SAMPLES* M. Tatsumoto, C. E. Hedge, R. J. Knight, D. M. Unruh, and B. R. Doe, U. S. Geological Survey, Denver, Colo. 80225

Seven crystalline rocks and three soils from the Apollo 15 mission and one breccia and three soils from the Apollo 16 mission were analyzed for U-Th-Pb and Rb-Sr systematics and for potassium concentrations by mass spectrometry and isotope dilution. Apollo 15 rocks contain less U, Th, Pb, Rb, and K (Tables 1 and 2) than rocks from all previous missions. The concentrations in Apollo 15 rocks (U: 0.03 to 0.15 ppm; Th: 0.13 to 0.49 ppm; Pb: 0.14 to 0.27 ppm), except for anorthosite 15415, are clearly smaller than for the low-K basalts from the Apollo 11 mission (U: 0.16 to 0.27 ppm; Th: 0.53 to 1.02 ppm; Pb: 0.29 to 0.51 ppm)[1] or Apollo 12 mission (U: 0.16 to 0.40 ppm; Th: 0.61 to 1.41 ppm; Pb: 0.28 to 0.64)[2]. Anorthosite 15415 contains a very small amount of uranium (0.0015 ppm) and thorium (0.0035 ppm) but a disproportionately great content of lead (0.25 ppm).

U, Th, and Pb concentrations in Apollo 15 soils (Table 1) are similar to those of soils from the Apollo 11 mission, but are far smaller than those in the KREEP-rich soils of the Apollo 12 and Apollo 14 missions. U and Th concentrations in Apollo 16 soils (Table 1) are similar to those in the Apollo 15 soils, but Pb concentrations are greater, indicating Pb enrichment in the soils as determined from the U-Pb concordia diagram.

The Th/U ratio (4.0) of the mare basalts (porphyritic clinopyroxene basalts) from Station 1 (Elbow Crater) and Station 4 (Dune Crater) is greater than that of Apollo 12 (3.6 to 3.9) and Apollo 14 rocks (3.7)[3], but is similar to that ratio in most of the Apollo 11 rocks. On the other hand, anorthosite 15415 and anorthositic gabbro 15418 from Station 7 (Spur Crater) display smaller ratios (2.4 and 3.5, respectively), and a mare basalt (porphyritic olivine basalt) from the Hadley Rille Station 9A exhibits a ratio of 3.8. The Th/U ratio (3.8) of soils from Stations 1 and 9A is between those of Apollo 14 soils (3.7)[3,4] and Apollo 11 soil (4.0), and is similar to that of Apollo 12 soils, but the Th/U ratio of Apollo 16 soils is distinguishably greater (4.1) than that of the other soils. There are clear regional differences in the Th/U ratios on the moon, and there seems to be a trend in which soils rich in anorthositic component have a smaller ratio. $^{238}U/^{204}Pb$ values (400 $\sim$ 600) for Apollo 15 rocks are not significantly different from those observed in low-K basalts from the Apollo 11 and 12 sites.

The lead isotopic compositions of Apollo 15 rocks are as radiogenic as those for the low-K basalts of Apollo 11 and 12 but less radiogenic than for the high-K basalts of Apollos 11, 12, and 14. Reflective of the high Th/U ratio, the $^{208}Pb/^{206}Pb$ of the Apollo 15 rocks is greater than 1.0. The

---

*Publication authorized by the Director, U. S. Geological Survey.

U-Th-Pb, Rb-Sr, and K Measurements

M. Tatsumoto

uranium and thorium contents in anorthosite 15415 are essentially nil, and the correction of U- and Th-derived Pb in situ for initial lead isotopic composition is very small. The $^{206}Pb/^{207}Pb$ of the anorthosite when it was formed (initial ratio) was calculated by use of a two-stage model and the observed $^{238}U/^{204}Pb$ to have been 0.67. This initial ratio indicates that the rock formed 3.87 b.y. ago from an environment with $^{238}U/^{204}Pb \sim 300$, a source perfectly normal for lunar igneous rocks. This age is a little less than the ^{40}Ar-^{39}Ar age obtained by Husain et al. (4.09 ± 0.19)[5] and by Turner (4.05 ± 0.15)[6], but is still in the error range. The 3.87-b.y. age agrees with the age of the Fra Mauro formation observed from Apollo 14 samples, and thus we interpret that this age probably represents an Imbrium excavation event but probably does not represent a portion of the original anorthositic crust formation.

The U-Pb concordia diagram for Apollo 15 is presented as Figure 1. The data fall into two distinct groups and separate rocks from soils. Rocks 15065, 15076, and 15085 from Elbow Crater and rock 15476 from Dune Crater (with a different $^{207}Pb/^{206}Pb$ value for the Dune Crater rock) lie on a 3.5-b.y. to 4.65-b.y. discordia line, while 15555 from a rille station lies on a 3.3-b.y. to 4.65-b.y. discordia line. The lower intercept at 3.3 b.y. agrees with ages obtained by Rb-Sr[7,8] and $^{40}Ar/^{39}Ar$ methods, and igneous rocks continue to contain no evidence of "third events" in accord with our previous observation[3]. A metaigneous rock, 15418, lies above concordia and indicates lead enrichment relative to uranium in the specimen analyzed. However, the uranium content determined in the sawdust of 15418 is higher than for the rock sample, and the data point for the sawdust is below concordia if the lead value of the rock specimen is used for the sawdust. The data of Apollo 15 soils (15071 and 15080 from Elbow Crater and 15600 from rille station) lie below concordia, indicating that the soils are a mixture of the Apollo 15 rocks and KREEP-rich material such as Apollo 14 breccia matrix (14307M, 14318M). The present data confirms our previous observation[3] that highlands-type soils and matrix of breccias (Apollos 14 and 16) continue to plot above concordia and are indicative of lead enrichment relative to uranium a long time ago, whereas mare-type soils and breccias (Apollos 11, 12, and 15 mare sites) continue to portray lead loss relative to uranium a long time ago. The mixing line for the soils intercepts concordia at about 3.5 b.y. and 4.85 b.y. This mixing relation is also clear in the $^{206}Pb/^{207}Pb$ versus $^{238}U/^{207}Pb$ diagram (Figure 2). The initial value of the tie line between the data points of the igneous rocks and soils from Elbow Crater matches that of the anorthosite 15415, and the tie line between rock and soil from the rille station also matches that of the 15415 data point at its initial value. The slope of the tie lines (3.57 and 3.46 b.y.) does not, however, necessarily indicate significant ages. It may indicate that significant magmatic activity on the moon occurred between 3.2 to 3.9 b.y. as indicated by ages of mare basalts from the Apollo 11, 12, and 14 missions. If KREEP material and acidic magma (like the source for 12013) had formed in this time interval, then most basalts and soils plot near a 3.5-b.y. isochron. The initial $^{206}Pb/^{207}Pb = 0.67$ (not corrected for the primordial lead) is close to the initial values for 14310

U-Th-Pb, Rb-Sr, and K Measurements

M. Tatsumoto

obtained by Tera and Wasserburg (0.69)[9] but does not match that reported by Tatsumoto et al. (0.613)[3]. In our previous paper[3], the smaller initial value was induced by the large common lead correction equivalent to all the ^{204}Pb observed in the mineral fractions.

Rb-Sr data (Table 2) for the soil samples 15071, 15080, and 15060 plot approximately on the 4.65-b.y. isochron defined by previous soil samples. The igneous rock samples which we have analyzed thus far contain unusually non-radiogenic strontium for lunar igneous rocks.

The study of the U-Th-Pb system on breccia 14063, one of the "white rocks," suggested that the black clasts appear to be closely related to grayish matrix. Howard Wilshire (oral communication) has suggested that possibly the black clasts could be the result of induced melting within a blanket of anorthositic tuff analogous to the formation of obsidian in rhyolitic tuffs on earth. The study of another gray matrix-black clast rock in which the clasts are much more abundant, 67015, is quite compatible with the Wilshire suggestion. The "clasts" appear to have lost lead (both radiogenic lead and "common lead") and the matrix gained lead relative to uranium about 3300 m.y. ago. These relations are those that might be expected upon the melting of a rock in vacuum. The great uranium and thorium contents of the "clast" are equal to KREEP samples rather than the anorthositic matrix and are indicative of greater complexity than expected in an anorthositic obsidian model.

REFERENCES AND NOTES

(1) TATSUMOTO M. (1970) *Proc. Apollo 11 Lunar Sci. Conf., Geochim. Cosmochim. Acta,* Suppl. 1, Vol. 2, pp. 1595-1612.
(2) TATSUMOTO M., KNIGHT R. J., and DOE B. R. (1971) *Proc. Second Lunar Sci. Conf., Geochim. Cosmochim. Acta,* Suppl. 2, Vol. 2, pp. 1521-1546.
(3) TATSUMOTO M., HEDGE C. E., DOE, B. R., and UNRUH D. M. (1972) *Proc. Third Lunar Sci. Conf., Geochim. Cosmochim. Acta,* Suppl. 2, Vol. 2 (in press).
(4) SILVER L. T. (1972) *Lunar Science-III* (abstract, editor C. Watkins), pp. 704-706.
(5) HUSAIN L., SCHAEFFER O. A., and SUTTER J. F. (1972) *Science 175,* pp. 428-430.
(6) TURNER G. (1972) *Earth and Planet. Sci. Letters 14,* pp. 169-175.
(7) MURTHY V. R., EVENSEN N. M., JAHN BOR-MING, and COSCIO M. R., Jr. (1972) *Science 175,* pp. 419-421.
(8) PAPANASTASSIOU D. A., and WASSERBURG G. J. (1972) *Earth and Planet. Sci. Letters* (in press).
(9) TERA F., and WASSERBURG G. J. (1972) *Earth and Planet. Sci. Letters 14,* pp. 281-304.
(10) We are indebted to Philip Reed for laboratory assistance and Robert Hildreth for mass spectrometer runs for strontium isotopes. Supported by NASA Interagency Transfer Order T-2407A.

U-Th-Pb, Rb-Sr, and K Measurements

M. Tatsumoto

Table 1. Pb-U-Th concentrations and composition for selected Apollo 15 and Apollo 16 samples.

Sample No.	Type	Concentration (ppm) U	Th	Pb	Pb composition* $^{206}Pb/^{204}Pb$	$^{207}Pb/^{204}Pb$	$^{208}Pb/^{204}Pb$	$^{232}Th/^{238}U$	$^{238}U/^{204}Pb$
				Apollo 15					
15065	basalt	0.1368	0.5244	0.236	495.0	201.8	524.4	3.96	611
15076	do.	0.1532	0.5901	0.266	374.4	155.8	393.1	3.98	460
15085	do.	0.1183	0.4588	0.208	308.9	130.7	335.7	4.01	382
15476	do.	0.1919	0.7334	0.354	379.6	170.6	402.6	3.95	447
15555A	do.	0.1264	0.4596	0.209	360.5	150.6	366.7	3.76	457
15555B	do.	0.1173	0.4296	0.191	--	--	--	3.78	
15418A	metabasalt	0.0380	0.1272	0.138	134.7	100.9	145.7	3.46	91.1
15418B	do.	0.0394	0.1377	0.132	--	--	--	3.61	
15418	sawdust	0.0578	0.2077	(1.927)**	--	--	--	3.71	
15071	soil	0.6801	2.456	1.555	328.5	203.4	327.0	3.73	324
15080	do.	0.7854	2.924	1.766	450.7	281.2	440.1	3.85	450
15600	do.	0.5225	1.889	1.098	438.5	264.1	430.3	3.73	466
15415A	anorthosite	0.0017	0.0036	0.268	79.71	116.8	96.63	2.24	
15415B	do.	0.0014	0.0034	0.246	--	--	--	2.41	1.5
				Apollo 16					
66041	soil	0.6383	2.546	1.980	301.2	244.9	293.8	4.12	243
66081	do.	0.6679	2.764	1.938	286.9	227.9	279.8	4.28	237
68501	do.	0.6414	2.553	2.178	284.3	238.3	276.6	4.11	203
67015,11	breccia (black clast)	1.210	4.449	2.486	1289	702.3	1247	3.80	1361
67015,12	breccia (gray matrix)	0.2003	0.7315	0.630	443.7	339.8	423.6	3.77	332

*Corrected for analytical blanks of Pb (2.7-4.8 ng/g sample).
**Indicates a large Pb contamination from sawing.

Table 2. Rb-Sr-K concentrations and $^{87}Sr/^{86}Sr$ in selected Apollo 15 samples.

Sample No.	Concentration Rb (ppm)	Sr (ppm)	K (percent)	K/U	Normalized $^{87}Sr/^{86}Sr$
15555	0.874	92.0	0.0538	4.62×10^3	0.70062
15418	--	--	--	--	0.69954
15418 (sawdust)	0.263	134.6	0.0126	2.18×10^3	0.69965
15071	3.098	116.3	0.0996	1.46×10^3	0.70435
15080	3.729	122.2	0.1188	1.51×10^3	0.70493
15600	2.294	108.1	0.1135	2.17×10^3	0.70373
15415	0.217	173.3	0.0151	9.02×10^4	0.69914

U-Th-Pb, Rb-Sr, and K Measurements

M. Tatsumoto

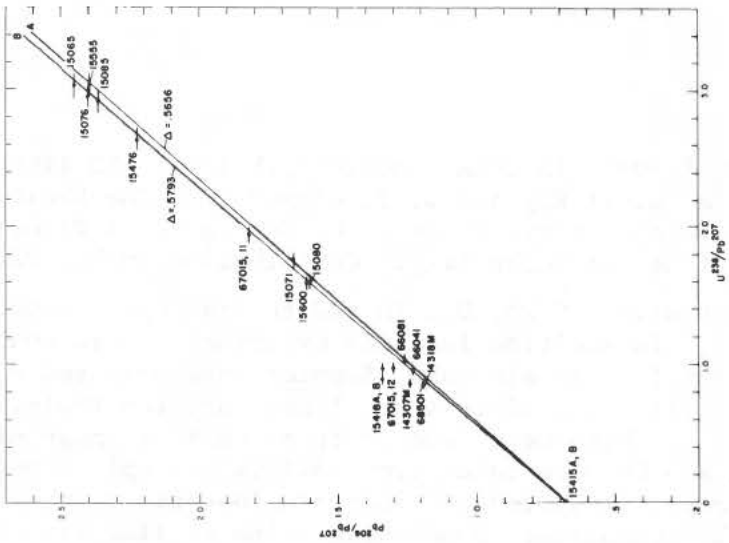

Fig. 2. Pb^{206}/Pb^{207} vs. U^{238}/Pb^{207} for Apollo 15 and 16 samples. Line A is for 15415, 15600, and 15555; line B is for all Apollo 15 samples analyzed except 15418. Samples are corrected for chemistry blank.

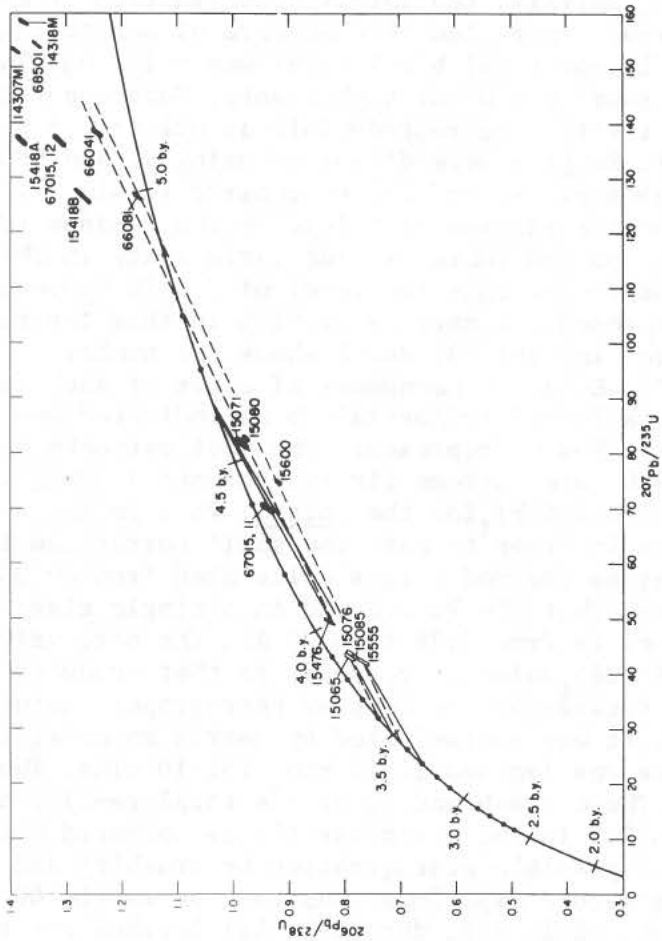

Fig. 1. U-Pb concordia diagram. Two-model discordia lines (4.65 b.y.-3.5 b.y. and 4.65 b.y.-3.3 b.y.) are indicated by solid lines; mixing lines are dashed.

DISTRIBUTION OF Pb-U-Th IN LUNAR ANORTHOSITE 15415 AND INFERENCES ABOUT ITS AGE. Fouad Tera, L. Ai Ray and G. J. Wasserburg, The Lunatic Asylum of the Charles Arms Laboratory, Division of Geological & Planetary Sciences, California Institute of Technology. Contribution Number 2221.

We report the concentration of Pb, U & Th and the isotopic composition of Pb in samples of 15415. In addition leaching experiments were done to ascertain the distribution of these elements. Samples were prepared with great care using freshly polished stainless steel and tungsten tools. Only interior fragments were used which were free of lunar dust or smear metal. Samples P-1, P-2, Coarse and CH were taken from 15415,40. Sample L was taken from 15415,34. Samples mostly consisted of clear plagioclase grains but with some grains having a milky appearance. Some white veins of fine material were present in varying amounts. All samples except 40CH were gently crushed or hand picked prior to any analysis. Laboratory contamination is a fundamental problem which could only be controlled through careful monitoring of procedures. Previously (1) our total blank level was ~ 1-2 ng. Two samples were processed during a short period of high blanks. Subsequent to this we have improved the blank level to be reproducible at 0.2 to 0.6 ng depending on sample size (Table 1). Samples were dissolved using HF and HNO_3. U & Th were determined on aliquots of P-1 and P-2 and Coarse (Table 2). The concentrations for 40 Coarse are the sum of C leach + the residue (C). The range in U was from 0.9 to 3.4 ppb and there is wide variability in Th/U due to sample heterogeniety. Inspite of this low level of U & Th concentrations neither dertemination represents a serious problem in this laboratory. Analyses of lead are given in Table 3. Row A shows the number of picomoles of each isotope, rows C′, D′, E′ show the number of atoms of each isotope in the sample corrected for blank Pb and primordial Pb as indicated and the <u>insitu</u> decay of U & Th (Table 2). Row C′ represents the best estimate based on actual blanks while D′ & E′ are extreme limits. Columns 7 & 8 give the values of $(208Pb/206Pb)_I$ and $(207Pb/206Pb)_I$ for the <u>initial</u> Pb assuming an age of 4.0 ± 0.5 AE for the rock in order to make the small correction for <u>insitu</u> decay. The last column gives the model ages calculated from column 8 assuming the moon to be 4.60 AE and that the Pb evolved in a single stage process. The <u>total range</u> for all values is from 3.78 to 4.29 AE. The best value is between 3.8 and 4.1 AE. The $(208/206)_I$ value corresponds to that produced by Th/U ≃4.6 between 4.6 and 4.0 AE. Because of the complex petrographic nature of 15415(2) and the possibility that it was contaminated by matrix material in the breccia, sample 40 Coarse was leached in 1N HNO_3 for 10 mins. The sample was not obviously attacked. The C leach had 3% of the total (a+b) U & Th but 41% of the total Pb. The 206/204 in the leach was 111 as compared with 76 in the residue (C). To eliminate possible contamination by crushing and to study these effects further, a second experiment was done on sample 40 CH in seven steps. Each leach step was of 10 min. duration. All leaches and rinses were

Distribution of Pb-U-Th in Lunar Anorthosite 15415 and Inference About Its Age

Fouad Tera

centrifuged and the supernate and residues analyzed.

The procedure was (a) wash the single chunk in 5 ml 1N HNO_3 (20°C), rinse with H_2O. HNO_3 + H_2O analyzed as step 1; (b) gently grind chunk in teflon under 5 ml of H_2O and analyze H_2O as step 2; (c) add 5 ml 1N HNO_3 (20°C) to ground material. Rinse in H_2O. HNO_3 + H_2O combined and analyzed as step 3; (d) same as (c) but HNO_3 at 85°C. Leach is step 4; (e) add 5 ml 5N HNO_3 and 1.5 ml 30% HF at 20°C. Wash with H_2O. Sample clearly attacked. Acid and H_2O combined as step 5. Remaining sample has gelatinous coat. Residue is somewhat fluffy and is combined with remaining sample. About 1/3 of the sample was dissolved by this treatment; (f) residues weighing ~ 5 mg from centrifuging leaches in (a) through (d) combined to make step 6; (g) remaining sample, about 2/3 of the original mass, was dissolved and analyzed as step 7. The general results of this procedure are seen in Table 4 and 5 and in Figs. 1 and 2. The following is a summary of observations and conclusions based on this study:

I. The bulk of Pb is easily leachable under very mild conditions. The leaches comprise 75% of the total Pb in 40 CH. Whether this Pb is deposited on surfaces by volatilization or is concentrated in easily soluble interstitial phases is not immediately obvious.

II. Pb composition is demonstrably heterogeneous and the Pb, U & Th concentrations are variable.

III. Highly radiogenic Pb with high α and β values is preferentially leached, leaving behind in the bulk of the material another radiogenic Pb relatively enriched in primordial Pb. It is not possible to explain the results in terms of a single initial Pb. The lack of simple 208/204 systematics leads us to the same conclusion (Fig.2). In general the average value of initial Pb in 15415 is similar to that in 14053 and 14310. The presence of highly radiogenic initial Pb appears to be characteristic of lunar rocks.

IV. As shown by the leached materials (Step 7 and 40 C which lie to the left of MT-A) there is a distinct suggestion that the plagioclase contains a radiogenic Pb which is <u>older</u> than that found in the leaches or in the "total"rock. Thus it appears that addition of radiogenic Pb took place subsequent to crystallization. This might have been associated with impact events (Imbrium impact?) causing partial redistribution of Pb.

V. While a simplistic age interpretation of this anorthosite is not fully valid, the data clearly shows that the Pb in 15415 represents the evolution of <u>about</u> 0.5 AE after the formation of the moon. There is thus no direct evidence that this anorthosite breccia represents ancient lunar crust. The study of initial leads in unmetamorphosed lunar anorthosites should permit an age determination of the lunar highlands. At present there is no indication that they comprise the ancient lunar crust.

VI. Insofar as any of the Pb in 15415 actually belongs to this rock we must visualize the anorthosites as contributing a significant amount of such Pb to lunar soils and thus causing high "ages".

Distribution of Pb-U-Th in Lunar Anorthosite 15415 and Inferences About Its Age

Fouad Tera

Table 2. U,Th & Pb in 15415 (measured amounts in picomoles)

Sample	Wt.(mg)	238_U	232_{Th}	Th/U	U(ppb)*	Th(ppb)*	Pb(B)(ppm)*
40 P-1	97.4	1.40	2.68	1.91	3.4	6.4	0.18
40 P-2	143	0.830	2.28	2.67	1.4	3.7	0.28
40, Coarse	436						
C	a	1.54	6.41	4.16	-	-	-
C leach	b	0.049	0.192	3.92	-	-	-
Total (a+b)		1.59	6.60	4.15	.87	3.5	0.16

For P-2 and 40-Coarse U blank ~ 0.005 ng, Th blank ⩽ 0.002 ng. Blank for P-1 ~ 0.03 ng U. Pb(B) is total Pb corrected for blank.

Table 1. Pb Blanks Associated with 15415 Experiments (in nanograms)

Sample	Measured	Calculated
40 P-1	3.9*	4.2
34 L	8.3*	8.8
40 P-2	0.37	0.37
40 C	0.47	0.47
40 CH Step 3	0.22	0.18
40 CH Step 7	0.56	0.65
Recent Blank (Aug)	0.37	0.31

* These high blanks were proved to be caused by a bad water supply.
** Blank calculated from the concentration of Pb in each of the reagents, the amounts used and a measured column blank of 0.15 ng.

Table 4. Pb in Leach Experiment on 15415, 40 CH

Step	Pb in(ng)†	α*	% of Pb
1	24.4	125	21.2
2	1.49	23.7	1.3
3	33.6	110	29.3
4	28.0	94.1	24.4
5	5.38	38.9	4.7
6	3.64	32.5	3.2
7	18.4	56.4	16.0

† The total Pb of 115 ng corresponds to 0.232 ppm in the orig. sample for a yield of 85%. Corrected for spike and blank.
* Uncorrected for blank.

References: (1) F. Tera and G. Wasserburg, U-Th-Pb Systematics in Three Apollo 14 Basalts and the Problem of Initial Pb in Lunar Rocks, Earth and Planetary Science Letters 14 (1972) 281. (2) H. G. Wilshire, G. G. Schaber, L. T. Silver, W. C. Phinney, E. D. Jackson, Geologic Setting and Petrology of Apollo 15 Anorthosite (15415) Geol. Soc. of America Bul. 83 (1972) 1083.

Distribution of Pb-U-Th in Lunar Anorthosite 15415 and Inferences About Its Age

Fouad Tera

Table 3 15415

Sample	Picomoles ^{208}Pb	^{207}Pb	^{206}Pb	^{204}Pb	$\left(\frac{208}{206}\right)_I$	$\left(\frac{207}{206}\right)_I$	T(4.6AE)
40 P-1							
A) Uncorrected Initial Pb	38.05	39.59	28.59	0.5412	–	–	–
C') ^{204}Pb blank + prim.	19.16	31.98	19.64	–	0.9756	1.628	4.10
D') ^{204}Pb all blank	17.12	30.74	17.52	–	0.9772	1.754	4.29
E') ^{204}Pb all prim.	21.79	33.57	22.34	–	0.9754	1.503	3.88
40 P-2							
A) Uncorrected Initial Pb	71.43	74.83	54.28	0.9890	–	–	–
C') ^{204}Pb blank + Prim.	41.02	63.66	43.02	–	0.9535	1.480	3.83
D') ^{204}Pb all blank	33.75	59.25	35.52	–	0.9502	1.668	4.16
E') ^{204}Pb all prim.	42.29	64.44	44.33	–	0.9540	1.454	3.78
40 C (a)							
A) Uncorrected Initial Pb	65.30	85.94	57.39	0.7643	–	–	–
C') ^{204}Pb blank + prim.	41.05	77.18	48.22	–	0.8513	1.600	(4.05)
D') ^{204}Pb all blank	35.15	73.58	42.12	–	0.8345	1.747	(4.28)
E') ^{204}Pb all prim.	41.75	77.60	48.94	–	0.8531	1.586	(4.03)
40 C leach (b)							
A) Uncorrected Initial Pb	39.20	47.58	32.10	0.2902	–	–	–
C') ^{204}Pb blank + prim.	30.66	44.54	29.25	–	1.048	1.523	(3.91)
D') ^{204}Pb all blank	28.25	43.08	26.76	–	1.56	1.610	(4.07)
E') ^{204}Pb all prim.	30.75	44.60	29.35	–	1.048	1.520	(3.91)
40 Coarse (a + b)†							
A) Uncorrected Initial Pb	104.5	133.5	89.49	1.054	–	–	–
C') ^{204}Pb blank + prim.	71.72	121.7	77.47	–	0.9258	1.571	4.00
D') ^{204}Pb all blank	63.40	116.7	68.88	–	0.9204	1.694	4.20
E') ^{204}Pb all prim.	72.50	122.2	78.28	–	0.9262	1.561	3.98

( ) indicate results on part of a leaching experiment not total sample.
† Total sample calculated from 40 C plus 40 C leach.

Distribution of Pb-U-Th in Lunar Anorthosite 15415 and Inferences About Its Age

Fouad Tera

Table 5 Leaching experiment on a single 0.5 g fragment of 15415

Step	^{206}Pb † picomoles	% used**	Data uncorrected for blank 206/204	207/204	208/204	207/206	208/206
1 Wash of fragment	31.95	Comp. (92.1)	124.9 ±3.6	187.2 ±5.4	148.0 ±4.1	1.499 ±0.014	1.185 ±0.006
		Yield* (7.9)	120.1 ±1.1	179.5 ±1.6	—	1.494 ±0.002	—
2 H_2O rinse of crushed fragment	2.10	Comp. (88.5)	23.73 ±0.08	23.01 ±0.08	43.11 ±0.13	0.9698 ±0.0029	1.817 ±0.004
		Yield* (11.5)	24.54 ±2.77	22.43 ±2.53	—	0.9088 ±0.0064	—
3 Cold HNO_3	44.23	Comp. (43.3)	110.4 ±0.5	164.2 ±0.7	134.2 ±0.6	1.487 ±0.0004	1.216 ±0.0003
		Yield* (6.2)	107.1 ±1.0	158.8 ±1.5	—	1.482 ±0.004	—
4 Hot HNO_3	37.37	Comp. (44.1)	94.06 ±0.19	141.3 ±0.3	108.7 ±0.2	1.502 ±0.001	1.156 ±0.0003
		Yield* (6.5)	90.36 ±0.48	135.2 ±0.7	—	1.495 ±0.001	—
5 HF + HNO_3	7.96	Comp. (46.4)	38.87 ±1.16	49.56 ±1.49	54.42 ±1.36	1.275 ±0.018	1.400 ±0.014
		Yield* (4.1)	36.40 ±0.44	45.59 ±0.55	—	1.252 ±0.005	—
6 Combined residue	5.66	Comp. (44.0)	32.47 ±0.13	37.60 ±0.15	51.96 ±0.20	1.158 ±0.0005	1.600 ±0.001
		Yield* (7.15)	28.68 ±0.20	31.67 ±0.22	—	1.104 ±0.001	—
7 Remaining bulk	26.22	Comp. (45.0)	56.35 ±0.32	80.10 ±0.46	68.90 ±0.39	1.421 ±0.003	1.223 ±0.002
		Yield* (6.2)	53.88 ±0.75	75.90 ±1.06	—	1.405 ±0.003	—
Total Blank Comp.			18.26	15.46	37.59	0.8466	2.058
Primordial Pb Comp.			9.346	10.22	28.96	1.093	3.099

* Aliquot spiked with ^{208}Pb † using a yield of 85%

**% used is the percent of the total step used for composition or yield.

Distribution of Pb-U-Th in Lunar Anorthosite 15415 and Inferences About Its Age

Fouad Tera

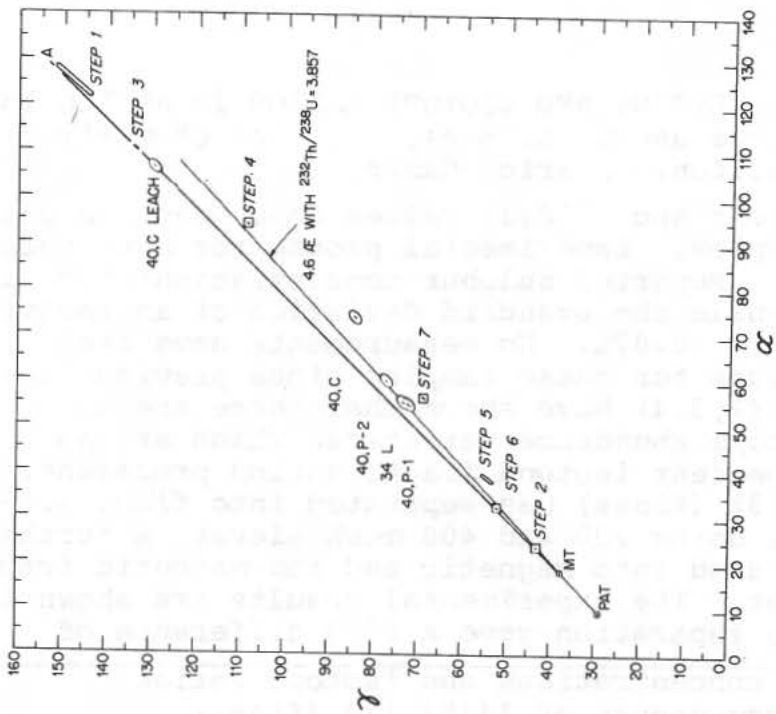

Fig. 2. Graph of γ (208/204) versus α. Same notation as in Fig. 1. The wide scatter of these data shows more clearly the complex nature of Pb in 15415. Note that the amounts of Pb in almost all fractions is far more than is accountable by in situ decay of U and Th.

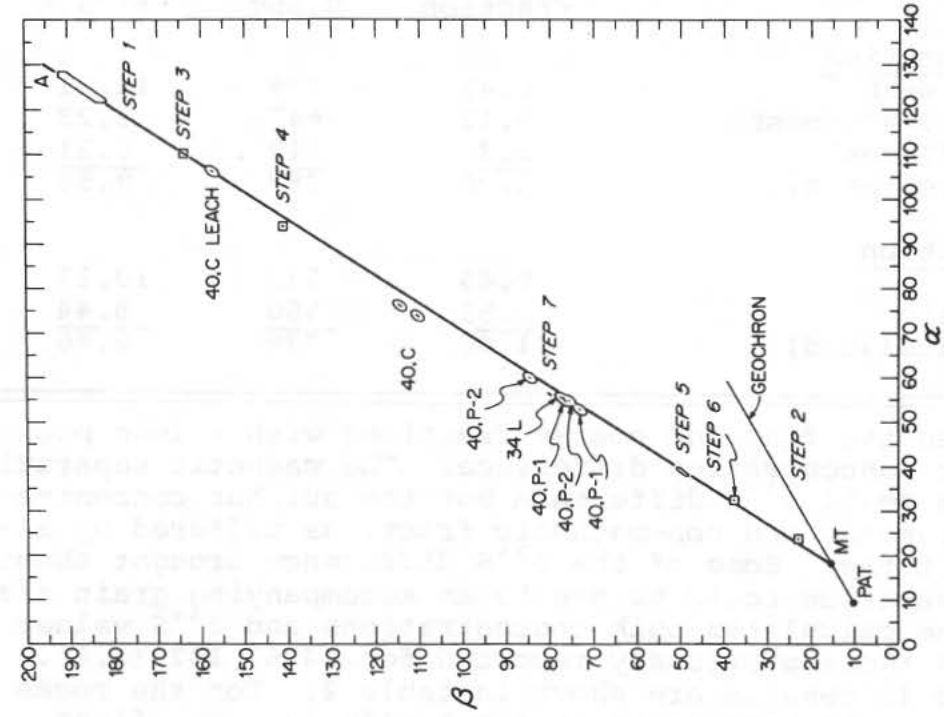

Fig.1.Graph of β (207/204) vs α (206/204) for samples of 15415. PAT is primordial Pb and MT is modern terrestrial. All data shown is uncorrected for blank. Line MT-A is for reference and is drawn through MT and Step 3. Steps of the leaching experiment on 40 CH are indicated on the right of line MT-A. With the exception of Steps 1 & 5 which have large errors and 7(small dot), all the data points are enclosed in squares for 40 CH and ellipses for other experiments. Note that data points lie on both sides of MT-A far outside of analytical errors. The data form a reasonable linear array but do not define a straight line even with corrections for blank.

SULPHUR CONCENTRATIONS AND ISOTOPE RATIOS IN APOLLO 14 AND 15 SAMPLES, H. G. Thode and C. E. Rees, Dept. of Chemistry, McMaster University, Hamilton, Ontario, Canada.

Sulphur concentrations and $\delta^{34}S$(1) values have been measured for Apollo 14 and 15 samples. Experimental procedures have been described elsewhere (2). Reported sulphur concentrations have an estimated error of ±3% while the standard deviation of an individual $\delta^{34}S$ determination is ±0.07‰. No measurements have been made of $\delta^{33}S$ or $\delta^{36}S$ values for these samples since previous results on lunar material (2,3,4) have shown that there are no significant sulphur isotope abundance variations which are not attributable to mass dependent isotope fractionation processes.

A sample of 14163,132 (fines) was separated into fine, medium and coarse fractions using 200 and 400 mesh sieves. A further sample was crudely separated into magnetic and non-magnetic fractions using a hand magnet. The experimental results are shown in table 1. The grain size separation gave a $\delta^{34}S$ difference of

Table 1. Sulphur concentrations and isotope ratios in separated components of 14163,132 (fines)

	Fraction	S,ppm	$\delta^{34}S$,‰
Grain size separation			
Fine,<400 mesh	0.49	879	11.91
Medium, 200-400 mesh	0.12	647	8.23
Coarse,>200 mesh	0.39	717	6.21
Total (calculated)	1.00	787	9.50
Magnetic separation			
Magnetic	0.45	953	10.17
Non-magnetic	0.55	560	8.44
Total (calculated)	1.00	739	9.46

about 5‰ between the fine and coarse fractions with a less pronounced sulphur concentration difference. The magnetic separation produced only a small $\delta^{34}S$ difference but the sulphur concentrations in the magnetic and non-magnetic fractions differed by almost a factor of two. Some of the $\delta^{34}S$ difference brought about by magnetic separation could be due to an accompanying grain size separation. The calculated bulk concentrations and $\delta^{34}S$ values agree well with those previously reported for 14163,132 (3,4).

The Apollo 15 results are shown in table 2. For the rocks the values lie in the same range as for Apollo 12. The fines

Sulphur Concentrations and Isotope Ratios in Apollo 14 and 15 Samp

H. G. Thode

samples show a trend of increasing $\delta^{34}S$ value with increasing sulphur concentration in agreement with the finding previously reported (4) for 14163. The samples with the highest and lowest $\delta^{34}S$ and sulphur concentration (15021 and 15531) also have respectively high and low ratios of agglutinates plus glass to basaltic components (5). The higher proportion of unaltered basaltic rock component in the 15531 soil could explain its lower $\delta^{34}S$ value since lunar basalts have $\delta^{34}S$ values which lie between 0 and +1‰.

Table 2. Sulphur concentrations and isotope ratios in Apollo 15 samples

	S,ppm	$\delta^{34}S$,‰
Rocks		
15495,60	569	0.24
15557,47	673	0.39
15076,23	452	lost
15076,23	499	0.57
Fines		
15021,91	694	10.22
15021,106	689	10.36
15933,22	612	8.30
15471,26	570	7.45
15531,31	565	5.34
15531,39	536	5.43

References and Notes

1. $\delta^{34}S,‰ = \{[(^{34}S/^{32}S)\ \text{sample}/(^{34}S/^{32}S)\ \text{standard}]-1\} \times 1000$; standard is Canyon Diablo troilite.
2. H. G. Thode and C. E. Rees, Earth Planet Sci. Lett. 12, 434 (1971).
3. H. G. Thode and C. E. Rees, in Lunar Science III (editor C. Watkins) pp 749-751, Lunar Science Institute Contr. No.88.
4. C. E. Rees and H. G. Thode, Proc. Third Lunar Sci. Conf., Geochim. Cosmochim. Acta Suppl. 3, Vol. 2, in press, M.I.T. Press.
5. Lunar Sample Information Catalog - Apollo 15, p. 58 and p. 247 NASA publication MSC 03209.

6. Supported by the National Research Council of Canada.

COSMONUCLIDES IN LUNAR SOIL FROM APOLLO 15, Y.Yokoyama, J.L.Reyss, F.Guichard, Centre des Faibles Radioactivités, CNRS, 91-Gif-sur-Yvette, France, and J.Sato, Faculty of Science, University of Tokyo, Tokyo, Japan

Two soil samples taken at the station 6 on the Apennine Front were studied. Sample numbers are 15261,47 and 15271,44: the former was taken at the bottom of a trench and the latter was collected at the surface near the trench.

A non-destructive analysis on Na-22, Al-26, Th and U was performed with a low back-ground gamma-gamma coincidence spectrometer. The experimental results are listed in Table 1 together with the results reported by Keith et al.(1) on the sample 15271. The errors given in the table are one standard deviation in the counting statistics.

The present results on the sample 15271 agree with those of Keith et al.(1) within experimental errors.

The production rates of Na-22 and Al-26 were calculated in the same way as that reported previously(2). A rigidity parameter of R_o=100 MV and an incident flux of J=70 protons/cm^2/sec/4π are adopted for solar particles, and for galactic cosmic rays slight modifications on some coefficients were made.

The variation in the activity of Na-22 and Al-26 as a function of depth is compared with the calculated production rates (Fig. 1). The results obtained by LSPET(3) from the Deep-drill core sample collected at the station 8 are also given in Fig. 1. Effects of solar particle bombardment are visible in the surface sample 15271. From the figure of Al-26, the mean depth of this sample can be estimated to be about 1 cm.

Since the effect of solar particles is negligible for samples deeper than 10 cm, the fossil record of galactic cosmic fluxes can be observed in those samples. The experimental results agree with the calculation based on a constant primary flux of F=4±1 nucleons/cm^2/sec/4π for past millions years.

Cosmonuclides in lunar soil

Y.Yokoyama

Table 1 Radioactivities in the lunar soil, 15271 and 15261

Sample	15271 surface Keith et al.	15271,44 surface this work	15261,47 trench bottom this work
Weight	527.9 g	10.2 g	10.0 g
Na-22	37 ± 4 dpm/kg	41 ± 13 dpm/kg	34 ± 13 dpm/kg
Al-26	130 ± 30 dpm/kg	104 ± 13 dpm/kg	36 ± 12 dpm/kg
Th	4.1 ± 0.4 ppm	3.67 ± 0.30 ppm	3.72 ± 0.31 ppm
U	1.21 ± 0.04 ppm	1.03 ± 0.10 ppm	0.93 ± 0.10 ppm

References:

(1) Keith, J. E., Clark, R. S. and Richardson, K. A.: Gamma Ray Measurements of Apollo 12, 14 and 15 Lunar Samples. Lunar Science - III, Revised Abstracts of Papers Presented at the Third Lunar Science Conference, Houston, 10-13 January, 1972, ed. by C. Watkins.

(2) Yokoyama, Y., Auger, R., Bibron, R., Chesselet, R., Guichard, F., Leger, C., Mabuchi, H., Reyss, J. L. and Sato, J.: Cosmonuclides in Lunar Rocks. Proceedings of the Third Lunar Science Conference (Supplement 3, Geochim. Cosmochim. Acta), vol. 2, 1972 (in press).

(3) Apollo 15 Preliminary Science Report, NASA SP-289 (1972).

Figure caption:

Observed and calculated production rates for Na-22 and Al-26. Dashed curves are for partial production by solar and galactic particles, and solid curves, for the total production rates.

Cosmonuclides in lunar soil

Y.Yokoyama

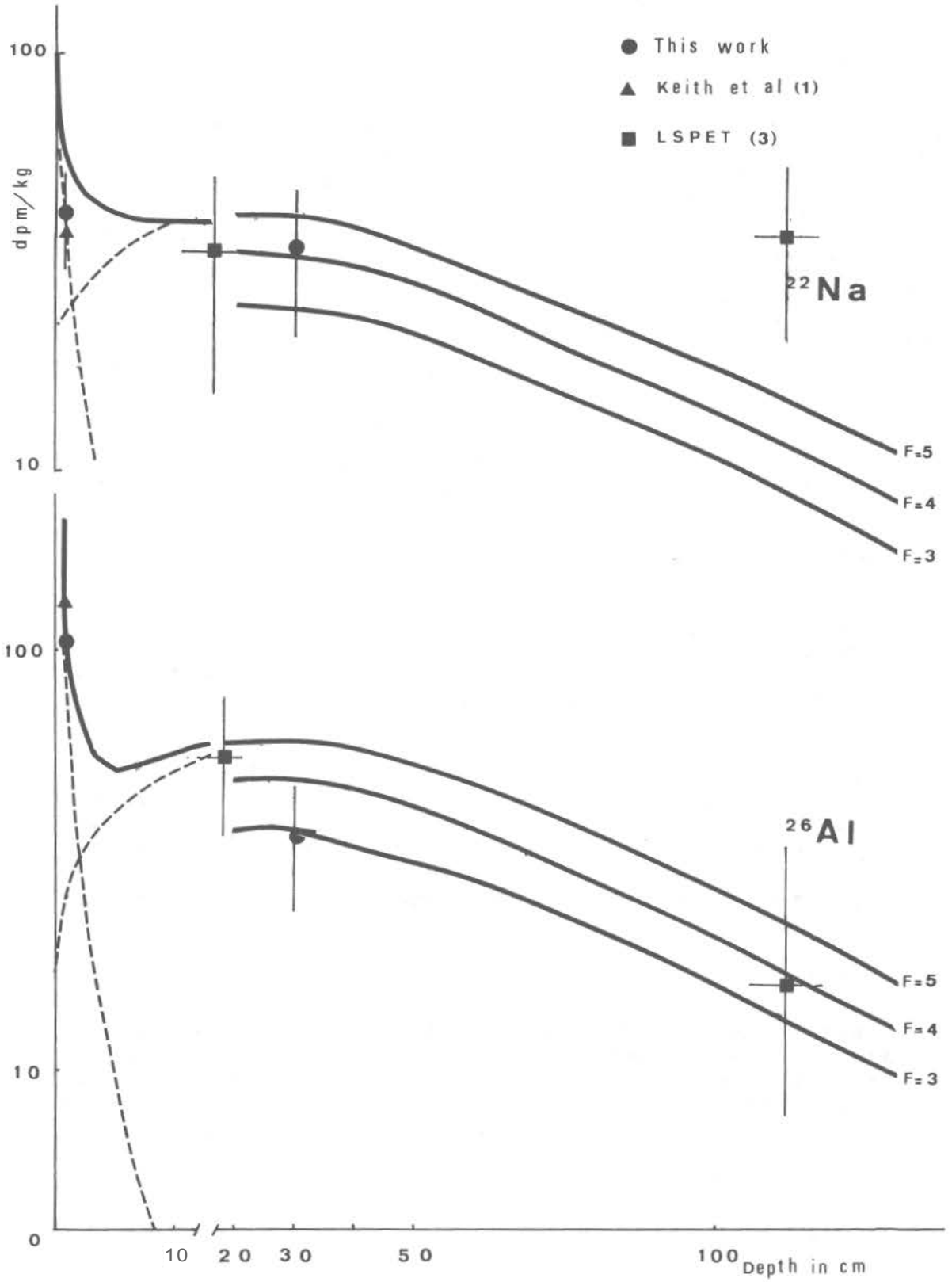

MICROMETEOROID CRATERS SMALLER THAN 100 MICRONS

D. E. Brownlee, University of Washington, Seattle, Washington; F. Hörz, NASA Manned Spacecraft Center, Houston, Texas; J. B. Hartung, NASA Manned Spacecraft Center, Houston, Texas; and D. E. Gault, NASA Ames Research Center, Moffett Field, California

INTRODUCTION

Binocular studies of whole rock surfaces have yielded information on the absolute and relative frequencies of 100-1000 μm size impact craters. The resulting mass-frequency calculations of the impacting micrometeoroids are in good agreement between Hartung et al., 1972; Morrison et al., 1972; and Neukum et al., 1972. In contrast, the relative frequencies of craters smaller than 100 μm and particular smaller than 5 μm are somewhat controversial. These small craters are of particular interest because of their importance in obtaining information on micrometeoroids in the approximately 10^{-10} to 10^{-15} g mass range. Our results are based on detailed SEM studies on glass-surface 15286,11 and a Luna 16 glass spherule.

CRATER MORPHOLOGY AND PROJECTILE PROPERTIES:

Using laboratory simulations for μm-sized craters (Vedder, 1971, 1972; Neukum et al., 1972) we feel that a few but important conclusions about physical properties of the projectiles can be drawn:

1) Although there are exceptions, the majority of craters we examined are roughly circular. According to Vedder (1971, 1972), this implies a fairly equidimensional if not spherical projectile. Thus the possibility that most interplanetary particles in the 10^{-10} to 10^{-15} g range have highly nonspherical shapes can be ruled out. Shapes such as rods and platelets have been predicted on the basis of grain growth processes in the solar nebula (Donn, 1964) and they were reported as constituents of primitive meteorites (Arrhenius, 1972). Our cratering studies, however, indicate that the far majority of (present day?) micrometeoroids must be fairly equidimensional, if not spherical (Figure 1a and b).

2) Our observations, however, do not rule out the possibility that some micron size meteoroids could consist of aggregates of much smaller rods, platelets, irregular fragments, etc. In fact, some few craters are highly irregular and appear to have been produced by particles of non-homogeneous density or mass distribution, i.e. of aggregate structure (Figure 1d). However, such features are rare.

3) The craters smaller than 10 μm examined on rock 15286 were relatively deep structures with depth/diameter (pit) ratios mostly exceeding 0.5. On the basis of cratering simulation experiments fired at 12 km/sec (Vedder, 1972) we tentatively can exclude projectile densities less than 1 g/cm^{-3}. It appears that the extreme porosity postulated for mm-sized meteoroids (e.g. Verniani, 1969) does not exist in micron sized particles.

RELATIVE CRATER FREQUENCIES:

As indicated above, various authors have reported differing relative abundances for craters smaller than 100 and especially below 5μm pit diameter. Our best (and new) results are illustrated in Figure 2 and compared to a variety of other results in

Figure 3. Figure 2 demonstrates the change in relative crater frequency as a function of SEM magnification. The fact that the absolute crater densities on both surfaces are similar is fortuitous. According to these two surfaces, our "best estimate" distribution is indicated. This distribution is used in Figure 3 as standard to which all other data were normalized. Depending on the crater size-range covered by the various investigators, the curves were normalized at either 100, 10 or 1 μm pit diameter. Significant differences in the .1 to 100 μm size range become apparent.

Admittedly the differences could be somewhat decreased if some curves were "normalized" at a different crater size, i.e. shifted vertically, to purposely obtain the very best fit. Though this would somewhat smoothen the general picture, it would not change the slopes of individual curves and therefore would have no influence on the relative frequencies discussed below.

Certain factors may influence the slopes, however, to a degree which is most difficult to assess:

1) As illustrated in Figure 2, varying SEM magnifications used even by the same operator will yield differently shaped curves on the same sample.

2) The total number of craters counted will influence the quality of the statistics. No error-bars are indicated, because the raw data of the literature references were not available; however, only curves are plotted which are based on more than 30 craters.

3) The positive recognition of impact craters especially in the submicron range is a difficult task. There is a high probability that some impact-craters are simply overlooked and thus a relatively larger decrease in frequency is simulated. More importantly, however, is the capability to distinguish between genuine impact phenomena and other circular depressions such as burst bubbles, "dimples" (Carter and McKay, 1971), etc. Cratering experiments by Neukum et al. (1972) and investigations about lunar crater geometry (Hartung et al., 1972) have shown that there are striking similarities between genuine impact craters and other circular depressions on lunar materials especially for submicron-sized features.

Because these factors are rather interpretative and subjective in nature, they are difficult to evaluate. However, some differences cannot be accounted for even with the above factors and we consider them as real differences in the mass-frequency distribution of micrometeoroids. Especially the curve of Schneider (1972, rock 15076) and our best estimate are incompatible. We offer two explanations for this difference:

a) The especially large number of submicron size craters observed on 15076 are due to secondary impacts in the fashion proposed by Carter and McKay (1971), and therefore the observed frequencies result from a mixture of primary and secondary projectiles.

b) The absolute crater density of rock 15076 is about a factor of 10 less than that of 15286 and the Luna 16 glass. Thus the various crater populations were accumulated over different time periods if not even at entirely different geologic times. It is possible that the mass frequency distribution of micrometeoroids in the 10^{-10} to 10^{-15} g mass range was not constant over geologic or even very recent time.

Though other and less likely processes may also be considered to explain the differences (e.g. exposure-geometry, deposition of thin glass films which would preferentially obscure the submicron size craters, differential erosion of submicron size features by solar wind sputtering, etc.), we think that the above two alternates are

Microcraters Smaller than 100 μm

D. E. Brownlee

the most plausible ones. At present it is very difficult to decide which of the explanations may be correct. However, it is demonstrated that Gault et al.'s (1972) model about the mass-frequency distribution of micrometeoroids is in good agreement with the findings for micrometeoroids 10^{-4} to 10^{-10}g in mass. The abundance of micrometeoroids smaller than 10^{-10}g is still subject to more detailed investigations. It is, however, apparent that a virtual cut off in the existence of micrometeoroids smaller than 10^{-12} g as previously postulated (e.g. Kerridge, 1970) on the basis of in situ measurements made from spacecraft does not exist. Micrometeoroid masses down to 10^{-14}gare observed, though their relative abundance is still subject to discussion (see also Hemenway et al., 1972).

References

1. Arrhenius, G., Paper presented at Astronomical Society, Pacific Section, Annual Meeting, Santa Cruz, Calif., June 26-29, 1972.
2. Carter, J. L. and McKay, D. S., Proceedings 2. Lunar Sci. Conf., Vol. 3, 2653-2670, 1971.
3. Donn, B., Ann. of the New York Academy of Sciences, 119, Art. 1, 5-16, 1964.
4. Gault, D. E., Hörz, F. and Hartung, J. B., Proceedings 3. Lunar Sci. Conf., in press, 1972.
5. Grossman, L., Geochim. Cosmochim. Acta 36, 597-619, 1972.
6. Hartung, J. B., Hörz, F., and Gault, D. E., Proceedings 3. Lunar Sci. Conf., in press, 1972.
7. Hemenway, C. L., Hallgren, D. S., and Schmalberger, D. C., Nature 238, 256-260, 1972.
8. Kerridge, J. F., Nature 228, 616-619, 1970.
9. Morrison, D. A., McKay, D. S., Moore, H., and Heiken, G. H., Proceedings 3. Lunar Sci. Conf., in press, 1972.
10. Neukum, G., Schneider, E., Mehl, A., Stortzer, D., Wagner, G. A., Fechtig, H., and Bloch, M. R., Proceedings 3. Lunar Sci. Conf., in press, 1972.
11. Schneider, E., Unpublished thesis, University of Heidelberg, Germany, 1972.
12. Vedder, J. F., Earth Planet. Sci. Letters, 11, 291-296, 1971.
13. Vedder, J. F., Personal communication, 1972.
14. Vernani, F., Smithsonian Contrib. Astrophysics 10, 230, 1967.
15. Cour-Palais, B. G.; Flaherty, R. E.; Brown, M. L.; and McKay, D. S.; "Lunar Science - III".

Microcraters Smaller than 100μm

D. E. Brownlee

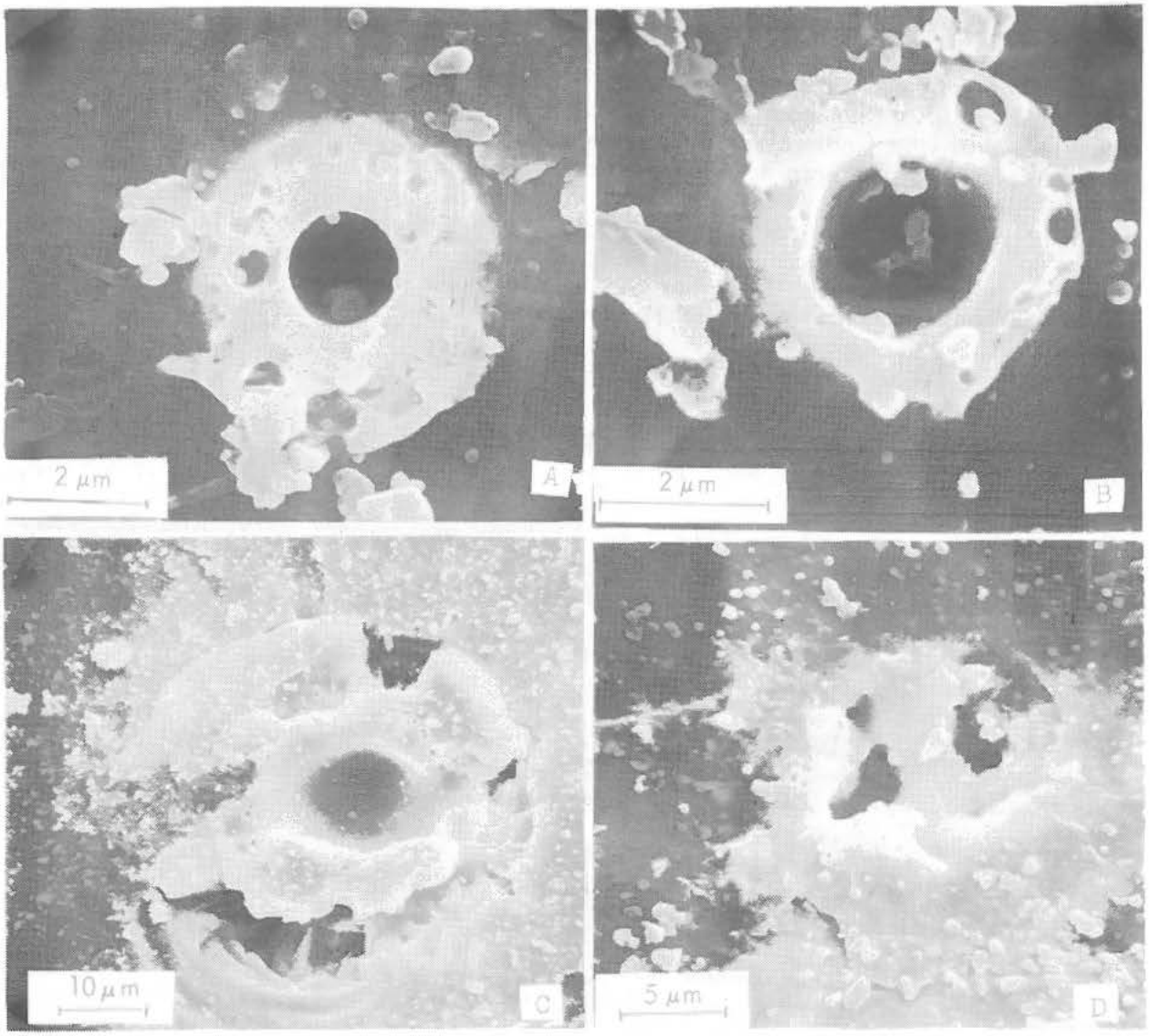

Fig. 1

a) Small, almost perfectly circular crater. Though crater geometry varies with absolute pit-size (Hartung et al., 1972) most lunar microcraters have centro-symmetric pits. All other craters in Fig. 1 are infrequent exceptions to this rule. 1b) Crater with somewhat polygonal outlines. Note that both craters in Fig. 1a and 1b have frothy rims, which are unique to lunar craters and which have not been reproduced in the laboratory. 1c) Elongated crater probably caused by ellipsoidal projectile. Oblique impact angle can probably be ruled out because spallation zone would be even more assymetric (according to Vedder (1971)). 1d) Impact feature characterized by a variety of individual depressions within the crater floor interpreted to be caused by a projectile of aggregate structure.

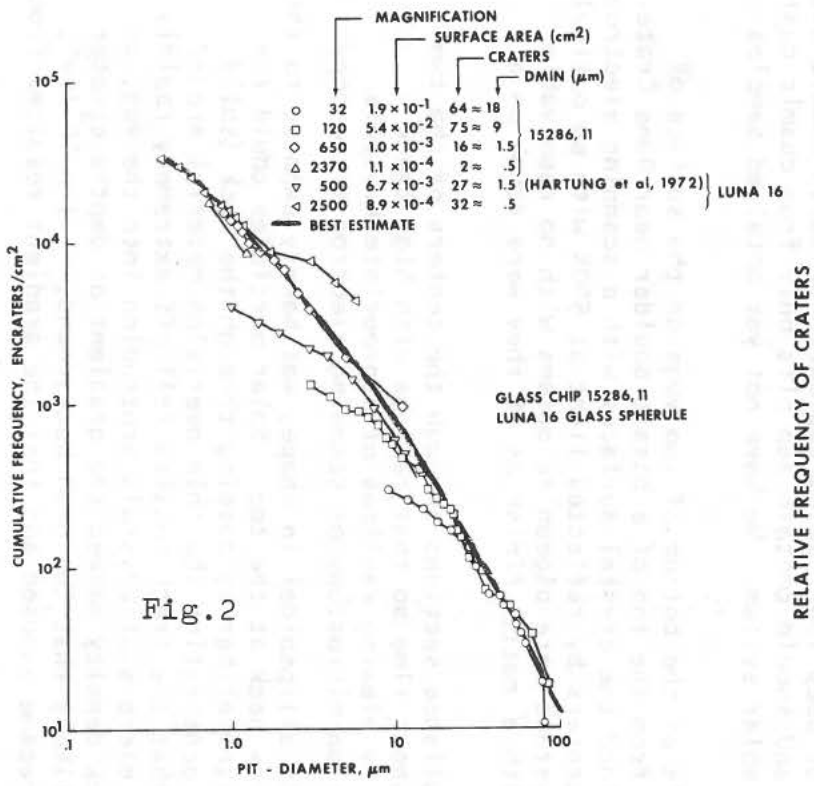

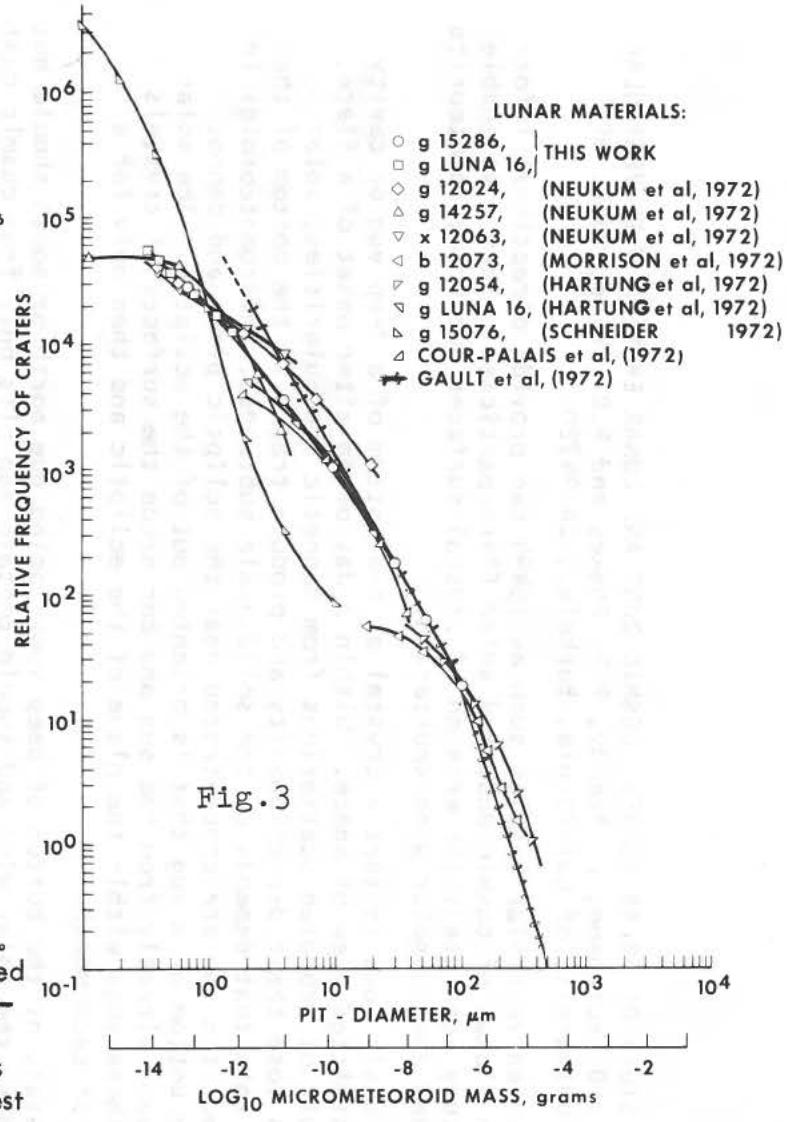

Fig. 2): New data on absolute crater densities for craters smaller than 100μm. The surfaces investigated had no overlapping craters etc. and thus a "production-state" can be ensured which should truly reflect the relative mass-frequency of impacting projectiles. Note the relative decrease of crater frequency as a function of SEM magnification. Our "best estimate" is indicated.

Fig. 3): Comparison of relative crater frequencies obtained from Fig. 2 with other data. All curves are normalized with respect to "best estimate" of Fig. 2. Note the significant differences in the slope of various curves. The inserted mass-scale is taken from calibration I of Hartung et al., 1972.

STUDY OF SOLAR FLARES, COSMIC DUST AND LUNAR EROSION WITH VESICULAR BASALTS, I.D. Hutcheon, D. Braddy, P.P. Phakey and P.B. Price, Dept. of Physics, University of California, Berkeley, CA 94720

Oriented vesicular basalts such as 15499 can provide directional information on fluxes of cosmic dust and solar flare particles. They also enable one to study separately the erosion of crystal surfaces due to micrometeorite impacts and due to solar wind sputtering.

The basic idea is that a crystal at the bottom of a deep vug or cavity has a restricted view of space. Within a day or so after onset of a flare, as a result of repeated scatterings from magnetic irregularities, solar particles lose their directionality and produce tracks at the bottom of the vug at a rate that depends on the solid angle subtended. Micrometeoroids in orbit about the sun are concentrated near the ecliptic plane and cannot reach the bottom of a vug that is oriented out of the ecliptic. The solar wind streams directly from the sun and can erode the surfaces of crystals only in those vugs within the plane of the ecliptic and then only for a fraction of each month.

Crystals at the bottom of deep vugs facing due north or south should not be eroded by the solar wind and should contain zap pits only from cosmic dust that originated outside the solar system. We have not yet obtained samples in such an orientation.

We have studied crystals at the bottom of two vugs on the surface of rock 15499 that was removed from the top of a basalt boulder near Dune Crater. Though we have not yet examined the crystal surfaces with a scanning electron microscope, we saw no microcraters by reflected light at 500X with an optical microscope. The largest crystals were pigeonite prisms with no resolvable rounding of the edges but with a matte finish as if they were rough on a submicroscopic scale.

We prepared vertical polished sections through the centers of the two vugs and etched for a very short time so that regions with high track densities could be resolved by viewing replicas of appropriate crystals either by transmission electron microscopy or scanning electron microscopy.

One of the vugs, roughly ellipsoidal in shape, was barely exposed to the outside world through a narrow neck at the top. Solar particles could impinge on crystals at the bottom either by passing through the neck (solid angle ~0.1 steradian) or by penetrating the thin overlying material around the neck. Though we found that the track density fell off extremely rapidly with depth in the outer few microns of crystals protruding into the vug, an overall high background track density masked the gradient at depths greater than a few microns. It is likely that the high background, $\sim 1 \times 10^8/cm^2$, accumulated before the vug became exposed and that the gradient resulted from

I.D. Hutcheon

a relatively short exposure after a chip was removed from above the vug.

When we examined a section through the second vug, it was immediately obvious that the track profile was far steeper than any ever before seen in a lunar rock or meteorite. The track density decreased from $\gtrsim 5 \times 10^{10}/cm^2$ near the external surface of the crystal to $\sim 10^8/cm^2$ a few tens of microns below the surface.

In Fig. 1 the profile of track density versus depth in the vug is compared with the profile previously observed[1-3] in the glass filter from the Surveyor III camera that was exposed on the moon for 2.6 years, and with a profile measured by Barber et al.[4] on the surface of rock 12022.

Crozaz et al.[5] have emphasized that, because of erosion, profiles on all lunar rock surfaces ever studied have been at least one power shallower than the Surveyor profile, taken to be representative of an uneroded surface. (In 2.6 years no more than a few angstroms thickness would be removed.) The profile in the vug appears comparable to that on Surveyor and is obviously much steeper than profiles on eroded surfaces.

What we have shown is that track profiles characteristic of solar flare spectra on uneroded surfaces (like the Surveyor glass) can be observed in certain regions of rocks that are protected from the normal kinds of erosion (or from handling by the astronauts).

If we naively assume that the track profile in the Surveyor glass was representative of the long-term average solar flare profile, and if we take into account differences in solid angle, track-recording characteristics, and mode of viewing tracks in the Surveyor glass and in the vug, we estimate an exposure time of $\sim 10^5$ years for the vug.

Brownlee[6] has recently made extensive crater counts on lunar rocks and spherules. From his data we would expect to have seen about five pits with diameter greater than 4 microns on the exposed surface of the crystal on which we made our measurements, assuming an exposure age of 10^5 years. About fifty pits with diameter less than 4 microns should have been produced during that same time. Recognizing that we only inspected the surface with an optical microscope, we cannot claim that our failure to see pits is incompatible with his data, or that the vug had to have been oriented out of the plane of the ecliptic. Unfortunately, only the location but not the orientation of our sample of 15499 was documented.

These first results on a track profile within a vug indicate that a statistical study of track profiles and microcrater counts in vugs of various known orientations would be very informative.

References

1. Crozaz, G., and Walker, R.M. (1971), Science 171, 1237-1239.

2. Fleischer, R.L., Hart, H.R., and Comstock, G.M. (1971), Science 171, 1240-1242.

3. Price, P.B., Hutcheon, I.D., Cowsik, R., and Barber, D.J. (1971), Phys. Rev. Lett. 26, 916-919.

4. Barber, D.J., Cowsik, R., Hutcheon, I.D., Price, P.B., and Rajan, R.S. (1971), Proc. Second Lunar Sci. Conf., Vol. 3, pp 2705-2714, MIT Press

5. Crozaz, G., Drozd, R., Hohenberg, C.M., Hoyt, H.P., Ragan, D., Walker, R.M., and Yuhas, D. (1972), Proc. Third Lunar Sci. Conf., Geochim. Cosmochim. Acta Suppl. 3, Vol. 0, pp. 0000-0000., MIT Press.

6. Brownlee, D. (1972), private communication.

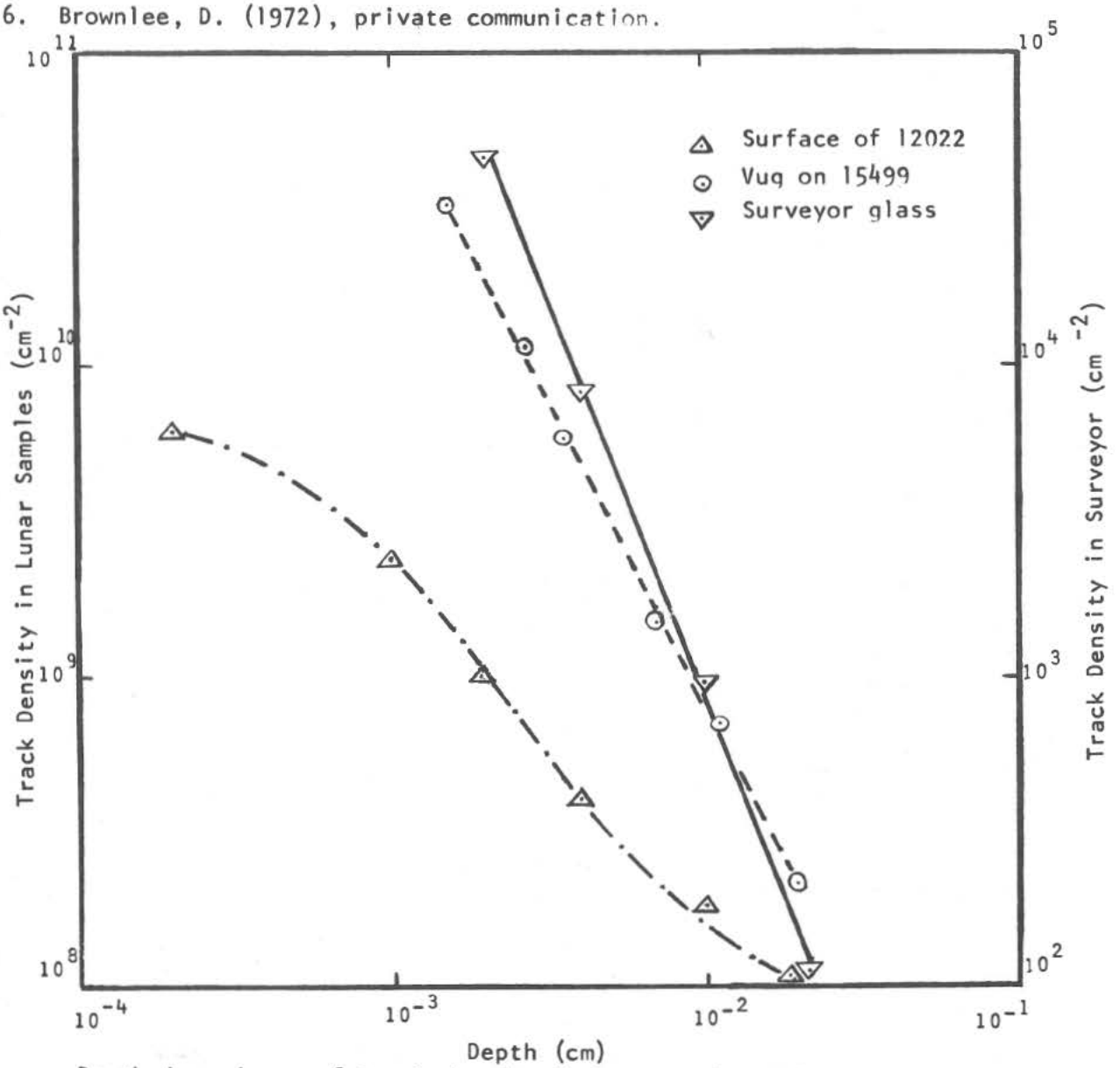

Depth dependence of track density in a crystal at the bottom of a surface vug in rock 15499, compared with depth dependence in a surface crystal in rock 12022 (ref. 4) and in glass from the Surveyor III camera (refs. 1-3). The gradient is steeper in 15499 than in 12022 because the usual lunar erosion processes have been thwarted at the bottom of the vug.

EXPOSURE AGES OF APOLLO 15 SAMPLES BY MEANS OF MICROCRATER STATISTICS AND SOLAR FLARE PARTICLE TRACKS.

E. Schneider, D. Storzer, and H. Fechtig, Max-Planck-Institut für Kernphysik, Heidelberg, Germany.

Crater number densities of various Apollo 15 samples have been measured using a scanning electron microscope (SEM).
For three samples (crystalline rock 15076,31, glass coated breccia 15015,24, and glass splash 15927,3) it was possible to determine exposure ages applying the solar flare track method. As there is evidence that the samples are in production state concerning the microcraters, the crater number densities and the solar flare exposure ages could be used to calculate the interplanetary dust flux in the range between 0.1 and about 2.5 μm particle diameter.

1. Microcrater statistics. Very smooth surfaces of the samples have been scanned with the help of the SEM. Using a scanning magnification of 20000, craters down to 0.1 μm diameter were identified and quantitatively counted. The crater frequencies are given in table 1. In order to identify such small craters correctly and distinguish them from other surface features crater simulation experiments[1,2] in the submicron size, high velocity range of projectiles have been performed using the 2 MV-Van-de-Graaff dust accelerator. These laboratory produced craters are very similar to the craters found on lunar samples and in some cases it is impossible to distinguish them from lunar ones. Carter and MacGregor (1970)[3] have reported similar micronsized craters on lunar glasses which they interpreted to be to a large extent secondary impacts of lunar debris particles having impacted the glass bodies when these were still in a molten or viscous state shortly after their formation. From our crater simulation experiments, however, there is no doubt that most of the craters (>90%) show typical high velocity impact features, whereas most of the secondary particles ejected during impact processes have velocities of about 1 km/s or lower[4]. At such low velocities the projectiles either stick in a small impact hole or they elastically rebound and leave a shallow depression on the target surface. As we found the submicronsized craters on glassy material as well as on crystalline rock surfaces we must conclude that they are mainly of primary, meteoritic origin.

2. Exposure ages by means of the solar flare track method. Residence times of glass and mineral faces at the very top of the lunar surface can be determined using the high density and steep gradient tracks of Fe-group nuclei emitted in solar flares[5,6,1].
In the glass coated breccia 15015,24, glass splash 15927,3 and crystalline rock 15076,31 the solar flare tracks were counted at different depths from the same surfaces which had been checked for microcraters. In the glasses as well as in the pyroxenes trapped in the glass splashes and the breccia the solar flare tracks were observed both with an optical and a scanning electron microscope. As noticed previously[1,7] the solar flare tracks in lunar

glasses are annealed to a considerable extent and therefore, the solar flare track densities are thermally reduced. This observation also holds for the glasses of this study. In the pyroxenes no track fading was detected. By correcting for the track fading effects in the glasses [1,7,8] concordant track densities were found in the glass splashes and their trapped pyroxenes.
In the three samples studied, the track densities p decrease with depth R from the surface according to $p = \text{const.} \cdot R^{-\alpha}$, α being 2.8, 2.5, 2.6 respectively (Fig. 1). Contrary to the α-values of most lunar samples these values agree well with the α-value found for the unetched surveyor III glass lens [9,10,11] indicating that our samples were not affected by erosion.
From the solar flare track densities vs. depth (Fig.1) solar flare exposure ages were calculated for samples 15015,24, 15927,3, 15076,31. Assuming the track production rates derived from the Surveyor III glass the exposure ages are 13 a, 1.6×10^3 a and 8.5×10^4 a, respectively.
Due to the uncertainty of the Surveyor III data these ages have an uncertainty of a factor of about 2.

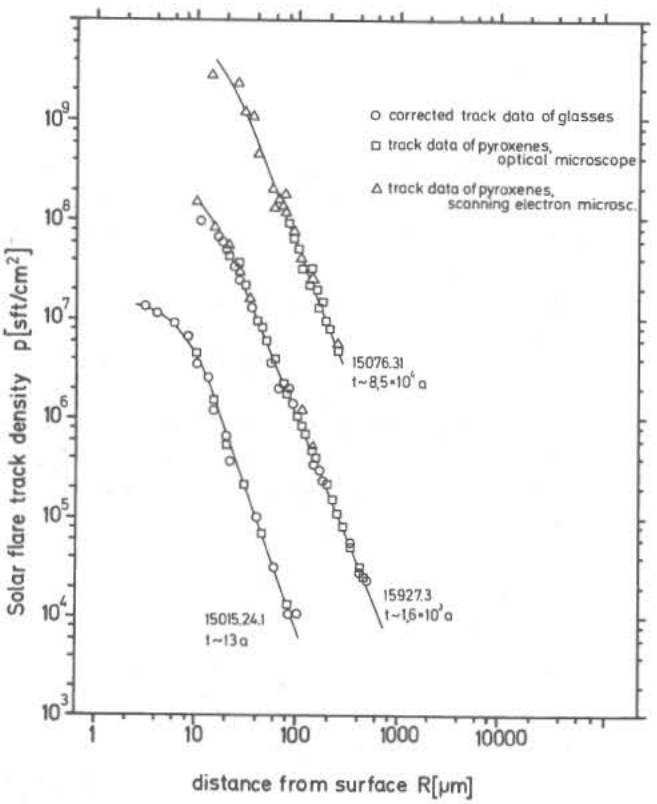

Fig. 1. Track density versus depth.

3. Interplanetary dust flux. As mentioned already the crater frequencies of the samples 15076,31 and 15927,3 showing production state conditions in connection with the solar flare track ages yielded the flux of interplanetary particles in the micron- and submicron-size range. It is plotted cumulatively versus the particle mass and diameter (Fig. 2). The conversion of crater data to flux values is based on a crater to projectile diameter ratio of 2 corresponding to a mean impact velocity of 20 km/s as it is known from simulation experiments [1,2]. A mean density value of 3 g/cm^3 for the projectiles has been assumed.
Both samples 15076,31 and 15927,3, which are different in exposure age by nearly two orders of magnitude indicate the same absolute flux values within the uncertainty of the solar flare track method, in particular both indicate the same considerable increase of the flux below about 1 µm particle diameter. With exception of the flux determined by Mehl (1972) [12] there is a general discrepancy between the fluxes derived from satellite measurements and those derived from lunar microcrater studies (Hartung et al. [13], Neukum et al. [1],

Sample No.	Crater frequency	Solar flare track age
15076,31	$5 \cdot 10^3$ cm^{-2} ≥ 1 µm $4 \cdot 10^4$ cm^{-2} ≥ 0.5 µm $\sim 10^6$ cm^{-2} ≥ 0.1 µm	$T_E = 8.5 \cdot 10^4$ a $(4 \cdot 10^4 \text{a} < T_E < 1.6 \cdot 10^5 \text{a})$
15927,3	$1.5 \cdot 10^2$ ≥ 1 µm $5 \cdot 10^3$ ≥ 0.5 µm $3 \cdot 10^4$ ≥ 0.1 µm	$T_E = 1.6 \cdot 10^3$ a $(5 \cdot 10^2 \text{ a} < T_E < 4.5 \cdot 10^3 \text{ a})$
15015,24	no craters	$T_E = 13$ a $(4 \text{ a} < T_E < 40 \text{ a})$

Table 1.: Crater densities and solar flare track ages of three Apollo 15 samples.

Schneider[2]). The fluxes calculated from crater statistics are about 2 orders of magnitude below the satellite data, a problem which is not yet solved[14]. It might be that the solar flare flux is not represented sufficiently by the Surveyor III glass standard.

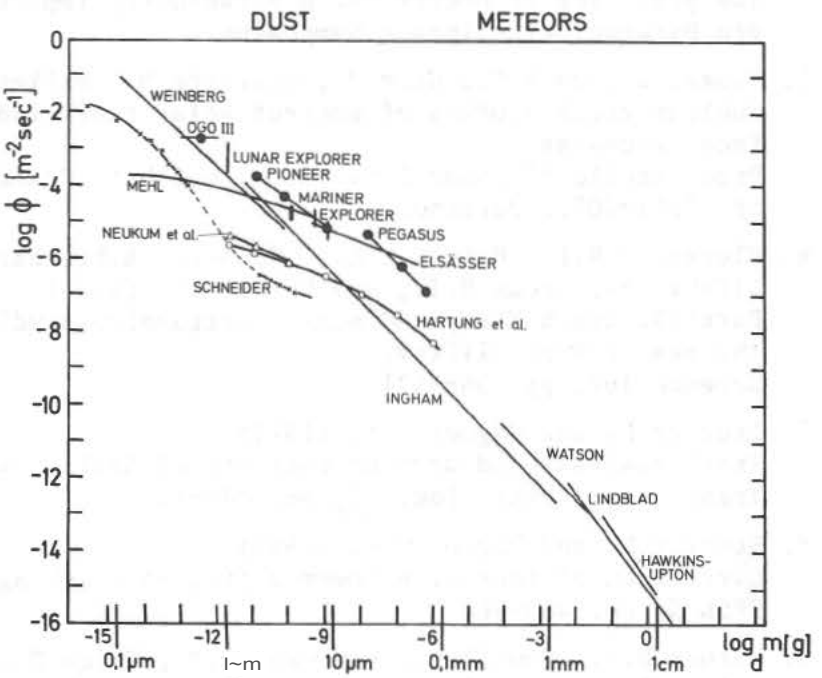

Fig.2. Cosmic dust flux versus particle mass and diameter.

References

1. Neukum G., Schneider E., Mehl A., Storzer D., Wagner G.A., Fechtig H., and Bloch M.R. (1972)
Lunar craters and exposure ages derived from crater statistics and solar flare tracks.
Proc. Third Lunar Sci. Conf., Geochim. Cosmochim. Acta Suppl. 3, Vol.3 (in press)

2. Schneider E. (1972) Mikrokrater auf Mondgestein und deren Laborsimulation Thesis, University of Heidelberg (unpublished)

3. Carter I.L., and MacGregor I.D. (1970)
Mineralogy, petrology and surface features of some Apollo 11 samples.
Proc. Apollo 11 Lunar Sci. Conf., Geochim. Cosmochim. Acta Suppl. 1, Vol.1 pp. 247-275, Pergamon

4. Gault D.E. and Heitowit E.D. (1963)
The partition of energy for hypervelocity impact craters formed in rock.
6th Hypervelocity Impact Symposium.

5. Crozaz G., Haak U., Hair M., Maurette M., Walker R., and Woolum D. (1970)
Nuclear track studies of ancient solar radiations and dynamic lunar surface processes.
Proc. Apollo 11 Lunar Sci. Conf., Geochim. Cosmochim. Acta Suppl. 1, Vol.3 pp. 2051-2070, Pergamon

6. Fleischer R.L., Haines E.L. , Hanneman R.E., Hart H.R., Kasper I.S., Lifshin E., Woods R.T., and Price P.B. (1970)
Particle track X-ray and mass spectrometry studies of lunar material from the Sea of Tranquillity.
Science 167, pp. 568-571

7. Storzer D. and Wagner G.A. (1972)
Track analyses and uranium contents of Apollo 14 glasses.
Trans. Amer. Nucl. Soc. 15, pp. 119-120

8. Storzer D. and Wagner G.A. (1969)
Correction of thermally lowered fission track ages of tektites.
EPSL 5, pp. 463-468

9. Barber D.I., Cowsik R., Hutcheon I.R., Price P.B., and Pajan R.S. (1971)
Solar flares, the lunar surface and gas-rich meteorites.
Proc. Sec. Lunar Sci. Conf., Vol. 3, pp. 2705-2714. MIT Press

10. Crozaz G. and Walker R.M. (1971)
Solar particle tracks in glass from Surveyor III spacecraft.
Science 171, pp. 1237-1239

11. Fleischer R.L., Hart H.R., and Comstock G.M. (1971)
Very heavy solar cosmic rays: energy spectrum and implications for lunar erosion.
Science 171, pp. 1240-1242

12. Mehl A. (1972) Nachweis von kosmischem Staub auf Mondproben und mit einem Detektor.
Thesis, University of Heidelberg (unpublished)

13. Hartung I.B., Hörz F., and Gault D.E. (1972)
Lunar microcraters and interplanetary dust.
Proc. Third Lunar Sci. Conf., Geochim. Cosmochim. Acta Suppl. 3, Vol. 3 (in press)

14. Gault D.E., Hörz F., Hartung I.B. (1972)
Abrasion and catastrophic rupture of lunar rocks: Some implications to the micrometeoroid flux at 1 AU.
Invited paper at XV COSPAR Meeting Madrid, Spain, May 10-24, 1972

DIFFICULTIES IN SEPARATING THE STABLE COMPONENT OF NATURAL REMANENT MAGNETIZATION IN LUNAR ROCKS. S. K. Banerjee, K. A. Hoffman and J. P. Mellema, Dept. of Geology and Geophysics, Univ. of Minnesota, Minneapolis, MN 55455.

It has been suggested [1,2] that the natural remanent magnetizations (NRM) of returned lunar samples owe their origin to the past magnetic field of a once-active dynamo in a small (radius=250 km) iron core. The birth and death of such a dynamo will be reflected in the variation of the intensity of an ancient lunar magnetic field (paleointensity) which, in turn, should be recorded in the size of the stable component of NRM in lunar rocks of different ages. Not all rocks, however, are suitable for a reliable paleointensity determination since they usually contain a variable amount of geologically unstable secondary components of NRM. From Apollo 15 mission we have obtained four different rock samples, three crystalline rocks and one recrystallized breccia. We report here our measurements of their NRM stability prior to paleointensity determinations and in particular, we present alternating field (AF) demagnetization data of one olivine basalt, 15535,28, which typifies in a grand manner one major problem encountered frequently with lunar rocks, that of variable NRM stability which we attribute in this paper to contributions from vastly different grain-sizes. AF demagnetization was carried out in a triple mu-metal-shielded environment where the residual steady field was less than 10 gamma. Peak values of AF for each demagnetizing run was increased usually in steps of 5 Oe, starting with an initial value of 5 Oe. AF frequency was 400 Hz, free of any dc bias and subharmonics or higher harmonics. The sweep from peak value to zero was accomplished electronically; the ramp or rate of decrement of AF was extremely slow, 100 gamma per half-cycle. Each sample was sequentially demagnetized, once along each of the three axes, before NRM measurement. Each set of NRM measurements (with Schoenstedt Spinner SSM-1A) yielded 4 independent measurements for each axis. Similar to what has been found by some previous workers [2], 10 to 35 Oe peak values of AF were required to remove the unstable components from most of our samples; the end-point of demagnetization was determined by a non-varying (less than 4°) NRM vector direction with regard to the sample axes and a slow (5% per Oe) rate of change of the vector amplitude. Occasionally, on demagnetization to a particular peak value of AF, the NRM vector would increase which could be explained by the removal of an unstable component with a fortuitously antiparallel contribution to the stable component. However, Fig. 1 shows a repeated, zig-zag

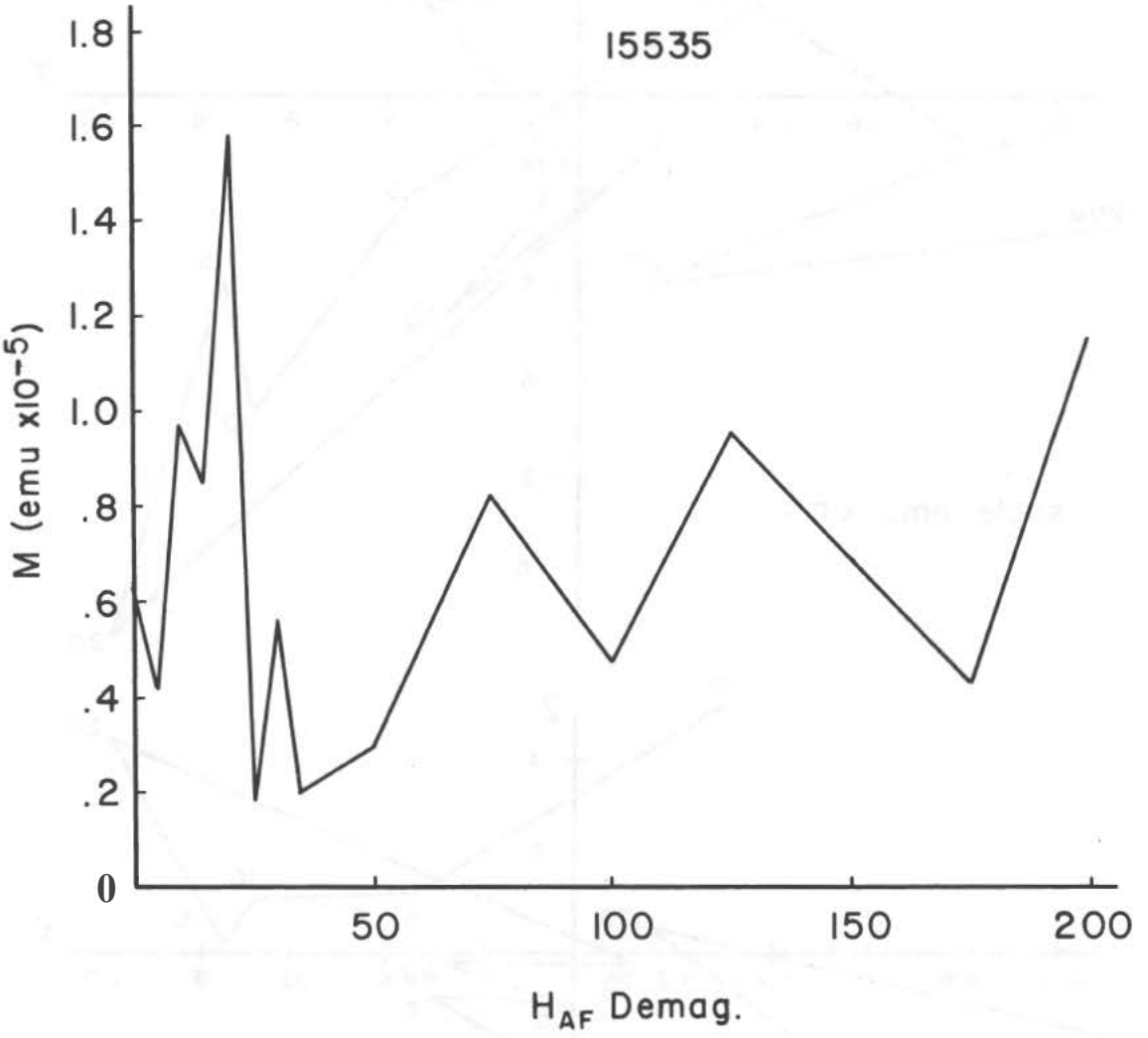

Fig. 1. Total NRM of 15535,28 (6.08 gram) versus peak values AF for demagnetization.

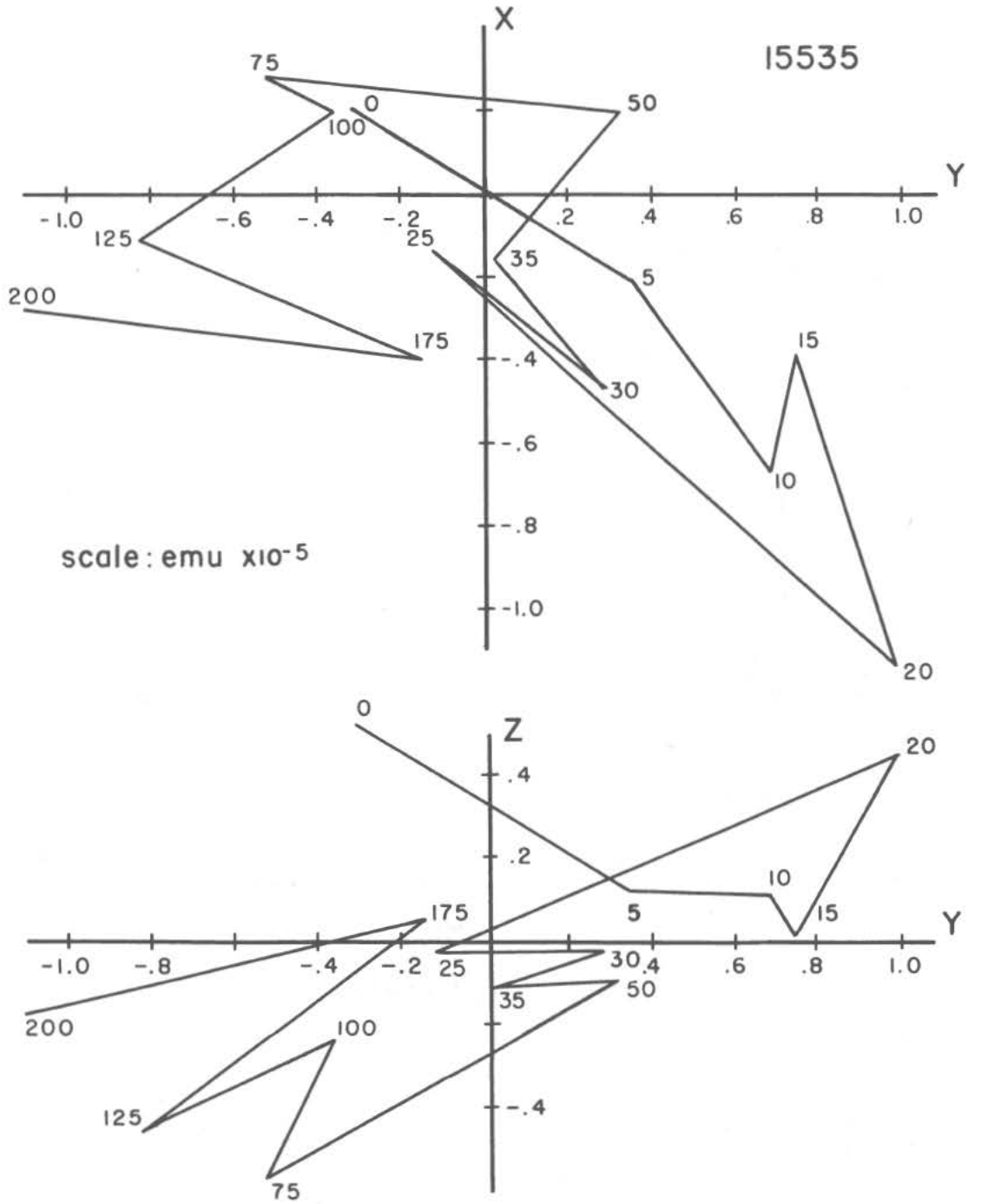

Fig. 2. Positions of NRM vectors in XY and YZ planes after stepwise demagnetization to the indicated peak values of AF.

behavior of this kind shown by sample no. 15535,28 which cannot anymore be attributed to the removal of antiparallel unstable components (1)because of the repeated nature, an increase followed by a decrease and (2), due to its persistence even at 200 Oe, a high coercivity indeed for an unstable component. An increase of NRM after AF demagnetization to a particular peak value could be caused by a spurious addition of anhysteretic remanent magnetization (ARM) due to substantial uncorrected dc bias in the AF demagnetizer. This was found not to be the case since successive AF demagnetization to higher peak values with the sample always in the same orientation with regard to the AF solenoid produced successive increase and decrease in NRM. A spurious ARM would have produced only successive increases. Fig. 2 shows the changes in the vector directions in two orthogonal planes in the sample. Under normal circumstances, when the unstable component is removed, the vector gradually decreases in size along a straight or nearly straight line. The observed irregular motion along a plane suggests that a moderate-sized and medium-stability secondary component was imprinted in the rock (due, perhaps, to mild reheating at a later time or to a magnetic storm) and is carried by a few large, planar multi-domain grains oriented in the above plane and with randomly located domain-wall-pinning-centers (defects, dislocation pile-ups, etc.). The applied AF is just large enough to move the walls from one shallow potential well to another but this does not truly randomize the positions of the walls, a process which alone would lead to an effective demagnetization. Instead, after every demagnetization to a certain peak AF the walls get pinned by different pinning centers and the net NRM shows either an increase or a decrease. A similar behavior was reported by Strangway et al.[3] for samples from Apollo 12 mission and was attributed by them to a "remagnetiz(ation) during the demagnetizing process," an observation with which we concur and forward the above physical explanation. In particular, we note that sometimes only one chip from a sample studied by the above group showed a zig-zag demagnetization curve which strongly supports our contention that sample inhomogeneity is the major culprit. Fuller (personal communication) has also made similar observations while demagnetizing rocks from Apollo 14 mission. It would appear then, that extreme caution is required in applying routine AF demagnetization technique to separate the stable component of NRM in rocks as commonly inhomogeneous as the lunar rocks. For example, it may be true that by proceeding to peak values of AF as large as 500 or 1000 Oe we will in the end be able to remove the secondary component of NRM in 15535,28 and thus recover the stable, primary component of interest. Alternatively, it can well be argued that the above procedure is likely to destroy the primary component itself. Under these circumstances, therefore, thermal demagnetization may be the preferred method for selective demagnetization

before proceeding with paleointensity measurements involving the stable component of NRM.

Acknowledgment: This work was supported by NASA grant NGR 24-005-248.

References

1. Runcorn, S. K., Collinson, D. W., O'Reilly, W., Stephenson, A., Battey, M. H., Manson, A. J. and Readman, P. W. (1971) Magnetic Properties of Apollo 12 Lunar Samples, Proc. R. Soc. Lond. A, 325, pp. 157-174.
2. Pearce, G. W., Strangway, D. W. and Larson, E. E. (1971) Magnetism of two Apollo 12 igneous rocks, Proc. Second Lunar Science Conference, 3, pp. 2451-2460.
3. Strangway, D. W., Pearce, G. W., Gose, W. A. and Timme, R. W. (1971) Remanent Magnetization of Lunar Samples, Earth and Planet. Sci. Letters, 13, pp. 43-52.

MAGNETIC PROPERTIES OF APOLLO 15 ROCKS AND FINES.

D.W.Collinson, S.K.Runcorn and A.Stephenson, Department of Geophysics and Planetary Physics, School of Physics, the University, Newcastle upon Tyne, England.

The magnetic properties of samples of Apollo 15 material have been investigated, following earlier work on lunar samples by this and other groups.[1,2,3] The existence of a hard component of magnetization in the latter rocks has aroused considerable interest, because its origin may be in an intrinsic lunar magnetic field which existed when the rocks were formed; this in turn bears on the internal structure of the moon at that time and subsequently during its history. The natural remanent magnetization (NRM) and other magnetic properties have now been studied in two chips each from samples 15085, 15499 and 15555 (basaltic) 15459 (fragmental) and 15086 (1 chip of soil breccia); a fines sample, 15101,75 has also been examined.

1. Remanent magnetization. Table 1 shows the intensity of NRM of the samples as received in the laboratory. Its response to A.F.demagnetization was similar to that found in earlier samples, namely soft and hard components were revealed, the intensity of the latter being about 1 x 10^{-6} emu/g in two of the basalts, but higher in the fragmental rock and soil breccia (Fig.1).

The direction of NRM of 15085,31 during demagnetization stabilises at about 120 Oe in an area about 110° away from that of the initial value, with an excursion of 60° off the path between the initial and final direction at 45 Oe, corresponding to the dip in the intensity curve (Fig.1). 15499,21 shows a steady movement of the NRM direction up to the maximum demagnetizing field of 350 Oe; in 15555,75 any hard component is clearly very weak, and above 75 Oe repeat readings at the same demagnetizing fields are rather scattered, although a roughly constant direction is indicated about 90° from the NRM direction. The fragmental sample, 15459,95 and soil breccia, 15086,12 showed a stable direction of NRM after removal of soft components up to 100 Oe, the hard component being associated with an intensity of around 10 x 10^{-6} emu/g.

Samples 15085,32, 15499,27 and 15459,96 were subjected to stepwise thermal demagnetization up to 810° C in a continuously pumped vacuum furnace ($< 5 \times 10^{-4}$ torr). No change in initial susceptibility was observed after each stage of heating in the basaltic samples, but the fragmental rock showed some changes above 600° C. All the samples showed an NRM which persisted up

Magnetic properties of Apollo 15 rocks

D.W.Collinson.

to the Curie point of iron, which, in keeping with previous results, points to iron or iron-nickel as the carrier of the remanence.

The intensity of NRM falls off rather rapidly up to between 100° C and 300° C, followed by an approximately constant intensity 'plateau' before decreasing again near the Curie point. 15459,96 shows a roughly constant direction in the plateau region, followed by a further change to another constant direction around 700° C; rather similar behaviour is shown by 15085, 32. As was found during A.F. demagnetization of 15499,21, sample 15499,27 showed a steady migration of NRM direction up to the Curie point.

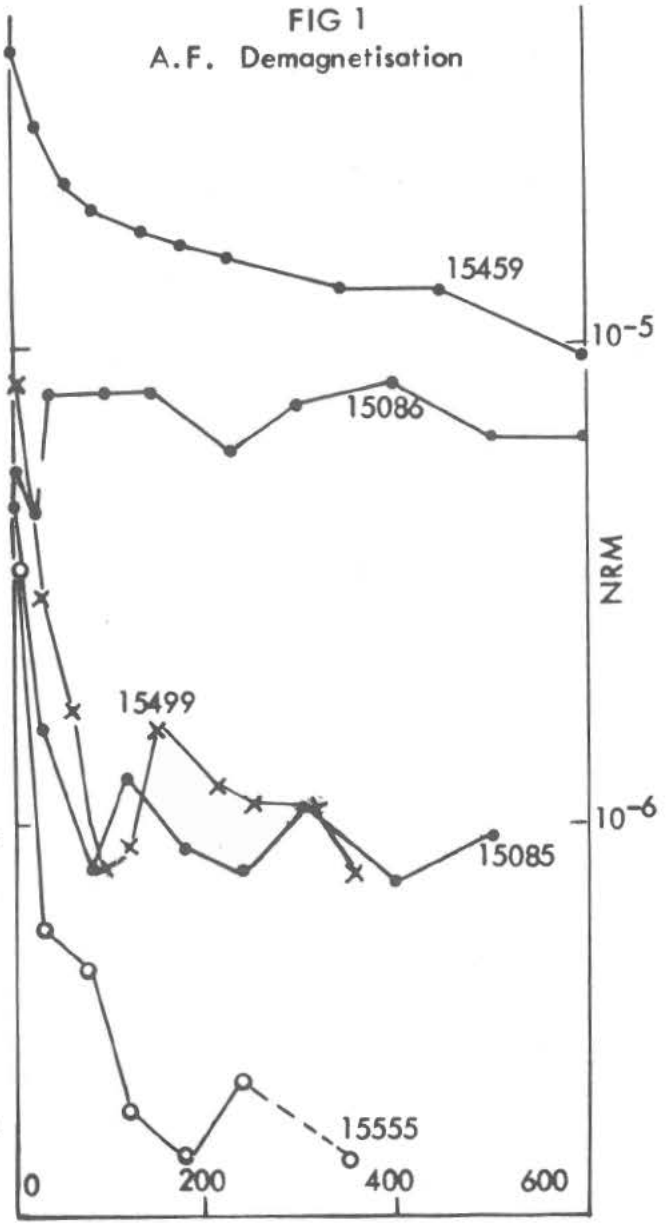

Viscous magnetization. The acquisition of VRM was measured in fields of 1.0 or 2.0 Oe. A strong VRM was acquired by 15459,95 and 15086,12, intensities of 214 and 130 x 10^{-6} emu/g being acquired in one week, with corresponding viscosity coefficients of 47.5 and 33.5 x 10^{-6} emu/g/Oe. This VRM was anomalously stable to A.F. demagnetization, fields in excess of 250 Oe and 150 Oe respectively being required to remove it in 15086,12 and 15459,95. The basaltic samples showed low viscosity coefficients of 0.7 x 10^{-6} (15499,21) and 0.08 x 10^{-6} (15555,75).

Artificial Thermoremanence. The TRM acquired by cooling samples from 800° C to room temperature in various weak fields was measured. In 15085,31 the A.F. demagnetization curve of the TRM acquired in 6000 and 2000 was similar in shape to that of the NRM, but the TRM intensity was not linear with the applied field. In 15499,21 the TRM intensity was proportional to field in the above range, and, by comparison of the 'hard' intensity of NRM and TRM an ambient field intensity of about 1000 ɣ is

Magnetic properties of Apollo 15 rocks.

D.W.Collinson.

estimated, on the assumption that the observed NRM was acquired as a TRM on the moon. Although any hard component of NRM in 15555,75 appears to be less than 0.3 x 10^{-6} emu/g in intensity, a very hard TRM is acquired which is proportional to field and of intensity 40 x 10^{-6} emu/g in 6000 γ.

2. Rock Magnetism. The samples can be divided magnetically into two distinct groups. The first consists of the fines, soil breccia and fragmental rock, in which the saturation isothermal remanent magnetization is 30 - 100 times greater than in the second group, the basaltic rocks (Table 1). The initial susceptibility of the two groups differ by an order of magnitude, with values of about 10^{-3} and 10^{-4} emu/g/Oe respectively, and significant differences between the two groups are also seen in the acquisition of VRM and the intensity of the hard component of NRM.

Sample	NRM x10^{6}	'Hard' NRM x10^{6}	IRM(sat) x10^{3}
15085,31	8.7	~ 1	-
32	7.1	-	0.65
15499,21	8.8	~ 1	-
27	15.4	-	0.67
15555,75	3.7	< 0.3	-
92	5.5		0.70
15086,12	5.5	"9	21
15459,95	42.6	~11	-
96	42.4	-	68

TABLE 1

The fines show almost identical behaviour to those of Apollo 11, the susceptibility being 2.2 x 10^{-3} emu/g/Oe and the Curie point 778°±3° C. Low temperature TRM amd IRM experiments yielded results which follow accurately theoretical curves proportional to log (293/T)[4]. This is indicative of a single domain size distribution of iron grains, with the number of grains within the volume range v to v +dv given by $N(v)dv = \beta v^{-2} dv$, where β is a constant. This holds at grain diameters of the order of 100 Å. 15459,95 also accurately followed the theoretical curve, and there is also evidence for this distribution in 15086,12. Calculated values for the coercivity (in the absence of thermal fluctuations) were not significantly different, being 1000 Oe and 1200 Oe respectively for the fines and 15459,95. The latter, when heated in air, exhibited a temperature-susceptibility curve very like that of the fines, with an iron Curie point (776°±3°), and on cooling, a second phase was produced with a Curie point of 333°±4° C. The fines, heated in an evacuated capsule, did not show this second phase.

When given a TRM in a field of 0.8 Oe between room temperature and - 196° C, subsequent demagnetization by warming in zero field produced a very marked transition at about - 140° C in samples 15555,75 and 15085,31. The low temperature TRM, which disappeared at the transition point, was 3.3 x 10^{-3} and 0.78 x 10^{-3} emu/g respectively. The transition temperature probably

represents a Curie point of a titanomagnetite very near to ulvöspinel in composition. This effect has also been observed in some Apollo 12 and 14 samples. None of the samples showed any evidence of magnetite.

ARM experiments. In a further attempt to obtain estimates of an ancient lunar field intensity, some samples were given an anhysteretic remanent magnetization in 0.6 Oe in a peak alternating field of 1200 Oe, which was sufficient to produce saturation of the ARM. The ARM was then demagnetized in an alternating field and the curves obtained compared with those of the NRM. While this process is not strictly comparable to giving the sample a TRM, it has the merit of avoiding irreversible changes which may take place on heating. In the three basaltic samples, the ARM in 0.6 Oe reached a saturation value which was within a factor of two of the NRM. However, for the soil breccia (15086,12) the saturation ARM in 0.6 Oe was 230 x 10^{-6} emu/g, about 50 times greater than the NRM. A possible explanation for this is that the original NRM of the sample has partly decayed after the disappearance of the lunar field. 15459,95 proved too unstable to measure. Comparison of the A.F. demagnetization curves of ARM and NRM showed comparable stability of the two magnetizations, but there was not sufficient correlation for an ancient field intensity to be derived, and thus for these samples the ARM experiments appear to be of limited value.

3. Discussion. As expected, iron (with or without a small nickel content) is the dominant magnetic material in the Apollo 15 rocks, and it carries the remanent magnetism. In all the samples measured, except perhaps 15555, a hard component of NRM is present which persists above 300 Oe during demagnetization. Of the basaltic samples, only 15085 provided an approximately stable direction of hard NRM; the direction in 15499,21 changed continuously up to 350 Oe (and up to 750° C during thermal demagnetization of 15499,27) and 15555,75, apart from possessing only a very weak or negligible hard magnetization, also showed very scattered directions after 75 Oe. This is puzzling, since the stable TRM that it can acquire shows that it possesses grains which might be expected to contribute a stronger hard component of NRM than is observed. The evidence in these samples for a simple magnetization history of a single thermoremanence event in a lunar field contributing the hard components is only good in the case of 15085, and the results from 15499 and 15555 are more difficult to interpret. As noted before[a], there appears to be the possibility of several components of magnetization being present, from the behaviour of the NRM directions and the shape of the demagnetization curves.

The soil breccia and fragmental rock have interesting properties. Not only do they possess a strong stable component

Magnetic properties of Apollo 15 rocks.

D.W.Collinson.

of NRM, but they also have the property of rapid acquisition of VRM, which itself shows high stability and may, in fact, contribute to the observed hard component of NRM in these samples. These two rocks clearly contain a wider range of grain sizes of iron than the basaltic rocks, and are comparable with the fines in this respect. The Apollo 15 fragmental rock, 15459, has quite different properties compared with those from Apollo 14 studied by the authors[3]; the latter were more similar magnetically to the Apollo 14 basaltic material. The evidence from the NRM of the Apollo 15 material is somewhat conflicting, but it may be said that it is not inconsistent with the NRM being acquired by thermoremanence in a weak lunar field, although the detailed magnetization history appears to be complicated.

No further evidence has been found for the origin of the soft component of magnetization. There are again significant decreases observed during thermal demagnetization up to 100°C, which suggests an origin (at least in part) after removal of the rocks from the lunar surface. There is also no evidence as to the cause of the very weak ambient magnetic field recorded at the Apollo 15 site ($6 \pm 6\gamma$). The initial NRM of the samples is comparable with that found in the rocks from previous missions, and one explanation may be that the site is further from an 'edge' or discontinuity in the rock underlying the site.

Acknowledgements. We are grateful to N.A.S.A. for providing the samples under the Lunar Sample Analysis Program, British participation in which is facilitated by the Science Research Council. One of us (A.S.) gratefully acknowledges the tenure of a N.E.R.C. Senior Research Associateship.

References.

1. Runcorn,S.K., Collinson,D.W., O'Reilly,W., Battey,M.H., Stephenson,A., Jones,J.M., Manson,A.J. and Readman,P.W. (1970). Proc. Apollo 11 Lunar Sci. Conf. 3, 2369.
2. Runcorn,S.K., Collinson,D.W., O'Reilly,W., Stephenson,A., Battey,M.H., Manson,A.J. and Readman,P.W. (1971). Proc.Roy. Soc.Lond. A. 325, 157.
3. Collinson,D.W., Runcorn,S.K., and Stephenson,A., (1972). Proc.3rd. Lunar Sci. Conf., MIT Press. (in press).

(Refs.1 and 3 contain reports by other groups investigating magnetic properties of lunar rocks.)

4. Stephenson,A. (1971). Phys. Earth and Planetary Interiors, 4, 353, 361.

MAGNETISM OF APOLLO 15 SAMPLES. W. A. Gose, LSI, Houston, TX 77058, G. W. Pearce, LSI, Houston, TX 77058 and University of Toronto, Toronto, Canada, D. W. Strangway, MSC, Houston, Texas 77058 and J. Carnes, Lockheed Electronics Co., Houston, TX 77058.

Natural Remanent Magnetism (NRM) - At this point we have examined the magnetic properties of five samples from the Apollo 15 mission in some detail. These samples are 15415, anorthosite; 15595, Rille edge basalt; 15498, breccia; 15076; gabbro; and 15016, basalt. The magnetization of these samples as received is shown in the histogram (figure 1). Here it can be seen that the anorthosite is weakly magnetic while the breccia is two orders of magnitude more magnetic. The remaining samples have remanent magnetizations that are very similar to the NRM values found on samples from other missions (1). In addition to these samples, we measured eighteen ZF samples using the Develco cryogenic magnetometer (ZF samples cannot be exposed to alternating fields or to the spinning of typical magnetometers). The data from these samples are also shown in the histogram of figure 1. The bulk of these rocks had NRM values much like those from the earlier missions confirming that most of the lunar igneous rocks have NRM close to 10^{-5}emu/gm. The few breccias measured tend to be somewhat more magnetic presumably due to the greater iron content.

Alternating Field Demagnetization - The results of demagnetizing by alternating fields are illustrated in figure 2. The anorthosite sample is very weak and quite hard to measure but it appears to have a stable component of about 2×10^{-7}emu/gm, far weaker than any other sample we have measured to date. The other igneous rocks have the now classical behavior showing a soft component in random directions which can be eliminated in a few tens of oersteds to yield a stable component of magnetization. As was shown by returning a sample to the moon on Apollo 16 (2) the soft component is likely of spacecraft origin. This finding is in agreement with earlier results by Strangway et al (3) as well as the NRM data for samples 15595,0, 15595,10 and 15596,0 all of which come from the same boulder at the rim of Hadley Rille. Their NRM directions of magnetization are random and thus unlikely of lunar origin. We were only permitted to demagnetize 15595,10 and 15595,13, a non-oriented chip. On demagnetization, a stable direction was found which should be the direction of magnetization of the bedrock since the boulder from which it comes is considered probable bedrock (Figure 3).

Sample 15498 is a very unusual sample among our studies to date. It is extremely stable magnetically and barely changes direction or intensity on demagnetization (figure 4).

Viscous Remanent Magnetization (VRM) - We have examined the time-dependent magnetic properties of several of our Apollo 15 samples continuing the detailed investigations reported by Gose et al, (4). Sample 15498, for example, a breccia of unknown metamorphic grade, shows a classical Richter-type after effect similar to that seen in class 1 and 2 metamorphic grade

MAGNETISM OF APOLLO 15 SAMPLES

W. A. Gose

breccias from Apollo 14 (figure 5). This behavior is typical of rocks which contain iron grains a few hundred Angstroms in size. The high magnetic stability is undoubtedly due to the presence of single domain grains.

Conglomerate Test - It has been pointed out earlier (5) that since most of the samples returned from the moon are believed to have been "tumbled" into their present position, that the directions of magnetization would be random if they come from a uniformly magnetized and magnetically stable bedrock. In the Apollo 15 samples we have been able to add three directions to our earlier results. As seen in figure 6 this suggests that the samples are indeed randomly magnetized (stable components only). This confirms, but does not prove, that the samples have preserved their magnetization for a long time. Certainly they have not been remagnetized by a recent uniform field.

Magnetic Properties - Hysteresis loops have been run on rock samples 15016, 15076, 15498, 15595 and soil samples 15301 and 15601. These results are tabulated in Table I. The igneous rocks, as we have reported for samples

TABLE I

Sample	Type	J_s emu/gm	χ_p (gm^{-1})	J_{rs} emu/gm	H_c oe.	H_{Rc} oe.	J_{rs}/J_s	Equiv. % Fe
15016	Igneous	0.145	41.2×10^{-6}	-	-	-	-	0.067
15076	Igneous	0.216	36.6	-	-	-	-	0.099
15301	Soil	1.05	33.0	0.050	20	400	0.047	0.48
15498	Breccia	0.75	36.9	0.066	78	770	0.088	0.34
15595	Igneous	.140	40.3	-	-	-	-	.064
15601	Soil	1.05	42.8	0.076	38	450	0.073	0.48

of previous Apollo missions (1), have less than 0.1% Fe while the soils and breccias approach 0.5% Fe. This continues to confirm earlier statements by many workers that the soils have excess iron. Only a small part of this can be of meteoritic origin since very little thermal hysteresis is seen (figure 7) although a high nickel alloy with a Curie temperature of 250 - 300°C is suggested. Rather it seems to us that much of the excess iron is due to subsolidus reduction during impact heating of the soils (6), or to other mechanisms liberating iron from the material of the soil itself. The high magnetic stability, referred to above, of 15498 is also shown by the unusually high remanence coercive force, H_{Rc}, possessed by this sample.

References:

1. W. A. Gose, G. W. Pearce, D. W. Strangway and E. E. Larson, The Moon, in press, 1972.
2. G. W. Pearce and D. W. Strangway, Apollo 16 Preliminary Science Report, in press, 1972.

MAGNETISM OF APOLLO 15 SAMPLES

W. A. Gose

3. D. W. Strangway, G. W. Pearce, W. A. Gose and R. W. Timme, Earth Planet. Sci. Letters, 13, 43-52, 1971.
4. W. A. Gose, G. W. Pearce, D. W. Strangway and E. E. Larson, Geochim. Cosmochim. Acta, Suppl. 3, in press, 1972.
5. G. W. Pearce, D. W. Strangway and W. A. Gose, Geochim. Cosmochim. Acta, Suppl. 3, in press, 1972.
6. G. W. Pearce, R. J. Williams and D. S. McKay, Earth Planet. Sci. Letters, in press, 1972.

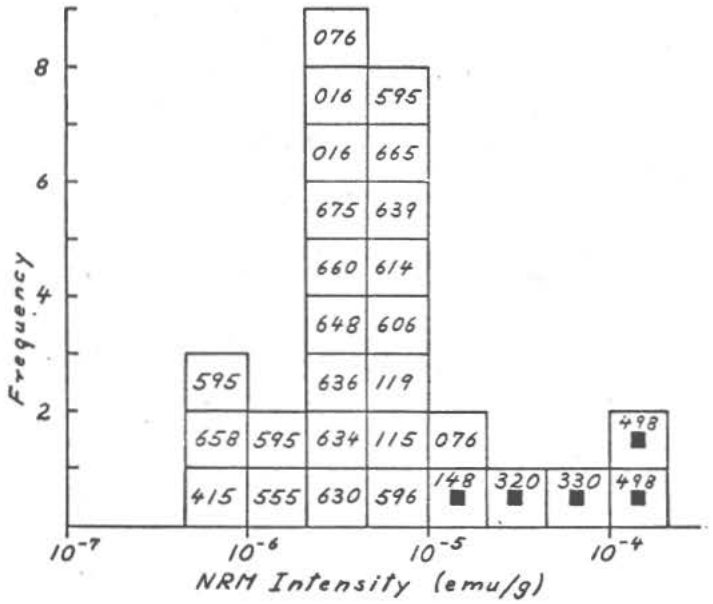

Figure 1

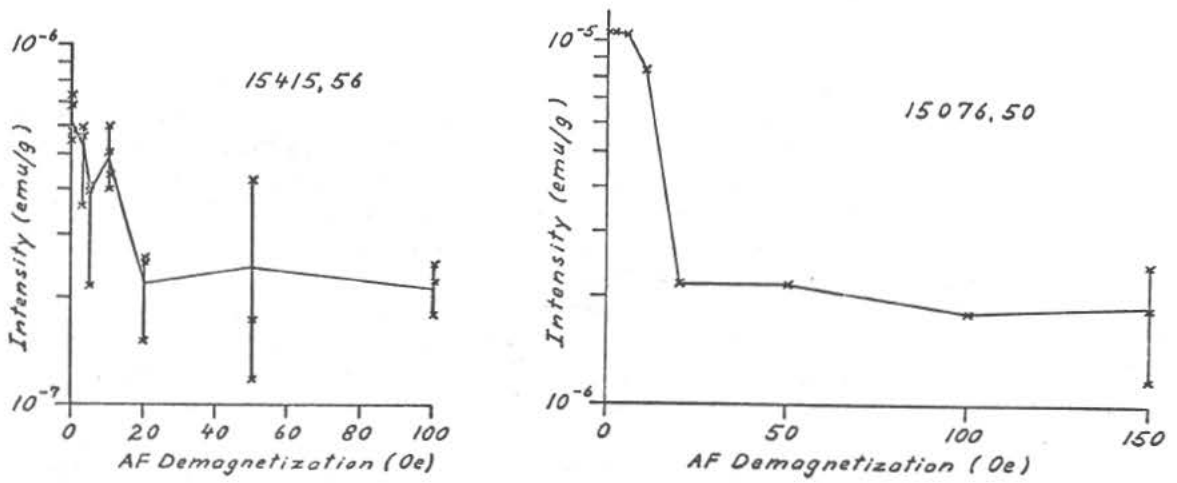

Figure 2

MAGNETISM OF APOLLO 15 SAMPLES

W. A. Gose

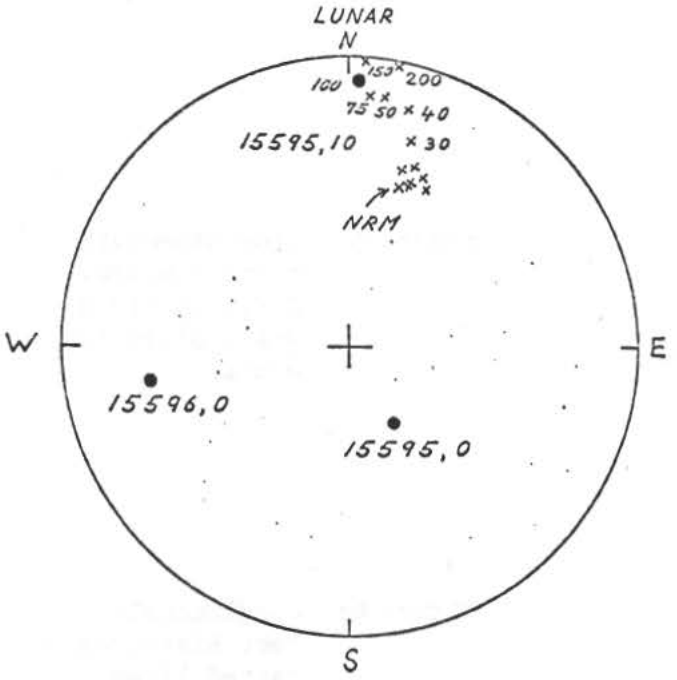

Figure 3: Direction of magnetization of three samples from the same boulder. X are lower hemisphere, ● are upper hemisphere.

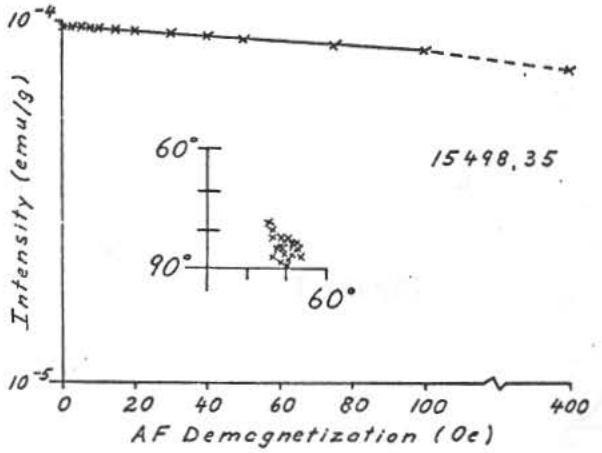

Figure 4

MAGNETISM OF APOLLO 15 SAMPLES

W. A. Gose

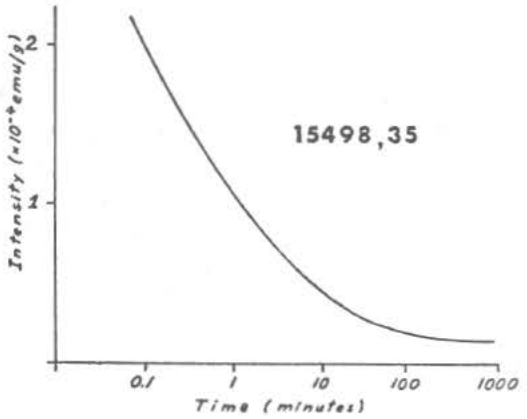

Figure 5: Time dependent magnetization. A 2.5 Oe field was applied for 8 min.

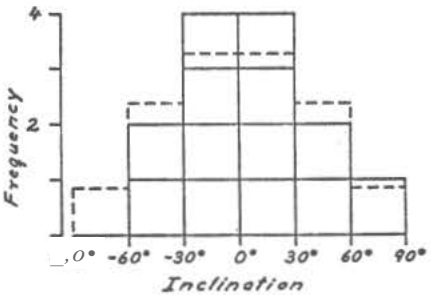

Figure 6: Conglomerate Test Histogram - dashed lines represent expected random distribution

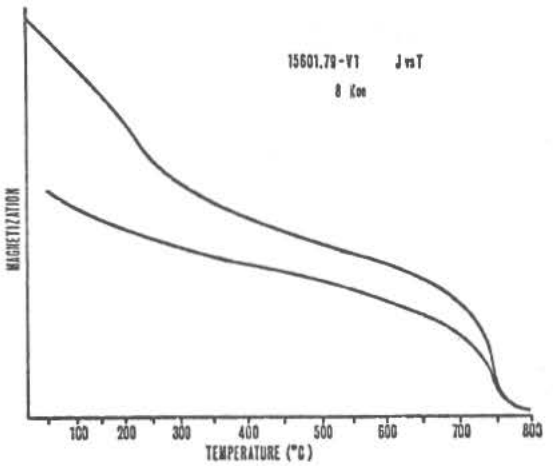

Figure 7

FERROMAGNETIC RESONANCE OF SMALL, MULTIDOMAIN IRON PARTICLES IN AN 0.5-CM FRAGMENT OF LUNAR GLASS, 15434, 62.

D. L. Griscom and C. L. Marquardt, Naval Research Laboratory, Washington, D. C. 20390

Ferromagnetic resonance (FMR) absorptions have been observed at X-band in a 130-mg fragment of Apollo 15 glass at 300°K and 77°K. Supplementary measurements were performed at Ka-band and 300°K on several < 1mg chips of this sample. The data, when compared with those for simulated lunar glasses known to contain metallic iron, lead to the conclusion that the primary resonance at X-band results from small, multidomain particles of iron. This resonance is distinct from the "characteristic" resonance[1] which was also identified in 15434, 62 with a specific intensity ~ 3000 times smaller than observed for typical < 1-mm fines, consistent with the observation[2] that the latter signal is generally proportional to the specific surface area of the as-returned sample.

Sample 15434, 62 was opaque to macroscopic viewing with ~ 70% of its surface comprising lusterous, conchoidal faces exhibiting faint flow banding but no obvious vesicles or inclusions. The remaining surface was dull gray and relatively smooth except for a number of cracks and fissures. Aside from some fine grained inclusions in this surface, no contacts were evident. Small chips were pale green in transmitted light.

Figure 1 shows the FMR spectra of 15434, 62 in comparison with those of a synthetic glass[3] known to contain octahedral crystals of iron ~3 μm. The field axes of the spectra obtained at 9.1 and 35.5 GHz have been telescoped to emphasize probable correspondences of spectral features. The splittings H_{A1}, H_{A2}, and H_D are ad hoc definitions. However, the significance of H_D will be emphasized. It has been noted that H_D is independent of changes in frequency between 9.1 and 9.53 GHz (the range of the X-band spectrometer), while no splitting H_D is manifest at Ka-band. These properties are not peculiar to the present samples but appear to be general to "Type-II" resonances[2] which have been attributed to metallic iron precipitates in silicate glasses.

The various laboratory fields H_{app} at which resonance occurs are given by

$$H_{app} = h\nu/g_{eff}\beta - H_{int} \quad , \qquad (1)$$

where ν is the spectrometer frequency, $g_{eff} \approx 2$ for metallic iron, h is Planck's constant, β is the Bohr magneton, and H_{int} is the net internal

FMR OF MULTIDOMAIN IRON IN LUNAR GLASSES

D. L. Griscom

field due to anisotropy, surface poles, etc. In a glass or powder, angular averaging gives rise to a broad, smeared-out range of values for H_{int}. However, in view of the sizeable term linear in ν, the frequency independence of H_D presents a seeming paradox which is resolved as follows:

It is postulated that X-band spectra of the type shown in Fig. 1 are due to small, multidomain particles of metallic iron. The resonance absorption between zero field and 3.2 kOe ($\approx h\nu/2\beta$) takes place in domains whose magnetization vectors have positive projections on H_{app}; i.e., in "aligned" domains where H_{int} assists H_{app}. The absorption for $H_{app} > 3.2$ kOe occurs in domains which are "anti-aligned", wherein H_{int} opposes H_{app}. However, as magnetic saturation is approached the sizes and numbers of anti-aligned domains go to zero. For a 400-Å, two-domain cube of iron, a theoretical treatment[4] indicates the anti-aligned domain will disappear at $H_{app} \approx 6$ kOe. This process, of course, is independent of the resonance phenomenon. Thus the frequency-dependent absorption of microwave energy by anti-aligned domains is limited by the frequency-independent saturation process, giving rise to the observed line shape. It is expected, then, that $H_D = DM_s(T)$, where D is a demagnetization factor (empirically determined to be $\sim 4\pi/3$) and $M_s(T)$ is the saturation magnetization at temperature T. Indeed, it has been found the temperature dependence of H_D for another lunar glass particle (10084, 170, 5a)[2] closely follows the magnetization-vs-temperature curve for 12%Ni-Fe.[5]

It is concluded that the resonance line shapes at X-band are determined by domain effects. For $H_{app} > 10$ kOe all particles become saturated and the Ka-band spectra can be described by Eq. (1) with $g_{eff} \approx 2.17$ and $H_{int} \sim \pm H_{A1,2}/2$. H_{A1} and H_{A2} are assumed to be anisotropy splittings. Both are too large to be accounted for by the magnetocrystalline anisotropy alone ($2K_1/M_s \approx 500$ Oe for Fe). H_{A1} is believed to result from the cubic shape anisotropy of the Fe octahedra. Since $H_{A2} < H_{A1}$, it is inferred that the iron particles in 15434, 62 are probably spheroidal. Both the magnitude and temperature dependence of H_D for this sample suggest that these particles may contain 25±5% Ni.[5] Comparisons of the specific signal intensities of the lunar and simulated[3] glasses lead to the estimate that 15434, 62 contains ~ 0.4 wt% metallic Fe in particle sizes ranging from ~ 300Å (threshold for multidomain behavior) to ~ 1μm (the microwave skin depth).

[1] For reasonably complete references, c.f., Ref. 2.

[2] D. L. Griscom and C. L. Marquardt, Proc. Third Lunar Sci. Conf., Geochim. Cosmochim. Acta, Suppl. 3, Vol. 3 (in press).

[3] This sample, which was quenched from a melt having the nominal composition of rock 10017, was generously provided by R. M. Housley who also

communicated the results of optical, susceptibility, and Mössbauer determinations of its iron content.

[4] H. Amar, Phys. Rev. 111, 149 (1958); J. Appl. Phys. 29, 542 (1958).

[5] D. L. Griscom and C. L. Marquardt, (to be published).

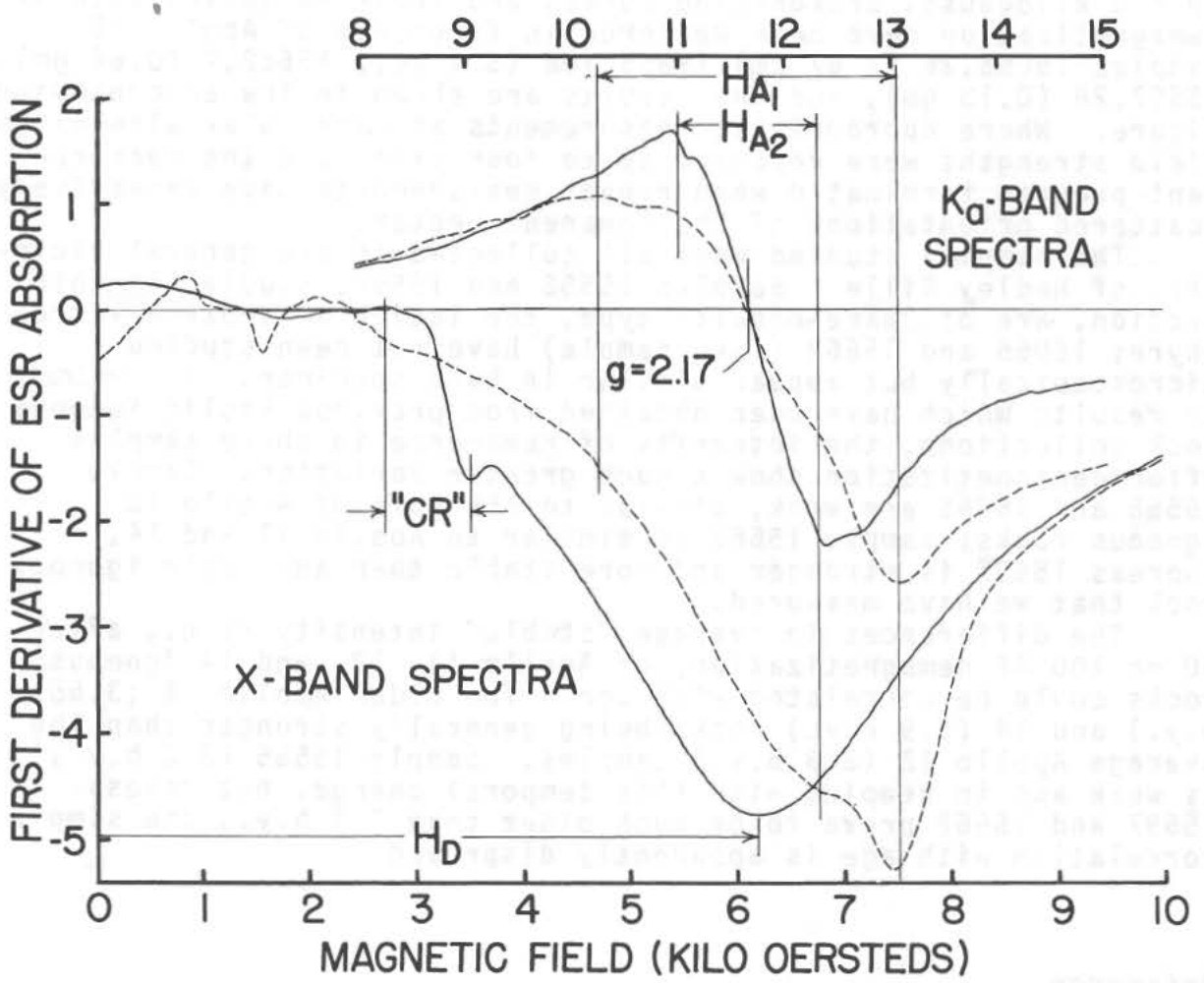

Figure 1. FMR spectra of lunar glass 15434, 62 are compared with those of a simulated lunar glass[3] containing metallic iron precipitates (dashed curves). "CR" designates the "characteristic" resonance.[1]

REMANENT MAGNETISM IN FOUR APOLLO 15 IGNEOUS ROCK FRAGMENTS: R. B. Hargraves and N. Dorety, Dept. of Geol. Geophys. Sci., Princeton Univ., Princeton, N. J. 08540.

Intensity of NRM (solid-line curves) and saturated IRM (H = 8 kilogauss, broken-line curve) and their variation with AF demagnetization have been measured in fragments of Apollo 15 samples 15065,26 (3.67 gm) 15555,108 (5.4 gm), 15662,2 (0.64 gm), 15597,28 (0.13 gm), and the results are shown in the accompanying Figure. Where appropriate, measurements at particular alternating field strengths were repeated up to four times and the measurement program terminated when repeat measurements gave excessively scattered orientations of the remanent vector.

The samples studied were all collected in the general vicinity of Hadley Rille. Samples 15555 and 15597, studied in thin section, are of "mare-basalt" type, the latter a pyroxene vitrophyre; 15065 and 15662 (rake sample) have not been studied microscopically but appear similar in hand specimen. In contrast to results which have been obtained from previous Apollo igneous rock collections, the intensity of remanence in these samples after demagnetization show a much greater variation. Sample 15555 and 15065 are weak, similar to the bulk of Apollo 12 igneous rocks; sample 15662 is similar to Apollo 11 and 14, whereas 15597 is stronger and more stable than any lunar igneous rock that we have measured.

The differences in average "stable" intensity (i.e., after 50 or 100 AF demagnetization) of Apollo 11, 12, and 14 igneous rocks could be correlated with age: The older Apollo 11 (3.65 b.y.) and 14 (3.9 b.y.) rocks being generally stronger than the average Apollo 12 (3.3 b.y.) samples. Sample 15555 (3.3 b.y.)[1] is weak and in keeping with this temporal change, but unless 15597 and 15662 prove to be much older than 3.3 b.y., the simple correlation with age is apparently disproved.

Reference

[1]Schaeffer, O. A., Husain, L., Sutler, J., Funkhouser, J., 1972 The ages of lunar material from Fra Mauro and Hadley Rille - Apennine Front area, (Abs.) Revised Abstracts Third Lunar Science Conference, 675-677.

Remanent Magnetism in Four Apollo 15 Samples

R.B. Hargraves

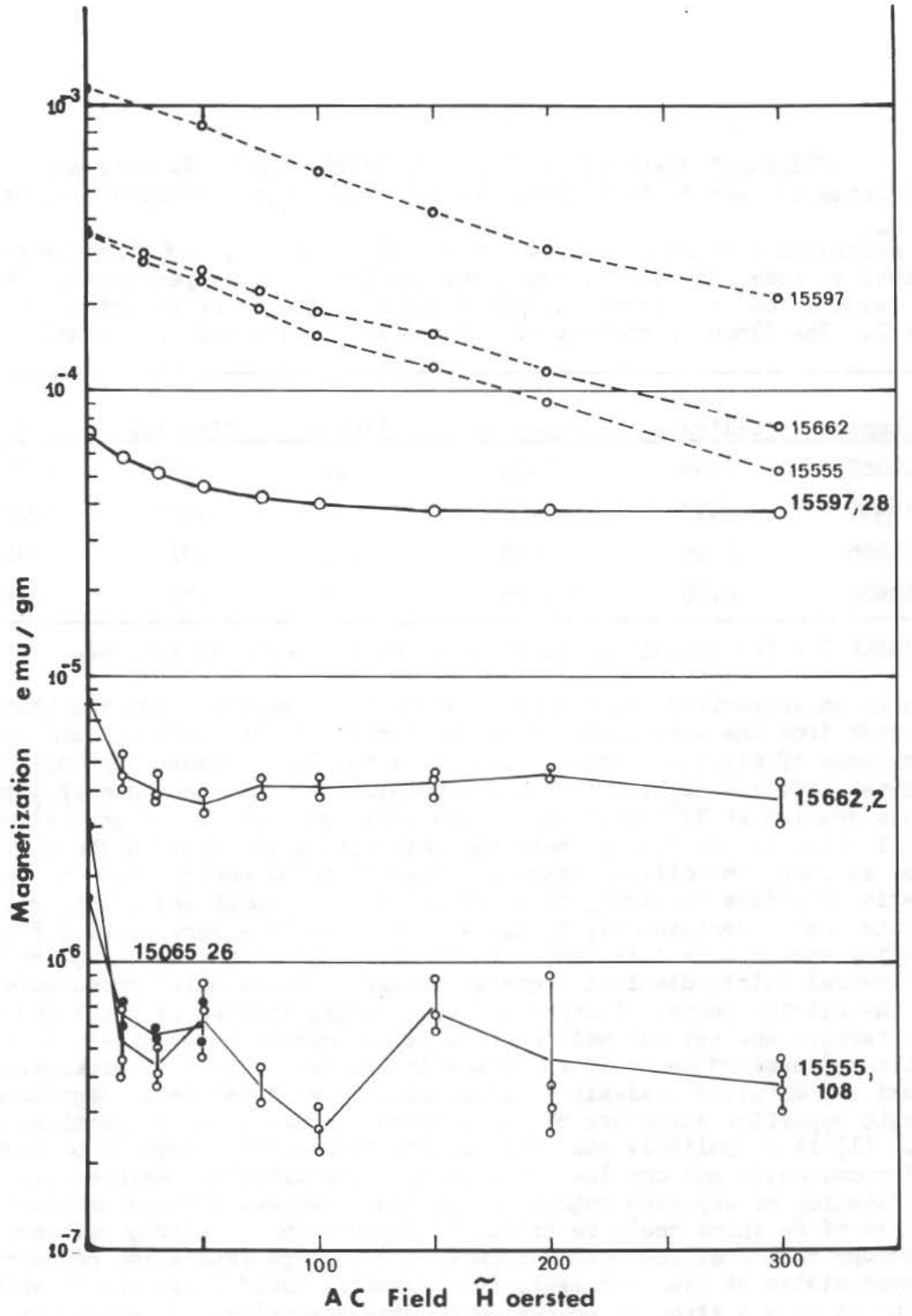

MÖSSBAUER ANALYSES OF APOLLO 15 SAMPLES by G. P. Huffman, F. C. Schwerer, and R. M. Fisher, U.S.Steel Res. Lab., Monroeville, Pa. 15146

Mössbauer spectra of samples 15058, 15495, 15555, and 15556 have been obtained at room, liquid nitrogen, and liquid helium temperatures. Preliminary results for the fractional phase distribution of Fe are given in Table I. The ilmenite content of all samples is low and only sample 15556

Sample	Total Silicate	Pyroxene	Olivine	Ilmenite	Fe
15058	0.98	0.98	~ 0.0	.012	<.01
15495	0.98	0.98	~ 0.0	.015	<.01
15555	0.98	~ 0.73	~ 0.25	.013	<.01
15556	0.96	~ 0.96	~ 0.15	.02	.02

TABLE I - Fractional distribution of Fe in Apollo 15 samples.

contains an appreciable amount of metallic Fe. Samples 15555 and 15556, collected from the same vicinity on the lunar surface, both contain sizable percentages of olivine. This is seen from the large quadrupole splitting of the outer silicate doublet at room temperature and the increase of intensity of this doublet at 77°K when the pyroxene M1 peaks shift outward,[1] as shown in Fig. 1. At 4.5°K, where the spin relaxation time in the silicate phases is long, the olivine makes a rather striking contribution to the magnetic hyperfine spectrum, as shown in Fig. 2. 15058 and 15495, whose silicate phases contain only pyroxene, both exhibit a very broad diffuse hyperfine spectrum at this temperature; 15555 and 15556, on the other hand show several fairly distinct magnetic hyperfine peaks which presumably arise from the olivine phase. Further low temperature studies of these and other lunar samples and several well characterized terrestrial minerals as a function of applied magnetic field are in progress and it is premature to attempt any detailed analysis of these spectra at this time. Regarding the magnetic hyperfine structure of the olivine, however, two suggestions can be made. (1) It is unlikely that the olivine is Fe-rich enough to be truly antiferromagnetic and our low temperature susceptibility measurements give no indication of any such magnetic ordering; however, superparamagnetic clusters of Fe spins could be frozen in orientation by strong exchange anisotropy fields at low temperatures. (2) A large separation between d electron states of $|xy\rangle$ and $|xz\rangle$, $|yz\rangle$ symmetry could cause the Fe spins in olivine to have a strongly preferred crystal direction.[1] Either of these

"MÖSSBAUER ANALYSES OF APOLLO 15 SAMPLES

G. P. Huffman

possibilities could give rise to rather distinct magnetic hyperfine structure of the type seen in Fig. 2.

(1) F. C. Schwerer, G. P. Huffman, R. M. Fisher and T. Nagata, Proc. 3rd Lunar Sci. Conf., Suppl. 3, Geochim. Cosochim. Acta, v. III.

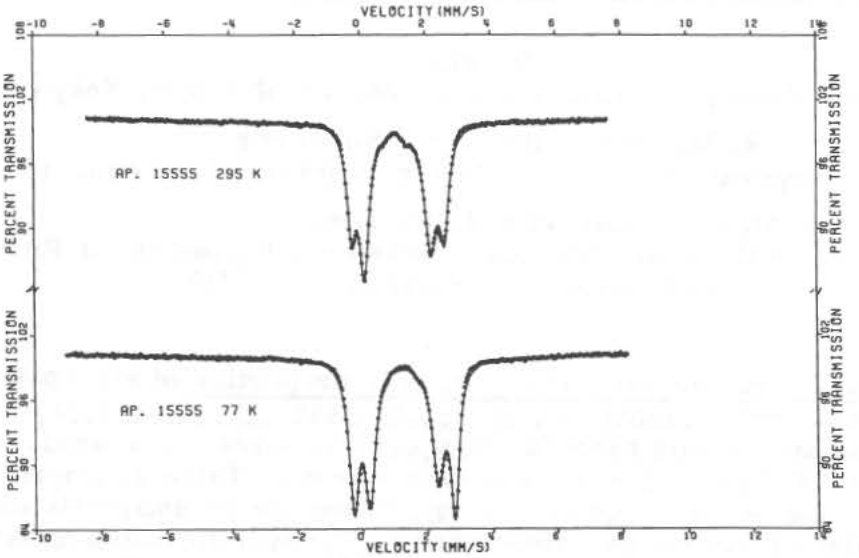

FIG. 1 - Spectra of 15555 at 295 (top) and 77°K (bottom).

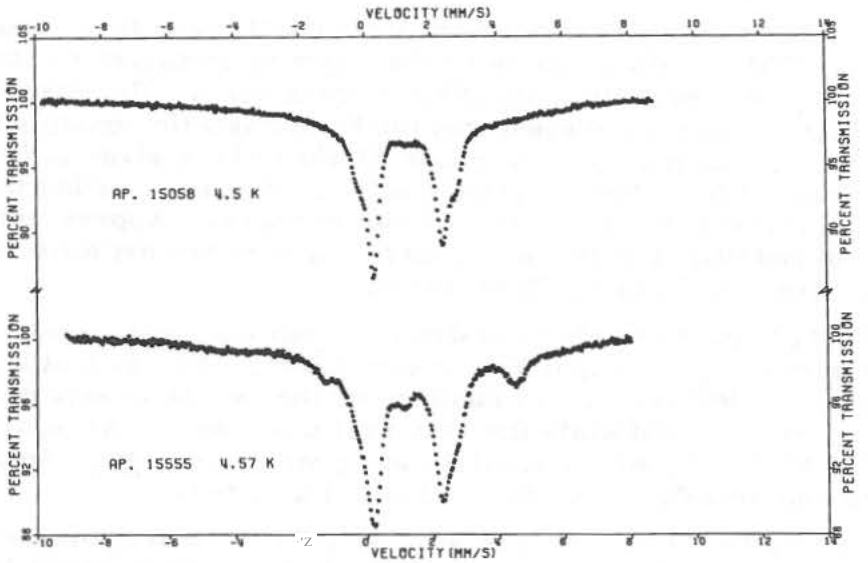

FIG. 2 - Spectra of 15058 (top) and 15555 (bottom) at 4.5°K.

Summary of Rock Magnetism of Apollo 15 Lunar Materials

T. Nagata
Geophysics Research Laboratory, University of Tokyo, Tokyo, Japan,

R. M. Fisher and F. C. Schwerer
U.S.Steel Corporation Research Center, Monroeville, Penn. 15146

and M. D. Fuller and J. R. Dunn
Department of Earth and Planetary Sciences, University of Pittsburgh, Pittsburgh, Pennsylvania, 15213

(1) Intrinsic and structure-sensitive magnetic properties of six Apollo 15 materials (igneous rocks, 15058,55, 15495,52, 15555,132, 15556,37, and 15556,38 and an anorthosite breccia 15418,41) have been measured. The magnetic properties of these materials are summarized in Table 1, where χ_o: initial specific magnetic susceptibility, χ_a : specific paramagnetic susceptibility, I_s : specific value of saturation magnetization, I_R : specific value of saturation remanent magnetization, H_c : coercive force, $(H)_c$: apparent Curie temperature, $(H)_c$*: apparent lower Curie temperature in the cooling process, I_n : specific intensity of natural remanent magnetization, and W(Fe): estimated weight percentage of contained metallic iron.

As shown in Table 1, an anorthosite breccia (15418) and three specimens of basaltic rock (15556) contain kamacite as the major ferromagnetic constituent, having upper and lower magnetic transition temperatures. Results of analyses of the thermomagnetic curves suggest that the ferromagnetic constituent in these sample consists of a kamacite phase, whose Ni/Fe ratio is given in the table, and a CoFe alloy phase of less than 1 weight % of Co. It must be noted that the kamacite phase is first found in the lunar igneous rocks. Approximate values of the abundance of metallic iron (W(Fe)) in these samples are estimated from I_s values to range from 0.052 to 0.076 weight %.

Sample 15556,38 consists of two distinctly separable phases, i.e.(1) a dark black colored part and (2) a bright gray colored part. The magnetic properties and the intensity of NRM have been examined for the two parts separately. The black part has a strong NRM while the gray part has a weak NRM which is roughly equal to NRM of 15556,37, which has the same gray color. χ_o, I_R and H_c of the former are appreciably larger than those of the latter.

I_R and H_c of Apollo 15 samples are very small at room temperature, but as shown in Fig. 1 for example, they discontinuously increase at about 105°K when these samples are cooled down to 4.2°K. In Table 1, the observed values of I_R and H_c at 4.2°K as well as at 300°K for other Apollo 15 samples are summarized,

Table 1. Magnetic Properties of Apollo 15 Lunar Materials

Magnetic Parameter	Temperature	15058,55	15418,41	15495,52	15555,132	15556,37	15556 38,1	15556 38,2	Unit
	(°K)								
χ_o	300	4.54	0.86	–	–	2.58	4.46	2.52	$\times 10^{-4}$ (*)
χ_a	300	3.5	1.46	3.82	3.82	3.8	4.3	4.1	$\times 10^{-5}$ (*)
	4.2	68.0	22.7	85.8	68.5	74.4	75.5	77.4	"
I_s	300	0.125	0.145	0.165	0.127	0.125	0.124	0.114	emu/gm
	100	–	0.190	0.167	0.125	0.131	0.14	0.14	"
I_R	300	10	13	7.5	10	15	19	7	$\times 10^{-4}$ (*)
	4.2	7	1.8	7.8	6.8	8.0	8.6	7.6	$\times 10^{-2}$ (*)
H_c	300	~10	~10	~10	7	<10	17	~10	Oe
	4.2	89	45	87	70	90	102	90	"
T*		110	No sharp change	120	105	110	105	105	°K
Ⓗc		790	765	–	–	784	786	782	°C
Ⓗc*			668			668	641	668	°C
I_n		10.6	7.6	–	7.3	3.5	88.4	5.8	$\times 10^{-6}$ (*)
W(Fe)		0.057	0.067	0.076	0.058	0.057	0.057	0.052	weight %
Ni/Fe Ratio		~0	4.0 (±.5)	–	–	4.0 (±.5)	5.5 (±.5)	4.0 (±.5)	weight %

(*) emu/gm in Unit.

where T* represents the temperature at which H_c and I_R sharply change. (However, no sharp change in H_c and I_R is observed for an anorthosite breccia 15418,41). Since no magnetic transition is observed around 100°K, the sharp change in H_c and I_R may represent the blocking phenomenon of extremely fine metallic iron particles; namely, T* may represent the blocking temperature Tb. If this interpretation is right, the mean diameter of the dominant metallic iron particles is estimated to be about 140 Å. It has been actually demonstrated that a basaltic rock, 15556,38, can have a conspicuous viscous magnetization at room temperature.

(2) The natural remanent magnetization (NRM) of Apollo 15 samples and its stability against the storage in a non-magnetic space, the AF-demagnetization and the thermal demagnetization have been examined.

Four samples (15058,70, 15418,46, 15556,37, and 15556,38) had been

Fig 1 (A)

COERCIVE FORCE (H_c) vs TEMPERATURE (T)

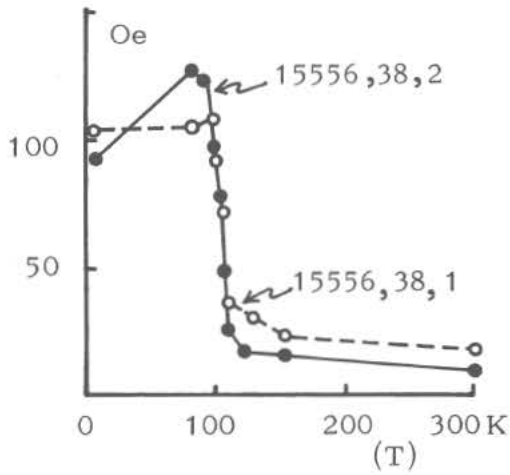

Fig. 1 (B)

SATURATION REMANENT MAGNETIZATION (I_R) vs TEMPERATURE (T)

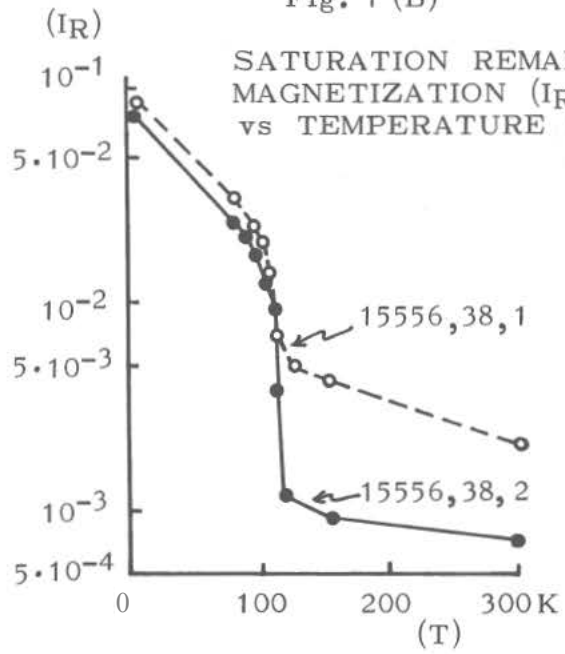

stored during about 90 days in a double-shielded high-μ metal capsule, in which the magnetic field intensity is less than 5 gammas. The observed change of NRM intensity during the storage is less than 10%. The direction of NRM also had been conserved within a solid angle of about 15 degrees in diameter. Thus, a hypothesis that the NRM's of these samples are acquired as VRM in the geomagnetic field, could be eliminated.

NRM's of five samples (15058,55, 15418,41, 15556,37, 15556,38,1, and -2) have been AF-demagnetized. The effective AF-demagnetization field, $\tilde{H}_o$ and the critical AF-demagnetization field, $\tilde{H}^*$, of these samples (Nagata et al 1971 and 1972) are summarized, together with the intensity of NRM's, in Table 2, where h represents the intensity of static magnetic field which can produce IRM whose intensity is the same as that of NRM, while $\tilde{H}'_o$ denotes the effective AF-demagnetization field for the IRM acquired in h. $\tilde{H}_o$ values of NRM's are considerably larger than $\tilde{H}'_o$ values of the equivalent IRM's. It may hardly be possible to attribute the observed NRM's (particularly for samples 15418 and 15556) to the artificial IRM's acquired in h field.

As already pointed out (Nagata et al 1972, Pearce et al 1972), some samples (15058,55, 15418,41, 15556,37, and 15556,38,2) have a hard component of NRM, whose intensity is about 1×10^{-6}emu/gm and whose direction is kept reasonably invariant for the AF-demagnetization fields larger than 100 Oe.rms. In these samples, the stability of the softer component is represented by $\tilde{H}_o$ and $\tilde{H}^*$ in Table 2.

Results of the thermal demagnetization experiments on samples 15058,70 and 15418,46 seem to suggest that NRM's of these two samples are attributable to TRM acquired by cooling from 300°C at most.

Table 2. NRM and its stability of Apollo 15 materials

Sample	15058,55	15418,41	15556,37	15556,38,1	15556,38,2	Unit
I_n	18.8	6.4	3.4	88.4	5.8	$\times 10^{-6}$ emu/gm
$\tilde{H}_o$	9	52	25	35	14	Oe.rms
$\tilde{H}^*$	15	60	10	40	20	Oe.rms
h	13	19	9	38	17	Oe
$\tilde{H'}_o$	4	4	3	17	5	Oe.rms

(3) Artificial acquisitions of remanent magnetization were experimentally demonstrated for four samples. Results of TRM acquisition experiments have indicated that PTRM of samples 15048 and 15556,37 is most efficiently acquired by cooling from 300°C to 20°C and from 800°C and 700°C. If the stable component of NRM of these two samples can be attributed to the PTRM, the ambient lunar magnetic field is estimated to be about 2,000 gammas. PTRM of sample 15418,46 is the largest for 800-600°C. The ambient lunar magnetic field deduced from the TRM hypothesis for the stable component of NRM is also about 2,000 gammas.

Experimental results of the acquisition of static pressure remanent magnetization (PRM) on sample 15418,41 have shown that the observed NRM could be produced by a pressure impact of 50 k bars in a magnetic field of about 800 gammas.

(4) Concluding remarks :

Because of the dominant presence of extremely fine particles of metallic iron in Apollo 15 basalts, the reliability of NRM of these samples is considerably less than that of the previous Apollo lunar rock samples. Nevertheless, it seems that the ambient lunar magnetic field of 1000-2000 gammas could produce TRM or PRM of the same intensity as observed as NRM of these Apollo 15 samples.

References

Nagata, T., Fisher, R. M., Schwerer, F. C., Fuller, M. D. and Dunn, J. R., (1971) ; Proc. Second Lunar Sci. Conf., Vol. 3, pp.2461-2476.

Nagata, T., Fisher, R. M., Schwerer, F. C., Fuller, M. D. and Dunn, J. R., (1972); Lunar Science-III. (Revised abstract, Third Lunar Sci. Conf.) pp. 573-575.

Nagata, T., Fisher, R. M. and Schwerer, F. C. (1972) ; The Moon 4, 160-186.

Pearce, G. W., Strangway, D. W. and Gose, W. A. (1972) ; Lunar Science-III. (Revised abstract, Third Lunar Sci. Conf.) pp. 599-601.

Magnetic Hysteresis Classification for the Lunar Surface-Peter Wasilewski-George Washington University, Washington, D. C.

Magnetic hysteresis and the derived magnetic hysteresis parameters adequately describe the irreversible magnetization behavior for any dilute ferromagnetic dispersion, i.e., the lunar samples. The magnetization of the lunar samples is due primarily to Fe-Ni-Co alloy whose magnetization values and the shape and size distribution determines the shape of the magnetic hysteresis loop. The magnetic viscosity, demagnetization stability, and remanence acauisition efficiency are directly related to magnetic hysteresis for any given sample. Measurement of the magnetic hysteresis properties for lunar samples provides a distinctive signature of the magnetic character of the sample, and as is the case for all natural materials the hysteresis is related to the mode of origin and general petrological consideration. The petrological classifications of Jackson and Wilshire (1972) and Warner (1972) are compatible with the magnetic hysteresis classification. Non-equilibrium subsolidus reduction (see Haggerty, 1971) in thermally metamorphosed breccia and basaltic samples (sample 14053, for example) is easily evaluated by magnetic hysteresis analysis. Magnetic analysis is a powerful stratigraphic tool and by itself can provide a measure of the natural history of iron in the regolith.

Magnetic Hysteresis-Definitions of symbols used in this paper are as follows: H_C=coercive force, H_R=remanent coercive force, I_R=remanent magnetization, I_S=saturation magnetization, $R_I=I_R/I_S$, $R_H=H_R/H_C$.

The size, shape, and composition of a ferromagnetic particle will determine its hysteresis properties; for a dispersion the variation in the size, shape, and composition will determine the hysteresis properties. Superparamagnetism is defined with $H_C=0$ and though it does not contribute to H_C, it will reduce H_C according to the argument $H_C \cdot q/\overline{I}_R$ and the amount present (ϵ) in the equation (Kneller and Luborsky, 1963), $\overline{H}_C=H_C/1+(H_C \cdot q/\overline{I}_R)(\epsilon/1-\epsilon)$ where $q=VM_S/3kT$ with V=volume, M_S=magnetization, k=Boltzman's constant, and T=absolute temperature. If large multidomain grains are present, the same arguments hold except that $q=(NM_S)^{-1}$, where N is the demagnetization factor.

Magnetic Hysteresis in Lunar Samples-Table I is a summary of the size, shape, and mode of origin of metal in lunar samples (Wasilewski, 1972a). Data presented by Nagata et al. (1970, 1971, 1972)

Hysteresis Classification

Peter Wasilewski

for Apollo 11, 12, and 14 samples is utilized (Table II). The samples are placed in two groups based on R_I and R_H values. The hysteresis ratios R_I and R_H are demonstrated to be characteristic for each group of natural materials (Wasilewski, 1970, 1972. , 1972 , 1972). The R_I and R_H values plot as two distinct groups. One group with $R_I < 0.02$ and $R_H < 10.0$ contains the igneous rocks and thermally metamorphosed breccia samples, the other group with $R_I > 0.04$ and $R_H > 10.0$ contains the fines and welded breccia samples.

The H_c values for all samples fall between 10 and 50 Oe. The R_I vs. H_R plot (Figure 1) results in two distinct and characteristic groups. For the first group, which includes the crystalline rocks and thermally metamorphosed breccia samples, $R_I < 0.02$, and H_R varies between 75 and 180 Oe., while for the second group, which includes the fines and welded breccias, $R_I > 0.04$, and H_R varies between 300 and 520 Oe. The R_I vs. H_R plot appears to be most informative. The presence of three discrete iron modes provides for a 10^3 range in grain H_c ranging from $H_c = 0$ for the superparamagnetic material to $H_c \sim 10^3$ for single domain material. All of the hysteresis loops thus far presented for lunar samples show constriction in the region of low measuring fields. This constriction can be found in partially oxidized terrestrial basalts (Wasilewski, 1972), chondrite meteorites (Wasilewski, 1972), and in the lunar samples (Nagata et al., 1970, 1971, 1972).

Discussion-The data presented in Table II is quite systemmatic despite the limited sampling. The samples were arranged in order of increasing R_H values, and all other parameters follow a systemmatic increase or decrease accordingly. It is also of interest to note that Nagata has defined two types of viscous (VRM) behavior for the analyzed lunar samples, and type I VRM behavior is associated with group A hysteresis characteristics, and type II VRM behavior is associated with group B hysteresis behavior (see also Gose et al., 1972). A direct sample to sample comparison of the H_R value is informative since it indicates the magnitude of the field needed to reverse half of the irreversible remanence left in the sample after saturation. The R_I value is also a relative indication of the amount of irreversible magnetization, and, as can be seen in the R_I vs. H_R plot, this value increases as H_R increases. The lower the H_R value the more viscous is the size fraction larger than single domain size. There are two components which are considered in time dependent changes, (a) the superparamagnetic fraction and (b) the multidomain fraction. This is reflected in the R_H values, the H_c values, and the initial susceptibility. For a constant H_R value the R_H value will depend on the amount of superparamagnetism. A more detailed study of viscous behavior based on low temperature analysis of the blocking spectrum will allow the size spectrum of superparamagnetism to be separated from the multidomain size spectrum. We can conclude that the relative significance of supermagnetism (SP) is

Hysteresis Classification

Peter Wasilewski

SP(Fines) > SP(Welded Breccia) > SP(Igneous Rocks) > SP(Thermally Metamorphosed Breccia).

Therefore, the H_c value will be reduced relatively more significantly in the reverse order of the list above, and the R_H value will depend on the H_R value almost exclusively, particularly since the H_c values (Table II) are limited to a narrow range.

The H_R value will depend on the shape and range of the size distribution. For igneous rocks and thermally metamorphosed breccia samples the H_R value is expected to be lowest since the majority of iron grains will be multidomain with single domain or small multidomain grains carrying any stable component. As the shape of the size distribution becomes wider, shifting to a smaller size range, or bimodal, as in the case of the fines and welded breccia, the H_R value should increase since a large fraction of the iron will be single domain or nearly so. The fines contain the broadest size distribution of ferromagnetic components, and welding the fines should not produce any significant alterations to the distribution. Thermal metamorphism will destroy some or all of the superparamagnetism, and an effective shift of the size distribution will result in a decrease in H_R, R_H, and R_I, as observed.

The data thus far accumulated provides distinct evidence that the lunar samples are quite different from terrestrial samples, mainly because there is iron in the lunar samples. The consistent R_H and H_R values for the lunar fines suggest a common origin and common size and shape modes for the ferromagnetic fraction in each group. Though data are sparse at present, there is a definite suggestion that the permanent remanence of each lunar sample can be understood in terms of the hysteresis properties of each sample. The path the hysteresis parameters will take depends on the mode of origin and acting chemical processes. A soil can be welded, thermally metamorphosed, or shock lithified. Each of the three processes will produce different effects depending on (a) the behavior of the SP component, (b) the change in the ferromagnetic component size distribution, (c) the magnetostatic interaction for subsolidus reduction, (d) the influence of the shape of the ferromagnetic components, (e) the composition of the alloy, i.e. Ni+Co content.

Conclusions-(1) There are well defined groups of lunar materials based on their magnetic hysteresis properties. (2) Natural remanence correlated directly with saturation magnetization, the R_I value, and the initial susceptibility for crystalline rocks. (3) In lunar samples the low H_c values are due in part to the presence of superparamagnetic iron and in part to multidomain iron. (4) The H_c value is a meaningless parameter for lunar samples. (5) The H_R value is important and diagnostic since it is due to near single domain and multidomain grains. It is independent of the superparamagnetic fraction. (6) Microbreccia samples can

be analyzed nondestructively and classified as to their mode of origin based on magnetic hysteresis. This approach will be more effective with a more systemmatic array of data. (7) It is possible that the measured surface fields can be due to a magnetized regolith. This requires further verification, but it is a distinct possibility which must be considered. (8) A soil can be subjected to welding, thermal metamorphism, or shock lithification. Each of the three processes will produce different hysteresis characteristics and remanent states depending on (a) the behavior of the SP component, (b) the change in the effective grain size distribution, (c) the development of eutectic intergrowths, (d) the phase composition, i.e. Ni+Co content, (e) the thermomagnetic anomalies of the ferromagnetic components. (9) Two distinct viscous or time dependent features are characteristic of iron in the lunar samples. The first concerns the superparamagnetic fraction, and the second concerns the soft multidomain iron fraction. Both features are temperature dependent. (10) From the hysteresis data and other published results it appears that relative superparamagnetism (SP) can be specified

SP (Fines)>SP(Welded Breccia)>SP(Igneous Rocks)
>SP(Thermally Metamorphosed Breccia).

The H_c value will be relatively reduced in the opposite order. (11) The natural history of iron in the lunar regolith can be analyzed using magnetic hysteresis. (12) Magnetic stratigraphy of regolith core samples can provide a sequential history of thermochemical events associated with makeup of the regolith.

This work was supported by the National Aeronautics and Space Administration.

Hysteresis Classification

Peter Wasilewski

TABLE I

Summary of (a) classes of metal in lunar rocks and fines based on mode of origin (b) size range of metal particles in lunar materials and (c) magnetic effects due to variations in size, shape, and composition of metal in lunar rocks.

(a) Mode of Origin of Metal

Class I - primary crystallization
Class II - subsolidus reduction of spinels
Class III - shock melting
Class IV - vapor deposition

(b) Size Range of Metal

Optical microscopy - 0.5 μm to 1000 μm
Scanning electron microscopy - 0.05 μm to 5 μm
Electron microscopy - 10 Å, 100 Å

(c) Magnetic Effects

1. Size:
   SUPERPARAMAGNETISM-ambient temperature relaxation effects-temperature dependent blocking temperature effects over the lunar cycle 100° K. to 400° K.-zero coercivity-reduces coercivity and R_H in a mixture
   MULTIDOMAIN-low coercivity-reduces coercivity and R_H in a mixture-time dependent magnetization acquisition in weak fields-source of noise in lunar samples
   SINGLE DOMAIN-high magnetic stability-high coercive force-spectrum variable over the lunar temperature cycle 100° K. to 400° K.
2. Shape:
   Spheres < 0.05 μm to 100 μm; cubes < 1 μm to 5 μm; needle shapes with length:diameter ratio > 10:1; magnetostatically interacting chains of spheres and platelets
   The shape fields $H_S=NI_S$ change resulting in discrete discontinuities in the magnetization curves.
3. Composition:
   FeNiCo variation: Co - 0 to 8%; Ni - 0 to 40%. Temperature dependent magnetization anomalies-Curie point variations-variable shock remagnetization mechanisms

TABLE II

(Tabulation of data from Nagata et al.)

Group A - Crystalline rocks and thermally metamorphosed breccia

Sample	$\chi_o(10^3)$	$I_n(10^5)$	I_s	R_H	R_I	$I_R(10^2)$	H_c	H_R
14053	2.24	203.0	2.2	4.0	0.019	4.0	20	80
14303	0.69	13.0	1.27	6.6	0.016	2.1	27	180
14311	0.46	0.81	0.74	8.2	0.006	0.43	17	140
Group B - Welded breccia								
10048		5.6	1.8	10.4	0.072		50	520
14047		1.23	1.4	13.4	0.044	6.1	26	350
- Lunar fines								
10084			1.17	12.78	0.072		36	460
14259			1.5	15.7	0.04	6.0	19	300
14161			0.98	16.5	0.044	4.3	26	430
12070			1.28	20.45	0.048		22	450

Hysteresis Classification

Peter Wasilewski

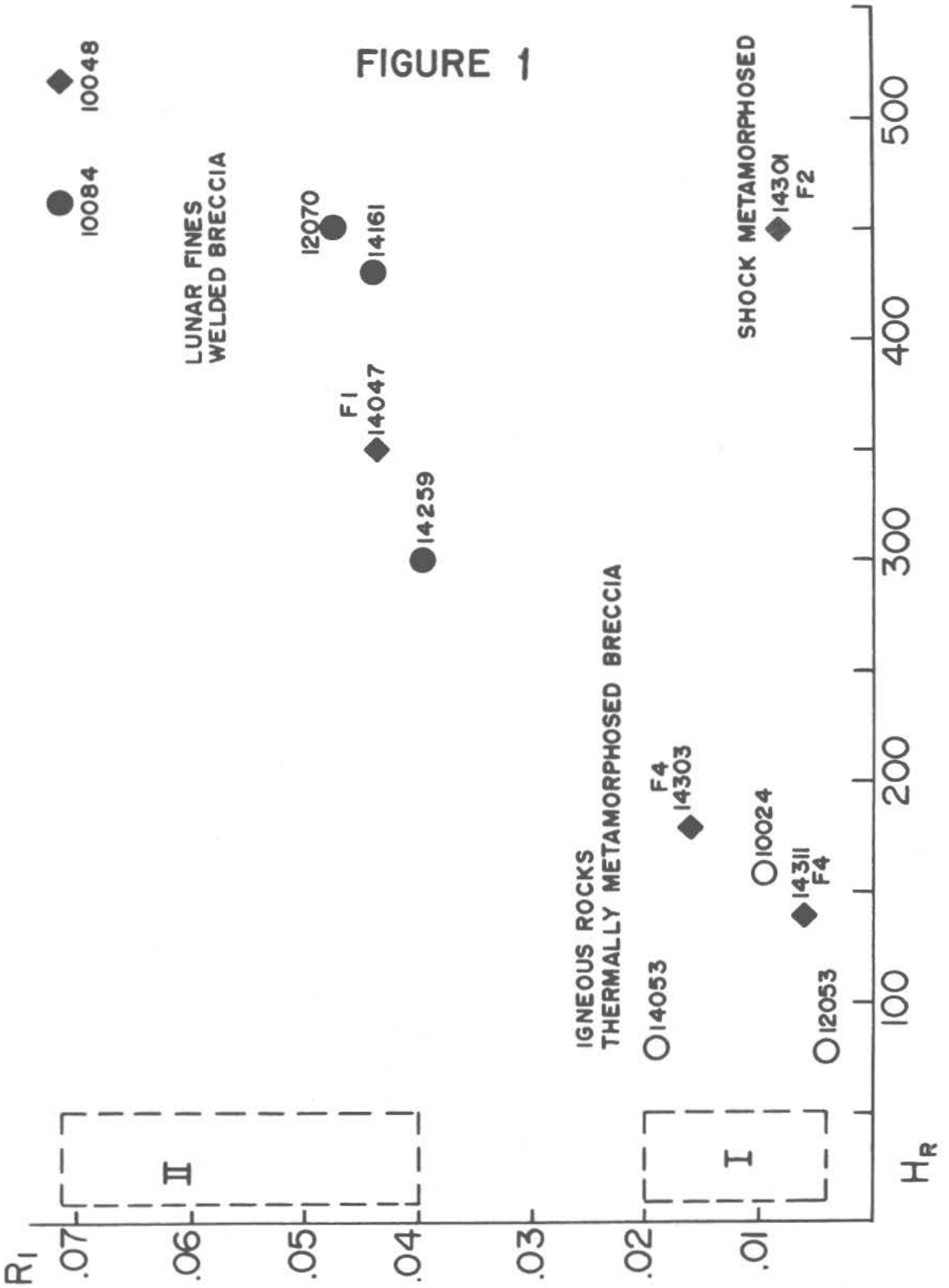

THERMOLUMINESCENCE OF APOLLO 15 LUNAR SAMPLES : (I) -196 to + 250°C

I. M. Blair and R. A. Jahn, A.E.R.E., Harwell, U.K.; J. A. Edgington, Department of Physics, Queen Mary College, London, U.K.; S. A. Durrani, Department of Physics, University of Birmingham, Birmingham, U.K.; M. Phillips, Department of Applied Physics, Lanchester Polytechnic, Coventry, U.K.; A. Kacperek, Department of Physics, University of Surrey, Guildford, U.K.

This paper records the results of a preliminary examination of four samples of <1mm fines : 15261,70 (hereafter termed A); 15271,90 (B), 15301,84 (C) and 15601,78 (D). Our sample nomenclature agrees with that of the companion paper[1], which discusses thermoluminescent (TL) properties at higher temperatures. Here we report the proton-induced luminescent and TL spectra and glow-curves, and the leakage and saturation properties of the trapping centres.

We shall summarize the experimental technique, as a detailed account has been given elsewhere[2]. With one exception, the samples were studied as received from NASA. The powder was sprinkled onto silicone vacuum grease thinly smeared on aluminium plates; specimen preparation and storage was in dry air. The exception was a portion of 15271,90, which was heated to 800°C for 15 hours at a pressure of 10^{-6} torr, before mounting on grease. The irradiations were performed at a pressure of 3×10^{-2} torr in the 160 MeV external proton beam of the A.E.R.E. synchrocyclotron. Whilst in the irradiation chamber, the samples were in complete darkness, and remained so until read-out was complete.

Luminescence spectra were taken at both room temperature and -196°C, using a set of seven wide-band interference filters covering the visible spectrum between 380nm and 750 nm. All spectra were normalized to a beam flux of 4×10^8 protons cm^{-2} sec^{-1} (approximately 280 rad sec^{-1}).

For the TL studies, samples were irradiated at -196°C using a dose rate of 700 rad sec^{-1}. After a 15 minute waiting period, to allow any short period phosphorescence to decay, samples were heated to~250°C at 0.8°C sec^{-1} (constant to within $\pm$ 10%). For spectral studies, doses were close to 400 krad and glow-curves were normalized to this dose. The silicone grease possesses glow peaks, predominantly blue, below -100°C, and this temperature region has consequently been omitted from the blue glow curves obtained.

TL of Apollo 15 : (I)

I. M. Blair

Proton-induced luminescence

At room temperature, spectra were similar for all samples, that is, whitish and of a low intensity comparable with that shown by samples from previous missions. Fig. 1 shows the spectra at -196°C. The salient feature is the much lower blue response of the pre-heated sample B, compared with the unheated specimen of this sample. After these spectra had been obtained, all samples were held at a little over 100°C for 1 hour in vacuum, and the low-temperature spectra then recorded again. Only A showed any change, its spectrum becoming almost identical with that of the pre-heated B. After exposing A to the atmosphere for some hours, its spectrum returned to its original form. This was not the case for the pre-heated B.

This behaviour is reminiscent of the disappearance of low-temperature glow-peaks as samples are heated above 100°C, a phenomenon noted previously in Apollo 11 samples and tentatively ascribed(3) to the driving off of adsorbed water. Possibly a similar effect is present here, the differences between samples being related to their mineralogy and surface characteristics.

The absolute luminescent efficiencies at -196°C were $\sim 3 \times 10^{-3}$, which is similar to that found for Apollo 11 and 12 samples.

Proton-induced TL.

Fig. 2 shows the glow curves, in three wavebands, for sample A. Samples B and C (including the preheated B) showed curves of similar structure, though absolute intensities differed by factors of ~ 1.5. Note the intense red glow peaks, below -50°C and near -25°C. The intensity of these peaks diminishes rapidly towards shorter wavelengths, and it is noteworthy that this is the first time a red TL has been seen, at these low temperatures, in lunar samples. In Ref. 1 we present evidence that the red TL continues to diminish, both absolutely and relative to the blue, at higher temperatures. The glow curves of all samples were well reproducible, apart from a peak in the blue at -75°C in sample C; after the first irradiation and read-out, this was no longer observed (Fig. 2). Such shallow traps are likely to be caused by shock-damage, and may well have been annealed out at 250°C.

Two separate specimens prepared from sample D showed much lower TL intensity. Specifically we found that D yielded only 20% as much light as A, B and C when samples were irradiated at, and heated from, room temperature. This agrees with the findings of Ref. 1. However, whereas A, B and C gave a strong red glow peak below 0°C, when heated from -196°C, this was absent from D, an upper limit on its intensity being 2% of A-C. In Ref. 1 the difference between A-C and D is attributed to D being an iron-rich mare-type basalt from the Rille, whereas A-C are plagioclase-rich material from the "Front".

TL of Apollo 15 : (I)

I. M. Blair

TL leakage and saturation effects

Fig. 3 shows the variation of TL peak height, with waiting time before read-out, for one of the peaks of sample A. Other peaks showed similar behaviour. During the waiting period the samples were kept in the dark at -196°C. Note a rapidly decaying short-term component and a longer term, apparently constant, component. The assumption of exponential decay of the short term component yields a mean life of ~45 minutes, the longer term component having about one third of the initial intensity. We observed similar, apparently non-thermal, decay of TL in Apollo 14 samples(4).

In Fig. 4 we show the magnitude of the same TL peak, as a function of radiation dose, for samples A and C. Saturation occurs at about 2.5 Mrad and 1.75 Mrad respectively. Each curve may be characterised by the "half dose", $R\frac{1}{2}$ (a shape parameter defined in Ref. 1); $R\frac{1}{2}$ is ~360 krad and 630 krad, for A and C respectively.

Study of these leakage and saturation effects is continuing.

References

(1) S. A. Durrani et al. (1972) Thermoluminescence of Apollo 15 lunar samples: (II) 20-550°C, (this volume).

(2) I. M. Blair and J. A. Edgington (1970). Proc. Apollo 11 Lunar Science Conference, 3, 2001.

(3) J. A. Edgington and I. M. Blair (1970). Mat. Res. Bull. 5, 947.

(4) I. M. Blair et al. (1972). Proc. 3rd Lunar Science Conf., (ed. C. Watkins) LSI Contr. No. 88, 86.

TL of Apollo 15 : (I)

I.M.Blair

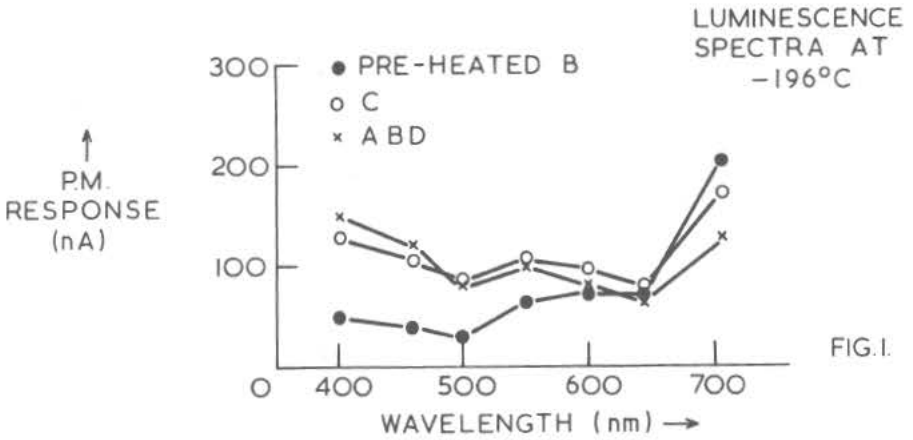

FIG.1.

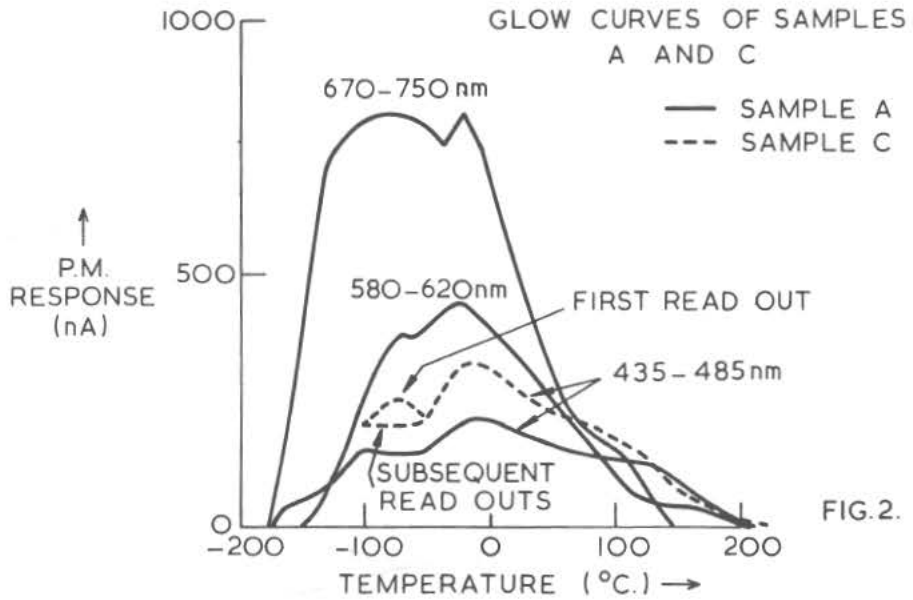

FIG.2.

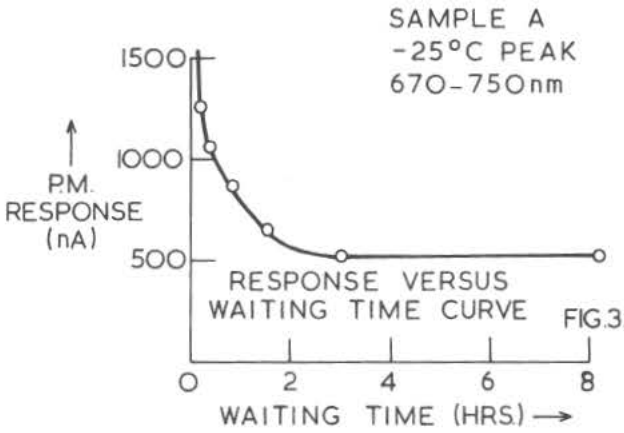

FIG.3.

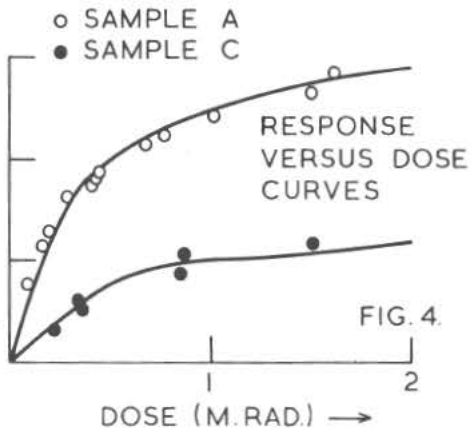

FIG.4.

THERMOLUMINESCENCE OF APOLLO 15 LUNAR SAMPLES: (II) 20 to 550°C

S.A.Durrani, W.Prachyabrued, Dept. of Physics, University of Birmingham, U.K.
J.A.Edgington, Dept. of Physics, Queen Mary College, London, U.K.
I.M.Blair, Nuclear Physics Division, AERE, Harwell, U.K.

Thermoluminescence (TL), both natural and that induced by γ and UV irradiation, has been studied in Apollo 15 fines samples. The rate of heating (in N_2 atmosphere) was 5°C/sec; readout temperature, 20-550°C; amount of sample (38-63 μm grains), ≈ 2 mg. A cooled quartz photomultiplier (EMI: 6256 SA) received the TL glow transmitted, normally, through an Ilford 'Bright Spectrum Blue' filter (no. 622:375-530 nm). For details see ref. 1.

Fig. 1 shows the natural TL from the four samples studied. Samples 15261, 70 (termed A), 15271, 90 (B) and 15301, 84 (C) all show two broad peaks, while sample 15601, 78 (D) shows the second peak only - and even that ~ $\frac{1}{2}$ as high as from A-C. It is significant that samples A-C come from neighbouring locations on the shoulder of Hadley Delta (the 'Front'), while D comes from level ground near the edge of Hadley Rille ~6 km away. Moreover, sample A, which has retained the largest amount of glow in peak I, comes from the bottom of a 20 cm deep (and hence presumably cooler) trench.

Fig. 2 shows the TL response of sample C to ^{60}Co γ-ray dose ranging from 82 to 545 krad. It is representative (in structure) of similar glow curves from samples A-D, thus suggesting an identity of nature of TL phosphors in all of them. The TL output from sample D for a given dose is, however, always lower (by a factor of ~ 5) than from A-C. A smaller proportion, or a lower TL-efficiency, of the relevant minerals in sample D (cf. the considerable chemical differences reported[2,3]) may account for this effect.

The growth of the TL output in the readout temperature intervals 20-300°C (peak I) and 300-500°C (peak II) has been studied as a function of γ dose; the latter is plotted in Fig. 3. (Note again the smaller TL output per unit dose, as well as the lower saturation level, for sample D.) By extrapolating the initial trend of the curves, a 'γ-ray equivalent natural (or equilibrium) dose 'R_{eq} of ~ 150 krad is obtained for all samples. Similarly, the dose needed to fill half the remaining traps at any point (termed I the 'half-dose' $R_{\frac{1}{2}}$ is found from

Thermoluminescence of Lunar Samples (II)

S. A. Durrani

Fig. 3 to be ~350 krad (for peak II) for all samples. Both R_{eq} and $R_{\frac{1}{2}}$ have values close to those found by us for Apollo 14 fines (to be published). The values of R_{eq} and $R_{\frac{1}{2}}$ for peak I in samples A-C are recorded in Table 1.

TL PARAMETERS AND T_{eff} Trap parameters E (depth in eV) and s (frequency factor in sec^{-1}) have been determined for peak I (at ~200°C) and for peak II (at ~420°C), using natural samples A-C and D, respectively, by the 'initial rise' method. Following the procedure described in an earlier paper[1] (and assuming an incident radiation dose rate of 10 rad/yr and a diurnal heat wavelength of 25 cm at the surface of the moon), the 'effective lunar storage temperature' T_{eff} has been calculated for the four fines samples. The relevant data and the results obtained are summarized in Table 1. It may be pointed out that the natural TL under peak I in samples A-C had, by the time of the experiment (~9 months after retrieval), been partially drained (cf. $\tau_{\frac{1}{2}}$ at 20°C in Table 1). This results in higher E (and s) values for the residual peak I, and hence in an overestimate (by ~10°C in the case of sample A) of the T_{eff} calculated. The importance of refrigerating lunar samples destined for TL investigations is again emphasized.

Table 1. Trap parameters and the calculated 'effective lunar storage temperature' T_{eff} (assuming a dose rate of 10 rad/yr)*

Sample and Peak	Trap depth E(eV)	Freq. factor s(sec^{-1})	Half-dose $R_{\frac{1}{2}}$ (krad)	Equilib. dose R_{eq} (krad)	N/n_{eq}**	T_{eff} (°K)	Half-life $\tau_{\frac{1}{2}}$(yr) at 20°C	Half-life $\tau_{\frac{1}{2}}$(yr) at T_{eff}
15261,70(A) I:190°C	1.12 ±0.05	~ 4×10^{11}	1150	25	42	251±5	1.0	1650
15271,90(B) I:225°C	1.20 ±0.05	~ 4×10^{11}	1150	15	92	271±5	23	1100
15301,84(C) I:225°C	1.28 ±0.05	~ 4×10^{11}	1150	10	160	290±5	500	800
15601,78(D) II:400-440°C	1.64 to 1.72	~ 2×10^{11} to ~ 3×10^{11}	350	150	3.1	363±10	~ 6×10^{9}	~ 1.6×10^{4}

*For method of calculation see ref. 1

** Proportion of filled traps at equilibrium

Thermoluminescence of Lunar Samples (II)

S. A. Durrani

UV IRRADIATION Natural samples as well as those previously subjected to TL readouts (i.e. heated up to 550°C) were exposed to ultraviolet radiation, which centred at 254 nm and had an intensity of $\sim 10^{-2}$ W/cm^2 at sample position (~ 10 cm from source). The samples (of grain size 38-63 μm) were spread out in roughly single-grain layers. UV radiation is found to fill low-energy traps preferentially. In a heated sample (i.e. drained during a previous TL readout), the growth of both peaks I and II with UV irradiation parallels that with γ irradiation. (Incidentally, the heated sample is 'sensitized' by a factor of ~ 2 in γ response in comparison with the unheated sample.) The 'half-dose' of UV radiation for TL traps in the readout interval 20-300°C is found to be that imparted in ~ 1 hr of irradiation (calculated to be ~ 400 Mrad of UV); this produces a TL glow equivalent to that resulting from ~ 40 krad of γ rays in an unheated (or ~ 20 krad in a heated) sample. The saturation level for UV irradiation (reached in ~ 6 hr) is equivalent to twice these γ-ray doses. Note that, as in the case of γ irradiation, sample D exhibits a much lower TL response (by a factor of ~ 5) to UV irradiation than do samples A-C. The same TL-efficiency factor between sample D and the rest is found for 160 MeV proton irradiation (see the preceding paper[3]).

SPECTRAL RESPONSE The TL emission spectra have been studied both from γ-irradiated natural samples and from UV-irradiated heated samples, using a set of interference filters (for discussion see ref. 1). Fig. 4 shows some representative curves. At low readout temperatures (covering peak I), the TL intensity in short wavelengths (violet to green, ~ 400-525 nm) is comparable to that in long wavelengths (green to red, ~ 525-650 nm). With the onset of peak II (~ 300°C onwards), however, the emission spectrum begins to be depleted in long wavelengths, until at 450°C there is hardly any intensity beyond ~ 500 nm (blue). The UV-irradiated heated samples show a distinctly different pattern. In peak I, there is a much greater proportion of short wavelength emission (~ 400-500 nm); these wavelengths are, however, not as predominant in UV-induced peak II as they are in the case of γ irradiation.

References

1. Durrani S. A. et al. (1972) Thermoluminescence of Apollo 12 samples: Implication for lunar temperature and radiation histories. Proc. Third Lunar Sci. Conf., Geochim. Cosmochim. Acta, Suppl. 3, Vol. 3. MIT Press.

2. Apollo 15 Preliminary Science Report (1972) NASA SP-289, p. 6-17.
3. Blair I. M. et al. (1972) Thermoluminescence of Apollo 15 lunar samples: (I) - 196 to +250°C. (This volume).

Thermoluminescence of Lunar Samples (II)

S.A.Durrani

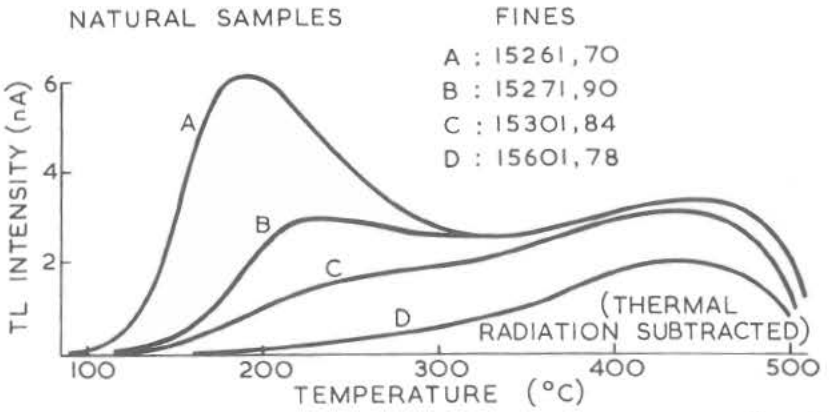

FIG. 1. TL OF NATURAL SAMPLES. HEATING RATE : $5^{\circ}C\ sec^{-1}$; EACH SAMPLE : 2·0mg, 38-63 μm; FILTER : ILFORD 'BRIGHT SPECTRUM' No. 622

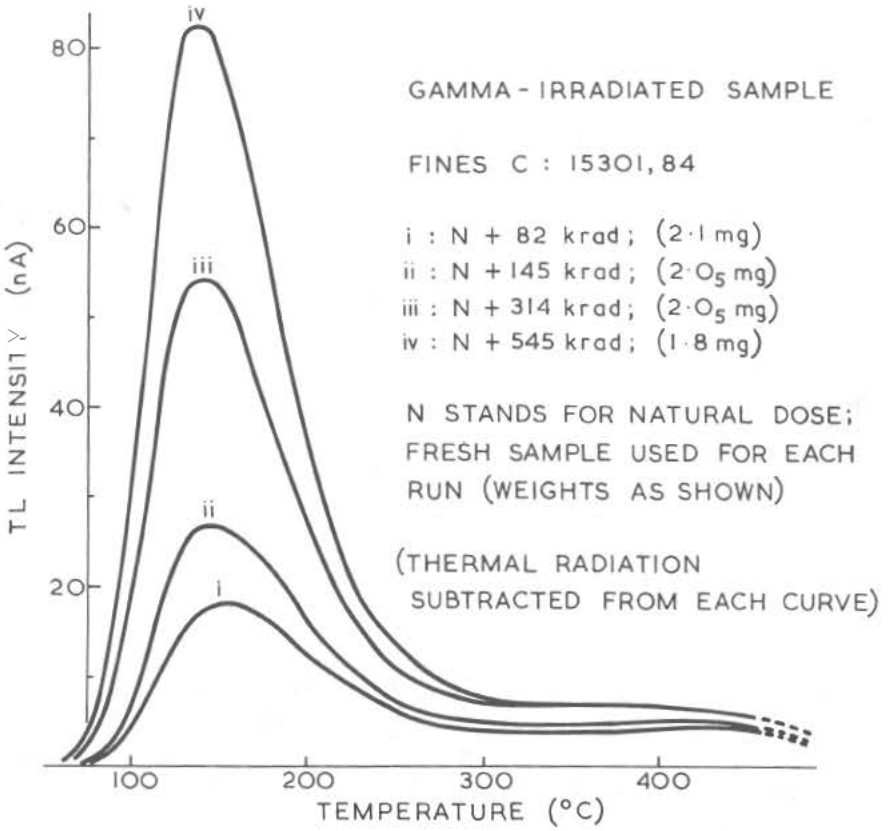

FIG. 2. TYPICAL RESPONSE OF A FINES SAMPLE (C) TO IRRADIATION WITH ^{60}Co γ-RAYS. THE ORDINATE SCALE AND EXPERIMENTAL CONDITIONS ARE THE SAME AS IN FIG. 1.

Thermoluminescence of Lunar Samples(II)

S.A.Durrani

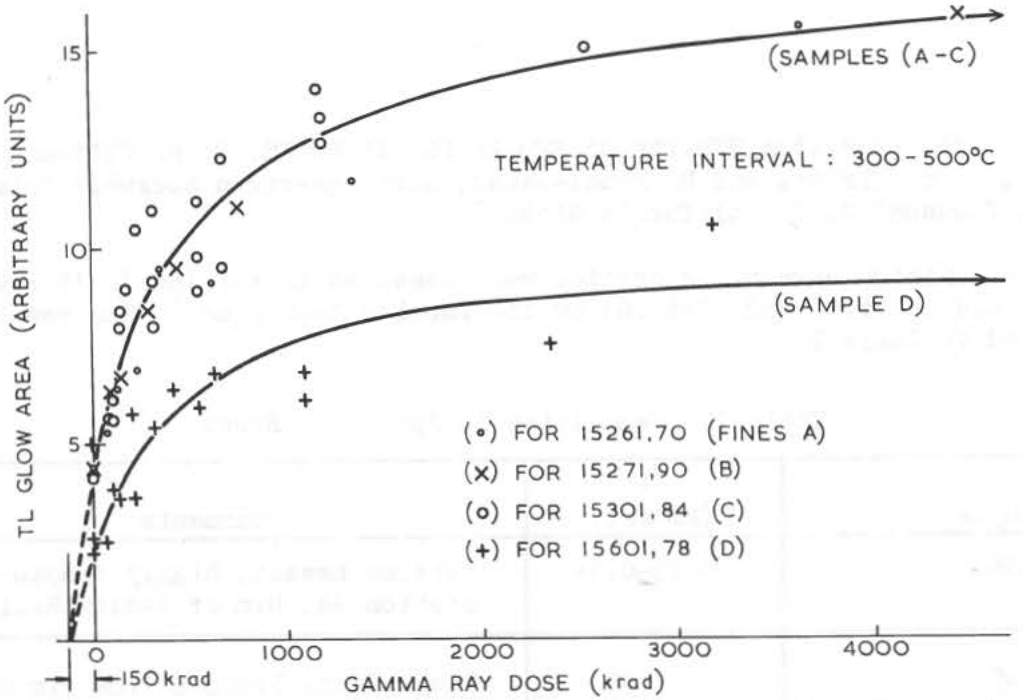

FIG. 3. DOSE RESPONSE OF FINES SAMPLES A-D (2·0 mg EACH). INTEGRATED GLOW AREA IN THE INTERVAL 300-500°C IS PLOTTED, AND 'NATURAL DOSE' (~150 krad) FOUND BY EXTRAPOLATION OF INITIAL TREND. EXPERIMENTAL CONDITIONS AS IN FIG. 1.

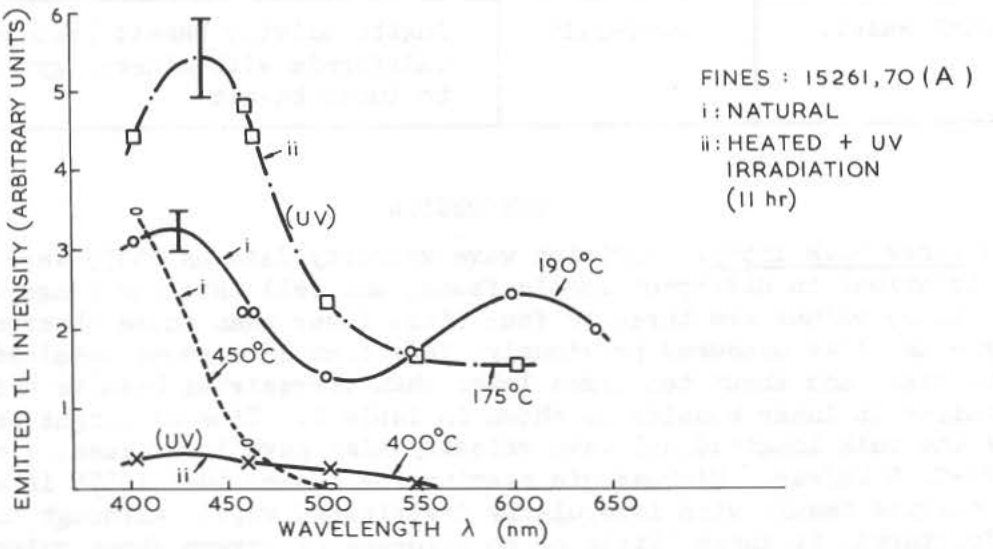

FIG. 4. TL EMISSION SPECTRA USING INTERFERENCE FILTERS. NATURAL TL (CURVES i) AS WELL AS THAT INDUCED BY UV IRRADIATION OF SAMPLES PREVIOUSLY HEATED TO 550°C (CURVES ii), IS SHOWN AT THE READOUT TEMPERATURES INDICATED.

RAYLEIGH WAVE STUDIES OF TWO APOLLO 15 ROCKS, B. R. Tittmann, R. M. Housley, E. H. Cirlin, and M. Abdel-Gawad, North American Rockwell Science Center, Thousand Oaks, California 91360

The Rayleigh wave v_R velocities were measured in two Apollo 15 returned lunar rocks 15555.90 and 15459.65 by the impulse technique.[1] The results are presented in Table I.

Table I. Velocities in Apollo 15 Rocks

Sample	v_R (km/sec)	Comments
15555	0.28-0.34	Olivine basalt, highly fractured, Station 9A, Rim of Hadley Rille
15459	$\leq$ 1.95	Tough dense breccia from rim of Spur Crater
Synthetic Analog	2.21-2.26	Basalt, analog of lunar rock 10017, very few fractures
Terrestrial Basalt	2.97-3.15	Augite olivine basalt from Northern California with mineralogy similar to lunar basalt

DISCUSSION

(a) Lunar Rock 15555: Rayleigh wave velocity data on 15555 were obtained[2] on many locations on different sample faces, and fell into the range 0.28-0.34 km/sec. These values are three to four times lower than those observed on lunar igneous rocks measured previously, less than half those obtained on lunar breccias, and about ten times lower than terrestrial basalts with mineralogy similar to lunar basalts as shown in Table I. Time of flight measurements of the bulk longitudinal wave velocity also gave low values, i.e., $v_p \approx 0.70$-0.95 km/sec. Microscopic examination showed that 15555 is a coarse grained olivine basalt with irregularly distributed vugs. Although the rock is highly fractured, it shows little or no evidence of severe shock metamorphism and appears coherent and competent in normal laboratory handling. Care was taken to make the Rayleigh wave velocity measurements on the more massive portions of the rock where the vugs were sparsely distributed and did not exceed about 0.1 mm in size.

Rayleigh Wave Studies of Two Apollo 15 Rocks

B. R. Tittmann

Scanning electron micrographs were obtained[3] on this rock and compared to those of other lunar rocks and synthetic analogs of lunar rocks. These studies coupled with velocity measurements on the same rocks revealed an apparent correlation between degree of fracture and compliance. While it is difficult to determine at this time any quantitative relationship, there seems little doubt that the presence of microfractures created in an environment devoid of liquids and gases contributes greatly in increasing the compliance of the lunar rock concomitant with a decrease in velocity.

The existence of a very low elastic wave velocity in this generally competent, igneous rock indicates that the existence of a thick, low velocity zone near the lunar surface does not necessarily require postulating the existence of a thick layer of fines on the moon's surface. From field observations, Swann et al.[4] have concluded that the regolith at the Hadley Rille rim where the sample was collected is very thin or absent and that most of the samples collected in this area are probably representative of the local volcanic bedrock exposed at the Rille rim. From the discussion by Swann et al.[4] we are not sure of the exact source of rock 15555. However, this rock is classified[5] as typical of the porphyritic olivine basalts and similar in this respect to 15535 which is judged most certainly representative of the bedrock. Thus the assumption that 15555 may have been derived from the upper part of volcanic bedrocks exposed in the vicinity of the Hadley Rille seems justified. If this conclusion is borne out by further studies, the unusually low velocities measured on this igneous rock should be taken into consideration in the interpretation of the low seismic velocities observed in the upper layer of the lunar surface.

(b) Lunar Rock 15459: This rock is a coarse breccia from the rim of Spur Crater. It is a tough dense breccia with a glassy matrix that makes up more than 50% of the volume. Imbedded in the matrix are many small clasts of anorthosite. When one face of the sample was polished it showed pronounced fractures running more or less parallel to one another at a spacing of about 1 to 2 mm. The Rayleigh wave velocity was measured in directions parallel and perpendicular to the fractures, and data such as shown in Fig. 1 were obtained. The data are plotted as a graph of signal arrival time as a function of transducer separation which in general gives a straight line, the reciprocal of whose slope is the Rayleigh wave velocity v_R. The most important feature to notice is that the velocity parallel to the fractures is very high, i.e., $v_R \approx 1.95$ km/sec. This value is higher than that for any of the lunar rocks measured by us previously and approaches the value found in the synthetic analog[3] of a lunar basalt (see Table I) with $v_R \approx 2.21$-2.26 km/sec. This is all the more remarkable since this rock is a breccia and generally this rock type has previously shown much lower velocities than the lunar basalts. This breccia, however, appears very compact except for the well defined set of fractures mentioned. The data in the direction perpendicular to the fractures do not give a straight line plot but show several steps in which the slope changes its value abruptly, reflecting the crossing of the receiving transducer over a fracture. A line drawn through the data points with the

Rayleigh Wave Studies of Two Apollo 15 Rocks

B. R. Tittmann

steps viewed as deviations from a mean gives a velocity of $v_R \approx 1.1$ km/sec. In the vicinity of the fractures, however, the velocity dips to values as low as $v_R \approx 0.5$ km/sec. Thus, it is clear again from this work that the presence of fractures plays an important role in determining the velocity value. The high value of $v_R \approx 1.95$ km/sec is therefore most likely closest to the intrinsic velocity value for the material.

IMPLICATIONS

With the inclusion of the Rayleigh wave velocity data obtained on these Apollo 15 rocks, a velocity range of about one order of magnitude from $v_R = 0.3$ km/sec to $v_R = 2.0$ km/sec is covered. These velocities have all been obtained at zero confining pressure and are therefore representative of the solid material in the upper few kilometers of the lunar surface. In view of this spread in velocities it is perhaps not surprising that seismic experiments show a high degree of scattering in this layer. Rock 15459, in being a tough and compact breccia, resembles the class of breccias which have been thermally recrystallized at some depth of the moon. Thus the elastic properties of 15459 might serve as an indication of the elastic properties expected of these thermally recrystallized breccias. If this surmise proves to be correct it will be very difficult to distinguish between hypotheses, which regard the lunar mare as largely igneous and those which regard them as deep accumulation of dust on the basis of seismic velocity measurements.

This work was supported in part by NASA Contracts NAS9-11542 and NAS9-11539.

REFERENCES

1. B. R. Tittmann, Rev. of Sci. Instr. 42, 1136 (1971).
2. B. R. Tittmann, M. Abdel-Gawad, and R. M. Housley, "Lunar Science --III", ed. C. Watkins (Houston: Lunar Science Institute), 1972.
3. B. R. Tittmann, M. Abdel-Gawad, and R. M. Housley, Proc. Third Lunar Sci. Conf. Geochim. Cosmochim. Acta, Suppl. 2, Vol. 3, MIT Press, in press.
4. G. A. Swann, M. H. Hait, G. G. Schaber, V. L. Freeman et al., "Prel. Descriptions of Apollo 15 Sample Environments", Interagency Rep. 36 (1971).
5. LSPET (Lunar Sample Preliminary Examination Team) Preliminary examination of the lunar samples from Apollo 15, Science 175, 363 (1972).

Rayleigh Wave Studies of Two Apollo 15 Rocks

B. R. Tittmann

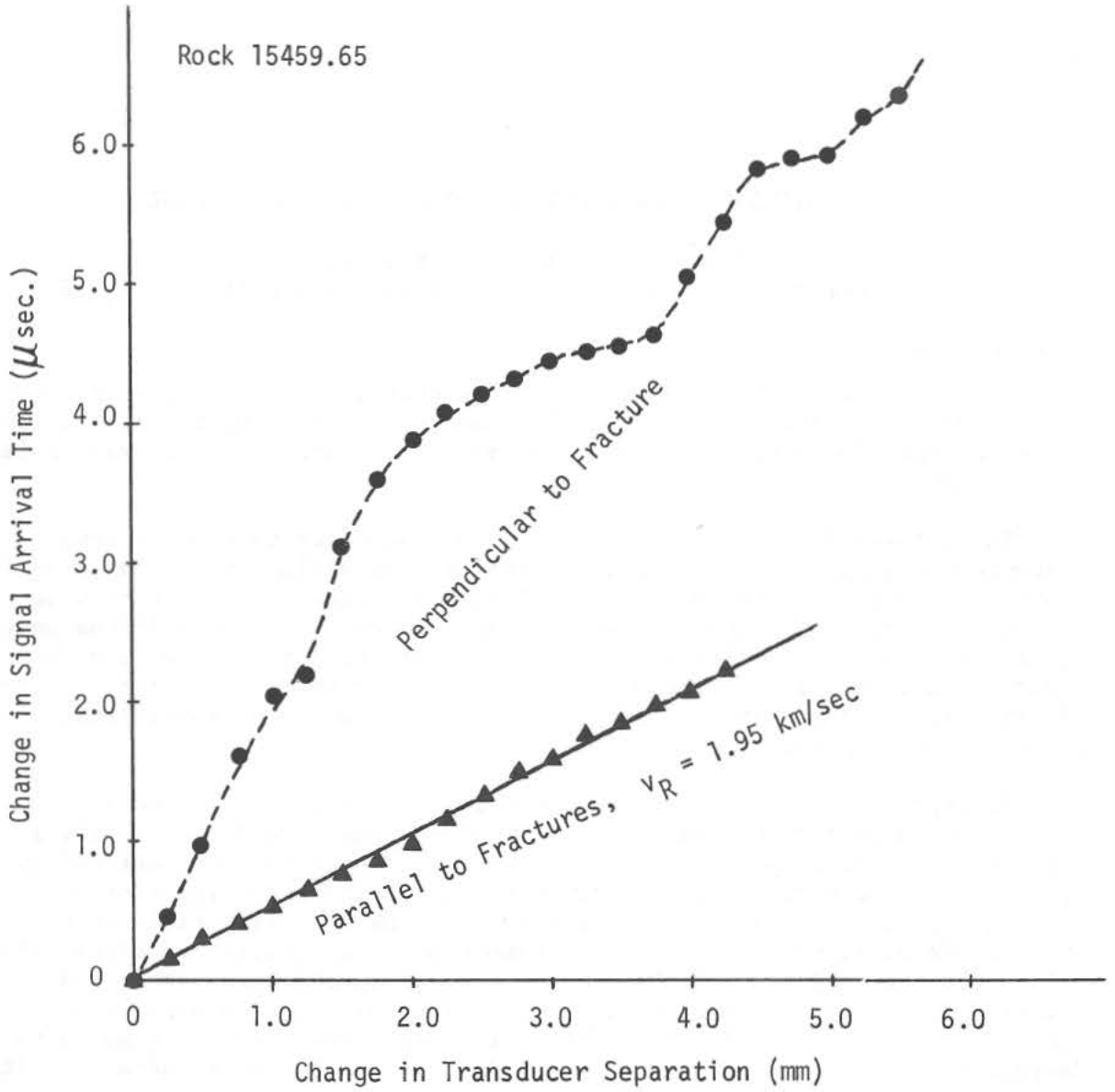

FIGURE 1

Sample data of change in signal arrival time versus change in transducer separation for rock 15459. The data were obtained by the impulse technique.[1] The reciprocal of the slope gives the Rayleigh wave group velocity.

ELECTROSTATIC INTERPARTICLE ADHESION IN APOLLO 15 FINES

S.K. Asunmaa and G. Arrhenius
University of California, San Diego,LaJolla,California 92037

Introduction

The objective of this program is to measure the adhesion forces between the grains in contact in Apollo 15 fines and to collect experimental evidence on the nature of charges and the mechanism of the persistent internal polarization inferred.

The information obtained has bearing on the understanding of lunar soil characteristics such as 1) microstructural features,clustering and anomalies observed in fossil track density profiles, 2)integral properties such as redistribution of soil material under varying electric field conditions on the sunlit side of the moon (Gold,1972,1), 3) polarized light reflection from the lunar surface and 4) the fundamental mechanism for non-gravitational accretion of particles in space and the embryonic growth of planets, satellites, asteroids and comets.

We reported on electrostatic properties of Apollo 11, 12 and 14 fines in (2) and on supporting experimental material and adhesion forces in (3,4). The electrostatic properties of the lunar soil dielectrics are defined by 1) a net surface charge and 2) a heterocharge in the grain interior, a condition that in an electric field,even in a low intensity field as on the lunar surface, renders the grains supramolecular dipoles.The inferred persistent internal polarization would promote the interparticle adhesion that primarily is based on a net surface charge.The polarization also would slow down the adhesion decay.The adhesion forces are measurably weakened in the deepest strata sampled by Apollo 12 double core, estimated to have deposition age of the order of at least 10^7 years.

High concentration of defects are observed throughout the material and especially in the surface layer of specific irradiated grains with high concentration of implanted gases.This suggests that the grain contact regions counteract any leakage current and prevent emission of exoelectrons (5). Consequently we believe that the extensive structural damage provides deep potential wells for charge storage and that the excessive modification of a 500-700 A thick surface zone is largely responsible for the persistent clustering of the lunar fines (even after storage under atmospheric conditions for several months) in the Apollo samples examined.

ELECTROSTATIC INTERPARTICLE ADHESION

S.K.Asunmaa and G. Arrhenius

Net Charge and Internal Polarization

The existence of a net surface charge on the grains (<1mm diameter) under laboratory conditions, was reported in our previous observations and estimated by fractionation of the grains by free fall through a low intensity electric field where they deviate from their vertical paths toward the electrode of opposite polarity.Clusters of new configurations were produced at the "landing sites" on the electrodes.Charge densities from 10^{-6} to 10^{-10} Coul/cm^2 were determined.The field intensity up to 350 V/cm was shown to be low enough to preclude charge induction in the lunar dielectrics.Such charge induction became pervasive only at field strengths exceeding 2000 V/cm.

Dipole effects were observed by imposing electric fields of 600 V/cm and higher on samples of small grains.The separation of internal heterocharge was also established in a number of grains without exposing them to the influence of an external field.This was done by placing the grains in a liquid crystal medium;charateristic low frequency scintillation and other optical effects were observed, demonstrating the presence of an electric field.

Adhesion Forces Counteracted by Shear Stress

Measurement of forces of interparticle adhesion in Apollo 15 fines was performed by balancing adhesion strength with the mechanical force required for releasing the fine particle coating from the host grain surfaces.This was achieved by shear stress in laminar flow of inert gas.

Evaluation of interparticle adhesion forces in lunar soil is complicated by variations in particle size and composition.Since the lunar soil dielectrics are susceptible to polarization and relocation of electric charges in an imposed electric field, we prefer to measure the electrostatic adhesion forces by balancing them with non-electric forces,for the present experiments inert gas shear was chosen.

A number of Apollo 15 grains (3 to 10 simultaneously) were subjected to gas shear under laminar flow conditions.Distribution patterns on collector substrates and grain size statistics of the micrograins dislodged by the gas, were evaluated.The average shear stresses at particle locations for steady state incompressible laminar flow through a circular tube were computed from the fluid dynamicslaw for laminar flow in viscous medium.Values ranging from 12 to 170 dynes were computed as shear forces required for detaching 20 to 2 μm grains from the host contact in sample 15601,116 using a flow rate of 169 cm^3/sec in one typical experiment.Final increase of flow rate by 50% to 255 cm^3/sec released only a small additional amount of coating grains,most of them of micron and submicron size.Forces of some 250 dynes thus were required for detaching the most tenaciously adhered but removable micrograins.This first approximation will be modified in further refinement of the experimental technique so that we will average over a limited size fraction of grains in each experimental stage rather than over some 1000 micrograins of various sizes and compositions as at the present time.

ELECTROSTATIC INTERPARTICLE ADHESION

S.K.Asunmaa and G. Arrhenius

The most significant error source is the contact area estimate if the shear stress is computed on the basis of the mass of the dislodged and collected micrograins.However,an alternative shear force evaluation that is applicable in gaseous systems where the fluid viscosity is low, is mainly concerned about the length of the obstacle meeting the flow velocity vector at right angle, hence the contact area estimate does not enter the calculations in this treatment.

A control calculation was performed by estimating the range of surface charges per unit area likely to produce the adhesion strength of the given magnitude.If the charge density is considered the main governing parameter for interparticle adhesion, electrostatic charges of 5×10^3 e.s.u. or 1.7×10^6 Coul/cm^2 will suffice for inducing adhesion forces of 170 dynes.This is a reasonable charge density in view of the similar values determined experimentally for the lunar soil grains using the electric field-gravitational field technique (2,3).

The prototype experimental device was designed to secure the laminar flow conditions for dry filtered argon gas at flow rates ranging from 130 to 255 cm^3/sec.The collector efficiency was optimized by choice of exit aperture size, flow rate and aperture-collector spacing as variable parameters.The host grains of sufficiently large size were placed on a retaining grid with a 90×100 μm^2 window size in the upper part of the apparatus.Successive fractions of micrograins were then dislodged from the host grain surfaces by stepwise increase of the argon flow rate.An SEM specimen holder was used as a collector for the micrograins, hence these were available for identification by electron microscopy and electron diffraction without exposing them to undue handling and contamination.

Feldspar host crystals proved to have particularly high surface densities of detachable micrograins, frequently of flake or lath shape.Other phases such as olivine,pyroxene,ilmenite and also glass agglutinates were examined for differences in specific adhesion and charging characteristics and for crystallographic relation between the carrier and its surface coating of micrograins.The host supported grains range in general from 20 to 0.07 μm diameter.The cumulative, shear detached particle mass in relation to the carrier grain surface area or mass was in general smaller in the glass agglutinates than in the units with a crystalline structure.The argon rinsed glassy units appear to contain a great many surface protuberances with "welding" contact.

After completed gas shear exposure,the host grains display some residual coating of micrograins whose substrate adhesion appears to be maximized by increased contact area (as in crevices) or perhaps due to optimum image forces based on the dielectric properties of the two materials in contact.Alternatively an uneven distribution of surface charges could induce the local,exceptionally high adhesion forces.Local variations in argon shear due to specimen geometry and location are also unavoidable.A detailed examination of the

lunar grains before the gas flow experiments is precluded by the fact that any electron beam and especially the high intensity SEM electron beam interferes with the original interparticle adhesion mechanism. Specific experiments were made to study this effect and enhanced mobility of the micrograins with increasing surface charge was noted, until finally the electrostatic repulsion cleaned the carrier grains completely.

Comments

The electrostatic interparticle adhesion forces in our experiments are comparable in magnitude to the (in other respects dissimilar) adhesion forces between fresh crystal cleavage surfaces in high vacuum. For lunar rocks Grossman (6) found such forces amounting to 800 dynes, decaying to 200 dynes in 2 minutes and in 15 minutes below the measurement capability limit. The interparticle forces observed in the lunar soil, ranging between 10 and 250 dynes certainly represent lower limits in view of the partial adhesion decay anticipated from sample handling and storage on Earth for several months before the measurements were made.

References

1. Gold,T. "The Depth of the Lunar Dust Layer" in Lunar Science III,1972 LSI Contribution No.88 p. 321.

2. Arrhenius,G.,Asunmaa,S.K. and Fitzgerald,R.W. "Electrostatic Properties of Lunar Regolith" in Lunar Science III,1972,p.30.

3. Asunmaa,S.K. and Arrhenius,G."Interpretation of Electrostatic Properties of Lunar Regolith" in Proc.30th Annual Meeting,Electron Microscopy Soc.America,Los Angeles,Ca.1972,ed.C.J.Arceneaux,Claitor's Publ. Div.,Baton Rouge,La. p.532.

4. Asunmaa,S.K. and Arrhenius,G. "Surface Damage in Lamellar Lunar Regolith Grains", ibid. p.534.

5. Gammage,R.B. and Becker,K. "Search for Exoelectrons in Apollo 12 Materials" Earth and Planetary Science Letters 12 (1971),155.

6. Grossman,J.J.,Ryan,J.A.,Mukherjee,N.R. and Wegner,M.W."Microchemical,Microphysical and Adhesive Properties of Lunar Material" in Proc. Apollo 11 Lunar Science Conference (1970) Vol.3. ed.A.A.Levinson, Pergamon Press,p.2171.

INFRARED STRUCTURAL CHARACTERIZATION OF SINGLE GRAINS FROM TWO APOLLO 15 DUSTS. P. A. Estep, J. J. Kovach, C. Karr, Jr., Morgantown Energy Research Center, U. S. Department of the Interior, Bureau of Mines, Morgantown, West Virginia, 26505.

Single grains ($>150\mu$) of minerals, basalts, and glasses from two Apollo 15 dusts have been structurally characterized by infrared absorption spectroscopy. The two comprehensive dusts were obtained from geologically different terrains—sample 15301,83 from the Apennine Front on the northeast rim of Spur Crater (Station 7), and lying on a narrow ridge that may be a ray formed from the craters Aristillus or Autolycus; and sample 15601,72, from the Mare-Rille terrain, collected approximately 20 meters northeast of the rim of Hadley Rille (Station 9a), lying off the ridge. The infrared spectral data show that grains from each dust have distinctive structural features that characterize the site of collection and may help to interpret its geology. Structural features of grains from the Front dust were similar to those in grains that we previously isolated from Apollo 14 Fra Mauro highland samples,[1] while those from the Rille dust were similar to those that we observed in grains from Apollo 11 and 12 mare basaltic samples.[1][2] Differences between the two Apollo 15 samples as determined by single-grain infrared analyses may further serve to distinguish ray material from non-ray material.

The dusts were dry-sieved and single grains isolated from only the +100 mesh fractions. The Front dust gave a smaller amount of +100 mesh (15.5 wt %) than the Rille dust (32.6 wt %), or any of the six other dusts that we previously studied from Apollo 11, 12 and 14 Missions (21.7 to 32.1 wt %). Infrared analyses for single grains from the dusts, as shown in Table 1, were obtained by recently developed microsampling techniques.[1] These made it possible to detect grain-to-grain structural variations in several different mineral classes within each dust sample, and to characterize the structures of some trace accessory minerals.

SILICATE MINERALS

Plagioclase Four plagioclase grains from the Front dust (An_{76}, An_{78}, An_{79}, An_{79}; snow-white granular, pink and yellow translucent) gave unusual infrared spectra. These had a well-defined absorption band triplet at 395, 385 and 375 cm^{-1}, as shown for example in curve (b), Fig. 1, that was not observed in spectra of other plagioclase grains from this dust. Moreover, only three such grains were previously isolated from a Fra Mauro dust (14259,15; An_{78}, An_{80}, An_{83}; snow-white granular) and two from a mare dust (10085,46; An_{92}, An_{100}; snow-white granular).[2] The 67 other lunar plagioclase spectra from all lunar rock and dust samples that we studied showed only one predominant absorption band in this region, similar to that shown in curve (d), Fig. 1, which varied in frequency from 395 to 380 cm^{-1}. We have observed the unique splitting in varying degrees in infrared spectra of terrestrial plutonic anorthite (An_{92}) from Grass Valley, Calif. (curve (a), Fig. 1), plagioclase (An_{80}) from three eucrites, and an anorthite synthesized under hydrothermal conditions.[3] The splitting was not observed in spectra of volcanic lava plagioclase (An_{94}) from Miyake, Japan (curve (c), Fig. 1) or the synthetic sample of curve (d), Fig. 1. It appears to be reversible and related to thermal history of the sample as shown in heating experiments on terrestrial samples in this laboratory. For example, heating the Grass Valley anorthite to near melting temperatures converted the triplet to a singlet (383 cm^{-1}). Conversely, the predominant absorption band at 383 cm^{-1} in spectra of the synthetic and Miyake anorthites was converted to the unique triplet by annealing at 1050° C for 76 hours. In spectra of both lunar and terrestrial samples,

INFRARED STRUCTURAL CHARACTERIZATION

P. A. Estep

TABLE 1. – Compositional Data for Single Grains Isolated from Apollo 15 Dusts

Mineral class	Sample	Description of mineral grains[1]	Number of grains	Analytical frequencies,[2] cm^{-1}	Derived composition
Silica					
α-Quartz	15601,72	Mixed with olivine; medium yellow, honey transparent	2	1075, 791, 773, 454, 392, 368	
		Composited with other lunar silicates, black, smooth surfaced, blocky	1		
Plagioclase	15301,83	Colorless transparent, tinted translucent, white granular	9	223-228	An_{76}-An_{79}
	15601,72	Colorless transparent, white granular	7	225	An_{79}
Pyroxenes					
Orthopyroxenes					
Bronzite[3]	15301,83	Light yellow opaque	2	396, 393	Fs_{11}, Fs_{16}
	15301,83	Light yellow transparent, light yellow to honey translucent	4	395-392	Fs_{13}-Fs_{17}
	15601,72	Light yellow transparent	1	390	Fs_{20}
Clinopyroxenes					
Pigeonite (Wo_5-Wo_{15})	15301,83	Light yellow transparent	1	390	Fs_{24}
	15601,72	Medium yellow to medium amber	5	393-380	Fs_{20}-Fs_{40}
Subcalcic Augite (Wo_{15}-Wo_{25})	15301,83	Golden yellow to medium amber transparent	3	387-375	Fs_{20}-Fs_{48}
	15601,72	Honey to medium amber transparent	15	390-372	Fs_{24}-Fs_{53}
Augite (Wo_{25}-Wo_{45})	15301,83	Light to dark amber transparent	5	387-383; 321-319	Fs_{29}-Fs_{35}, Fs_{43}-Fs_{46}
	15601,72	Yellow to dark amber transparent	8	394-385; 320-315	Fs_{18}-Fs_{32}, Fs_{44}-Fs_{53}
Pyroxenoid	15601,72	Honey transparent; 400 x 400 μ	1	726, 705, 670, 659, 632, 572, 556	
Olivines	15301,83	Light yellow to honey, green, transparent to opaque; some rounded	8	402-391	Fa_{26}-Fa_{43}
	15601,72	Light yellow to honey, green, transparent to opaque; some rounded	21	402-390	Fa_{26}-Fa_{45}
Ilmenite	15301,83	Black lustrous grains; 150 μ	2	310	> Type I
	15601,72	Black lustrous grains; 300, 400 μ	2	280, 270	Inter. I-II, < Type II
Ulvöspinel	15601,72	Black lustrous grain; 200 μ	1	564, 410, 280	Fe, Ti-rich
Basalts	15301,83	Light to dark grey, granular	3	1000	50% SiO_2
	15601,72	Light to dark grey, granular	2	990, 980	46, 42% SiO_2
Glasses	15301,83	True glass; green transparent, beads and fragments	9	980-970; 500-510	42-38% SiO_2
		Partially crystalline; yellow, green and amber transparent, beads and fragments	14	1000-980; 460-501	
	15601,72	True glass; dark amber transparent fragment, green transparent bead	2	985, 970; 470, 500	44, 38% SiO_2
		Partially crystalline; light yellow to green, brown, transparent to opaque, beads and fragments	4	990-980; 475-500	

(1) Isolated single grains ranged 1500-150 μ and were typically 400-200 μ.

(2) Only selected diagnostic frequencies are listed.

(3) Two types of bronzite spectra were obtained from dust 15301,83; see ref. (1).

INFRARED STRUCTURAL CHARACTERIZATION

P. A. Estep

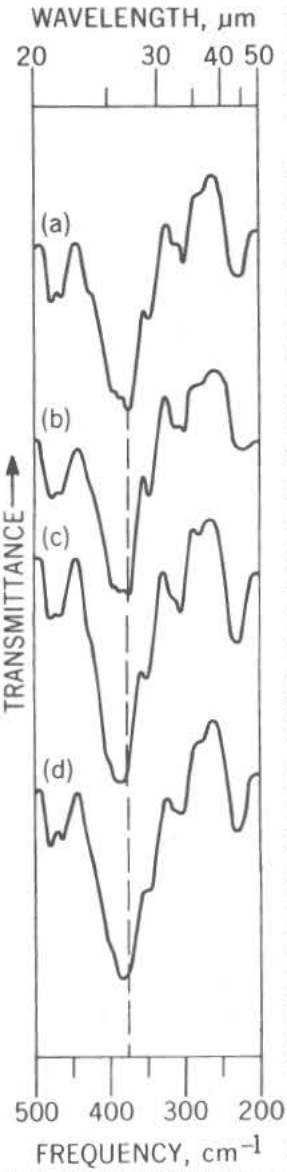

Figure 1. Infrared Spectra of Plagioclase (a) An_{92}, Grass Valley, Calif. (b) An_{79}, 400μ White Granular Grain, from Dust 15301,83 (c) An_{94}, Miyake, Japan (d) An_{100}, Synthetic, Temp-Pres Research, State College, Pa.

relative intensities of the doublet at 477 and 465 cm^{-1} (Fig. 1) were observed to reverse in a continuous manner, but these variations did not correlate systematically with the degree of triplet splitting. Single crystal X-ray studies have shown for plagioclase from these same terrestrial sources,[4][5] that slow-cooling (plutonic) produces cation ordering on the lattice sites, while rapid crystallization from a melt (volcanic) produces cation disordering, and that the degree of ordering is also dependent on Ab content. Such ordering could produce splitting of infrared bands, but it is difficult to determine until infrared and X-ray data are available on the same crystals, if the splitting and the doublet intensity changes are due to Al, Si ordering[6] or Ca(Na) ordering.[4] Plagioclase bands in the triplet region have been assigned to (Si, Al)-O-(Si, Al) deformations and torsions, and bands in the doublet region to a coupling between O-Si-O bending and Ca-O stretching.[3] Infrared frequencies for all these vibrations could be cation site dependent. Thus the variations in infrared spectra of lunar plagioclase indicate a range of different thermal histories, and the within-sample grain variations shown by the Front dust suggest a complex history of events at this site. Further data from infrared and heating studies on both lunar and terrestrial plagioclase samples with known An contents will be useful in deducing specific thermal histories. Since it was shown that the infrared triplet can be produced by annealing, the unique plagioclase grains from Fra Mauro and Apennine Front material could have been slow-cooled at depth. They could represent fragments of the original lunar crust and support the proposed formation of these areas from the Imbrium impact event. Support for this possibility can be obtained from the fact that lunar anorthosite 15415 (Genesis Rock), found by X-ray studies to contain a highly ordered anorthite,[7] was collected near the same site as the Front dust, and that the Apollo 11 dust from which the unique grains were isolated is the same dust in which proposed original crustal anorthositic fragments were found.[8]

Pyroxenes The isolation of more pyroxene grains from the Rille dust than from the Front dust, as seen in Table 1, indicates a higher pyroxene content and a more basaltic composition. An anomaly was observed in spectra of orthopyroxene grains from both Apollo 15 dusts, and is demonstrated in Fig. 2. A band of medium intensity near 450 cm^{-1} in a bronzite grain from the Front dust (curve b) is considerably weaker than that in the spectrum of a terrestrial metamorphic bronzite (curve a) with an equivalent ferrosilite content. In previous studies[1] we have shown that the intensity of the 450 cm^{-1} band in spectra of terrestrial orthopyroxenes decreases systematically with increasing temperature (up to 1000° C) and increasing pressure (up to 1 megabar), and that it correlates with an increasing disorder of Fe^{2+} over the nonequivalent octahedrally coordinated sites M1 and M2 in the pyroxene lattice. The 450 cm^{-1} band was considerably weaker in spectra of orthopyroxene grains from an Apollo 14 breccia (14321,108) and an Apollo 14 dust (14259,15), both with probable shock histories, than in spectra of orthopyroxenes from other samples (10085,46, 14163,80, 14310,93, 15601,83). The band ranged from very weak to moderately weak in spectra of orthopyroxene grains from the Front dust, and this grain inhomogeneity further indicates a complex history for this dust.

INFRARED STRUCTURAL CHARACTERIZATION

P. A. Estep

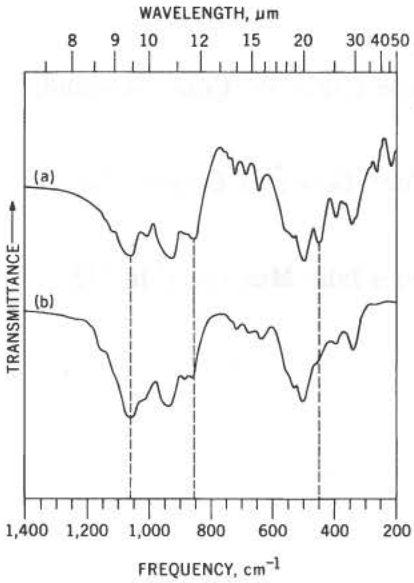

Figure 2. Infrared Spectra of Orthopyroxenes (a) Bronzite (Fs_{11}), Jackson Co., N. C. (USNM 47530) (b) Bronzite (Fs_{11}), 300μ Pale Yellow Transparent Rounded Grain from Dust 15301,83

Pyroxenoids The identification of a metastable pyroxenoid in the Rille dust gave further evidence that this dust is composed largely of material formed by a rapid near-surface crystallization. The spectrum of this pyroxenoid was distinctly different from that of the pyroxenoid which we previously isolated from an Apollo 12 basalt (12021,24), indicating structural differences and different conditions of formation for the parent basalts from which these grains were derived.

Olivines Two unique olivine grains containing minor amounts of α-quartz were isolated from the Rille dust, suggesting a reheating history. A more basaltic composition for the Rille dust was indicated from the larger number of isolated olivine grains and their higher average fayalite content (Fa_{37}) than those from the Front dust (Fa_{32}).

OPAQUE OXIDES

Spectra of ilmenite grains from the dusts were classified, according to the position of the lowest frequency absorption band, as Type I or Type II (at 305 and 275 cm^{-1}, resp.) in end-membered terrestrial samples. This band was at 310 cm^{-1} in spectra of ilmenite from the Front dust and at 270 cm^{-1} in a grain from the Rille dust, and thus exceeded the range for terrestrial samples. In previous studies of ilmenite spectra from other lunar samples,[1] we observed that highland samples were generally Type I, while those from the mare basalts were Type II. A single grain of ulvöspinel was isolated from the Rille dust and its composition further indicated a similarity of this dust to mare basalts.

BASALT GRAINS AND SIEVED FRACTIONS

Infrared spectra of bulk-composition samples from the two Apollo 15 dusts indicated the same distinctions between highland and mare compositions as was observed in studies on mineral grains. Spectra of basalt grains and the -100 mesh sieved fraction from the Front dust matched those of previously studied Apollo 14 highland samples (shown to be predominant in plagioclase), while spectra of the basalt grains and -100 mesh fraction from the Rille dust matched those of previously studied Apollo 11 and 12 mare samples (shown to be predominant in pyroxenes). From a previously derived correlation relating the Si-O stretching frequency (near 1000 cm^{-1}) to silica content,[2] we determined that bulk compositions of the Front dust basalt grains (50 wt % SiO_2) and -100 mesh fractions (45 wt % SiO_2) were slightly less basic than those of the Rille dust basalt grains (42-46 wt % SiO_2) and -100 mesh fractions (42 wt % SiO_2).

GLASS

The abundant green glass from the Front dust gave unique infrared spectra in which the background absorption decreased from high to low frequencies, while that in spectra of glasses from Apollo 11, 12 and 14 samples and the Rille dust increased from high to low frequencies. Such a spectral behavior may be related to the structural homogeneity and the high refractive index of this unique glass. Using the previously described correlation plot, we determined that the compositions of true glasses from Apollo 15 dusts were more basic (38-44 wt % SiO_2) than those from Apollo 14 dusts (42-54 wt % SiO_2), as were those from Apollo 11 and 12 dusts (34-50 wt % SiO_2).

INFRARED STRUCTURAL CHARACTERIZATION

P. A. Estep

REFERENCES AND NOTES

1. Estep P. A., Kovach J. J., Waldstein P., and Karr C., Jr., Proc. Third Lunar Sci. Conf. Geochim. Cosmochim. Acta Suppl. 3, 3 (1972) 3047. MIT Press.

2. Estep P. A., Kovach J. J., Karr C., Jr., Proc. Second Lunar Sci. Conf. Geochim. Cosmochim. Acta Suppl. 2, 3 (1971) 2137. MIT Press.

3. Iiishi K., Tomisaka T., Kato T., Yamaguchi, and Umegaki Y., Neues Jahr. Mineral. Abh. 115 (1971) 98.

4. Laves F. and Goldsmith J. R., Acta Cryst. 7 (1954) 465.

5. Gay P., Mineral. Mag., 30 (1954) 428.

6. Laves F. and Goldsmith J. R., Z. Krist., 106 (1955) 227.

7. Steele I. M. and Smith J. V., Nature, 234 (1971) 138.

8. Wood J. A., Dickey J. S., Jr., Marvin U. B. and Powell B. N., Proc. Second Lunar Sci. Conf. Geochim. Cosmochim. Acta Suppl. 1, 1 (1970) 965. MIT Press.

9. We thank A. A. Angotti, R. C. Berkshire, Jr., E. E. Childers, and B. D. Stewart for obtaining infrared spectra. This work was sponsored by NASA contract No. T-1760A.

INFRARED EMISSION SPECTRA OF APOLLO 15 SOILS. L.M. Logan, G.R. Hunt and J.W. Salisbury, Terrestrial Sciences Laboratory, Air Force Cambridge Research Laboratories, L.G. Hanscom Field, Bedford, Mass. 01730

In a previous paper[1] we reported on the spectral emission properties of two Apollo 15 soil samples. One sample (15101) was collected at Station 2 on the edge of the Apennine Front, while the other (15601) was collected at Station 9A on the margin of Hadley Rille. These samples yielded spectra that were entirely consistent with spectra previously obtained with a balloon-borne telescope system of the Apennine Mts. and Mare Imbrium, respectively, demonstrating the validity of that remote sensing effort[1]. The spectra were also consistent with the systematic variation of effective emissivity peaks (Christiansen peaks) with rock type, as shown in laboratory experiments on terrestrial rocks in a simulated lunar environment[2]. Most important, the fact that the infrared emission spectra of two different soils only 4 km apart were different, showed that cross-contamination was not sufficient to disguise their compositionally diagnostic infrared spectral signatures.

In this paper we present spectra of two additional Apollo 15 soil samples recorded in a simulated lunar environment as described in detail elsewhere[3]. Sample 15271 was collected at Station 6 and sample 15301 at Station 7. These stations are 450 meters apart on the Apennine Front about 2½ km ESE of Station 2.

As shown in Figure 1, the emission spectra of all three Apennine Front soil samples are identical, with Christiansen peaks located at 8.30 $\pm$ .02 microns. This indicates either that cross-contamination effectively homogenizes lunar soils at distances up to 2½ km or, more likely, that the provenance of all three soils is the same. Assuming the latter case, the emission spectrum of Apennine Front material can be considered well enough known for this area to be used as a remote sensing calibration source.

Comparing spectra of Apennine Front material with spectra of soil derived from the Frau Mauro formation at the Apollo 14 site is of interest. It is generally assumed that the Frau Mauro formation was derived from rocks such as those exposed on the Apennine Front during the gigantic impact that produced the Imbrian Basin. Yet, Frau Mauro soil spectra are distinctly different from those of Apennine Front material, displaying a Christiansen peak at 8.24 $\pm$ .02 microns (Fig. 1). This suggests significant vertical or lateral inhomogeneity in the source rocks of the Frau Mauro formation, which should result in lateral inhomogeneities within the Frau Mauro formation itself.

Infrared Soil Spectra

L.M. Logan

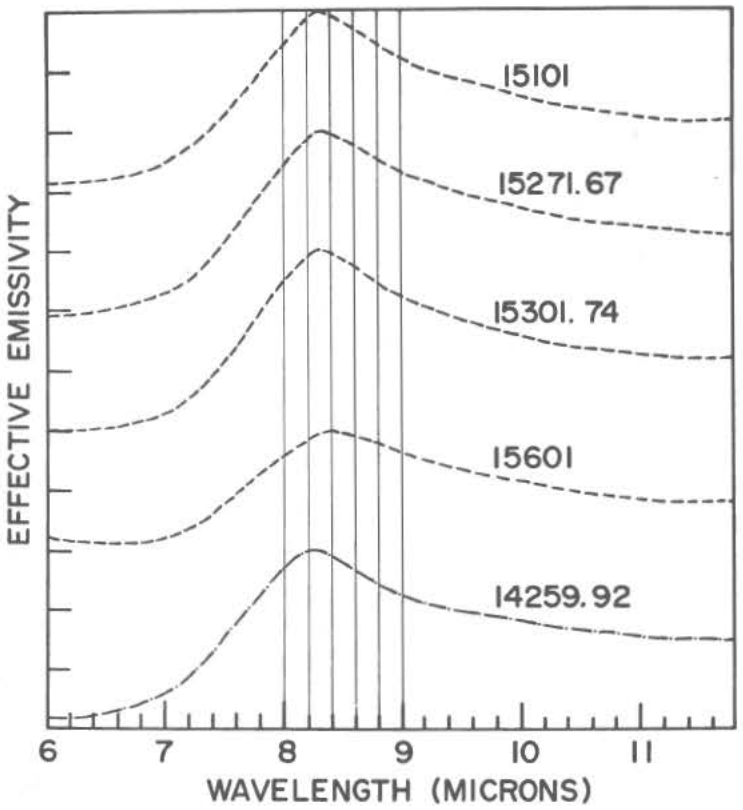

Figure 1. Effective emissivity spectra of lunar soils recorded in the laboratory under simulated lunar conditions. Each spectrum is normalized to an emissivity of 1 at the Christiansen peak. Curves have been separated vertically for clarity. Vertical scale divisions are 10 percent.

REFERENCES

1. Logan, L.M., Hunt, G.R., Balsamo, S.R. and Salisbury, J.W. (1972) Mid-infrared emission spectra of Apollo 14 and 15 soils and remote compositional mapping of the moon. Geochimica et Cosmochimica Acta (in press).

2. Logan, L.M. and Hunt, G.R. (1970) Infrared emission spectra: Enhancement of diagnostic features by the lunar environment. Science 169, 865-866.

3. Logan, L.M. and Hunt, G.R. (1970) Emission spectra of particulate silicates under simulated lunar conditions. Journal of Geophysical Research 75, 6539-6548.

FREQUENCY AND TEMPERATURE DEPENDENCE OF THE ELECTRICAL PROPERTIES OF A SOIL SAMPLE FROM APOLLO 15. G. R. Olhoeft, Lockheed Electronics Co., Houston TX 77058, A. L. Frisillo, NRC/NAS Fellow, MSC, Houston, TX 77058 and D. W. Strangway, MSC, Houston, TX 77058.

The dielectric constant, loss tangent and D.C. conductivity of soil sample 15301,38 have been measured using a three terminal technique in vacuum (2×10^{-7} torr) as a function of temperature to 827° C. The sample density was determined to be 1.47±0.06 gm/cc with an estimated porosity of 55%.

The D.C. conductivity data is graphically represented in Figure 1. This figure represents data accumulated as temperature was cycled from room to some maximum (T_{max}) and then back to room temperature. In the subsequent run, T_{max} was increased by approximately 100° C beyond the previous value and data taken as temperature was decreased. This process continued until the largest value of T_{max}=827°C was reached. As may be observed from Figure 1, no hysteresis in the D.C. conductivity was observed as has been reported by other authors using solid samples (Refs. 1 and 2). The activation energy, as calculated from Figure 1, is 0.50±0.08 ev.

Representative dielectric properties are given in Tables 1 and 2 and are illustrated in Figure 2. The dielectric constant at room temperature is nearly frequency-independent with a value of about 3.2. The loss tangent values at room temperature are somewhat frequency-dependent, but, as in earlier studies, they are extremely low (Ref. 3). The dielectric constant and loss tangent increase with temperature and a very distinct frequency dependence appears, suggesting a Maxwell-Wagner relaxation process due to intergranular effects. The dielectric properties show three distinct regions where the properties vary as a function of temperature. These are 25 - 200°C, 200 - 600 or 700°C and over 700°C. At least one of these break points roughly corresponds to the maximum temperature reached during a lunation.

Although no hysteresis was seen in the D.C. conductivity, a definite dielectric hysteresis was observed when the sample temperature exceeded about 700°C. To illustrate the observed hysteresis, the loss tangent (Tan δ) for f = 100 Hz has been plotted as a function of temperature in Figure 3. When $T_{max} \leq 700°C$, Tan δ was easily reproducible within experimental limits during each temperature cycle (middle curve). However, when T_{max} was brought to 827°C, Tan δ returned to a new value (top curve) indicating a hysteresis effect that was reproduced several times. This effect is further illustrated in Figure 4 in which curve A represents the previously observed behavior of Tan δ vs. frequency at T = 25° C ($T_{max} \leq 700°C$) and curve B indicates the new "irreversible" data at T = 25° C (T_{max}=827°C). Curves C and D show the behavior of Tan δ at the two pertinent values of T_{max}.

After completion of the temperature cycles, the sample was then exposed to air and measured at several different times. This data is presented in Figure 5 in which curve A represents Tan δ for $T_{max} \leq 700°C$ and B is for T_{max} = 827°C which was obtained prior to exposure to air. Curve C in this figure is

for data recorded immediately after the sample was exposed to air with no time allowed for temperature equilibrium with ambient conditions to be established. Data recorded after 3.5 hours (curve D) shows a tendency toward higher values of Tan δ at all frequencies. After 19.5 hours (curve E), enough moisture has been absorbed by the sample to raise Tan δ by approximately an order of magnitude. These results are consistent with those reported earlier by our laboratory on an Apollo 14 sample (Ref. 3).

Several days after exposing the sample to air, the sample was again placed into the apparatus and allowed to remain in a vacuum of 2×10^{-7} torr for three days. The density of the sample in this run was determined to be 1.63 ± 0.06 gm/cc. The final measurement of Tan δ vs. frequency at 25°C (curve F in Figure 5) does not show the earlier observed hysteresis. In fact, this data seems to indicate that if the remaining moisture was removed from the sample, nearly identical results as those for $T_{max} \leq 700^{\circ}$ C would be obtained. In this sense, the hysteresis appears to be reversible. Investigations are continuing to resolve the cause of the observed hysteresis.

References:

1. Schwerer, F. C., T. Nagata and R. M. Fisher, Electrical conductivity of lunar surface rocks and chondritic meteorites, The Moon, 2, pp. 408-422, 1971.

2. Schwerer, F. C., G. P. Huffman, R. M. Fisher and T. Nagata, D.C. electrical conductivity of lunar surface rocks with complementary Mossbauer studies, Lunar Science III, Rev. Abst. of papers presented at Third Lunar Science Conference, Houston, 10-13 January, 1972, pp. 686-687, ed. by C. Watkins.

3. Strangway, D. W., G. R. Olhoeft, W. B. Chapman and J. Carnes, Electrical properties of lunar soil - dependence on frequency temperature and moisture, Earth Planet. Sci. Letters, in press.

Table 1

Dielectric Constant

Freq/Temp (°C)	25	330	610	827
10^2	3.24	3.86	21.4	-
10^3	3.20	3.49	7.54	-
10^4	3.18	3.35	4.75	30.2
10^5	3.17	3.29	3.80	10.6
10^6	3.17	-	3.55	4.35

Frequency and Temperature Dependence

G. R. Olhoeft

Table 2

Loss Tangent

Freq/Temp (°C)	25	330	610	827
10^2	0.010	0.11	0.69	-
10^3	0.0058	0.046	0.56	-
10^4	0.0033	0.017	0.28	1.1
10^5	0.0032	0.0052	0.12	0.53
10^6	0.001	0. -	0.032	0.24

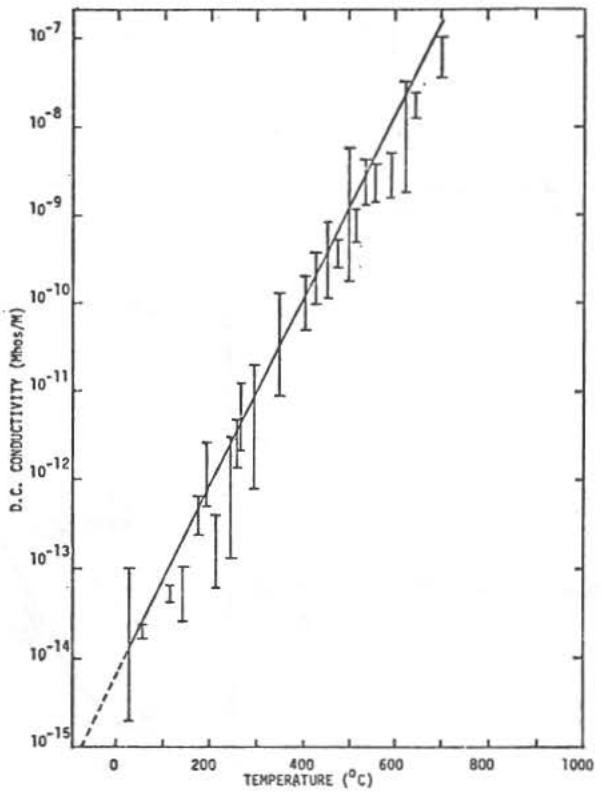

Figure 1: D.C. conductivity as a function of temperature.

Frequency and Temperature Dependence

G. R. Olhoeft

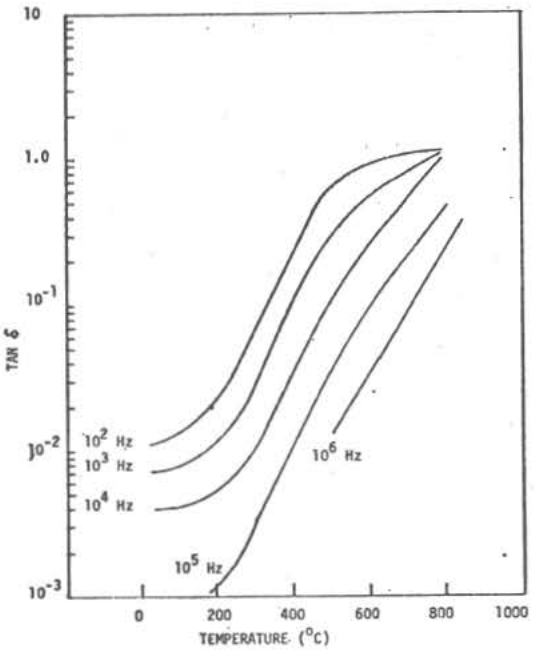

Figure 2: Representative data showing temperature dependence of loss tangent at constant frequency.

Figure 3: Tan δ vs. Temperature for constant frequency, f = 100 Hz.

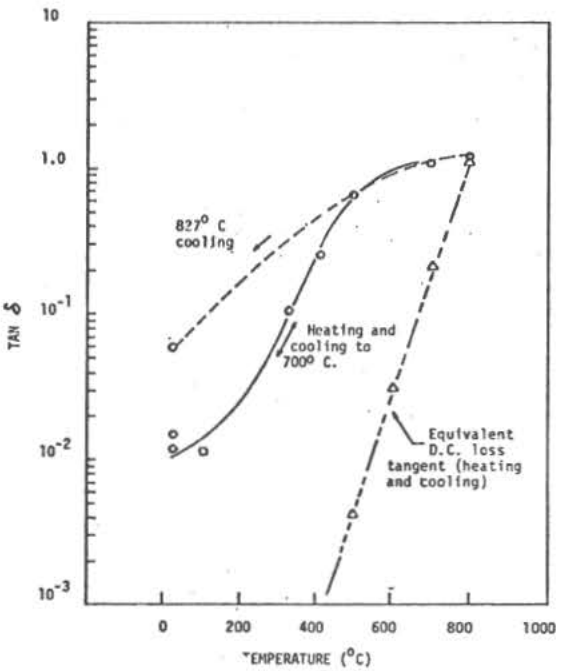

Frequency and Temperature Dependence

G. R. Olhoeft

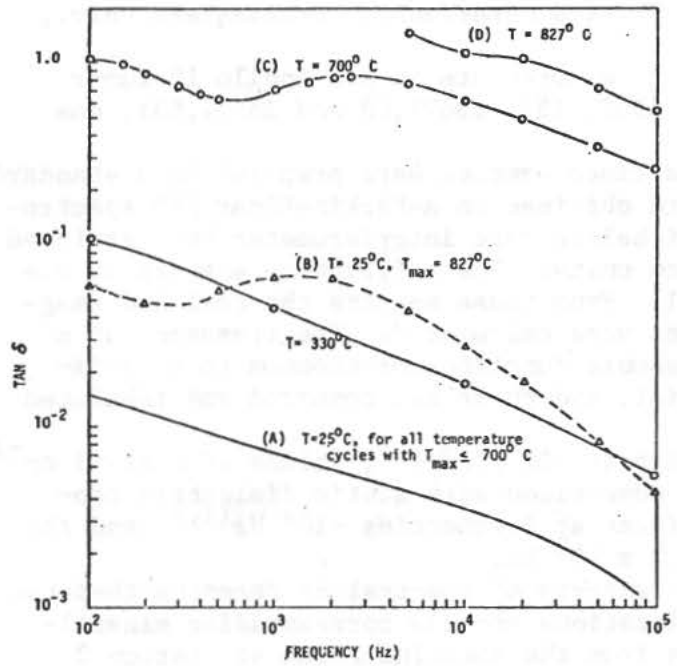

Figure 4: Tanδ vs. frequency for constant temperature showing hysteresis.

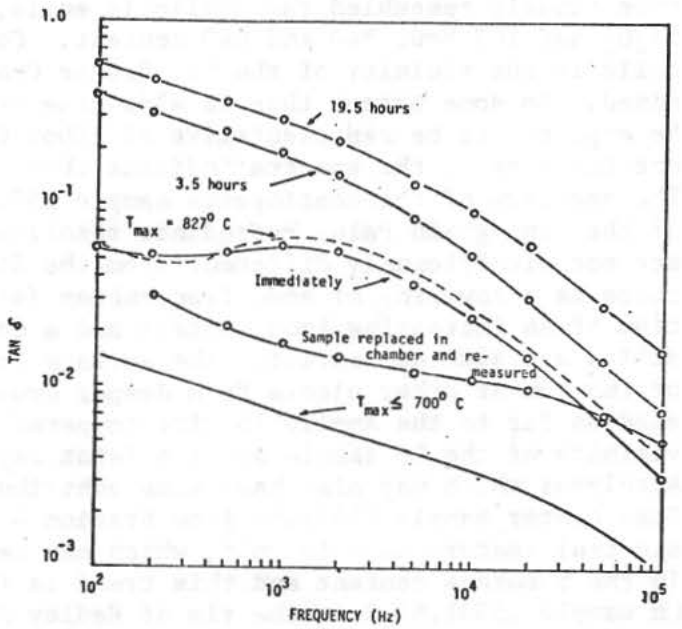

Figure 5: Tanδ vs. frequency at T = 25°C showing effect of exposing sample to air and subsequent data after sample was placed in vacuum for 3 days.

INFRARED STUDIES OF APOLLO 15 FINES.* C.H.Perry and R.P. Lowndes, Solid State Spectroscopy Laboratory, Physics Department, Northeastern Univ., Boston, Mass. 02115.

We have made infrared reflectance measurements on six Apollo 15 lunar fines (15091,65, 15221,71, 15071,60, 15021,159, 15471,68 and 15531,63), one rock sample (15426,2).

Pressed disks ∿1 mm thick of the fines samples were prepared in a standard 5 mm diameter die and the spectra were obtained on a Perkin-Elmer 180 spectrophotometer and a Fourier-transform Michelson type interferometer both equipped with near normal incidence reflectance units. The reflectance spectra of the Apollo 15 samples are shown in Fig. 1. From these spectra the real and imaginary parts of the dielectric constant were calculated. The frequency of a given resonance in the dielectric response function corresponds to a fundamental vibrational mode of the material, and these are compared and tabulated in Table 1.

At limiting frequencies, where $R = (\varepsilon^{\frac{1}{2}}-1)^2/(\varepsilon^{\frac{1}{2}}+1)^2$, values of ε at ∿5 cm^{-1} (i.e., $\sim 10^{11}$ Hz) were calculated for comparison with static dielectric constants obtained using standard techniques at frequencies $<10^6$ Hz[1,2] and the data obtained by Gold et al.[3] at 4.3×10^8 Hz.

The Apollo 15 soils show a large variety of spectral differences that can be associated with their geographic locations and the corresponding mineralogical compositions. The two samples from the Apennine Front at Station 2 (15091,65 and 15221,71) comprise St. George Crater ejecta and other ejecta materials. The two showed some very slight spectral variations but in fact more closely resembled the Apollo 14 soils,[2] having about a 48% SiO_2; 18% Al_2O_3 and 10% MgO, FeO and CaO content. Consequently, it would appear that soils in the vicinity of the St. George Crater rim are substantially intermixed. To some extent this is also true of 15071,60 from Station 1 which might be expected to be representative of Elbow Crater ejecta but apparently this is not the case as the spectra indicate that the soil is again well intermixed. The spectrum of the contingency sample 15021,159 is presumably representative of the fine-grain Palus Putredinis regolith. Although the spectral features are not significantly different from the St. George and Elbow Crater ejecta, there is a lowering of some frequencies (see Table 1) which is usually indicative of an increasing iron content and a corresponding slight decrease in the silica and alumina content. The surface layer here may be more representative of Imbrium or other ejecta from deeper crust levels that would not have traveled as far to the Apollo 15 site compared to the Apollo 14 site. Also in the vicinity of the LM sample are the faint rays from the craters Aristillus and Autolycus which may also have some contributing effect. The spectrum of the Dune Crater sample 15471,68 from Station 4 shows further enhancement of the spectral feature at ∿450 cm^{-1}, which can be associated with a slight increase in the pyroxene content and this trend is further enhanced as seen in Fig. 1 in sample 15531,63 from the rim of Hadley Rille. These spectra are similar to

INFRARED STUDIES OF APOLLO 15 FINES

C.H. Perry and R.P. Lowndes

some of the Apollo 12 rocks[2] such as 12002,186 or 12009,48 which have high pyroxene contents. It may be expected that these young ejecta materials are more representative of bedrock whereas the material from the Apennine Front contains largely gardened mixtures. The SiO_2 and Al_2O_3 contents in the Hadley Rille rim sample have probably dropped to less than 45% and 15% respectively with a subsequent slight increase in the abundance of FeO and TiO_2.

In contrast, the 15426,2 breccia from Station 7 at Spur Crater is spectroscopically different from the Apollo 15 soils that we have examined. It is also obviously richer in pyroxene than the Fra Mauro breccias but does not show the same spectroscopic features observed in the Apollo 12 samples. It bears some resemblance to the Cone Crater sample 14321,263[2] which has a high magnesium and a low calcium content.

The Christianson frequencies corresponding to peaks in the fine powder emissivity spectra show a variation of $\sim$1225 cm^{-1} for the Elbow and St. George Crater ejecta to $\sim$1205 cm^{-1} for the Hadley Rille sample. This again indicates a lowering of the SiO_2 content by a few percent as the surface sampled material becomes more basic and characteristic of bedrock. Exactly similar trends are observed in the dielectric constant values at $\sim 10^{11}$ Hz where there is a marked increase in the Hadley Rille 15531,63 sample for sample densities which varied from about 2400-2600 Kgm/m^3.

References

Proc. Third Annual Lunar Science Conference (Supplement 3, Geochimica et Cosmochimica Acta), Vol. 3 (in press):

1. C.H. Perry, D.K. Agrawal, E. Anastassakis, R.P. Lowndes and N.E. Tornberg.
2. D.H. Chung and W.B. Westphal.
3. T. Gold, E. Bilson and M. Yerbury.

*This work was supported by NASA Grant NGR 22-011-069 and partial equipment support was provided under NASA Cooperative Agreement NCAw 22-011-079.

Table 1 - The infrared vibrational mode frequencies (cm^{-1}), ω_c (Christianson frequency) and ε_o (dielectric constant values at $\sim 10^{11}$ Hz) for the Apollo 15 samples.

Suggested Assignment	St. 1 Elbow Crater Ejecta	St. 2 St. George Crater Ejecta		Ray Area (LM)	St. 4 Dune Crater	St. 9a Hadley Rille	St.7 Spur Crater Ejecta
	15071,60	15221,71	15091,65	15021,159	15471,68	15531,63	15426,2
Combinations		1100	1090	1040	1100	1070	1040
M-O Stretch	1000	1000	1000		1000,950	960	
	920			890		930,910	
	870,820	890	880		860	870	850
Cation-Oxygen	780	790	790		770	790	810
Lattice	670	670	670	660	680	700	710
Vibrations	610	610	600		620	630	640,610
	580	550	550		560		570
M-O-M Bend	460	440	440	470	450	510,450	450
	370	370	360	370	370	380	370
Lattice	290	280	280	300	280	280	280
Modes	230	230	220	210	230	220	
ω_c (cm^{-1})	1225	1220	1220	1220	1210	1205	1220
ε_o	3.8	4.2	4.0	4.0	4.2	4.9	6.5

INFRARED STUDIES OF APOLLO 15 FINES

C.H. Perry and R.P. Lowndes

15071,60 (Fines) Station 1
Elbow Crater ejecta.

15091,65 (Fines) Station 2 St.
George Crater ejecta, etc.
Mature Regolith.

15221,71 (Fines) Station 2 St.
George Crater ejecta, etc.
Mature Regolith.

15021,159 (Contingency Sample)
LM. Fine grained Regolith
(Ray area).

15471,68 (Fines) Station 4 S.E.
Dune Crater (secondary crater
ejecta).

15531,63 (Fines) Station 9a
Rim Hadley Rille.

15426,2 (Breccia) Station 7
Spur Crater ejecta.

Fig. 1 Infrared reflectance spectra of six Apollo 15 fines and one rock sample from 0-2000 cm^{-1}.

INFRARED STUDIES OF APOLLO 15 FINES

C. H. Perry and R. P. Lowndes

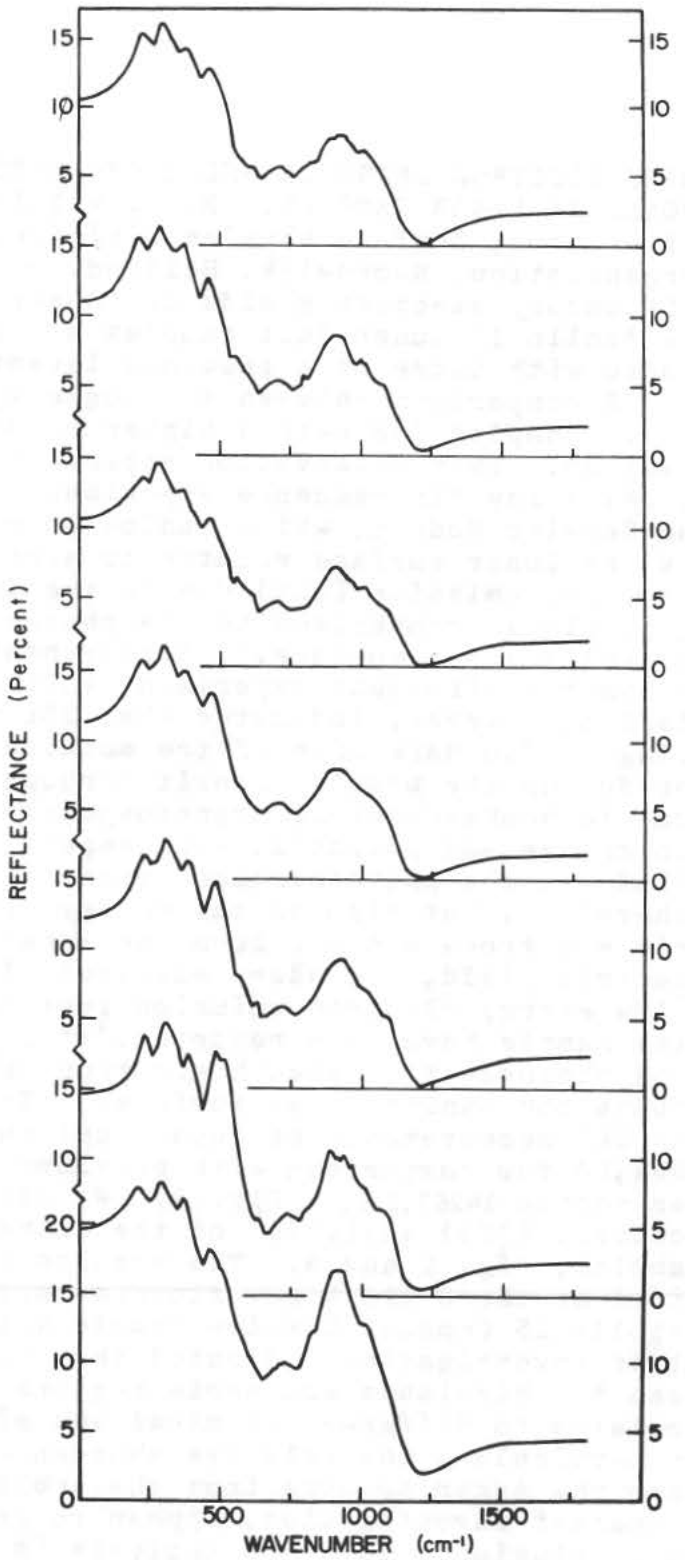

SECONDARY ELECTRON EMISSION AND AUGER ELECTRON SPECTROSCOPY FROM APOLLO 15 LUNAR SAMPLES. R. F. Willis, M. Anderegg, B. Feuerbacher, B. Fitton, Surface Physics Division, European Space Research Organization, Noordwijk, Holland.

ABSTRACT - Secondary electron yields and Auger spectroscopic analysis of three Apollo 15 lunar dust samples are reported and the results compared with those of a previous investigation on an Apollo 14 sample. A comparison between the Auger spectra from the Apollo 14 and 15 samples indicate a higher relative abundance of Al/Si in the latter. This observation appears to support the results of the S-161 X-ray fluorescence experiment on board the Apollo 15 Command Service Module, which indicated compositional variations across the lunar surface related to albedo variations.

Secondary electron emission (SEE) due to the impacting solar wind flux is negligible in comparison to the photoelectron continuum above the sunlit lunar surface.[1] Measurements by the charged particle lunar environment experiment (CPLEE)[2,3], during the Apollo 14 mission, however, indicated that SEE may give rise to surface charging on the dark side of the moon and along the moon's terminator during the moon's transit through the geomagnetic tail, due to bombardment by magnetospheric electrons. The lunar surface charge and potential will depend not only on the solar wind flux and the photoemission properties of the lunar material therefore, but also on the energy distribution of the magnetospheric electrons and SEE from the lunar surface.

The photoelectric yield, secondary electron yield and energy distribution of low energy electron emission from an Apollo 14 lunar surface fine sample have been reported,[4,5] together with a calculation of the photoelectron sheath electron density and electric field above the sunlit lunar surface.[4] In this paper, we report similar SEE measurements on lunar dust samples 15101,77, 15021,98 and 15601,68 for comparison with previous measurements[4,5] on lunar sample 14259,116, Fig. 1. We also report Auger electron spectroscopic (AES) analysis[6] of the elemental composition of these samples, Fig. 2 and 3. The results are compared with those obtained by the S-161 X-ray fluorescence experiment carried on the Apollo 15 Command Service Module while in lunar orbit.[7] The latter investigation indicated that the albedo difference between the highlands and maria regions of the lunar surface may be related to different chemical and mineralogical compositions, in particular, the relative abundance of Al/Si. A comparison between the Auger spectra from the Apollo 14 and 15 samples, in the present investigation, appear to provide some support for this conclusion. This AES analysis is in substantial

agreement with the results obtained from Apollo 12 samples.[6]

The samples were handled in a dry nitrogen atmosphere and the secondary electron yield and AES measurements were obtained using a hemispherical collector system, details of which have been described.[4,5] The procedure for obtaining the energy distribution of Auger electrons by electronic differentiation of the secondary electron energy distribution function with respect to energy, N(E) vs. E, is well documented.[6,8] The dN(E)/dE vs. E Auger spectra in this paper were recorded at an incident beam energy and current of 1500 V and 1μA and modulation voltage peak-to-peak amplitudes of 0.5,5 and 20 V. Bakeout of the ultra-high vacuum system and sample was limited to 150°C for 1 week in order to simulate lunar thermal conditions and to remove absorbed gaseous impurities. In situ sputter cleaning by Ar ion bombardment was not used[6] in view of chemical reduction effects which are known to occur.[9]

The secondary electron yield curves from the Apollo 15 samples show a maximum of 1.5 ± 0.1 in the energy region 300-700 ev, similar to that observed previously[5] from the Apollo 14 sample. Values of the yield greater than unity cause the dust to charge positively i.e., for incident electron flux energies in the range 100-200 ev to 1500-2500 ev. Some of the curves, notably those from samples 14259,116 and 15101,77 show a pronounced 'kink' about 1000 ev, which is indicative of secondary electron emission from a mixture of high yield and low yield components. All the curves are typical of those expected for highly particulate, insulating samples as described previously.[5]

Auger electron spectra from an Apollo 15 sample, 15601,68 (Fig. 2) are compared with those from the Apollo 14 sample, 14259,116 (Fig. 3). Spectra from all of the Apollo 15 samples were very similar to that of sample 15601,68. The following elements were identified: Al, Si, K. C, Ca, O and Fe were the major constituents, small amounts of S and Cl appearing in some cases in close agreement with an Apollo 12 sample analysis reported previously.[6] A major difference between the Apollo 14 and 15 samples were the more pronounced Fe peaks at 560, 600, 650 and 700 ev in the latter and the high Al/Si abundance in the Apollo 15 samples (Fig. 2). This would appear to endorse similar compositional differences reported for the two lunar regions from X-ray fluorescence analysis.[7]

If distinct compositional differences between maria and highlands regions of the lunar surface do exist, as these and the results of the Apollo 15 X-ray fluorescence experiment suggest, it would appear that horizontal transport of electrostatically charged dust is not effective over large distances since this would tend to smear out any such differences in the lunar dust layer. This finding reinforces the argument frequently put forward against electrostatic transport, namely the persistence of albedo differences arising from compositional variation in the

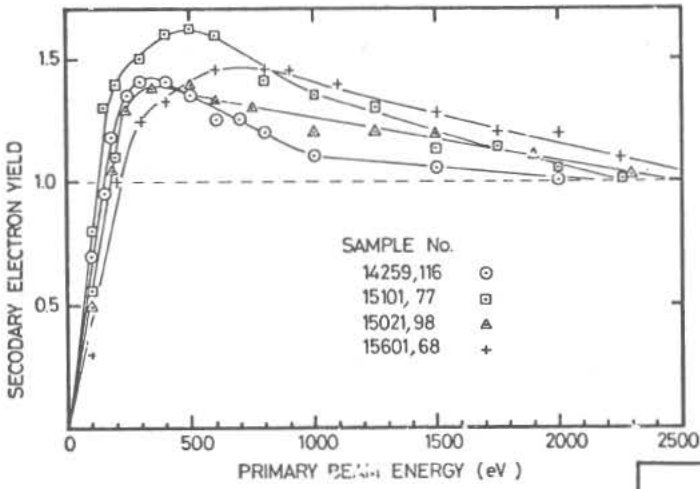

Fig. 1

Secondary electron yield from Apollo 14 and 15 lunar dust samples for incident primary energies of 50 to 2500 ev.

Fig. 2

Auger electron spectra of lunar sample 15601,68. The relative gain for the three curves (left to right) is approximately x1, x10, and x40 corresponding to modulation voltage amplitudes of 0.5, 5.0 and 20.0 V peak-to-peak.

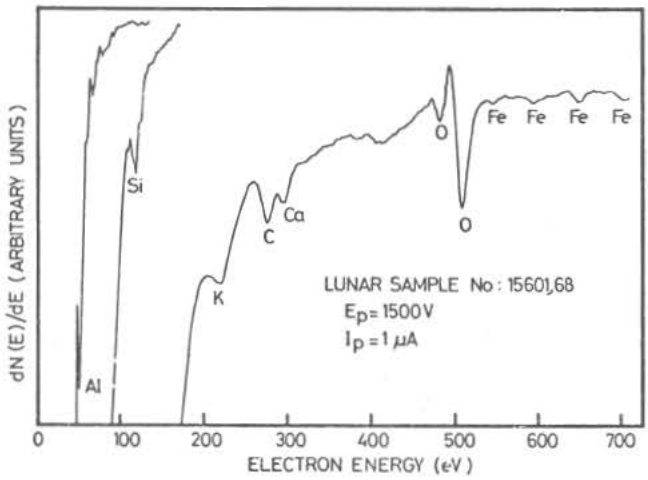

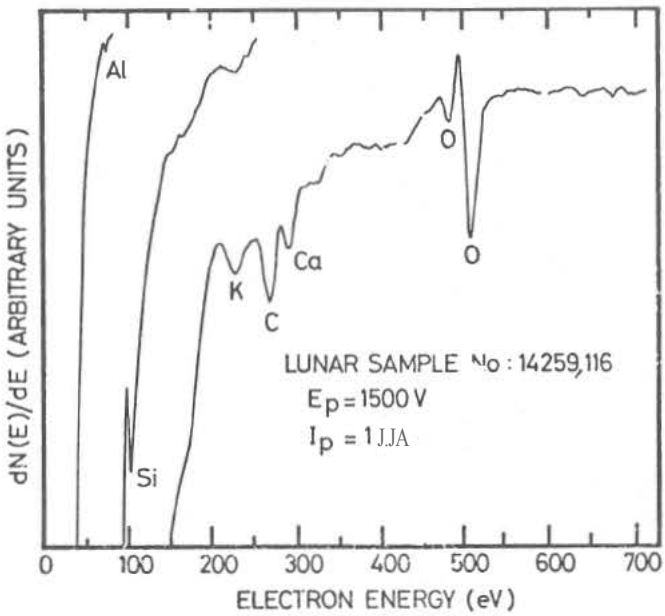

Fig. 3

Auger electron spectra of lunar sample 14259,116
The relative gain for the three curves is identical to that of Fig. 2.

Al/Si content.[7] It is hoped to perform similar measurements on clean Apollo 16 samples to further clarify these results.

References

1. Grobman W. D. and Blank J. L. (1969 J. Geophys. Res. 74 3943.
2. O'Brien B. J. and Reasoner D. L. (1971) Apollo 14 Prelim. Science Report, p. 193 NASA SP-272.
3. Reasoner D. L. and Burke W. J. (1972) Proc. Third Lunar Sci. Conf., Geochim. Cosmochim. Acta Suppl., Vol. 3, MIT Press.
4. Feuerbacher B., Anderegg M., Fitton B., Laude L. D., Willis R. F., and Grard R. J. L. (1972) Proc. Third Lunar Sci. Conf., Geochim. Cosmochim. Acta Suppl., Vol. 3, MIT Press.
5. Anderegg M., Feuerbacher B., Fitton B., Laude L. D., and Willis R. F., (1972) Proc. Third Lunar Sci. Conf., Geochim, Cosmochim. Acta Suppl. Vol. 3, MIT Press.
6. Connel G. L., Schreidmiller R. F., Kraatz P., and Gupta Y. P., (1971) Proc. Second Lunar Sci. Conf., Geochim. Cosmochim. Acta Suppl. Vol. 3, p. 2083, MIT Press.
7. Adler I., (1972) Proc. Third Lunar Sci. Conf., Geochim, Cosmochim. Acta Suppl. Vol. 3, MIT Press.
8. Chang. C. C., (1971) Surface Sci. 25 53, for a review.
9. Yin L. I., Ghose S., and Adler I, (1971) Goddard Space Flight Center Report, to be published.

SAMPLE NUMBER INDEX

AUTHOR INDEX

G

H

SUBJECT INDEX*

*Pagination refers to first page of paper in which subject is cited.